KARST WATERS INSTITUTE

Special Publication 5

$i, j+1$

i, j

Karst Modeling

Proceedings of the symposium held
February 24 through 27, 1999
Charlottesville, Virginia

Edited by Arthur N. Palmer, Margaret V. Palmer, and Ira D. Sasowsky

REPORT DOCUMENTATION PAGE

Form Approved
OMB NO. 0704-0188

1. AGENCY USE ONLY *(Leave blank)*	2. REPORT DATE	3. REPORT TYPE AND DATES COVERED
	June 1999	Final

4. TITLE AND SUBTITLE

Karst Modeling

5. FUNDING NUMBERS

DAAG55-98-1-0510

6. AUTHOR(S)

John W. Hess, principal investigator

7. PERFORMING ORGANIZATION NAMES(S) AND ADDRESS(ES)

Karst Waters Institute
Charles Town, West Virginia 25414

8. PERFORMING ORGANIZATION REPORT NUMBER

9. SPONSORING / MONITORING AGENCY NAME(S) AND ADDRESS(ES)

U.S. Army Research Office
P.O. Box 12211
Research Triangle Park, NC 27709-2211

10. SPONSORING / MONITORING AGENCY REPORT NUMBER

ARO 39202.1-EV-CF

11. SUPPLEMENTARY NOTES

The views, opinions and/or findings contained in this report are those of the author(s) and should not be construed as an official Department of the Army position, policy or decision, unless so designated by other documentation.

12a. DISTRIBUTION / AVAILABILITY STATEMENT

Approved for public release; distribution unlimited.

12 b. DISTRIBUTION CODE

13. ABSTRACT *(Maximum 200 words)*

ABSTRACT NOT AVAILABLE

14. SUBJECT TERMS

15. NUMBER IF PAGES

16. PRICE CODE

17. SECURITY CLASSIFICATION OR REPORT	18. SECURITY CLASSIFICATION OF THIS PAGE	19. SECURITY CLASSIFICATION OF ABSTRACT	20. LIMITATION OF ABSTRACT
UNCLASSIFIED	UNCLASSIFIED	UNCLASSIFIED	UL

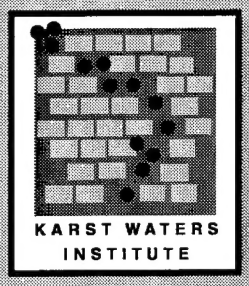

Special Publication 5

Karst Modeling

Proceedings of the symposium held
February 24 through 27, 1999
Charlottesville, Virginia

Edited by Arthur N. Palmer, Margaret V. Palmer, and Ira D. Sasowsky

Published by: Karst Waters Institute, Inc.
P.O. Box 490
Charles Town, West Virginia 25414
http://www.uakron.edu/geology/karstwaters

Please visit our web page for ordering information.

The Karst Waters Institute is a non-profit 501(c)(3) research and education organization incorporated in West Virginia. The mission of the Institute is improvement of the fundamental understanding of karst water systems through sound scientific research, and the education of professionals and the public. The Institute does not issue or have memberships.

Library of Congress Catalog Card Number: 99-60215

ISBN 0-9640258-4-1

Printed in the U.S.A. by the Department of Printing Services, University of Akron.

Text 10 point Times New Roman; titles 12 point Times New Roman on 28/70# Futura Laser White.
Cover stock 12 point Mead Mark V.
Composed using Adobe Pagemaker® software.

Original cover layout by Ron Sill, Nittany Geoscience, Inc.
Original cover illustration by Arthur N. Palmer.

CONFERENCE SUPPORTERS

The Karst Waters Institute greatly appreciates the financial support of the following organizations for the Karst Modeling Symposium:

National Science Foundation

U.S. Army Research Office
(Corps. of Engineers Waterways Experiment Station)

American Chemical Society
(Petroleum Research Fund)

Cave Conservancy of the Virginias

Endless Caverns

CONFERENCE ORGANIZERS AND STAFF

Karst Waters Institute:
Conference Planning:
Arthur N. Palmer
William K. Jones
Publications:
Ira D. Sasowsky
Registration:
Lee F. Elliott
Paul A. Woodell

Field Trip:
William K. Jones
David Hubbard

Production Assistance:
Selena M. Walko
Paul A. Woodell

KARST WATERS INSTITUTE OFFICERS

President	David C. Culver, Ph.D.	**Executive Vice-President**	William K. Jones
Treasurer	Daniel W. Fong, Ph.D.	**Secretary**	Rane L. Curl, Ph.D.

Vice-President for Communications	Ira D. Sasowsky, Ph.D.
Vice-President for Education	Horton H. Hobbs, III, Ph.D.
Vice-President for Research	William B. White, Ph.D.

KARST WATERS INSTITUTE BOARD OF DIRECTORS

	John W. Hess, Ph.D. **(Chair.)**	
Margaret A. Colgate, Ph.D.	William K. Jones	John E. Mylroie, Ph.D.
David C. Culver, Ph.D.	Thomas C. Kane, Ph.D.	Robert E. Putz
Rane L. Curl, Ph.D.	Philip E. LaMoreaux, Ph.D.	Ira D. Sasowsky, Ph.D.

Many others also contributed to the success of the symposium.

Table of Contents

Introduction

Arthur N. Palmer
Department of Earth Sciences, State University of New York
Oneonta, NY 13820-4015

The concept of karst modeling

Karst includes some of the world's most impressive landscapes, but they are also some of the most challenging in terms of groundwater and engineering problems. Topics such as yield of water and petroleum to wells, contaminant fate and transport, contaminant monitoring, and remediation involve many uncertainties because the nature of the porosity and permeability of soluble rocks is not easily predicted. Solutional porosity is what sets karst apart from other geologic settings. Thus in karst it is essential to recognize a triple porosity that includes intergranular (matrix) pores, fractures and partings, and solutional voids.

"Modeling" is of course one of the great buzz-words of contemporary science. Many researchers feel that their work will not be taken seriously unless it is forged into some kind of model. Overused though it is, the word and concept behind it are essential to organizing complex topics. Karst modeling, as envisioned in this volume, includes not only the various ways of organizing karst science, but also, in the more traditional sense, the methods of reproducing karst processes in the laboratory so that the natural phenomena can be better understood.

Conceptual models are based on field observation and guided by knowledge of karst-forming processes. They are able to stand alone without mathematical or numerical analysis, although many have been partly substantiated by these quantitative approaches. **Analytical models** are derived from the functional relationships inherent in natural "laws" such as flow equations and conservation of mass. **Digital models** come in two forms: (1) commercial software for interpreting groundwater flow patterns and geochemical equilibria, and (2) specialized numerical models designed to investigate complex physical relationships, e.g. in the evolution of karst conduits. Digital models have almost entirely supplanted analog models, for example those those in which resistor-capacitor networks or heat flow are used to simulate groundwater flow. **Statistical models** draw upon field evidence to allow quantitative predictions of the nature of karst by fitting the data to ideal distributions (e.g. fractal patterns). **Scale models** are hardware reconstructions of field conditions, usually at reduced scale. The title page of each section of this volume includes a more detailed description of each modeling approach. In practice these subdivisions tend to overlap, since they are often combined in various ways. They also rely on abundant field information, and a large part of this volume focuses on field methods and interpretations.

Practical applications

The field practitioner who seeks answers to real problems may imagine that some topics in this volume are too theoretical to be easily applied. On the contrary, they define the basic karst concepts that allow field conditions to be anticipated, so they do not come as an unpleasant surprise. Without this framework one's understanding is fragmentary, and isolated pieces of field information rattle about with no conceptual glue to hold them together.

Practical goals of karst modeling include interpretations of the following:

- Groundwater flow patterns, velocities, and divides
- Distribution of porosity and permeability
- Interaction of fluids among porosity types
- Storage characteristics of the pore network
- Groundwater geochemistry
- Well-head protection areas
- Fate and transport of contaminants
- Groundwater monitoring and remediation strategies
- Land subsidence and foundation stability
- Stormwater management

A valid karst field study requires familiarity with karst features and processes, carbonate geochemistry, and flow mechanics in closed conduits and open channels as well as in fissures and granular material. It also demands proficiency in specialized field methods such as dye tracing, analysis of spring hydrographs, thermographs, and chemo-graphs, in addition to the conventional hydrologic tools such as well tests. Finally, sufficient field data must be available so that the functioning of the entire karst system can be described, rather than just isolated bits. It is rare for all these skills to be possessed by a single individual or group. It is necessary to take advantage of the great amount of information already available (see references), and to use the models described here as a framework for organizing the data. Certain specialized methods, such as tracer tests and cave mapping, are best subcontracted to those who have extensive experience in such fields.

By acquiring these extra skills, many of which lie outside the normal range of hydrology, one's personal involvement in the field is enhanced. Traditional groundwater hydrology can seem a rather narrow field, as its practice often boils down to a few tried and true methods that may easily become repetitive. The specialized skills required in karst broaden the scope of hydrology and enhance its stature as a science.

The fragmentary nature of karst studies

The greatest source of controversy in karst studies is the tendency for researchers to focus on a narrow range of topics without viewing the karst system as a whole. Most karst specialists center their attention on solution conduits (especially caves, which are voids large enough to enter). To this group, karst hydrology involves the hydraulics of pipes and open channels. In contrast, traditional hydrologists view karst mainly from well data, and petroleum geologists rely mainly on borehole data and geophysics. These latter methods provide useful information about porosity and geologic structure but tend to overlook the influence of solution conduits.

Which approach is correct? In fact, all are. Most water wells in karst draw their supply from narrow fissures and intergranular pores that support laminar flow, just as in any other type of fractured bedrock aquifer. The majority of the storage volume is normally in the laminar-flow openings. Most carbonate petroleum reservoirs consist of porous dolomites in which matrix porosity is dominant, whereas paleokarst reservoirs with discrete conduits are in the minority.

Karst specialists are usually alone in emphasizing the turbulent-flow portions of the aquifers. Although conduits represent only a small percentage of the porosity, they carry most of the discharge, and at velocities that are extraordinarily high by groundwater standards. They behave in the same manner as surface rivers -- serving as outlets for the surrounding laminar flow during low flow, leaking water to the surrounding parts of the aquifer when perched, supplying "bank storage" during floods, and influencing local heads within the aquifer. Any karst study involving contaminant studies or well-head protection zones that does not consider conduit flow is seriously flawed.

Clearly a full understanding of karst relies on a comprehensive view of ***all*** these aspects, and real advances in karst science cannot be achieved until all field evidence and approaches are combined and widely acknowledged. This is one of the major goals of this volume and the symposium for which it was compiled.

Terminology

Many of the papers in this volume use terms that are considered outdated by most groundwater hydrologists, but which in fact are chosen with care. For example, in the karst literature the terms ***vadose*** and ***phreatic*** zones are preferred to the more commonly accepted ***unsaturated*** and ***saturated*** zones, because the latter terms confuse the distinction between aqueous and chemical saturation, both of which are important in karst studies. It is also possible to use the former terms as adjectives (e.g. "phreatic conduits" and "vadose cements"). Another convenient term is ***water table***. Although ***potentiometric surface*** is often preferred, even by karst researchers, it should be used only where the former term is not appropriate, or in generalized discussions. The water table in an unconfined karst aquifer, however irregular and discontinuous it may be, is the discrete boundary between gravitational and pressure-related phenomena. It can be clearly distinguished in the morphology of solution conduits, even those that have long been abandoned by the water that formed them. Finally, even the term ***karst*** is avoided by most groundwater hydrologists, because it is viewed as a geomorphic term. Most hydrologists prefer instead to speak of ***carbonate aquifers***. Our editorial view is that the features that distinguish karst, such as sinkholes, sinking streams, and caves, are of critical importance in controlling the subsurface hydraulics in such terrains. Not every carbonate aquifer contains these features, and they are rare at considerable depth beneath the surface. Thus the term ***carbonate aquifer*** is useful in a general context, or where karst features are absent, but ***karst aquifer*** is preferred where recognizable karst features are present.

Goals of the Karst Modeling Symposium

The goal of the Karst Modeling Symposium and of this proceedings volume is to bring together researchers from diverse fields who share a desire to understand the internal workings of karst systems. This volume gives an example of the paths that are being taken today. Besides including most of the papers presented at the Symposium, it contains several additional papers that serve as topics of discussion.

Assembled here is some of the recent work of the world's leading contributors to karst modeling and the majority of America's most active karst field researchers. Their ideas do not necessarily coincide, nor are they all universally accepted. But they are all complementary, heading toward the same goals by different routes. The Symposium will open a dialog among karst modelers in an effort to reveal which approaches are most applicable, and to show promising new paths.

Further information on karst

This volume is not intended to cover all aspects of karst. For further information on the physical karst sciences we recommend the following comprehensive books:

Beck, B.F. (ed.), 1993, Applied karst geology: Proceedings of the Fourth Multidisciplinary Conference on Sinkholes and Engineering and Environmental Impacts of Karst, Rotterdam, A.A. Balkema, 295 p. (This and other proceedings of the annual "Sinkhole Conferences" hosted by P.E. LaMoreaux Assoc. provide a wealth of information on environmental aspects of karst.)

Bögli, A., 1980, Karst hydrology and physical speleology: Berlin, Springer-Verlag, 284 p.

Bonacci, O., 1987, Karst hydrology: Berlin, Springer-Verlag, 184 p.

Bosák, P., D. Ford, J. Glazek, and I. Horácek (eds.), 1989, Paleokarst: Prague, Czechoslovakia, and Amsterdam, Netherlands, Academia and Elsevier, 725 p.

Budd, D.A., A.H. Saller, and P.M. Harris (eds.), 1995, Unconformities and porosity in carbonate strata: American Association of Petroleum Geologists Memoir 63, 313 p.

Dreybrodt, W., 1988, Processes in karst systems: physics, chemistry and geology: Berlin, Springer-Verlag, 288 p.

Ford, D.C., and P.W. Williams, 1989, Karst geomorphology and hydrology: London, Unwin Hyman, 601 p.

Gillieson, D., 1996, Caves: processes, development, and management: Oxford, UK, Blackwell Publishers, 324 p.

Herak, M., and V.T. Stringfield (eds), 1972, Karst: important karst regions of the northern hemisphere: Amsterdam, Elsevier, 551 p.

James, N.P., and P.W. Choquette (eds.), 1988, Paleokarst: New York, Springer-Verlag, 416 p.

Jennings, J.N., 1985, Karst geomorphology: Oxford, U.K., Basil Blackwell, 293 p.

Klimchouk, A., D. Ford, A. Palmer, and W. Dreybrodt (eds.), 1999, Speleogenesis: the evolution of karst aquifers: Huntsville, Ala., National Speleological Society (in press).

Milanović, P.T., 1981, Karst hydrogeology: Littleton, Colorado, Water Resources Publications, 434 p.

Moore, C.H., 1989, Carbonate diagenesis and porosity: Amsterdam, Netherlands, Elsevier, Developments in Sedimentology 46, 338 p.

Moore, G.W., and G.N. Sullivan, 1997, Speleology: caves and the cave environment: St. Louis, Cave Books, 176 p.

Northup, D., E. Mobley, K. Ingham, and W. Mixon (eds.), 1998, A guide to speleological literature of the English language, 1794-1996: St. Louis, Cave Books, 539 p.

Ruehl, P.O., and P.W. Choquette, 1982, Carbonate petroleum reservoirs: New York, Springer-Verlag, 622 p.

Sweeting, M.M., 1972, Karst landforms: London, Macmillan, 362 p.

Trudgill, S., 1985, Limestone geomorphology: New York, Longman Group, Ltd., 196 p.

White, W.B., 1988, Geomorphology and hydrology of karst terrains: New York, Oxford University Press, 464 p.

White, W.B., and E.L. White (eds.), 1989, Karst hydrology: concepts from the Mammoth Cave region: New York, Van Nostrand Reinhold, 346 p.

Additional information on karst is available from the following organizations:

Karst Waters Institute
P.O. Box 490, Charles Town, WV 25414-0490
www.uakron.edu/geology/karstwaters/kwi.html

National Speleological Society
2813 Cave Avenue, Huntsville, AL 35810-4431
www.caves.org

Cave Research Foundation
P.O. Box 443, Yellow Springs, OH 45387
www.cave-research.org

American Cave Conservation Association
P.O. Box 409, 119 East Main St.
Horse Cave, KY 42749
www.cavern.org

The photographs on the following pages illustrate many of the karst features and concepts discussed by the papers in this volume. Photos by A. N. Palmer.

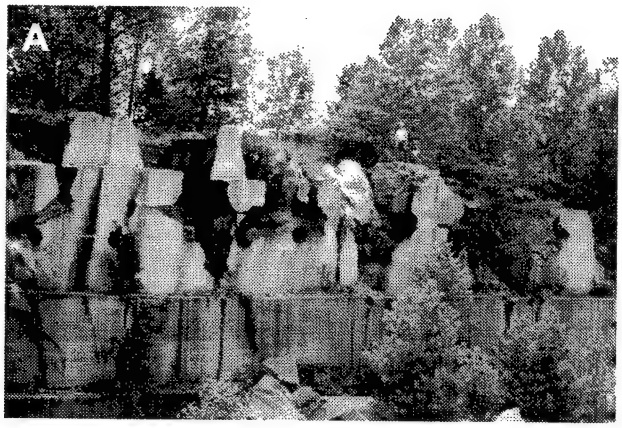

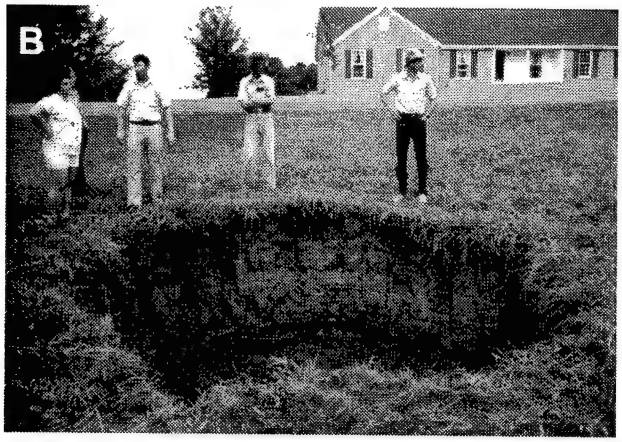

A: Epikarst exposed in Salem Limestone quarry, Indiana. **B:** Sinkhole development in a suburban lawn, Bowling Green, Kentucky. **C:** Mature sinkhole configuration, McClung's Cave, West Virginia. **D:** Karren topography and sinkholes (dolines), Croatia. **E:** Spring in Slovenia fed by a large cave system, Planinska jama (water-supply flume on left). **F:** Artesian karst spring rising into a valley filled with 30 m of late Pleistocene glacial and alluvial deposits, N.Y.

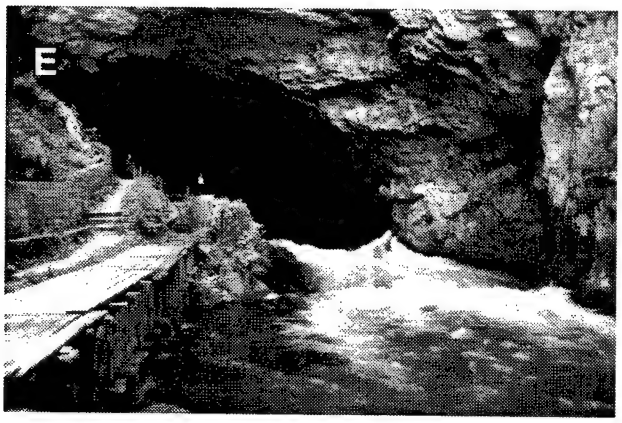

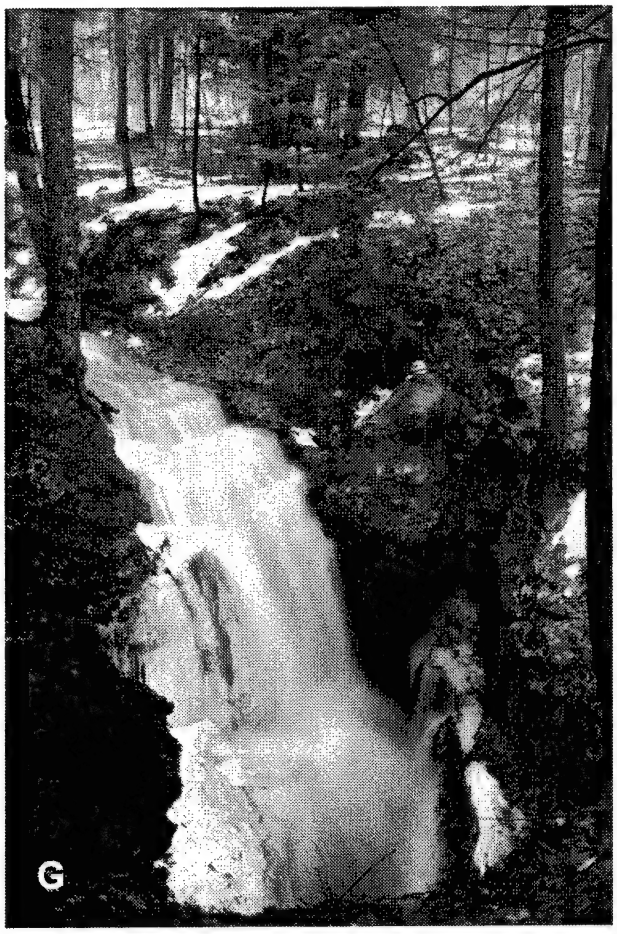

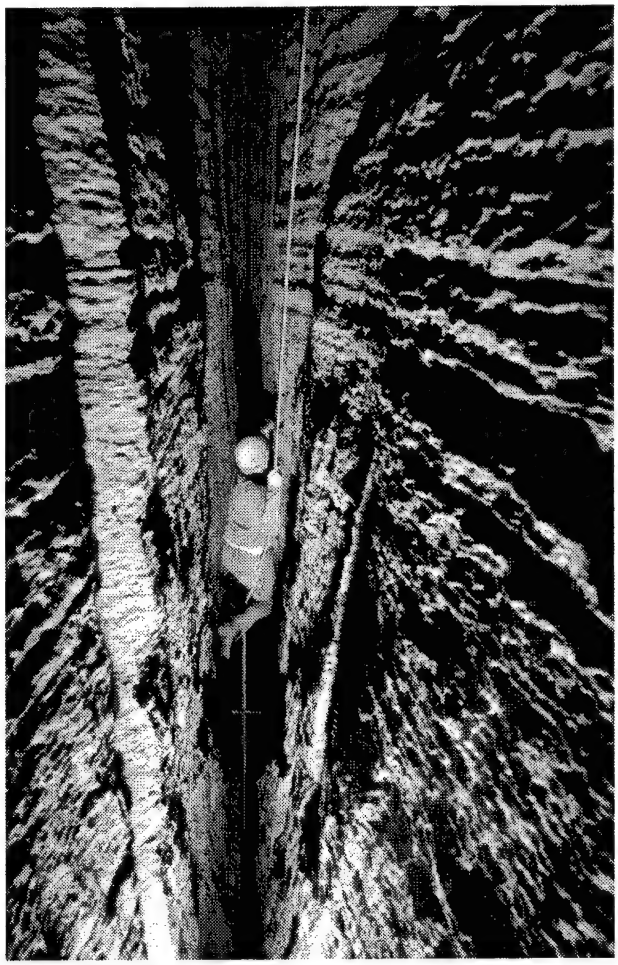

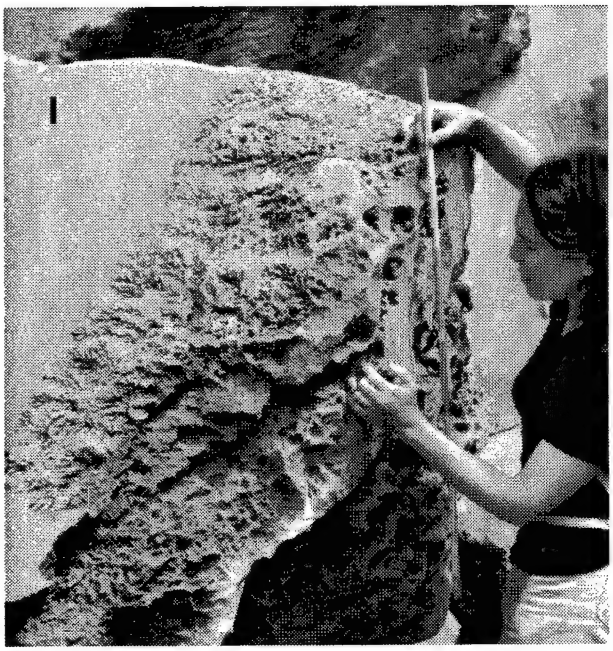

G: Sinking stream in flood, Carlisle, New York. The water drops 16 m into a shaft in the Coeymans Limestone and is a major inlet to McFail's Cave (see photos H and K). **H:** Nearby vadose fissure, 25 m deep, developed along a prominent joint in the Coeymans Limestone. **I:** Matrix (intergranular) porosity in massive Salem Limestone, Indiana, solutionally enlarged by injection of water from neighboring fissures during floods. **J:** Porous zone in brecciated Ellenburger Group, Texas, a major petroleum reservoir at depth. (Pen for scale.)

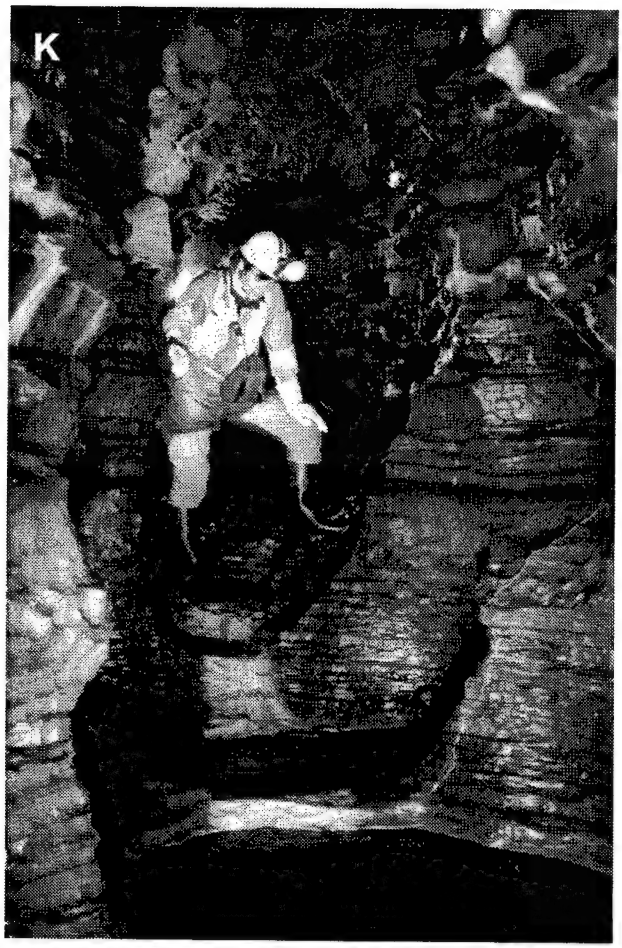

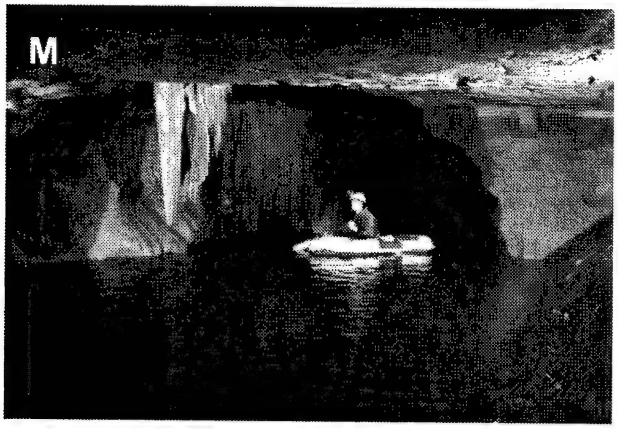

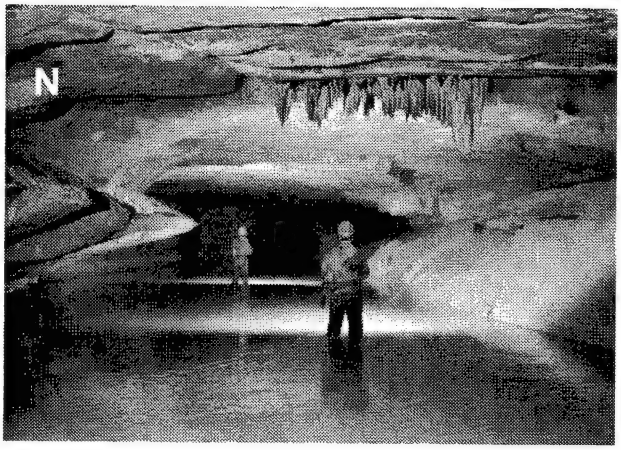

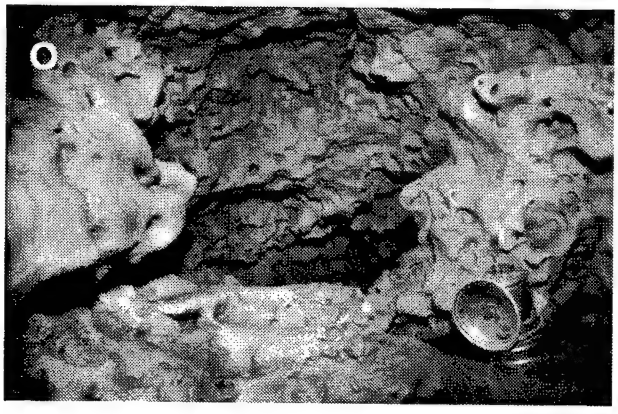

K: Actively downcutting vadose canyon in the Manlius Limestone, McFail's Cave, N.Y. **L:** Headward-retreating waterfall fed by vadose stream perched on chert, Norman Cave, West Virginia. **M:** Phreatic tube in thick-bedded Salem Limestone, Blue Spring Cave, Indiana. Jointing imposes a rectilinear plan-view pattern. **N:** Phreatic tube in St. Louis Limestone, Indiana. Bedding-plane partings foster a sinuous passage pattern. Both M and N flood to the ceiling during high flow. **O:** Porosity in former freshwater/seawater mixing zone, Pleistocene Paget Formation, Bermuda. Miner's lamp, 10 cm high, for scale.

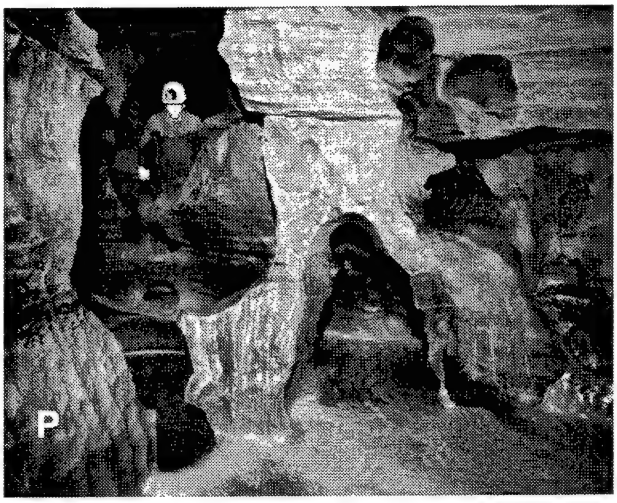

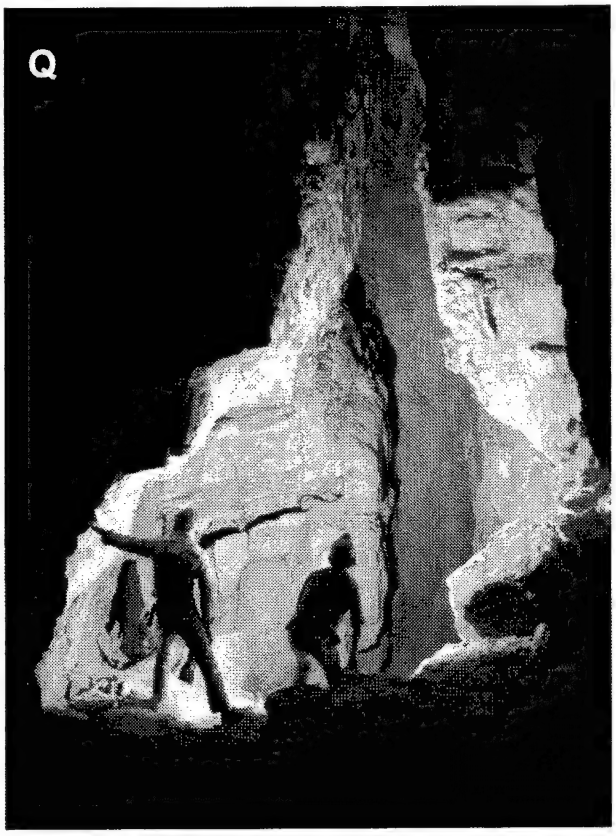

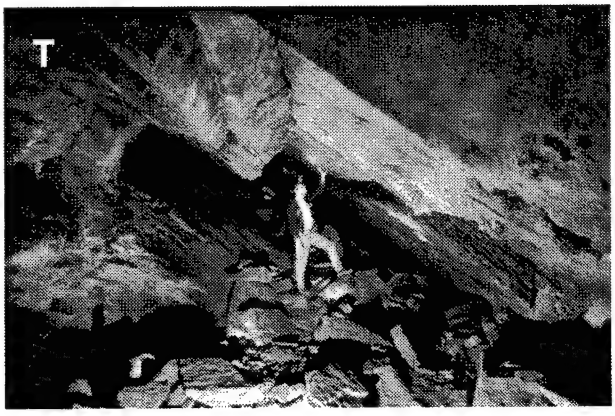

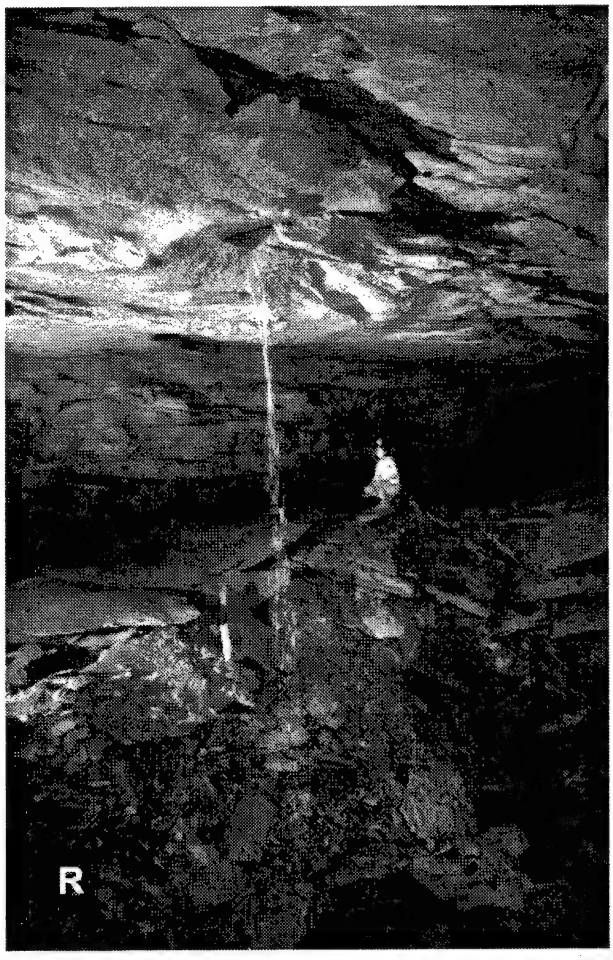

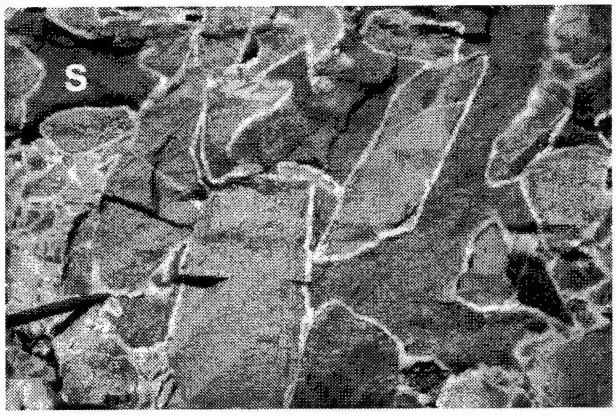

P: Maze development caused by floodwater bypassing of a collapse in the main stream passage of Blue Spring Cave, Indiana. **Q:** Former "phreatic lift" in Cottonwood Cave, New Mexico, where the cave-forming water rose along prominent fractures. The cave was formed by sulfuric acid derived from the oxidation of rising hydrogen sulfide. **R:** Perched vadose water passing through a relict phreatic tube, Mammoth Cave, Kentucky. **S:** Karst-hosted breccia formed at depth in the Ellenburger Group, Texas. Clasts are rimmed by saddle dolomite. (Pen for scale in lower left.) **T:** Relict strike-oriented phreatic tube in steeply dipping Helderberg Limestone, New Trout Cave, West Virginia.

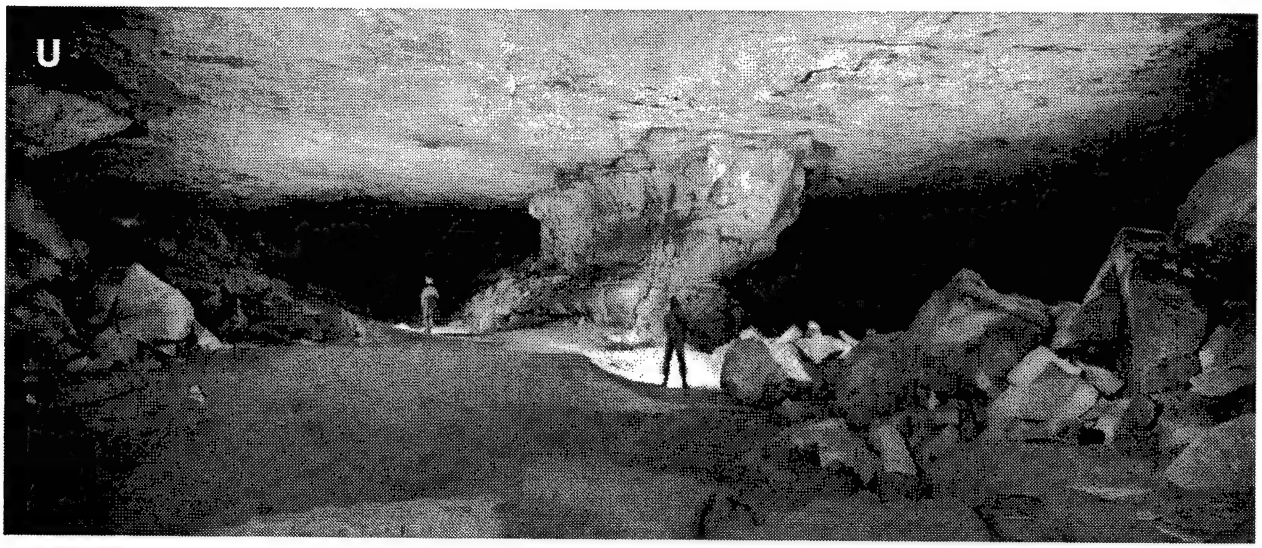

Relict conduits: U: Phreatic tube, Mammoth Cave, Kentucky, developed at a former static base level at and just above the contact between the Ste. Genevieve and St. Louis Limestones. **V:** Canyon formed by headward retreat of a perched waterfall, Mammoth Cave, Kentucky. Note vertical flutes formed by descending water. **W:** Phreatic tube in Cretaceous limestone, Dent de Crolles, in the pre-Alps of eastern France. Intense faulting has allowed passages to follow irregular flow paths, producing a saw-toothed profile. **X (next page):** Fissure network enlarged by thermal water rising along a paleokarst zone in the Madison Limestone, Wind Cave, South Dakota.

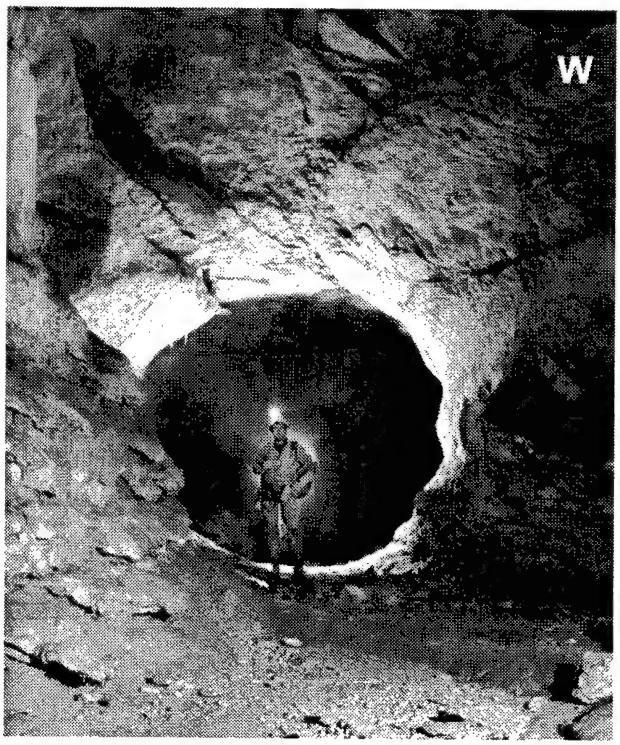

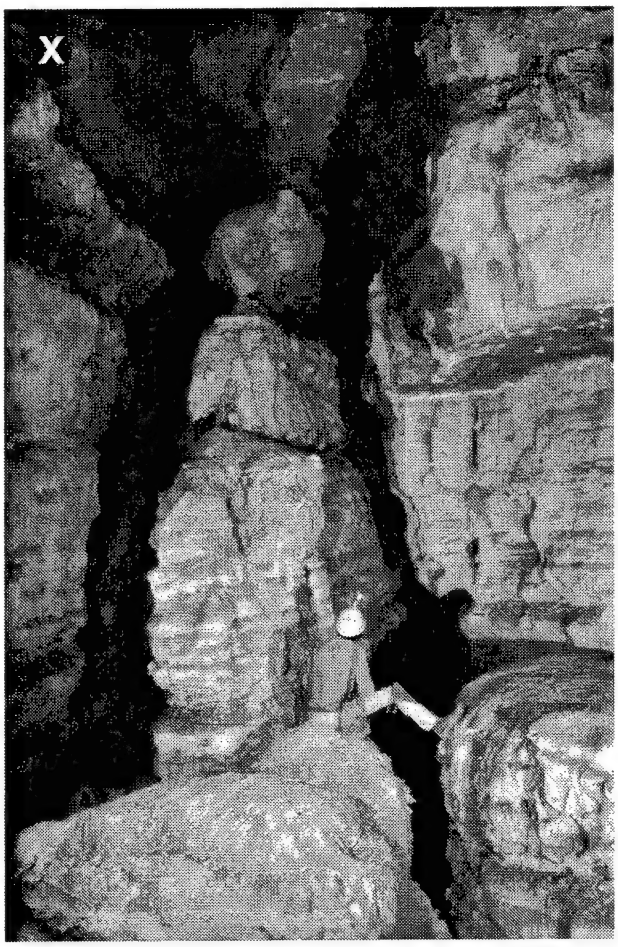

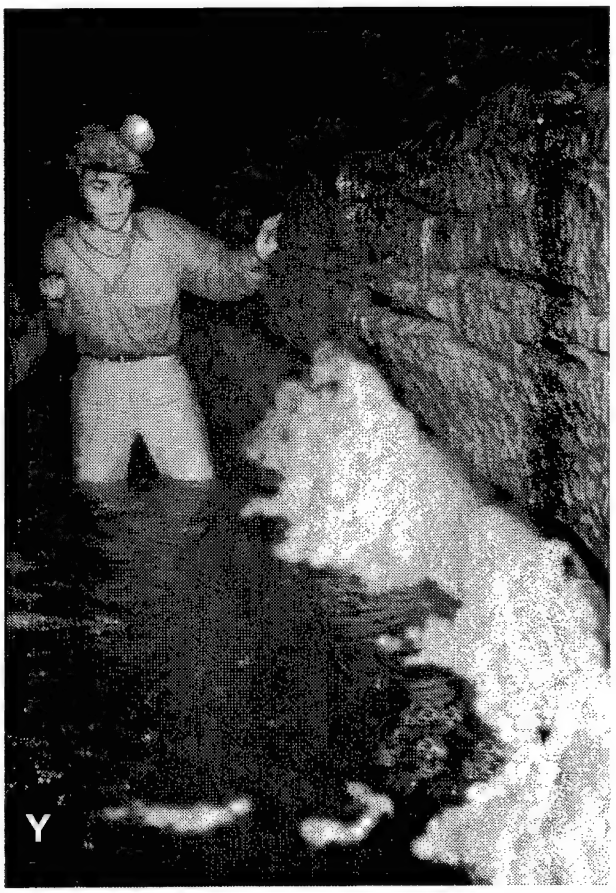

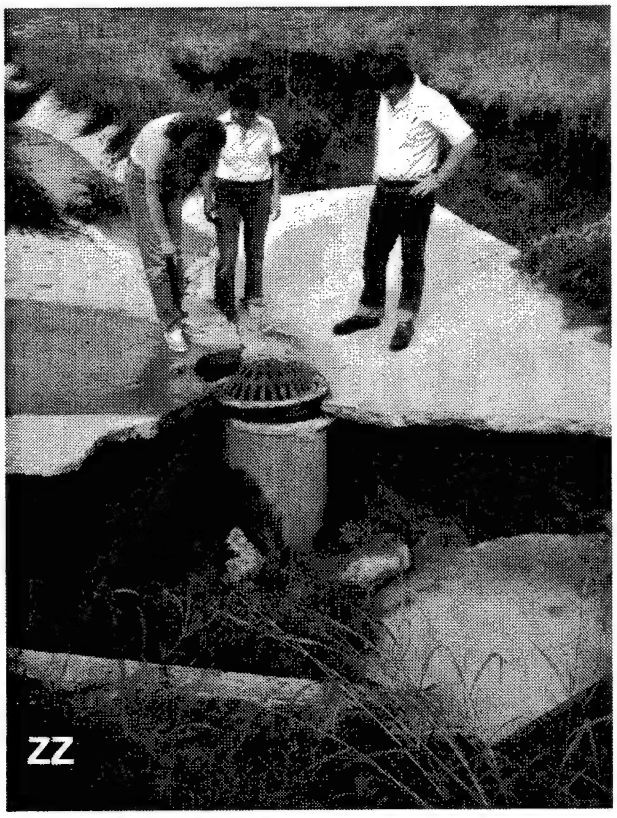

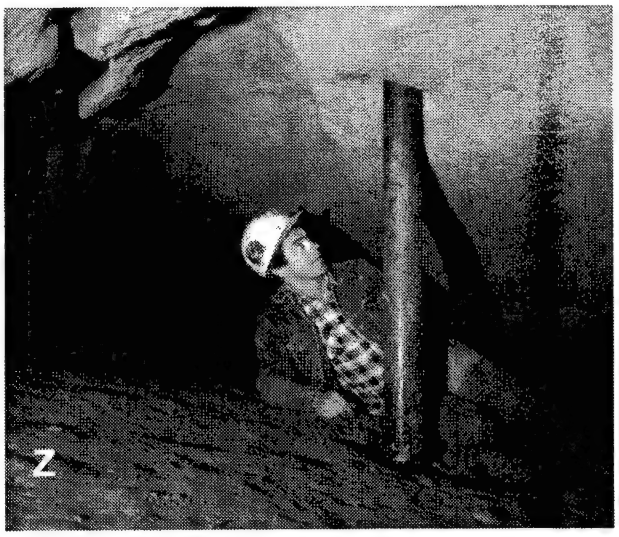

Typical karst problems (see also Photo B): Y: Because of rapid transit times and lack of filtering, water in karst conduits is usually of low quality and subject to severe contamination (Onesquethaw Cave, N.Y.). **Z:** If water wells encounter active conduits, they should be cased and sealed (Blue Spring Cave, Ind.). **ZZ:** Artificial drain in sinkhole, Bowling Green, Kentucky, installed to prevent depression from filling with water during heavy rains. Subsidence of overburden in the sinkhole floor has damaged the drain.

CONCEPTUAL MODELS

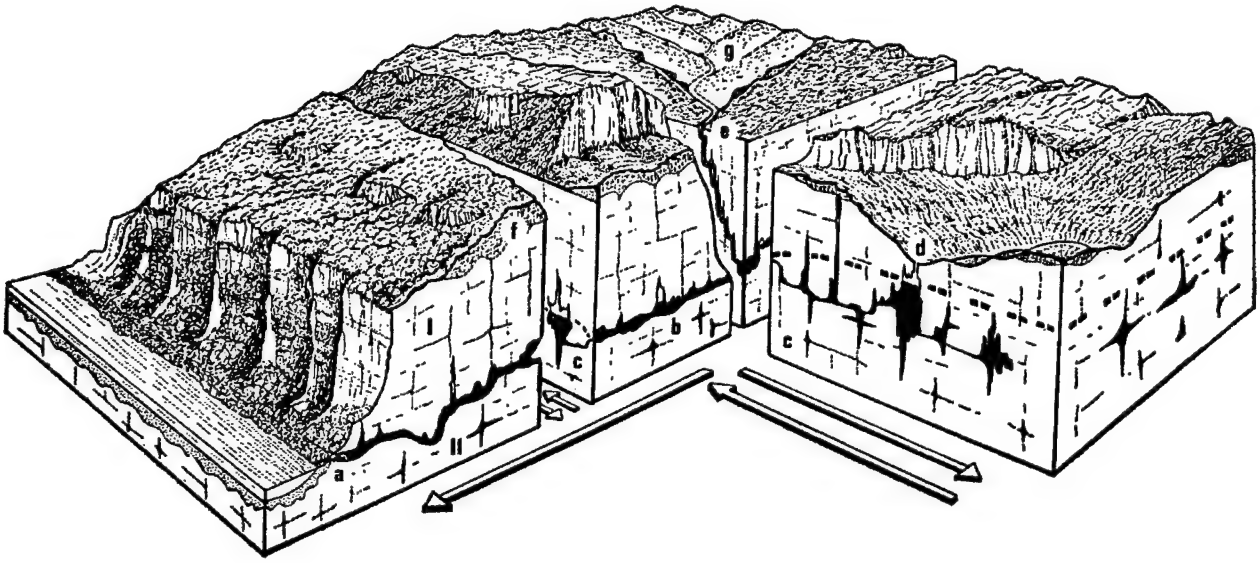

In the geosciences a conceptual model is a synthesis of ideas based on field observation and coupled with an understanding of the pertinent physical and chemical principles. Many conceptual models rely upon analytical elements, particularly hydraulics and geochemistry, but the status of a true conceptual model is achieved when the model is able to stand alone without quantitative support.

For example, the above karst model, developed by Alain Mangin (1975) at the CNRS Underground Laboratory at Moulis, France, is based on exhaustive hydrologic field data and analytical methods. However, the diagram speaks for itself, even when lacking its original labels. It shows the organization of conduits and groundwater flow, including periodic pulses of water into and out of subsidiary voids ("karst annexes") in response to flooding.

Early models of cave development were almost wholly conceptual -- e.g. those of Davis, Bretz, Swinnerton, and others (see paper by Ford in this section). But they restricted the process to too narrow a hydrologic range. Field data were limited, and geochemical principles were treated sparingly. Still, this early literature is valuable not only for its historic context but also for the questions that it poses about the origin of caves and karst aquifers. Many of these questions are still pertinent today.

The first comprehensive conceptual model of karst aquifers was that of White (1969, 1975), and the title of this section is a tribute to his insight. The papers in this section represent the state of the science in an easily accessible form.

References cited

Mangin, A., 1975, Contribution à l'étude hydrodynamique des aquifères karstiques: Annales de Spéléologie, v. 29, p. 283-332, 495-601; v. 30, p. 21-124.

White, W.B., 1969, Conceptual models of carbonate aquifers: Ground Water, v. 7, no. 3, p. 15-21.

White, W.B,, 1977, Conceptual models of carbonate aquifers, revisited, *in* R.R. Dilamarter and S.C. Csallany (eds.), Hydrologic problems in karst regions: Bowling Green, Ky., Western Kentucky University, p. 176-187.

CONCEPTUAL MODELS FOR KARSTIC AQUIFERS

William B. White
Department of Geosciences and Materials Research Laboratory
The Pennsylvania State University, University Park, PA 16802

Abstract

Karstic carbonate aquifers are extremely heterogeneous with a distribution of permeability that spans many orders of magnitude. They often contain open conduit flow paths with hydraulic characteristics more like surface streams than ground water. Karstic carbonate aquifers have highly efficient interfaces with surface water through swallets and springs. Characterizing parameters include: area of groundwater basin, area of allogenic recharge basins, conduit carrying capacity, matrix hydraulic conductivity, fracture hydraulic conductivity, conduit system response time, and conduit/fracture coupling coefficients. The geologic setting provides boundary conditions that allow the generalized conceptual model to be applied to specific aquifers.

Introduction

In order to model karst aquifers, it is necessary to know what one is attempting to model. That is, one must have a conceptual model before building geochemical, mathematical, or computer models. The conceptual model is usually physical -- an interconnected sequence of recharge areas, permeability distributions, and geologic substrates that collectively provide a visualization of the way in which water is added to the system, stored in the system, transmitted through the system, and discharged from the system. However, a well-structured conceptual model should be translatable into mathematics -- the physical picture replaced by a set of coupled differential equations that describe the transport processes along with the boundary conditions imposed by the geologic setting. In practice, of course, this translation is at the core of the problem of karst aquifer modeling.

Modeling of karst aquifers in the contemporary meaning of the term "modeling" has not been easy. Anderson and Woessner (1992) in their treatise on ground water modeling list "karst" as one of the advanced topics, and summarize a few of the attempted models up to the time of writing, none of which work very well.

Investigators, in their efforts to sort out the essential features of karst aquifers have often taken one of two essentially different viewpoints. One might be called a view through space. The aquifer with all its parts is taken as a given condition. The discussion then focuses on recharge and groundwater movement without consideration for modifications in the aquifer itself. Many of the groundwater flow models take this viewpoint. The other might be called a view through time. The discussion begins with a mass of fractured carbonate rock and then focuses on the evolution from a fracture aquifer to a fully developed conduit aquifer. Many of the geochemical models take this viewpoint.

It is the objective of this paper to revisit the physical framework within which all mathematical or computer models must be constructed. Of necessity, this will be a view through space -- a description of the varieties of aquifer that actually exist.

One early attempt at conceptualizing karst aquifers (White, 1969) focused attention on the variety of geologic settings and their controlling influence on groundwater flow patterns. This scheme was later expanded (White, 1977) to take into account the overall area of the groundwater system. Based only on the type of permeability, Shuster and White (1971) divided aquifers into "conduit flow" aquifers, which contain well-developed conduit systems, and "diffuse flow" aquifers which do not. This binary classification was soon recognized as inadequate, and further attempts to organize a classification scheme were made. Smart and Hobbs (1986) added recharge source and aquifer storage as two additional "coordinates" to construct a three-parameter aquifer classification. Ray et al. (1994) carried this concept a step further to arrive at a combined risk factor for plotting a groundwater sensitivity map for the State of Kentucky.

As more details concerning the variety and properties of karst aquifers have been filled in over the past decade or two, it was inevitable that the same concepts would be formulated by different researchers more or less independently and more or less at the same time. As a result there exists in the literature a certain jockeying for position, for setting the language of the concepts, that is not easy to untangle. The matter is not made easier when many important conceptual insights are hidden in abstracts of unpublished papers, in theses, and in government reports.

Plumbing

The essential components of the karst aquifer flow system are sketched in Figure 1. Not all of these components are present in all aquifers, and their presence and relative importance are an important part of distinguishing one aquifer from another.

Recharge

At least four sources of recharge for karst aquifers can be recognized:

1. Allogenic recharge: Surface water injected into the aquifer at the swallets of sinking streams.
2. Internal runoff: Overland storm flow into closed depressions where it enters the aquifer through sinkhole drains.
3. Diffuse infiltration: Precipitation onto the land surface, where it infiltrates through the soil and may be held for days or weeks in the epikarst before it migrates downward through the rock matrix or along fractures to reach the water table.
4. Recharge from perched catchments: Many geologic environments support locally perched groundwater systems above carbonate aquifers. This water reaches the main aquifer by means of vadose shafts and open fracture systems along the margins of the perched aquifers.

Permeability

The "karstification" of an aquifer is in large part measured by its permeability distribution. For many years, this has been discussed in terms of the "triple permeability" model. Karst aquifer permeability consists of

1. The matrix (or granular) permeability of the bedrock itself.
2. Fracture permeability
3. Conduit permeability

The flow fields through each of these permeability types operate on different scales (Teutsch and Sauter, 1991). The hydraulic conductivity of the rock matrix can be measured on test blocks at the laboratory scale. The hydraulic conductivity produced by the fracture permeability must be averaged over a large volume of rock at a scale of hundreds of meters. Values calculated from pump and packer tests on appropriately sited wells can probe the aquifer at the fracture scale. The conduit system operates on the scale of the entire groundwater basin -- a scale of kilometers to tens of kilometers. Travel times in the conduit system can be very short and although both have units of velocity, it is not appropriate to speak of a hydraulic conductivity of the conduit system.

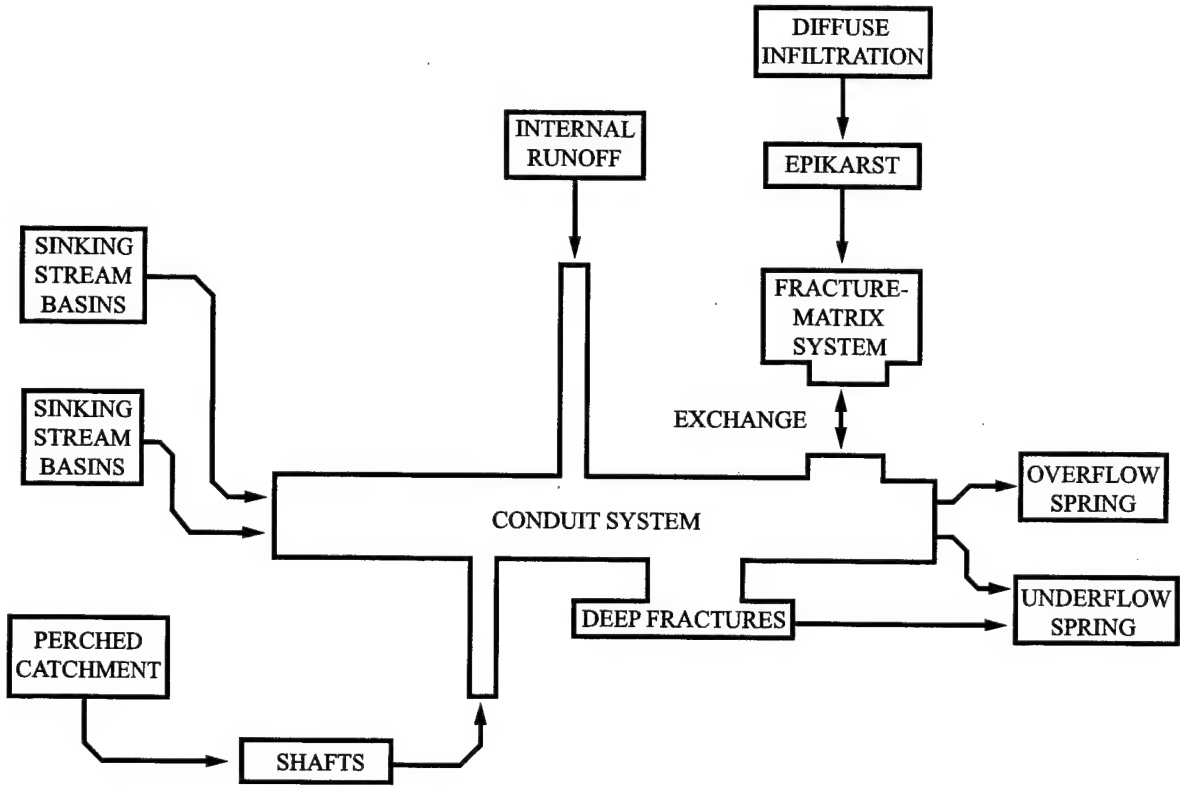

Figure 1: Conceptual model for a carbonate aquifer.

The matrix permeability of many Paleozoic limestones and dolomites is very low and can often be ignored. Young limestones such as those of Florida and the Caribbean islands may have very high matrix permeabilities. There is indeed a continuum, and actual measurements are needed to determine the importance of matrix permeability.

Fracture permeability requires two parameters, the fracture aperture and the fracture spacing. Both are statistical and have a range of values within the same aquifer. Fracture permeability is modified by solution so that fracture apertures range from tens or hundreds of micrometers in unmodified limestone up to 10 millimeters. The latter is the aperture at which non-linear effects begin to appear in the flow field and marks a useful boundary between large fractures and very small conduits.

Conduits can range in size from 10 mm to tens (sometimes hundreds) of meters. Hydrologically, they behave much like storm drains. In map view, conduits take on many different patterns depending on local geology and various characteristics of the flow field itself.

To understand the dynamics of a karst aquifer, then, it is necessary to understand the rate of recharge into the various components of the permeability and the exchange of water between these components.

Discharge

A distinguishing feature of karst aquifers is that most of the groundwater is discharged through a small number of large springs. In some aquifers, the entire discharge is through a single spring. In other aquifers there is a distributary system to a small number of springs. One or a few of these carry the base-flow discharge and are called "underflow springs" while other springs flow only during periods of high discharge and are called "overflow springs" (Worthington, 1991).

The discharge from karst springs is a composite of all water moving through the aquifer. The spring (or springs) therefore is an optimum location for measuring hydrographs, chemographs, and also for monitoring the aquifer for contaminants.

Groundwater basins

Although aquifer thickness is an important parameter in granular aquifer modeling, the lateral extent of the aquifer is often only loosely defined. Karst aquifers, in contrast, borrow a concept from surface water, that of the "groundwater basin." Much like surface-water basins, but without the definitive boundary provided by topographic highs, groundwater basins can be delineated, although basin boundaries may shift with water levels and piracy and flood-overflow routes across basin divides are common. Within the confines of a karst groundwater basin, all recharge water makes its way to a single spring or related group of springs. The spring outlets define the downstream end of the basin.

Mostly, groundwater basins have been established by systematic tracer tests (Jones, 1973; Quinlan and Ray, 1981; Quinlan and Ewers, 1989) but other evidence is provided by the patterns of explored caves, water-table gradients, geological constraints, and area/discharge relationships.

Parameters for karst aquifers

Instead of trying to pigeonhole aquifers into specific categories along the lines of "conduit-diffuse" or the three-dimensional scheme of Smart and Hobbs (1986) and its embellishments, an alternative approach might be to set down the important parameters that characterize karst aquifers. These parameters should lend themselves to numerical measurement. Then, if it were really necessary to classify a particular karst aquifer, it would be represented by a point in an n-dimensional parameter space where n is the number of characterizing parameters.

Area of the groundwater basin

The total area of the groundwater basin, including surface catchments of allogenic streams, is easily determined once the underground divides of the groundwater basin have been established.

Allogenic recharge

Two parameters arise:

1. The total area of the allogenic basins, which is simply the sum of the areas of individual sinking-stream basins.
2. The total allogenic recharge, Q_a.

Allogenic recharge can be measured by direct gauging of allogenic surface streams at their swallets, taking account that many sinking streams lose their water at a series of swallow points upstream from the main swallet. The total allogenic recharge is then obtained by summing the contributions of the individual allogenic basins. Allogenic recharge will have a rapid response to storms.

Conduit carrying capacity

Karst groundwater basins often have a surface component. In some karst basins the drainage is completely underground with no remnant of a surface stream or, indeed, of a surface stream channel. Other basins retain a dry stream bed that carries water only during flood flows. Still others re-

tain a perennial surface stream that loses only part of its flow to the subsurface.

The conduit system has a certain carrying capacity, Q_c, which can be compared with Q_a:

1. $Q_c > Q_a$ (max): All allogenic recharge including storm peak can be accommodated by the conduit system.
2. Q_a (max) > Q_c > Q_a (base): The conduit system can accommodate base flow, but flood flows that exceed Q_c spill over into the surface channel.
3. $Q_c > Q_a$ (base): The conduit system cannot accommodate all of the base flow, so the excess allogenic runoff must travel through the karst basin as surface flow.

It seems that the critical flow when $Q_a = Q_c$ would be a useful parameter for characterizing the conduit permeability. It would require gauging the surface channels above and below the swallet and recording the discharge at which the swallet is exactly overtopped.

Matrix hydraulic conductivity

K_m is best measured on bedrock cores using a permeability cell. The rock cores must be selected carefully to avoid fractures. For most Paleozoic carbonates, K_m will be too small to be significant.

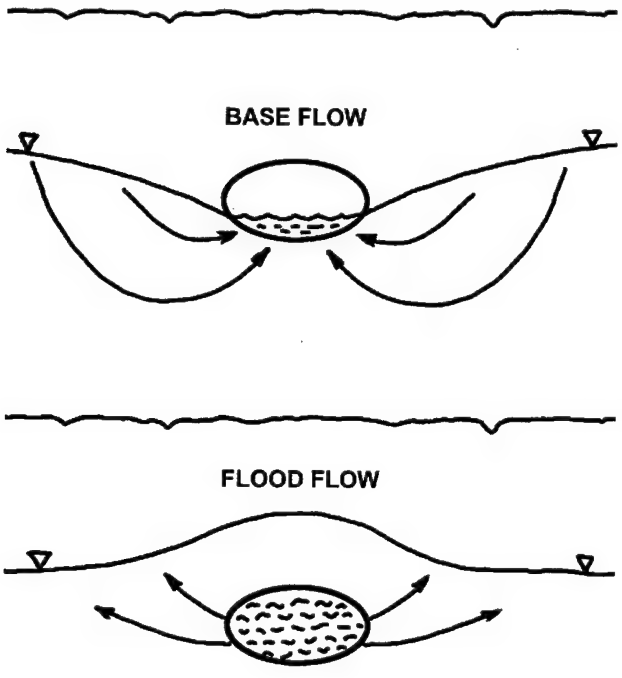

Figure 2: Sketch showing exchange of groundwater between conduit system and matrix and fracture system during base flow and flood flow.

Fracture system hydraulic conductivity

K_f must be determined by pumping tests or packer tests. The difficulty is in siting wells that will intersect a representative sampling of the fractures. Fracture-trace mapping on aerial photographs can often be used to identify fracture swarms and intersections of fracture swarms. These represent the high-permeability pathways within the fracture permeability. Assignment of a hydraulic conductivity to random joints and bedding-plane partings is very difficult without drilling an unrealistic number of wells.

Conduit-system response time

Because conduit flows are often turbulent, it is not appropriate to speak of a conduit hydraulic conductivity. Two measurements can provide a surrogate. One is travel time determined by quantitative tracer breakthrough curves from swallets to spring. The other is response time(s) computed from the recession limbs of storm hydrographs measured at the springs. Travel time and response time are not equivalent measurements, but each will tell something of the rate of movement of water through the conduit system and thus indirectly how well the conduit system is developed.

What no quantitative measurement will provide, however, is the geometry of the conduit system itself. Direct exploration and survey of active conduits, including water-filled portions mapped by divers, gives very precise information, albeit in descriptive form. In very few karst aquifers, however, is a sufficient sampling of the conduit system possible.

Conduit/fracture coupling coefficients

Conduit systems act as low-hydraulic-resistance drains, so that the flow field in the surrounding matrix and fracture system is directed toward the conduit rather than toward groundwater discharge zones on the surface. During base flow conditions, groundwater recharged from diffuse infiltration and stored in the fracture and matrix porosity will drain toward the conduit system (Figure 2). However during storm flows, the conduit system may flood to the roof and indeed establish a substantial piezometric head above the roof of the conduit. During intervals of storm flow, the flow field will reverse and water will move from the conduit into the surrounding fracture and matrix porosity. The effectiveness with which these two (or three) systems are coupled, combined with the intrinsic hydraulic conductivity of the matrix and fracture systems, will determine the rate of movement of groundwater into and out of storage and also the base-flow discharge of the springs.

Possible routes to the calculation of conduit/fracture coupling coefficients include:

1. Deconvolution of spring hydrographs, particularly the relationships of peak flow to base flow.
2. Analysis of the normalized base flow for various families of drainage basins. Base flow is proportional to basin area, but the proportionality constant varies with different hydrogeologic settings.
3. (Speculative.) Comparison of storm response in a well drilled on a fracture swarm near a conduit, vs. the storm response of a second well placed in the conduit to act as a piezometer.

Geologic boundary conditions

The aquifer system described above is the naked plumbing. It must be clothed in the geologic framework before the concept is complete. If we knew the mathematics, the previous description would give us the differential equations and identify the coefficients within the equations. The geology provides the boundary conditions that allow us to select the correct solution. The geology is also what links the generalized model for karst aquifer behavior to the specific aquifer of interest.

Karst aquifer/surface basin architecture

In regions of fluviokarst such as eastern United States, karst aquifers and karst drainage basins are embedded in larger basins that include areas of non-carbonate rock. The placement of the carbonate sequence within the larger basins is the primary constraint that determines areas of allogenic recharge, location of springs, and general limitations on possible flow paths.

Basin relief

The head difference between recharge area and springs is the primary driving force for the movement of water through the aquifer.

Lithologic and stratigraphic factors

Factors having to do with the carbonate bedrock are:

1. Thickness of the carbonate rock sequence.
2. Lithologic character of the carbonate rock. Limestones tend to develop more elaborate conduit systems than dolomites. Sandy limestones can be as karstic as nearly pure limestones, but shaly limestones tend to have limited conduit- and surface-karst development. Variation of lithology in the stratigraphic section focuses groundwater flow and conduit development into favorable rock units.
3. Confining layers. Shales, primarily, but also sandstones and igneous dikes, interbedded within the carbonate section can block groundwater flow, limit vertical circulation, confine flow in artesian conditions below the confining layer, and perch the groundwater flow above the confining layer.
4. Clastic rock units below the carbonate sequence can perch groundwater flow and prevent deep circulation. Clastic rock units above the carbonate sequence act as capping beds and limit or rearrange recharge.

Structural influence and control

Structural influences combine with stratigraphic and lithologic factors to place boundaries on possible routes of groundwater flow. Structural controls operate on many size scales from regional features down to individual joint orientations. These are outlined only in very general terms:

1. Degree of folding. In regions of strongly folded rock, conduits tend to be oriented along the structural strike, both because of the larger aperture of strike joints and because of the orientation of favorable lithologies for conduit development. In regions with little folding, the nearly flat-lying rocks provide two-dimensional flow paths along bedding-plane partings with the development of more highly integrated drainage patterns.
2. Regional dip. Aquifers where the bedrock dip is (more or less) in the downgradient direction tend to develop shallower flow paths than in aquifers where groundwater must move across the structure. Deeper circulation and completely flooded conduits are more common.
3. Faults. Faults play several roles. Active faults can act as paths of high permeability and concentrate groundwater flow. Old, stable faults tend to be sealed by secondary mineral deposition and have little influence on flow paths. Faults that have moved poorly soluble or non-soluble rocks into potential paths of groundwater flow create groundwater dams which can divert flow.

From conceptual models to mathematical and computer models

Comparison of the aquifer components in Figure 1 with the large number and diverse character of aquifers that have been examined in detail, suggests that the conceptual model is reasonably complete or can at least be easily modified to new situations. The processes of groundwater flow are individually amenable to theoretical analysis and mathematical description. Most of the hydraulic conductivities, recharge terms, and exchange terms have been identified, and there is at least the beginning of a methodology for obtaining numerical values for these parameters. Most of the geologic boundary conditions are sufficiently well understood to also be reduced to mathematical terms. What remains is our general inability to predict the layout of the conduit system. In the most realistic models that have been constructed so far, the conduits are put in "by hand" and the success of the model depends on how accurately this can be done.

References cited

Anderson, M. P., and W. W. Woessner, 1992, Applied Ground Water Modeling : Academic Press, San Diego.

Jones, W. K., 1973, Hydrology of limestone karst in Greenbrier County, West Virginia: West Virginia Geol. Survey Bull. 36, 49 pp.

Quinlan, J. F., and J. A. Ray, 1981, Groundwater basins in the Mammoth Cave Region, Kentucky: Occasional Pub. No. 1, Friends of Karst, map sheet.

Quinlan, J. F., and R. O. Ewers, 1989, Subsurface drainage in the Mammoth Cave Area, *in* W. B. White and E. L. White (eds.) Karst Hydrology: Concepts from the Mammoth Cave Area: Van Nostrand Reinhold, New York, p. 65-103.

Ray, J. A., J. S.Webb, and P. W. O'dell, 1994, Groundwater sensitivity regions of Kentucky: map sheet, Kentucky Dept. for Environmental Protection.

Shuster, E. T., and W. B. White, 1971, Seasonal fluctuations in the chemistry of limestone springs: A possible means for characterizing carbonate aquifers. Jour. Hydrology, vol. 14, p. 93-128.

Smart, P. L., and S. L. Hobbs, 1986, Characterization of carbonate aquifers: A conceptual base: Proceedings of the Environmental Problems in Karst Terranes and Their Solutions Conference, Bowling Green, KY, p. 1-14.

Teutsch, G., and M. Sauter, 1991, Groundwater modeling in karst terranes: Scale effects, data acquisition and field validation: Proc. Third Conf. Hydrogeology, Ecology, Monitoring, and Management of Ground Water in Karst Terranes, Nashville, TN, p. 17-35.

White, W. B. (1969) Conceptual models for limestone aquifers: Groundwater, vol. 7, no.3, p.15-21.

White, W. B., 1977, Conceptual models for carbonate aquifers: revisited: *in* Hydrologic Problems in Karst Terrains, R. R. Dilamarter and S. C. Csallany, Eds., Western Kentucky University, Bowling Green, KY, 176-187.

Worthington, S. R. H., 1991, Karst hydrogeology of the Canadian Rocky Mountains: Ph.D. thesis, McMaster University, Hamilton, Ontario, 227 p.

PERSPECTIVES IN KARST HYDROGEOLOGY AND CAVERN GENESIS

Derek C. Ford
School of Geography and Geology, McMaster University
Hamilton, ON L8S 4K1 Canada

Abstract

Hydrogeology and speleology both began during the 19th Century. Their approaches to limestone aquifers diverged because hydrogeologists tend to measure phenomena at very local scales between drilled wells and generalize from them to basin scales, while speleologists study the large but sparse conduits and then infer conditions around them. Convergence of the two approaches with modern computing should yield important genetic models of aquifer and cave.

Genesis of common cave systems by dissolution is a three-dimensional problem, best broken down into two-dimensional pairs for purposes of analysis. Historically, the dimensions of length and depth have received most attention, especially the question of the location of principal cave genesis with respect to the water table. Between 1900 and 1950, different scientists proposed that caves develop principally (1) in the vadose zone; (2) at random depth in the phreatic zone; (3) along the water table in between. Empirical evidence suggests that these differing hypotheses can be reconciled by a four-state model in which the frequency of penetrable fissuration controls the system geometry.

For the dimensions of length and breadth (plan patterns) there is widespread agreement that dendritic (or branchwork) patterns predominate in common caves. Irregular networks or anastomose patterns may occur as subsidiary components. When hydraulic conditions in a fissure are anisotropic (the usual case), dissolutional conduit development is competitive: local hydraulic gradients are reoriented toward the first conduits to break through to outlet points, redirecting others toward them in a cascading process. Plan patterns are most complex where there have been multiple phases ("levels") of development in a cave system in response to such effects as river channel entrenchment lowering the elevation of springs.

Introduction

Scientific study of groundwaters (geohydrology and hydrogeology) and of dissolutional cave systems (speleology) both became established in the second half of the 19th Century. Since then, development of the two subjects has been quite divergent. Groundwater hydrologists generally make physical investigations of most kinds of aquifers by means of a few wells and cored holes, measuring the very local rock properties and applying local drawdown and slug tests. Recharge to the aquifers is normally diffuse and thus to be approximated only in a similarly generalized manner, while the discharge (springs and seepages) is often dispersed into wetlands or alluvial channels and so is also difficult to isolate. In contrast, speleologists and karst hydrologists have focused on those conduits and fissures sufficiently large and unobstructed to permit human entry, which will be a tiny proportion of the totality in most cases. They have sought to investigate inaccessible regions of the aquifer between, above and beneath conduits by means of dye traces from the largest points of recharge (stream sinks, which are not necessarily the quantitatively dominant sources of recharge) to the most apparent regional springs. At the recent 6th Conference on Limestone Hydrology and Fissured Media (Switzerland, August 1997), Bakalowicz (1997) and Bonacci (1997) also commented on the contrasts of hydrogeological and speleological approaches.

This dichotomy of approach was made plain early in our century with the publication of the two radically different groundwater models for the classical Dalmatian karst that are shown in Figure 1. Grund (1903) proposed a Darcian

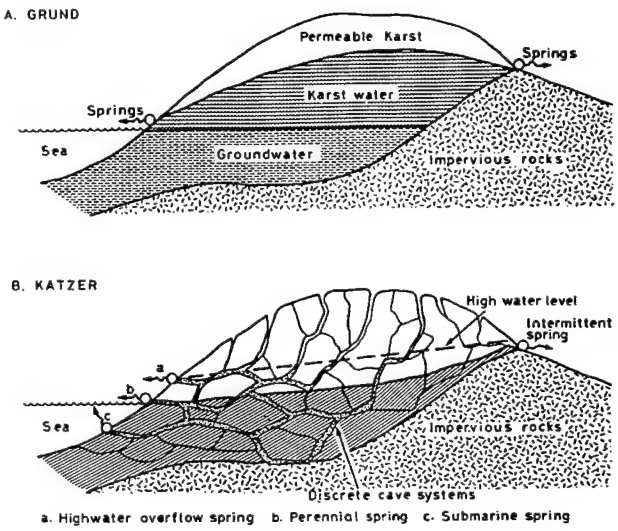

Figure 1: Groundwater flow models for the Dalmatian karst according to **(A)** Grund (1903); **(B)** Katzer (1909).

solution, with fresh karstic recharge circulating in an essentially isotropic and homogeneous aquifer above deeper, stagnant waters; Katzer (1909) imagined the karst waters to be circulating independently in rather inchoate cave river networks.

It is now appreciated that the truth is more complex than either model. If karst aquifers are defined simply as those in which groundwater transmission and storage have been and are being significantly enhanced by bedrock dissolution, they can exhibit many different conditions. Some display strictly single porosity, either as matrix only (common in young reefal and eolian limestones) or as fissure only (e.g. incipient karst in marble or porcellaneous limestones). Large volumes of most karst aquifers will display at least dual porosity, however, exhibiting significant matrix plus fissure, matrix plus conduit, or fissure plus conduit transmission. True triple porosity (matrix-fissure-conduit) can be recognized in at least some portions of most large explored caves.

The difficulties that this natural variety and inhomogeneity can pose in the design and operation of quantitative models for groundwater flow in karst rocks will be appreciated. In addition, within saturated fissures the flow may be simply laminar (Darcian), or non-linear laminar requiring an approximation such as the Hagen-Poisseuille equation. Conduits may be permanently water filled (pipefull, Hagen-Poisseuille or Darcy-Weisbach equations), permanently open channel (free surface, Manning equation or similar; see, e. g., Hauns et al., 1997), or switching between the two as the discharge varies. Evaluation of the friction factors to be applied to these or similar turbulent flow equations in cave passages is especially difficult. For the friction factor (f) in the Darcy-Weisbach equation, for example, I have obtained a range of values from 0.1 to 340 in "back of an envelope" estimates for various situations underground.

Figure 2 is an attempt to illustrate these difficulties with an imaginary karst. In situation 2A, there are only reconnaissance hydrogeological data. A couple of streams are observed to sink underground at an upgradient boundary to the karst, and one large and one incipient spring are detected along the downgradient edge. In between, outcrops of vuggy, reefal limestone exhibiting diffuse permeability are noted, flanked by patches of thin, densely jointed, inter-reefal beds. Elsewhere, soil obscures the bedrock but a few lineaments show up on air photos. To approximate flow patterns and velocities, we may apply a Darcian equation with a regional value for the hydraulic conductivity, K, such as that which Böcker (1969) derived for the largely

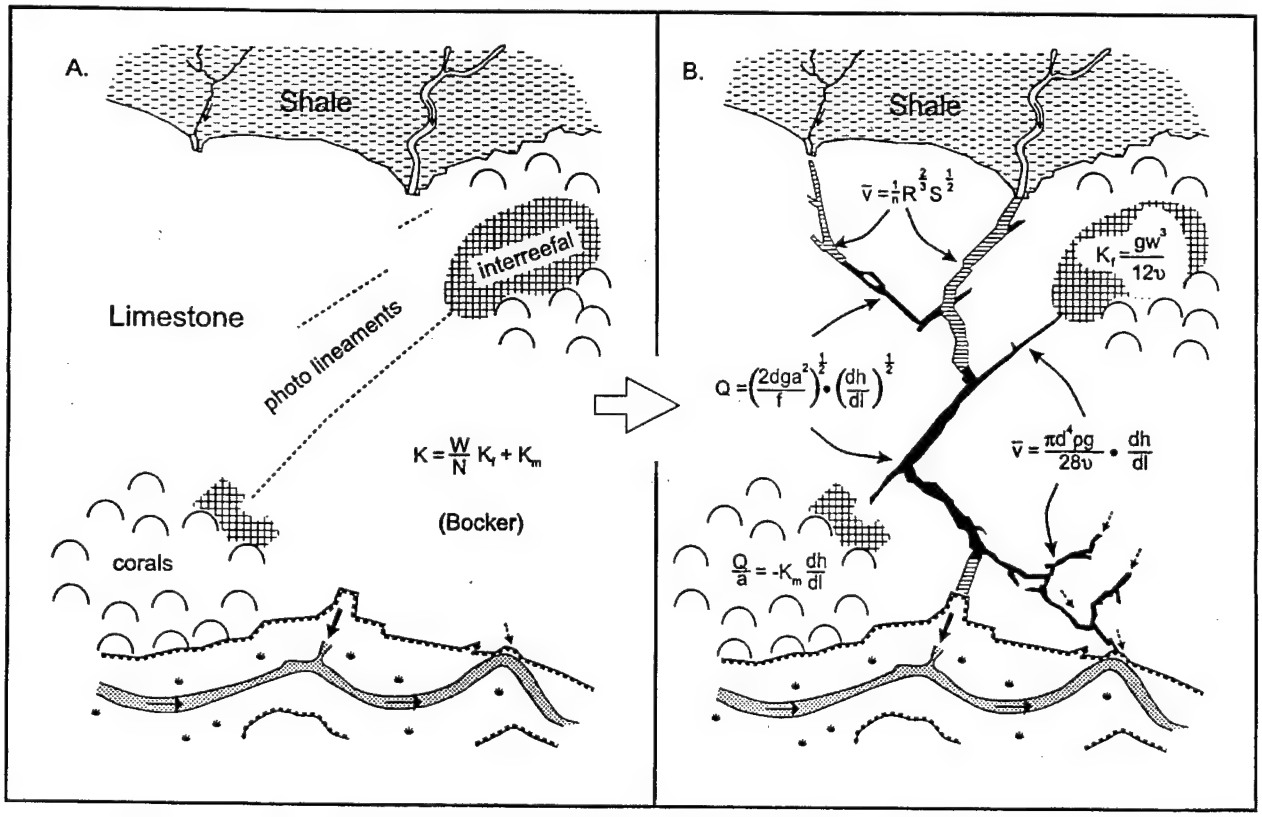

Figure 2: The analytical structure of an imaginary karst aquifer **(A)** at the hydrogeological reconnaissance level; **(B)** following detailed cave exploration and dye tracing. See text for details.

obscured karstlands of Hungary:

$$K = \frac{W}{N} k_f + k_m \quad (1)$$

(W = mean width of fissures in a set, N = mean spacing; kf, hydraulic conductivity of fissures; km, hydraulic conductivity of the matrix).

Figure 2B puts the principal karst conduits (which might be detected by exploration) onto the map, plus some smaller conduits or enlarged fissures whose location and role could be determined by subsequent detailed programs of dye tracing. There is no information at all for large areas of the map. We might choose to approximate the conditions in them by drilling and coring (Worthington and Ford, 1997); to be confident of intercepting representative principal conduits (i.e. dispensing with cave exploration altogether) it would be necessary to drill traverses on not more than one-meter centers in a majority of karsts, which is clearly infeasible: small conduits and enlarged fissures will be missed even at this exploration density.

The representative, comparatively simple, triple-porosity karst drainage system in Figure 2B is not analytically intractable, I suggest. However, modeling its hydrologic and hydrochemical behavior offers opportunities to adopt many different theoretical approaches (see Hobbs and Smart, 1986; Clemens et al., 1977). There is scope for much imagination in the operational designs for the models, and the application of supercomputing resources is invited. The formation of computer-focused karst hydrogeological analytical groups at centers such as the Universities of Bremen, Neuchâtel, Tübingen, and Waterloo is among the most exciting developments in karst studies in recent years. There is a large, intellectually exciting and economically important field of work open to them.

Conceptual models of cave-system development in fissured limestone aquifers

The review that follows is brief and makes no claim to be comprehensive. It presents my own perspectives on some of the main features in the evolution of our understanding about the development of the great integrated systems of cave galleries and shafts discovered during this century. Speleologists appreciate that, in truth, the natural variation that occurs in the systems is immense and that, as a consequence, no one genetic explanation is likely to be complete. We can never be truly certain what will be found around the next bend in the passage; that is a good part of the joy of the game.

This review is limited to cave systems created by normal meteoric groundwaters circulating in limestone or other soluble rocks without any major artesian confinement. These have been termed "common caves" (Ford and Williams 1989, p. 246) because they are probably 90% or more of all known and mapped dissolutional caves longer than a few hundred meters. It does not include caves created by waters (thermal or otherwise) ascending into the cavernous rock from deeper strata, or marine mixing-zone caves.

Common cave systems are usually large in all three spatial dimensions. For genetic analysis, it is conventional to divide such three-dimensional phenomena into singlets or two-dimensional pairings, and this happened historically in the case of caves. Most early proposals focused on their development in length and depth (i.e. in projected long sections) and were greatly concerned with the relationships between cave and water table. With the benefit of hindsight, I believe that it might have been more useful to have considered length and breadth first, i.e. the genesis of the plan patterns of cave systems. The focus on length and depth probably reflects the early European speleologists' attention to the deep shaft-and-drain types of caves that were beginning to be explored in the Alps, Pyrenees, and elsewhere. E.A. Martel, widely considered to be "the father of speleology," was certainly attracted to them (e.g. Martel, 1921).

Development in Length and Depth

The models advanced between (roughly) 1900 and 1950 A.D. are a striking example of the evolution of scientific ideas. They were concerned to determine what was the principal locus of cave genesis in relation to the water table. By the close of this period, every alternative possibility seems to have been advocated by one group of scientists or another. These conflicting models are summarized in Figure 3.

(a) Vadose hypotheses

A general vadose model is not presented explicitly in the work of any one author but is implicit in the writings of several such as Dwerryhouse (1907) and Martel (1921). A first, very important, assumption is either that a water table is already established at depth in the rock before there is significant cave genesis (its elevation being determined by some external control such as an entrenched river channel or an impermeable sill) or that it rapidly becomes established during the early cave genesis. Thereafter, it remains essentially fixed in elevation. In this early writing the role of soil CO_2 in enhancing the solubility of limestone was not appreciated. As a consequence, dissolution was believed to be restricted to the 45 - 75 mg/L $CaCO_3$ supported by atmospheric CO_2 pressure at normal temperatures. It was believed that this small solvent capacity would be largely

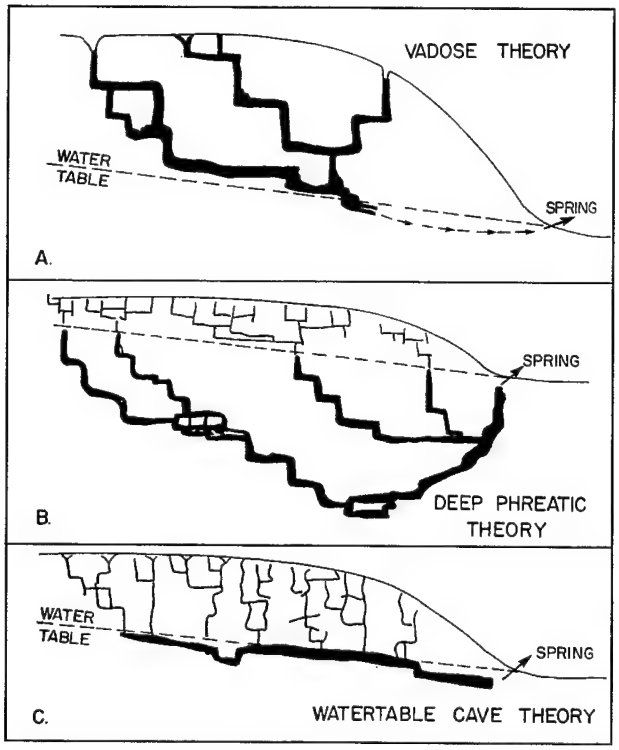

Figure 3: Schematic diagram to depict the vadose, deep-phreatic and water-table theories of common cave genesis.

exhausted in the zone that the groundwaters encountered first -- the vadose zone. Groundwater velocities would also be greatest in the zone, exposing its cave passages to enlargement by the mechanical erosion of the stream bedload. At the water table, bedloads would be dropped and the passages would shrink to the small dimensions that could be created by the (largely expended) solvent capacity of slowly flowing waters.

Vadose caves of this form can be found. The best examples known to the author are reported in Mt. Sedom, a salt dome that is rising on the western shore of the Dead Sea (Frumkin, 1994). The climate is very arid, favoring a deep water table. Anhydrite caprocks concentrate the occasional rains into streams that reach the salt at a few specific points; dissolutional shafts are drilled beneath these (following fractures or intergranular pores) and fizzle out at an approximate regional water (brine) table where the waters become saturated with the salt. Similar, though less distinctive, shaft-and-drain caves can be found in very young limestones on oceanic islands, where the rock has high matrix porosity and the water table oscillates 70 m or more during each Quaternary sea-level cycle, exposing the mixing zone porosity at each low sea stage. Some high mountain caves in ancient limestones may also be ideally vadose as consequences of rapid uplift accompanied by the opening of the fractures by pressure release, but this is not established. The majority of simple shaft-and-drain vadose caves in mountainous regions are probably of "invasion origin," i.e. they have developed where new streams are able to invade a vadose zone that was drained by cave enlargement during earlier speleogenetic phases. This is frequently a consequence of glaciers deranging earlier surface channel patterns.

(b) Deep-phreatic hypotheses

In flat contradiction to the vadose proposals, W. M. Davis (1930, 1931) and J H. Bretz (1942, 1953) developed a general model proposing that predominant cave development takes place at depth in the phreatic zone. The model was empirical in origin, based on a wealth of field evidence of cave forms that could only have developed under pipefull flow conditions. Certain prime categories of these evidences are now seen to be invalid; for example, the great maze caves of the Black Hills, South Dakota, (prominent in Davis' 1930 discussion) are undoubtedly phreatic in origin but they are not common caves, having been created by thermal waters invading paleokarst under an artesian cover (Ford et al. 1993). Other important pipefull morphologic forms are widespread to predominant in common cave systems around the world, however, and the sum of their evidence is incontrovertible. In Davis' formulation the dissolutional caves essentially follow the stream tubes in a Darcy flow net. Bretz (1942) elegantly linked this pattern, and the cave clastic fillings, to Davis' "Geographical Cycle of Erosion" (1898), suggesting that most cave enlargement occurs during the mature stage of the landscape cycle when local relief and, thus, hydraulic gradients will be greatest and that in the old-age stage of diminishing gradients the caves will slowly fill with insoluble residuum (mostly clays) from the overlying soils.

The deep-phreatic common cave systems that are well known and explored are relatively few. This is because, where they remain water-filled, they are often too deep for exploration by divers. Where they are now drained and relict, their lower sections are prone to local blockage or complete infilling with detritus, while upper sections are modified or destroyed by vadose invasion processes.

Davis and Bretz explained the paucity of examples of ideal vadose caves (Figure 3A) in the literature of their time by supposing that all limestone cave genesis was very slow; they, too, did not appreciate the potential significance of soil CO_2. As a consequence, in their model most terrain above regional water tables (i.e. the vadose zone) would have been destroyed by surface erosion processes before the caves had attained large dimensions.

(c) Water-table hypotheses

In the English-speaking world, American hydrologists are considered the first to recognize the importance of soil CO_2 as a significant booster of limestone solubility (Adams and Swinnerton, 1937). This finding weakened the strength of one of the principal points in the arguments supporting both the vadose and deep-phreatic models, that limestone dissolution is a weak process. In 1932 Swinnerton introduced a water-table speleogenetic model (Figure 3C, Figure 4A). The principal new contention was that, from the outset, groundwater flow in karst aquifers is not constrained by Darcian rules because the physical conditions are always anisotropic and heterogeneous. At the water table a given parcel of groundwater, "A", may split up and flow along several different fissures (A1, A2, A3 - Figure 4A). As he drew the two-dimensional geometry, it is evident that Route 1 would win in a race to enlarge to conduit dimensions and so capture most or all of the flow. It is the shortest route and thus will experience the most rapid renewal of fresh, acidic groundwaters. Note that, if we insert a wider initial fissure along, e.g., most of Route 2, than occurs along Routes 1 or 3, this argument breaks down. Similarly, by adding the third dimension, Route 2 can be drawn as direct

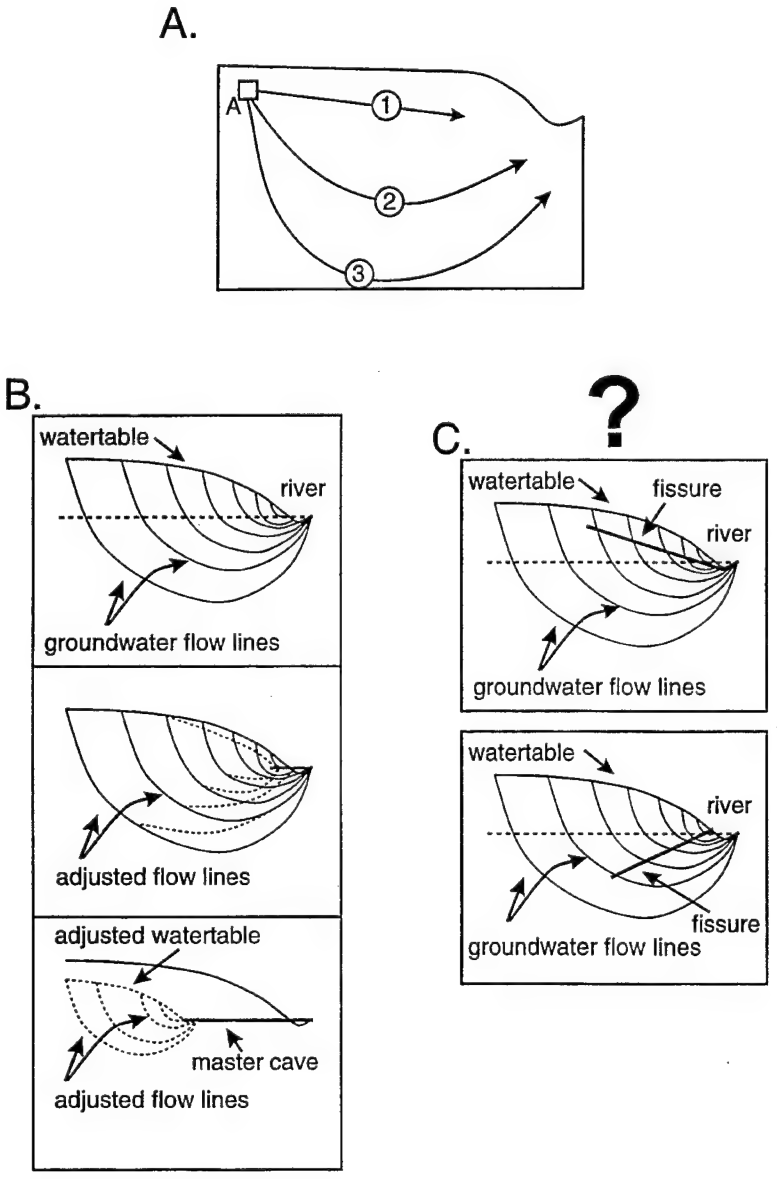

Figure 4: (A) Detail of the water-table cave model proposed by A. C. Swinnerton (1932). **(B)** The water-table cave model of Rhoades and Sinacori (1941). **(C)** How will the Rhoades and Sinacori model evolve if inappropriately oriented fissures are superimposed on it?

and Route 1 as very sinuous, also destroying its advantage.

In the Swinnerton model the water table is again believed to be established at depth before the cave-system building begins. He allowed that it might be lowered as much as several tens of meters as a consequence of greater hydraulic conductivity due to conduit enlargement along Route 1, and stressed the importance of speleogenesis in an epiphreatic zone that is inundated by seasonal or shorter-period floods. Preferential cave development in the epiphreatic zone was first advocated by Cvijić (1918) and is repeatedly emphasized in later studies (e.g. Warwick, 1953; Glennie, 1954; Audra, 1997). In the Swinnerton model the cave is propagated along the water table from the head of the system toward the spring. Significant cave development is not prohibited in the vadose zone, but this essentially serves as a collector to deliver flow to the big caves along the water table.

Ten years after Swinnerton, Rhoades and Sinacori (1942) presented the significantly different water-table model depicted in Figure 4B. The great advance in conceptualizing here is that the water table is no longer a fixed entity preceding the cave. Instead, it is progressively lowered as the cave (underground plumbing and reservoir) is enlarged. In this formulation the cave propagates headward (upgradient) into the rock from the spring, creating a water-table master drain to which any lateral waters (i.e. from the third dimension) will flow.

This type of cave can develop in the ideally simple form that Rhoades and Sinacori imagined. It is found in young limestones where matrix porosity is predominant and the dissolution is enhanced by freshwater/saltwater mixing along a halocline, i.e. it is the basic model for marine mixing-zone caves such as those analyzed by Mylroie and Carew (1990). These are not "common caves," however. If fissure porosity is predominant (the initial conditions in most limestone aquifers), then the locus of the master cave depends upon the distribution and orientation of whichever fissures happen to be the most penetrable by groundwaters and also efficiently directed towards potential spring discharge points, as indicated in Figure 4C.

(d) An amplified four-state model

My Ph. D. thesis was a study of cave systems in the central Mendip Hills, England, that drain to two major regional springs, Cheddar and Wookey Hole (Waltham et al., 1997). The limestone lithology and geologic structure are complex and the cave systems are ancient, multi-phase and incompletely known. As yet, none of them have been explored all the way through from sink to spring. The morphology and geologic locational controls of the accessible passages were mapped in great detail as a data base. From this information, attempts were made to reconstruct the sequence of passage development and integration in order to establish what factors had controlled the pattern building. The process can be likened to constructing one of the new three-dimensional jigsaw puzzles of famous buildings (St. Peter's, Chartres, Taj Mahal, etc.) that are now on the market, except that in the case of the caves the puzzle pieces are progressively broken or missing above the ground floor until entire wings are gone in the upper storeys, and one rarely finds any remaining piece of the roof!

From these reconstructions and later cave studies in North America and continental Europe, however, the model shown in frames 1-4, Figure 5, was constructed. It is the product of several iterations (Ford 1971, Ford and Ewers 1978, Ford and Williams 1989, p. 261 *et seq.*) and is intended to apply to those aquifers in limestone, dolostone, gypsum, and anhydrite in which fissure porosity and transmission is predominant before the integrated dissolutional conduit systems develop. The water table does not precede the cave at depth in the rock; at the outlet boundary its elevation may be determined by some allogenic control (river channel, impermeable barrier, etc.) but behind this position it is lowered by the evolving three-dimensional geometry of the cave system (the master plumbing), as in the Rhoades and Sinacori (1942) formulation. Where penetrable fissures are sparse but large, cave systems may thus be compelled to follow deep loops below the spring elevations. Where the fissure density is greater, loop amplitude tends to diminish and may be further reduced by subsequent gradational processes such as entrenchment of loop crests (see Ford and Williams, 1989, p. 271-4. Rossi et al. (1997) describe excellent new examples from the Cantabrian Mountains, Spain). Bedding-parting planes, joints, and faults all serve as important links in most large cave systems. Bedding planes may be more significant because their greatest apertures tend to be more continuous than those of fractures, except at shallow depths (e.g. Knez, 1997); quite often certain of them will have been a little enlarged over wide areas by dissolution in sluggish regional flow preceding the phases of linear conduit development ("nothephreatic conditions" of Jennings, 1983; "inception horizons" of Lowe, 1992). Deep loops are favored where strata dip steeply and shallower caves where dip is gentle. Many cave systems may display mixtures of State 2 and 3 or 3 and 4 along their length. Major cave development is not inhibited in the vadose zone, (as it is in the Davis/Bretz, Swinnerton, Rhoades and Sinacori formulations), but a majority of enterable vadose passages are guided by initial phreatic tubes of lesser dimension. Further details may be found in Ford and Williams (1989, p. 261-278).

The four-state model seeks to encompass the range of conditions encountered in common caves that are of explorable

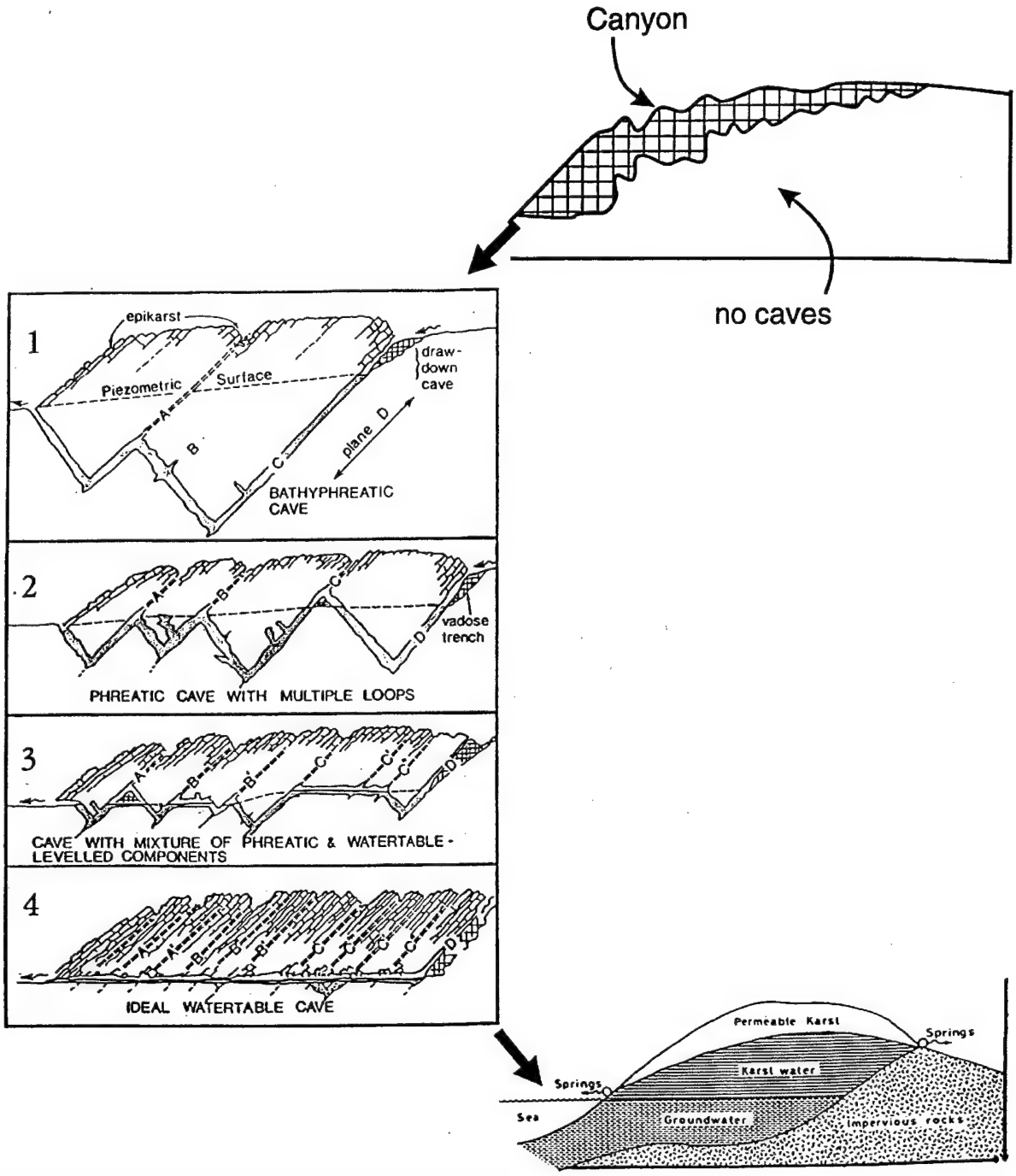

Figure 5: The four-state model of cave system geometrics (Ford 1971 *et seq.*) amplified to include: above right State O, where fissure frequency and/or aperture is too low to permit cavern genesis; below right, State 5, where fissure frequency and/or matrix porosity are too high to permit caves to develop to an enterable scale.

dimensions. It is an incomplete description of the meteoric groundwater conditions found in carbonate and sulfate rocks, however, as indicated in the two extra illustrations in Figure 5. There is also a State 0 in which the penetrable fissuration is so sparse (at least, beneath the epikarst) that integrated cave systems have not been able to develop in the available hydrogeologic time. This is true of many marble outcrops because metamorphism sealed their fissures, and of dolostones because of their lesser solubility. At the other extreme, in State 5, matrix porosity is so great and/or fissure frequency is so high that groundwater flow and dissolution are too diffuse to create significant caves; piezometric surfaces and groundwater circulation can be approximated by a simple Darcian formulation such as Grund's model, repeated to round out the Figure. This is the condition that prevails in most chalks, much gypsum

and many thin-bedded or very young limestones. Note, however, that allogenic streams may be able to establish and maintain caves through such rocks because their waters are focused into channels before arriving at the karst.

For the practice of hydrogeology in cavernous limestones the most important feature of this model, perhaps, is the emphasis that it places upon the heterogeneity of conditions such as fissure frequency, continuity, and aperture that may be encountered. There are no precise and global values for the spatial frequency of penetrable fissures that can be cited as probable boundaries between, e.g., predominantly State 2 and predominantly State 3 caves, because of the significance of varying aperture within fissure sets. However, it is often possible to calibrate the model at the regional scale within a given geologic formation with a uniform tectonic history.

Plan patterns of common caves and development in length and breadth

During the first 70 years of this century, there was much less effort to develop general models for evolution of the plan patterns of common cave systems than for their long sections. There is general recognition by authors in many nations that the patterns are broadly dendritic or branchwork in their form, focusing flow toward a single spring point. Worthington (1991) analyzed 96 published cases where river cave passages have been explored and mapped along their full length from input points to output points. He found that sinuosity (measured length along the passages/straight line distance from input to output) falls between 1.4 and 1.7 in most instances, indicating that the conduit systems tend to evolve with fairly direct connections.

Palmer (1991) has proposed the general model for the plan patterns of all genetic cave types that is shown in Figure 6. Common caves display chiefly the branchwork forms that

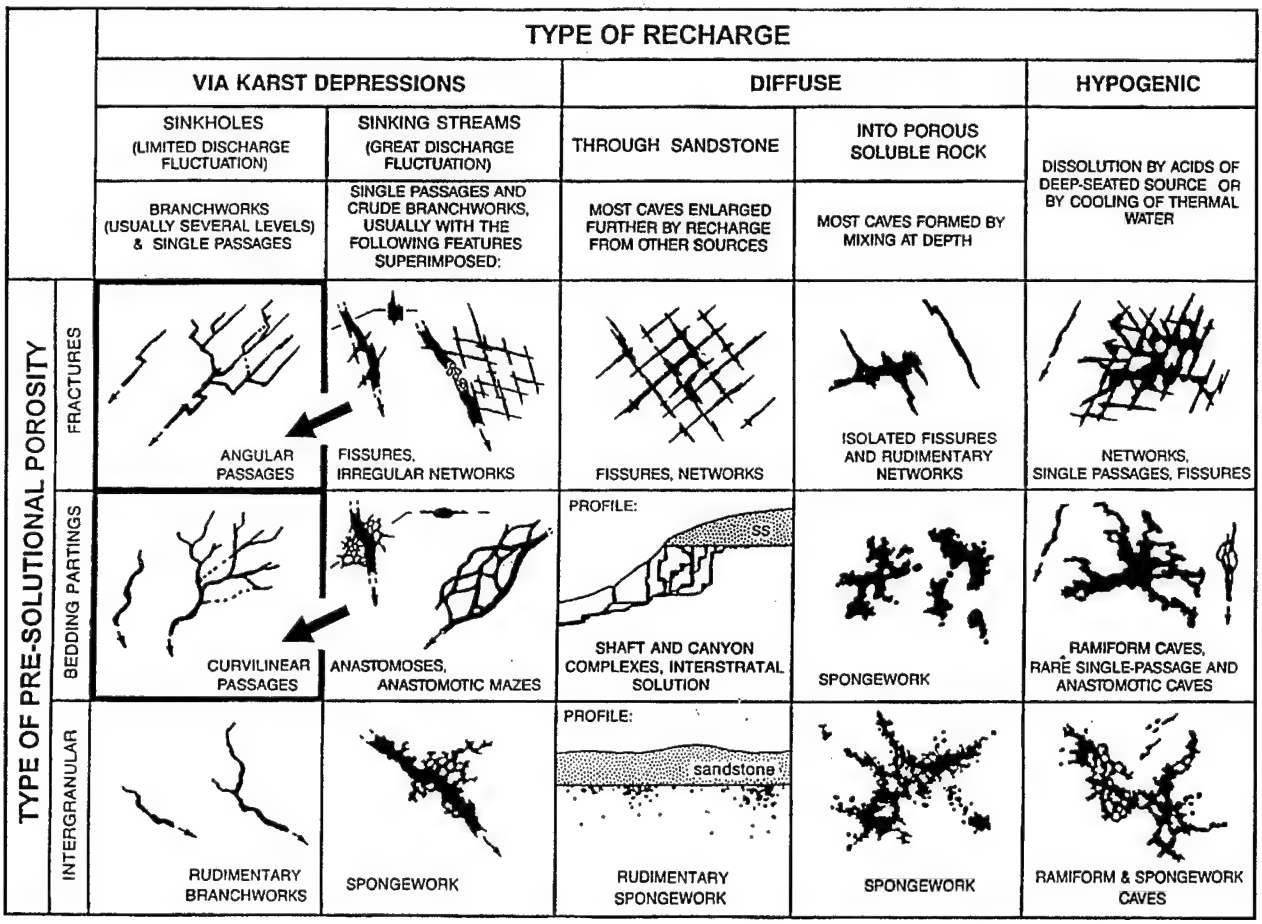

Figure 6: The general model for plan patterns of caves proposed by Palmer (1991), modified to emphasize the branchwork patterns that are predominant in common cave systems. Irregular networks and anastomotic mazes tend to be subsidiary components of the branchworks, as indicated.

I have highlighted in his figure. Angular connections dominate these where joints and faults are the principal structural guides of the conduits, and curvilinear forms where they develop primarily along bedding planes. Many cave systems will display mixtures of the two patterns. The "irregular networks" and "anastomotic mazes" shown in the figure tend to occur as subsidiary components of the branchwork patterns, usually at their upstream ends where flash floods from surface channels can create extreme but short-lived hydraulic gradients. Groves and Howard (1994), Clemens et al. (1997) have published computer model studies of such maze generation.

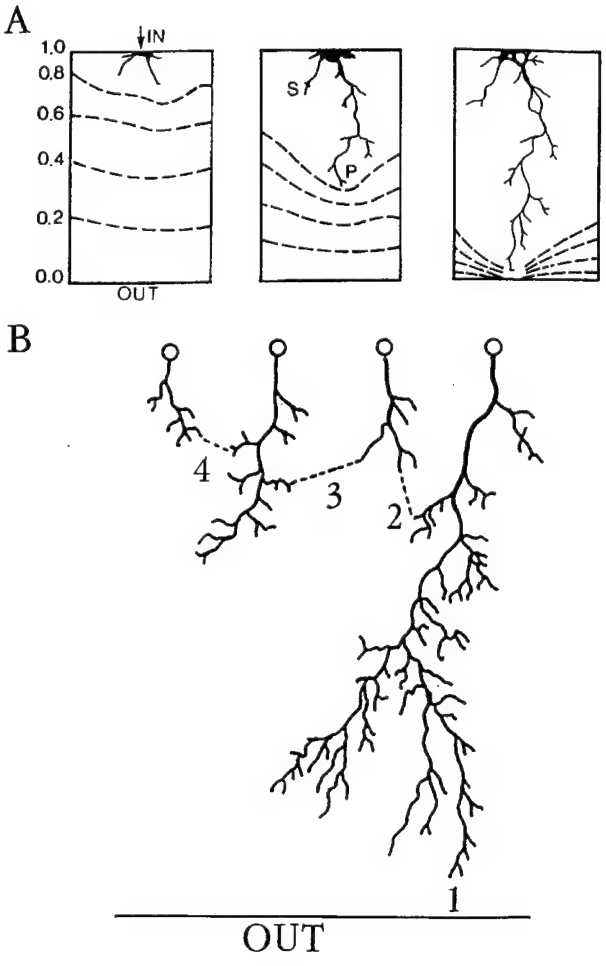

Figure 7: (A) The competitive extension of dissolutional proto-conduits across a fissure with anisotropic porosity. "P" = principal tube; "S" = secondary tubes. Dashed lines are equipotentials. **(B)** Competitive extension where there are multiple inputs in a rank. Numbers and dashed lines indicate the predicted sequence of breakthrough connections that will occur and their location. (Both figures based on hardware simulations by R.O. Ewers, 1982.)

In a fully developed branchwork cave the dissolutional conduits will occupy only a tiny proportion of the total length or area of penetrable fissures that is available to the groundwaters. The rules that govern the selection of the successful linkages that will be enlarged into the branchwork pattern were investigated by Ewers (1982) by means of comprehensive series of electrical and sand model flow-field analogs and direct solutional simulations with plaster of Paris; Lauritzen (1986) and Dreybrodt (1997) have supported many of the results with finite-element and lattice analyses. Figures 7 and 8 summarize the principal features of Ewers' findings.

The models explore conduit propagation across a single fissure that is anisotropic. They will also apply to systems of many interconnected fissures where aperture is anisotropic within and between the individual fractures. The most important feature of the dynamic behavior is the "breakthrough," when a dissolutional proto-conduit approximately one centimeter in diameter reaches an output boundary such as a spring or an earlier cave passage. This abruptly drops the resistance to flow along its line by one or more orders of magnitude because non-linear laminar or turbulent flow can commence (Ewers, 1982; White, 1988), thereby accelerating dissolutional conduit development.

The most simple case of propagation is that of a single groundwater input to the fissure, as shown in Figure 7A. Competing proto-conduits form distributary patterns by exploiting the wider pores and throats in the fissure until the breakthrough creates one winner or principal tube, "P". When there are competing inputs in one rank, one of them will get ahead (Figure 7B); upon breakthrough the piezometric surface is drawn down above it, reorienting the local hydraulic gradient toward it. Nearest neighbor inputs then connect to it (breakthrough - dashed lines) in steps A2, A3, A4, etc. In General Systems terminology, common caves evolve as "cascading systems" (von Bertalanffy, 1962), one breakthrough (or energy cascade) re-orienting the local water table and so tripping off the next cascade. The main system of Hölloch, Switzerland (Bögli, 1970) is the finest example that I know of cascade linkage across a fissure (i.e. strike-oriented) in what has been essentially a one-rank-of-inputs situation: there have been four or more successive cascades as the system adjusted to allogenic lowering of the outlet springs. In Switzerland also, the pattern of Siebenhengste (Bitterli and Jeannin, 1997) appears to exhibit similar features.

The most complex patterns arise where there are many successive ranks of inputs. This is the case in most areas of holokarst, ranging in scale from local limestone pavements (clints-and-grikes) to extensive sinkhole plains such as those of Indiana, Kentucky, and Tennessee. Figure 8A shows that there is the same sequence of competition as above, first

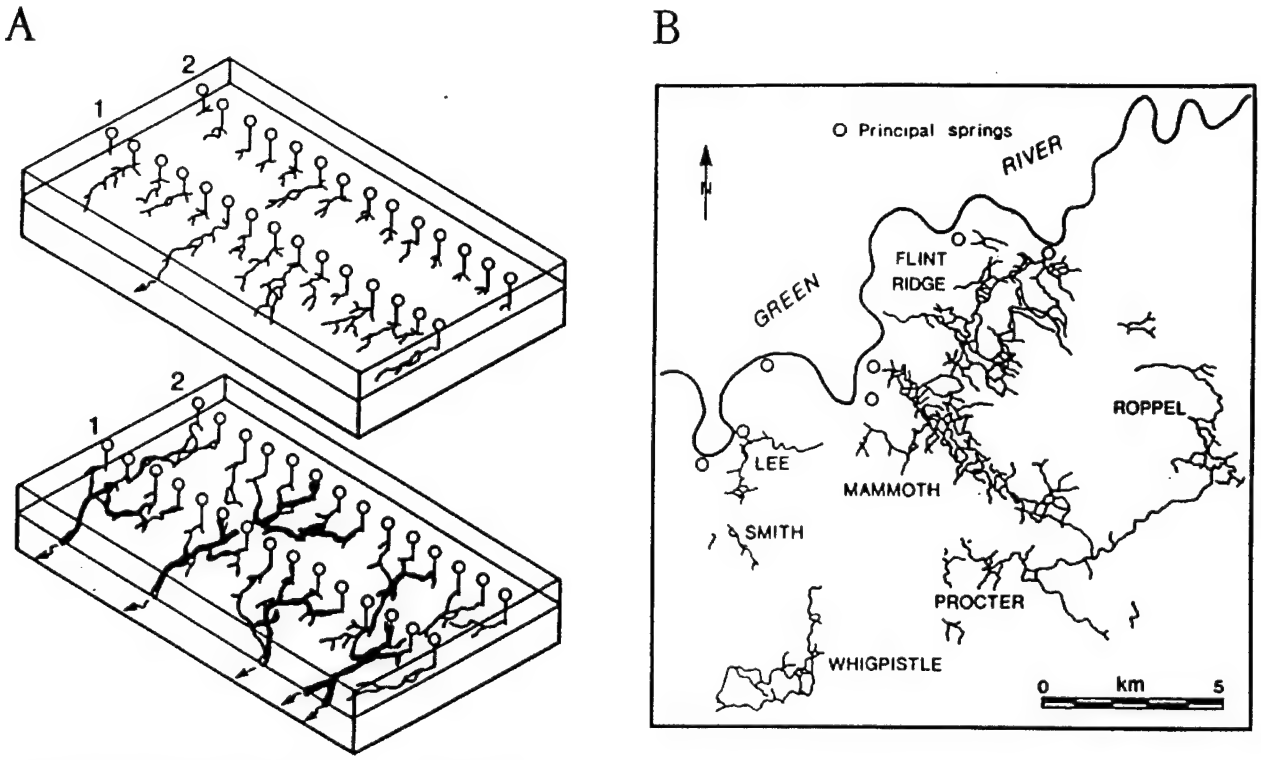

Figure 8: (A) Patterns of proto-conduit breakthrough and connection where there are multiple ranks of inputs. **(B)** Map of the major galleries in Mammoth Cave and neighboring cave systems, Kentucky, to illustrate multi-rank cave genesis.

among the distributaries of the individual inputs, next by lateral connection of nearest neighbors to the first breakthrough principal tubes. Ranks of inputs that are further from the output boundary then link to winners in the nearer ranks in successive cascades. This pattern may be broadly discerned in the organization of conduits in Mammoth Cave and nearby systems that drain to springs along the Green River, Kentucky (Figure 8B). This is the lengthiest regional aggregation of known and mapped conduits and shafts (>600 km). Note, nevertheless, that the many gaps in the map indicate that information about the conduit system remains very incomplete, especially if we compare it to channel patterns in surface river basins of the same scale. The Mammoth map is also complicated by the fact that it mingles many successive phases of cave development targeted at different spring locations and elevations; the older passages are now hydrological relicts.

A final initial genetic pattern is found where the limestone is exposed only along a narrow valley floor and groundwater drains to springs at the valley mouth. In this "restricted input" case the sinkpoints tend to line up behind one another in a single file, with breakthrough commencing at that which is closest to the spring (see Ford and Williams, 1989, p. 259-260).

It is emphasized that the construction of these comparatively simple patterns of conduits is liable to major distortions (1) by local lithologic and structural factors such as perching on a chert bed or direction down the axis of a syncline; (2) by great differences in the quantities of water supplied to different inputs in a group, for example when allogenic flow to a stream sink is compared to seepage into nearby holokarst dolines. The pattern-building is analogous to that of the development of dendritic channel networks on the earth's surface, but with one very significant difference: the ideal river pattern is wholly stochastic, the individual channel being initiated at some random point on a surface, from which it can extend upslope and downslope until it chances to encounter another channel segment and so amalgamates. In a certain sense the location of initial input points in a karst branchwork can also be considered to be stochastic, but the successive link-ups of the principal tubes are deterministic because they are directed by local reorientation of the water table following breakthrough. Despite the strong deterministic factors in cave-pattern building (lithological and structural as well as hydraulic), however, it is rarely feasible to predict the exact locations where principal conduits will be found underground, for the reasons made evident in Figure 7B.

Multiphase (multi-level or multi-stage) cave systems

The great majority of the large common caves that are known appear to be multi-phase systems. These display different "levels" of major conduits that have been created

in response to changes in the elevation of the springs. Normally, these changes are lowerings of elevation as consequences of erosional base level lowering around the margins of the karst. Upper galleries are progressively abandoned by the streams that generated them until they become completely relict. Of course, there are also instances of the converse, i.e. cave systems reconstructed progressively above one another where base level is rising because land is sinking or the sea is rising. There are probably many such around the limestone shores of the Mediterranean and Black Sea that are responses to the Messinian Crisis (the dry-up of these seas), for example. However, they are difficult to explore and will play a less important hydrogeologic role in most regions.

In many multiphase systems the lower, younger main galleries are located close to or directly beneath the older passages that they replace hydrogeologically. But in others the new galleries may follow new directions into previously non-cavernous rock. This usually occurs where there is a major shift in the geographic location of the springs accompanying their opening at lower elevation. Re-orientation of the trend of the main drainage conduits can be 90^0 or more. The effect is especially important in regions of low topographic relief and stratal dip such as central Kentucky, where lowering of 2-3 meters in spring elevation can be associated with a lateral displacement of more than 1000 meters.

In addition to the younger main conduits, the multiphase patterns will be complicated by the presence of many shorter, smaller passages and shafts that interconnect the different levels. Some are hydrogeologically active, conveying tributary streams, while others functioned genetically only for brief periods during the system readjustment to a new level (Ford and Williams, 1989, p. 274-276). Where there have been small readjustments to many successive levels that were separated by only a few meters in elevation, as at Mammoth Cave, Kentucky, the final pattern can be likened to that of a tangled spaghetti.

These relict systems will be contained within the modern vadose zone. Considering the total volume of that zone within a drainage basin, the aggregate volume of all relict passages and shafts will be small, amounting to a few percent at most. However, much of the drainage of the epikarst is organized to connect to them. They intercept this drainage and may convey it laterally as underfit streams on the floors of relict galleries for many hundreds of meters before the flow can find an escape route on downward. This is to suggest that the standard assumption when modeling, that recharge descends vertically through the vadose zone, may not be strictly correct. Factors for local concentration and lateral diversion must be introduced for areas proximate to known or suspected cave systems. Very little work has been done on the problem, but see the pioneering studies of Friederich and Smart (1981, 1982).

Conclusions

Large common cave systems are very heterogeneous in space and time. Working alone and with their differing techniques, neither speleologists nor hydrogeologists can obtain a comprehensive picture of their functioning within complex karst aquifers. The processes that create them and the factors influencing those processes now appear to be sufficiently understood that quite realistic multifactorial process-oriented computer modeling of system genesis is feasible. In the future there is great potential for computer scientists, hydrogeologists and speleologists to work together at this task. It is essential and exciting.

Acknowledgments

A version of this paper was first presented at the 6th Conference on Limestone Hydrology and Fissured Media, La Chaux-de-Fonds, Switzerland. I thank its staff for arranging this meeting and inviting me to participate. It was an excellent occasion. I also thank my graduate students, international colleagues and other companions in the field for stimulating ideas and discussion: the international karst community is one of warm, open and friendly enthusiasts everywhere. The Natural Sciences and Engineering Research Council of Canada have given generous support to my research endeavors for many years.

References Cited

Adams, C., and A.C. Swinnerton, 1937, The solubility of calcium carbonate: Transactions, American Geophysical Union, 11(2), p. 504-08.

Audra, P., 1977, Le rôle de la zone épinogée dans la spéléogenèse: Proceedings of the 12th International Congress of Speleology, Volume 1, La Chaux-de-Fonds, Switzerland, p. 165-167.

Bakalowicz, M., 1977, Hydrogéologue versus spéléologue, ou de qui relève l'étude et l'exploration des eaux souterraines kartiques? Proceedings of the 12th International Congress of Speleology, Volume 11, La Chaux-de-Fonds, Switzerland, p. 23-26.

Bitterli, T., and P.-Y. Jeannin, 1997, Entwicklungsgeschichte der Höhlen im Gebiet Hohgant-Sieben Hengste-Thunersee (Berner Oberland, Schweiz): Proceedings of the 12th International Congress of Speleology, Volume 1, La Chaux-de-Fonds, Switzerland, p. 349-354.

Böcker, T., 1969, Karstic water research in Hungary:

International Association of Scientific Hydrology, Bulletin 14, p. 4-12.

Bögli, A., 1970, Le Hölloch et son karst: Editions la Baconnière, Neuchâtel.

Bonacci, O., 1977, Role of speleology in karst hydrology and hydrogeology: Proceedings of the 12th International Congress of Speleology, Volume 11, La Chaux-de-Fonds, Switzerland, p. 27-30.

Bretz, J Harlen, 1942, Vadose and phreatic features of limestone caverns: Journal of Geology, vol. 50, p. 675-811.

Bretz, J Harlen, 1953, Genetic relations of caves to peneplains and big springs in the Ozarks: American Journal of Science, vol. 251, p. 1-24.

Clemens, T., D. Hückinghaus, M. Sauter, R. Liedl, and G. Teutsch, 1997, Simulation of the evolution of maze caves: Proceedings, 12th International Congress of Speleology, vol. 2, p. 65-68.

Cvijić, J., 1918, Hydrographie souterraine et evolution morphologique du karst: Receuilles Travaux de l'Institute de Géographie Alpine, vol. 6(4), p. 375-426.

Davis, W.M., 1898, The geographical cycle of erosion. Geographical Journal, vol. 14, p. 481-504.

Davis, W.M., 1930, Origin of limestone caverns: Geological Society of America, Bulletin, vol. 41, p. 475-628.

Davis, W.M., 1931, The origin of limestone caverns: Science, vol. 73, p. 327-33.

Dreybrodt, W., and J. Siemers, 1997, Early evolution of karst aquifers in limestone: Models on two-dimensional percolation clusters: Proceedings, 12th International Congress of Speleology, vol. 2, p. 75-80.

Dwerryhouse, A.R., 1907, Limestone caverns and potholes and their mode of origin: Yorkshire Ramblers Club Journal, vol. 2, no. 7, p. 223-8.

Ewers, R.O., 1982, Cavern development in the dimensions of length and breadth: Ph.D. thesis, McMaster University.

Ford, D.C., 1971, Geologic structure and a new explanation of limestone cavern genesis: Cave Research Group of Great Britain, Transactions, vol. 13(2), p. 81-94.

Ford, D.C., and R.O. Ewers, 1978, The development of limestone cave systems in the dimensions of length and breadth: Canadian Jour. of Earth Sci., vol. 15, p. 1783-98.

Ford, D.C., and P.W. Williams, 1989, Karst geomorphology and hydrogeology: London, Unwin & Hyman, 601 p.

Ford, D.C., J. Lundberg, A.N. Palmer, M.V. Palmer, W. Dreybrodt, and H.P. Schwarcz, 1993, Uranium-series dating of the draining of an aquifer: The example of Wind Cave, Black Hills, South Dakota: Geological Society of America Bulletin, vol. 105, p. 241-250.

Friederich, H., and P.L. Smart, 1982, The classification of autogenic percolation waters in karst aquifers: a study in G.B. Cave, Mendip Hills, England: Proceedings, University of Bristol Speleological Society, vol. 16(2), p. 143-159.

Friederich, H., and P.L. Smart, 1981, Dye tracer studies of the unsaturated zone: recharge of the Carboniferous Limestone aquifer of the Mendip Hills, England: Proceedings, 8th International Speleological Congress Kentucky, USA, p. 283-6.

Frumkin, A., 1994, Morphology and development of salt caves: National Speleological Society of America, Bulletin vol. 56, p. 82-95.

Glennie, E.A., 1954, The origin and development of cave systems in limestone: Cave Research Group of Great Britain, Transactions III, No. 2, p. 73-83.

Groves, G.G., and A.D. Howard, 1994, Early development of karst systems: 1. Preferential flow path enlargement under laminar flow: Water Resources Research, vol. 30(10), p. 2837-2846.

Grund, A., 1903, Die Karsthydrographie: Pencks geographische Abhandlung, vol. 7(3), p. 103-200.

Hanns, M., F. Hermann, and O. Atteia, 1977, Application of a computational fluid dynamics model to cave river hydrodynamics: Proceedings of the 12th International Congress of Speleology, Volume 11, La Chaux-de-Fonds, Switzerland, p. 141-144.

Hobbs, S.L. and P.L. Smart, 1986, Characterization of carbonate aquifers: a conceptual base: Proceedings 9th International Speleological Congress, Barcelona, vol. 1, p. 43-46.

Horton, R.E., 1945, Erosional development of streams and their drainage basins: Geological Society of America Bulletin 56, p. 275-370.

Jennings, J. N., 1983, The problem of cavern formation, *in* H.S. Sharma (ed.), Perspectives in Geomorphology: New Delhi, Concept, p. 223-53.

Katzer, E., 1909, Karst und Karsthydrographie: Zur Kunde der Balkan Halbinsel, vol. 8, Sarajevo.

Knez, M., 1997, Speleogenesis of phreatic channels in bedding-planes in the frame of karst aquifer (Skocjanske jama Caves, Slovenia): Proceedings of the 12th International Congress of Speleology, Vol. 11, La Chaux-de-Fonds, Switzerland, p. 279-282.

Lauritzen, S.-E., N. Odling, and J. Petersen, 1992, Modelling the evolution of channel networks in carbonate rocks, *in* J.A. Hudson, (ed.), ISRM Symposium: Eurock '92. London, Thomas Telford, p 57-62.

Lowe, D.J., 1992, The origin of limestone caverns: an inception horizon hypothesis: Ph.D. thesis, Manchester Polytechnic University, 512 p.

Martel, E.A., 1921, Nouveau traité des eaux souterraines: Paris, Editions Doin.

Mylroie, J.E., and J.L. Carew, 1990, The flank margin model for dissolution cave development in carbonate platforms: Earth Surface Processes and Landforms, vol. 15, p. 413-424.

Palmer, A.N., 1991, Origin and morphology of limestone caves: Geological Society of America Bulletin vol. 103, p. 1-21.

Rhoades, R., and M.N. Sinacori, 1941, The pattern of ground-water flow and solution: Journal of Geology, vol. 49, p. 785-94.

Rossi, C., A. Munoz, and A. Cortel, 1997, Cave development along the water table in Cobre System (Sierra de Penalabra, Cantabrian Mountain, N. Spain: Proceedings of the 12th International Congress of Speleology, vol. 1, La Chaux-de-Fonds, Switzerland, p. 179-182.

Swinnerton, A.C., 1932, Origin of limestone caverns: Geological Society of America Bulletin, vol. 43, p. 662-93.

Von Bertalanffy, L., 1962, General systems theory: a critical review: General Systems VII.

Waltham, A.C., M.J. Simms, A.R. Farrant, and H.S. Goldie, 1977, Karst and caves of Great Britain: London, Chapman and Hall, 358 p.

Warwick, G.T., 1953, The origin of limestone caves, *in* C.H.D. Cullingford (ed.), British Caving: London, Routledge and Kegan Paul, p. 41-61 .

White, W.B., 1988, Geomorphology and hydrology of karst Terrains: New York, Oxford University Press, 464 p.

Worthington, S.R.H., 1991, Karst hydrogeology of the Canadian Rocky Mountains: Ph.D. thesis, McMaster University, 370 p.

Worthington, S.R.H., and D.C. Ford, 1997, Borehole tests for megascale channeling in carbonate aquifers: Proceedings of the 12th International Congress of Speleology, vol. 11, La Chaux-de-Fonds, Switzerland, p. 195-198.

A COMPREHENSIVE STRATEGY FOR UNDERSTANDING FLOW IN CARBONATE AQUIFERS

Stephen R. H. Worthington
School of Geography and Geology, McMaster University
Hamilton, Ontario, Canada, L8S 4K1

Abstract

Studies of carbonate aquifers usually either concentrate on sampling the channel flow (e.g. sink-to-spring tracer testing, spring monitoring) or on sampling the non-channel flow (e.g. borehole measurements). A comprehensive approach is advocated here, involving the integration of both sources of information, as well as measurements of the porosity and permeability of the unfractured rock. Representative sampling can be achieved by treating carbonates as triple-porosity aquifers, with one-, two-, and three-dimensional porosity elements. The division of carbonate aquifers into "karstic" or "non-karstic" types is unwarranted.

Introduction

In the past three decades, carbonate aquifers have usually been considered in one of three ways. The simplest and most commonly used approach has been to assume that fractures may be locally important, but that fracture density is great enough that the aquifer can be treated as an equivalent porous medium and can be modeled using a package such as MODFLOW. A second approach has been to recognize that fractures may be laterally continuous for considerable distances and that these are much more conductive than the matrix of the rock. In this case a double-porosity (or double-permeability) model is used for the aquifer. In both cases it is assumed that boreholes facilitate representative sampling of the aquifer. A third approach has been to recognize the existence of a high-permeability network of conduits within the aquifer, and to concentrate on studying the conduits. Techniques include tracer testing from dolines or sinking streams to springs and monitoring of spring discharge or hydrochemical parameters. This approach is most commonly used where there are abundant surficial karst landforms.

The use of *a priori* assumptions on the behavior of carbonate aquifers tends to result in studies that only partially characterize an aquifer. Studies of spring flow or tracer testing from sinkholes to springs succeed in characterizing channel flow in the aquifer, but little is learned about non-channel flow. Conversely, studies using wells as sampling and monitoring points may characterize fracture and matrix flow but often give little or no indication of the rapid solute transport that is occurring in the channel network located between the wells. A full understanding of flow in carbonate aquifers can only be gained by studying all the flow components in the aquifer.

The conceptual model described below incorporates the techniques used for monitoring wells and those used for monitoring springs to gain a more holistic understanding of carbonate aquifers.

A conceptual model for carbonate aquifers

One way of studying carbonate aquifers that may prove useful is to consider aquifers in terms of the three fundamental geometric elements that can exist within it. These are shown in Figure 1 and are: (i) One-dimensional, or linear elements. These are often referred to as *channels*. In carbonate aquifers, large channels in which there is turbulent flow are commonly termed *conduits*, and if they are accessible by people they are called *caves*. (ii) Two-dimensional, or planar elements, such as bedding planes, joints and faults. (iii) The three-dimensional matrix.

Carbonate aquifers can be considered as triple-porosity aquifers since they contain these three porosity elements. Analysis of an aquifer in terms of three porosity elements results in a better understanding of flow and storage than if the aquifer is treated as having only two porosity components. Furthermore, there have been two different ways in which two porosity components in carbonate aquifers have been studied; a double-porosity aquifer is not the same as a conduit and diffuse-flow aquifer (Table 1). Analysis as a triple-porosity aquifer can avoid potential confusion and lead to more accurate insights on aquifer behavior.

Formation, size and distribution of channels

Fracture planes commonly have variable apertures, and most of the flow is concentrated along the more open portions of fractures, which are called channels. For instance, in granites in Great Britain and in Sweden it has been found that such channels may occupy 5-20% of a given fracture plane (Tsang, 1993). However, in carbonate rocks some channels may be greatly enlarged by solution processes. This is due to two factors:

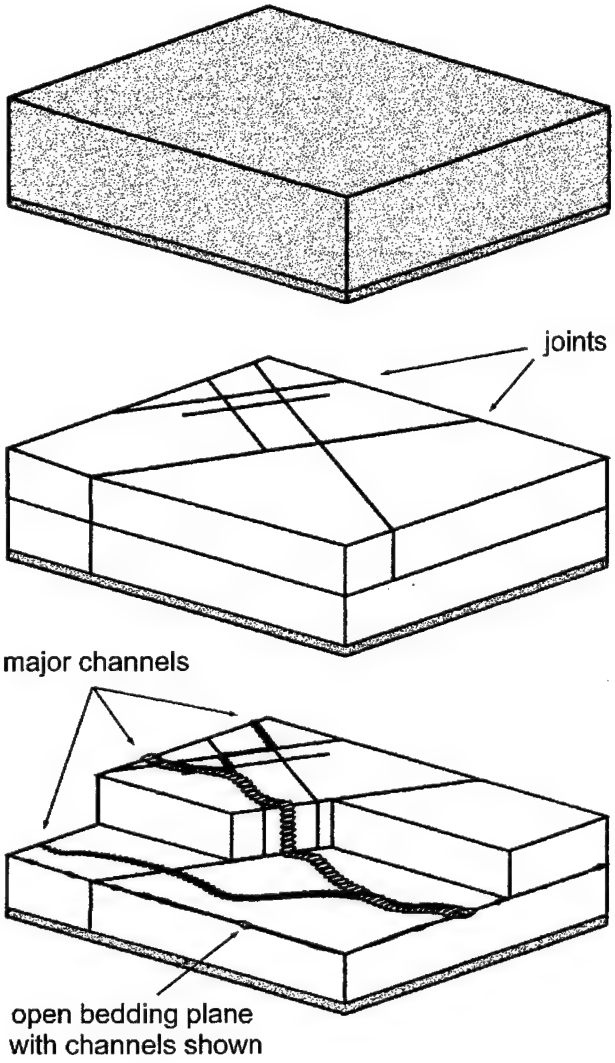

Figure 1: Model for a single-porosity aquifer with matrix flow (top), a double-porosity aquifer with matrix and fracture flow (center), and a triple-porosity aquifer with matrix, fracture, and channel flow (bottom).

(a) The non-linear nature of carbonate dissolution. As thermodynamic equilibrium is approached, the solution rate decreases by several orders of magnitude (Plummer and Wigley, 1976). This results in carbonate groundwater being slightly undersaturated with respect to calcium (or magnesium) carbonate at most sites where there is notable flow.

(b) The positive-feedback relationship between dissolution rate and discharge, which permits larger channels to grow at the expense of smaller ones (Ford and Williams, 1989, p. 249 *et seq.*).

These two factors combine to create broadly dendritic networks of channels. In unconfined carbonate aquifers in moist climates, channeling should always develop. An example of a dendritic channel network is shown in Figure 2. Fifty-three small tributaries converge in this well-mapped cave to form a flow path which discharges to the surface at a spring. The channels shown in Figure 2 are all accessible to people, and are all >0.3 m in diameter.

There are also smaller channels than cave passages. These channels are sometimes encountered in boreholes (Waters and Banks, 1997), but are better visible in quarry walls, outcrops and in cave passages. Figure 3 shows the calculated apertures of two sets of small channels. The "minor flows" are from measurements at 44 drip points from stalactites into four New Zealand caves (Gunn, 1978), and the "major flows" are from the 25 largest flows into GB Cave, England (Friederich and Smart, 1982). Apertures were calculated using the Hagen-Poiseuille equation and the maximum recorded discharge at each flow point, assuming a hydraulic gradient of unity and a circular channel shape. The calculated apertures are only estimates, as channel roughness and surface-tension effects are ignored, and the measured flow may be much less than the channels are capable of delivering. However, the calculated values are likely to be fairly accurate, since discharge varies with the fourth power of pipe diameter. Natural-gradient tracer tests were carried out from the surface to the input points in GB Cave, which were on average 60 m below the surface. Tracer arrival times varied from less than one day

Element geometry	Flow regime	Karst spring studies	Double porosity	Triple porosity
3D	laminar	diffuse	matrix	matrix
2D	laminar	diffuse	fracture	fracture
1D	laminar	diffuse	not included	channel
1D	turbulent	conduit	not included	channel (conduit)

Table 1: Comparison of classification schemes for porosity elements in carbonate aquifers.

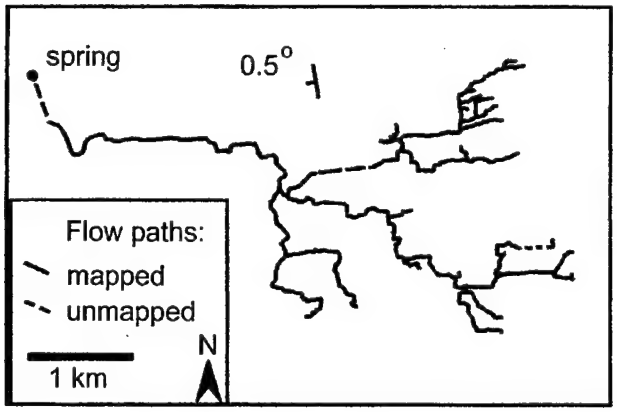

Figure 2: Convergent flow paths draining to a spring, as mapped in Blue Spring Cave, Indiana (after Palmer, 1969).

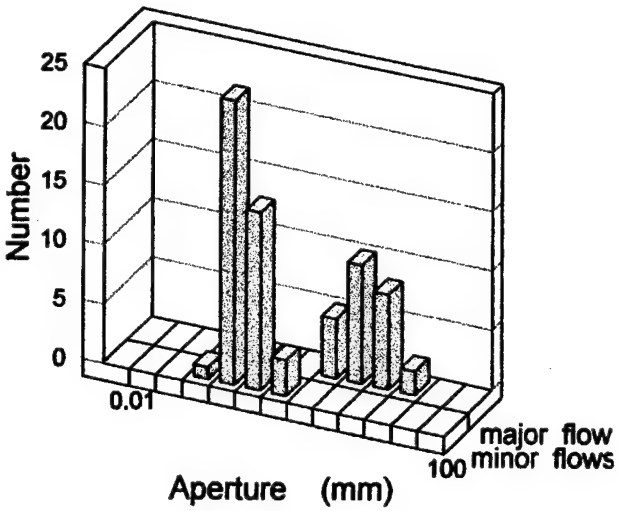

Figure 3: Calculated apertures of minor flows into four New Zealand caves and major flows into GB Cave, England (calculated from measurements by Gunn (1978) and Friederich and Smart (1982).

to several weeks, giving velocities mostly in the range of 10-100 m/day (Friederich and Smart, 1981). These velocities are between the 1700 m/day average velocity for sink-to-spring tracer tests (Worthington et al., 1999a) and calculated velocities of a meter per day or less derived from equivalent porous-medium analysis.

Dolines are input points to channels. The channel at the base of a doline is an efficient drain point which promotes centripetal drainage and facilitates the enlargement of the doline. The channels draining dolines are likely to be at least some millimeters in diameter, and are often found to be much larger. Such channels not only must be able to carry the discharge from the depression, but also the suspended load of insoluble material resulting from erosion of the bedrock within the doline. Furthermore, the channels must be part of a continuous channel network with its outlet at a spring; if this were not the case, then the doline-draining channels would becomes choked with insoluble material, and doline formation would be halted at an early stage.

Sampling and monitoring the three porosity components

(i) Channels: Springs in carbonate strata represent the output points for channel networks and provide a sampling point that integrates the groundwater flow from what is often a considerable area, e.g. 10-1000 km^2. They are thus ideal for sampling off-site migration from contaminant sites. Tracer testing from dolines or sinking streams to springs is common and serves to establish flow direction and velocity. If both spring discharge and the hydraulic gradients in the aquifer are known, then an "equivalent hydraulic conductivity" for the aquifer can be calculated (Worthington and Ford, 1999a). This is an average value across the cross section of the catchment draining to a spring, and ignores turbulent flow, which may be important. The use of an equivalent hydraulic conductivity facilitates comparisons of channel flow with matrix and fracture flow.

Boreholes are of limited use in studying channeling. Table 2 gives data on channeling in a number of well-studied carbonate aquifers where extensive caves have been found. From this data set, a borehole would have a probability of only 0.0037 - 0.075 of intercepting one of these mapped cave passages. In volumetric terms the caves only occupy between 0.004% and 0.48% of the bedrock in which they are located. Thus it would be fallacious to assume that an absence of major bit drops in drilling a number of wells at a study site signifies an absence of channeling.

(ii) Fractures: The permeability of horizontal or sub-horizontal fractures (usually bedding planes) is routinely determined from hydraulic testing (e.g. packer, slug, or pump tests) in vertical boreholes. Fracture aperture can be determined by the cubic law from narrow-interval packer testing. The permeability of vertical or sub-vertical fractures is usually estimated rather than measured. For instance, in horizontally-bedded strata it is often assumed that vertical permeability is 10 or 100 times less than horizontal permeability.

(iii) The matrix: The matrix is the solid unfractured rock. Samples may be collected from boreholes, quarry walls, or natural outcrops for testing porosity and permeability. Alternatively, *in situ* packer testing in unfractured sections of boreholes will give values of matrix permeability (Price et al., 1982).

Cave	Volume of rock length x width x height m (1)	Volume of cave x 10^6 m^3 (2)	Length of cave km (2)	Cave porosity % (3)	Areal coverage of cave % (4)
Ogof Agen Allwedd - Ogof Daren Cilau, Wales	6200 x 1900 x 50	0.9	75	0.15	1.7
Blue Spring Cave, Indiana	5100 x 2600 x 45	0.5	32	0.08	1.1
Kingsdale Cave System, England	2600 x 1500 x 100	0.17	20	0.04	1.8
Nohoch Nah Chich, Mexico	5500 x 1900 x 80	4	39	0.48	6.5
Mammoth Cave, KY, USA	11000 x 9000 x 90	8	550	0.09	1.4
Castleguard Cave, Canada	6500 x 1200 x 400	0.12	20	0.004	0.51
Friars Hole System, WV, USA	6000 x 2000 x 80	2.7	70	0.28	2.5
McFail's Cave, New York	3500 x 2300 x 90	0.12	11	0.016	0.37
Skull Cave, New York	1300 x 940 x 60	0.046	6	0.064	1.2
Caves in Southern Gunung Api, Malaysia	7000 x 2500 x 400	30	110	0.43	7.5

Table 2: Cave porosity and areal coverage for some well-mapped caves. **(1)** This represents the minimum rectangular block of rock that can contain the 3-D array of mapped passages in each cave. **(2)** These refer to the explored and mapped cave passages. Increases in these values are likely as the caves are more completely explored. **(3)** Cave porosity is defined as the volume of mapped cave divided by the minimum rectangular block of rock that can contain the cave. **(4)** The areal coverage is the plan area of the cave divided by the minimum rectangular area that can contain the cave, which represents the probability of a borehole intersecting the cave.

The extent of channel networks

Dolines represent the upgradient ends of channels, and it is possible to gain a better understanding of channel distribution by using doline distribution to construct a model of the channel network. For instance, Figure 4a shows the northeast portion of Blue Spring Cave, Indiana (Figure 2), with the doline watersheds shown. A simple map of channeling could be constructed by linking the low points in each of the 38 dolines with either the eight major inputs into this section of the cave or into other major channels (Figure 4b). Such a procedure obviously simplifies the geometry of the major channels and ignores smaller channels (e.g. channels feeding drip points at stalactites), but it does represent an important fraction of flow in the aquifer.

The above procedure is a starting point to modeling channeling in a polygonal terrain such as at Blue Spring Cave, where the whole surface is occupied by contiguous dolines. However, many surfaces above carbonate aquifers have dolines that are widely spaced. These can be linked in the same fashion as at Blue Spring Cave to give a channel network draining to a spring, but this network will be a great simplification of the true channel network. Furthermore, some carbonate aquifers have no dolines overlying them, such as where the aquifer is overlain by non-carbonates or by glacial sediments. Prominent examples are the most extensive cave in Canada (Castleguard Cave) and the most extensive cave in the USA (Mammoth Cave); the majority of both caves underlie surfaces where dolines are absent, so the channel network in these aquifers cannot be inferred from the surface landforms. However, in both cases channel networks have been demonstrated from tracer testing (Smart, 1988; Quinlan and Ray, 1981) as well as from cave exploration.

Where there are no dolines or sinking streams above a carbonate aquifer, then it is most difficult to estimate the extent of channeling. If there are no faults or high-permeability facies at a spring to explain the concentration of aquifer discharge at one point, then the best explanation is that the spring is the outlet for a channel network, and this is likely to extend throughout the spring's catchment. Some carbonate aquifers discharge into thick alluvium, lakes, or the sea, so that the location of springs may be extremely difficult, as will the characterization of channeling.

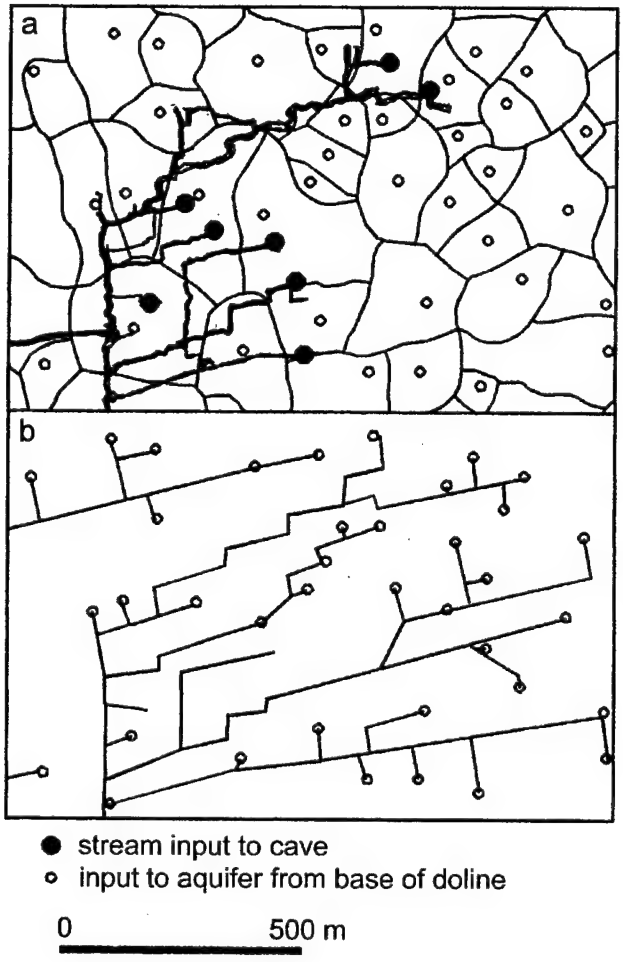

Figure 4: Channeling in the northeast section of Blue Spring Cave, Indiana, showing (top) doline watersheds and underlying cave passages (after Palmer, 1969); and (bottom) a dendritic network of the major channels

Sampling boreholes for channeling

Boreholes are not ideal for investigating channeling because of the low probability of intercepting channels, as explained above. However, there are some aquifer testing and monitoring techniques that can give an indication that there may be channels close to the borehole. The following list of the techniques for inferring channeling is based on the discussion in Worthington and Ford (1995):

(a) Well-to-well or well-to-spring tracer tests. Tracer tests from sinking streams or dolines to springs were established in the 1870s as an excellent method of determining channel velocities and connections. Well tests are much more problematic, as wells may be poorly connected to channels. It is likely that longer-distance traces (e.g. >100 m) are more likely to show evidence of channeling than shorter-distance traces, as the widely spaced channels are more likely to be encountered along a longer tracer path.

(b) Combination of core, packer, slug, and pump tests. Kiraly (1975) first suggested that there is a scaling effect in carbonate aquifers, with larger-scale tests encountering more permeable fractures and channels.

(c) Variable-rate pumping tests. Hickey (1984) showed that the pumping rate should be proportional to the drawdown in observation wells if Darcy's Law is valid within the cone of depression. If there are major channels within the cone of depression, and if these are well-connected to the pumping well, then there should be a non-linear pumping-rate / drawdown response.

(d) Matrix and fracture packer tests to calculate fracture extent. Price (1994) described a method for estimating the extent of interconnected fractures intersected by wells by using steady-state packer testing.

(e) Symmetry of cones of depression at pumping wells. The cone of depression at a pumping well is symmetrical in a homogeneous porous medium. However, the cone of depression is likely to be irregular if there is extensive channeling nearby.

(f) Continuous water-level monitoring. Interconnected channel networks transmit water quickly, so a prompt water-level response following rainfall can be expected in boreholes that are well connected to the channel network.

(g) Frequent water-quality monitoring. Precipitation that rapidly infiltrates along channel networks commonly has a much lower solute concentration than long-residence matrix water. Thus variation in solute concentration at a well should be an indicator of connectivity to major channel networks. Frequent sampling (e.g. at least daily) is necessary to detect the rapid response following rainfall. Continuous measurement of electrical conductivity is ideal.

(h) Troughs in the water table. The combination of high permeability in channels and tributary flow to channels means that there are lower heads in channels than in the surrounding aquifer. Quinlan and Ray (1981) showed that such water-table troughs correspond to flow in channels and that they terminate in the downstream direction at springs.

(i) Decreasing hydraulic gradients in the downflow direction. The water-table map of the Central Kentucky karst, which is based on measurements in 1500 wells, the results from 500 dye traces, and the mapping of 700 km of cave passage (Quinlan and Ray, 1981) shows that there are decreasing hydraulic gradients in the downflow direction

along water-table troughs. This contrasts with flow in a porous medium, where increasing gradients are needed in a downflow direction to drive the increasing discharge.

(j) Use of environmental isotopes to characterize age distribution of water in the aquifer. In a porous medium there will be increasing age with depth in recharge areas. Where channels provide rapid recharge to the subsurface, then younger water in channels will underlie older water in overlying fractures and the matrix.

The problem with all of these tests is that they cannot unequivocally demonstrate the presence of channeling. For instance, major fractures opened by tectonic forces could give many of the above results. However, the evidence from caves, from tracer testing, and from the kinetics of dissolution suggest that channeling is ubiquitous in unconfined carbonate aquifers. Thus the first assumption in a carbonate aquifer should be that a well-developed channel network is likely to be present.

Examples of triple-porosity analysis of carbonate aquifers

Worthington et al. (1999b) examined matrix, fracture and channel flow in four carbonate aquifers. The four aquifers are **(a)** a Silurian dolostone aquifer in a glaciated area, where there have been a large number of studies at a PCB spill site (Smithville, Ontario); **(b)** the Mississippian aquifer at the world's most extensive known cave (Mammoth Cave, Kentucky); **(c)** the most important aquifer in Britain (the Cretaceous Chalk); **(d)** a tropical Cenozoic limestone aquifer (Nohoch Nah Chich, Yucatan, Mexico); in recent years scuba divers have mapped more than 60 km of submerged channels in this cave.

Porosity and permeability measurements from these four aquifers are given in Tables 3 and 4, respectively. In all four cases more than 90% of the aquifer storage is in the matrix and more than 90% of the flow is in channels (Table 5), with fractures playing an intermediate role. Thus there are considerable similarities between the four aquifers. However, only the aquifer at Mammoth Cave has been traditionally treated as a karst aquifer. The majority of studies of the other three aquifers have treated them as double-porosity aquifers or equivalent porous media.

Discussion and conclusions

It has often been considered that there is a range in carbonate aquifers between "karstic" and non-karstic" end members. For instance, Atkinson & Smart (1981) classify the English Chalk as being close to the "non-karstic fissured aquifer" end of the spectrum, while the Carboniferous Limestone in England (in which most of the well-known caves are found) is classified as being closer to the

Area	Porosity (%)		
	Matrix	Fracture	Channel
Smithville, Ontario	6.6	0.02	0.003
Mammoth Cave, Kentucky	2.4	0.03	0.06
Chalk, England	30	0.01	0.02
Nohoch Nah Chich, Mexico	17	0.1	0.5

Table 3: Matrix, fracture, and channel porosity in four carbonate aquifers.

Area	Hydraulic conductivity (m s^{-1})		
	Matrix	Fracture	Channel
Smithville, Ontario	1×10^{-10}	1×10^{-5}	3×10^{-4}
Mammoth Cave, Kentucky	2×10^{-11}	1×10^{-5}	3×10^{-3}
Chalk, England	1×10^{-8}	4×10^{-6}	6×10^{-5}
Nohoch Nah Chich, Yucatan, Mexico	7×10^{-5}	1×10^{-3}	4×10^{-1}

Table 4: Matrix, fracture, and channel permeability in four carbonate aquifers.

Area	Fraction of storage in the matrix %	Fraction of flow in channels %
Smithville, Ontario	99.7	97
Mammoth Cave, Kentucky	96.4	99.7
Chalk, England	99.9	94
Nohoch Nah Chich, Yucatan, Mexico	96.6	99.7

Table 5: Principal flow and storage components in four carbonate aquifers.

"karstic" end of the spectrum. Worthington et al. (1999b) compared inflow data to adits in the two aquifers. Both had irregularly spaced inputs, and in both cases there were water-yielding fissures with discharges up to several hundred liters per second. Most of the permeability in both adits is attributable to widely spaced inputs. Consequently, dissolution in both aquifers has resulted in channel networks that contribute minimally to enhancing aquifer porosity, but which have greatly enhanced aquifer permeability. Therefore these aquifers have marked similarities in terms of hydraulic functioning.

One reason why these two limestone aquifers have been viewed differently is the presence of surficial karst features and of known caves in the Carboniferous Limestone and their scarcity in the Chalk. The presence or absence of the surficial features has led to assumptions about aquifer behavior. A second reason is the lack of comprehensive sampling and monitoring in either aquifer in most studies. Few wells have been drilled in the Carboniferous Limestone, and most aquifer studies have used springs. Conversely, most aquifer studies in the Chalk have used wells, and the many springs that exist have been ignored in most hydrogeological studies. Consequently, there is widespread knowledge of channel flow in the Carboniferous Limestone, and of fracture and matrix flow in the Chalk.

The similarity between the matrix, fracture and channel flow and storage proportions in the four contrasting carbonate aquifers, documented in Tables 3, 4 and 5, suggests there is likely to be a similarity between all unconfined carbonate aquifers. This can be explained by fracturing and followed by dissolution, resulting in low-porosity, high-permeability channel networks. Differences cited in the literature are often largely attributable to sampling differences. This problem can be diminished by considering carbonate aquifers as triple-porosity aquifers. Data collection and analysis of the three components of matrix, fracture, and channel flow can give an overall understanding of how a carbonate aquifer functions.

Acknowledgments

Art Palmer's sharing of cave statistics is gratefully acknowledged..

References cited

Atkinson, T.C., and P.L. Smart, 1981. Artificial tracers in hydrogeology, *in* A survey of British hydrogeology, 1980: Royal Society, London, p. 173-190.

Ford, D.C., and P. Williams, 1989, Karst geomorphology and hydrology: Unwin Hyman, London, 601 p.

Friederich, H., and P.L. Smart, 1981, Dye trace studies of the unsaturated-zone recharge of the Carboniferous Limestone aquifer of the Mendip Hills, England, *in* B.F. Beck (ed.), Proceedings 8th International Congress of Speleology, Bowling Green: National Speleological Society, Huntsville, Alabama, p. 283-286.

Friederich, H., and P.L. Smart, 1982, The classification of autogenic percolation waters in karst aquifers: a study in G.B. Cave, Mendip Hills, England: Proceedings, University of Bristol. Speleological Society, vol. 16, no. 2, p. 143-159.

Gunn, J., 1978, Karst hydrology and solution in the Waitomo district, New Zealand: Unpublished Ph.D. thesis, University of Auckland

Hickey, J.J., 1984, Field Testing the Hypothesis of Darcian Flow through a carbonate aquifer: Ground Water, vol. 22, p. 544-547.

Kiraly, L., 1975, Rapport sur l'état actuel des connaissances dans le domaine des charactères physiques des roches karstiques, *in* A. Burger and L. Dubertret (eds.), Hydrogeology of karstic terrains: International Union of Geological Sciences, Series B, 3, p. 53-67.

Palmer, A.N., 1969, A hydrologic study of the Indiana karst: Unpublished Ph.D. thesis, Indiana University, 181 p.

Plummer, L.N., and T.M.L. Wigley, 1976, The dissolution of calcite in CO_2-saturated solutions at 25°C and 1 atmosphere total pressure: Geochimica et Cosmochimica Acta, vol. 40, p. 191-202.

Price, M., 1994, A method for assessing the extent of fissuring in double-porosity aquifers, using data from packer tests: IAHS Publ. no. 222, p. 271-278.

Price, M., B. Morris, and A. Robertson, 1982, A study of intergranular and fissure permeability in Chalk and Permian aquifers, using double packer injection testing: Journal of Hydrology, vol. 54, p. 401-423.

Quinlan, J.F., and J.A. Ray, 1981, Groundwater basins in the Mammoth Cave Region, Kentucky: Occasional Publication #1, Friends of the karst, Mammoth Cave.

Smart, C.C., 1988, Artificial tracer techniques for the determination of the structure of conduit aquifers: Ground Water, vol. 26, p. 445-453.

Tsang, C-F., 1993, Tracer transport in fracture systems, *in* J. Bear, C.-R. Tsang, and G. de Marsily (eds.), Flow and contaminated transport in fractured rock: San Diego, Academic Press, p. 237-266.

Waters, A., and D. Banks, 1997, The Chalk as a karstified aquifer: closed circuit television images of macrobiota: Quarterly Journal of Engineering Geology, vol. 30, p. 143-146.

Worthington, S.R.H., and D.C. Ford, 1995, Borehole tests for megascale channeling in carbonate aquifers: Proceedings, XXVI Congress of the International Association of Hydrogeologists, Edmonton, Alberta, June 5th - 9th 1995.

Worthington, S.R.H., G.J. Davies, and D.C. Ford, 1999a, Quantification of matrix, fracture and channel contributions to storage and flow in a Paleozoic carbonate, *in* C. Wicks and I. Sasowsky (eds.), Approaches to understanding groundwater flow and contaminant transport in carbonate aquifers, Geological Society of America Special Paper (accepted).

Worthington, S.R.H., D.C. Ford, and P.A. Beddows, 1999b, Porosity and permeability enhancement in unconfined carbonate aquifers as a result of solution, *in* A. Klimchouk, D.C. Ford, A.N. Palmer, and W. Dreybrodt (eds.), Speleogenesis: Evolution of karst aquifers, (accepted).

STRUCTURAL EFFECTS ON CARBONATE AQUIFERS

Ira D. Sasowsky
Department of Geology, University of Akron
Akron, OH 44325-4101

Abstract

Structural geology affects the behavior of karst aquifers by controlling the overall placement and orientation of the limestone and through fractures. The placement and orientation affect the position of recharge and discharge boundaries to the system, while the fractures serve as pathways for water movement. When creating a conceptual or numerical model of a karst site, it is useful and cost-efficient to consider all of these effects, as well as the geologic and geomorphic history of the area. By understanding structural controls on the genesis of the aquifer, predictions can be made regarding current-day behavior in terms of heterogeneity and anisotropy of flow. Because conduits and fissures mainly form along structurally created discontinuities, structural data can be very useful for understanding aquifer behavior, and determining specific high-conductivity flowpaths.

Introduction

The structural geology of an area plays two crucial roles in defining the behavior of a groundwater flow system in karst terrane. First, it establishes general flow directions in the aquifer, and second, it serves as a template for development of specific flowpaths (routes of high hydraulic conductivity). Understanding these structural controls for a given site is an important early step in the construction of a conceptual model. Furthermore, it may give direct insight regarding position and orientation of high-conductivity features such as caves, fissures, etc. Identifying such features is commonly a significant goal within a site investigation.

The broadest structural control is the placement of the rocks in certain orientation and positions by folding, faulting, erosion, etc. When taken in consideration with topography, this establishes the input, output, and no-flow boundaries to the system. Hence, this determines the general direction of flow in the aquifer. The second control is exerted by discontinuities (fractures) present in the rock mass. These include joints, bedding planes, and faults. The position, orientation, and aperture of these features, taken together with the input and output boundary positions, strongly controls the way the system will behave. Both of these controls are strong determinants of the form the aquifer will take as it evolves. In particular, they control the development of high-conductivity pathways (caves, conduits, fissures). A very compelling illustration of the importance of structural effects was developed by Palmer (1975), and is shown in Figure 1. As with most hydrogeologic investigations, geologists working in karst are handicapped by the fact that they are trying to "remotely" understand the aquifer. Only limited parts can be seen (either through wells, caves, springs, outcrops, etc.) and these parts may not be representative of the aquifer as a whole. What conclusions might

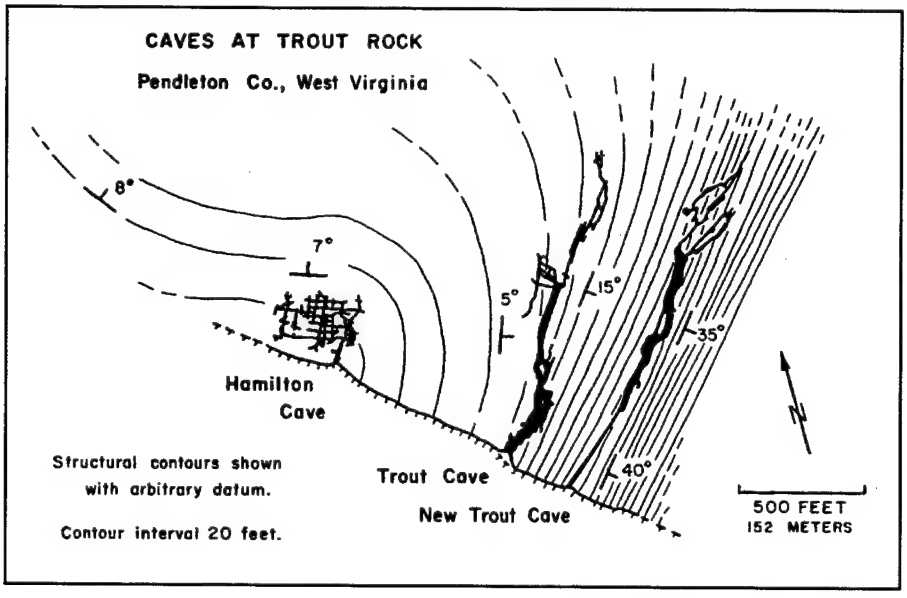

Figure 1: Illustration of one possible effect of structural controls on conduit porosity development. All three caves illustrated were developed simultaneously under similar boundary conditions. Differences in form may result from differences in rock orientation and fracturing. Note that where rocks are gently dipping towards the discharge boundary (southwest) a maze has formed, whereas in the rock steeply dipping normal to the boundary, a simple linear conduit has formed. From Palmer (1975).

a scientist have drawn in the area shown in Figure 1 if the caves had been intersected by boreholes, but had not been mapped? Maybe that there were disconnected voids of similar orientation. Or what if boreholes had not found the caves? Perhaps the assumption of isotropic fracture flow might have been made.

In many cases the approach left to the scientist or engineer is inference. Any tools that can guide that inference are a great aid, and should be used. For these reasons, it is recommended that any site investigation in limestone terrane include an evaluation of structural effects on the system. This has proven to be a successful and cost-effective step in various projects including water supply, contaminant transport, and sinkhole prediction. If a digital model of the site is required, this information will also help in deciding the appropriate code to employ. For the purposes of this paper, *structure* is taken in its broadest definition, including both classical structural features, as well as physical boundaries of the aquifer.

Genesis of carbonate aquifers

The history of an aquifer is a strong determinant of its present-day behavior. It is therefore useful to consider a generic conceptual model of carbonate-aquifer genesis, while recognizing that there will be departures from the model in a given setting. This model can serve as a basis for evaluating a given site by emphasizing the consideration of site-specific conditions.

In a limestone rock mass in a humid erosional setting (Figure 2A), initial boundaries are established by the topography. The stream defines local base level and the outputs to the system, while the uplands provide recharge points and input boundaries. In this state, one might envision a flow system approximating slow, Darcian conditions. The overall porosity is usually low in this initial state unless the rock is very young. Because of this, flow will tend to concentrate in the rock discontinuities (fractures). This focused flow results in the enlargement of certain of the discontinuities, a process that may become self-propagating as they grow larger, garnering more flow (Figure 2B). In turn, this leads to shifts in the aquifer boundary conditions.

Given the proper geochemistry, and extensive time periods (usually hundreds of thousands of years), the caves, sinkholes, and conduit-fed springs that characterize most karst areas will develop (Figure 2C). It is of particular interest to determine just which discontinuities are "chosen" for enlargement, and why, because this may allow prediction of preferred flowpaths in the aquifer. Several excellent references are available that cover the evolution of carbonate aquifers (Ford and Ewers, 1978; Ford and Williams, 1989;

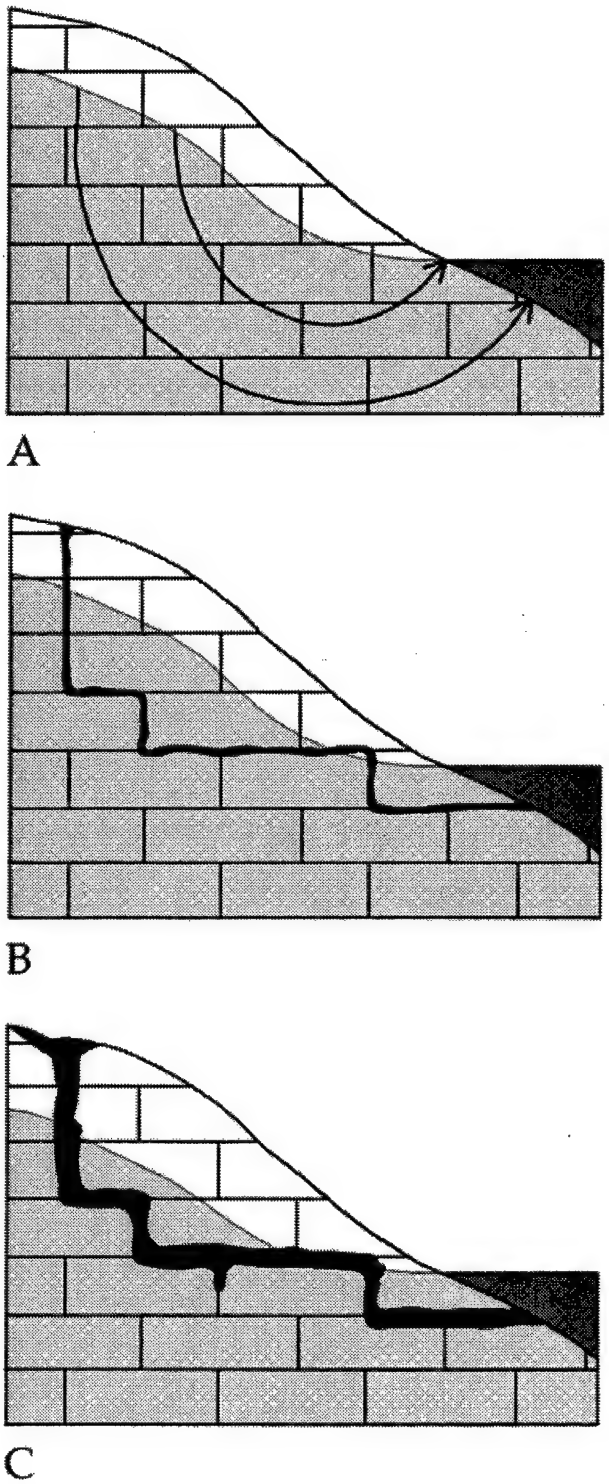

Figure 2: Hypothetical carbonate rock mass in initial, intermediate, and advanced stages of aquifer development. Arrows in Stage A show predicted flowlines for Darcian conditions. In Stage B a preferential flowpath has developed along structural discontinuities, focusing flow in this portion of the aquifer. In Stage C, extended growth of the path has captured most of the flow in the upper part of the aquifer, causing lowering of the water-filled zone.

Palmer, 1991; White, 1969; White, 1977; White, 1988). In addition, a number of works have been specifically concerned with which discontinuities are enlarged (Dreybrodt, 1992; Groves and Howard, 1994; Jameson, 1985)

Methods for gathering and using structural data in carbonate aquifers

Regional and local setting

At the beginning of a project, basic background information on the area should be collected. Frequently this will come from published literature and can include such structural elements as position and orientation of beds, fracture-set orientation, fault position, etc. Depending upon the needs of the project, new field data may be collected by traditional mapping methods (e.g. outcrop mapping of bedding contacts, faults, etc.), or by non-traditional methods (surface geophysics to locate the top of the bedrock, zones of fracture concentration, etc.).

Such information is essential for defining boundary conditions and evaluating geologic effects on aquifer development. This information will initially be evaluated by placing it on maps and cross-sections. In addition, regional information on tectonic and erosional history may also be important. Has the area undergone uplift? The rates may affect the development of porosity at different levels in the rock mass (Polyak et al., 1998; White and White, 1974). Have there been episodes of inundation with seawater? This could result in unique porosity development (Ewers et al., 1989; Michalski and Torlucci, 1988; Mylroie et al., 1995). Is the area on an escarpment or topographic margin? Stress-release fracturing may generate topographically oriented conduits (Sasowsky and White, 1994). Other settings will host different features that control porosity development, and every new area should be examined from this perspective.

Outcrop fracture studies

The statistical characterization of fracture direction and frequency is a well-established technique for evaluating aquifer anisotropy in insoluble rocks. The method relies upon measuring joint orientation along natural or artificial outcrops, with the data usually presented in rose diagrams. Preferred fracture directions may be considered to be preferential flow directions and used to construct an anisotropic hydraulic-conductivity ellipse.

In carbonate aquifers a similar technique can be used, but there is additional complexity. First, it has been shown that bedding planes, as opposed to joints, may be the most preferential flowpaths and loci for conduit growth (Jameson, 1985; Palmer, 1991). In a typical outcrop survey, these may be either unmeasured or undersampled. Second, joint aperture may be more important than the frequency at which jointing occurs. The conductivity of a joint increases as the cube of its aperture, making this a dominant control. It is very difficult to characterize joint aperture, though attempts have been made (Mace and Hovorka, in press). Nevertheless, outcrop data have been successfully used to provide information on preferential flow directions (Jancin and Ewart, 1995).

Borehole studies

While outcrops in the vicinity of a site provide general information on potentially conductive pathways, it is often desirable to gather data directly on-site. In some cases there may not even be exposed bedrock on site to allow outcrop measurement. The availability of inexpensive borehole video equipment now allows the gathering of such data, both in the vadose and phreatic zones. Open bedrock holes as small as 2 inches in diameter can be viewed, and, with an integral depth indicator, the position of fractures can be logged. The addition of a magnetic compass allows measurement of fracture orientation, and side-looking mirrors and lights actually allow viewing and photography of large-aperture fissures and conduits. It is common to be able to identify a single structural feature that is carrying the majority of flow by looking for the movement of fine sediments. Aquatic vertebrates (such as cave fish) or macro-invertebrates (such as springtails) may be occasionally observed, confirming to the most doubting scientist that one is indeed working in an aquifer where fissure/conduit flow is significant.

Incidentally, the importance of conductive fractures in boreholes is well known to well drillers working in limestone. They may drill far below the water table before producing significant water from the well, because productivity is frequently correlated to the interception of a single conductive fracture.

Integration of borehole structural information into models may require creativity. Although a great amount of information will be available at individual boreholes, data between them will be limited, and correlation may be difficult. Cross-well packer tests or other techniques may confirm connectivity but add expense. The identification of conductive features in a borehole is clearly useful in designing monitoring and remedial well completions. Appropriate zones can be packed off, thereby reducing the amount of water that must be purged or treated.

Mapping fracture traces

The mapping of fracture traces (also called lineaments, or photolinears) via aerial photography has emerged as a strategy for locating high-yielding water supply wells (Lattman

and Parizek, 1964) with great success. Fracture traces are straight topographic, drainage, or tonal features, and are the surface representations of vertical fracture zones. By drilling into these features, a borehole has the double advantage of tapping an extensive vertical feature as well as all of the sub-horizontal openings that the fracture zone intercepts. Well yields have been statistically shown to be greatest when drilling at the intersection of two fracture traces, compared to one or none. These zones not only represent high-conductivity pathways within the aquifer; they also represent preferential zones of recharge to the aquifer. Injection wells drilled on such features are likely to have higher injection capacities.

These factors need to be taken in to account when, for example, anticipating subsidence due to pumping stress, input boundaries to digital models, or siting landfills. Application of the method has its pitfalls, and care needs to be taken when ground-truthing the mapped features. For example, old fence lines or roads typically make excellent photolinear features but have no significance to the underlying bedrock. A useful handbook on the method has been produced (Meiser & Earl Hydrogeologists, 1982).

A similar method involves measuring the orientation of sinkholes. The thought is that elongation of sinkholes will reflect a direction of preferential flow. Ogden, et al. (1989) found that the orientation of sinkholes also mimicked the orientation of cave passages (see also below).

Mapping caves

A cave represents either a past or present route of preferential flow in the aquifer. Former routes are dry, while the presently active ones are wet (at least seasonally). In both instances a map of the cave may provide useful information for modeling present-day behavior of the aquifer. If the cave is presently active, it will show the direction and velocity of water movement in the aquifer. If the active cave is perennially flooded, the mapping may be conducted by SCUBA divers, which is a difficult and dangerous task. If the cave is dry (no longer active), or seasonally dry, it may be mapped with a magnetic compass and fiberglass tape, plus the proper safety gear. Thousands of published maps are available in regional or local compilations. Many more have been produced but not issued as formal publications. Scientists are advised to contact local groups that are knowledgeable about a particular area.

Cave maps can serve many uses in an investigation, dependent upon what is being attempted. The concern of this paper is extracting structural information from cave maps. Remembering that caves usually form along preferential discontinuities in the rock (not along preferentially soluble beds), it is possible to extract information about unseen preferential flow paths by analyzing which paths the cave development has followed. The assumption can be made that unknown caves (or proto-caves) in the general region will follow a similar pattern. For example, Ogden, et al. (1989) accomplished this by measuring the orientation of segments of cave passage and using the statistical distribution of these directions to predict regional flow-direction preferences.

Conclusions

Structural geology controls the overall position and orientation of the limestone, as well as the fractures that develop in the rock and serve as pathways for water movement. Conduits within the aquifer develop by preferential dissolution along some of these structural elements. Using structural data from a variety of sources will aid in the development of conceptual or numerical models of aquifer behavior. The regional structural setting is responsible for setting aquifer input and output boundaries. Outcrop or borehole studies of fracture position, aperture, and frequency allow prediction of anisotropy in the rock mass. Mapping of fracture traces via aerial photography identifies inputs to a high-conductivity network within the rock mass and is useful for siting high-capacity water-supply wells. Mapping of caves provides detailed information regarding which structural pathways were (or are) most preferred for conducting flow in the aquifer.

References cited

Dreybrodt, W., 1992, Dynamics of karstification: A model applied to hydraulic structures in karst terranes: Applied Hydrogeology, v. 1, no. 3, p. 20-32.

Ewers, R.O., D. Keagy, J.F. Quinlan, and M. Field, 1989, Discussion of "'Testing' a limestone aquifer using water-table response to stormwater discharged into sinkholes", by Andrew Michalski and Joseph Torlucci, Jr.: Ground Water, v. 27, no. 5, p. 715-716.

Ford, D. C., and R.O. Ewers, 1978, The development of limestone caverns in the dimensions of length and depth: Canadian Journal of Earth Sciences, v. 15, p. 1783-1798.

Ford, D.C., and P.W. Williams, 1989, Karst geomorphology and hydrology: London, Unwin Hyman, 601 p.

Groves, C.G., and A.D. Howard, 1994, Early Development of karst systems 1. Preferential flow path enlargement under laminar flow: Water Resources Research, v. 30, no. 10, p. 2837-2846.

Jameson, R.A., 1985, Structural segments and the analysis of flow paths in the North Canyon of Snedegar Cave, Fri-

ars Hole Cave System, West Virginia [Master of Science thesis]: West Virginia University, 421 p.

Jancin, M., and J. Ewart, 1995, Prediction and testing of hydraulic parameters in the interstratal karst of the Valley and Ridge Province, Pennsylvania, in B.F. Beck, (ed.), Karst Geohazards: Engineering and environmental problems in karst terrane: Rotterdam, A.A. Balkema , p. 125-130.

Lattman, L.H., and R.R. Parizek, R. R., 1964, Relationship between fracture traces and the occurrence of ground water in carbonate rocks: Journal of Hydrology, v. 2, p. 73-91.

Mace, R.E., and S.D. Hovorka, in press, Estimating porosity and permeability in a karstic aquifer using core plugs, well tests, and outcrop measurements, *in* Sasowsky, I. D., and C. Wicks, (eds.), Special Paper: Groundwater flow and contaminant transport in carbonate aquifers: Boulder, Geological Society of America .

Meiser & Earl Hydrogeologists, 1982, Use of fracture traces in water well location: A handbook: Office of Water Research & Technology, OWRT TT/82 1, 55 p.

Michalski, A., and J. Torlucci, Jr., 1988, "Testing" a limestone aquifer using water-table response to stormwater discharged into sinkholes: Ground Water, v. 26, no. 6, p. 751-760.

Mylroie, J.E., J.L. Carew, and H.L. Vacher, 1995, Karst development in the Bahamas and Bermuda, *in* H.A. Curran, and B. White, (eds.), Terrestrial and shallow marine geology of the Bahamas and Bermuda: Boulder, Colorado, Geological Society of America, Geological Society of America Special Paper 300, , p. 251-267.

Ogden, A.E., W.A. Curry, and J.L. Cummings, 1989, Morphometric analysis of sinkholes and caves in Tennessee comparing the Eastern Highland Rim and Valley and Ridge physiographic provinces, *in* B.F. Beck, (ed.), Engineering and environmental impacts of sinkholes and karst: Proceedings of the Third Multidisciplinary Conference on Sinkholes and the Engineering and Environmental Impacts of Karst: Rotterdam, A.A. Balkema, p. 135-142.

Palmer, A.N., 1975, The origin of maze caves: National Speleological Society Bulletin, v. 37, no. 3, p. 56-76.

Palmer, A.N., 1991, Origin and morphology of limestone caves: Geological Society of America Bulletin, v. 103, p. 1-21.

Polyak, V.J., W.C. McIntosh, N. Güven, and P. Provencio, 1998, Age and origin of Carlsbad Cavern and related caves from 40Ar/39Ar of Alunite: Science, v. 279, p. 1919-1922.

Sasowsky, I.D., and W.B. White, 1994, The role of stress release fracturing in the development of cavernous porosity in carbonate aquifers: Water Resources Research, v. 30, no. 12, p. 3523-3530.

White, W.B., 1969, Conceptual models for carbonate aquifers: Ground Water, v. 7, no. 3, p. 15-21.

White, W.B., 1977, Conceptual models of carbonate aquifers: revisited, *in* R.R. Dilamarter and S.C. Csallany, (eds.), Hydrologic problems in karst regions: Bowling Green, Kentucky, Western Kentucky University, p. 176-187.

White, W.B., 1988, Geomorphology and hydrology of karst terrains: Oxford, Oxford University Press, 464 p.

White, W.B., and E.L. White, 1974, Base-level control of underground drainage in the Potomac River basin, *in* H.W. Rauch, and E. Werner, (eds.), Fourth Conference on Karst Geology and Hydrology Proceedings: Morgantown, West Virginia Geological and Economic Survey , p. 41-53.

THE SURFACE-SUBSURFACE INTERFACE AND THE INFLUENCE OF GEOLOGIC STRUCTURE IN KARST

Ernst H. Kastning
Department of Geology, Radford University, Box 6939
Radford, Virginia 24142

Introduction

Early studies on the development of karst focused principally on surface features (Sweeting, 1973) and dissolutional enlargement in relation to positions of the water table, influence of the lithologic and stratigraphic character of the bedrock, and geologic structure. In recent decades such studies have broadened to include the hydrodynamics of fluid flow through conduits and the geochemical kinetics of dissolution and mass transport. The history of physical speleology has been well documented by several authors (Davies, 1966; Kastning, 1981; LaMoreaux, 1994; LeGrand and Stringfield, 1973; Moore, 1960; Powell, 1975; Shaw, 1992; Sweeting, 1981; White, 1987).

Emerging conceptual models of cavern development and subsurficial karst processes, in general, have evolved to include not only the characteristics of groundwater flow within the bedrock, but also the relationship of these systems to inputs and outputs at the surface (zones of recharge and discharge respectively). The general premises of conceptual models of cave and karst processes were proposed by White (1969) and expanded in subsequent revisions (White, 1977; White, this volume). Some recent landmark papers on speleogenesis include those of Ford and Ewers (1978), Palmer (1984, 1991), and White (1976). For further information on karst, see the references cited in the Introduction to this volume.

Groundwater flow in a karst area

The surface-subsurface interface influences groundwater flow through a karst aquifer by controlling the recharge to the flow network and the discharge from it. The collective sizes of openings dictate the maximum rate of throughput. No more water can pass through the system than is allowed at recharge sites. The evolution of karst systems is self-accelerating, having a positive feedback: the rate of recharge governs the rate of dissolutional enlargement of conduits, and conversely, the enlargement of conduits augments the rate of discharge. As more flow is accommodated, networks become well integrated, typically in dendritic systems where flow paths converge as tributaries to master conduits. This maturation process is well understood and documented (Palmer, 1991; White, 1988; Ford and Williams, 1989). Surface features such as sinkholes and springs also grow as favorable cracks enlarge and accommodate more water in the system.

Recharge zones

Recharge in a karstic terrane occurs in two ways. First, meteoric water may percolate through the soil and into fractures in the carbonate rock over large areas of the surface (diffuse, or dispersed, recharge). Secondly, surface streams may be entirely swallowed where they flow into caves or sinkholes (discrete recharge). Most karst regions are characterized by both.

The role of fractures in conveying water to the subsurface is well known. Where soluble rocks are mantled with a soil or regolith, fractures may not be readily apparent. Larger ones may be mapable as lineaments in aerial photographs, but most smaller fractures are unseen. The degree of fracturing of rocks in karst regions is easily observed where the soil has been removed or where the bedrock surface is exposed as a karst pavement. Some fine examples include the extensive karst pavements on the benches of the Yorkshire Dales in Great Britain and in semi-arid and arid regions of the southwestern United States (for example, in the Edwards Plateau of central Texas; see Kastning, 1983). Such karst pavements may exhibit a variety of small karstic landforms, collectively called karren or lapiés (Figure 1).

The morphology of fractures is of course most dependent on the tectonic history of the region. Most fractures occur as sets of parallel and conjugate joints. Dissolutional activity may greatly alter the initial morphology of fractures and bedding-plane partings (Figure 1), producing sizable openings. Folding and tilting of the rock will likely control the flow of water through these planar openings and this, in turn, will modify dissolutional landforms. For example in Figure 1, beveled slopes have formed on clint blocks on one fracture wall but not on the other.

Similarly, sinkhole morphology varies greatly from one area of karst to another. As with fractures, sinkholes provide insight into the role of structure in shaping karst (Kastning, 1984, 1989). Sinkholes are often aligned along major fractures in a karstic landscape (Kastning, 1984; Kastning and Kastning, 1981). In such cases, zones of

enhanced recharge may consist of linear swaths at the surface-subsurface interface. Where bedrock exhibits appreciable dip, or where erosion of the land surface has established sufficient relief, development of dissolutional features (e.g. sinkholes) may be confined to narrow bands corresponding to outcrops of soluble beds, producing an aligned pattern similar to that caused by fractures.

The influence of folding on recharge and discharge patterns is demonstrated in the example of Figures 2 and 3. Longhorn Cavern State Park, Burnet County, central Texas, lies on an elevated landscape known as Backbone Ridge. This upland is the surface of a former graben that now stands in relief above lowlands to the northwest and southeast, produced by differential erosion whereby granitic rocks have been lowered at a greater rate than were the dense, crystalline, Ordovician carbonate rocks of the graben (Kastning, 1983). This has resulted in inversion of the topography, as well as sufficient relief and steepened hydraulic gradients to allow groundwater circulation within the Gorman Formation of the Ellenburger Group. A significant network of conduits evolved within the Upper Calcitic Facies of the Gorman Formation, including several sizable sinkholes (dolines) with feeder conduits that serve as tributaries for recharge to the master conduit of the cave (Longhorn Cavern). The primary zone of discrete recharge points (sinkholes) lies at the nose of the fold, where the outcrop pattern is widest owing to the gentle (7 degree) dip

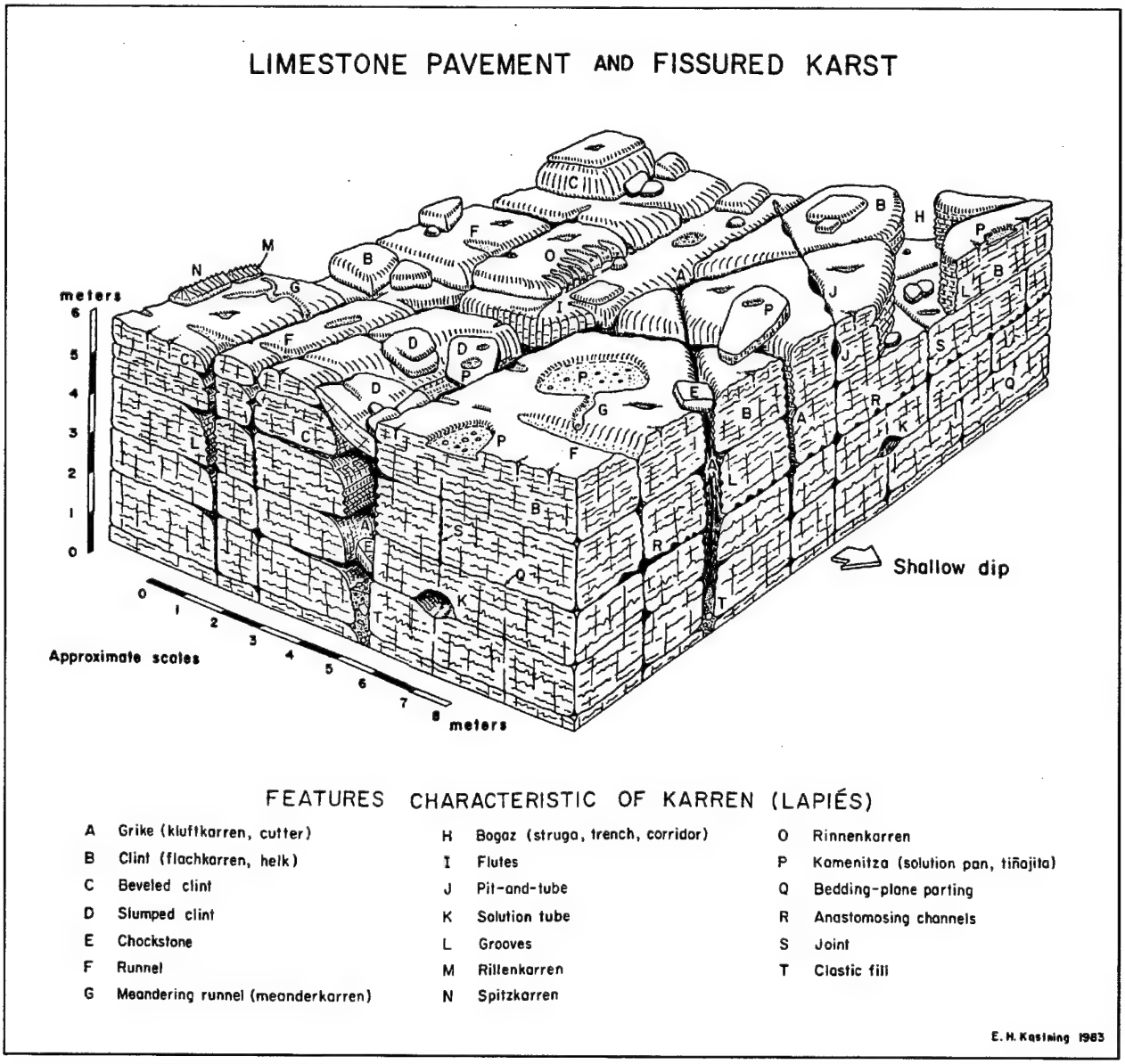

Figure 1: Morphological features commonly occurring on and below an exposed limestone pavement that is cut by joints and bedding-plane partings. Note that there is a shallow dip to front-right of the block diagram, resulting in asymmetry of some features. The landforms depicted are well described in textbooks on karst, in particular that by Sweeting (1973), and definitions of terms can be found in Monroe (1970). From Kastning (1983).

down the axis of the plunging syncline (Figure 2). The master conduit (main passage of Longhorn Cavern) lies within the Upper Calcitic Facies and convey water subhorizontally along strike to a spring along the fault scarp at the northwestern margin of Backbone Ridge. This is consistent with cavern development in the shallow phreatic zone where master conduits follow the strike of the bed just below the potentiometric surface, where fractures and bedding-plane partings are most open and discharge rates are greatest (Figure 3).

Recharge to many karstic aquifers is derived from surficial runoff originating on relatively insoluble rock in adjacent uplands. This overland flow typically sinks where it comes in contact with soluble bedrock at lower elevations. This is commonly referred to as allogenic recharge. Recharge zones established in this manner are controlled by the erosional exposure of rock units on the surface, geologic structure, and topographic conditions of the contributing fluvial system. The surface-subsurface interface for the underground karst system is normally congruent with the contact between the insoluble and soluble rock units.

Discharge zones

As with zones of recharge, natural outlets such as springs or seeps may become clustered or aligned along fractures or narrow outcrops of soluble rock. This is exemplified in the case of Longhorn Cavern (Figures 2 and 3), where water flowing through the master conduit of the cave discharges at a spring where the Upper Calcitic Facies meets the fault scarp..

Influence of topographic evolution

The surface-subsurface interface changes as the topography evolves, allowing potentiometric surfaces to change and speleogenesis to progress to new levels. In some cases these changes may be minor, especially where differential erosion is of low intensity. However, where surficial streams have cut large valleys or have become steeply entrenched, geologic structure may exert the dominant control over the process. Where beds have moderate or steep dips and where stream incision has produced a high local relief, deep phreatic systems may develop. In many

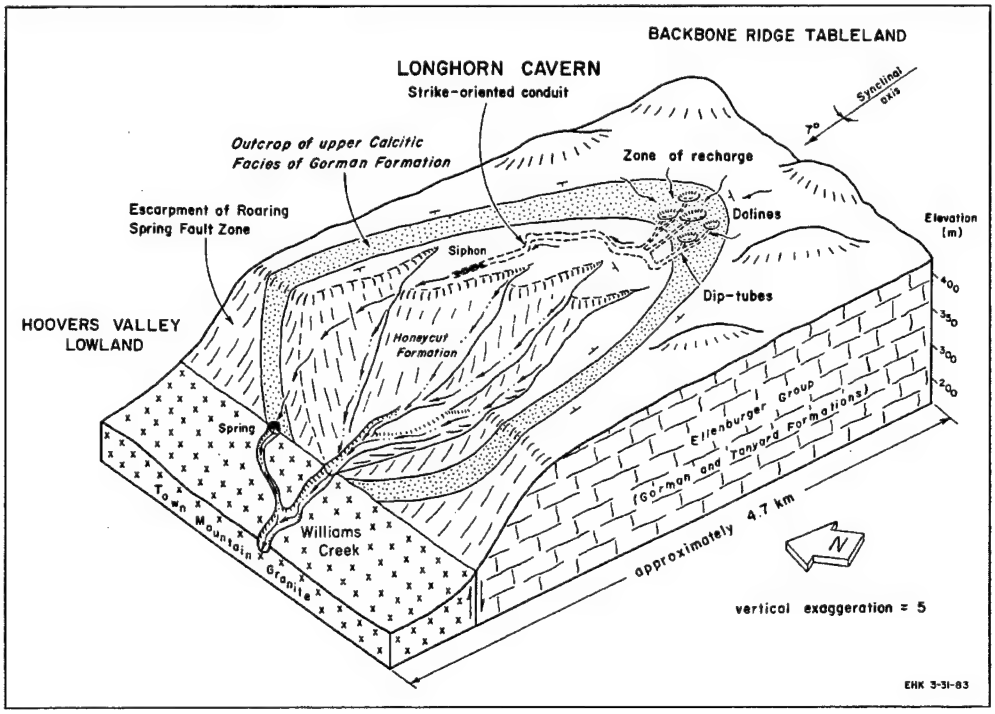

Figure 2: Block diagram of part of Backbone Ridge, Burnet County, Texas, in the vicinity of Longhorn Cavern State Park. The strike-oriented cave has developed along the northern flank of a plunging syncline and within the Upper Calcitic Facies of the Gorman Formation (Ordovician), a relatively soluble bed among otherwise dolomitic units (see text). Note that the zone of recharge for the system is a series of sinkholes in the widest part of the outcrop at the nose of the fold. Sinkholes contribute infiltration through a series of tributary feeders that are aligned in a down-dip direction. Discharge from the system emerges at a discrete spring along the fault scarp to the northwest (see Figure 3 for additional details). Backbone Ridge is an erosionally exposed graben (inverted topography) produced as adjacent granitic rocks were eroded at a differentially higher rate than were the carbonate units of the Ellenburger Group. From Kastning (1983).

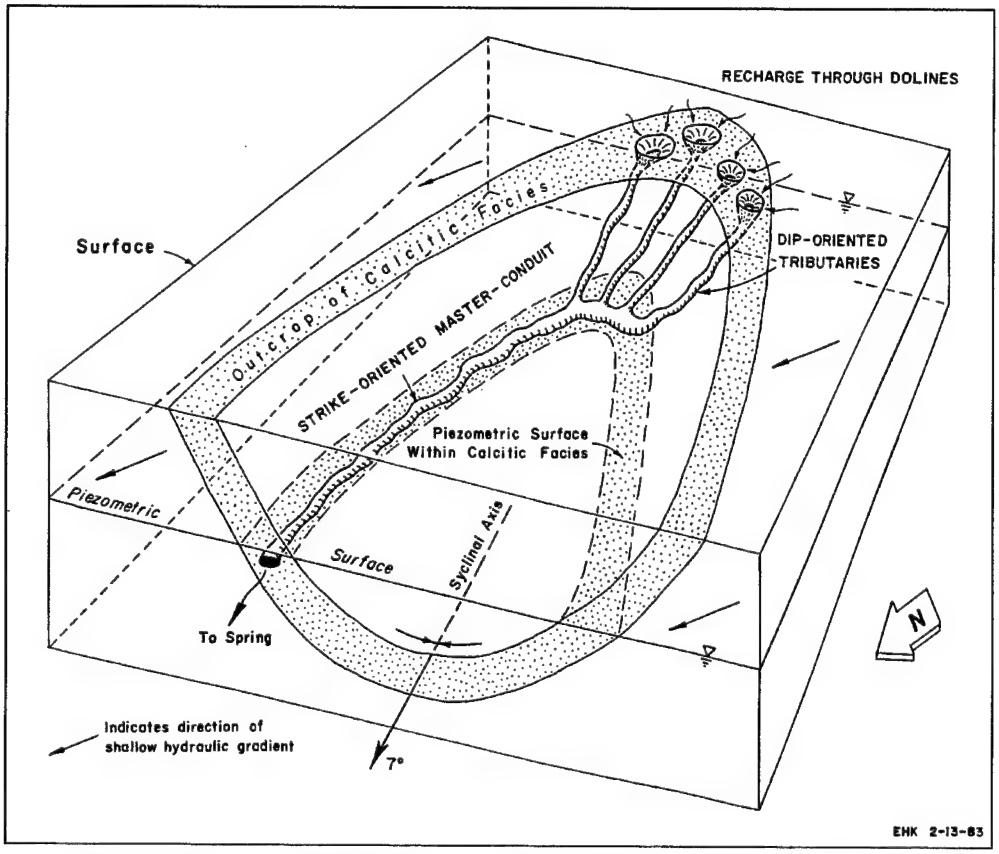

Figure 3: Groundwater conditions at Longhorn Caverns and relationships of cave passages to lithostratigraphy, structure, and position of the local potentiometric (piezometric) surface. Note that dip-oriented tributaries in the vadose zone contribute recharge to the strike-oriented master conduit in the shallow phreatic zone. From Kastning (1983).

cases this has resulted in a concentration of caves and springs along the outside valley walls of meander bends of surface streams. Natural phenomena other than fluvial or karstic processes may alter a pre-existing surface-subsurface interface. One of the most influential modifying mechanisms is glacial deposition. In areas where continental glaciation has covered an evolving karst landscape, zones of recharge and discharge may become occluded with till (e.g. Kastning, 1975; Mylroie, 1977).

Relation to environmental problems

Because environmental problems are most conspicuous at the surface, they have been extensively studied here (see LeGrand and Stringfield, 1973; White, 1988; and data bases such as GeoRef of the American Geological Institute). Environmental problems include (1) alteration of discharge or recharge by construction, paving, erosion, and siltation; (2) introduction of contaminants into recharge zones by sinkhole dumping, faulty landfills, accidental spills on highways, inappropriate land application of sludge; and (3) lowering of water tables and inducement of subsidence or collapse by overpumping of wells or dewatering of mines or quarries. The quantity and quality of groundwater is increasingly at risk in many places. Ultimately the only workable solution to these problems is through education about karst processes (Kastning and Kastning, 1991; Zokaites, 1997). The surface-subsurface interface is the zone that must be given the highest priority in management of karst terranes. In order to do this, recharge zones must be protected with appropriately designed buffer zones. Knowledge of the pattern of recharge-discharge and the effect of bedrock structure is an essential part of this strategy.

References cited

Davies, W.E., 1966, The earth sciences and speleology: National Speleological Society Bulletin, v. 28, p. 1-14.

Ford, D.C. and R.O. Ewers, 1978, The development of limestone cave systems in the dimensions of length and depth: Canadian Journal of Earth Sciences, v. 15, p. 1783-1798.

Ford, D.C. and P. Williams, 1989, Karst geomorphology and hydrology: Boston, Unwin Hyman, 601 p.

Kastning, E.H., 1975, Cavern development in the Helderberg Plateau, east-central New York: New York Cave Survey Bulletin 1, 194 p. plus 8 plates.

Kastning, E.H., 1981, Pioneers of North American cave and karst science prior to 1930, *in* B.F. Beck, (ed.), Proceedings of the Eighth International Congress of Speleology, Bowling Green, Kentucky: National Speleological Society, Huntsville, Alabama, v. 1, p. 247-249.

Kastning, E.H., 1983, Geomorphology and Hydrogeology of the Edwards Plateau Karst, Central Texas: Ph.D. dissertation (unpublished), The University of Texas at Austin, 657 p. plus 6 plates.

Kastning, E.H., 1984, Hydrogeomorphic evolution of karsted plateaus in response to regional tectonism, *in* R.G. LaFleur (ed.), Groundwater as a geomorphic agent: Boston, Allen and Unwin, Inc., p. 351-382.

Kastning, E.H., 1989, Surficial karst patterns: Recognition and interpretation, *in* B.F. Beck (ed.), Engineering and environmental impacts of sinkholes and karst: Proceedings of the Third Multidisciplinary Conference on Sinkholes and the Engineering and Environmental Impacts of Karst: Rotterdam, A.A. Balkema, p. 11-16.

Kastning, E.H., and K.M. Kastning, 1991, Environmental education regarding karst processes in the Appalachian region, *in* E.H. Kastning and K.M. Kastning (eds.), Appalachian karst: Proceedings of the Appalachian Karst Symposium, Radford Virginia: Huntsville, Ala., National Speleological Society, p. 123-134.

Kastning, K.M., and E.H. Kastning, 1981, Fracture control of dolines, caves, and surface drainage: Mississippian Plateau, western Kentucky, U.S.A., *in* B.F. Beck (ed.), Proceedings of 8th International Congress of Speleology, Bowling Green, Ky.: Huntsville, Ala., National Speleological Society, v. 2, p. 696-698.

LaMoreaux, P.E., 1994, History of Karst Studies: The Professional Geologist, v. 31, no. 9, p. 9-11.

LeGrand, H.E., and V.T. Stringfield, 1973, Karst hydrology -- A review: Journal of Hydrology, v. 20, p. 97-120.

Monroe, W.H., 1970, A glossary of karst terminology: U.S. Geol. Survey Water-Supply Paper 1899-K, 26 p.

Moore, G.W., 1960, Introduction to the origin of limestone caves: National Speleological Society Bull., v. 22, p. 3-4.

Mylroie, J.M., 1977, Speleogenesis and karst geomorphology of the Helderberg Plateau, Schoharie County, New York: New York Cave Survey Bulletin No. 2, 336 p.

Palmer, A.N., 1984, Geomorphic interpretations of karst features, *in* R.G. LaFleur (ed.), Groundwater as a geomorphic agent: Allen & Unwin, Inc., Boston, p. 173-209.

Palmer, A.N., 1991, Origin and morphology of limestone caves: Geological Society of America Bulletin, v. 103, no. 1, p. 1-21 .

Powell, R.L., 1975, Theories of the development of karst topography, *in* W.N. Melhorn and R.C. Flemal (eds.), Theories of landform development: Publication in Geomorphology, Binghamton, New York, p. 217-242.

Shaw, T.R., 1992, History of cave science: Speleological Research Council, Sydney, Australia, 338 p.

Sweeting, M.M., 1973, Karst landforms: Columbia University Press, NY, 362 p.

Sweeting, M.M. (ed.), 1981, Karst geomorphology: Benchmark Papers in Geology, v. 59, Hutchinson Ross Publishing Company, Stroudsburg, Pennsylvania, 448 p.

White, W.B., 1969, Conceptual models for carbonate aquifers: Ground Water, v. 7, p. 15-21.

White, W.B., 1976, The geology of caves, *in* W.B. White, Geology and biology of Pennsylvania caves: Pennsylvania Geological Survey, Fourth Series, General Geology Report 66, p. 1-71.

White, W.B., 1977, Conceptual models for carbonate aquifers: revisited, *in* R.R. Dilamarter and S.C. Csallany (eds.), Hydrologic problems in karst regions: Western Kentucky University, Bowling Green, Ky., p. 176-187.

White, W.B., 1987, Introduction to speleogenesis: National Speleological Society Bulletin, v. 49, p. 29-30.

White, W.B., 1988, Geomorphology and hydrology of karst terrains: Oxford University Press, New York, 464 p.

Zokaites, C.A. (ed.), 1997, Living on karst: a reference guide for landowners in limestone regions: Richmond, Va., Cave Conservancy of the Virginias, 26 p.

A CONCEPTUAL VIEW OF CARBONATE ISLAND KARST

J. E. Mylroie
Dept. of Geosciences, Mississippi State University Mississippi State MS 39762

H. L. Vacher
South Florida University, Tampa FL 33620

Abstract

Conceptually, the karst of carbonate islands can be modeled as the result of eogenetic diagenesis, freshwater/saltwater mixing, and glacioeustasy. The resulting eogenetic karst occurs in small, youthful limestone islands where the evolution of the karst is concurrent with meteoric diagenesis of the host rock, which has never been out of the active circulation of meteoric water. The rearrangement of the material of high porosity / low permeability sediments into moderate porosity / high permeability rock feeds back to the nature of the diagenetic environment as the flow volume of the lens is reduced by increasing flow efficiency.

Limestone islands are a constrained and simple environment, defined as carbonate islands (no noncarbonate rock) and composite islands (mixture of carbonate and non carbonate rock). Simple carbonate islands lack noncarbonate rocks within the active hydrological zone; carbonate-cover islands contain a noncarbonate contact that limits the freshwater lens and deflects vadose flow. The type of island greatly influences the subsequent karst hydrology. Increasing island size appears to cross a threshold favoring conduit flow. The karst features resulting from these island types, combined with mixing geochemistry and glacioeustasy, differ from those in continental settings and require a unique conceptual approach to modeling.

Introduction

Karst development occurs in coastal carbonate rocks of continents (e.g. Yucatan, Adriatic coast), in carbonate outcrops on complex islands (e.g. Guam, Barbados), and in small islands made up primarily of carbonate rocks (e.g. Bermuda, San Salvador). The development of karst in these peri-marine environments differs from that of the well-studied continental interiors of the mid-latitudes in at least three basic ways: (1) freshwater/saltwater mixing is present; (2) glacioeustatic history is relevant to the geologic history; and (3) the rocks are young and still experiencing diagenesis as a result of the meteoric water passing through them. All of these result from the fact that the karst is developing close, in both space and time, to the origin of the limestone. Small islands consisting mainly of carbonate rocks that are located in the world's well-known regions of "modern carbonates" are particularly good places to see a kind of karst that cannot be seen in continental interiors.

Classification of carbonate islands

Carbonate islands can be defined in a variety of ways. Vacher (1997) discussed the role of size, height, age, hydrology, depositional facies, relation to noncarbonate rocks, and tectonics in the introduction of a large book on geology and hydrogeology of carbonate islands (Vacher and Quinn, 1997). Table 1 gives a summary of the organizational scheme Vacher (1997) derived from those considerations. In contrast, Mylroie and Carew (1997) produced a simpler scheme based on the development of karst features on carbonate islands (Figure 1). The purpose of this paper is to combine the geologic and hydrologic perspective with the cave and karst perspective.

It can be stipulated that all carbonate islands contain, at least in part, freshwater overlying saltwater. These islands also have been subjected to repeated glacioeustatic sea-level changes. The carbonate rocks are young, Tertiary and Quaternary in age, and have not undergone deep burial. The carbonates to be discussed here, in fact, have never been out of active circulation. Choquette and Pray (1970) call this the environment of "eogenetic diagenesis," and we (Vacher and Mylroie, in prep.) call the karst of this environment "eogenetic karst." Three major factors appear critical in describing the hydrology of this type of karst: (1) island size, (2) carbonate depositional history, and (3) the presence of noncarbonate rock.

Island size has a direct impact on carbonate island hydrology by controlling, for a given climate, the total amount of recharge that passes through the lens and the length of the periphery for that groundwater discharge to pass through as it exits at the shoreline. The UNESCO guide for island hydrology (Falkland, 1991) describes islands with a surface area of less than 2,000 km^2 (or long islands with a width less than 10 km) as "small" islands, and islands with an area less than 100 km^2 (or width less than 3 km) as a subclass, "very small" islands. For this paper, size will be used as an adjective to modify a classification based on the presence or absence of noncarbonate rock.

I. Reef islands and reef composite islands
- **Atolls**
  - **Mururoa, Fangataufa (Fr. Polynesia)**
  - **Tikehau (Fr. Polynesia)**
  - **Rakahanga, Manuihiki, Pukapuka (Cook Islands)**
  - **Tarawa, Christmas Island (Kiribati)**
  - **Majuro, Kwajalein, Bikini (Republic of Marshall Islands)**
  - **Enewetak (Republic of Marshall Islands)**
  - **Mwoakiloa, Pingelap, Sapwuahfik (Fed. St. Micronesia)**
  - **Cocos (Keeling) Islands (Indian Ocean, near Indonesia)**
  - **Diego Garcia (Chagos Archipelego, central Indian Ocean)**
- **Modern reefs**
  - **Great Barrier Reef**
  - **Heron Island (Great Barrier Reef)**
- **Low Quaternary reef islands**
  - **Upper Keys (Florida)**
  - **Cozumel (northeastern Yucatan)**
  - **Houtman Abrolhos Islands (western Australia)**
- **Uplifted atolls, other elevated reef islands**
  - **Makatea (Fr. Polynesia)**
  - **Niue (south Pacific)**
  - **Nauru (central Pacific)**
  - **Isla de Mona (Puerto Rico)**
  - **Henderson Island (Pitcairn Islands)**
  - **Tongatapu (Tonga)**
- **Almost-atoll**
  - **Aitutaki (Cook Islands)**
- **Composite islands with elevated reef limestone**
  - **Barbados (Lesser Antilles)**
  - **Atiu, Mitiaro, Mauke, Mangaia (Cook Islands)**
  - **Guam (Mariana Islands)**

II. Eolianite islands
- **Bemuda**
- **Bahamian islands**
- **Cancun (northeastern Yucatan Peninsula, Mexico)**
- **Rottnest Island (Western Australia)**

III. Other carbonate islands
- **Lower Keys (Florida): Pleistocene oolitic shoals**
- **Islands of Florida Bay: Holocene mud islands**
- **Grand Cayman Island: Low islands with varied Sangemonian shallow-water deposits against Tertiary platform carbonates**
- **St. Croix: Composite island with Tertiary pelagic to shallow-water carbonates**
- **Lau Group (Fiji): Composite and solely carbonate islands with carbonates of various facies built up on submerged volcanic cones**

Table 1: Classification of carbonate islands, as discussed by Vacher and Quinn (1997).

One of the easiest observations to make about a carbonate island is whether or not noncarbonate rock is exposed in significant amounts. Nunn (1994) and Vacher (1997) propose the breakdown of oceanic islands into (1) volcanic islands, (2) composite islands, and (3) carbonate islands. Volcanic (and other noncarbonate) islands (e.g. Tahiti, Hawaii) lack significant exposed carbonates and are not considered further here. Composite islands contain significant outcrops of noncarbonate rock, whereas carbonate islands have only carbonate rocks cropping out on the surface. Vacher (1997) notes that carbonate islands may have a simple veneer of carbonates overlying noncarbonate rocks, or may consist of carbonate rock to a significant depth. Mylroie and Carew (1997) used a similar approach (Figure 1). They called composite islands "carbonate rimmed islands," which suffers from implying a certain geometry for the carbonate-noncarbonate rock distribution that is not essential to the concept. However, they also divided carbonate islands into "simple carbonate islands" and "carbonate-cover islands," a distinction that calls attention to the presence of a contact between carbonate and noncarbonate rocks within the reach of circulating meteoric water. This contact has been shown to be important to the kind of cave development that occurs in Bermuda (Mylroie et al., 1995a), although the noncarbonate rocks (volcanics) are completely buried.

For the purpose of discussing carbonate island karst development, we will describe islands as either carbonate or composite. We recognize that the composite island designation can be quite variable, depending on the relative amounts of carbonate versus noncarbonate rock and the various geometries that can occur between these two rock types. Furthermore, carbonate islands will be subdivided into simple carbonate islands and carbonate-cover islands. Simple carbonate islands have carbonates extending downward well below the maximum glacioeustatic sea-level lowstand of the Quaternary, and therefore the internal hydrology of these islands is unaffected at all sea levels by noncarbonate rock. Carbonate-cover islands, on the other hand, contain a carbonate/noncarbonate contact within the island, such that phreatic lenses may abut against the contact and (in some cases) vadose waters may be directed by this contact (Figure 1). In these carbonate-cover islands, the contact may come into play hydrologically only during glacioeustatic lowstands; Bermuda is an example.

With these definitions in mind, Bermuda (50 km^2) is a very small carbonate-cover island, whereas San Salvador Island, Bahamas (50 km^2) and Isla de Mona (55 km^2) are very small simple carbonate islands. Guam (549 km^2) and Barbados (430 km^2) are small composite islands, whereas Niue (259 km^2) and Grand Cayman Island (196 km^2) are small simple carbonate islands. Jamaica, Puerto Rico, and New Guinea are all islands that are famous for their karst landforms but those karsts are located in the island interiors; they are not influenced by marine water, and they are somewhat buffered from the effects of glacioeustasy. In that regard, these famous island karst areas behave more like those found in continental interiors than karst found in composite or carbonate islands. Continental coastal carbonates, such as those found in the Yucatan or along the coast of the Adriatic Sea, are influenced by marine water and by glacioeustasy; however, they are also influenced by the enormous continental catchment areas that feed them. Understanding them seems a more difficult task than approaching, first, the karst development of isolated, circumscribed, small, composite and carbonate islands.

Island karst hydrology

Conceptualizing island lenses can profitably begin with the small, or very small, simple carbonate island. Simple carbonate islands contain their fresh groundwater as a mass floating on underlying marine water. The idealized first approximation is that of a homogeneous island ("homogeneous" meaning that hydraulic conductivity is everywhere the same), in which the fresh groundwater occurs as a symmetric lens, thickest in the center of the island and thinning toward the shorelines. The size of the lens, as measured by the thickness of the fresh groundwater in the interior of the island, varies directly with island size and amount of recharge and inversely with hydraulic conductivity (Budd and Vacher, 1991). In extreme cases of very small size and/or recharge and high hydraulic conductivity, the lens is thin enough that the tidal forcing at the shoreline causes mixing of the fresh and saline groundwater to the extent that the lens is at best brackish. At the other extreme of large recharge and/or small hydraulic conductivity, the freshwater lens can be tens, and even hundreds, of meters thick, but even so, the ratio of lens thickness to island cross-width is always small in the eogenetic karst of carbonate islands (see Budd and Vacher, 1991, for figures and graphs). The ratio is so small, in fact, that if one should draw the typical iceberg-like lenses at true scale, the lenses would rarely show on a page.

Whereas the size of the equilibrium lens is a function of recharge and hydraulic conductivity, the shape of the lens depends on how those variables are distributed. In heterogeneous islands, the lens is thicker in the regions of lower hydraulic conductivity. In some cases, the areal variation in hydraulic conductivity is due to differences in depositional facies, sediment type, or grain-size variations in bioclastic-grainstone buildups. More generally, however, the areal variation in hydraulic conductivity is due to differences in secondary permeability related to differences in age (Figure 2).

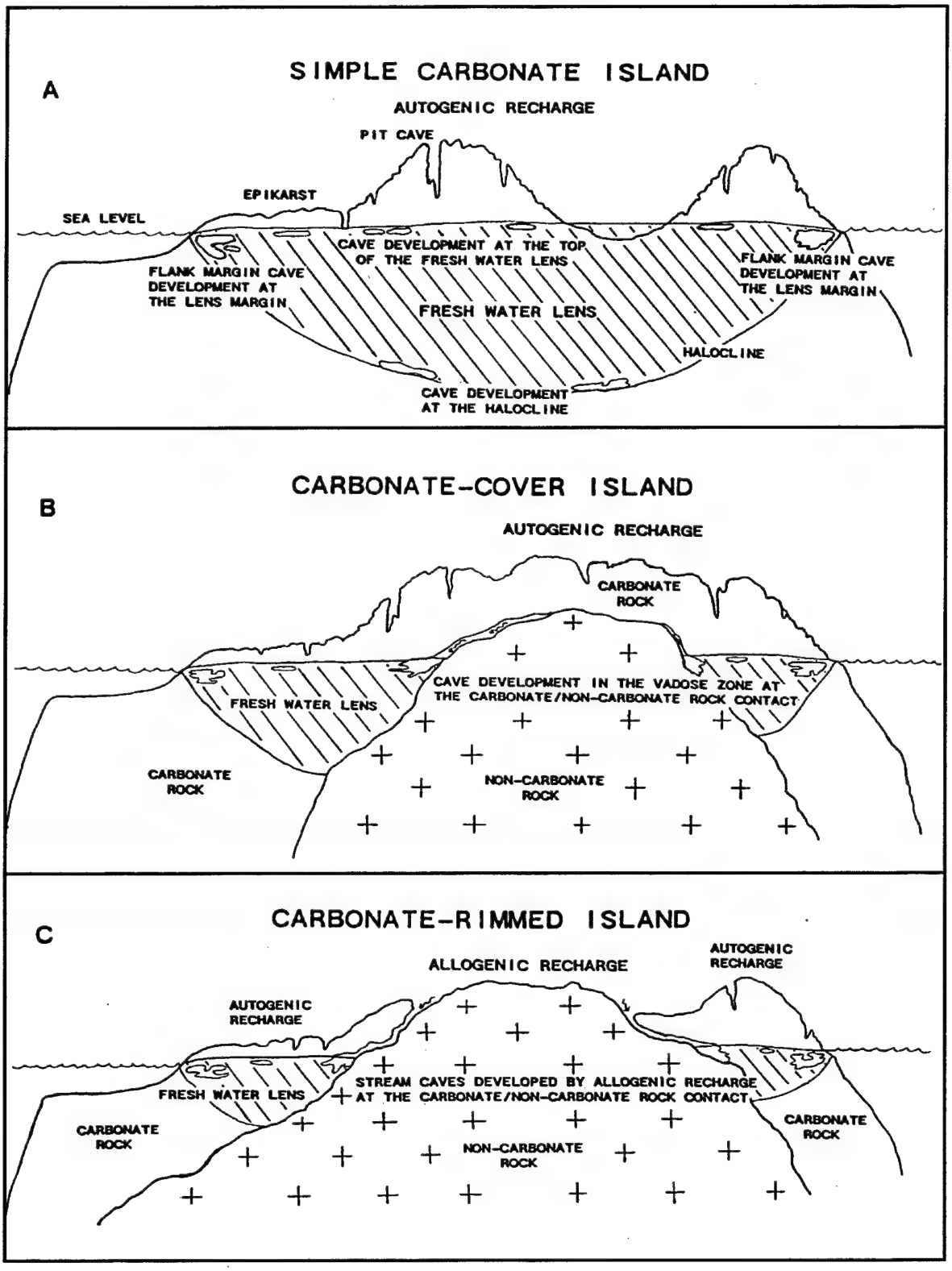

Figure 1: Conceptual presentation of carbonate islands, showing the influence of noncarbonate rock on karst processes. **(A)** The simple carbonate island, where no noncarbonate rock exists within the region of active hydrology. **(B)** The carbonate-cover island, where noncarbonate rock at depth influences both vadose flow and fresh-water lens configuration. **(C)** The "carbonate-rimmed" island, now described as a composite island, where noncarbonate rock influences both surface and subsurface flow. From Mylroie and Carew (1997).

Heterogeneity due to stratigraphically correlated differences in secondary permeability seems to be a hallmark feature of the eogenetic karst of carbonate islands composed of rocks of late Tertiary or Quaternary age. These limestones have not been buried and therefore not subjected to depth-related porosity reduction ("mesogenetic" diagenesis of Choquette and Pray, 1970). This eogenetic karst of carbonate islands involves a different type of pore space than that of the "telogenetic" realm (Choquette and Pray, 1970), where the porosity is related to fractures and solution-enlarged fractures lacing through a rock that has emerged from the mesogenetic realm. Paralleling differences in the types of karst are differences in the rocks themselves. Whereas telogenetic karst is established in mineralogically stabilized carbonates, many of the limestones of eogenetic karst in carbonate islands still retain some aragonite and, even, some Mg calcite. It cannot be emphasized enough that this karst, and the hydrology of the lenses occupying the limestones, occurs in rocks that are still in the general area of their formation.

Numerous studies (Vacher, 1978, 1988; Vacher and Wallis, 1992; Cant and Weech, 1986; chapters in Vacher and Quinn, 1997) have documented the orders-of-magnitude increase in hydraulic conductivity that attends the exposure of the carbonate islands to the meteoric water in the eogenetic realm. Fewer studies show reduction in hydraulic conductivity. If the porosity is reduced from 0.4 to 0.2, it is as nothing compared to the increase in hydraulic conductivity from 10 m/day to 100 m/day and, then, 1000 m/day. This increase in hydraulic conductivity with constant (or diminishing) porosity indicates a rearrangement of the matter in the rock. Preferential flow channels are created reducing the surface-to-volume ratios of the fluid passages. As the process continues, the hydraulic conductivity increases and there is progressively more isolation of passage water from the water within the still-porous material between the passages. The pore space is dual in nature, with preferred passages worming through porous, relatively unaltered limestone. This is an entirely different kind of dual porosity from the telogenetic variety where solutionally enlarged, preferred fractures lace through a mesh of unenlarged fractures.

The larger hydraulic conductivity of the older limestones in eogenetic karst means a greater flow efficiency for conducting the recharge on the island to the peripheral coastline (Figure 2). This greater efficiency thins the lens. For the given recharge (and there is no reason for it to change), the head difference is less between interior and coastline, and so the thickness of the Bahamas, where younger (hence less-conductive limestones) cover the older units, then the lenses reach down to the more-conductive limestones if the islands are large enough. The thinning of the lens brought about by the larger hydraulic conductivity means that the lens is effectively truncated at the geologic contact, and so the lens is effectively limited to the upper unit (Figure 3). In the Bahamas this occurs at the boundary between the Quaternary and the Pliocene (Cant and Weech, 1986); in many Pacific atolls, it occurs at the Holocene/Pleistocene contact, which has been called the "Thurber Discontinuity" by some Pacific hydrogeologists (see Vacher, 1997, for citations of earlier references).

In Bermuda, deposition of beach-and-dune complexes during successive interglacial highstands has resulted in a pattern of younger eolianites alongside older eolianites. At the present relatively high position of sea level, the lower portions of these eolianites host Bermuda's freshwater lenses. The older eolianites are more permeable, and so the lenses are thinner in those areas (Figure 4). The lenses are thicker in the younger, less-conductive eolianites (Vacher, 1988). Similar pinching and swelling of lenses occur in the Bahamas in Holocene and Pleistocene limestones. Commonly lakes occur at the inland boundaries between the Holocene strandplain sands and Pleistocene limestone, and, in the dry climate of the Bahamas, the lakes are groundwater sinks thinning the cross-island lenses; in some

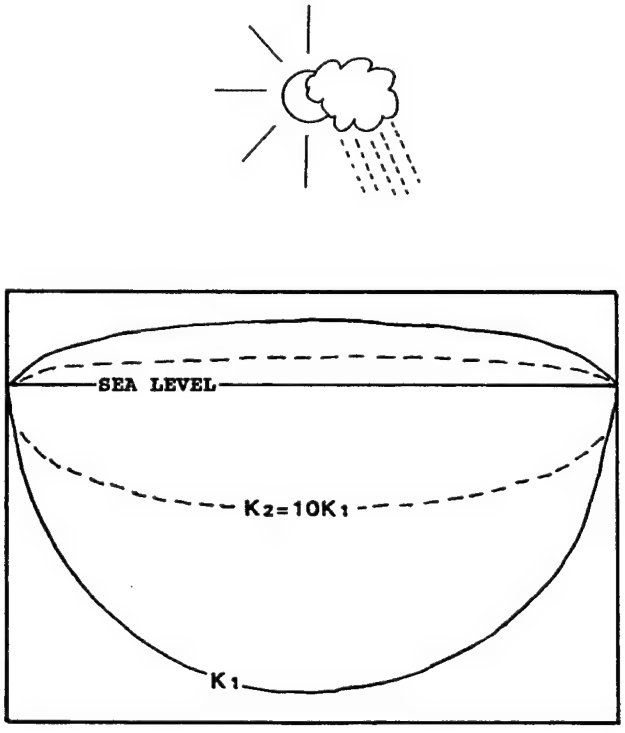

Figure 2: Loss of freshwater lens volume with rock age as permeability increases. K_1 is low hydraulic conductivity associated with young rocks. After time, dissolution increases the rock hydraulic conductivity to K_2 (here, ten times K_1), and the freshwater lens thins. Diagram is vertically exaggerated. See Vacher (1988) for a quantitative treatment.

cases the lakes are saline, implying that the lens that would have occurred without the evaporative losses has been thinned to nonexistence at the lakes. Nevertheless, the lenses remain in the Holocene strandplains and the inland Pleistocene limestones. Remarkably, the lenses in the strandplain deposits can be as thick as, or thicker than, those in the limestones, although the area of the strandplain bights is only a small fraction of the area of the main limestone island. The reason for the thick buildup of the lens is the relatively low hydraulic conductivity of the young, unaltered bioclastic sand of the strandplain complex.

Cave and karst development

Eogenetic karst differs from the telogenetic karst of indurated Paleozoic rocks, such as those of the continental United States, in that the karst pathways develop as the eogenetic rock undergoes diagenesis. A multitude of flow paths develop, uninfluenced by faults, joints and other structures, which generally do not yet exist. In the case of vertical accretion of carbonate units, the age-flow bias that concentrates flow in the older eogenetic rocks is self-limiting in that the flow is preferentially removed from the older (deeper) rocks, being concentrated in the area near the boundary with overlying and less permeable younger rocks. These small karst flow paths are therefore preferentially produced in the less permeable rocks. Unlike conduit development in dense Paleozoic limestones, competition for flow in vertically stacked eogenetic rocks does not result in the capture of more flow. In fact, the opposite occurs: the flow pathways, as they become more efficient, lose their recharge, which is held in the less transmissive overlying (or adjacent) younger units. Through time (at a given sea level position), less and less of a cross section of the older rocks experiences freshwater

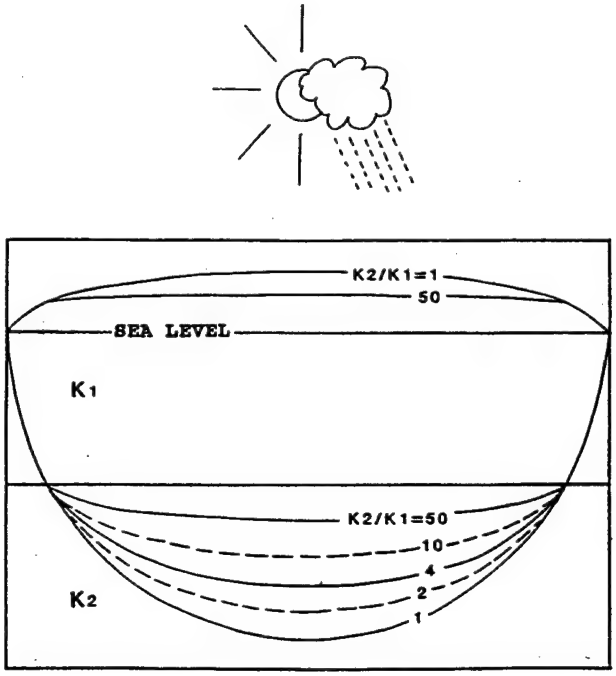

Figure 3: Change in freshwater lens structure when carbonate rock units of two different ages are stacked vertically. K_1 is the hydraulic conductivity of the overlying younger unit; K_2 is the hydraulic conductivity of the lower, older unit. The K_2 hydraulic conductivity value increases with increasing age of the lower unit, so that the ratio of K_2 to K_1 increases with time. The freshwater lens is preferentially contained in the upper, younger unit as the K_2/K_1 ratio increases. Diagram is vertically exaggerated. See Vacher (1988) for a quantitative treatment.

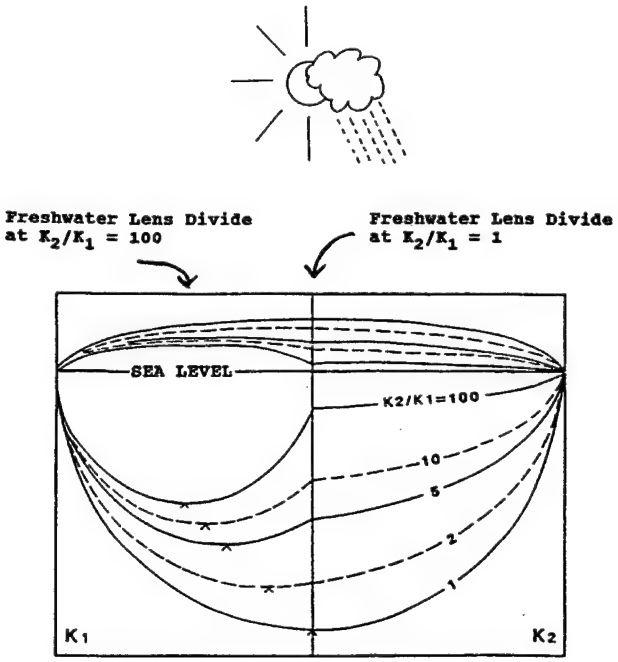

Figure 4: Diagrammatic representation of the migration of the watershed divide of a freshwater lens as a result of the lateral juxtaposition of carbonate units of different ages and hence hydraulic conductivities. When $K_2/K_1 = 1$, the units are hydrologically homogeneous and the lens divide is centered on the island axis. If the K_2 unit is older than K_1, then $K_2 > K_1$ and the ratio rises. The increased efficiency of the K_2 unit in transmitting water in the lens results in a shift of the lens divide into the K_1 unit, and when $K_2/K_1 = 100$, the lens divide is centered approximately at the midway point of the K_1 unit , or 1/4 of the island width in from the left side of the figure. Diagram is vertically exaggerated. See Vacher (1988) for a quantitative treatment.

lens flow, and the lens is retained only in the less permeable unit (Figure 3).

In contrast, in the case of lateral accretion of carbonate units, such as the eolianites of Bermuda (Vacher, 1978), the juxtaposition of older, more permeable rocks next to younger, less permeable rocks results in capture of ground water from the younger rocks by the adjacent, more flow-efficient older rocks. The groundwater divide therefore shifts laterally into the younger rock material. Through time, the divide moves from the mid-point of the combined young and old rock hydrological system to nearly the midpoint of the young rock unit alone (Figure 4).

One could argue that in the absence of glacioeustasy, which continually overlays carbonate platforms with young (and less permeable) sediment, islands would become progressively more permeable until they could no longer support a freshwater lens. However, because of glacioeustasy, the freshwater lenses in carbonate islands have repeatedly migrated over 130 m during the Quaternary, re-invading and overprinting rock units of a variety of ages and producing complicated porosity variations with depth. The overall trend of greater permeability with age (as related to depth) persists, however. The maximum alteration of the rock occurs at the crests and troughs of sea-level oscillation, where the lens soaks a given position for a longer time period than on the rising or falling limb of the sea-level change.

Dissolution in carbonate islands is enhanced by the mixing of fresh and marine waters at the boundary of the lens. This boundary can be a sharp halocline or a broad mixing zone, but in either case, if marine and fresh (or brackish) waters are mixed, dissolution can occur even if both waters are saturated with respect to calcium carbonate before mixing (Plummer, 1975). The phenomenon is similar to that known for mixing freshwaters that have reached saturation under different initial conditions ("mischungskorrsion;" Bögli, 1980); in continental systems, mischungskorrsion commonly involves vadose water mixing with phreatic water, or the junction of two cave streams of dissimilar initial P_{CO2}. The potency of fresh and marine water mixing has been noted in many environments, such as the Yucatan (Back et al, 1986) and the Bahamas (Smart et al, 1988). The dissolution has been modeled (e.g. Sanford and Konikow, 1989; Raeisi and Mylroie, 1995), and the production of porosity and karst voids is rapid.

In simple carbonate islands, void production is accentuated at the edge of the freshwater lens. At this location, the freshwater/marine-water mixing zone at the base of the lens is immediately overlain by the vadose/phreatic mixing area at the top of the lens, placing two dissolutionally active areas in close proximity (Mylroie and Carew, 1995; Mylroie et al, 1995a) . In addition, both the top and base of the lens represent a density boundary, and, as such, tend to collect organic material. This organic material is a source of CO_2 which can further drive rock dissolution. If sufficient organic matter is present, the boundary may become anoxic, allowing a variety of oxidation-reduction reactions to occur, some biologically mediated by bacteria, that produce H_2S, eventually leading to sulfuric acid. This H_2S mechanism has been observed in Bahamian blue holes (Bottrell et al, 1991). If the lens is thin and highly permeable, tidal mixing may blend the organic loads at the top and bottom of the lens. The role of organics in cave production in karst areas has become an important new area of study (e.g. Groves and Meiman, 1998).

The voids developed in this manner have been termed "flank margin caves," as they form in the distal margin of the freshwater lens, immediately under the flank of the land mass enclosing them (Mylroie and Carew, 1990). These voids are mixing chambers and not true conduits, in that they receive and discharge their water as diffuse flow. Field evidence indicates that these voids expand inland, and therefore the mixing front migrates landward. Production of individual flank margin cave chambers has been estimated at 1 m^3/yr in the Bahamas (Mylroie et al., 1991), and flank margin caves with volumes over 1 million m^3 are known from Isla de Mona, where paleomagnetic data indicate the voids developed almost 2 million years ago (Panuska et al., 1998). In other words, these voids develop rapidly but can persist through time.

Cave divers have reported that voids can be followed along the halocline (Palmer and Williams, 1984), but it is unclear if these voids formed at the current halocline or represent voids formed in another dissolutional environment that is now overprinted by current sea level and lens position. It is also apparent that small isolated voids develop at the top of the freshwater lens. In the Bahamas, many such voids formed when the land was emergent by only a few meters, such that the voids had only a thin bedrock roof. In the time since the last interglacial (oxygen isotope substage 5e) when they formed, these voids have collapsed in great numbers, producing what are locally termed "banana holes;" spatial densities commonly exceed 1,000/km^2 (Harris et al., 1995). It is less clear whether macroscopic voids (caves) develop at deeper levels in the lens; hydrodynamic data (Vacher, 1978; Whitaker and Smart, 1997) appears to indicate that dissolutional flow paths at a scale of a few centimeters dominate. In very small carbonate islands there is no evidence that macroscopic (human-size) dissolutional voids form an integrated conduit-flow network, as is commonly seen in continental karst areas.

In composite islands, the noncarbonate rock forms a catchment surface from which allogenic water can be

directed to the adjacent carbonates as point inputs of large discharge. Unlike the uniform autogenic catchment of carbonate islands, where the dissolutional potential of the meteoric water is mostly expended in forming the epikarst of the upper few meters, this allogenic water enters the carbonates and penetrates deeply while still maintaining significant ability to dissolve the carbonate rock.

In many cases, these allogenic streams flow within the carbonate rock at the contact with the underlying noncarbonate rock. In that regard, they behave as vadose streamways commonly seen in continental settings. Eventually, however, these streams will reach the top of the freshwater lens and the hydrologic environment changes dramatically. It is not clear what happens under these conditions, but preliminary evidence from Guam indicates that broad, low chambers develop at the top of the lens, most likely from mixing of the vadose stream water with the lens. In Guam, vadose streamways at the volcanic/carbonate contact can be followed below a series of such broad chambers. Each such chamber may represent a pause in sea-level position, and, given the uplift of Guam, these chambers were probably abandoned by the freshwater lens and undercut by the vadose streamways.

On Bermuda, a carbonate cover island, the basalt/carbonate contact is present everywhere beneath the carbonate cover. During glacioeustatic sea-level lowstands, this contact becomes exposed above the elevation of the fresh-water lens and becomes part of the vadose zone. There the contact directs autogenic recharge along the buried contact topography. This action undercuts the overlying carbonates, and large progradational voids develop by collapse (Mylroie et al., 1995a). On Guam and Barbados today, and on Bermuda in the Pleistocene, these contact streams feed water to the part of the lens that rests on noncarbonate rock, as opposed to floating on marine water. This water has been termed "parabasal water" on Guam (see Mink and Vacher, 1997, for a review of terminology).

As noted earlier, cave divers in the Bahamas and elsewhere have reported long linear caves that penetrate deep into carbonate platforms. The divers' descriptions indicate that these caves appear to be former phreatic conduits (Palmer and Williams, 1984). They are found at depths of 15 m or deeper on Great Bahama Bank and Little Bahama Bank. Under current sea-level conditions, these banks are almost entirely flooded by shallow marine water, with islands such as New Providence, Andros, Grand Bahama and Abaco rising from them. During glacial maxima and sea-level lowstands, however, these banks would be extremely large islands. Bank area today is 136,000 km^2; of which only 11,400 km^2 is subaerial (Meyerhoff and Hatten, 1974). A drop in sea level of only 10 m would produce land area over 100,000 km^2 Does island size affect conduit development? Mylroie and Carew (1997) offer some speculation about island size and karst development.

Given a circular island with a radius of 1 km; the perimeter (P) is 6.28 km, the area (A) is 3.14 km^2, and the A/P ratio is 0.5. If a circular carbonate island has a 100-km radius, the perimeter is 628 km, but the area is 31,416 km^2 for a ratio A/P of 50. It appears that some threshold exists, such that when island size becomes large enough, macroscopic (i.e. diver-sized) conduit flow is favored. Such conduit flow would work only if it could out-compete the diffuse flow network of the fresh-water lens. In a very small island, there is not enough recharge to support a large conduit. In addition, the close proximity of the island margin to all parts of the lens gives little advantage to conduit flow. However, if the island is very large, the available recharge is very large, and much of the island is isolated from the island periphery, making diffuse flow uncompetitive with conduit flow. Hence conduits may develop. It is interesting to note that divers have not located true conduits on very small isolated platforms, such as San Salvador Island. In that case, sea-level fall provides no significant increase in island size.

Surface karst on carbonate and composite islands is not unique to the island environment; in other words, the features are comparable to what would be expected on rocks of similar age in continental settings. As carbonate islands have entirely autogenic recharge, a complex epikarst extending several meters downward from the surface results. Because of the high initial porosity of the young rocks found on carbonate islands, vadose bypass flow routes called pit caves (Pace et al., 1992) commonly develop. These features rarely are more than 10 m deep in the Bahamas, but in Guam, on older rocks, depths can reach 50 m.

On composite islands, the carbonate outcrop contains features found on carbonate islands, but the carbonate/noncarbonate contact will produce classic karst features seen in continental settings, such as sinking streams and blind valleys. The dissolutional retreat of the carbonates away from the contact can form a marked topographic feature. In the Pacific, where carbonates commonly ring an interior volcanic edifice, a moat-like feature forms between the volcanic high ground and an erosionally retreating limestone scarp. Such islands are termed "makatea islands" (see Vacher, 1997, for a review of terminology). Given that carbonate islands and composite islands have very young limestones with eogenetic characteristics, any unique quality of the surface karst landforms reflects the age and nature of the rock more than directly reflecting the marine environment in which they are found.

One major karst landform that does seem more common in carbonate and composite islands than in continental karsts developed on old rock is the collapse sinkhole (or collapse doline). As noted above in the discussion of the Bahamian banana holes, voids develop, apparently at random locations at the top of the fresh-water lens. They can form in time spans of 10,000 years or less, reaching diameters of 10 m or more. If the land surface is at low elevation, these voids will have thin roofs and collapse readily. In the case of flank margin caves, they can form rapidly and with large volumes in specific locations (lens margin). Subsequent collapse can result in a preferential position for the collapse sinkholes (Mylroie and Carew, 1997). Such collapse may be favored during sea-level regressions, which would result in the loss of buoyant support for the rock. It has also been recognized that in composite and carbonate-cover islands, vadose flow along the carbonate/noncarbonate contact can produce very large voids in short periods of time. These voids may progradationally collapse to the surface, even from depths of 50 m or more, as has occurred in Bermuda (Mylroie et al., 1995a).

The karst hydrology of carbonate islands includes deep water-filled shafts called blue holes. These have been defined as follows: "Blue holes are subsurface voids that are developed in carbonate banks and islands; are open to the earth's surface; contain tidally-influenced waters of fresh, marine, or mixed chemistry; extend below sea-level for a majority of their depth; and may provide access to submerged cave passages" (Mylroie et al., 1995b, p. 225). Blue holes are polygenetic in origin, having developed by flooding of vadose shafts during glacioeustasy, by progradational collapse from deep-seated voids, and by fracture of the bank margin (Mylroie et al., 1995b). While they may play an important role in carbonate island hydrology today, it is unclear whether they developed as active components of that hydrology, or preexisted from an earlier hydrologic regime and were in place to influence modern hydrology. Whitaker and Smart (1997) offer a thorough review of blue-hole hydrology in the Bahamas.

Modeling carbonate island karst

The conceptual view of island karst depicts water flow in carbonate islands as the result of both fluid flow and the resulting diagenetic alteration of the rocks hosting that fluid flow. The result is a host rock with constantly changing hydraulic parameters. Dissolutional processes work rapidly in these youthful or eogenetic carbonates, but the geochemical and hydraulic boundaries of the flow system concentrate fluid flow to certain specific areas within the aquifer. The freshwater lens, by rearranging the host rock from a high-porosity / low-permeability rock to a moderate-porosity / high-permeability rock creates the conditions of its own modification. Under long-term stable conditions, the host carbonates become so permeable by dissolution that the freshwater lens will be replaced by a shore-to-shore zone of freshwater/saltwater mixing at and below the water table. The freshwater lenses found in today's carbonate islands owe their existence to glacioeustasy, which has moved the freshwater lens vertically and laterally over time, limiting permeability development at any given horizon. At the same time, during sea-level highstands, new sediment is added to the bank top, creating new high-porosity / low-permeability carbonate rock that can host a freshwater lens in the future.

References cited

Back, W., B.B. Hanshaw, J.S. Herman, and J.N. Van Driel, 1986, Differential dissolution of a Pleistocene reef in the ground-water mixing zone of coastal Yucatan, Mexico: Geology, v. 14, p. 137-140.

Bögli, A., 1980, Karst hydrology and physical speleology: Springer-Verlag, Berlin, 284 p.

Bottrell, S.H., P.L. Smart, F. Whitaker, and R. Raiswell, 1991, Geochemistry and isotope systematics of sulphur in the mixing zone of Bahamian blue holes: Applied Geochemistry, v. 6, p. 97-103.

Budd, D.A., and H.L. Vacher, 1991, Predicting the thickness of fresh-water lenses in carbonate islands: Journal of Sedimentary Petrology, v. 61, p. 43-53.

Cant, R. V., and P.S. Weech, 1986, A review of the factors affecting the development of Ghyben-Herzberg lenses in the Bahamas: Journal of Hydrology, v. 84, p. 333-343.

Carew, J.L., and J. E. Mylroie, 1997, Geology of the Bahamas, *in* H.L. Vacher and T.M. Quinn, (eds.), Hydrogeology of carbonate islands: Elsevier Science Publishers, Developments in Sedimentology 54, p. 91-139.

Choquette, P.W., and L.C. Pray, 1970, Geological nomenclature and classification of porosity in sedimentary carbonates: American Association of Petroleum Geologists Bulletin, v. 54, p. 207-250.

Falkland, A. (ed.), 1991, Hydrology and water resources of small islands: A practical guide: UNESCO, Paris, 317 p.

Groves, C., and J. Meiman (eds.), 1998, Friends of Karst - IGCP 379 Program with Abstracts: Western Kentucky University, Bowling Green, 42 p.

Harris, J.G., J.E. Mylroie, and J.L. Carew, 1995, Banana holes: Unique karst features of the Bahamas: Carbonates and Evaporites, v. 10, no. 2, p. 215-224.

Meyerhoff, A. A., and C.W. Hatten, 1974, Bahamas salient of North America: tectonic framework, stratigraphy, and petroleum potential: Association of American Petroleum Geologists Bulletin, v. 58, p. 1201-1239.

Mink, J.F., and H.L. Vacher, 1997, Introduction: Hydrogeology of northern Guam, *in* H.L. Vacher and T.M. Quinn (eds.), Geology and hydrogeology of carbonate islands: Elsevier Science Publishers, Developments in Sedimentology 54, p. 743-761.

Mylroie, J.E., and J.L. Carew, 1990, The flank margin model for dissolution cave development in carbonate platforms: Earth Surface Processes and Landforms, v. 15, p. 413-424.

Mylroie, J.E., J.L. Carew, N.E. Sealey, and J.R. Mylroie, 1991, Cave development on New Providence Island and Long Island, Bahamas: Cave Science, v. 18, no. 3, p. 139-151.

Mylroie, J.E., and J.L. Carew, 1995, Karst development on carbonate islands, *in* D.A. Budd, P.M. Harris, and A. Saller (eds.), Unconformities and Porosity in Carbonate Strata: American Association of Petroleum Geologists Memoir 63, p. 55-76.

Mylroie, J.E., J.L. Carew, and H.L. Vacher, 1995a, Karst development in the Bahamas and Bermuda, *in* H.A. Curran and B. White (eds.), Terrestrial and shallow marine geology of the Bahamas and Bermuda: Geological Society of America Special Paper 300, p. 251-267.

Mylroie, J.E., J.L. Carew, and A.I. Moore, 1995b, Blue holes: Definition and genesis: Carbonates and Evaporites, v. 10, no. 2, p. 225-233.

Mylroie, J.E., and J.L. Carew, 1997, Land use and carbonate island karst, *in* B.F. Beck and J.B. Stephenson (eds.), The Engineering Geology and Hydrogeology of Karst Terranes: Brookfield, A. A. Balkema, p. 3-12.

Nunn, P.D., 1994, Oceanic Islands: Blackwell, Oxford, 413 p.

Pace, M.C., J.E. Mylroie, and J.L. Carew, 1993, Petrographic analysis of vertical dissolution features on San Salvador Island, Bahamas, *in* B. White (ed.), Proceedings of the 6th Symposium on the Geology of the Bahamas: Port Charlotte, Florida, Bahamian Field Station, p. 109-123.

Palmer, R., and D.W. Williams, 1984, Cave development under Andros Island, Bahamas: Cave Science, v. 13, p. 79-82.

Panuska, B.C., J.M. Mylroie, D. Armentrout, and D. McFarlane, 1998, Magnetostratigraphy of Cueva del Aleman, Isla de Mona, Puerto Rico and the species duration of Audubon's Shearwater: Journal of Cave and Karst Studies, v. 60, no. 2, p. 96-100.

Plummer. L.N., 1975, Mixing of sea water with calcium carbonate ground water, *in* E. H. T. Whitten (ed.), Quantitative studies in geological sciences: Geological Society of America Memoir v. 142, p. 219-236.

Raeisi, E., and J.E. Mylroie, 1995, Hydrodynamic behavior of caves formed in the fresh-water lens of carbonate islands: Carbonates and Evaporites, v. 10, no. 2, p. 207-214.

Sanford, W.E., and L.F. Konikow, 1989, Porosity development in coastal carbonate aquifers: Geology, v. 17, p. 249-252.

Smart, P.L., J.M. Dawans, and F. Whitaker, 1988, Carbonate dissolution in a modern mixing zone: Nature, v. 335, p. 811-813.

Vacher, H.L., 1978, Hydrogeology of Bermuda – Significance of an across-the-island variation in permeability: Journal of Hydrology, v. 39, p. 207-226.

Vacher, H. L., 1988, Dupuit-Ghyben-Herzberg analysis of strip-island lenses: Geological Society of America Bulletin, v. 100, p. 580-591.

Vacher, H.L., and T. N. Wallis, 1992, Comparative hydrology of Bermuda and Great Exuma Island, Bahamas: Ground Water, v. 30, p. 15-20.

Vacher, H.L., 1997, Introduction: Varieties of carbonate islands and a historical perspective, *in* H.L. Vacher and T.M. Quinn (eds.), Geology and hydrogeology of carbonate islands: Elsevier Science Publishers, Developments in Sedimentology 54, p. 1-33.

Vacher, H.L., and T.M. Quinn, eds., 1997, Geology and hydrogeology of carbonate islands: Elsevier Science Publishers, Developments in Sedimentology 54, 948 p.

Whitaker, F.F., and P.L. Smart, 1997, Hydrogeology of the Bahamian archipelago, *in* H.L. Vacher and T.M. Quinn (eds.), Geology and hydrogeology of carbonate islands: Elsevier Science Publishers, Developments in Sedimentology 54, p. 183-216.

TOWARD A SUITABLE CONCEPTUAL MODEL OF THE NORTHERN GUAM LENS AQUIFER

J. W. Jenson
Water and Environmental Research Institute of the Western Pacific, University of Guam
Mangilao, Guam 96923

Abstract

The Northern Guam Lens Aquifer is a carbonate-island aquifer in an uplifted limestone sequence consisting of a Miocene-Pliocene detrital facies grading upward into a Pliocene-Pleistocene coral-algal reef-lagoon facies. The limestone sequence rests atop Eocene-Oligocene submarine volcaniclastic basement. Basement topography is complex, varying from a maximum of about 200 m, where it crops out to form the highest point above the limestone plateau, to a minimum of more than 150 m below sea level. The island has been generally emergent over Pleistocene time; the entire Pleistocene section is currently above sea level, the highest elevation of the plateau being about 180 m. Relative sea-level stillstands are recorded in several notches and marine terraces incised in cliff faces surrounding the plateau. The entire sequence has undergone fresh-water diagenesis as it was uplifted through the fresh-water lens. How karst processes have modified the subsequent porosity is of fundamental concern to those attempting to interpret or predict aquifer behavior. Three especially compelling questions include: (1) What is the relative importance of cavernous, fracture, and diffuse porous flow in the current vadose and phreatic zones, and what controls the occurrence of each type of porosity? (2) How strongly has horizontal conductivity been modified by water-table dissolution at previous still-stand levels? (3) What is the relative importance of concentrated versus diffuse infiltration? Answers to such questions are crucial for assessing the reliability of models in evaluating pump-test results and predicting groundwater flow directions, fresh-water lens geometry, and response to withdrawal.

A MODEL OF KARST DRAINAGE BASIN EVOLUTION, INTERIOR LOW PLATEAUS, USA

Joseph A. Ray
Kentucky Division of Water
Frankfort, KY 40601

Abstract

Trunk groundwater circulation within gently dipping soluble rocks has originated by leakage or base-flow piracy beneath stream channels. The subsurface flow capacity was initially inadequate to accept the higher stream discharges which eroded and maintained surface channels. ***Overflow Allogenic, or Type I basins (a)*** are common karst drainage basins characterized by the maintenance of surface valleys by overflow discharges.

The subsurface diversion route of a stream evolves over time to a large enough capacity that no flow can bypass the insurgence. The valley becomes blind and runoff from the entire watershed is conducted through the groundwater basin. This is termed an ***Underflow Allogenic, or Type II basin (b).*** Turnhole Spring basin, at Mammoth Cave, Kentucky, represents an underflow allogenic basin that has evolved from an overflow allogenic basin. This evolution is shown by an abandoned stream valley that begins near Mill Hole and meanders northwest six miles to Green River.

Local Autogenic, or Type III basins (c) are smaller karst basins predominantly recharged by surface infiltration and runoff into sinkholes. They tend to evolve on sinkhole plateaus adjacent to entrenched streams or by derangement of Type I or II basins.

Understanding the major karst basin types and their evolution can be useful in hydrogeologic surveys and tracer studies, and in interpreting spring behavior and water quality. A contaminated flood crest may bypass the spring of an Overflow Allogenic basin via surface routes and reduce flood impacts, for example.

ORIGIN AND ATTRIBUTES OF PALEOCAVE CARBONATE RESERVOIRS

Robert G. Loucks
ARCO Technology and Operation Services, 2300 West Plano Parkway
Plano, TX 75075

Abstract

Paleocave systems form an important class of carbonate reservoirs that are products of near-surface karst processes and later burial compaction and diagenesis. Origins of fractures, breccias, sediment fills and other features associated with paleocave reservoirs have been studied in modern and ancient cave systems. Information about such cave systems can be used to reconstruct the general evolution of paleocave reservoirs and understand their associated scale, pore networks, and spatial complexities.

Introduction

Paleocave reservoirs tend to have complex histories and pronounced lateral and vertical spatial complexity. In order to define reservoir geometry, scale, pore networks, and spatial complexities of these reservoirs for purposes of hydrocarbon exploration and development, their near-surface history and later burial modifications must be understood. Integrating studies of modern cave systems with those of paleocave systems from outcrops and cores provide the data necessary to develop geologic models of paleocave reservoirs that describe their major characteristics. Studies of modern systems provide data on cave origin and early modification, as well as information on factors controlling cave geometry. Data from paleocave systems show end products resulting from burial processes, but this data are limited to well information and relatively rare good outcrop exposures.

Concepts for this study come from the author's investigations of a series of modern cave systems (Blanchard Springs Caverns and Ennis Cave in northern Arkansas, Mammoth - Flint Ridge Cave system in Kentucky, and Longhorn Cavern and Inner Space Cavern in central Texas) and ancient cave systems (several oil and gas fields in Lower Ordovician and Siluro-Devonian strata in west Texas, as well as an outcrop study of Lower Ordovician paleokarst strata in central Texas). Data from published reports on modern cave systems and paleocave systems were also used.

Breccias and fractures are important components of cave systems. Figure 1 presents a classification showing the relationships between breccias, fractures, and cave-sediment fill. Crackle breccias are highly fractured rock with thin fractures separating breccia clasts. Individual clasts can be fitted back together. Mosaic breccias are similar to crackle breccias, but displacement between clasts is greater and some clast rotation is evident. A continuous gradation occurs between crackle breccias and chaotic breccias. Chaotic breccias are characterized by extensive rotation and displacement of clasts. The clasts can be derived from several sources producing a polymictic breccia. Chaotic breccias grade from matrix-free, clast-supported breccias to matrix-supported breccias. They can form by cave-wall and cave-ceiling breakdown or by mechanical transport. There is a break in the continuum between the crackle breccia and sediment fill (this is noted by the shaded area in the triangle shown in Figure 1) because mosaic breccia clasts do not have a transition into sediment. Cave sediment can fill passages or interbreccia pores in chaotic, mosaic, and crackle breccias.

Modern near-surface cave systems

Modern cave systems are well studied (e.g. Ford, 1988; White, 1988; Ford and Williams, 1989; Palmer, 1991, 1995; Loucks and Handford, 1992; White et al., 1995), but data from these studies have not been well integrated into studies of paleocave systems. This paper focuses on paleocave systems and the reader is referred to the voluminous literature on modern caves.

Paleocave systems

The processes by which cave systems evolve with burial and collapse cannot be monitored directly. These processes have to be inferred from analyzing the differences between modern cave systems and paleocave systems. It is very difficult to obtain three-dimensional quantitative measurements about collapse-paleocave size, geometry, or percentage of pore types. Because of these limitations the following section is basically conceptual in approach, but numerous observations about paleocave systems were used to develop these concepts.

Burial-evolution processes affecting cave passages

Collapsed-paleocave passages display complex histories resulting from many stages of modification including near-surface excavation, sedimentation, breakdown, and burial-related mechanical compaction. Figure 2 displays the

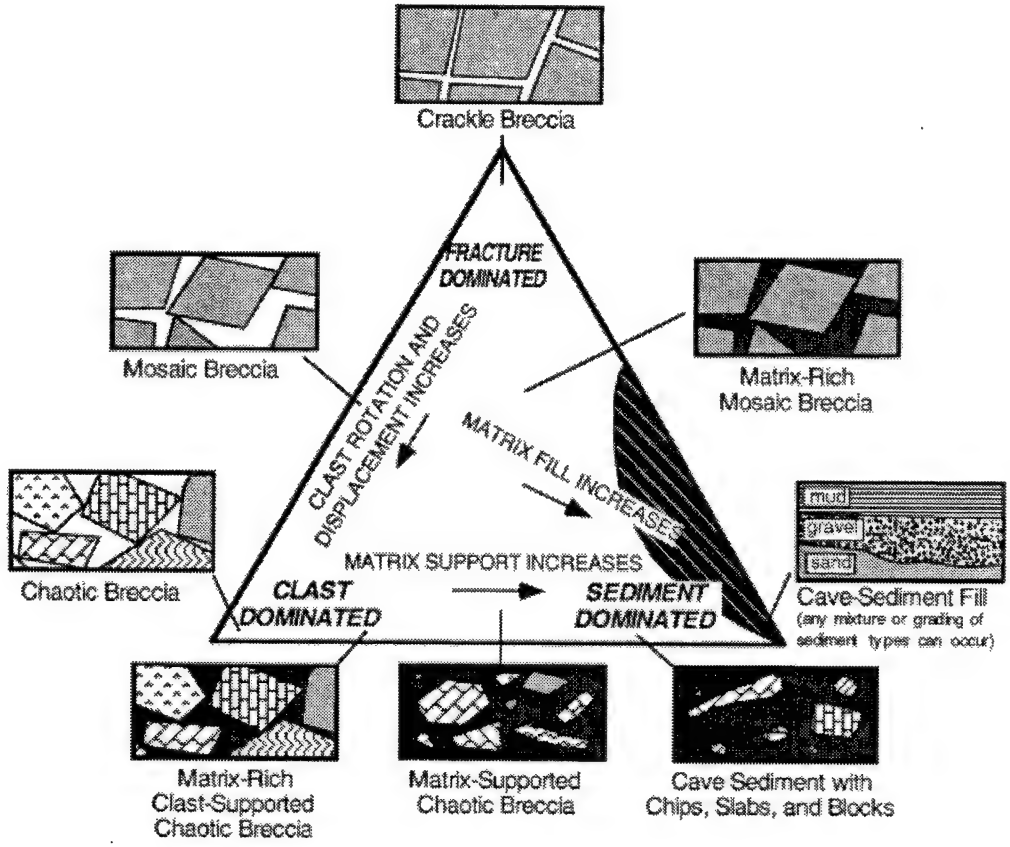

Figure 1: Classification of breccias and clastic deposits in cave systems. From Loucks (in press).

evolution of a passage from development in the phreatic zone, subsequent modification in the vadose zone, and through several stages of mechanical compaction during burial.

As cave-bearing strata are buried into the subsurface, extensive mechanical compaction is initiated, commonly resulting in collapse of remaining passages and restructuring of existing breccias (Figure 2). Collapse appears to occur over a broad depth range (near-surface to more than 2600 m). As the cave passages collapse, new breakdown breccias form from the ceiling and walls (Figure 2). These multistage breakdown breccias have been recognized in several studies of ancient paleocave systems (e.g. Kerans, 1988; Loucks and Handford, 1992; Lucia, 1995). The volume of interbreccia porosity increases, whereas the cavernous porosity decreases. The cross-sectional extent of brecciation and fracturing is commonly greater than that of the original passage because cave ceilings and cave walls are affected.

After initial burial collapse, passages are filled with clasts having a wide range of sizes. Original interbreccia pores may be as large as several meters across. Differentially compacted but relatively intact strata over the collapsed chamber are fractured and form burial cave-ceiling crackle and mosaic breccias with loosely to tightly fitted clasts (Figure 2). Sag features and faults may occur over the collapsed passages.

Continued burial leads to more extensive mechanical compaction of previously formed breakdown clasts. This causes blocks with large void spaces between them to fracture, brecciate, and pack closer together (Figure 2). Interbreccia pores decrease in size as a result. The resulting product is a rebrecciated chaotic breakdown breccia composed predominantly of small clasts. During burial of uncemented cave breccias, there is a general evolution from large clasts with large interbreccia pores to smaller clasts with smaller interbreccia pores (Figure 3). Mechanical compaction of clasts decreases where cementation stabilizes the breccia framework and ceases where cements fill the interbreccia pores.

As burial compaction continues, more fracturing occurs in the surrounding host rock as well as in the chaotic breccias. This mechanical process expands the volume of crackle breccias and fractures further into the host rock. The resulting brecciated zone is neither as simple nor as well defined as the original passage. It now consists of a zone of compacted chaotic breccias, commonly overprinted with

stress fractures. Radiating out from this larger pod of compacted chaotic breccia is a zone of crackle and mosaic breccias and fractures (Figure 2).

Burial evolution of cave systems

The author believes that most paleocave hydrocarbon reservoirs are not products of isolated collapsed passages, each only meters across and tens to hundreds of meters long, but are a product of coalesced, collapsed-cave systems hundreds to several thousand meters across and thousands of meters long (Figure 4). This is an important concept, because it indicates that exploration targets in collapsed-paleocave systems are likely to be much larger than individual collapsed caverns.

Coalesced collapsed-paleocave hypothesis

It is postulated that the development of a large collapsed-paleocave reservoir is the result of several stages of

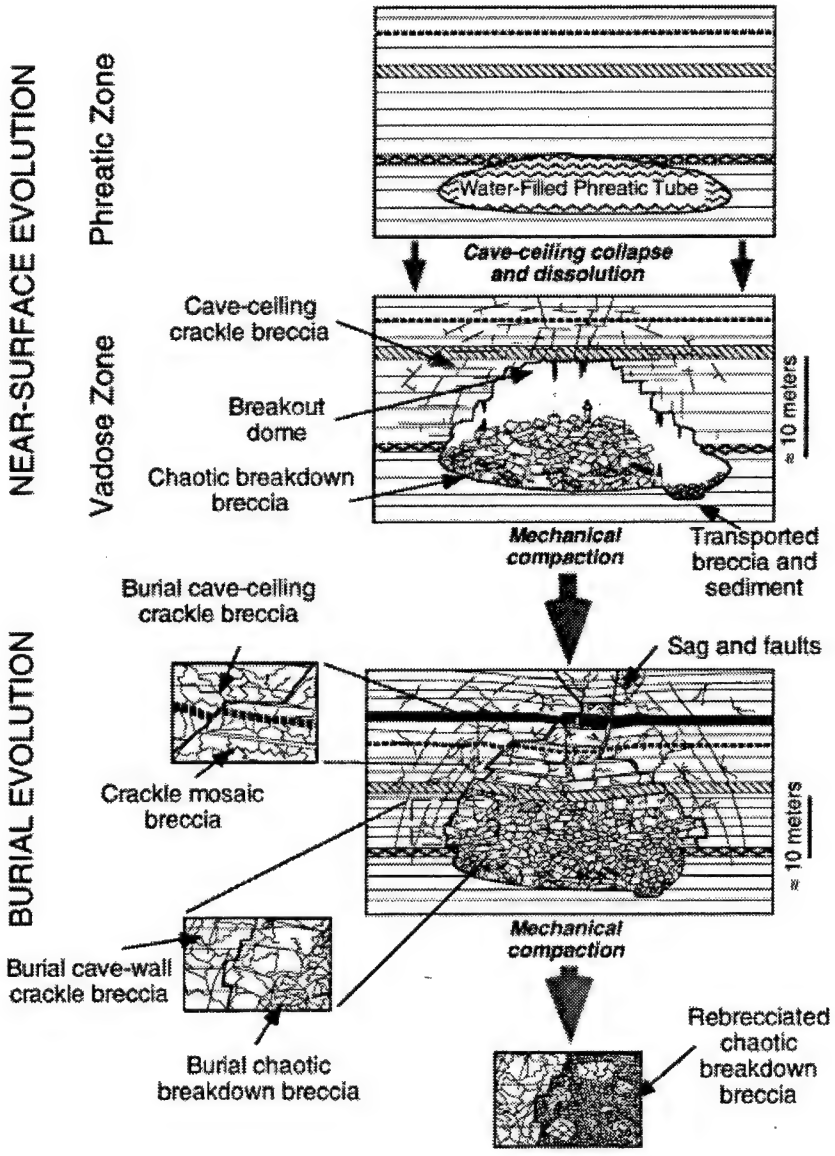

Figure 2: Schematic diagram showing evolution of a single cave passage from its formation in the phreatic zone of a near-surface karst environment to burial in the deeper subsurface where collapse and extensive brecciation occur. Near-surface phreatic-zone passage is modeled after passages seen in Mammoth and Longhorn caverns, and near-surface vadose-zone passage is modeled after passages seen in Mammoth and Blanchard Springs Caverns. The near-surface evolution of a cave passage is based on a falling base level. The burial diagram is based on outcrop studies in central Texas and in the Franklin Mountains, as well as subsurface studies from core and seismic data. Modified from Loucks and Handford (1992) and Loucks (in press).

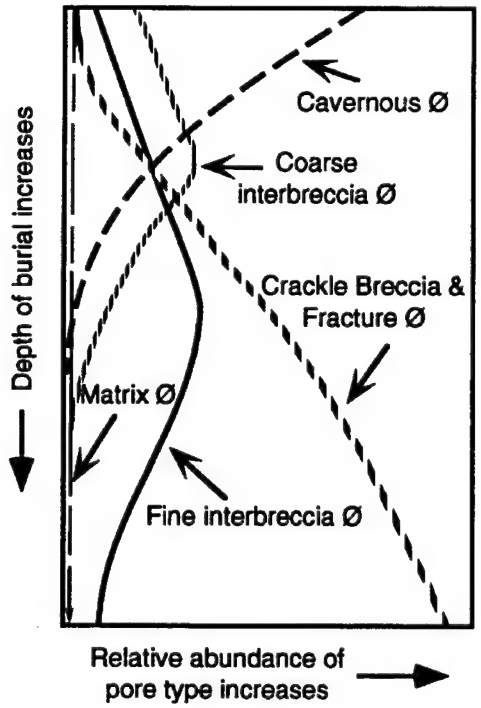

Figure 3: Generalized burial evolution of a cave-system pore network with relative proportions of pore types. The dividing line between fine-interbreccia and coarse-interbreccia pores is put at six centimeters by the author. The relative abundance of pore types and relative depth of burial are estimates based on review of near-surface and buried paleocave systems. From Loucks (in press).

development. This concept is referred to as the coalesced collapsed-paleocave hypothesis.

According to this concept, at a composite unconformity (more than one period of exposure), cave systems develop and partly collapse during each period of prolonged subaerial exposure (Figure 4). During each regional sea-level rise, the karst and cave system are inactive and partly filled with sediment. Preburial-cave systems, developed at a composite unconformity, would consist of closely spaced passages created over a vertical section of several hundreds of meters. Many passages might be partially collapsed or filled with debris. The surface might also have a well-developed system of dolines (sinkholes) partly filled with breccia and terrestrial and/or marine sediment.

As the multiple-episode cave system subsides into the deeper subsurface, wall and ceiling rock surrounding open passages collapses, forming breakdown breccias and fractures. These breccias and fractures radiate out from the collapsed passage and commonly intersect fractures from other collapsed passages and breccias within the system. The result is the interconnection of cave-passage chaotic breccias by crackle and mosaic breccias and fractures (Figure 4). This process produces a much larger exploration target with enhanced reservoir continuity; however, all of the porosity types are not necessarily well connected.

Conclusions

Paleocave reservoirs have complex histories of formation. They are products of near-surface cave development including dissolutional excavation of passages, breakdown of passages, and cave-passage sedimentation. The near-surface cave systems are three-dimensional megapore networks containing varying amounts of breccias and sediments. Between the passages is relatively tight host rock with minor fracturing. Statistics from modern cave systems indicate that cave passages are generally less than 8 m wide. Near-surface dissolutional excavation and cave sedimentation terminate as cave-bearing strata are buried into the subsurface. Extensive mechanical compaction is initiated, however, resulting in the collapse of remaining passages, rebrecciation of existing large breccia clasts, slabs, and blocks, and extensive redistribution of porosity types (Figures 2 and 3). As cave passages collapse, new breakdown breccias and fractures form from associated ceilings and walls.

Collapsed-paleocave reservoirs are commonly much larger and continuous than can be accounted for by the collapse of a single cave passage or simple cave system. It is postulated that the development of a large collapsed-paleocave reservoir is the result of several stages of development starting with the formation of a multiple-episode cave system in the near surface. As a multiple-episode cave system subsides into the deeper subsurface, wall and ceiling rock surrounding open passages collapses and forms breakdown breccias and associated crackle breccias and fractures. These fractures and breccias radiate out from the collapsed passage and intersect with fractures from other collapsed passages and breccias within the system. The result is the interconnection of cave-passage chaotic breccias by crackle and mosaic breccias and fractures. This process produces a spatially complex zone of brecciation up to a thousand or more meters wide and a hundred or more meters thick.

The study of modern cave systems is instrumental in understanding collapsed-paleocave systems. The initial cave systems, along with their burial evolution, have a strong influence on the architecture of the final paleocave system. This influence must be understood in order to recognize the complex spatial heterogeneity seen in associated hydrocarbon reservoirs.

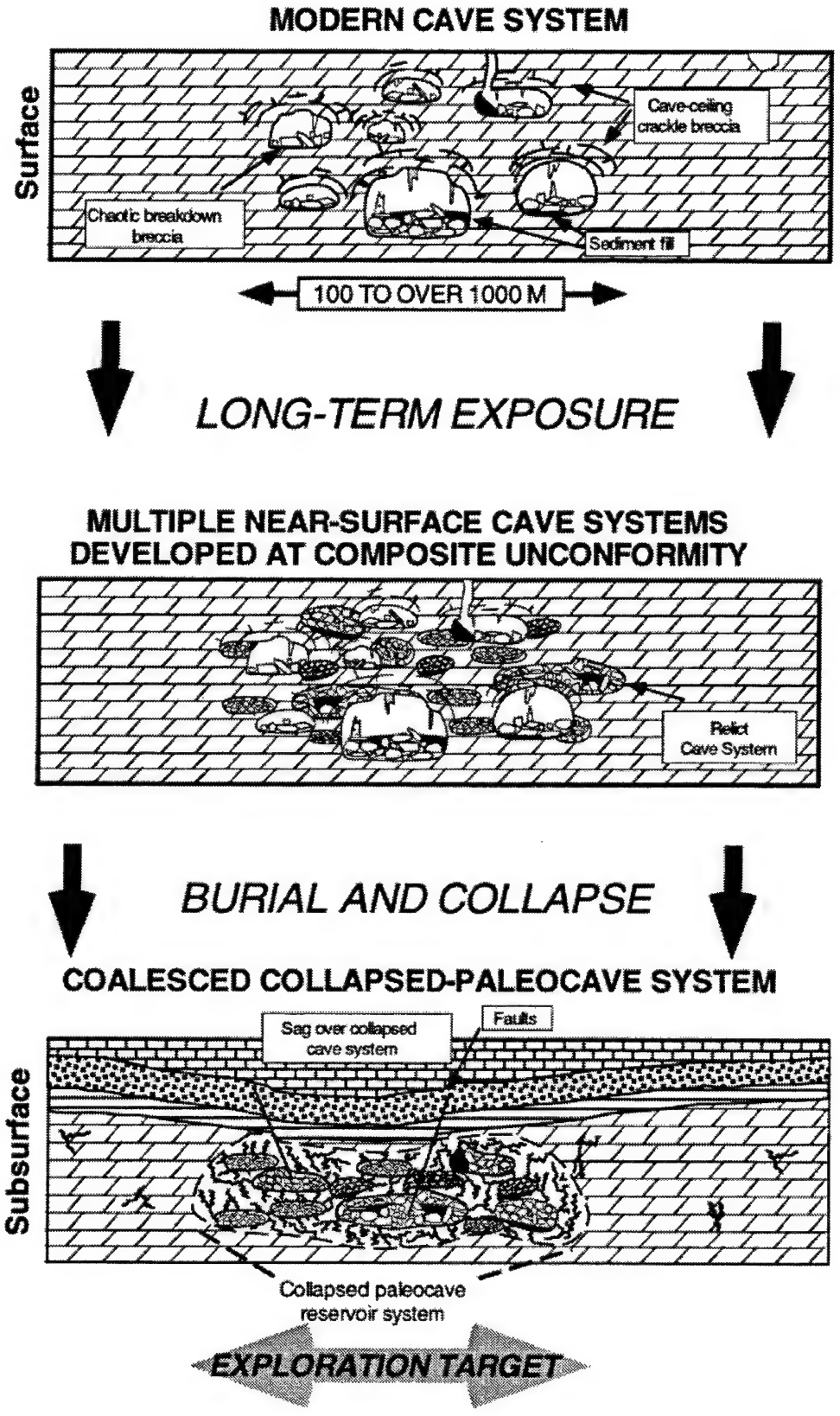

Figure 4: Schematic diagram of the coalesced, collapsed-paleocave model. From Loucks (in press).

References cited

Ford, D.C., 1988, Characteristics of dissolutional cave systems in carbonate rocks, *in* N. P. James and P. W. Choquette (eds.), Paleokarst: Springer-Verlag, p. 25-57.

Ford, D.C., and P.W. Williams, 1989, Karst geomorphology and hydrology: Unwin Hyman Ltd., London, 601 p.

Kerans, C., 1988, Karst-controlled reservoir heterogeneity in Ellenburger Group carbonates of west Texas: AAPG Bulletin, v. 72, p. 1160-1183.

Loucks, R.G., (in press) Paleocave carbonate reservoirs: origins, burial-depth modifications, spatial complexity, and reservoir implications: AAPG Bulletin (June 1999).

Loucks, R.G., and C.R. Handford, 1992, Origin and recognition of fractures, breccias, and sediment fills in paleocave-reservoir networks, *in* M.P. Candelaria and C.L. Reed (eds.), Paleokarst, karst related diagenesis and reservoir development: examples from Ordovician-Devonian age strata of west Texas and the Mid-Continent: Permian Basin Section SEPM Publication no. 92-33, p. 31-44.

Lucia, F.J., 1995, Lower Paleozoic cavern development, collapse, and dolomitization, Franklin Mountains, El Paso, Texas, *in* D.A. Budd, A.H. Saller, and P.M. Harris (eds.), Unconformities and porosity in carbonate strata: AAPG Memoir 63, p. 279-300.

Palmer, A.N., 1991, Origin and morphology of limestone caves: GSA Bulletin, v. 103, p. 1-21.

Palmer, A.N., 1995, Geochemical models for the origin of macroscopic solution porosity in carbonate rocks, *in* D.A. Budd, A.H. Saller, and P.M. Harris (eds.), Unconformities and porosity in carbonate strata: AAPG Memoir 63, p. 77-101.

White, W.B., 1988, Geomorphology and hydrology of karst terrains: University Press, New York, 464 p.

White, W.B., D.C. Culver, J.S. Herman, T.C. Kane, and J.E. Mylroie, 1995, Karst lands: American Scientist, v. 83, p. 450-459.

FROM A CONCEPTUAL MODEL OF KARST HYDROLOGICAL SYSTEMS TO WATER-VULNERABILITY MAPPING

Pierre-Yves Jeannin, François Zwahlen, and Nathalie Doerfliger
Center of Hydrogeology, University of Neuchâtel, Rue Emile-Argand 11
CH-2007 Neuchâtel, Switzerland

Abstract

A conceptual model of karst hydrological systems is presented here. It considers that water flows through four cascading subsystems: soils, epikarst, unsaturated zone, and saturated zone. This model lead us to define four criteria which appear to be significant for intrinsic vulnerability assessment with respect to a spring or a well: characteristics of epikarst (E), characteristics of protective cover (P), recharge or infiltration type (I) and presence/absence of a well-developed conduit network (K). The method has proved to be adequate for karst in Central Europe. In the future, it should be tested in other areas and compared to numerical approaches of karst systems.

Introduction

Delineation of water-protection zones in karst aquifers is generally problematic, because zones tend to be very large and often quite inefficient. Since 1991, within the framework of a contract for the Swiss Water Agency and a European scientific cooperation program (COST-65 and -620 actions), a method called EPIK has been developed for attempting to include karst specificity to the assessment of the vulnerability of water to pollution. The intrinsic vulnerability with respect to a spring or well can be assessed with this method. By intrinsic vulnerability, we consider possible water-quality degradation depending only on the aquifer characteristics, but neither on the type of pollutant (specific vulnerability), nor on the pollution probability (risk assessment). If required, these two steps (specific vulnerability and risk assessment) could be worked out after the intrinsic vulnerability mapping has been carried out. For each country, according to the existing laws and regulations, an adaptation of the vulnerability map to the protection zones is necessary.

The EPIK method has been developed in order to remain a reasonable compromise between investigation efforts (time and money) and meaningful results according to the special characteristics of karst.

This short note aims to make clearer the relation between such a method and the conceptual model on which the method is based. This can help hydrogeologists to adapt such a method to their own conceptual scheme in specific karst areas. Details about the method can be found in other papers (Doerfliger et al., 1999; Doerfliger 1996).

Conceptual model of karst groundwater flow systems in central Europe

Based on the existing literature and on our own observations, the following description of karst hydrological systems has been considered to adequately describe natural systems for the purpose of vulnerability assessment. As a first assumption, transit time is considered as the key parameter for controlling water intrinsic vulnerability. We assume that the karst groundwater flow system is a cascade of four subsystems, each having its own characteristics and behavior (Figure 1). These are soil, epikarst, unsaturated zone and saturated zone. It is assumed that water flows through all of them before reaching a spring or well.

Soil subsystem

This subsystem encompasses all superficial deposits of porous nature, which is assumed to filter and slow down water flow, i.e. to increase transit time. Besides evapotranspiration, which takes place mostly this subsystem, thickness and permeability are its most significant characteristics. As a first approximation, only these two parameters have been integrated into the EPIK method. Cation exchange capacity, clay content, and organic content may also play a role and should probably be considered in certain cases.

Epikarst subsystem

This subsystem has been first identified and defined by Mangin (1975) and further described by many authors. This subsystem is a karst-specific feature and plays a fundamental role in karst groundwater flow. It is a zone of weathered and dissolved limestone, varying from 0 to about 15 meters thick, located near the ground surface just below the soil (if present). Epikarst ranges from wonderful karren fields incised into compact limestone to piles of dislocated limestone boulders.

Hydraulically, the epikarst has both a high permeability and high porosity. These characteristics make it possible to absorb a fair amount of infiltration in a very short time.

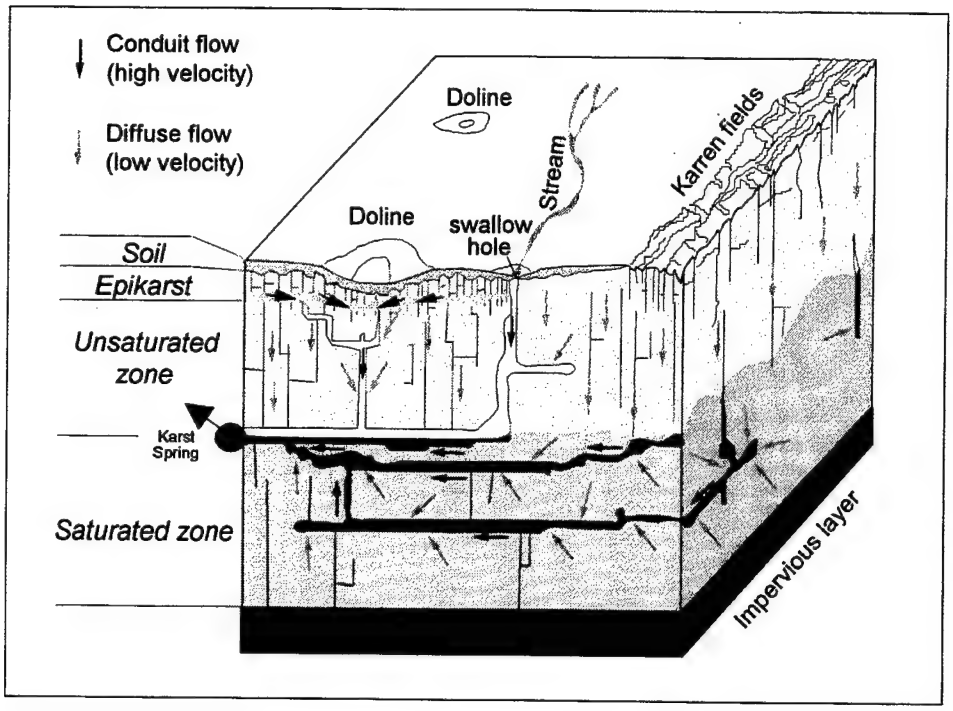

Figure 1: Conceptual model of a karst hydrological system (modified from Doerfliger and Zwahlen, 1995). Our model assumes that water flows through four cascading subsystems: soil, epikarst, unsaturated zone, and saturated zone. Vulnerability is derived from a qualitative assessment of the transit time in each subsystem.

Epikarst is a key factor in the absence of surface streams in most karst areas. Figure 2 shows a schematic diagram of epikarst behavior. Part of the water infiltrating into the epikarst is released very quickly into small conduits possibly present in the epikarst and connected to vertical conduits (shafts) in the unsaturated zone. As the bottom of the epikarst is irregular, part of the infiltrating water cannot be drained by the small conduits and is trapped in the lowest parts of the epikarst. This water can remain in storage for days or weeks and is slowly released downward through tiny fissures and cracks in the low-permeability parts of the unsaturated zone. In summary, it can be pointed out that epikarst plays a key role in the allotment of infiltrated water between rapid flow through conduits and slow flow through fissures and cracks.

The epikarst can be observed directly in roadcuts or drillholes. Beside these locations, especially in soil-covered karst, it is difficult to observe it and furthermore to map it over a catchment area. Nevertheless, many approaches to karst hydrological behavior point out the significant role played by the epikarst. For vulnerability it is essential to know, at any location, if part of the infiltration can reach the conduit network within hours, as is possible through a well-developed epikarst. The development of methods for investigating epikarst characteristics and behavior, as well as for mapping it, is an essential task for the near future.

Unsaturated zone subsystem

Also called the ***vadose zone***, this subsystem is characterized by vertical conduits (shafts) separated by zones of fissured limestone. Shafts are outlet points for the small conduits within the epikarst. Their typical spacing is on the order of some tens to hundreds of meters. Water flowing through shafts joins the saturated zone within a few hours. Zones of fissured limestone in the vadose zone are poorly documented so far. Their hydraulic conductivity is about 10^6 - 10^9 times lower than those of shafts. As a consequence, travel times are significantly longer than in shafts. Travel time is probably on the order of weeks, months or even years in the low-permeability parts of the unsaturated zone.

Saturated zone subsystem

This zone is called the ***phreatic zone*** in the karst technical language. It includes a network of connected conduits, leading to the outlet of the system, the karst spring. Various conduit network geometries and densities can be observed (Palmer 1991). A typical spacing between major conduits is on the order of 100 to 1000 meters. The porosity due to the conduit network is generally low (a few ‰). This low storage capacity, accompanied by rapid infiltration, induces flash-flooding of the conduits located above the phreatic zone. Water may rise several tens or even hundreds of meter in this "epiphreatic zone." When water rises so much in the conduits, it happens that heads are much higher in the conduits than in the surrounding matrix of fissured limestone. During these high-water periods, a flow from conduits into the matrix may take place. This water is released later when heads in the conduits have lowered again.

This means that the retarded flow can have two different origins: (1) slow flow from the lowest parts of the epikarst,

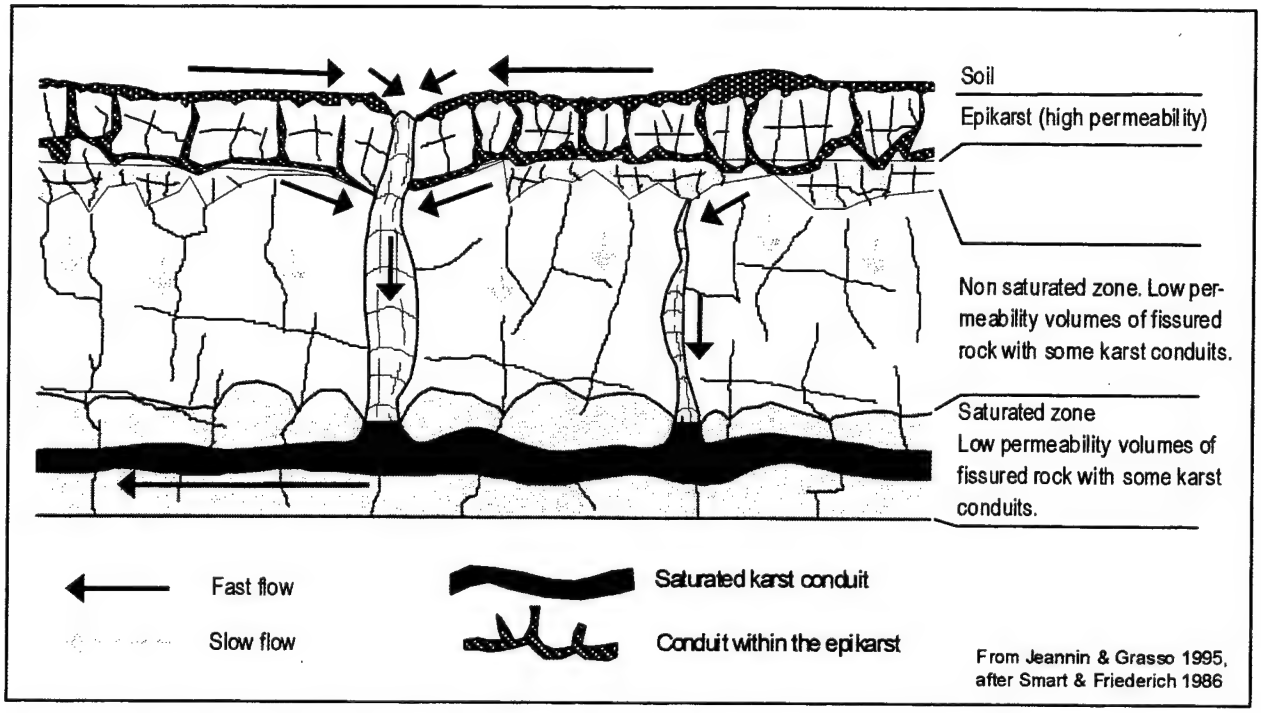

Figure 2: Schematic depiction of epikarst hydrological behavior (from Jeannin and Grasso, 1995, after Friederich and Smart, 1986). The epikarst plays a key role in the allotment of infiltrated water between rapid flow through conduits and slow flow through fissures and cracks.

through the low-permeability parts of the unsaturated zone, down to the low-permeability parts of the saturated zone; and (2) "injection" from the conduit network into the low-permeability volumes of the epiphreatic zone during high-water periods.

This retarded flow explains the well-known sustainability of karst springs through very long dry periods. This water, with a long transit time, is filtered and generally of good quality. Both components of the slow flow can be identified in the field (Jeannin, 1995). Their relative percentages are probably highly variable from one region to another. In the Swiss Jura mountains it appears that the total retarded flow represents some 50 - 60 % of the total flow and that most (60 - 80 %) of the retarded flow appears to be of type 1 (Jeannin and Grasso 1995).

Significant criteria for vulnerability assessment

Depending on the system to be investigated, the conceptual scheme described above may vary. For instance, one of the subsystems is sometimes not present (soil for example). In such a situation the vulnerability assessment method has to be modified according to the conceptual model.

In central Europe, and probably many karst areas of temperate climate, we could assume that water flows through all four of the subsystems described above. By further assuming that rapid flow leads to high vulnerability and slow flow to low vulnerability, the following criteria have been considered as the most significant ones for water vulnerability assessment.

(1) Characteristics of the epikarst (parameter E)

If the epikarst leads 90% of the infiltrated water very quickly into the conduit network, vulnerability is high. Alternatively, if the epikarst stores and slowly releases 90% of the infiltrated water, then vulnerability will be much lower.

(2) Characteristics of the protective cover (parameter P)

Soils and other sediments overlying the bedrock are very significant for protecting the aquifer against the rapid infiltration of pollutants.

(3) Type of recharge as infiltration (parameter I)

Classically, two types of recharge are distinguished: (1) concentrated recharge (swallowholes or sinking streams), which is a typical feature of karst hydrological systems, and (2) diffuse recharge. In the case of concentrated recharge, the protective cover and the epikarst criteria are of no significance because we can assume that point infiltration is more

or less directly linked to the conduit network and the spring. Point recharge is an easy criterion to map on the field.

(4) Characteristics of the karst conduit network (parameter K)

This is a key factor because the whole flow system is strongly influenced by the existence or absence of a well-developed conduit network. The vadose and phreatic zones are not distinguished in the present approach because it is assumed that the detailed characteristics of the conduit network (vadose, phreatic, or both) is of no significance compared to the existence or absence of such a network. It should be noticed here that the simplification of considering both zones together may not be adequate for extreme cases. If so, a refinement is necessary. Otherwise the method will consider a system with a 5 or 10 meter thick unsaturated zone exactly the same as another with 500 or even 1000 meters of vadose zone.

Case study

Having defined the criteria, we developed a similar approach to DRASTIC, but especially adapted to karst characteristics. This is the so called "EPIK" method. Each of the four criteria has been subdivided into three or four classes. Investigative methods have been proposed for recognizing and mapping the various classes for each criteria. Once those have been mapped, a GIS approach makes it possible to combine these data to obtain a vulnerability map.

So far, the EPIK-method has been applied to at least 5 different catchments in central Europe. Figure 3 shows the maps obtained for the E, P, and I criteria on the Milandre test field in northern Switzerland. This catchment includes a large cave system with an underground stream. For parameter K (karst conduit network) a single value ("well developed") has been assigned to the whole catchment area. The resulting vulnerability map is shown in the last box (bottom right). Several tracing experiments were carried out for verification and showed the method to be adequate. All examples proved the EPIK method to be feasible even by private consulting companies. The work effort is slightly higher than what is generally carried out in this type of study, but this slight disadvantage is largely compensated for by the fact that the resulting vulnerability zone is the result of a standard, explainable, and reproducible method adequate for the special characteristics of karst.

Conclusions

A sound understanding – a conceptual model – of the specific behavior of karst is necessary to develop a meaningful approach to karst water vulnerability. In central Europe our model has lead us to consider four major criteria: characteristics of epikarst, characteristics of protective cover, recharge or infiltration type, and presence/absence of a well-developed conduit network. In our opinion, based on our conceptual modeling, these criteria are the most significant for assessing vulnerability of a spring or well to pollution. These criteria, or similar ones depending on the selected conceptual model, should be considered in any study of this type. Applications of the EPIK method, or similar approaches in other areas, as well as comparisons with numerical studies of karst systems, will help to refine the conceptual models and thus the methods. In our opinion, the most interesting idea is that several criteria have to be selected to form the basis of a meaningful conceptual model of the karst system under investigation. This model has to take into account the special characteristics of karst systems in general, as well as those of the particular system investigated. Then all the selected criteria should be simultaneously assessed at every location of the catchment in order to evaluate the vulnerability to pollution of any particular point. E, P, I, and K are the four criteria derived from our conceptual model, which is probably adequate for many karst systems in temperature climates.

References cited

Doerfliger, N., 1996, Advances in karst groundwater protection strategy using artificial tracer tests analysis and multi-attribute vulnerability mapping (EPIK method): Ph.D. thesis, University of Neuchâtel, Switzerland, 308 p.

Doerfliger, N., P.-Y. Jeannin, and F. Zwahlen (in press), Water vulnerability assessment in karst environments: a new method of defining protection areas using a multi-attribute approach and GIS tools (EPIK method): Environmental Geology.

Jeannin, P.-Y., and D.A. Grasso, 1995, Recharge respective des volumes de roche peu perméables et des conduits karstiques, rôle de l'épikarst: Bulletin d'hydrogéologie no. 14, Neuchâtel, p. 95-111.

Jeannin, P.-Y., 1995, Comportement hydraulique mutuel des volumes de roche peu perméables et des conduits karstiques: conséquences sur l'étude des aquifères karstiques: Bulletin d'hydrogéologie no. 14, Neuchâtel, p. 113-148.

Mangin, A., 1975, Contribution à l'étude hydrodynamique des aquifères karstiques: Thèse de doctorat d'Etat, Université de Dijon, 124 p. (also published in Annales de Spéléologie, 1974-29(3), 283-332; 1974-29(4), 495-601; 1975-30(1), 21-124).

Palmer, A. (1991): Origin and morphology of limestone caves: Geol. Soc. of America Bull., vol. 103, p. 1-21.

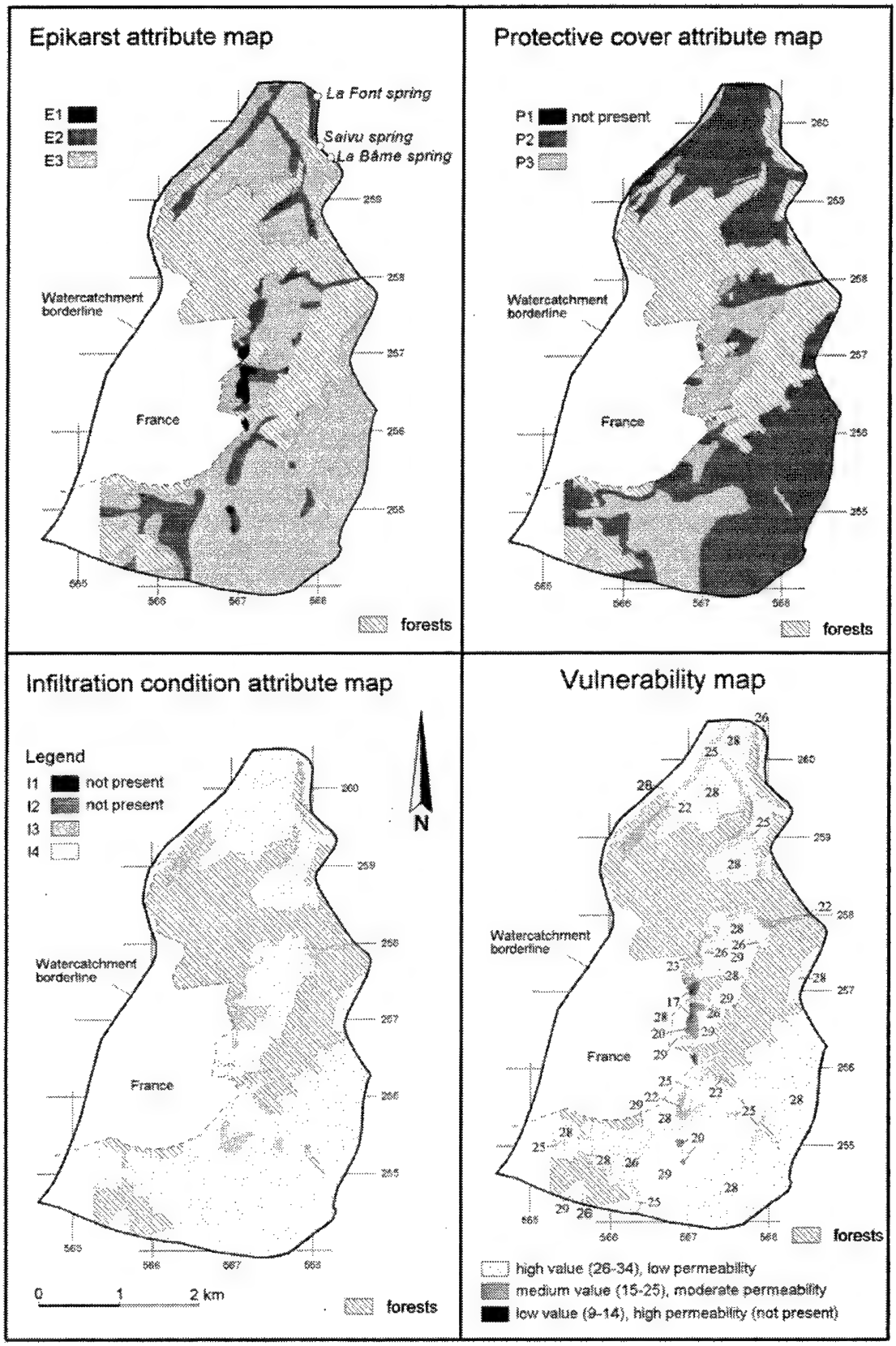

Figure 3: Maps of epikarst (E), protective cover (P) and recharge type (I) of the Milandre catchment area in northern Switzerland. The conduit network is known to be well developed over the whole catchment area. Combining the first three maps gives the vulnerability map shown at the bottom right (from Doerfliger 1996).

ANALYTICAL MODELS

Analytical models are based on quantitative relationships derived from known (or assumed) physical laws. Although most such models contain coefficients that must be determined experimentally, the relationships among variables are based on well-accepted principles such as equations for fluid flow, chemical kinetics, and conservation of mass. Their refined pedigree tends to make them more convincing to the scientific community than purely conceptual models, but it is difficult to combine the many interrelated processes by purely analytical methods. Thus analytical models are not often able to achieve the great breadth that their conceptual and digital cousins do.

Perhaps the earliest analytical karst model was that of Weyl (1958), who, in an attempt to show rates of solutional enlargement of conduits, came away puzzled as to how solution conduits could form at all, since the solvent water seemed to approach saturation too quickly. Howard (1964) calculated that the enlargement rate should increase several times at the laminar-turbulent transition. Wigley (1975) brought the subject still farther by using an analogy with heat flow. Cave patterns observed in the field were explained in purely hydraulic terms by Palmer (1975).

Laboratory experiments since the mid-1970s (see references cited in the first paper of this section) provide an accurate means for calculating rates of cave development (e.g. White, 1977; Palmer, 1981; Dreybrodt, 1996), which agree fairly well with those measured in the field and also resolve the puzzle faced earlier by Weyl. Dreybrodt (1996) has carried analytical methods for dissolution rate to a surprisingly high level.

Analytical methods have also been used to solve more specific karst problems. For example, Curl (1974) developed a method for determining the former flow velocity of water from the length of solutional scallops in cave walls. This work was based on a combination of dimensional analysis and laboratory experiments, combined with purely analytical methods for integrating the flow velocity across the entire passage cross section. The result is a handy tool for interpreting paleo-hydrology by calculating former flow velocity and discharge in relict conduits.

These are a few representative examples of analytical models in karst. In the general field of groundwater, the most widely used analytical model of all is the Theis method for interpreting aquifer characteristics from well tests, later simplified by Jacob (1940). Use of the Jacob method is demonstrated in the paper by Jones in the final section of this volume.

Not all of the papers that follow are purely analytical. The first is an elaboration of a conceptual model, and one or two others are highly empirical. However, they are all based primarily on analytical expressions.

References cited

Curl, R.L., 1974, Deducing flow velocity in cave conduits from scallops: Natl. Speleological Soc. Bull., v. 36, p. 1-5.

Dreybrodt, W., 1996 Principles of early development of karst conduits under natural and man-made conditions revealed by mathematical analysis of numerical models: Water Resources Research, v. 32, p. 2923-2935.

Howard, A.D., 1964, Processes of limestone cave development: International Jour. of Speleology, v. 1, p. 47-60.

Palmer, A.N., 1975, The origin of maze caves: National Speleological Society Bulletin, v. 37, p. 56-76.

Palmer, A.N., 1981, Hydrochemical controls in the origin of limestone caves: 8th International Speleological Congress, Proceedings, Bowling Green, Kentucky, p. 120-122.

Jacob, C.E., 1940, On the flow of water in an elastic artesian aquifer: American Geophysical Union Transactions, v. 2, p. 574-586.

Weyl, P.K., 1958, Solution kinetics of calcite: Journal of Geology, v. 58, p. 163-176.

White, W.B. 1977, Role of solution kinetics in the development of karst aquifers, *in* J.S. Tolson and F.L. Doyle (eds.), Karst hydrogeology: International Association of Hydrogeologists, 12th Memoirs, p. 503-517.

Wigley, T.M.L., 1975, Speleogenesis: a fundamental approach: Proceedings of 6th International Congress of Speleology, Oloumec, Czechoslovakia, vol. 3, p. 317-324.

PATTERNS OF DISSOLUTION POROSITY IN CARBONATE ROCKS

Arthur N. Palmer
Department of Earth Sciences, State University of New York
Oneonta, NY 13820-4015

Introduction

Unlike most geologic processes, the origin of dissolution porosity lends itself readily to analytical solutions. Four salient "laws" govern the process: two mass balances (water balance and chemical mass balance) and two kinetic equations (which describe the dissolution rate and the flow rate of water), and in combination they provide a theoretical basis for quantifying the solutional history of karst aquifers. The greatest difficulty is in applying these clean-cut analytical tools to the complex and rather disordered world of geology. It is impossible to model a karst aquifer in all its details, because most of the details are unknown.

However, a great deal can be learned about the origin and distribution of dissolution porosity by using the analytical approach to obtain a battery of governing concepts that can be applied to all karst aquifers. This paper summarizes the evolution of a conceptual model whose details were first developed on the basis of field observation and hydraulics, and only later substantiated by chemical kinetics. It applies specifically to carbonate rocks, although the general approach can be modified to fit any geologic setting by substituting the appropriate expressions for kinetics and fluid flow.

General distribution of karst porosity

The appropriate first step relies on concepts that are well known to everyone. Water, where it first enters a soluble rock, is undersaturated with respect to the minerals in that rock. Its saturation ratio (C/C_S) with respect to these minerals is at, or close to, zero. (C = concentration of dissolved mineral, e.g. calcite; C_S = saturation concentration, which is greatly enhanced by acids. C_S for calcite in typical groundwater is about 2-3 mmol/L.) Dissolution is most rapid where C/C_S is lowest, and its rate diminishes as the dissolved load increases. The greatest dissolution occurs where the water first enters the soluble rock and diminishes with flow distance. Thus most of the water's solutional aggressiveness is usually squandered at and near the bedrock surface, simply lowering the surface and widening the upstream ends of fissures that penetrate the rock (Figure 1). Underground water circulating through the rock has greatly diminished aggressiveness, but unless C_S decreases (e.g. by CO_2 degassing, rising temperature, or common-ion effects) the water will never quite reach saturation. Since the flow of water is con-tinuous from recharge source to outlet, and the relatively high C/C_S allows dissolution to proceed only at a slow rate, the dissolution porosity is drawn out along the entire length of the flow paths. Aggressiveness can be maintained by a gradual rise in C_S, for example by oxidation of organic compounds. Aggressiveness can also undergo a local burst because of mixing of different waters or by oxidation of hydrogen sulfide. However, in a typical karst aquifer the solutional porosity tends to form continuous conduits rather than isolated voids (Figure 1). The diminution of dissolution porosity with depth in karst aquifers is well documented by borehole data (Figure 2).

Introductory geology textbooks typically portray karst porosity in cross sections that resemble blocks of Tilsit cheese, with the holes elongated along beds and fractures as a gratuitous nod to the influence of geology. This portrayal would be amusing, were it not for the fact that many scientists and engineers, perhaps subconsciously, use the same conceptual view of karst when attempting to solve environmental problems. The real distribution of karst porosity is more complex, but also more predictable.

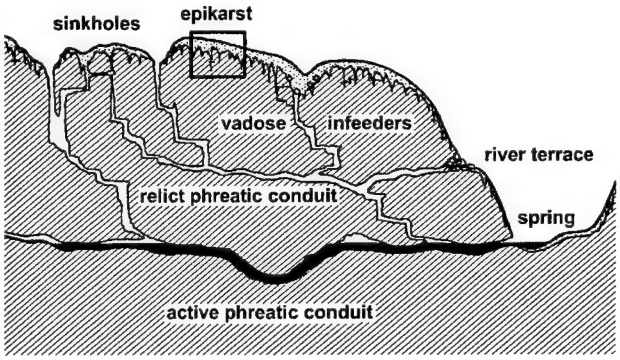

Figure 1: Generalized cross section of a karst aquifer formed by meteoric water, showing relative distribution of dissolution voids. The apparent porosity is exaggerated in the diagram for clarity. Below the epikarst the total dissolution porosity rarely exceeds a few percent and is commonly far less (see paper by Worthington in this volume).

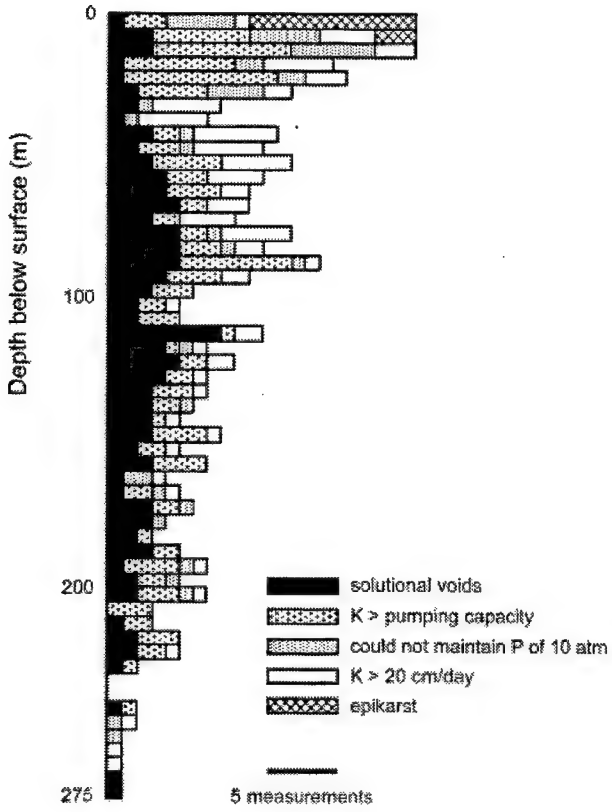

Figure 2: An example of the variation in karst porosity with depth, as observed in deep boreholes in Herzegovina (Modified from Milanović, 1981).

Within karst aquifers, most of the dissolution porosity consists of conduits, usually arranged in dendritic patterns in which tributaries join each other to produce fewer but larger conduits in the downstream direction. When we visit a cave of this kind, our conception of dissolution porosity can easily be skewed. The impression is that the overall dissolution porosity must be enormous. However, it is concentrated in only a relatively few conduits, which, if compared to the overall rock volume, yield only a tiny porosity, usually less than a percent (see Worthington, in this volume, for representative examples). In the most complex part of Mammoth Cave, Kentucky, Palmer (1995) calculated the total dissolution porosity to be only 4%, even though the figure includes many more inactive relict passages than active ones. Most accessible caves are surrounded by rock in which the vast majority of openings have hardly enlarged at all. The conduits are not surrounded by porous zones, with walls like a sponge, where progressively smaller openings extend indefinitely into the cave wall. The conduits are quite discrete.

As shown by the morphology of cave passages, the flow of aggressive water through karst aquifers takes place mainly along fractures and bedding-plane partings, and much less so along primary pores. It is important to note that fractures and partings diminish in width and number with depth (see Ford and Ewers, 1978, and Ford in this volume). Provided the openings are too small to admit turbulent flow, the flow is described by the Hagen-Poiseuille equation:

$$Q = \frac{w^3 b \gamma}{12 \mu} \left(\frac{dh}{dL} \right) \qquad (1)$$

where Q = discharge, w = fissure width, b = fissure breadth (long dimension of fissure cross section), γ = specific weight of water, μ = dynamic viscosity of water, and dh/dL = hydraulic gradient. Although groundwater can pass through all openings in varying amounts, note the strong dependence of flow on fissure width. Since w diminishes downward, one can assume that the water will preferentially follow shallow paths, far more so than in aquifers whose pore size does not decrease so significantly with depth (for example, gravel). This applies to fractured bedrock aquifers of all types, but especially in soluble rocks where the initial openings are enlarged by the flow. As these openings grow, some will enlarge more rapidly than others. They are the ones that grow to cave size and which eventually dominate the flow pattern within the aquifer. The onset of turbulent flow is often used to distinguish the birth of a karst conduit.

This discussion applies mainly to phreatic water. Gravitational vadose water is easily perched for some distance on resistant or relatively insoluble beds, providing a strong lateral com-ponent to the flow, interrupted by shafts where the perching beds are breached by fractures (see paper by Palmer under Statistical Models).

The tendency for conduits not to penetrate far below the potentiometric surface is disrupted to some extent by faulting and folding. In tectonically disturbed areas it is possible for certain flow paths to extend to considerable depths, especially along faults. For example, in a catalog of solutional voids encountered beneath river beds during drilling by the Tennessee Valley Authority (Moneymaker, 1941), the deepest voids are encountered in the folded and faulted Appalachians and in the fault zone of western Kentucky. Ford (1971) emphasized low fissure frequency as the main criterion for why certain caves extend deep beneath the potentiometric surface, whereas Palmer (1969) emphasized fissure width. The two contrasting views are nevertheless compatible.

Despite this disruption, the shallowest paths are still the most favorable, even in tectonically disturbed areas, and deep conduits are relatively rare. Pervasive deep flow is

likely only in confined settings, or where favorable stratigraphic boundaries allow deep dissolution (for example, along sulfate-carbonate interfaces). Worthington (1991) cites many examples of sulfate-rich springs fed by groundwater that follows deep basin-wide paths.

Rates of conduit growth

In a fissured aquifer with myriad flow paths, which ones are most likely to enlarge into solution conduits? This is not a trivial question, because the presence and distribution of conduits is one of the most important variables in the assessment of a karst aquifer. Phreatic conduits form potentiometric lows and are the main paths of groundwater discharge, as well as the major paths of contaminant transport. The configuration of vadose channels determines how sources at the surface relate to the points of recharge at the underlying water table.

In most carbonate aquifers only a small percentage of flow routes enlarge into turbulent-flow conduits. Early in the flow history of the aquifer, fissures are narrow and the flow is dispersed among many different routes, each with its own overall hydraulic gradient, mean fissure width, total flow length, and mean discharge. Groundwater discharge and velocity are so small that the water becomes nearly saturated with dissolved bedrock long before it emerges at the surface. This can be verified by measuring the chemistry of inflowing seepage through narrow openings into accessible caves. Even some substantial flows of several cm^3/sec arrive essentially at C/C_s =1.0 after less than 50 m of flow. Therefore, in any single flow route, the rate of dissolutional enlargement depends simply on the chemical mass balance. The mass of material removed from the walls of the opening is equal to the mass removed in solution by the groundwater flow. This rule is independent of the shape of the opening (tube, fissure, etc.).

The chemical mass balance can be stated as follows: Mass removed from the walls of the opening = mass carried away in solution. Change in mass with time = $\rho\, \Delta V/\Delta t = Q\Delta C$, where ρ = rock density, $\Delta V/\Delta t$ = change in volume with time, and ΔC = change in dissolved load over the length of the conduit. A conduit of circular cross section is assumed for convenience; the actual conduit shape is not important, since the functional relationships are the same. Thus, within any single conduit segment of rather uniform dimensions, the rate of wall retreat (S) can be stated

$$S = \frac{31.56\, Q\,(C - C_o)^n}{2\pi r\, \rho\, L} \qquad \text{[cm/yr]} \quad (2)$$

where C_o = initial concentration of dissolved bedrock (mg/L), r = conduit radius (cm), and L = conduit length (cm). All other terms are in cgs units. The numerical coefficient converts the result to cm/yr. A uniform radius is not required, since we are concerned only with mean values of S, Q, and r, and again the functional relationships are not affected.

Early in the evolution of a karst aquifer, when the water emerges from each opening essentially at saturation, if we assume that $C_o = 0$, then $\Delta C = C_s$, which is constant at a given temperature and CO_2 partial pressure. Under these conditions, the mean rate of wall retreat within each conduit is therefore a linear function of Q/rL.

The mean S values plot as the family of lines shown in group A of Figure 3 (10° C, P_{CO2} = 0.01 atm). At any value of r, the larger the Q/L ratio, the greater the rate of enlargement. Large Q and/or small L favor rapid enlargement. Dashed lines show the corresponding values of i/L, where i = hydraulic gradient, are also shown on Figure 3, valid only for laminar flow (derived from the tubular version of eq. 1, where $w^3b/12$ is replaced by $\pi r^4/8$).

The numerical values for S in Figure 3 are misleading, because (1) they assume that the water enters each conduit at zero saturation; (2) most of the dissolution is concentrated in the upstream end of the conduit, so that the rate throughout the majority of the conduit is less than the mean; and (3) they do not consider mixing or branching between different conduits. However, it is the relative values -- the general relationships among the terms -- that concern us here, not the specific numerical values. Actual growth rates are best determined with finite-difference calculations or analytical methods (e.g. Palmer, 1984, 1991; Dreybrodt, 1990, 1996; Groves and Howard, 1994a

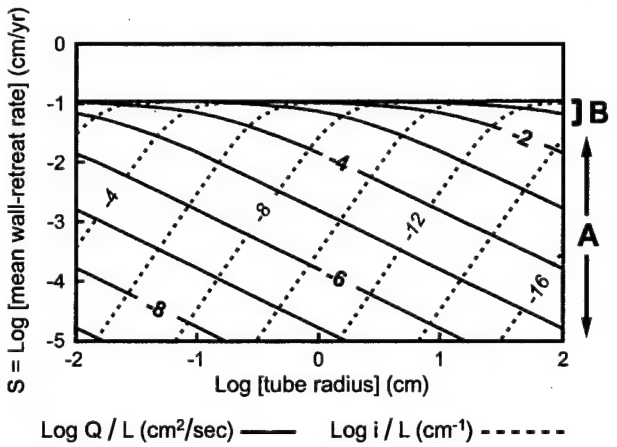

Figure 3: Mean rate of wall retreat (cm/yr) as a function of discharge (Q), flow distance (L), hydraulic gradient (i), and tube radius (r) in tubular conduits at 10° C and P_{CO2} = 0.01 atm (C_s = 212 mg/L $CaCO_3$). Values of i/L are valid only for laminar flow. **A** = region of varied growth rates (Q/rL < 0.001 cm/sec); **B** = maximum possible solutional growth rate, limited by chemical kinetics. (From Palmer, 1981.)

and b; Clemens et al, 1996; Hanna and Rajaram, 1998).

The earliest conduit growth usually begins somewhere in (or beyond) the lower left portion of Figure 3. Growth rates are far too low to allow turbulent-flow conduits to develop in a geologically feasible time. Within any given conduit, the growth rate can increase only if Q increases, since L does not change. If Q does not increase, the enlargement rate will remain static or actually decrease, as shown by the negative slope of the lines in group A as the conduit radius increases. (Conduits of non-circular cross section would have more gently sloping lines in group A.)

But the growth rate reaches an upper limit beyond which it cannot rise. This is typically about 0.001-0.01 cm/yr, depending on the chemical conditions. So far the analysis has been focused on narrow openings in which the water emerges near saturation. Now consider a conduit with such a large Q/L ratio that water is able to pass through the conduit while retaining nearly all its aggressiveness. The entire conduit enlarges at a nearly uniform rate (shown as B in Figure 3), which is a function of the dissolution kinetics, rather than of the mass balance. Rates of wall retreat are almost uniform and independent of Q/L.

Experiments by Berner and Morse (1974), Plummer and Wigley (1976), Plummer et al. (1978) show that in turbulent flow the dissolution rate for calcite is governed mainly by the chemical reactions at the wall, rather than by mass transfer within the fluid, and that turbulence and flow velocity have little effect on. Mass transfer does have an effect at low flow rates in limestone conduits (Curl, 1968; Buhmann and Dreybrodt, 1985a and b, Dreybrodt, 1988), and in evaporites at any flow rate, but the pattern of lines in group A in Figure 3 is not affected.

For carbonate rocks, the dissolution rate is expressed by

$$\frac{dC}{dt} = \frac{A'k}{V}\left(1 - C/C_s\right)^n \qquad \text{[mg/L-sec]} \quad (3)$$

where A' = surface area of rock in contact with water, V = water volume, k = reaction coefficient, and n = reaction order. It is more common for the parenthetical term to be expressed as $(C_s - C)$, but the form shown in eq. 3 avoids the problem of having to adjust the units of k whenever n changes. Values of k and n depend on the acid content of the water (for example, P_{CO2}), and k also varies with temperature and lithology (Palmer, 1991, derived from the original lab measurements of Plummer et al., 1978, Plummer and Wigley, 1976, Rauch and White, 1977, and other sources). The reaction order (n) increases rather abruptly from 1-2 to 4 or more at C/C_s values that range from about 0.6 to 0.9, depending on temperature and P_{CO2} (Palmer, 1991; Dreybrodt et al. in this volume). In typical groundwater, $n \approx 2$ (or 1, in narrow conduits) and $k \approx 0.01$ at C/CS $<\approx 0.65$. At greater C/C_s, $n \approx 4$ (occasionally more; see Dreybrodt et al., this volume) and $k \approx 0.1$.

Because $C/C_s < 1$, an increase in reaction order represents a decrease in dissolution rate. Ironically, this decrease appears to be essential to the origin of nearly all solution conduits (Palmer, 1984). If the low-order (rapid) kinetics were to prevail throughout the initial opening, virtually all the aggressiveness would be consumed within a few meters of flow, except in usually wide fissures, and the growth rate would be so slow in the rest of the conduit that it would never achieve turbulent flow within a geological feasible time. On the other hand, the high-order (slow) kinetics alone are too slow to enlarge the conduits to the size of traversable caves. White (1977) called the change from slow to rapid dissolution a "kinetic trigger" that represents the beginning of true cave development. Thus cave origin enjoys the best of both worlds: slow growth when the aggressiveness must persist for long distances through narrow fissures, and later rapid growth to achieve large size.

Combining eqs. 2 and 3, and substituting $Q = V/t$ and $A' = 2\pi rL$, gives the following general equation for dissolutional wall retreat in carbonate rocks:

$$S = \frac{31.56\,k\,(1 - C/C_s)^n}{\rho} \qquad \text{[cm/yr]} \quad (4)$$

which is valid for all types of flow and conduit geometries (Palmer, 1991). The maximum rate of wall retreat (aside from occasional mechanical erosion during floods in large conduits) can be determined by this equation, where C/C_s = saturation ratio where the water enters the conduit. In Figure 3, the maximum rate at B is for $C/C_s = 0$. Higher saturation ratios, even as high as 0.9, still provide enlargement rates that are rapid by geological standards, and the overall shape of the graph in Figure 3 remains valid.

The composite graph in Figure 3 shows both the early laminar flow (S dependent on Q/L) and the late-stage flow (S independent of Q/L). The curvature of the lines where Zone A meets Zone B was determined by finite-difference analysis.

It is not realistic to assume that water can pass through an entire aquifer without changing its saturation ratio. The water acquires most of its solute load at the upstream end, especially where it accumulates in small openings that feed the main conduits. The maximum enlargement rate in a conduit is thus limited in part by the value of C_o at its upstream end, which is rarely less than 0.5. High-Q flow can pass through a cave-size conduit for great distances while gaining only a few mg/L of dissolved load. Because of the large Q, this still represents a substantial rate of mass flux.

Competition between enlarging flow paths: unitary conduits and branchworks

The specific configuration of conduits within the aquifer is determined by the relative growth rates of competing flow paths. The most common situation, where meteoric groundwater passes through a carbonate unit from an upland recharge surface to outlets at lower elevation, can be described as follows:

1. Early in the flow history of the aquifer, the many alternate flow routes have low Q/L ratios and plot in or beyond the lower left corner of Figure 3. Their Q/L values and rates of conduit growth span a wide range of many orders of magnitude. All growth rates are small, but some will be much greater than others. The dots on Figure 4 show some representative flow paths early in the aquifer development. These are idealizations, because no single flow path behaves entirely independently.

2. Growth rate can increase only if the Q/L ratio increases. For any given path, this can be achieved only by an increase in discharge. As each opening grows, its discharge tends to increase because more water is able to pass through. But there is a maximum amount of available infiltration, and eventually a conduit can acquire additional Q only at the expense of its neighbors. This is achieved in two ways: (a) As a conduit grows, its hydraulic head decreases (despite increasing Q) because of the reduced amount of head loss required to transmit the flow. Water is drawn from neighboring openings in which the head is greater, which increases the discharge in the major conduits. (b) Sinkholes develop as the major openings and their tributaries enlarge, especially at the upstream ends, funneling water into the largest conduits but bypassing lesser openings. As a result, the openings with the largest initial Q/L or i/L are those that are most likely to acquire increasing flow and to increase their enlargement rate. As shown by the arrows in Figure 4, some openings are favored over their neighbors and increase rapidly in both Q and S. Others languish with negligible and generally decreasing Q and S.

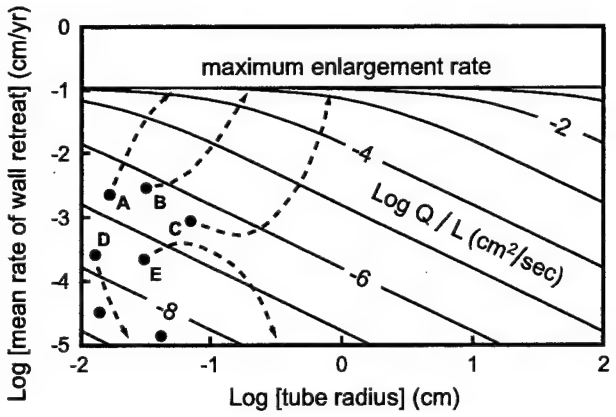

Figure 4: Varied growth histories of competing flow paths in the early stages of a karst aquifer. Paths A, B, and C accelerate in growth and reach the maxium rate by increasing their discharge. These are the routes that become major dissolution conduits. In contrast, other paths (e.g. D and E) stagnate at low and usually diminishing enlargement rates.

3. Enhanced discharge is able to increase the enlargement rate only up to a certain point, beyond which the rate becomes insensitive to further increases in Q. The enlargement rate is now limited mainly by the dissolution kinetics. Those relatively few conduits that reach this state grow at approximately the same rapid rate, with only minor differences caused by local variations in chemistry, flow, and passage configuration. Traversable caves are formed by water that has achieved this state.

Single-passage stream caves and branchwork caves are the normal result. Branching caves are by far the most common, because of the tendency for convergence of flow toward the relatively low head of the major conduits, and because of fortuitous intersections between passages. The typical passage pattern is similar to that in Figure 5a. This example is located in prominently bedded, low-dip strata. Greater structural complexity leads to comparable passage complexity, but the overall cave pattern is usually a branchwork.

Uniform dissolution among many competing flow routes: labyrinthine porosity

Under certain conditions, nearly every competing flow route enlarges at comparable rates, and a labyrinth of interconnected openings is formed. According to Figure 3, the only way this can happen is to expose many openings simultaneously to high values of Q/L or i/L. Beyond a certain threshold (Q/rL > 0.001 cm/sec in tubes, Q/bL>0.001 cm/sec in fissures), they will all enlarge at rather similar rates, regardless of size, discharge, gradient, or flow length. The result is a labyrinth of interconnected passages consisting of openings that have grown simultaneously to cave size. Caves formed under these conditions have maze patterns (Figure 5 b, c, and d). Favorable conditions include the following:

Where aggressive water first enters the soluble rock (small values of L). Distances of flow from the entry points are short, and all openings have large Q/L values regardless of opening size or discharge. The most common example is the epikarst, the zone of extensive dissolution in the upper few meters or tens of meters of the soluble rock, located either beneath a soil cover or exposed directly at the surface (Figure 1). The same approximate result is achieved where

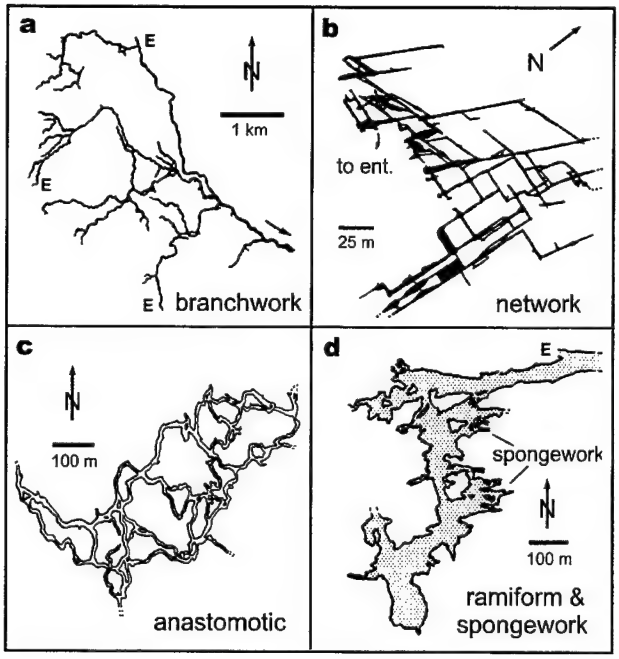

Figure 5: Examples of solutional cave patterns: **(a)** Crevice Cave, Missouri, **(b)** part of Crossroads Cave, Virginia, **(c)** part of Höloch, Switzerland, **(d)** main rooms of Carlsbad Cavern, New Mexico. Maps courtesy of Paul Houck, H.H. Douglas, Alfred Bögli, and Cave Research Foundation, respectively. E = entrance.

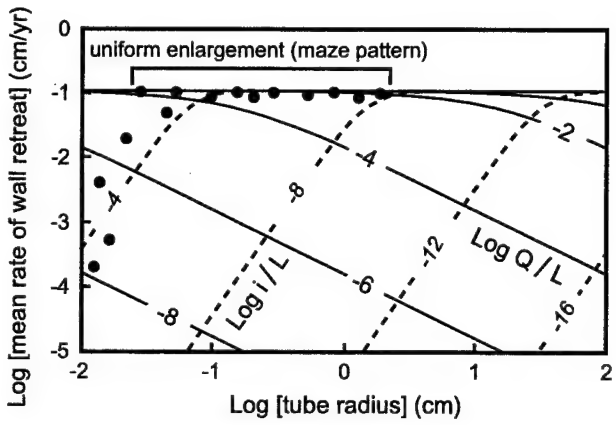

Figure 6: Many alternate routes are able to enlarge simultaneously at roughly the same rate, regardless of size, if they are all able to sustain high discharges (e.g. because of steep hydraulic gradients) or short flow distances. Maze caves, epikarst, and pervasive labyrinthine porosity are produced in this way. Very small openings, or those with low *Q/L* or *i/L* will not be competitive.

water passes through a porous, non-soluble rock before entering the carbonate rock, forming a maze cave. Network caves formed along intersecting fractures are the most common type (Figure 5b). The flow of water can be downward from the overlying surface or upward as artesian flow from an underlying formation (provided the water has not encountered substantial amounts of carbonate rock beforehand).

It is also possible to enlarge many alternate flow routes simultaneously where steep hydraulic gradients are imposed by flooding. This is most noticeable where soluble rock is exposed adjacent to entrenched rivers that flood severely. Water enters the ground as bank storage having high *i/L* ratios because of the steep gradients and short flow distances. The same effect is achieved in local areas within preexisting caves where flow constrictions (breakdown, sediment fill, interference by relatively insoluble beds) cause floodwater to pond upstream from them. Seasonal or storm-related flooding periodically injects aggressive water into every available opening, enlarging them rapidly and simultaneously. Irregular network caves (western part of Figure 5b) are formed where vertical or steeply inclined fractures dominate. Anastomotic caves are formed where bedding-plane partings or low-angle faults are the main cave-forming units. Where matrix porosity provides the major flow paths, for example in diagenetically young limestones, breccias, or reef rock, a spongework pattern will form (as illustrated in parts of Figure 5d).

Where steep hydraulic gradients are sustained (e.g. beneath dams), growth rates rise steeply in all conduits as *r* increases, as shown by the dashed lines in Figure 3, until they all reach the maximum rates of wall retreat at or near the top of the graph. A network of similarly enlarged conduits is expected (Palmer, 1988; Dreybrodt, 1996; Bauer et al., Digital Modeling section of this volume).

Solutional aggressiveness can be renewed in zones of mixing between chemically contrasting waters, for example between infiltrating high-CO_2 freshwater and low-CO_2 seawater. Local network and spongework patterns are produced, not only because the flow distances from the source of aggressiveness are short, but because of the diffuse nature of most water flow under these circumstances. Carbonate aquifers in coastal and island settings are noted for this kind of porosity (Back and others, 1984; Mylroie and Carew, 1990; Mylroie and Vacher, this volume).

Mixing between rising (often thermal) waters and meteoric water is capable of producing considerable aggressiveness (see abstract by Luiszer in this volume). Caves formed in this way tend to have network or irregular ramiform patterns (Figure 5 b and d).

Oxidation of rising hydrogen sulfide rising from depth into oxygen-rich zones at or near the water table produces a burst of localized dissolution. This process usually results in network and ramiform caves, consisting of large irregular rooms with sequential branches exiting to the surface (Figure 5d). The outflow usually coalesces into discrete conduits as aggressiveness is lost and flow length increases.

Summary

This simplified view of the distribution of karst porosity leads to several conclusions, which are summarized below:

Karst porosity is greatest near the land surface in areas of groundwater recharge (for example, in the epikarst). It diminishes in the downflow direction but coalesces into relatively few major conduits that are continuous through the entire aquifer. Except in mixing or redox zones, karst porosity rarely occurs as isolated voids. Branching conduit patterns are the most common.

Conduits form only where the setting is favorable for certain flow paths to gain discharge at the expense of their neighbors, e.g. by development of sinkholes.

Dissolution labyrinths, in which every accessible opening is enlarged to comparable amounts, form in several settings: (a) within short distances of flow from where aggressive water first enters a soluble rock, or where mixing or redox reactions produce local zones of undersaturated water within a karst aquifer; (b) in areas of steep hydraulic gradient, where Q/L and i/L are large.

Dissolution porosity diminishes greatly at depths beneath the local base level because of the very strong influence of fissure widths on resistance to flow.

Use of these concepts can aid in the prediction of porosity distribution and geometry. However, it must be recognized that relict karst porosity can also occur where conditions favorable to its origin are no longer present. Also, details of geologic structure must be considered. These ideas are developed further in the literature, including many papers in this volume and the references that they cite.

The concepts described here have not changed significantly since their first brief publication in 1981, although they have been explored at greater length since by more advanced geochemical and digital models (see Palmer, 1991, 1995, and the papers in the Digital Modeling section of this volume). The model described in Figure 3 was generalized from the behavior of individual conduits. However, subsequent digital modeling of multiple-conduit networks has validated these concepts.

References Cited

Back, W., B. Hanshaw, and J.N. Van Driel, 1984, Role of groundwater in shaping the eastern coastline of the Yucatan Peninsula, Mexico, *in* R. G. LaFleur (ed.), Groundwater as a geomorphic agent: Boston, Mass., Allen and Unwin, Inc. p. 281-293.

Berner, R.A., and J.W. Morse, 1974, dissolution kinetics of calcium carbonate in sea water, IV: Theory of calcite dissolution: American Journal of Science, v. 274, p. 108-134.

Buhmann, D., and W. Dreybrodt, 1985a, The kinetics of calcite solution and precipitation in geologically relevant situations of karst areas. 1: Open system: Chemical Geology, v. 48, p.189-211.

Buhmann, D., and W. Dreybrodt, 1985b, The kinetics of calcite solution and precipitation in geologically relevant situations of karst areas. 2: Closed system: Chemical Geology, v. 53, p. 109-124.

Clemens, T, D. Hȗckinhaus, M. Sauter, R. Liedl, and G. Teutsch, 1996, A combined continuum and discrete network reactive transport model for the simulation of karst development, *in* Calibration and reliability in groundwater modeling, Proceedings of the ModelCARE 96 Conference held at Golden, Co., Sept. 1996: UAGS Publ. No. 237.

Curl, R.L., 1968, Solution kinetics of calcite: Proceedings of 4th International Congress of Speleology, Ljubljana, Slovenia, p.61-66.

Dreybrodt, W., 1988, Processes in karst systems: physics, chemistry and geology: Berlin, Germany, Springer-Verlag, 288 p.

Dreybrodt, W., 1990, The role of dissolution kinetics in the development of karst aquifers in limestone: a model simulation of karst evolution: Journal of Geology, vol. 98, no. 5, p. 639-655.

Dreybrodt, W., 1996 Principles of early development of karst conduits under natural and man-made conditions revealed by mathematical analysis of numerical models: Water Resources Research, v. 32, p. 2923-2935.

Ford, D.C., 1971, Geologic structure and a new explanation of limestone cavern genesis: Transactions of the Cave Research Group of Great Britain, v. 13, no. 2, p. 81-94.

Ford, D.C., and R.O. Ewers, 1978, The development of limestone cave systems in the dimensions of length and

depth: Canadian Journal of Earth Sciences, v. 15, p. 1783-1798.

Groves, C.G., and A.D. Howard, 1994a, Minimum hydrochemical conditions allowing limestone cave development: Water Resources Research, v. 30, no. 3, p. 607-616.

Groves, C.G., and A.D. Howard, 1994b, Early development of karst systems, 1. Preferential flow path enlargement under laminar flow: Water Resources Research, v. 30, no.10, p. 2837-2846.

Hanna, R.B., and H. Rajaram, 1998, Influence of aperture variability on dissolutional growth of fissures in karst formations: Water Resources Research, v. 34, no. 11, p. 2843-2853.

Milanovic, P.T., 1981, Karst hydrogeology: Littleton, Colorado, Water Resources Publications, 434 p.

Moneymaker, B.G., 1941, Subriver solution cavities in the Tennessee Valley: Journal of Geology, vol. 49, p. 74-86.

Mylroie, J. E., and J.L. Carew, 1990, The flank margin model for dissolution cave development in carbonate platforms: Earth Surface Processes and Landforms, v. 15, p. 413-424.

Palmer, A.N., 1969, A hydrologic study of the Indiana karst: Ph.D. thesis, Indiana Univ., Bloomington, Ind., 181 p.

Palmer, A.N., 1981, Hydrochemical controls in the origin of limestone caves: 8th International Speleological Congress, Proceedings, Bowling Green, Kentucky, p. 120-122.

Palmer, A.N., 1984, Recent trends in karst geomorphology: Journal of Geological Education, v. 32, p. 247-253.

Palmer, A.N., 1988, Solutional enlargement of openings in the vicinity of hydraulic structures in karst regions: Association of Ground Water Scientists and Engineers, 2nd Conference on Environmental Problems in Karst Terranes and their Solutions, Proceedings, p. 3-15.

Palmer, A.N., 1991, Origin and morphology of limestone caves: Geological Society of America Bulletin, v. 103, p. 1-21.

Palmer, A.N.,1995, Geochemical models for the origin of macroscopic solution porosity in carbonate rocks, *in* D.A. Budd, P.M. Harris, and A. Saller (eds.), Unconformities in carbonate strata: their recognition and the significance of associated porosity: American Association of Petroleum Geologists, Memoir 63, p. 77-101.

Plummer, L.N., and T.M.L. Wigley, 1976, The dissolution of calcite in CO_2-saturated solutions at 25° C and 1 atmosphere total pressure: Geochimica et Cosmochimica Acta, v. 40, p. 191-202.

Plummer, L.N., T.M.L. Wigley, and D.L. Parkhurst, 1978, The kinetics of calcite dissolution in CO_2-water systems at 5° to 60° C and 0.0 to 1.0 atm CO_2: American Journal of Science, v. 278, p. 179-216.

Rauch, H.W., and W.B. White, 1977, Dissolution kinetics of carbonate rocks. 1. Effects of lithology on dissolution rate: Water Resources Research, v. 13, p. 381-394.

White, W.B. 1977, Role of solution kinetics in the development of karst aquifers, *in* J.S. Tolson and F.L. Doyle (eds.), Karst hydrogeology: International Association of Hydrogeologists, 12th Memoirs, p. 503-517.

Worthington, S.R.H., 1991, Karst hydrogeology of the Canadian Rocky Mountains: Ph.D. dissertation, McMaster University, Hamilton, Ont., 227 p.

KARSTIC PERMEABILITY: ORGANIZED FLOW PATHWAYS CREATED BY CIRCULATION

Peter W. Huntoon
Department of Environmental Studies, University of Nevada
Las Vegas, NV 89154-4030

Abstract

Most karstic permeability in soluble rocks is created by the circulation of a solvent through the rock. Given a bit of geologic time, karstic permeability develops a hierarchal structure of highly organized conduits that facilitates the movement of the fluid in the downgradient direction. Consequently, karst permeability is not an independent, inherited static attribute of the rock; rather it adjusts dynamically to changing boundary conditions in the flow system.

Karstic permeability tends to be the most anisotropic of all the permeability types found in nature. The permeabilities of the dissolution channels generally overwhelm the transmissive characteristics of all the other types of permeability present. Consequently, when dealing with assessments of the impacts of withdrawals or the migration of contaminants in carbonate aquifers, the professional is obligated to find and unravel the character of the organized conduit network; otherwise the essence of the transmissive and storage properties of the flow regime is inadequately formulated, so predictive failures are inevitable.

Karstic permeability

Carbonate aquifers are readily soluble (Palmer, 1991). The single most distinguishing feature of karst aquifers when contrasted with other aquifer types is that the permeability structure within them is predominantly created by the flow regime. As a result, the permeability is not an independent, inherited static attribute of the rock, but rather is highly dynamic over geologic time. Because karstic permeability is created by fluid flow, it has a highly organized structure that facilitates circulation in the downgradient direction (see Bakalowicz and Mangin, 1980).

An equally important consideration is that the permeability structure can adjust as the flow regime responds to changing hydraulic boundary conditions. Thus, the hierarchy of permeability pathways and their organization within the aquifer are dictated by the hydrodynamic characteristics of the flow system operating within the recent geologic past and, to a variable degree, the characteristics of older flow systems (Ewers, 1982; Huntoon, 1985).

The dynamic evolution of karstic permeability can be intuitively illustrated. Lateral flow through an extensive carbonate aquifer can be adequately described using a two-dimensional partial differential equations such as:

$$\frac{\partial(T_x\frac{\partial h}{\partial x})}{\partial x}+\frac{\partial(T_y\frac{\partial h}{\partial y})}{\partial y}=S\frac{\partial h}{\partial t}+W \qquad (1)$$

where:

b = saturated thickness,
h = hydraulic head,
K = hydraulic conductivity,
S = storage coefficient,
t = time,
T = Kb,
T_x, T_y = anisotropic transmissivities at each point,
x, y = spatial coordinates, and
W = source-sink term.

Linkage between permeability and circulation in a soluble aquifer takes the form:

$$q_s=-K_s\frac{\partial h}{\partial s} \qquad (2)$$

where:

q = specific discharge,
s = general spatial coordinate, and
$\partial h/\partial s$ = hydraulic gradient;

but wherein:

$$K_{s(t)}=f(q_s)K_{s(t-1)} \qquad (3)$$

where t-1 and t indicate time progression.

Notice that equations 2 and 3 comprise a feedback mechanism that adjusts the hydraulic conductivity as dissolution progresses as a function of the latest available specific discharge through the rock (Worthington, 1991; Dreybrodt, 1988). Continual adjustment of the permeabilities in geologic time will inevitably produce a highly anisotropic permeability structure regardless of the permeability configuration in the initial state.

Genesis of karstic permeability is a hydrodynamic process that occurs over time. Successive views of the permeability structure in the aquifer are simulated by cycling through a loop comprised of equations 1, 2, and 3. A solution to equation 1, using appropriate boundary conditions, yields a map of the hydraulic head for a time step. Those heads are used in equation 2 to calculate the current specific discharges in the x and y directions at all points, and those specific discharges are in turn used in equation 3 to adjust T_x and T_y throughout the flow field.

Adjustments to T_x and T_y result in progressive increases in transmissivity and reorientations of the flow pathways. This is accomplished in nature by the successive imprinting of new, ever more favorably oriented dissolution voids through the rock mass, as well as by enlargement of those that already have favorable orientations. As the optimally oriented conduits become established, their size grows, allowing them to accommodate increasingly greater percentages of the total circulation through the aquifer. The progressive capture of flow increases the rate of dissolution enlargement within them, and their locations become increasingly fixed within the rock mass. The earlier tubes can become abandoned or hydraulically deactivated.

Conduit localization in soluble aquifers is a function of specific discharge. Consequently the primary variables governing the location of the conduits are hydraulic conductivity and gradient, as shown in equation 2. However, the hydraulic conductivity in a soluble aquifer is dependent on the hydraulic gradient, as revealed in equation 3. Accordingly, the independent variable that ultimately dictates conduit localization, given enough geologic time, is the hydraulic gradient. Heterogeneous geologic fabrics within aquifers, including tectonic structures and rocks with differing solubilities, ultimately become of secondary concern.

Competition between hydraulic conductivity and gradient

Important in the early stages of karstification, or after a significant reorganization of hydraulic boundary conditions, is the fact that both permeability and hydraulic gradient compete for dominance in determining where the conduits will localize in the aquifer. Geologic variables such as lithology and tectonic structure are of supreme importance early on because they allow for the establishment of the initial flow pathways through the rock. Fracture permeability associated with tectonic structures is often an especially important early consideration, because intercrystalline permeabilities within carbonate sequences are commonly negligible. In contrast, hydraulic gradient is a secondary factor at the beginning of the karstification process because the permeabilities through the unfractured parts of the aquifer are so small, and thus dissolution rates through those masses are negligible even if gradients are very large across them.

However, as time passes, the hydraulic gradient increasingly wins dominance, a condition forced by equation 3. It is apparent from this cursory analysis that conduits ultimately will develop in areas where gradients are steepest because those regions are subjected to the greatest flow and thus the greatest dissolution rates. The conduits will tend to adjust to orientations that parallel the gradient, given a bit of geologic time. The karst system can be considered mature when the adjustment is complete.

Unconfined and confined organization

There are organizational distinctions between conduit networks found in unconfined and confined karst aquifers. Unconfined karst systems usually have a permeability structure which has a hierarchal organization with similarities to a surface-water drainage network. Unconfined systems contain collector structures at or just below the surface, such as epikarst and sinkholes, which often occupy the unsaturated zone. These features feed to low-order tubes which in turn coalesce downgradient into successively better organized and higher-order caves similar in function to the branching tributaries found in surface-water basins. The higher the order, the more widely spaced the conduits in the rock mass. The Mammoth Cave system of Kentucky is an excellent example of this type of architecture (Quinlan and Ray, 1989). Complicated hydraulic short circuits, often stage dependent, commonly interconnect adjacent passage networks.

In contrast, dissolution cavities are more thoroughly interconnected and far more pervasively distributed in confined karst aquifers. Consequently, fully integrated 2- and even 3-dimensional maze-type tube networks tend to develop. The resulting architecture mimics the interconnections between pores in intergranular media, but vastly differs in scale. Wind Cave, South Dakota, is such a dewatered two-dimensional maze (Scheltens, 1984).

The explanation for the differing passage morphologies appears to be a function of the degree of saturation. Saturation in unconfined systems tends to be minimal because the highly permeable conduits that are present drain the rock, minimizing the volume of rock that is bathed in the solvent. In contrast, confined aquifers are fully saturated, thus maximizing the volume of rock interacting with the solvent. The result in unconfined systems is localized dissolution along fairly well-defined flow pathways in contrast to ubiquitous 2- and 3-dimensional dissolution in confined systems. Consequently develop-

ment of tube networks are favored in unconfined systems versus 2- and 3-dimensional mazes in confined systems. In addition, the distribution of passages tends to be more homogeneous and spread more widely in plan in confined systems. Thus artesian cave networks tend to exhibit considerably less hierarchal organization in the downstream direction then is found in unconfined networks. Large karstic permeabilities ensure that hydraulic gradients are very small. Gentle gradients facilitate the development of dissolution mazes which in turn maximizes storage within the aquifer

Mazes are not restricted to confined systems. They also develop in unconfined systems where gradients are small, which minimizes flow rates.

The greater the flow rate, the greater the anisotropy with respect to hydraulic conductivity. Unconfined systems therefore tend to be far more anisotropic then confined systems. Even so, there is a moderate to strong degree of anisotropy in the confined-aquifer mazes with the maximum principal permeability tensor aligned roughly parallel to the modern gradient, some paleo-hydraulic gradient, or a geologic fabric within the host rock that caused localization of dissolution.

Conclusion: karstic organization

The transmissive characteristics of a soluble aquifer are dominated by the presence of the highly organized, integrated network of dissolved conduits. There is a hierarchy among the tubes in which those in the downstream direction generally exhibit the greatest degree of organization and size.

One ramification of conduit organization is that it creates an extremely anisotropic permeability architecture. Velocities measured in the undissolved matrix and the largest conduits in Paleozoic carbonates range over 30 orders of magnitude (Quinlan and others, 1996). This range hints at the extreme permeability contrast that is possible between the minimum and maximum principal hydraulic conductivity tensors in karstified rocks. For example, contrast the hydraulic conductivities measured along a cave and perpendicular to the cavern wall.

An obvious consequence is that the bulk of the circulation takes place in the caves. More to the point, the disproportionately large transmissivities of well-developed cave networks in carbonate rocks so totally overwhelm the mechanical function of other permeability features that the latter are often almost inconsequential when assessing the bulk movement of fluids or the rates of migration of contaminants through the rock.

References cited

Bakalowicz, M., and A. Mangin, 1980, L'aquifère karstique, sa definition, ses characteristiques et son identification: Memoires hors Serie Société Geologique de France, no. 11, p. 71-79.

Dreybodt, W., 1988, Processes in karst systems: physics, chemistry, and geology: Berlin, Germany, Springer-Verlag, 288 p.

Ewers, R.O., 1982, An analysis of solution cavern development in the dimensions of length and breadth: McMaster University (Hamilton, Ontario, Canada), Ph.D. dissertation, 398 p.

Huntoon, P. W., 1985, Gradient controlled caves, Trapper-Medicine Lodge area, Bighorn Basin, Wyoming: Ground Water, v. 23, p. 443-448.

Palmer, A.N., 1991, Origin and morphology of limestone caves: Geological Society of America Bulletin, v. 103, p. 1-21.

Quinlan, J.F., G.J. Davies, S.W. Jones, and P.W. Huntoon, 1996, The applicability of numerical models to adequately characterize ground-water flow in karstic and other triple-porosity aquifers, *in* J.D. Ritchey and J.O. Rumbaugh (eds.), Subsurface fluid-flow (ground-water and vadose zone) modeling: American Society for Testing and Materials, Special Technical Paper 1288, p. 114-128.

Quinlan, J.F., and J.A. Ray, 1989, Groundwater basins in the Mammoth Cave region, Kentucky, showing springs, major caves, flow routes, and potentiometric surface: Friends of Karst, Mammoth Cave, KY, Occasional Publication 1 (map).

Sheltons, J.P., 1984, map of Wind Cave, Wind Cave National Park, Hot Springs, South Dakota: Wind Cave/ Jewel Cave Natural History Association.

Worthington, S.R.H., 1991, Karst hydrology of the Canadian Rocky Mountains: McMaster University (Hamilton, Ontario, Canada), Ph.D. dissertation, 227 p.

INTERPRETING FLOW USING PERMEABILITY AT MULTIPLE SCALES

Todd Halihan[a], John M. Sharp, Jr.[a], and Robert E. Mace[b]

[a] Department of Geological Sciences, The University of Texas at Austin, Mail Code C1100 Austin, TX 78712
[b] Bureau of Economic Geology, The University of Texas at Austin, University Station, Box X Austin, TX 78713

Abstract

Two difficulties that karst aquifers can present are permeability that varies with the scale of measurement (up to nine orders of magnitude), and permeability that is so high that standard pump tests obtain no measurable drawdown. Though it is difficult to quantify, permeability is the most sensitive parameter for either laminar or turbulent groundwater equations and must be accurately estimated.

Permeability data at the small-scale (laboratory and outcrop) were used to reproduce permeabilities measured at the well- and regional-scales in the San Antonio segment of the Edwards aquifer. These calculations provided an understanding of how features observed at the small-scale affect permeability measurements at larger scales. Conversely, these calculations can be performed on the well- and regional-scale to estimate what small-scale features are influencing the aquifer. In this paper, equations and techniques are presented to help answer questions such as: (1) How can small-scale data be combined to determine an effective well- or regional-scale permeability? (2) What size high-permeability features are influencing an aquifer on the well- or regional-scale? (3) Is the flow in an aquifer Darcian? (4) What velocities should be expected in an aquifer?

Introduction

This paper is broken up into sections that may be digested separately. There are various combinations of high-permeability features, and usually someone is interested in certain combinations. Unfortunately, this format may make the paper as a whole somewhat segmented. A longer discussion of how these techniques may be applied to answer specific questions in a fractured karst aquifer can be found in Halihan et al. (in press). The averaging and inversion techniques presented are useful "back of the envelope" calculations which can be used to estimate the effects and dimensions of high-permeability features in karst aquifers. Some definitions are provided for those who are not familiar with karst hydrogeology (Appendix A), and a section is devoted to explaining the permeability scale effect. There are also short sections explaining the concept of permeability combination modeling and its application to the San Antonio segment of the Edwards aquifer. Finally, equations are presented with examples to aid in understanding how standard hydrogeologic measurements of permeability are affected by the high-permeability features present in karst aquifers for matrix, fracture, and conduit combinations.

Permeability scale effect

Kiraly (1975) first mentioned the scale effect in karst aquifers of Switzerland, in which permeability continually increased from the small- to the regional-scale (Figure 1). He hypothesized that the increase from small- to well-scale was caused by fractures, and that the largest permeabilities on the regional-scale were caused by karstic conduits. Quinlan and others (1992) compiled over 1800 dye traces from 25 countries, and concluded that average flow velocity values continually increased with scale. Extending the work of Brace (1984), Clauser (1992) noted that permeability increased approximately three orders of magnitude from the small-scale to the well-scale in crystalline rocks. However, Clauser suggested that the permeability of fractured media measured on the well-scale would not continue to increase when measured on the regional-scale. Other authors have also suggested that if a

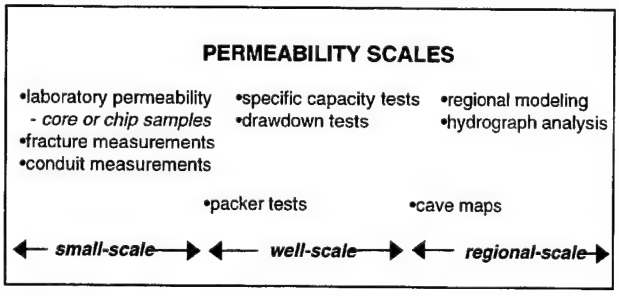

Figure 1: Permeability or intrinsic permeability measurements made on different scales. Over this range, aquifer permeability measurements can vary over nine orders of magnitude (Halihan et al., in press). The figure does not include micro-scale measurements of permeability performed in thin sections.

sufficiently large volume of rock was selected, a single, representative value for permeability could be determined (Long and others, 1982; Odling, 1997). Rovey (1994) examined carbonate aquifer permeability with variogram models; he found that for fractured unkarstified carbonates, a range could be determined in which the permeability reached a constant value. But for mature, well-developed karst aquifers, he suggested that permeability increased to "practical infinity." Halihan et al. (in press) tested Kiraly's (1975) hypothesis using a permeability database for the San Antonio segment of the Edwards aquifer of central Texas and found that Kiraly's hypothesis was applicable for that aquifer.

Small-scale permeability distributions

Small-scale permeabilities in carbonate aquifers have a few common trends. Published matrix permeabilities tend to lie in the range of $5x10^{-17}$ to $5x10^{-13}$ m^2 for limestone and dolomite (Freeze and Cherry, 1979). These values can extend from below 10^{-17} m^2, where they become difficult to measure, up to values of 10^{-11} m^2, which may include some small solutional voids or fractures (Hovorka et al., 1993; Hovorka et al., 1995) (Figure 2). The permeability of the matrix is often log-normally distributed (Halihan et al., in press), as it is for many lithologies.

Fracture permeabilities are highly variable in aquifers. However, the distribution of apertures is generally assumed to follow a log-normal or power-law distribution (Bianchi and Snow, 1969; Barton and Zoback, 1992; Marrett, 1996). When the log-normal or power-law distribution is modified to permeability using the cubic law (Lamb, 1932), generally a single fracture or a small number of fractures will dominate the flow. Although thousands of fractures may be present, the distribution of apertures indicates that only a few will control the aquifer.

Conduit permeabilities are difficult to estimate. Most conduits have variable diameters and limited lengths. Permeability calculations indicate that on a regional-scale, a meter-scale conduit would dominate the flow field (Halihan et al., in press), but the values are very high and not often observed because of either pump-test limits or incorrect modeling assumptions in regional models. However, some work suggests that conduits should follow a log-normal or power-law distribution as well, with the result being that, when present, generally a single conduit will dominate an aquifer (Curl 1986; Laverty, 1987; Ford and Williams, 1989).

Results of modeling for the Edwards aquifer

Halihan et al. (in press) used permeability combination models combined with a database of small-scale permeability distributions to reproduce observed well- and regional-scale permeability measurements in the San Antonio segment of the Edwards aquifer of central Texas (Figures 2, 3, and 4). The modeling suggested that Kiraly's (1975) hypothesis worked in the Edwards and that permeability will depend on scale in a fractured karst aquifer. They concluded that the well-scale permeability in the aquifer could be generated as a function of fracture aperture distribution.

The difficulty that Halihan et al. (in press) had to overcome was that, for the Edwards aquifer, approximately 15% of the well tests had no measurable drawdown. They explained this phenomenon as being the measurement limit of pumping tests, but the modeling suggested that these results could be caused by either millimeter-sized fractures or centimeter-scale conduits, both of which are observed in

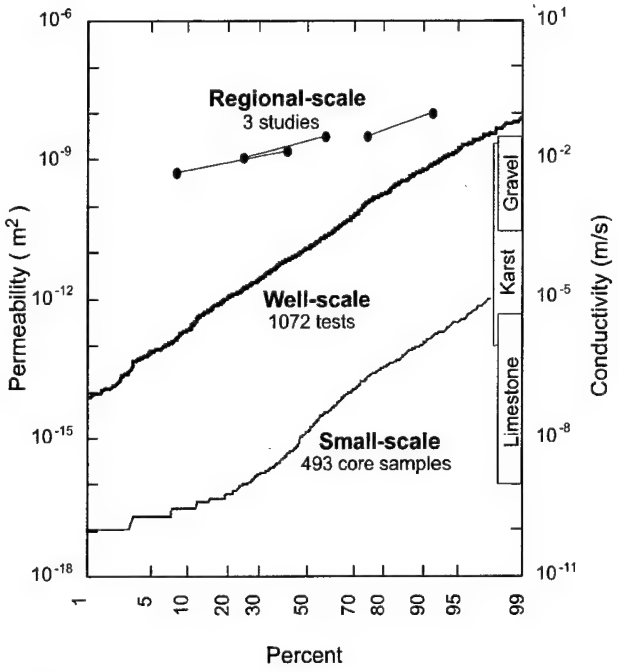

Figure 2: Permeability scale effect for the San Antonio segment of the Edwards aquifer. Cumulative distribution function for permeability values measured from cores (Hovorka et al., 1993; Hovorka et al., 1995; Hovorka, personal communication), wells (Hovorka et al., 1995; Mace, 1997), and regional models (Klemt et al., 1979; Maclay and Land, 1988; Thorkildsen and McElhaney, 1992). Permeability values for 3 regional modeling studies were calculated using a range of thickness (110 m -230 m) to convert from the highest model transmissivity to permeability. Permeability ranges for limestone, karst, and gravel (Freeze and Cherry, 1979) are illustrated for comparison. The individual data points for matrix and well data are not indicated because the quantity of data available provides nearly continuous lines.

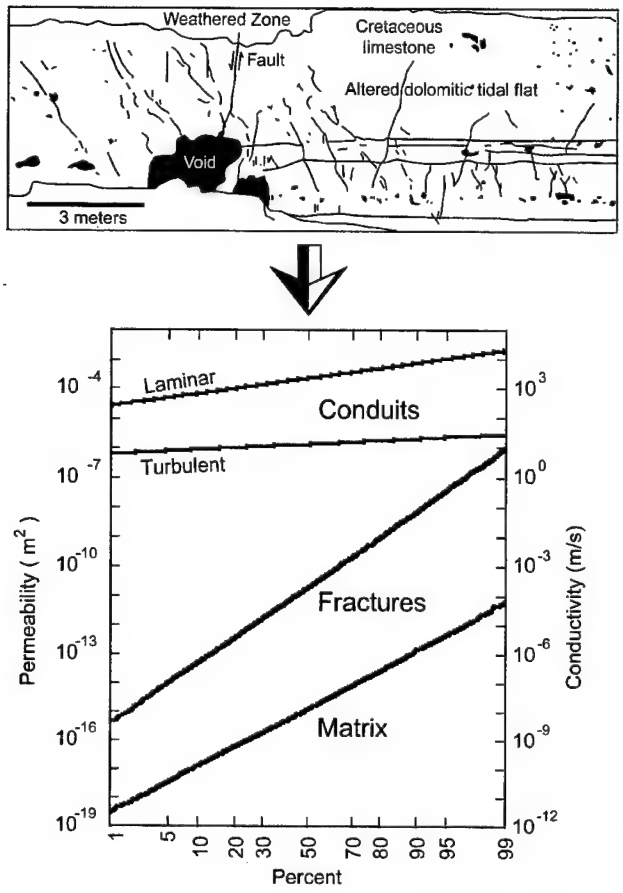

Figure 3: Small-scale permeability information for the San Antonio segment of the Edwards aquifer. The upper diagram is a digital outcrop interpretation of the Lake Medina outcrop that provides the basis for some of the data in the graphical lower diagram. Graphical data compiled from 493 matrix permeability measurements from 1-inch cores (Hovorka et al., 1993; Hovorka et al., 1995; Hovorka, personal communication), 776 fracture aperture measurements from roadcuts (Hovorka et al., 1998), and 2685 conduit measurements from roadcuts (Hovorka et al., 1995). Fracture permeability was calculated using equation (4a). Laminar and turbulent conduit permeability was calculated using equations (7c) and (7e), respectively. It is assumed that a homogenous aquifer would yield a straight horizontal line on the diagram.

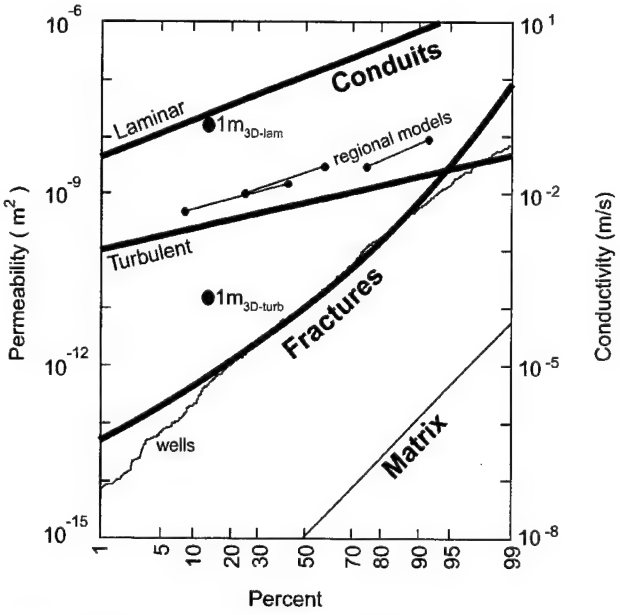

Figure 4: Permeability scale effect (thin lines, and points connected with lines; see Figure 2) and permeability combination models (thick lines, and individual points) for the San Antonio segment of the Edwards aquifer. Permeability combination model is shown for a 50-fracture Monte Carlo model using the distributions for matrix and fracture permeability (Figure 3) and equation 6. 2D single-conduit models are shown for laminar and turbulent flow using the distributions for matrix and conduit permeability (Figure 2) and equation 7a. 3D conduit model calculation (individual points) shown for 1-meter laminar and turbulent models using equation (8b) with $k_m = 10^{-11}$ m^2, and $A_\perp = 1.7\text{x}10^6$ m^2.

outcrop. The study illustrated the difficulty in applying standard pump tests to a fractured carbonate aquifer due to the limitations of pumping tests, and the highly heterogeneous nature of the high permeability features in the aquifer.

Permeability combination models

Permeability combination models provide a method for performing estimates of 1) averaged permeabilities caused by a mixture of different permeable features in an aquifer (Halihan et al., in press; Figures 3 and 4), or 2) size of small-scale permeable features from well- or regional-scale permeability data. These models are steady-state geometric models that estimate the effects of different heterogeneities on aquifer permeability. The models assume that measurements of permeability on different scales are all valid estimates, which simply average different heterogeneities.

Permeability combination models are modifications of equations for layered aquifers (Leonards, 1962; Fetter, 1994). In addition to the assumptions used for layered aquifers, three additional assumptions are necessary for these models: (1) the hydraulic gradients used in the estimates are uniform between different heterogeneities (2) equation 4g is valid for fractures and equations 7d and 7f are valid for laminar and turbulent flow in conduits; (3) there are no strong interactions between regions with different permeabilities. While the standard techniques for

measuring permeability yield average values that generally underestimate flow velocities, these model estimates will likely overestimate flow velocities. These calculations are approximations and are highly dependent on the orientations of the permeable features.

In order to illustrate the use of these models, three cases are given for matrix, fracture and conduit combinations with example problems. For combining regions of varying matrix permeability, one case is given for combining small-scale measurements, and two cases for inverting well- or regional-scale measurements. For combinations of fractures and matrix, two cases discuss how to combine small-scale data to obtain estimates of larger-scale permeabilities, and one case illustrating how to estimate fracture aperture from well data. Finally, two cases are presented to estimate how a conduit flowing under laminar or turbulent conditions would affect well- or regional-scale estimates, and one illustrating the problem of estimating conduit size from regional models. The problems are simplified and ask some rhetorical questions, but do illustrate the basic ways in which the high-permeability features present on the small-scale in aquifers can be combined to affect measurements at larger scales. A more formal derivation of the equations is presented for the case of a single fracture intercepting a well (case 4).

Matrix

How thick would a high-permeability layer in an aquifer need to be to supply the water flowing to a well? How high would be the permeability detected in a well if it intercepts a known high-permeability zone? What is the permeability of a conductive zone that was encountered during drilling? How much faster does water move through the high-permeability zone than the rest of the aquifer? Often, the permeability of a given lithology is known, or can be estimated using small-scale measurements. Using the small-scale data and information about the well, these questions can be answered with the equations and examples provided (Figure 5).

Case 1: Using small-scale lithology information to predict well -test results

Need: (1) total thickness of the aquifer (b_{total}); (2) thickness of high-permeability layer (b_{high}); (3) permeability or conductivity of the two lithologies (k_m, k_{high} or K_m, K_{high}).

Calculation:

Permeability:

$$k_e = k_m + (k_{high} - k_m)\left(\frac{b_{high}}{b_{total}}\right) \qquad (1a)$$

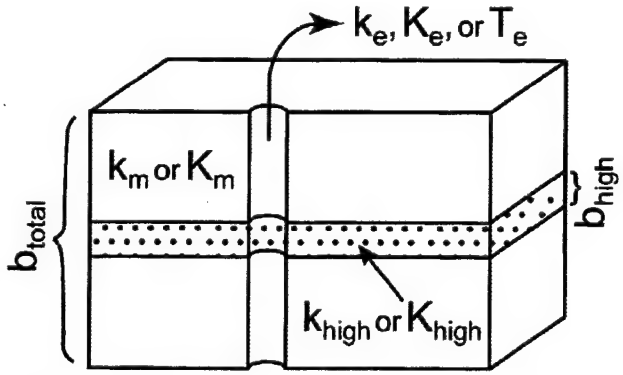

Figure 5: High-permeability matrix layer located in a lower-permeability aquifer. See Case 1, 2, and 3.

Conductivity:

$$K_e = K_m + (K_{high} - K_m)\left(\frac{b_{high}}{b_{total}}\right) \qquad 1b)$$

Transmissivity:

$$T_e = K_m(b_{total} - b_{high}) + K_{high}(b_{high}) \qquad (1c)$$

Case 2: Inverting pump-test results to find high-permeability layer size

Need: (1) transmissivity from pump test (T_e); (2) conductivity of the two lithologies (K_m, K_{high}); (3) thickness of aquifer (b_{total}).

Calculation:

$$b_{high} = \frac{T_e - K_m b_{total}}{K_{high} - K_m} \qquad (2a)$$

Approximation:

If $T_m \ll T_e$, equation (2a) can be approximated:

$$b_{high} \cong \frac{T_e}{K_{high}} \qquad (2b)$$

Case 3: Inverting pump-test results to find high-permeability layer conductivity

Need: (1) Transmissivity from pump test (T_e); (2) conductivity of the low-permeability matrix (K_m); (3) thickness of aquifer and the high-permeability layer (b_{total}, b_{high}).

Calculation:

$$K_{high} = \frac{T_e - K_m(b_{total} - b_{high})}{b_{high}} \quad (3a)$$

Approximation:

If K_m is negligible, equation (3a) can be approximated:

$$K_{high} \cong \frac{T_e}{b_{high}} \quad (3b)$$

Example 1:

A 100 m well is drilled though a well-characterized aquifer with a matrix hydraulic conductivity of 10^{-5} m/s. A distinct 2.0 m high-permeability zone is encountered. The well test yields a transmissivity of 3.0×10^{-3} m^2/s. What is the hydraulic conductivity of the 2.0 m zone?

Solution 1:

Using equation 3a, the hydraulic conductivity would be:
K_{high} = [(3.0×10^{-3} m^2/s - 10^{-5} m/s (100 m - 2.0 m)) / 2.0 m]
= 1.0×10^{-3} m/s

Approximation using equation 3b:
K_{high} = [3.0×10^{-3} m^2/s / 2.0 m] = 1.5×10^{-3} m/s

Example 2:

The same well as example 1, except the aquifer is unfractured limestone with a matrix hydraulic conductivity of 10^{-7} m/s. What is the specific discharge of the aquifer (a) assuming a homogeneous aquifer, (b) through the limestone matrix, and (c) through the high-permeability matrix, if the hydraulic gradient in the area is 10^{-3}?

Solution 2:

Using equation 3a, the hydraulic conductivity would be:
K_{high} = [(3.0×10^{-3} m^2/s - 10^{-7} m/s (100 m - 2.0 m)) / 2.0 m]
= 1.5×10^{-3} m/s

Approximation using equation (3b):
K_{high} = [3.0×10^{-3} m^2/s / 2.0 m] = 1.5×10^{-3} m/s

As can be seen comparing this example to example (1), the low matrix permeabilities of limestones make approximations of high-permeability zones easier.

Specific discharge:

(a) $K\,i = 3.0 \times 10^{-5}$ m/s * $10^{-3} = 3 \times 10^{-8}$ m/s = 0.002 m/day
(b) $v = 10^{-7}$ m/s * $10^{-3} = 10^{-10}$ m/s = 0.000009 m/day
(c) $v = 1.5 \times 10^{-3}$ m/s * $10^{-3} = 1.5 \times 10^{-6}$ m/s = 0.1 m/day

Since the specific discharge reflects the transport velocity, the difficulties with using a homogeneous assumption can be observed. The specific discharge of the high-permeability zone is 50 times greater than estimated, assuming a homogenous aquifer.

Fractures

What would be the permeability detected in a well if it intercepted a fracture of a given aperture? What size fracture would have to be encountered to obtain a specific transmissivity? Is flow in a fracture Darcian? What would the flow velocity in the fracture be? Using small-scale data and information about a well, these questions can be answered with the equations and examples provided (Figures 6 and 7). Case 4 includes a derivation of the equations used throughout this paper.

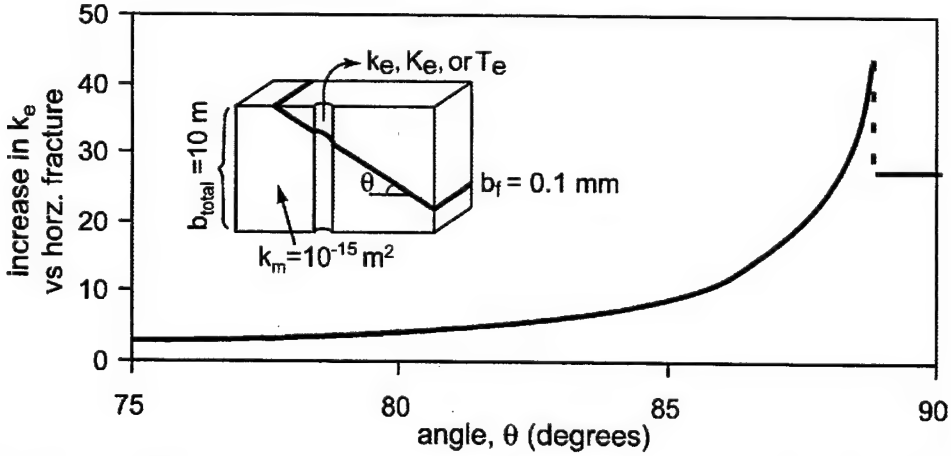

Figure 6: Effect of a single 0.1 mm aperture fracture at angle θ, located in a 10 m thick aquifer with matrix permeability of 10^{-15} m^2 (example 3). The increase in permeability due to the horizontal fracture over the matrix alone is approximately an order of magnitude. At angles less than approximately 80°, the effect of fracture angle is negligible. Above this value, increases in permeability of more than an order of magnitude over the horizontal case are possible.

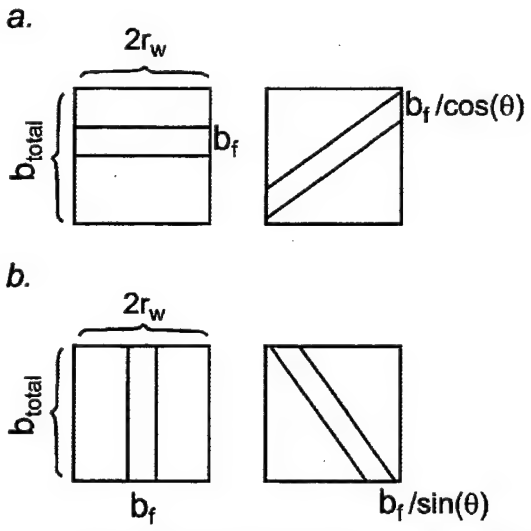

Figure 7: Projected profile view for two cases of a fracture intercepting a well. **(a)** For most wells, the increase in effective permeability due to a fracture at an angle can be estimated using equation 4h. In this low-angle case, the end member is a horizontal fracture, and the effective permeability is independent of the well radius. **(b)** For angles greater than arctan (b_{total} / $2r_w$) (usually an angle greater than 80°), the effective permeability can be calculated using equation 4*k*. For this high-angle case, the effective permeability is no longer a function of the total aquifer thickness, but is now a function of the well radius.

Case 4: Single fracture at an angle -- predicting well test results

Need: (1) permeability or conductivity of the matrix (k_m); (2) permeability or aperture of the fracture (k_f or b_f); (3) Fracture angle (θ), measured from the horizontal; (4) Total thickness of the aquifer (b_{total}); (5) Well radius (r_w).

Calculation (derivation for equations used throughout): We consider the case of an infinite fracture located in a permeable matrix of finite thickness but infinite extent. The system is sampled by a well intercepting the fracture at an angle (θ). The conceptualization of this system is shown in Figure 6. We start with the solution for a vertical averaging of transmissivity within a well:

$$T=\sum T_i \tag{4a}$$

where T is the transmissivity. Expressing transmissivity as a function of fluid properties, permeability, and thickness:

$$\left(\frac{g}{\nu}\right)k_e b_{total}=\left(\frac{g}{\nu}\right)\sum k_i b_i \tag{4b}$$

where g is the gravitational acceleration [L t^{-2}], ν is the kinematic viscosity [L^2 t^{-1}], k_e is the effective permeability (m^2), b_{total} is the formation thickness [L], k_i is the permeability of the individually permeable regions, and b_i is the thickness of those regions. For this problem, there are two possibilities (Figure 7): (1) the fracture intercepts the well bore (low angle), or (2) the fracture penetrates the entire well vertically (high angle).

For the case of the fracture intercepting the well bore (low-angle case) (Figure 7a):

Dividing by the fluid properties, and separating the quantities into matrix and fracture values:

$$k_e b_{total}=k_m b_m+k_f\left(\frac{b_f}{\cos(\theta)}\right), \quad if\ \theta<\arctan\left(\frac{b_{total}}{2r_w}\right) \tag{4c}$$

where θ is the angle that the fracture makes relative to horizontal. The subscripts *m* and *f* represent matrix and fracture, respectively. Note that the equation is only valid when θ < arctan ($b_{total}/2r_w$) which occurs at θ = 78.7° for a 1 m thick aquifer with a 0.1 m well and at θ = 88.9° for a 10 m aquifer with the same well. Replacing b_m and rearranging, we obtain:

$$k_e b_{total}=k_m\left[b_{total}-\left(\frac{b_f}{\cos(\theta)}\right)\right]+k_f\left(\frac{b_f}{\cos(\theta)}\right) \tag{4d}$$

$$k_e=k_m-k_m\left(\frac{b_f}{b_{total}\cos(\theta)}\right)+k_f\left(\frac{b_f}{b_{total}\cos(\theta)}\right) \tag{4e}$$

$$k_e=k_m+(k_f-k_m)\left(\frac{b_f}{b_{total}\cos(\theta)}\right) \tag{4f}$$

Lastly, if we replace b_f using the intrinsic permeability of a fracture (Lamb, 1932):

$$b_f=(12k_f)^{1/2} \tag{4g}$$

we obtain:

(4h)

$$k_e=k_m+(k_f-k_m)\left(\frac{(12k_f)^{1/2}}{b_{total}\cos\theta}\right), \quad if\ \theta<\arctan\left(\frac{b_{total}}{2r_w}\right)$$

Approximation:

If $k_m << k_f$ then equation 4h can be approximated as:

$$k_e \cong \frac{3.46(k_f)^{3/2}}{b_{total}\cos(\theta)} \quad (4i)$$

which gives the effective permeability in terms of the matrix and fracture permeability, the aquifer thickness, and the angle of the fracture. For the horizontal case ($\theta = 0°$), we obtain:

$$k_e = k_m + (k_f - k_m)\left(\frac{(12k_f)^{1/2}}{b_{total}}\right) \quad (4j)$$

This is analogous to the case for a high-permeability matrix intercepting a well, as illustrated in equation 1a. For the low-angle case of a fracture intercepting a well, the effective permeability is independent of the well radius (Figure 7a).

For the second case (high angle), where $\theta >$ arctan (b_{total} / $2r_w$), we obtain (Figure 7b):

$$k_e = k_m + (k_f - k_m)\frac{(12k_f)^{1/2}}{\pi r_w \sin(\theta)} \quad (4k)$$

Approximation:

If $k_m << k_f$ then equation 4k can be approximated as:

$$k_e = \frac{3.46(k_f)^{3/2}}{\pi r_w \sin(\theta)} \quad (4l)$$

In the limit of the high-angle case, for a vertical fracture ($\theta = 90°$), we obtain:

$$k_e = k_m + (k_f - k_m)\frac{(12k_f)^{1/2}}{\pi r_w} \quad (4m)$$

In the high-angle case, the effective permeability is now dependent upon the well radius but is independent of the aquifer thickness (Figure 7b). There is a third possible case of a fracture that straddles the side of the bore and the top and bottom of the bore, but this case would be rare, if not nonexistent, in real-world well bores with typical fractures.

Example 3:

How much does the effective permeability of a 10 m thick limestone with a small-scale permeability of 10^{-15} m^2 increase if intercepted by a single 0.1 mm fracture that intercepts a 0.1 m radius well (a) horizontally, (b) at 45°, (c) at 75°, or (d) vertically (Figure 6)?

Solution 3:

First, calculate the critical angle for determining when the low-angle case is valid.

$\theta <$ arctan(10 m / 2*0.1 m) = arctan(50) = 88.85°. So equation 4h is valid for most fracture angles, but above 88.85° equation 4k is valid.

Calculate k_f for the problem using equation 4g:

$k_f = b_f^2/12 = (1\text{x}10^{-4}\text{ m})^2 /12 = 8.33\text{x}10^{-10}\text{ m}^2$

(a) $\theta = 0°$, using equation 4h: $k_e = 10^{-15}\text{ m}^2 + (8.33\text{x}10^{-10}\text{ m}^2 - 10^{-15}\text{ m}^2)[\ 10^{-4}\text{ m} / 10\text{ m} * \cos(0)\ ]$; $k_e = 10^{-15}\text{ m}^2 + (8.33\text{x}10^{-10}\text{ m}^2 * 1\text{x}10^{-5})$; $k_e = 9.33\text{x}10^{-15}\text{ m}^2$ -- an increase of nearly an order of magnitude over the matrix value

Approximation using equation 4i:

$k_e \approx (\ 3.46 * (8.33\text{x}10^{-10}\text{ m}^2)^{3/2} /10\text{ m} = 8.32\text{x}10^{-14}\text{ m}^3 /10\text{m} = 8.32\text{x}10^{-15}\text{ m}^2$

(b) $\theta = 45°$: $k_e = 1.28\text{x}10^{-14}\text{ m}^2$ -- an increase of 0.4 times over the horizontal case.

(c) $\theta = 75°$: $k_e = 3.32\text{x}10^{-14}\text{ m}^2$ -- an increase of 2.6 times over the horizontal case.

(d) $\theta = 90°$, using equation 4k: $k_e = 10^{-15}\text{ m}^2 + (8.33\text{x}10^{-10}\text{ m}^2 - 10^{-15}\text{m}^2)[\ 10^{-4}\text{m} / 3.14 * 0.1\text{ m} * \sin(90)\ ]$; $k_e = 2.66\text{ x }10^{-13}\text{ m}^2$ -- increase of 27.5 times over the horizontal case.

Approximation using equation 4l:

$k_e \approx (\ 3.46 * (8.33\text{x}10^{-10}\text{ m}^2)^{3/2} / 3.14 * 0.1\text{ m} * \sin(90) = 2.65\text{x}10^{-13}\text{ m}^2$

From this example it is observed that the angle at which a fracture intercepts a well does not make a significant difference in the calculated permeability for angles less than 80° in most situations (Figure 6). For angles less than 75°, the difference is insignificant compared to the other uncertainty in most field data. For high angles, the difference is more than an order of magnitude. So although fractures intercept wells at all angles, the permeability of the fractures can be closely approximated by the two end-member cases. Additionally, it is unlikely that a vertical well will intercept a large number of high-angle fractures; therefore, it is reasonable to approximate the permeability encountered in a vertical well as a series of horizontal fractures.

Case 5: Calculating the hydraulic aperture of a single low-angle fracture

Need: (1) transmissivity from pump test (T_e); (2) conductivity of matrix (K_m); (3) thickness of the aquifer (b_{total}); (4) fracture angle ($\|$).

Calculation:

Starting with equation 4h, and substituting back the fluid properties and the fracture aperture, we obtain,

$$K_e = K_m + (K_f - K_m)\left(\frac{b_f}{b_{total}\cos(\theta)}\right), \quad if\ \theta < \arctan\left(\frac{b_{total}}{2r_w}\right) \tag{5a}$$

If we then assume that $K_f >> K_m$ and solve for b_f, we obtain:

$$b_f = \left[\left(\frac{12\nu\cos(\theta)}{g}\right)(T_e - K_m b_m)\right]^{1/3} \tag{5b}$$

Since b_m is approximately equal to b_{total}, substituting:

$$b_f \cong \left[\left(\frac{12\nu\cos(\theta)}{g}\right)(T_e - K_m b_{total})\right]^{1/3} \tag{5c}$$

Approximation: If $T_m << T_f$ then equation 5b can be approximated as:

$$b_f \cong \left(\frac{12\nu\cos(\theta)T_e}{g}\right)^{1/3} \tag{5d}$$

Example 4:

A pump test returns a value of transmissivity of 10^{-3} m^2 /s in a 10 m limestone aquifer. Core samples reveal the matrix conductivity to be 10^{-8} m/s. What size single horizontal fracture could explain this pump test (Figure 8)? Would flow through that fracture follow Darcy's law if the regional hydraulic gradient were 10^{-3}? What is the specific discharge of the aquifer (a) assuming a homogeneous aquifer, (b) through the limestone matrix, and (c) through the fracture if the hydraulic gradient in the area is 10^{-3}?

Solution 4:

Using equation 5c, the size of the fracture is

b_f= [(12 (10^{-6} m^2/s) / 9.81 m/s^2) * (10^{-3} m^2/s - (10^{-8} m/s * 10 m))]$^{1/3}$; b_f= 0.00106 m = 1.06 mm horizontal fracture. By approximation, $b_f \cong$ [(12x10^{-7} m-s) * (10^{-3} m^2/s)]$^{1/3}$ ≅ 1.06 mm. Would the flow be Darcian? Checking the Reynolds number:

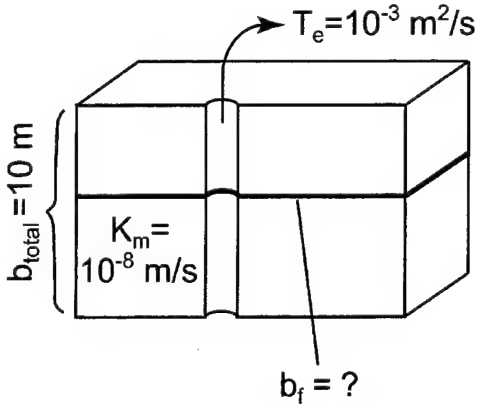

Figure 8: Often, the hydraulic aperture of a fracture intercepting a well is of interest (example 4). Using the transmissivity from a pump test combined with equation (5c), the hydraulic aperture can be determined.

$R_e = v b_f/\blacktriangleright = K_f i\, b_f/\blacktriangleright = 0.94$ m/s*10^{-3}*1.06x10^{-3} m*10^6 s/m^2 = 0.996

Since the Reynolds number is below 10, the flow in this system would be Darcian, but the value is high, and under pumping conditions the flow near the well would likely be non-Darcian.

Specific discharge (v):

(a) v = $K\,i$ = 10^{-4} m/s * 10^{-3} = 10^{-7} m/s = 0.009 m/day - for a homogenous assumption; (b) v = 10^{-8} m/s * 10^{-3} = 10^{-11} m/s = 9x10^{-7} m/day - for the matrix; (c) v = 0.9 m/s * 10^{-3} = 9x10^{-4} m/s = 80 m/day - for the fracture.

This example illustrates why using homogenous assumptions fails to estimate transport velocities in this type of aquifer. The homogeneous estimate of specific discharge is 4 orders of magnitude below the specific discharge of the fracture (Figure 8).

Case 6: Multiple horizontal fractures - combining small-scale data to reproduce well- and regional-scale data

Need: (1) permeability of matrix (k_m), or distribution of k_m; (2) fracture aperture distribution (b_f); (3) aquifer thickness distribution (b_{total}); calculation (Halihan et al., in press):

$$k_e = k_m - k_m\left(\frac{\sum b_f}{b_{total}}\right) + \left(\frac{\sum b_f^3}{12 b_{total}}\right) \tag{6}$$

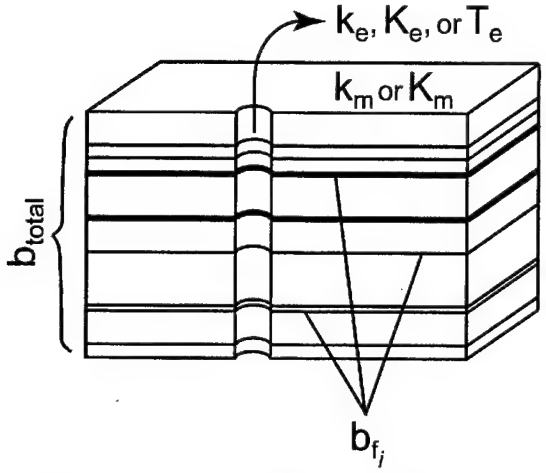

Figure 9: Multiple horizontal fractures with log-normal or power-law aperture distribution intercepting a well (case 6; example 5).

Example 5:

This formulation was used by Halihan et al. (in press) to reproduce well-scale permeabilities in the Edwards aquifer using small-scale data (Figures 4 and 9).

Solution 5:

The k_e distribution was estimated from the distributions of k_m, b_f, and b_t using Monte Carlo simulations with 10,000 trials per simulation (Jensen et al., 1997, p. 61-64). These simulations were performed using the distribution for the full aquifer thickness, and the open interval length for b_t. Each fracture was generated separately for the simulations. These simulations were performed for models of 1, 10, 50, and 100 horizontal fractures.

The best fit of the multiple horizontal fracture model to the well-test data occurred with 50 fractures (average connected fracture density of 1 fracture every 3.4 meters). At this density the model fit approximately 80 percent of the well-test data with an error in the median values of 8% (Figure 4). The model predicted higher values for the effective permeability below the 10th percentile and above the 90th percentile.

To determine the relative effects of the 50 horizontal fractures and the matrix, 20 trials of the model were examined. In the random trials, the matrix contributed less than 0.5% of the permeability in all but one case. The largest number of fractures contributing more than 1% of the total effective permeability was 6 of 50 fractures, which occurred in 4 of the 20 trials. These four trials had an effective permeability range of 1.9×10^{-13} to 6.0×10^{-12} m^2. The largest fracture had an aperture of 1.77 mm, contributing 46.2% of the permeability. The smallest number of fractures contributing greater than 1% of the permeability was 1 of 50, which occurred in 6 of the 20 trials. These six trials had an effective permeability range of 1.3×10^{-12} to 1.3×10^{-8} m^2, with the largest single fracture of 29.0 mm contributing 99.9% of the permeability. These limited tests indicate that flow occurs in a limited number of fractures in the model, and that some of these fractures are flowing under non-linear laminar ($10<R_e<2000$) to turbulent ($R_e>2000$) flow conditions.

Conduits

Conduit modeling is very difficult in groundwater settings. The sizes, location, length, and orientation of conduits are often ill defined or unknown. The following calculations allow first estimates of conduit sizes or regional permeability based on available permeability data (Figures 3 and 10). Equations are provided to calculate hydraulic conductivity and flow for laminar and smoothly turbulent conduits. Conduits in natural settings may not follow either laminar or smoothly turbulent flow laws exactly, but by using the two different formulations, the effect of turbulence on the aquifer can be compared with a Darcian assumption.

Case 7: Single horizontal conduit - 2D

Need: (1) permeability of matrix (k_m); (2) conduit size estimate (d_c); (3) aquifer thickness (b_{total}) calculation (Halihan et al., in press):

$$k_{e,2D} = k_m + (k_c - k_m)\frac{d_c}{b_{total}} \qquad (7a)$$

This is analogous to equation (1a) and equation (4h).

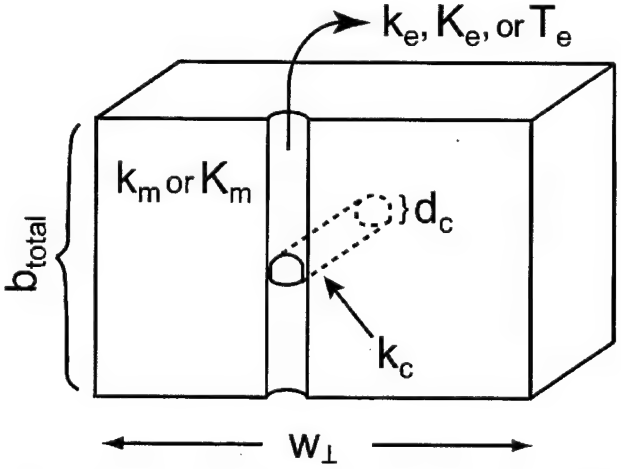

Figure 10: Single horizontal conduit intercepting a well (case 7; example 6).

Approximation:

If $k_m << k_c$ then equation 7a can be approximated as:

$$k_{e,2D} \cong \frac{k_c d_c}{b_{total}} \tag{7b}$$

Conduit conductivity and permeability:

For laminar flow (Gupta, 1989, p. 549-551):

$$K_{c,lam} = \frac{g d_c^2}{32 \nu} \tag{7c}$$

$$k_{c,lam} = \frac{d_c^2}{32} \tag{7d}$$

For smoothly turbulent flow (Halihan et al., 1998):

$$K_{c,turb} = 4.706 \frac{g^{4/7}}{\nu^{1/7}} \left(\frac{d_c}{2} \right)^{5/7} \tag{7e}$$

$$k_{c.turb} = K_{c.turb} \frac{\nu}{g} \tag{7f}$$

Modeling conduits is intrinsically different when compared to fractures or matrix layers. One difficulty occurs because conduits are modeled by lines, not planes, and equation 7a is valid only for the width of the conduit (Figure 10). This would be a good approximation for a well permeability, but the well would be violating radial-flow assumptions and would be following linear flow equations. The well permeabilities calculated for centimeter- to meter-scale conduits are generally too high to measure with a standard pump test. For regional permeability estimates, the estimated effective permeability would also include the matrix to the sides of the conduit, as illustrated in case (8) (Figure 11).

Example 6:

Equation 7a was used by Halihan et al. (in press) to estimate well-scale permeabilities in the Edwards aquifer using small-scale data (Figures 3 and 4).

Solution 6:

The k_e distribution was estimated from the distribution of k_m, k_c, d_c, and b_t using Monte Carlo simulations (see example 5). The permeabilities for the conduit distributions were calculated using both laminar and turbulent flow equations (equations 7d and 7f, respectively).

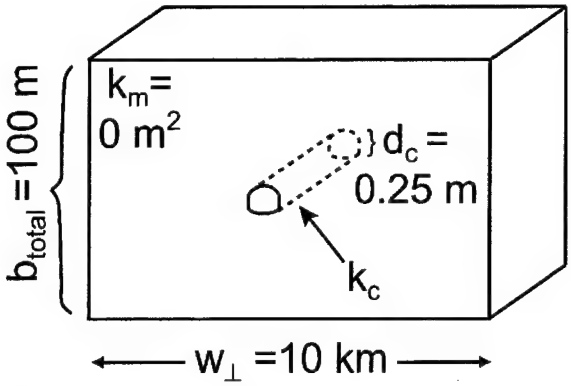

Figure 11: Examples 8 and 9 for a single conduit extending through an aquifer. The difficulty in this problem is determining whether Darcy's law is valid for the aquifer, and how the initial assumptions affect the resulting values.

The laminar horizontal conduit model resulted in a predicted effective permeability increase of over 7 orders of magnitude compared to the matrix alone (Figure 4). This prediction is significantly above the calculated well-test permeabilities and the regional permeabilities. The turbulent horizontal conduit model resulted in a predicted effective permeability increase of over 5 orders of magnitude. It is not expected that every well in the Edwards intersects a conduit of significant dimensions, so it is appropriate to compare the horizontal conduit model prediction either with the upper end of the well-permeability distribution or with the regional values. The median value of the turbulent model is 20 times larger than the median well-test value. However, these values are similar to some of the calculated values for the highest-permeability wells.

Case 8: Single horizontal conduit - 3D - calculating estimated regional permeability

Need: (1) permeability of matrix (k_m); (2) conduit size or permeability (d_c or k_c); (3) aquifer thickness (b_{total}); (4) Aquifer width perpendicular to conduit ($w_\perp$).

Calculation:

$$k_{e,3D} = k_m + (k_c - k_m) \frac{d_c^2 \pi}{4 b_{total} w_\perp} \tag{8a}$$

$$k_{e,3D} = k_m + (k_c - k_m)\frac{d_c^2 \pi}{4A_\perp} \quad (8b)$$

where:

$$A_\perp = b_{total} * w_\perp \quad (8c)$$

Approximation:

If $k_c >> k_m$, then equation 8b can be approximated as:

$$k_{e,3D} \cong \frac{k_c d_c^2 \pi}{4A_\perp} \quad (8d)$$

Example 7:

A 1 m diameter cave runs though an aquifer that is 50 m thick and 10 km wide. The average well-scale permeability from pump tests is 10^{-12} m^2. What is the expected regional permeability parallel to the conduit, for (a) Darcian flow, (b) smoothly turbulent flow?

Solution 7:

For this problem, $A_\perp = 5x10^5$ m^2 from equation 8d, $k_{c,\,lam} = 3x10^{-2}$ m^2 from equation 7d, and $k_{c,\,turb} = 8x10^{-6}$ m^2 from equation 7f.

(a) Using equation 8b, $k_{e,\,3D} = 10^{-12}$ m^2 + ($3x10^{-2}$ m^2 - 10^{-12} m^2)[(1 m^2 * 3.14)/ (4 * $5x10^5$ m^2)]; $k_{e,\,3D} = 5x10^{-08}$ m^2 for Darcian flow.

Using the approximation (equation 8d), $k_{e,\,3D} = 5x10^{-8}$ m^2.

b) Using equation 8b, $k_{e,\,3D} = 10^{-12}$ m^2 + ($8x10^{-6}$ m^2 - 10^{-12} m^2)[(1 m^2 * 3.14)/ (4 * $5x10^5$ m^2)]; $k_{e,\,3D} = 1x10^{-11}$ m^2 for smoothly turbulent flow.

For this example, the aquifer matrix has an area that is over 600,000 times greater than the conduit area. But under laminar flow conditions the flow in the conduit is nearly 50,000 times greater than the flow for the entire matrix.

Case 9: Single horizontal conduit - 3D - estimation of regional conduit size

Need: (1) regional-scale aquifer permeability ($k_{e,3D}$); (2) aquifer area perpendicular to conduit ($A_\perp$); (3) $k_m << k_c$.

Calculation:

Assuming laminar flow, $k_m << k_c$, and solving equation 8b for d_c we obtain

$$d_c \cong \left[\frac{128A_\perp}{\pi}(k_{e,3D} - k_m)\right]^{1/4} \quad (9a)$$

or

$$d_c \cong \left[\frac{128\nu A_\perp}{g\pi}(K_{e,3D} - K_m)\right]^{1/4} \quad (9b)$$

Assuming turbulent flow, $k_m << k_c$, and solving equation 8b for d_c we obtain

$$d_c \cong \left[\frac{1.395 g^{3/7} A_\perp}{\nu^{6/7}\pi}(k_{e,3D} - k_m)\right]^{7/19} \quad (9c)$$

or

$$d_c \cong \left[\frac{1.395 \nu^{1/7} A_\perp}{g^{4/7}\pi}(K_{e,3D} - K_m)\right]^{7/19} \quad (9d)$$

Example 8:

A hypothetical confined karst aquifer 10 km wide and 100 m thick contains a single 0.25 m diameter conduit running the length of the aquifer (Figure 11). The permeability of the remainder of the aquifer is negligible. Assume that flow in the conduit follows the equation for smoothly turbulent pipe flow:

$$Q = 4.706\pi \frac{g^{4/7}}{\nu^{1/7}}\left(\frac{d_c}{2}\right)^{19/7} i^{4/7} \quad (9e)$$

If the hydraulic gradient parallel to the conduit is 10^{-3}, what would the aquifer discharge be? Would flow be Darcian? Using a simple Darcian regional model, what would the regional hydraulic conductivity be parallel to the conduit?

Solution 8:

Aquifer discharge, using equation 9e: $Q = 4.706 * \pi * (9.8\ m/s^2)^{4/7} * (10^{-6}\ m^2/s)^{-1/7} * (0.125\ m)^{19/7} * (10^{-3})^{4/7}$;
$Q = 0.027\ m^3/s = 27\ L/s$.

Is the flow Darcian? Checking the Reynolds number (R_e):
$R_e = v\, d_c/\nu = (Q/A)\, d_c/\nu = (4\,Q) / (\pi d_c \nu)$;
$R_e = (4*0.027\ m^3/s)/(0.25\ m*3.14*10^{-6}\ m^2/s)$;
$R_e = 140{,}000$ -- flow is turbulent, non-Darcian

What is the regional conductivity? This would generally be calculated for a Darcian model by examining the discharge and inputs to the system and calibrating a model to

available head data. For this example, the calculation would look like:

$K_{e,\,3D} = Q/iA_{\perp} = (0.027\ m^3/s)/(10^{-3}*10^6\ m^2) = 2.7x10^{-5}$ m/s.

This calculation is in error, since the aquifer is not actually flowing under Darcian conditions, but most groundwater models make this type of error when applied to non-Darcian karstic aquifers.

Example 9:

Using the regional hydraulic conductivity estimate from example 8 ($2.7x10^{-5}$ m/s) and assuming that the matrix permeability is negligible, what is the approximate size of a conduit in the aquifer (a) assuming laminar flow, and (b) assuming turbulent flow? If the hydraulic gradient is 10^{-3}, would the flow be Darcian (Figure 11)?

Solution 9:

For this problem, $A_{\perp} = 10^6\ m^2$, $K_{e,\,3D} = 2.7x10^{-5}$ m/s.

(a) Using equation 9b,
$d_c \cong [128 * 10^{-6}\ m^2/s * (9.8\ m/s^2 * \pi)^{-1} * 10^6\ m^2 * 2.7x10^{-5}\ m/s]^{1/4}$; $d_c \cong 0.10$ meters -- assuming laminar flow.

(b) Using equation (9d),
$d_c \cong [1.4 * (9.8\ m/s^2)^{-4/7} * (10^{-6} m^2/s)^{1/7} / \pi * 10^6 m^2 * 2.7x10^{-5}\ m/s]^{7/19}$; $d_c \cong 0.74$ meters - assuming turbulent flow.

Would the flow be Darcian? Checking the Reynolds number:

$R_e = v\, d_c/\nu = K i^x d_c/\nu$

(a) Assuming laminar flow: $R_e = g\, i\, d_c^3 / 32\nu^2$; $R_e = [9.8\ m/s^2 * 10^{-3} * (0.10\ m)^3] / [32 * (10^{-6} m^2/s)^2]$; $R_e = 3x10^5$.

(b) Assuming turbulent flow: $R_e = 2.868\, g^{4/7}\, \nu^{-8/7}\, i^{4/7}\, d_c^{12/7}$; $R_e = 2.868*(9.8\ m/s^2)^{4/7} * (10^{-6}\ m^2/s)^{-8/7}\ (10^{-3})^{4/7}\ (0.74\ m)^{12/7}$; $R_e = 9x10^5$.

For this problem, the question of laminar vs. turbulent flow using regional modeling is simple enough. The calculation showed that the aquifer flows under turbulent conditions, but neither calculation derived the correct conduit diameter.

What happened in this example? Which diameter is correct? Actually, neither approach was truly correct. The regional modeling was incorrect in assuming Darcy's law is valid for this aquifer. The turbulent calculation was wrong because it assumed that the value obtained using the Darcian calculation was correct. If we modify the turbulent calculation by altering the regional conductivity to account for turbulent loss, we may improve our calculation.

Regional conductivity from the Darcian model, $K_{e,\,3D} = 2.7x10^{-5}$ m/s. Turbulent correction: $K_{e,\,turb} = K_{e,\,3D} * i^{3/7} = 2.7 \times 10^{-5}*(10^{-3})^{3/7} = 1.4x10^{-6}$ m/s.

Recalculating conduit size using equation 9d:

$d_c \cong (1.395 * (9.8\ m/s^2)^{-4/7} * (10^{-6}\ m^2/s)^{1/7} * \pi^{-1} * 10^6 m^2 * 1.4x10^{-6}\ m/s)^{7/19}$; $d_c \cong 0.25$ m.

This answer is the same as was established in example 8 assuming that the 0.25 m diameter pipe flowed following the equation for smoothly turbulent flow. In actual aquifers the flow may not follow this exact equation, but turbulence will have the same effects on the equations in (1) reducing the value of the hydraulic conductivity and (2) lowering the effective hydraulic gradient. Calculations of expected conduit diameter will always be approximations. This example illustrates some of the difficulties encountered when applying Darcian assumptions to potential non-Darcian aquifers.

Conclusions

Estimating permeability in karst aquifers is not simple. The flow is often far from the typical assumptions of homogeneous and isotropic aquifers. Permeability measurements vary by many orders of magnitude, depending on the scale and direction of measurement. The difficulty is that while permeability is difficult to estimate, it is also the most sensitive parameter in both laminar and turbulent groundwater flow equations (Halihan and Wicks, 1998). In order to manage these aquifers effectively, permeability must be quantified as accurately as possible for the scale of interest. Fortunately, quantifying the size of small-scale features that affect well- and regional-scale permeability estimates makes understanding these aquifers easier. By quantifying the permeabilities or dimensions of high-permeability matrix, fractures, or conduits, a better understanding of aquifer structure and rates of transport can be obtained.

Appendix A: definitions

Intrinsic permeability or permeability (k) - the ease with which a porous medium transmits water [length^2]. Permeability may be defined for either laminar (Darcian) or non-laminar (non-Darcian) flow.

Hydraulic conductivity or conductivity (K) - Darcy's proportionality constant [length/time], or the coefficient of proportionality between fluid flux and hydraulic gradient. The difficulty with using hydraulic conductivity to describe

karst aquifers is that not only does the parameter include the properties of the fluid, but generally assumes Darcian flow (that the flux is indeed proportional to the gradient). In many cases in karst aquifers, Darcy's law may not be valid (non-Darcian flow), thus making the hydraulic conductivity also a function of the hydraulic gradient. Halihan and Wicks (1998) defined a turbulent hydraulic conductivity for the turbulent-flow law as the portion of the flow laws that do not include the hydraulic gradient or flow area.

Small-scale - Similar to the definitions of Bradbury and Muldoon (1990), small-scale refers to permeameter tests, fracture measurements, or conduit measurements that take place in the laboratory or outcrop and generally make a measurement over a volume of 0.01 m^3 to 10 m^3. This is also referred to as laboratory-scale (Dagan, 1986) or outcrop-scale.

Well-scale - refers to the scale of well or packer tests that occur on a scale of 100-1000 m^3. This scale can have a wide variation, depending on the depth of well or size of packer configuration. Well-scale is also referred to as local scale (Dagan, 1986).

Regional-scale - refers to volumes greater than 1000 m^3. This common term can be used in karst settings to refer to something on the scale of a cave map up to the entire aquifer.

Permeability scale effect - An effect first noted by Kiraly (1975) that indicates that permeability is dependent upon the scale of measurement (Figure 1). There is anywhere from a 3 to 9 order of magnitude increase in permeability from small- to regional-scale measurements.

Matrix - rock where no fractures visible to the unaided eye are present. For karst aquifers this is generally limestone or dolomite with intrinsic permeabilities of $5x10^{-17}$ to $5x10^{-13}$ m^2 (Freeze and Cherry, 1979).

Fracture - crack visible to the unaided eye that is open, not filled by minerals. In models, fractures commonly are considered two-dimensional uniform slots.

Conduit - dissolution feature that extends for a range greater than that of the well-scale and is visible to the unaided eye. In models, conduits are generally treated as one-dimensional pipes.

Non-Darcian - a situation that occurs when the flow through an aquifer no longer follows Darcy's law (i.e. the flux is not directly proportional to the gradient). This is generally predicted by Reynolds numbers greater than 10 (Linquist, 1933; Scheidegger, 1974, p. 152-187; Fetter, 1994, p. 143-144).

Appendix B: variables used

$A_\perp$ = cross-sectional area perpendicular to the long axis of a conduit, [L^2]
b_f = fracture aperture, [L]
b_{high} = thickness of high permeability layer, [L]
b_i = thickness of individual permeable feature, [L]
b_m = thickness of aquifer matrix, [L]
b_{total} = total thickness of aquifer, (or penetration length of well), [L]
d_c = diameter of conduit, [L]
g = gravitational constant, [L t^{-2}]
i = hydraulic gradient, [dimensionless]
k_c = conduit permeability, [L^2]
$k_{c,\ lam}$ = laminar conduit permeability, [L^2]
$k_{c,\ turb}$ = turbulent conduit permeability, [L^2]
k_e = equivalent or averaged permeability, [L^2]
$k_{e,\ 2D}$ = equivalent or average permeability over conduit diameter, [L^2]
$k_{e,\ 3D}$ = equivalent or averaged 3D conduit permeability, [L^2]
k_f = fracture permeability, [L^2]
k_{high} = permeability of high permeability layer, [L^2]
k_i = permeability of individual permeable feature, [L^2]
k_m = permeability of aquifer matrix, [L^2]
K = hydraulic conductivity, [L t^{-1}]
$K_{c,\ lam}$ = laminar conduit hydraulic conductivity, [L t^{-1}]
$K_{c,\ turb}$ = turbulent conduit hydraulic conductivity, [L t^{-1}]
K_e = equivalent or averaged hydraulic conductivity, [L t^{-1}]
$K_{e,\ turb}$ = equivalent or averaged 3D turbulent conduit conductivity, [L t^{-1}]
$K_{e,\ 3D}$ = equivalent or averaged 3D conduit conductivity, [L t^{-1}]
K_f = fracture hydraulic conductivity, [L t^{-1}]
K_{high} = hydraulic conductivity of high permeability layer, [L t^{-1}]
K_m = matrix hydraulic conductivity, [L t^{-1}]
Q = discharge, [L^3 t^{-1}]
R_e = Reynolds number, [dimensionless]
r_w = well radius, [L]
T = transmissivity [L^2 t^{-1}]
T_e = equivalent or averaged transmissivity [L^2 t^{-1}]
T_f = fracture transmissivity, [L^2 t^{-1}]
T_i = transmissivity of individual permeable feature, [L^2 t^{-1}]
T_m = matrix transmissivity, [L^2 t^{-1}]
v = specific discharge, [L t^{-1}]
$w_\perp$ = width perpendicular to the long axis of a conduit, [L]
ν = kinematic viscosity, [L^2 t^{-1}]
π = pi = 3.14
θ = angle between fracture and horizontal

Acknowledgments

We thank Sue Hovorka of the Texas Bureau of Economic Geology for providing access to her matrix permeability data. We also thank John Bye, Neville Robinson, and Craig Simmons for their helpful discussions. Funding for Todd Halihan was provided by a National Science Foundation Traineeship in Hydrology (NSF grant GER-9454098). Funding for permeability data collection was provided by the Edwards Aquifer Authority. Manuscript preparation was supported by the Owen-Coates Fund of the Geology Foundation of The University of Texas at Austin.

References cited

Barton, C.A., and M.D. Zoback, 1992, Self-similar distribution and properties of macroscopic fractures at depth in crystalline rock in the Cajon Pass scientific drill hole: Journal of Geophysical Research, vol. 97, p. 5181-5200.

Bianchi, L., and D.T. Snow, 1969, Permeability of crystalline rock interpreted from measured orientations and apertures of fractures: Annals of Arid Zone, vol. 8, no. 2, p. 231-245.

Brace, W.F., 1984, Permeability of crystalline rocks: new *in situ* measurements: Journal of Geophysical Research, vol. 89, no. B6, p. 4327.

Bradbury, K.R., and M.A. Muldoon, Hydraulic conductivity determinations in unlithified glacial and fluvial materials, *in* D.M. Nielsen and A.I. Johnson (eds.), Ground water and vadose zone monitoring, ASTM STP 1053: Philadelphia, American Society for Testing and Materials, p. 138-151.

Clauser, C., 1992, Permeability of crystalline rocks: EOS, Transactions American Geophysical Union, vol. 73, no. 21, p. 233-238.

Curl, R.L., 1986, Fractal dimensions and geometries of caves: Mathematical Geology, vol. 18, no. 8, p. 765-783.

Dagan, G., 1986, Statistical theory of groundwater flow and transport: Pore to laboratory, laboratory to formation, and formation to regional scale: Water Resources Research, vol. 22, no. 9, p. 120S-134S.

Fetter, C.W., 1994, Applied Hydrogeology: New York, Macmillan, 691 p.

Ford, D.C., and P.W. Williams, 1989, Karst Geomorphology and Hydrology: London, Unwin Hyman, 601 p.

Freeze, R.A., and J.A. Cherry, 1979, Groundwater: Englewood Cliffs, New Jersey, Prentice Hall, 604 p.

Gupta, R.S., 1989, Hydrology and Hydraulic Systems: Englewood Cliffs, New Jersey, Prentice Hall, 739 p.

Halihan, T., R.E. Mace, and J.M. Sharp, Jr., in press, Flow in the San Antonio segment of the Edwards aquifer: matrix, fractures, or conduits? Geological Society of America Special Paper.

Halihan, T., C.M. Wicks, and J.f. Engeln, 1998, Physical response of a karst drainage basin to flood pulses: example of the Devil's Icebox cave system (Missouri, USA): Journal of Hydrology, vol. 204, p. 24-36.

Halihan, T., and C.W. Wicks, 1998, Modeling of storm responses in conduit flow aquifers with reservoirs: Journal of Hydrology, vol. 208, p. 82-91.

Hovorka, S.D., R.E. Mace, and E.W. Collins, 1995, Regional distribution of permeability in the Edwards aquifer, Report 95-02: San Antonio, Texas, Edwards Underground Water District, 128 p.

Hovorka, S.D., R.E. Mace, and E.W. Collins, 1998, Permeability structure of the Edwards aquifer, south Texas -- Implications for aquifer management: Austin, Texas, Bureau of Economic Geology, University of Texas at Austin, Report of Investigations No. 250, 55 p.

Hovorka, S.D., S.C. Ruppel, A.R. Dutton, and J. Yeh, 1993, Edwards aquifer storage assessment, Kinney County to Hays County, Texas: Austin, Texas, Bureau of Economic Geology, University of Texas at Austin, report prepared for the Edwards Underground Water District, 101 p.

Hovorka, S.D., 1997, personal communication.

Jensen, J.L., L.W. Lake, P.W.M. Corbett, and D.J. Goggin, 1997, Statistics for Petroleum Engineers and Geoscientists: Upper Saddle River, New Jersey, Prentice Hall, 390 p.

Kiraly, L., 1975, Rapport sur l'état actuel des connaissances dans le domaine des caractères physiques des roches karstiques, *in* A. Burger and L. Dubertret (eds.), Hydrogeology of karstic terrains: Paris, International Association of Hydrogeologists, Series B, no. 3, p. 53-67.

Klemt, W.B., T.R. Knowles, G.R. Elder, and T.W. Sieh, 1979, Ground-water resources and model applications for the Edwards (Balcones fault zone) aquifer in the San Antonio region, Texas: Austin, Texas, Texas Water

Development Board, Report 239, 88 p.

Lamb, 1932, Hydrodynamics, 6th edition: New York, Dover, 738 p.

Laverty, M., 1987, Fractals in karst: Earth Surface Processes and Landforms, vol. 12, no. 5, p. 475-480.

Leonards, G.A., 1962, Foundation Engineering: New York, McGraw-Hill, 1136 p.

Lindquist, E., 1933, On the flow of water through porous soil: Stockholm, Premier Congres des grands barrages, p. 81-101.

Long, J.C.S., J.S. Remer, C.R. Wilson, and P.A. Witherspoon, 1982, Porous media equivalents for networks of discontinuous fractures: Water Resources Research, vol. 18, p. 645-658.

Mace, R.E., 1997, Determination of transmissivity from specific capacity tests in a karst aquifer: Ground Water, vol. 35, no. 5, p. 738-742.

Maclay, R.W., and L.F. Land, 1988, Simulation of Flow in the Edwards Aquifer, San Antonio Region, Texas, and Refinement of Storage and Flow Concepts: U.S. Geological Survey Water-Supply Paper 2336-A, 48 p.

Marrett, R, 1996, Aggregate properties of fracture populations: Journal of Structural Geology, vol. 18, no. 2/3, p. 169-178.

Odling, N.E., 1997, Scaling and connectivity of joint systems in sandstones from western Norway: Journal of Structural Geology, vol. 19, no. 10, p. 1257-1271.

Quinlan, J.F., G.J. Davies, and S.R.H. Worthington, 1992, Rationale for the design of cost-effective groundwater monitoring systems in limestone and dolomite terranes: cost-effective as conceived is not cost-effective as built if the system design and sampling frequency inadequately consider site hydrogeology, *in* Symposium on Waste Testing and Quality Assurance (8th, Washington, D.C., July 1992): Washington, D.C., U.S. Environmental Protection Agency, p. 552-570.

Rovey, C.W., II., 1994, Assessing flow systems in carbonate aquifers using scale effects in hydraulic conductivity: Environmental Geology, vol. 24, p. 244-253.

Scheidegger, A.E., 1974, The physics of flow through porous media, 3rd edition: Toronto, University of Toronto Press, 353 p.

Thorkildsen, D., and P.D. McElhaney, 1992, Model refinement and applications for the Edwards (Balcones fault zone) aquifer in the San Antonio region, Texas: Austin, Texas, Texas Water Development Board, Report 340, 33 p.

LINEAR SYSTEMS APPROACH TO MODELING GROUNDWATER FLOW AND SOLUTE TRANSPORT THROUGH KARSTIC BASINS

Carol M. Wicks[1] *and John A. Hoke*
Department of Geological Sciences, University of Missouri
Columbia, MO 65211

Abstract

Modeling groundwater flow and solute transport in karst aquifers is complicated by the highly heterogeneous nature of the aquifer. A linear systems approach provides a basin-scale perspective that does not require specific details of internal geometry. In this study, three kernel functions were derived: one that relates excess recharge to spring discharge; one that relates solute input from a point source to concentrations of the solute in the spring discharge; and one that relates input from a non-point source to concentrations of solute in the spring water. Results indicate that these kernel functions can be used to predict groundwater flow and solute transport through a large karstic basin.

Introduction

The linear systems approach is very useful in karst aquifers because it describes regional (basin) scale transport in terms of the distribution of travel or residence times without requiring detailed knowledge of the internal structure (location and geometry of conduits) in the aquifer (Knisel, 1972; Ashton, 1966). Using a linear systems approach, Dreiss (1989a, b) was able to reproduce the discharge and composition records of a spring as a result of a storm event with an average 3% error. While she was not able to predict the discharge or concentrations, she was able to show that the linear systems approach warranted further investigation.

A lumped, time-invariant linear system is completely and uniquely characterized by its response to various inputs or forcing functions (Blank and others, 1971). This relation between the input and the response of the system is given by:

$$o(t) = \int_{-\infty}^{\infty} h(t-\tau) * i(\tau)\ \partial\tau \qquad (1)$$

where $o(t)$ is the observed output from the system, $i(\tau)$ is the input into the system, and $h(t-\tau)$ is the kernel function of the system. The response of a linear system to any input can be evaluated once the kernel function is known. It is critical, therefore, that the kernel function be determined as accurately as possible.

When applied to karst aquifers, one input function is excess precipitation (precipitation minus evapotranspiration and changes in soil moisture) and the corresponding output function is the spring discharge. The derived kernel function relates recharge over a spatial area (that delivered to the basin) to changes in the discharge at the spring. Another input function of importance to the karst hydrologist is the mass of a solute entering the karst system of interest. The method by which the solute enters the karst system must be considered in order to accurately derive the kernel function. A spatially and uniformly distributed non-point source solute to the basin will exhibit a different response than a discrete-input, point-source solute to the basin due to a difference in kernel functions. Once the unique kernel functions for an area have been determined, inputs that are available through monitoring programs can be used to determine groundwater movement and solute transport through a karst basin.

Kernel function derivation

Kernel functions were calculated for Maramec Spring Basin (Figure 1) that relate a point-source solute to its concentration at the spring, a non-point source solute to its concentration at the spring, and excess precipitation to spring discharge. Derivation of this suite of kernel functions required the use of the linear systems approach similar to that represented in equations 2 and 3:

$$h_{i,\ solute} = \frac{q_i\ C_i\ A\ \Delta t}{\sum_{i=1}^{n} q_i\ C_i\ A\ \Delta t} \qquad (2)$$

$$h_{i,\ discharge} = \frac{q_i * \Delta t}{\sum_{i=1}^{n} q_i * \Delta t} \qquad (3)$$

where the h_i values are the kernel functions for the solutes and discharge, q_i is the discharge, C_i is the concentration, A is the basin area, and Δt is the time step. The end result will be to determine whether or not these kernel functions will collectively characterize the physical and chemical

[1] Corresponding author.

transport of groundwater and aqueous-phase solutes through the Maramec Spring Basin.

Point-source kernel function

A well-documented nitrogen fertilizer pipeline break in Maramec Spring Basin provided an excellent opportunity to test the ability of the linear systems approach to characterize the transport of aqueous-phase solutes introduced as a point source. In November 1981, a pipeline carrying liquid fertilizer released an estimated 24,100 gallons of nitrogen-rich fluid directly into a losing stream reach (Figure 1). Collection of quantitative total nitrogen and dissolved oxygen concentration data was initiated shortly after the pipeline break in order to document changes in the spring-water composition and their effect on the local biota (Vandike, 1985; Crunkilton, 1985).

A point-source kernel function for the nitrogen pipeline break location was derived using the kernel derivation method described by Dreiss (1989b) and available daily nitrogen concentration and spring discharge data for the period of November 23, 1981 to January 1, 1982. The nitrogen concentrations that were measured in the spring water were total nitrogen, representing the sum of all nitrogen-bearing aqueous species regardless of oxidation state. Values of daily nitrogen concentration, C_i, were multiplied by the daily spring discharge, q_i, for a time step Δt equal to one day. The products of each daily nitrogen concentration and spring discharge for the period of record were then summed. The daily values of the point-source kernel were calculated on the basis of equation 2 (Figure 2).

Dye-trace kernel function

In early May 1982, a follow-up study to confirm the hydrologic connectivity between the nitrogen-pipeline spill location with Maramec Spring was initiated. Three gallons of an inert fluorescent dye were injected into the same losing stream reach downstream from the pipeline break location (Vandike, 1985). First arrival of the dye occurred 11 to 12 days after injection and confirmed the connectivity of the nitrogen-fertilizer pipeline break with Maramec Spring via subsurface karst conduits. Dreiss (1989b) derived a point-source kernel function for the dye trace using equation 2 and daily spring-water dye concentrations and discharge measurements recorded at Maramec Spring (Figure 2).

Non-point-source kernel function

A kernel function for non-point-source solute transport through Maramec Spring Basin was derived using daily measurements of spring-water conductivity and spring discharge recorded at Maramec Spring from January 1, 1994, to December 31, 1995 (Vandike, 1996). Spring-water conductivity predominantly represents mass concentrations of Ca^{2+}, Mg^{2+}, and HCO_3^- in the spring discharge that has been integrated over the entire karst basin. Using daily spring-water conductivity to represent the mass concentration of cations, C_i, in the spring discharge, q_i, equation 2 was used to derive a kernel function characterizing the behavior of an areally distributed non-point-source solute. To remove the effect of previous storm events in the kernel derivation, baseflow levels of specific conductivity and spring discharge were subtracted from the data by straight-line baseflow separation (Bedient and Huber, 1992). The daily product of spring-water conductivity and spring discharge for the period of the storm response was divided by the summed value of spring-water conductivity and spring discharge to obtain a non-point-source kernel function for Maramec Spring Basin.

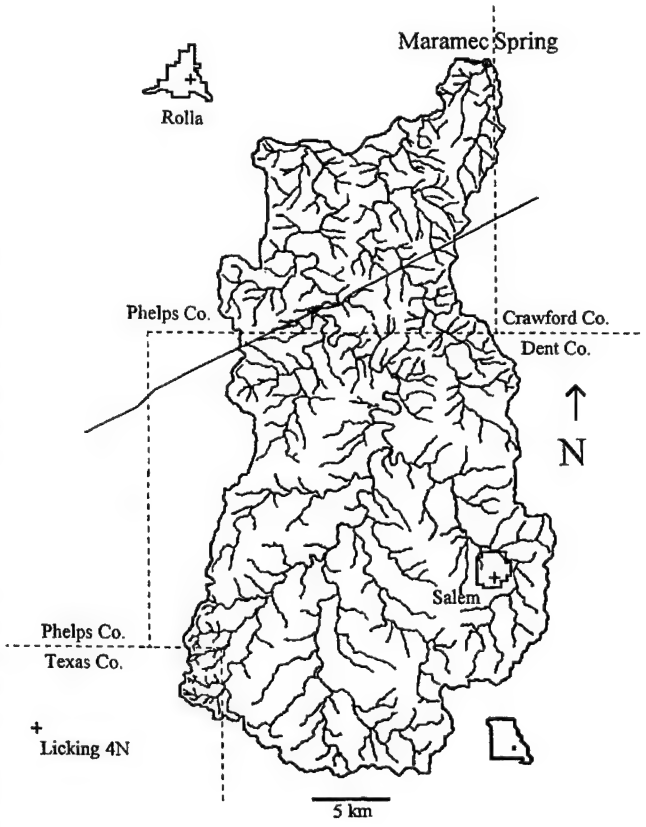

Figure 1: Map of the recharge area of Maramec Spring.

Non-point-source kernel functions were derived for isolated rainfall events of similar duration that had complete specific conductivity records. Spring-water conductivity and spring-discharge data from the June 27, July 6, and November 20, 1994, rainfall events and the May16, 1995, rainfall event were used in the derivation. A characteristic non-point-source kernel function for Maramec

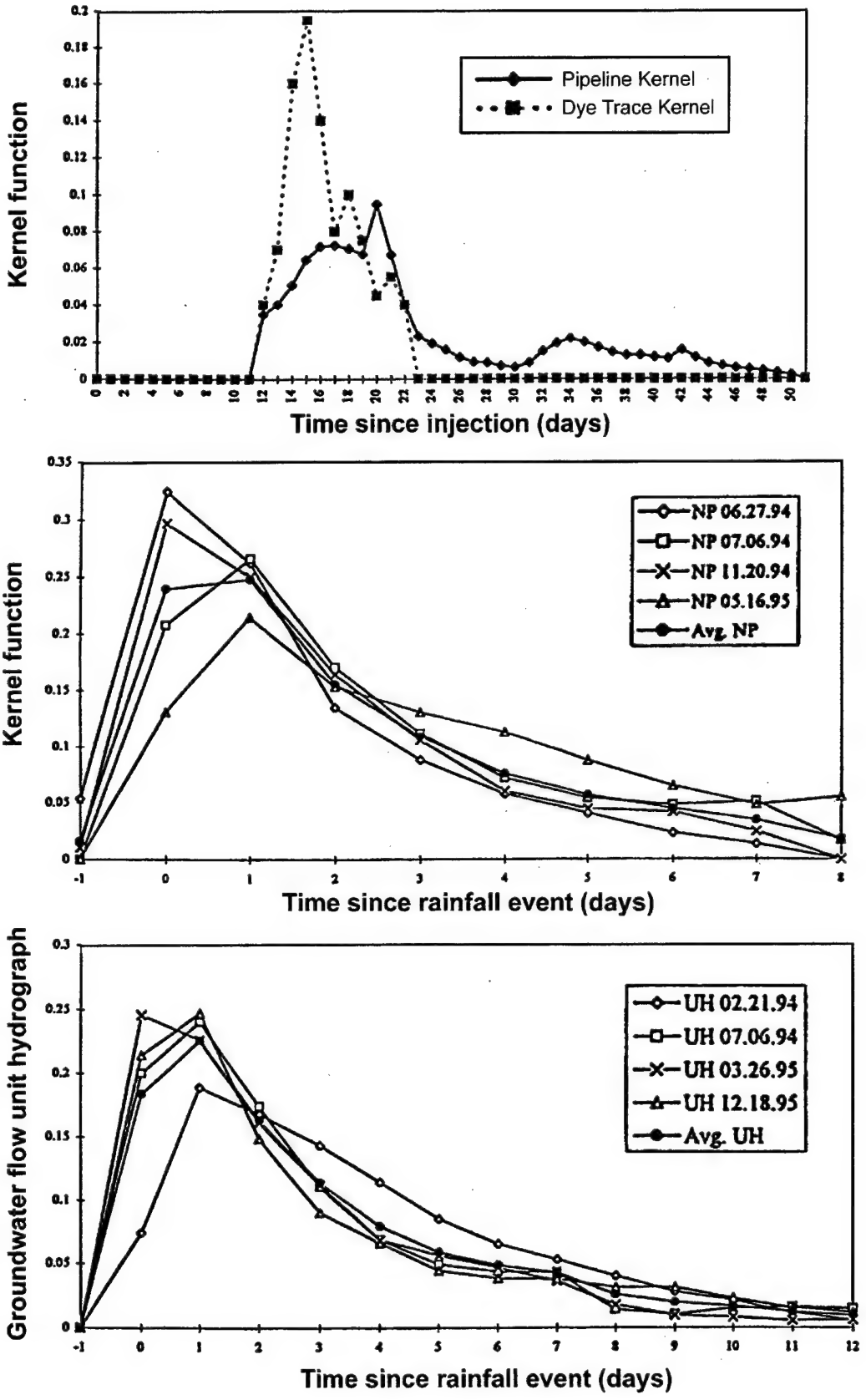

Figure 2: Kernel functions for Maramec Spring basin, **(a)** for point-source introduction of solutes, **(b)** for non-point introduction of solutes, and **(c)** for groundwater.

Spring Basin was calculated by taking the average of the four derived non-point-source kernel functions (Figure 2).

Groundwater-flow unit hydrograph

A groundwater-flow unit hydrograph was derived for the Maramec Spring Basin using observed discharge data at the spring for the period of record from January 1, 1994, to December 31, 1995 (Vandike, 1996). The groundwater-flow unit hydrograph was derived using discharge data from isolated storm events and a unit-hydrograph derivation method similar to that used for the point and non-point source kernel functions (Dingman, 1994). To isolate the influence of rainfall-event-derived water from water already in the karst system, baseflow levels of spring discharge were removed from daily spring discharge values using straight-line baseflow separation (Bedient and Huber, 1992). Daily spring discharge values were summed over the response time of Maramec Spring to the isolated storm event. To calculate the values of the unit hydrograph for the storm event, each daily discharge value was divided by the summed discharge response of Maramec Spring to the isolated storm event.

Groundwater-flow unit hydrographs were derived using observed discharge values from the February 21 and July 6, 1994, rainfall events and the March 26 and December 18, 1995, rainfall events. A characteristic groundwater-flow unit hydrograph was calculated by taking the average of the four derived unit hydrographs (Figure 2).

Interpretation

The time to peak (maximum value of a kernel function) represents the average transit time for groundwater and solutes (point and nonpoint) to move through the aquifer. The lag time represents the length of time that the recharge front takes to move through the aquifer.

The agreement between the lag time and time to peak for the two point-source kernel functions was expected, as the dye was injected at the location of the pipeline break. The agreement between the groundwater kernel and the non-point-source kernel also makes sense, as both input functions are areally distributed over the basin. Our ability to resolve the lag time for the groundwater and non-point-source kernel is limited by the resolution of the data, which are daily. The lag time is less than one day.

Significance

Since these results indicate that linear kernel models can be used to model karst solute transport, this technique becomes useful in describing solute problems in other karst basins. Of the large number of karst terrains known, a significant portion of these have been dye traced in the past. Some karst systems, such as Mammoth Cave, have been meticulously traced and copious amounts of data collected. Given dye traces for a particular karst terrain, kernel functions for the karst basin of interest can be computed. Once the kernel functions for a karst basin have been calculated, solute and groundwater behavior in the karst system can be characterized and anticipated for any input of solute concentration and excess precipitation. The use of the three kernel functions provides a handle on groundwater flow and solute transport through karst basins.

References cited

Ashton, K., 1966, The analysis of flow data from karst drainage systems: Transactions of the Cave Research Group, v. 7, p. 163-203.

Bedient, P.B., and W.C. Huber, 1992, Hydrology and floodplain analysis, 2nd ed.: Addison-Wesley Publishing Company, Reading, Mass., 692 p.

Blank, D.J., J.W. Delleur, and A. Giorgini, 1971, Oscillatory kernel functions in linear hydrologic models: Water Resources Research, v. 7, no. 5, p. 1101-1117.

Crunkilton, R., 1985, Subterranean contamination of Maramec Spring by ammonium nitrate and urea fertilizer and its implication on rare cave biota: Missouri Speleology, v. 25, p. 151-158.

Kernel function	Lag time (days)	Time to peak (days)
Groundwater	<1	1
Non-point-source solute	<1	1
Dye trace	11	15
Pipeline	11	17 (20)

Table 1: Comparison of values of the various kernel functions.

Dingman, S.L., 1994, Physical Hydrology: Macmillan Publ. Co., New York, 575 p.

Dreiss, S. J., 1982, Linear kernels for karst aquifers: Water Resources Research, v. 18, p. 865-876.

Dreiss, S. J., 1989a, Regional scale transport in a karst aquifer: 1. Component separation of spring flow hydrographs: Water Resources Research, v. 25, p. 117-125.

Dreiss, S. J., 1989b, Regional scale transport in a karst aquifer, 2. Linear systems and time moment analysis: Water Resources Research, v. 25, p. 126-134.

Knisel, W.G., 1972, Response of karst aquifers to recharge: Hydrology Papers, Colorado State University, Fort Collins, Colorado, December , 1972.

Vandike, J.E., 1982, The effects of the November 1981 liquid-fertilizer pipeline break on groundwater in Phelps County, Missouri: unpublished report, Water Resources Data and Research, Missouri Department of Natural Resources, Division of Geology and Land Survey, Rolla, Missouri, p. 28.

Vandike, J.E., 1985, Hydrogeologic aspects of the November, 1981 liquid fertilizer pipeline break on groundwater in the Maramec Spring recharge area, Phelps County, Missouri: Missouri Speleology, v. 25, p. 93-101.

Vandike, J. E., 1996, The hydrology of Maramec Spring: Water Resources Report No. 55, Missouri Department of Natural Resources, Division of Geology and Land Survey, Rolla, Missouri, 104 p.

TOWARD UNDERSTANDING TRANSPORT IN THE FLORIDAN KARST

David Loper
Geophysical Fluid Dynamics Institute, Florida State University
Tallahassee, FL 33431

Abstract

There is a strong need for better scientific knowledge of groundwater behavior in Floridan-type karstic aquifers and for better mechanisms to transfer such knowledge into practice. To facilitate this transfer, a new scientific organization called the Hydrogeology Consortium has recently been established. The Consortium is described in detail elsewhere in this volume. Its mission is to cooperatively provide scientific knowledge applicable to groundwater resource management and protection.

A necessary adjunct to the mission of the Consortium is the development of better models of transport and dispersion in karstic aquifers. A first step in this development is elucidation of the shortcomings of the standard model of dispersion. In this model, dispersion is represented by an effective diffusivity, called the dispersion coefficient, which is the product of the mean flow speed and the decorrelation distance. It is shown that this model does not correctly describe dispersion in an aquifer having porosity that is weakly correlated on a large scale. That is, *the concept of a decorrelation distance is not viable for a non-homogeneous aquifer*.

One approach toward the quantification of transport and dispersion in karstic aquifers to model the aquifer as a classic Darcian porous medium riddled by a distribution of macroscopic conduits. The flow properties of this model are compatible with the standard Darcian model, but its transport equation is non-autonomous; it has coefficients that depend on the elapsed time.

Problems modeling transport and dispersion in karst

Transport of water-borne material in an aquifer is the result of the large-scale flow of water, while dispersion results from the small-scale flow through the individual pores, mechanically spreading the material. The traditional method of modeling transport and dispersion is to use the classic advection-diffusion equation with the cumulative effect of the small-scale motions being modeled by an effective diffusion or dispersion coefficient. The standard parameterization of the dispersion coefficient, D, is as the product of the mean (macroscopic) flow speed, $\bar{v}$, times the *dispersivity* or "*decorrelation length*," δ, which is the distance over which flow trajectories become decorrelated:

$$D \approx \bar{v}\delta \tag{1}$$

Decorrelation is usually defined in the context of a Lagrangian description of motion and is quantified using the velocities at two different positions of a given particle of fluid as it wends its way through the porous medium. When the distance between the two positions is much less than the decorrelation length, δ, the two velocities are strongly correlated, and they are decorrelated when this distance is much greater than δ.

A definitive treatment of this approach is given by Phillips (1991, p. 13-22), who argues that δ is either the grain size or the characteristic distance between fracture intersections. A related quantity is the *decorrelation time*:

$$T=\delta/\bar{v} \tag{2}$$

which is the time it takes fluid, moving at the mean flow speed, to travel the decorrelation distance. Phillips' argument relies on the assumption that the porous medium is homogeneous on the macroscale, though irregular on the microscale.

A basic postulate of this approach to modeling transport (by means of the advective-diffusion equation) is that the dispersion coefficient is intensive: a function only of the local mechanical and thermodynamic conditions, and insensitive to the size of the system being modeled. It follows from the parameterization given in equation 1 that the dispersivity δ must be intensive as well. A strong indication that the standard parameterization of transport is fundamentally flawed is provided by field observations, which show that the dispersivity varies with the scale of the experiment (Gelhar et al, 1985, reproduced as Figure 6.15 in Dullien, 1992).

A necessary preliminary to the construction of an improved model of transport is the development of an understanding why the traditional approach fails. To that end, the analysis of Phillips is discussed in the next section where it is shown that the assumption of large-scale homogeneity is conceptually flawed and mathematically singular. A small amount of large-scale heterogeneity can invalidate the standard parameterization of dispersion.

A fundamental flaw in the standard parameterization of dispersion

Consider the flow of water through an aquifer. As noted above, transport is accomplished by the mean (macroscale) velocity, while the (microscale) velocity deviations cause dispersion. The vigor of the deviations is quantified by the *covariance* of velocity, which is the average product of velocity deviations of a microscopic fluid parcel, initially at position $\mathbf{x} = \mathbf{a}$, at two instants of time, t and $t\phi$ as it moves along its trajectory. The average is in fact an ensemble mean of all possible (microscale) initial states within the macroscale volume element located at $\mathbf{x} = \mathbf{a}$. Since position $\mathbf{a}$ is arbitrary, we may set $t\phi = 0$ without loss of generality. Following Phillips, the covariance may be expressed as

$$\overline{\mathbf{w}(\mathbf{a},t)\cdot\mathbf{w}(\mathbf{a},0)} = \overline{w^2}W(t) \qquad (3)$$

where $\mathbf{w}$ is the deviation of the point-wise velocity from the macroscopic average, $w = |\mathbf{w}|$ and W is the *autocorrelation function*. Note that, since on average a parcel travels with the mean transport speed $\bar{v}$, its mean displacement in time interval t is given by

$$l = \bar{v}t \qquad (4)$$

Two important properties of the autocorrelation function are the decorrelation time, T, defined by

$$T = \int_0^\infty W(t)dt \qquad (5)$$

and the decorrelation distance,

$$L = \bar{v}T \qquad (6)$$

If the decorrelation time is of the order of $\delta/\bar{v}$, as Phillips (1991) argues, then $L = \delta$; the parcel velocity becomes decorrelated at the grain or fracture scale. A basic assumption of the standard parameterization of dispersion is that the velocity deviation of the fluid parcel becomes completely decorrelated for time intervals t much greater than T, or, equivalently, for length scales l much greater than L. The stability of this assumption of homogeneity will now be investigated and attention will be focused on whether the standard parameterization remains valid if a weak, large-scale correlation exists in the aquifer.

For a homogeneous porous medium the function W is quite simple, as illustrated by Figure 2.11 in Phillips' book. An obvious form for this simple autocorrelation function is

$$W(t) = \exp(-\pi t^2/4T^2) \qquad (7)$$

Now what if the porous medium is not simple? For example, suppose that the autocorrelation function has a weak tail, perhaps representing a small-volume fraction of conduits of large radius. To investigate the consequences of this, let

$$W_1(t) = (1-\varepsilon)\exp\left(-\frac{\pi t^2}{4T_o^2}\right) + \varepsilon\exp\left(-\eta^2\frac{\pi t^2}{4T_o^2}\right) \qquad (8)$$

where T_0 is the decorrelation time when $\varepsilon = 0$. The dimensionless parameter is a measure of the strength of the large-scale correlation, while η is the ratio of the pore scale to the scale of correlation. Both ε and η are much smaller than unity. The decorrelation time, T_1, for the autocorrelation function given by (6) is

$$T_1 = \left(1 + \frac{\varepsilon}{\eta} - \varepsilon\right)T_0 \qquad (9)$$

The last factor in the parenthesis is small, but the size of the middle term is unconstrained. This means that *the concepts of a decorrelation time and a decorrelation distance cannot be applied to an aquifer having porosity with a large-scale correlation.*

Generalizing, suppose that there is a spectrum of correlation functions. Let

$$W_c(t) = \int_0^\infty A(\theta)\exp(-\pi t^2/4\theta^2)d\theta \qquad (10)$$

where the amplitude function A satisfies the normality condition

$$\int_0^\infty A(\theta)d\theta = 1 \qquad (11)$$

If $A(\theta) = \delta(\theta - T)$, then equation 7 is recovered. The decorrelation time for the autocorrelation function defined by equation 10 is

$$T_c = \int_0^\infty A(\theta)\theta d\theta \qquad (12)$$

Suppose, for example, that the hierarchy of scales is uniformly distributed in the porous medium:

$$A(\theta) = \begin{cases} \dfrac{\bar{v}}{L} \text{ for } 0<\theta<L/\bar{v} \\ 0 \text{ for } L/\bar{v} < \theta \end{cases} \qquad (13)$$

where L is the downstream spatial extent of the porous medium. The cutoff in the distribution of A given in equation 13 is dictated by the fact that when $L/\bar{v} < \theta$ at least one of the two parcels has moved out of the aquifer. In this case,

$$T_c = \frac{L}{2\bar{v}}; \qquad (14)$$

that is, the decorrelation time is half the residence time of a particle in the aquifer.

Now in order to get to the standard parameterization given by equation 1, one must assume that the elapsed time t is much larger than the decorrelation time T. But it is not possible to satisfy this condition if the aquifer has a hierarchy of scales for which equation 13, or anything like it, applies. This reaffirms the earlier conclusion that the standard parameterization is not valid for a porous medium having any significant correlation on the scale of the aquifer.

Toward the development of a better model of transport

A karstic-aquifer model is being developed in which the aquifer consists of a classical Darcian porous medium containing a number of macroscopic conduits or pipes of varying sizes and orientations. The flow properties of this model are compatible with those of a Darcian porous medium, but the model has novel transport properties. These novel properties arise from the fact that advection of material cannot be ignored in the transport equation if the conduits are sufficiently large. The typical conduit occurring in Floridan karst (which is large enough to swim through) is sufficiently large that advection is an important component of transport. In this case the transport equation is non-autonomous; it has coefficients that depend on the elapsed time.

References cited

Dullien, F. A. L., 1992, Porous Media: Fluid Transport and Pore Structure: Academic Press.

Gelhar, L. W., A. Mantoglou, C. Welty, and K. R. Rehfeldt, 1985, RE. EA-4190: Elect. Power Res. Inst., Palo Alto, Calif.

Phillips, O. M., 1991, Flow and Reactions in Permeable Rocks: Cambridge University Press.

DIGITAL MODELS

When analytical models begin to approach the complexity of real systems, the only way to solve them quantitatively is to break the model into tiny discrete space and time increments. Conditions within each increment can then be solved simultaneously or by successive approximation. This is the topic of digital modeling. It was originally known as numerical analysis, but this term is rarely used today because the only satisfactory way of solving complex numerical problems is with a computer. Like the limb of a tree that has grown larger than the main trunk, digital modeling is simply an outgrowth of analytical modeling, and it shares the same analytical roots.

There is theoretically no limit to the complexity of a digital model, and it can be safely said that any natural system in which the processes and dimensions are accurately known -- no matter how large or complex -- can be modeled accurately by digital methods. The giant fly in the ointment, of course, is our limited knowledge of the physical systems and processes.

There are two basic kinds of digital model. In the geosciences the most popular are the groundwater models designed to calculate head, flow patterns, and contaminant transport within an aquifer. The popular software package MODFLOW, originally designed by the USGS, is the leading example. The other type of model, which is well represented by the papers in this section, is designed to investigate the processes that operate within idealized systems, rather than in real field sites.

Digital modeling of real karst aquifers has acquired a dubious reputation, especially among karst researchers themselves. Some models (e.g. Cullen and LaFleur, 1984) have been designed to handle the specific characteristics of karst, and although they provide insight into how karst groundwater behaves, even the modelers realize that they cannot be used for predictive purposes. Probably no natural system is less suited to predictive digital modeling than karst. The figure on the cover of this volume expresses the fantasy of attempting to do so. The late James Quinlan, the world's most prolific karst groundwater tracer, repeatedly claimed that "A single dye trace is worth a thousand digital models."

No perceptive hydrologist would disagree. But digital modeling also forces us to come to grips with what is going on in the field. Each step in designing a model requires an intimate knowledge of the physical system and the processes operating within it. The conscientious modeler uses these design steps as a guide to what information must be obtained from the field -- and how much is not known. And the results should be used only as an idealized comparison with what is actually observed in the field. The discrepancy between observed conditions and the ideal model can be a great help in clarifying field conditions.

Unfortunately it is easy for a modeler to slip around these requirements by making spurious or tentative assumptions when designing a predictive model. The result is a bogus model whose seemingly elegant output takes on a reality of its own and can lead to seriously flawed decisions.

The validity of a site-specific digital model depends on the accuracy with which the aquifer variables can be quantified within the model. The heterogeneity of karst aquifers is so severe that it is virtually impossible to acquire sufficient field information to construct a predictive digital model trustworthy enough to allow extrapolation of heads and flow conditions from known to unknown locations, let alone into the future. It can even be argued that digital models are inadequate to realize these goals in any kind of bedrock aquifer.

On the other hand, digital models are well suited to revealing the interactions among water flow, chemistry, and geologic setting under idealized conditions. The entire evolution of a conceptual karst aquifer can be modeled in this manner. This kind of digital model combines scientific rigor, realistic boundary conditions, and easily refereed procedures. As shown by the following papers, digital modeling is the most promising quantitative tool for investigating karst processes.

Reference cited

Cullen, J.J., and R.G. LaFleur, 1984, Theoretical considerations on simulation of karstic aquifers, *in* R.G. LaFleur (ed.), Groundwater as a geomorphic agent: Boston, Allen and Unwin, p. 249-280.

DYNAMICS OF THE EARLY EVOLUTION OF KARST

Wolfgang Dreybrodt, Franci Gabrovšek, and Jörg Siemers
Institute of Experimental Physics, University of Bremen, Germany

Abstract

The evolution of karst conduits by calcite-aggressive water flowing in initially narrow fractures requires a non-linear rate law $F_n(c) = k_n(1 - c/c_{eq})^n$ for limestone dissolution close to equilibrium with respect to calcite. A mathematical analysis of the evolution of limestone dissolution rates of water in such early, narrow fractures as a function of the distance from the input reveals an exponential decrease of dissolution rates for linear rate laws ($n = 1$), such that subsurface karstification is prevented.

For non-linear kinetics ($n > 2$), however, the decrease of rates proceeds by a hyperbolic relation, such that dissolution rates at the exit of the fracture are still sufficiently high to create a feedback mechanism by which after a long time of gestation a dramatic increase in the widths of the conduits is established. After this breakthrough event, uniform widening along the entire channel determines the further evolution. The time to achieve breakthrough is given by $T \approx a_0 / 2\gamma F(l,0)$, where $2\gamma F(l,0)$ is the initial widening in cm/year at the exit of the conduit. This equation defines the parameters that determine karstification. The equation above, however, is valid only when the calcite concentration of the inflow solution is less than 99% of saturation. Otherwise the positive feedback loop is switched off and the conduit widens evenly along its entire length with rates of 10^{-9} cm/year to enlarge extremely narrow fractures with initial widths of several ten microns over distances of kilometers to sizes of about 0.1 mm within several ten millions of years. This provides a general explanation for the concept of inception horizons, where usually other mechanisms have been assumed.

The results in one-dimensional conduits were applied to two-dimensional nets of initial fractures. These are constructed on a square lattice by occupying the lines between nearest neighbor sites by a water-conducting fissure of width a_0 and length l with an occupation probability p. For $p > 0.5$, percolating nets occur that transmit water. To simulate cave genesis in step 1, we calculate the water flow rates driven by the hydraulic head h through all fissures. Then in step 2 the one-dimensional transport-dissolution model is applied to each of these fractures and the evolution of their widths is calculated during a time step Δt. Iterating step 1 and step 2 the evolution of the two-dimensional system is modeled. At the onset of karstification, flow is evenly distributed among all fractures. As the system develops, solutional widening creates preferred pathways, which attract more and more flow, until at breakthrough both widening and flow increase dramatically. A numerical analysis of breakthrough times dependent on the parameters a_0 (width of the initial fractures), L (horizontal dimension of the aquifer), h (hydraulic head acting on it), and on the chemical parameters of the dissolution kinetics reveals that the relation valid for one-dimensional conduits is also valid for two dimensions. The consequences of the dependence of breakthrough time on the various parameters determining karstification are finally discussed.

Introduction

The dissolution rate of limestone by CO_2 containing calcite- aggressive water flowing through a narrow fracture with a width of several tenths of a millimeter is given (Dreybrodt and Eisenlohr, 1997; Dreybrodt et al., 1996; Eisenlohr et al., 1997; Svensson and Dreybrodt, 1992) by

$$F_1(c) = k_1(1 - c/c_{eq}) \quad \text{for} \quad c \le c_s \qquad (1a)$$

$$F_n(c) = k_n(1 - c/c_{eq})^n \quad \text{for} \quad c > c_s \qquad (1b)$$

where c is the concentration of dissolved calcite in the solution and c_{eq} the equilibrium concentration with respect to calcite in mole/cm^3. The rate constants k_1 and k_n are related by

$$k_n = k_1(1 - c_s/c_{eq})^{(1-n)} \quad [\text{mole/cm}^2/\text{sec}] \qquad (2)$$

c_s is the switch concentration, where the reaction order changes from 1 to n. Typically $0.75 < c_s < 0.9$ for natural limestone.

To answer the question of how the profile of an initially uniform fracture develops in space and time when an aggressive solution is forced through, numerical models have been used that assume a constant pressure head driving the water through the fracture. These models show (Dreybrodt, 1990, 1996; Palmer, 1991; Groves and Howard, 1994a, 1994b) that a positive feedback loop is operative. Widening of the fracture causes increasing flow through it, and therefore the dissolution rates increase along the entire fracture and so on, until finally a dramatic increase of flow rates causes a dramatic enhancement of the widening of the fracture. This breakthrough event terminates the initial state of conduit evolution. To

gain more insight into this positive feedback mechanism, we present a simple mathematical model, which avoids numerical modeling by finite differences. In the second part of this work we extend this model to two-dimensional networks of such fractures and show that the important results of the one-dimensional model apply also to the more realistic network model.

Dissolution of limestone in a plane-parallel fracture

We replace a natural irregular fracture by a uniform fracture with initial aperture width a_0 and a breadth b_o. We furthermore assume that $a_0 << b_0$ (typically $a_0 \approx 0.01$cm, $b_o \approx 100$cm). The length of the fracture is l, and the hydraulic head h is acting on it.

A part of this fracture is illustrated by Figure 1. At a distance x from the input the calcite concentration is $c(x)$. It increases by the material dissolved from the walls between x and $x+dx$ to a value $c(x+dx)=c(x)+dc$. The flow velocity of the water is $v(x)$. $A(x)$ is the cross sectional area of the fracture, and $P(x)$ its perimeter at position x. According to the law of continuity, the flow rate through the conduit does not depend on the distance x and is given by

$$Q = v(x)\cdot A(x) \tag{3}$$

Now conservation of mass requires that the amount of calcite dissolved per time from the walls between x and $x+dx$ must be equal to the difference of calcite transported by the flow Q out of the fracture at $x+dx$ to that entering it at x. Thus

$$Q\cdot dc = F(c(x))\cdot P(x)\cdot dx; \tag{4a}$$

Integration yields

$$\int_{c_o}^{c}\frac{dc}{F(c)} = \int_{0}^{x} P(x)dx / Q \tag{4b}$$

c_0 is the concentration at the entrance $x=0$ of the conduit. During the initial state of speleogenesis, flow is laminar and the flow rate $Q(t)$ at time t through the fracture is given by

$$Q(t)=\frac{h}{R},\quad R=\frac{12\eta}{\rho g}\int_0^1 a^{-3}(x,t)b^{-1}(x,t)\cdot M^{-1}(x,t)dx \tag{5}$$

where $a(x,t)$ and $b(x,t)$ are its dimensions, which now vary in space and time, η is the dynamic viscosity of the solution, ρ its density, and $M(x,t)$ is a geometric shape factor with values between 0.3 and 1 (Beek and Mutzall, 1975), g is the earth's gravitational acceleration, and l is the length of the conduit. Units are [g], [cm], [sec], [mole/cm^3].

Equations 2-5 specify the parameters that determine

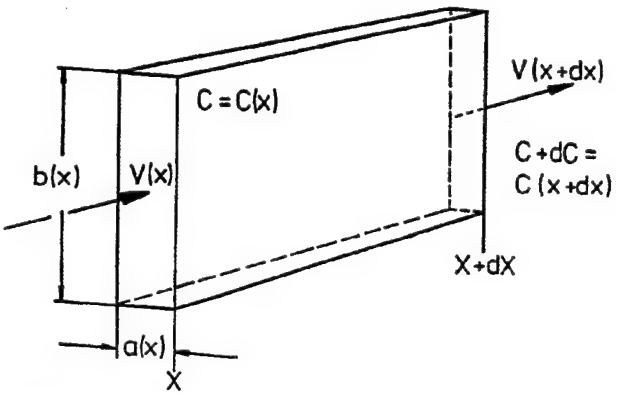

Figure 1: Part of a fracture along the percolating pathway at distance x from input between x and $x+dx$. The concentration increases along the distance by dc.

karstification in its initial state. The first group of parameters represents the chemical driving forces. They are k_1, k_n, n, c_s, c_0 and the equilibrium concentration c_{eq}. The kinetic constants k_1 and k_n depend on temperature, and k_n also depends on the lithology of the bedrock (Eisenlohr et al., 1997). The kinetic exponent n takes values, $2<n<11$. The equilibrium concentration c_{eq} is related to temperature and to the amount of carbon dioxide available at the surface of the karst terrain. Finally c_0 is the calcite concentration of the solution entering the fracture.

The physical driving forces are mainly related to the hydraulic head h, i.e. the relief of the fracture system. If meteoric precipitation is high, such that an ample amount of water is available at the surface, this value remains constant in time. In the early state of karstification this can be assumed as realistic, since the narrow fractures cannot transport large quantities of water and therefore the water table remains close to the surface. In the later state of mature karst the amount of water available might not suffice to keep this high water table. Therefore the amount of meteoric precipitation determines the further development of the karst aquifer.

The hydrogeologic setting is characterized by the geometry of the fracture, which determines its resistance R (eq. 5). Thus the corresponding parameters are the aperture width a_0, the breadth b_0 and the length l of the fracture. Furthermore, the dynamic viscosity η depends on temperature ($\eta = 1.8\cdot10^{-2}$ at 0° C, $\eta = 1.33\cdot10^{-2}$ at 10° C, and $\eta = 0.90\cdot10^{-2}$ dynes/cm^2 at 25° C). Therefore the amount of water transported through a system of fractures almost doubles if the temperature is raised from 2° C (alpine karst) to 25° C (tropical karst).

As a first step we calculate the initial dissolution rates along the initial fracture, which at the onset of karstification has not yet been widened. By use of eqs. 1 - 5 one finds

$$\int_{c_o}^{c} \frac{dc}{k_1(1-c/c_{eq})} = 2(a_0+b_0)\cdot x/Q_0 \qquad (6)$$

when linear dissolution kinetics acts to a distance x (of eq. 1a). As the water flows along the fissure its calcite concentration increases until at location x_s it attains the value c_s, where the rates switch to a non-linear rate law (cf. eq. 1b). In this case one finds

$$\int_{c_s}^{c} \frac{dc}{k_n(1-c/c_{eq})^n} = 2(a_0+b_0)(x-x_s)/Q_0 \qquad (7)$$

Q_0 is the initial flow rate, and is found from eq. 5 as

$$Q_0 = \frac{\rho g a_0^3 \cdot b_0 \cdot M_0}{12\eta} \cdot \frac{h}{l} \qquad (8)$$

Integration of eq. 6 and eq. 7 and employing eq. 2 yields

$$F(x) = k_1 \exp(-x/L_1)(1-c_0/c_{eq}) \text{ for } x \le x_s \qquad (9)$$

and

$$F(x) = \frac{k_n(1-c_s/c_{eq})^n}{(\frac{x-x_s}{L_n}+1)^{n/(n-1)}} \quad \text{for } x > x_s \qquad (10)$$

where

$$L_1 = \frac{Q_0 c_{eq}}{2(a_0+b_0)\cdot k_1} = \frac{\rho g h}{12\eta l} \frac{a_0^3 \cdot b_0 \cdot M_0}{2(a_0+b_0)} \cdot \frac{c_{eq}}{k_1} \qquad (11)$$

and

$$L_n = L_1/(n-1);\ n \neq 1 \qquad (12)$$

Figure 2 illustrates this with the following scenario: Water with concentration $c0 = 0$ enters into the fracture with $b_0 >> a_0$. The dissolution rate at the entrance is $F(0)$. We have plotted $F(x)$ in units of $F(0)$ versus x/L_1. At the entrance the dissolution rates are determined by linear kinetics and drop exponentially until at $x = 2L_1$ the concentration has reached the switch point at $c_s = 0.86 \cdot c_{eq}$ (dotted line). From then on dissolution proceeds by a non-linear rate law and the rates drop by a hyperbolic relation. This is shown by the solid lines for $n = 2$, 4, and 10.

If, however, no switch were to occur, the rates would continue to drop exponentially as shown by the dotted line, and within a short distance of $x = 30\,L_1$ they are reduced by 13 orders of magnitude. In contrast to that the rates are reduced only moderately by about 3 orders of magnitude, when non-linear kinetics are active.

To translate the data of Figure 2 into real situations one has to know the values of L_1 and $F(0)$. Using $c_{eq} = 2 \times 10^{-6}$ mole/cm^3 and $k_1 = 5 \times 10^{-11}$ mole/cm^2/sec one finds $L_1 \approx 1.6 \times 10^8\ a_0^3 h/l$. In natural karst systems $a_o \approx 2 \times 10^{-2}$ cm and $h/l \approx 10^{-2}$. Therefore $L_1 \approx 10$ cm. Initial dissolution rates are converted from mole/cm^2/sec into cm/year by the factor 1.17×10^9. Thus the initial rates at the entrance are about 5×10^{-2} cm/year. If only first-order kinetics were operative, the dissolution rates would drop to about 10^{-45} cm/year at a distance of 10 m away from the entrance. Therefore, caves never could develop. The key to the evolution of caves is the non-linear kinetics, which allows the water to penetrate deep into the rock without losing its solutional power. This was first pointed out by Palmer (1984). From Figure 2 one reads that at a distance of about 1 km, dissolutional widening is about 5×10^{-9} cm/year for $n \ge 4$.

The initial dissolution rates at the exit of a yet-unwidened initial fracture of length l and width a_o can now be obtained from eqs. 10, 11, and 12 by considering that $l >> x_s$, $l >> L_n$, and $a_o >> b_o$:

$$F(l,0) = k_n\left(\frac{\rho g h}{24\eta l^2} \cdot a_0^3 \cdot \frac{c_{eq}}{k_n(n-1)}\right)^{\frac{n}{n-1}} \qquad (13)$$

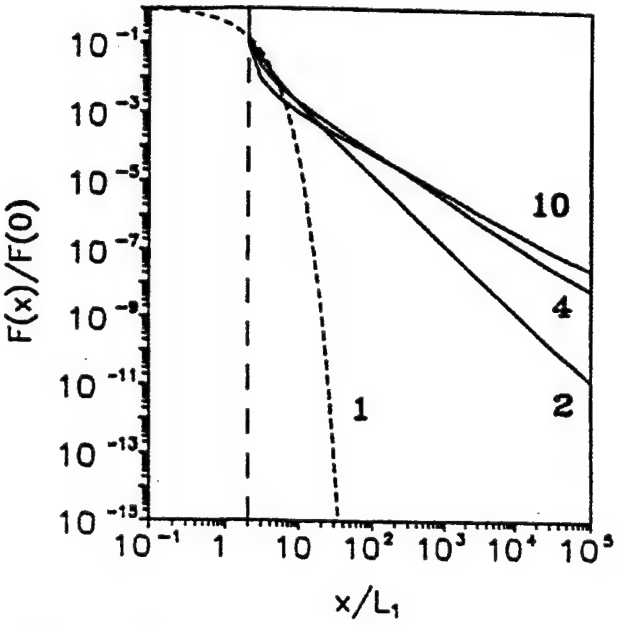

Figure 2: Dissolution rate in units of the initial rate *F(0)* as a function of distance, measured in units of L_t. The water flows to a distance $2L_t$ and dissolves calcite with linear kinetics, then switches to kinetics with $n_2 = 2$, 4, or 10 (as shown in solid lines). The dashed line shows dissolution with linear kinetics, when no switch occurs.

Note that the dissolution rates are independent of c_O and k_1 and that this equation represents an approximation, which is valid as long as $L_n >> L_0$. In this case they are entirely determined by the higher-order kinetics. The reason is that first-order kinetics acts only close to the entrance at a distance up to about $x_s \approx 10\text{cm}$, which is orders of magnitudes smaller than l. Therefore, the non-linear kinetics is active practically along the entire fracture.

Evolution of an one-dimensional conduit

To illustrate the evolution of a cave under such conditions, Figure 3 shows the results of a numerical model described elsewhere (Dreybrodt 1988, 1990, 1996). In this special case the parameters used are: $a_0 = 0.02$ cm, $b_0 = 100$ cm, $l = 10^5$ cm, $c_{eq} = 2 \cdot 10^{-6}$ mole/cm^3, $k_1 = 4 \cdot 10^{-11}$ mole/cm^2/sec, k_n = mole/cm^2/sec, $n = 4$, $c_s = 0.9 c_{eq}$.

Figure 3a shows the flow rate $Q(t)$ as a function of time. After a long gestation time of about 32,000 years, where $Q(t)$ increases by no more than one order of magnitude, there is a dramatically steep increase within a very short time span. We call this event breakthrough, and the time at which it occurs, the breakthrough time T_B. Figure 3b depicts the profiles of the initially uniform fracture as they evolve in time. Note that the scale of width is logarithmic. At the input of the fracture, dissolution rates are high and a funnel-like shape is created. Since the rates drop rapidly, this shape is restricted to distances close to the input. The rest of the fracture opens up more evenly with a slow widening at the exit, which finally accelerates dramatically, and within a short time span of about a hundred years opens up, allowing breakthrough to occur. During this evolution the kinetic length L_n increases in a similar way as $Q(t)$ (cf. eqs. 11 and 12.). As a consequence the concentration of the solution at the exit decreases slowly until at breakthrough it drops rapidly to values close to the concentration c_0 at the input.

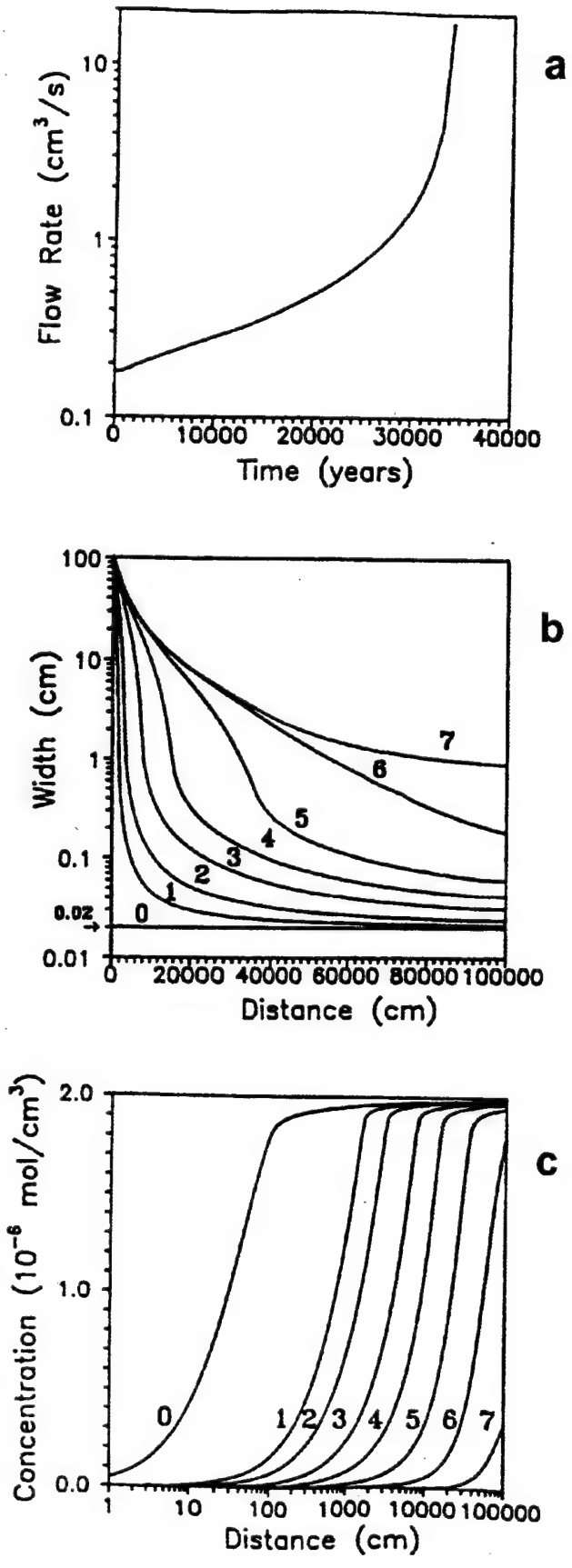

Figure 3: **(a)** Flow rate $Q(t)$as a function of time for a conduit with $a_o = 0.02$ cm, $b_o = 100$ cm, $l = 10^5$ cm, $i = 0.05$, $c_{eq} = 2 \times 10^{-6}$ mole/cm^3, $c_s = 0.9\ c_{eq}$, $k_1 = 4 \times 10^{-11}$ mole/cm^2/sec, $n = 4$, and $k_n = 4 \times 10^{-8}$ mole/cm^2/sec. The steep increase in flow rate marks the breakthrough time. Note the logarithmic scale of Q. **(b)** Profiles of the widths along the distance x for increasing times. From bottom to top, $T_0 = 0$ years, $T_2 = 20{,}000$ years, $T_3 = 30{,}000$ years, $T_4 = 33{,}000$ years, $T_5 = 34{,}000$ years, $T_6 = 34{,}100$ years, $T_7 = 34{,}110$ years. Note the dramatic increase in diameter in the last hundred years. Note also the logarithmic width scale. **(c)** Concentration profiles along the distance x for the times T_0 to T_7 listed above. The concentration front, i.e. the steep increase of the curves, moves slowly toward the exit as the conduit enlarges slowly. Note that the distance scale is logarithmic here.

From then on the fast first-oreder kinetics governs dissolution rates along the entire conduit, and during this new state of maturity a uniform and comparatively quick widening of the conduit results. This is illustrated in Figure 3c, which shows the concentration profile $c(x)$ for various times until breakthrough. Note that in Figure 3c the length scale is logarithmic. After the breakthrough event, turbulent flow sets in and furthermore the amount of water needed to sustain the hydraulic head may no longer be available. Therefore the hydraulic head drops to a new value, which is determined by the amount of meteoric precipitation. Consequently the upper entrance parts become vadose and further phreatic evolution of the conduits proceeds below the new water table.

Estimation of breakthrough time

To obtain a deeper understanding of the processes illustrated in Figure 3 we give an derivation of the breakthrough time which does not require numerical models.

From the knowledge of the dissolution rates at the exit of a plane-parallel fracture, it is possible to give an estimation of how the width of the exit develops with time. To this end we assume that the fracture is widened evenly along its entire length, with the dissolution rate acting on its exit. In reality this is not the case, since the dissolution rate at the exit is lower than everywhere else in the fracture. Therefore the fracture, instead of developing a bell-shaped profile, would maintain an even width *a(t)* after time *t*. This is illustrated by Figure 4. The initial tube has widened to a bell-shaped form. The width at the exit is *a(t)*. The dashed profile would have evolved if the dissolution rate at the exit had been active along the entire length.

We now, by use of eq. 13, calculate the dissolution rate $F(l,t)$ at the exit of the idealized uniform fracture with uniform width *a(t)*.

$$F(l,t) = F(l,0)\cdot\left(\frac{a^3(t)}{a_0^3}\right)^{n/(n-1)} \qquad (14)$$

This rate is smaller than the real rate, since the flow rate through the even fracture is less than that through the bell-shaped one.

The time to widen the initial fracture evenly by Δa is given by

$$T_1 = \frac{\Delta a}{2\gamma F(l,0)} = \frac{a_0}{2\gamma F(l,0)}\cdot\frac{\Delta a}{a_0} = T\cdot\frac{\Delta a}{a_0} \qquad (15)$$

where T is the time needed for doubling the width of the fracture

$$T = \frac{a_0}{2\gamma\, F(l,0)} \qquad (15a)$$

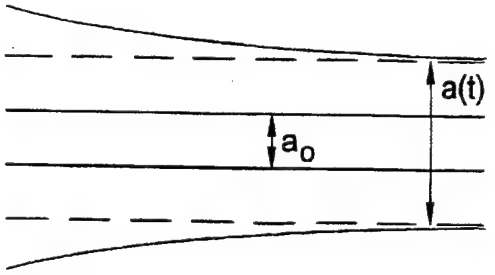

Figure 4: Profile of a fracture with initial width a_0 at time t after onset of karst evolution (solid line). The dashed line illustrates the profile that would have developed if the dissolution rate at the exit had been acting along the entire length of the fracture.

where $\gamma\cdot F(l,0)$ is the retreat of bedrock in cm/year, and the factor $\gamma = 1.17\cdot 10^9$ transforms the rates from mole/cm²/sec to cm/year.

After this time the dissolution rates have increased and a further even widening by Δa needs the time

$$T_2 = \frac{\Delta a}{2\gamma\, F(l,T_1)} = T\left(\frac{\Delta a}{a_0}\right)\cdot\left(\frac{a_0}{a_0+\Delta a}\right)^{3n/(n-1)} \qquad (16)$$

After m time steps the width has increased to $(a_o + m\cdot\Delta a)$ and the time T_m for further widening by Δa is given by

$$T_m = \frac{\Delta a}{2\gamma F(l,T_{m-1})} = T\left(\frac{\Delta a}{a_0}\right)\left(\frac{a_0}{a_0+m\Delta a}\right)^{3n/(n-1)} \qquad (17)$$

Therefore, the total time T_M necessary for widening the fracture to $(a_0 + M\Delta a)$ is

$$T_M = \sum_{m=1}^{M} T_m = T\cdot\sum_{m=1}^{M}(\Delta a/a_0)(1+m\Delta a/a_0)^{-3n/(n-1)} \qquad (18)$$

Figure 5 shows the widths of the fracture as it develops in time for several values of n and $\Delta a/a_0 = 0.001$. The curves depict the plot of T_M versus $a_0 + M\Delta a$.

After an initially slow widening, the widths increase rapidly and diverge at breakthrough time T_B. This time is given in the limit $M\to\infty$, and one finds by numerical calculations, that

$$T_B = \frac{n-1}{2n+1}\cdot T \qquad (19)$$

This becomes numerically practically independent of the ratio $\Delta a/a_0$ for $\Delta a/a_0 < 10^{-3}$. It should be noted that this value of T_B represents an upper limit owing to the approximation of uniform widening along the entire fracture (cf. Figure 4). In reality the fracture is wider, and therefore

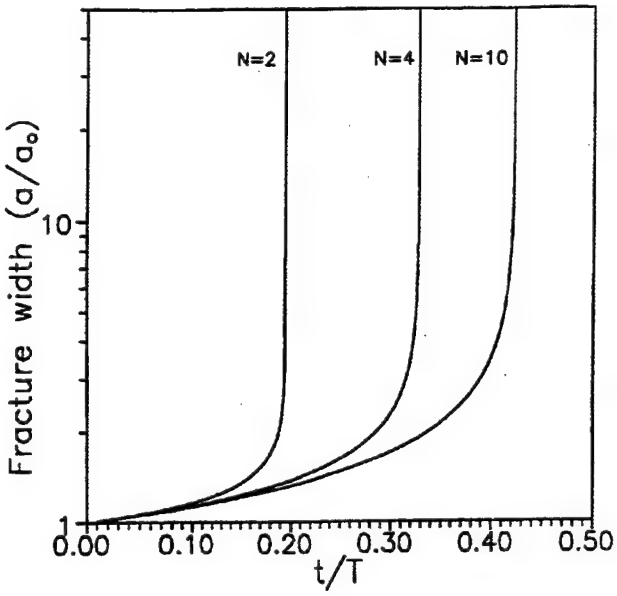

Figure 5: Evolution of the width of the idealized fracture as a function of time. The width is in units of a_0, and the time in units of T (cf. eq. 15a). The numbers on the curves give the order of the kinetics acting at the exit. Note that T depends on n. Therefore the time scales are different for n = 10, 4, and 2. The evolution of the fracture width is calculated from eq. 18 ($M = 10^4$ and $\Delta a/a_0 = 10^{-2}$.

---

it carries a larger flow. Therefore, according to eq. 13 the dissolution rates are larger, and correspondingly T_B becomes smaller.

After breakthrough the flow rate Q increases with $a(t)^3$. Therefore the length $L_1(t)$ increases correspondingly, such that the concentration approaches c_0 at the exit and the dissolution rates are uniform along the entire fracture.

The positive feedback is nicely demonstrated by eq. 17. Due to the increase of the dissolution rates at the exit by a power law of $a(t)$ with exponent $3n/(n-1)$ the times for widening the exit by Δa decrease correspondingly. Thus with increasing fracture width the dissolution rates are enhanced, and this accelerates widening until breakthrough occurs. This, however, is only possible if the hydraulic head remains constant. It is the increase of discharge under constant hydraulic head due to the increasing width of the fracture that causes the positive feedback. After breakthrough the flow rate will become limited, and the dissolution rates become constant with time.

Using eqs. 13 and 15, the breakthrough time can be written as a function of all parameters, which determine the evolution of the conduit along a fracture:

$$T_B = \frac{1}{\gamma}\cdot\frac{n-1}{2n+1}\left(\frac{1}{a_0}\right)^{\frac{2n+1}{n-1}}\left(\frac{24\eta l^2(n-1)}{\rho g h c_{eq}}\right)^{\frac{n}{n-1}}(k_n)^{\frac{1}{n-1}} \quad (20)$$

[years]

Units in eq. 17 are cm, mole, g, and sec. $\gamma = 1.17 \times 10^9$ converts the units of T_B into years.

So far we have assumed that the length L_n in eq. 10 is several orders of magnitude smaller than the length of the conduit, such that $l >> L_n$ and the value 1 in the denominator of eq. 10 can be safely neglected. In this case the dissolution rate F_{in} at the input is orders of magnitude higher than the initial rate $F(l,0)$ at the output. The feedback mechanism expressed by eq. 14 is valid only under these conditions.

However, $F(l,t)$ cannot increase beyond F_{in}. The general valid expression for $F(l,t)$ can be derived from eq. 10 as

$$F(l,t) = F_{in}\cdot\left(\frac{(l-x_s)\cdot a_0^3}{L_n\cdot a^3(t)}+1\right)^{-n/(n-1)} \quad (21)$$

Therefore, when $a(t)$ has increased to a sufficiently large value, the increase in growth rate at the exit slows until finally it reaches the constant value F_{in}. From then on the conduit increases linearly in time and evenly along its entire length. In most cases the flow becomes restricted to a constant value before this happens. But also then the feedback mechanism is no longer active and the conduit increases linearly in time.

If, however, the solution enters into the conduit with a concentration c_o sufficiently close to equilibrium with respect to calcite, and $c_o > c_s$, eq. 7 has to be changed by replacing $c_s = c_o$ and $x_s = 0$. By integration of the modified eq. 7 one finds

$$\tilde{L}_n = \frac{\rho g a_0^3 b_o h\cdot M_0\cdot c_{eq}}{24\eta(a_o+b_0)\,l\cdot k_n(1-c_o/c_{eq})^{n-1}\cdot(n-1)} \quad (22)$$

The dissolution rates in this case are given by eq. 21, considering $x_s = 0$ and $L_n = \tilde{L}_n$.

In any case the feedback mechanism expressed by eq. 14 is only operative as long as $la_0^3/(\tilde{L}_n a^3(t)) >> 1$ and it is effectively switched off when this ratio reaches values of about 0.1 (cf. eq. 10). Therefore, when the width $a(t)$ has reached the value

$$a_s(t_s) \approx 2a_0\left(\frac{l}{L_n}\right)^{1/3} \quad (23)$$

the exit rate takes the value $F_s(l,t_s) \approx 0.9\cdot F_{in}$ and beyond that time t_s the feedback mechanism is no longer active. Consequently the width of the conduit increases linearly with time and evenly along the entire conduit. This is

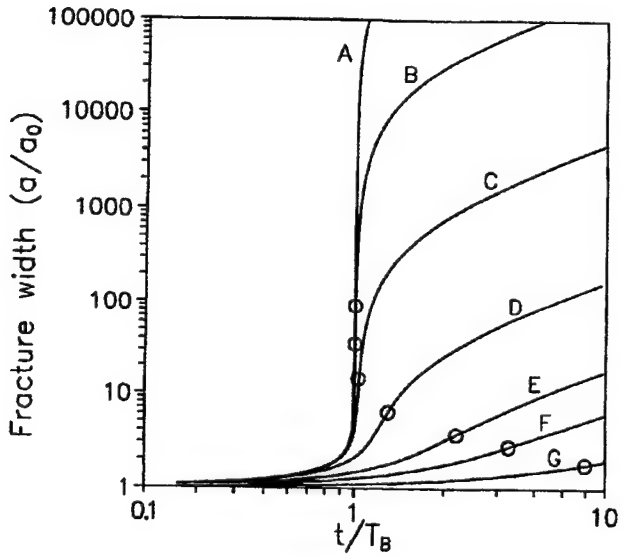

Figure 6a: Evolution of the idealized fracture for various input concentrations c_0 in a double logarithmic plot. A: $c_0 = 0.75\, c_{eq}$; B: $c_0 = 0.9\, c_{eq}$; C: $c_0 = 0.96\, c_{eq}$; D: $c_0 = 0.9825\, c_{eq}$; E: $c_0 = 0.99\, c_{eq}$; F: $c_0 = 0.9925\, c_{eq}$; G: $c_0 = 0.995\, c_{eq}$. The open circles mark the switch-off points, beyond which the positive feedback loop is no longer operative.

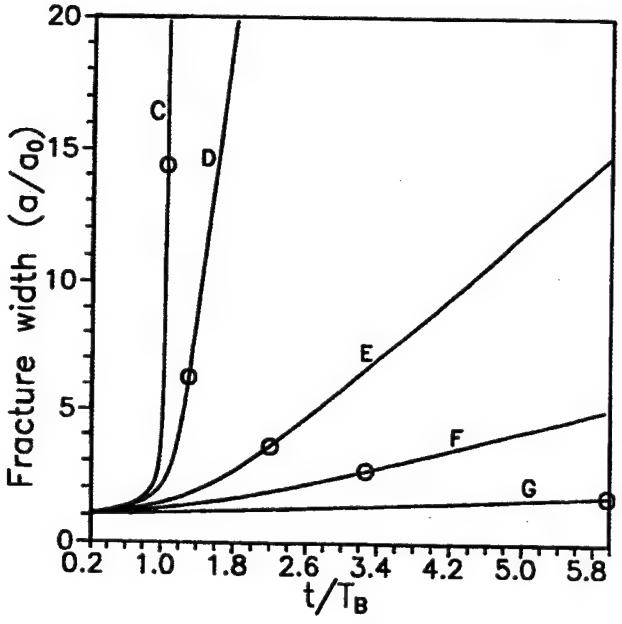

Figure 6b: Figure 6a in a linear plot to illustrate the linear growth during the time after the switch-off. The open circles mark the switch-off points, beyond which the positive feedback loop is no longer operative.

illustrated by Figure 6a, which shows the evolution of the idealized conduit for several values of c_0. Figure 6a depicts in a double logarithmic plot the width $a(t)/a_0$ versus T/T_B. Curves A and B visualize the case where the input concentrations $c_0 < c_s$, $c_A = 0.75\, c_{eq}$ and $c_B = c_s = 0.9\, c_{eq}$. In both cases breakthrough is independent of c_0. This is generally true as long as $c_o \le c_s$. As soon as $a(t)$ reaches $a_s(t_s)$, growth continues with a constant rate $2\gamma \cdot k_1(1 - c_o / c_{eq})$, given by eq. 1. This is shown by curve B. The open circle marks the switch-off point (a_s, t_s). A similar behavior is also shown by curves C $(c_0 = 0.96\, c_{eq})$ and D $(c_0 = 0.9825\, c_{eq})$. In this case $c_0 > c_s$ and therefore the higher-order kinetics acts along the entire conduit from the very beginning of its evolution. The switch-off points are marked by open circles on the curves in Figures 6a and 6b. For curve C, $l / \tilde{L}_n \approx 300$, and $l / \tilde{L}_n \approx 25$ for curve D.

For curves E, F, and G these values are 4.6, 2, and 0.6 respectively, since the input concentrations are sufficiently close to equilibrium. (E: $c_0 = 0.99\, c_{eq}$; F: $c_0 = 0.9925\, c_{eq}$, G: $c_0 = 0.995\, c_{eq}$. Therefore the initial dissolution rates at the exit (cf. eq. 21) are $0.1F_{in}$, $0.23F_{in}$, and $0.53F_{in}$ respectively. Consequently the feedback mechanism is reduced so efficiently that breakthrough does not occur. It should be noted that the logarithmic plot distorts the linear growth beyond t_s. To illustrate this region we have replotted curves A - G at a linear scale (Figure 6b). Clearly curves C, D, E, F, and G exhibit maximal constant growth rates beyond t_s and comparatively lower rates before this time.

Therefore when hydrogeologic conditions favor concentrations sufficiently close to equilibrium, $\tilde{L}_n$ achieves values of several kilometers, and even widening of the order of 10^{-9} cm/year may enlarge narrow fractures with aperture widths of several tens of μm over distances of kilometers in time scales of several tens of millions of years. This might be a general and ubiquitous mechanism creating sufficiently wide fractures as a prerequisite for later karstification, which then can occur under changing hydrogeologic conditions, which deliver solutions of sufficiently low input concentrations to the fractures in this way. In this way, "inception horizons" as postulated by Lowe (1992) may find a general explanation based entirely on the dissolution kinetics of limestone.

Evolution of two-dimensional conduit networks

Real karst systems are three-dimensional or at least two-dimensional. Aquifers leading water from an input to an output can develop only if percolating pathways exist. To give an answer as to whether such pathways do exist, we employ some basic results of percolation theory (Stauffer, 1985). Imagine a set of joints represented by a square lattice,

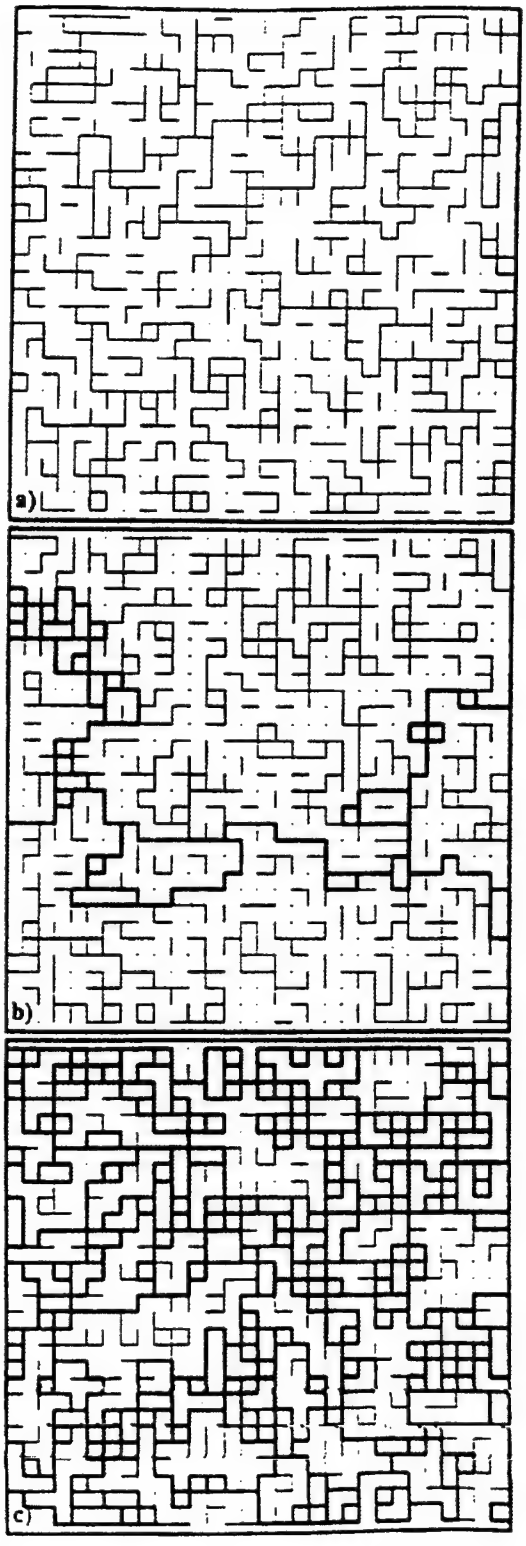

Figure 7: Percolation networks in a square lattice with occupation probability p = 0.4 (**a**, upper diagram), p = 0.5 (**b**, middle diagram), and p = 0.7 (**c**, lower diagram). The thin lines represent fractures that cannot transmit flow. The fat lines are fractures within a cluster and transmit water from the left-hand side to the right-hand side of the square lattice.

as depicted in Figure 7. Each space between neighboring points represents a possible location of a fracture; but fractures are not evenly distributed. Therefore we assume that each of these spaces is occupied by a real fracture with an occupation probability $p \leq 1$.

Figure 7a, for example, displays a small net of 30*x*30 with a probability p = 0.4, which means that on the average 40% of the possible locations contain a real fracture. We further assume that water enters at the left-hand side of the grid and leaves at the right-hand side, whereas the top and the bottom of the grid are impermeable. In Figure 7a we have plotted the real fractures by thick lines. We see that there are clusters of fractures that are not connected between the input and output, and which therefore cannot transmit water. In such a case a conduit cannot develop. Figure 7b illustrates the situation for p = 0.5. In this case the clusters have merged into each other and percolating pathways appear. All fractures conducting water to the output are marked by extra thick lines. From the shape of the percolation cluster we would expect a dentridic cave system. Figure 7c gives the situation with p = 0.7. Here we obtain a water-conducting network and the resulting cave system might be maze-like. Percolation pathways only can exist if $p \geq pc$, where *pc* is called the critical percolation threshold (Stauffer, 1985; Balberg, 1986; Sahimi, 1995). Therefore, in each setting having fractures with $p < pc$, karst development would not be possible. For values of $p \geq pc$, but still close to *pc*, the water is transmitted through a few pathways that may evolve to large conduits until the water table drops. If p, however, is close to 1 all the many fractures are employed to carry the water and the water table may drop even when the diameters of the evolving conduits are still small. Therefore, in highly fractured rock, karstification may be intense, but major cave systems may be missing. The boundary conditions, i. e. the regions of input and output, which are simple in Figure 7, may be restricted to a few input and output points. Correspondingly, even though a cluster extending over the entire area may exist, it may not lead water to the output. It is obvious, therefore, that the hydrologic setting is of utmost importance in the evolution of a system of conduits.

Furthermore, each of the fractures in the network has statistically distributed aperture widths a_o, breadths b_o, and lengths *l*. Among all the percolating pathways these will exhibit short breakthrough times, which on the average have a small flow resistance, i. e. a small average length and large average width, and which are also subject to the most favorable dissolution conditions. After breakthrough of one of these pathways the boundary conditions change due to a dropping water table, and only those pathways connecting the new water table to the output will develop further, whereas others will cease to grow. The first crude models using brickwork patterns of fractures in small 7*x*6 nets have

been presented by Groves and Howard (1994b). Their networks, however, were too small to provide sufficient spatial resolution. But, they all show that breaktrough, as in one-dimensional fractures, does occur, and therefore they provide the basis for more extended investigations such as those reported in this work.

From these arguments one may expect that the concept of breakthrough as derived from one-dimensional models (Dreybrodt 1996) is also valid for two-dimensional fracture networks. Correspondingly, one has to ask the question whether the equation for breakthrough time derived for single one-dimensional fractures (Dreybrodt 1996) is still meaningful. This is by no reasons trivial, since depending on the occupation probability the total length of a percolating pathway can vary quite considerably.

To answer this question we present a model of two-dimensional karstification in sufficiently large networks to reveal the details of cave evolution. Then we will use numerical sensitivity analysis to investigate the dependence of breakthrough times on the various physical, hydrogeologic, and chemical parameters involved.

Model structure

As the first step, a percolation network with given p is created. Next the boundary conditions for input and output are defined and all fractures which cannot transport flow are omitted. The remaining percolation cluster represents all percolating pathways. To calculate the flow rates in each fracture, a yet-unknown hydraulic head h_i is assigned to each node where three or more fractures are connected. The series of single fractures connecting such a point i to the next possible intersection point j constitutes an isolated flow resistance R_{ij}, which for laminar flow is given (Beek and Mutzall, 1975) by

$$R_{ij} = \frac{12\eta}{\rho g}\int_i^j \frac{dx}{a^3(x)b(x)M(x)} \qquad (24)$$

x represents the distance from node i along the series of fractures connected to the node j, and $a(x)$ and $b(x)$ are the profiles of the fracture diameters; ρ is the density of water, η its dynamic viscosity, and g earth's gravitational acceleration. Flow rates within these elements of the network are calculated by a mass-conservation equation for each of the nodes:

$$\sum Q_{in} - \sum Q_{out} = \sum_j Q_{ij} = 0 \quad ; \quad \frac{h_i - h_j}{R_{ij}} = Q_{ij} \qquad (25)$$

Q_{in} is the flow rate towards i, whereas Q_{out} is the flow rate away from it. Q_{ij} the flow rate in the pathway connecting nodes i and j. This set of linear equations is solved by standard methods, using a special CG-iteration procedure for sparse matrices (Jacobs, 1977). Once the heads h_i and h_j are known, the flow rates Q_{ij} are given (eq. 2). Then we calculate dissolutional widening for all tubes in the following way.

(A) First we select an input point at the boundary of the network. We specify the concentration c_{in} of the solution that flows into the input tube. Then we apply the one-dimensional transport-dissolution model (Dreybrodt 1996) to calculate the concentration profile along this tube, including the concentration of the solution leaving it at the next node, where this tube is connected to another one. Furthermore we calculate the new profile of the tube after a time step Δt. We repeat this procedure for all input points at the boundary. In the dissolution model the dissolution kinetics in eqs. 1 and 2 is used.

(B) In the next step we select all nodes where the concentrations of all the inflowing solutions are known. We assume complete mixing of these solutions before they are transferred into conduits transporting the flow away. For these, as described above, the one-dimensional transport-dissolution model is used to obtain the concentration of the solution at their exits, and also their new profiles after the time step Δt. Then we repeat procedure B until the new profiles of all conduits have been obtained.

For the new network, we calculate the new flow rates at time Δt and the new profiles at time $2\Delta t$. By repeating procedures A and B the profiles of all conduits and their flow rates can be obtained as a function of time. It should be noted that the boundary conditions and the input concentrations can be changed after each time step, thus considering external changes by climate or geological changes (e.g. uplifting or downcutting of base level). It is also possible, instead of specifying hydraulic heads at each arbitrary mode, to use fixed input flow rates. Thus a variety of geologic and climatic conditions can be simulated by the model.

Breakthrough in two-dimensional networks

Figure 8 gives an example of the breakthrough behavior typical for all simulations. The network with p = 0.7 simulates the initial hydrogeologic setting. The length L of the square is 3 km. The left-hand side contains a variety of input points at a hydraulic head of h = 150 m. The right-hand side contains output points, all at a hydraulic head of 0. The upper and lower sides of the square are assumed to be impervious. The width of the fractures is a_0 = 0.03 cm and their breadth b_0 = 100 cm. The concentration of the inflowing solution is c_0 = 0. The equilibrium concentration with respect to calcite is $c_{eq} = 2 \times 10^{-6}$ mole/cm^3. The rate constants of reaction kinetics are $k_1 = 4 \times 10^{-11}$ mole/cm^2/sec, $k_4 = 4 \times 10^{-8}$ mole/cm^2/sec, n = 4, and c_s = 0.9.

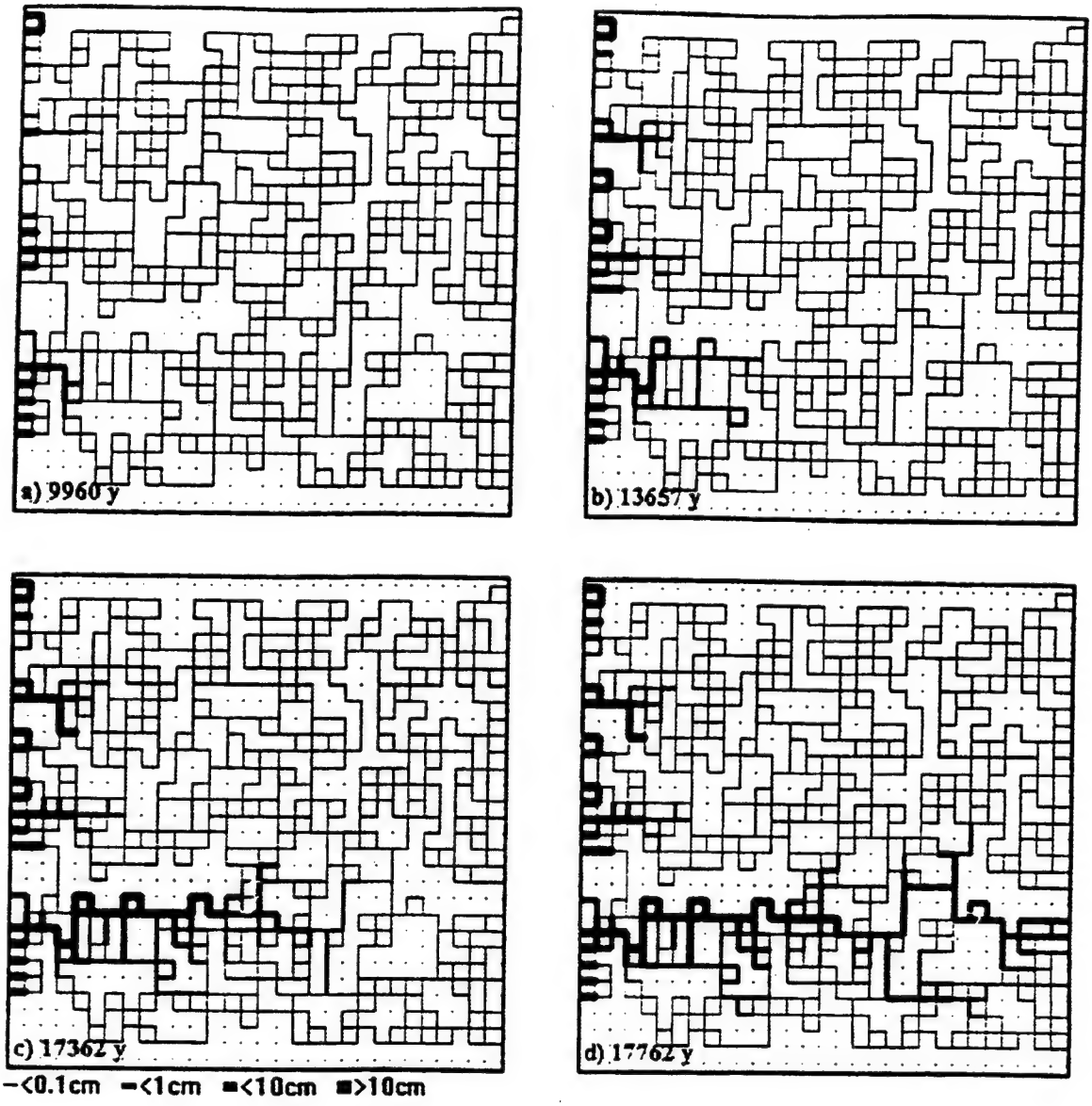

Figure 8: Evolution of a karst aquifer with p = 0.7 at 9960 years **(a)**, 13,657 years **(b)**, 17,362 years **(c)**, and 17,762 years **(d)**. The upper and lower boundaries are impervious. The left-hand boundary is at constant head (h) = 150 m, whereas the head at the right-hand boundary is 0 m. The thickness of the lines represents the average aperture of the fractures, as shown at the bottom of the figure. Parameters $a_0 = 0.03$ cm, $b_0 = 100$ cm, $\Delta h = 15{,}000$ cm, $L = 3 \times 10^5$ cm, $n = 4$, $c/c_{eq} = \hat{c}_s = 0.9$, $c_{eq} = 2 \times 10^{-6}$ mole/cm^3, and $k_4 = 4 \times 10^{-8}$ mole/cm^2/sec.

Figure 8a shows the average widths of the fractures after 9960 years. These average widths are those which a uniform conduit with even spacing $\bar{a}$ would exhibit, if it had the same resistance as the real conduit with a profile $a(x)$. Figure 8(b and c) illustrates the further evolution as the conduits penetrate into the system. Finally, after 17762 years, the first channel has reached an exit point. The distance of penetration $Lp(t)$ can now be defined by the largest distance from the input, where channels have been widened to 0.1cm. Breakthrough at time T_B is achieved when $Lp(T_B) = L$.

Figure 9 shows the following as a function of time: Lp/L, the width $a(t)/a(T_B)$, the water flow $Q(t)/Q(T_B)$, and the concentration $c(t)/c_{eq}$ of the solution at the breakthrough exit point. All these quantities show a typical breakthrough behavior. We define the breakthrough time by the time at which the concentration of the water leaving the major exit point drops below $10^{-3} \cdot c_{eq}$. In all cases flow was laminar, as checked by calculating the Reynolds Number to be below 1000.

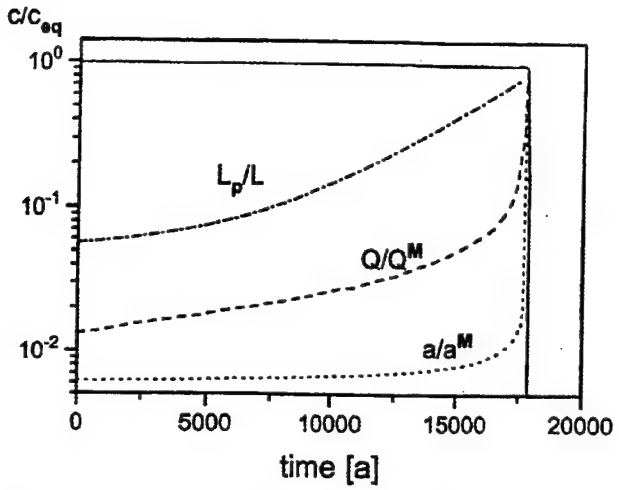

Figure 9: Evolution of penetration length L_p/L, flow rate Q/Q_M, fracture width a/a_M and the concentration $c/c_{eq} = \hat{c}_s$ at the exit of the winning pathway. Q_M and a_M are the values achieved at breakthrough. $Q_M = 518$ cm³/sec, and $a_M = 4.86$ cm. At breakthrough the concentration switches to values close to zero.

Numerical sensitivity analysis of breakthrough time

Using such a network but changing only one of its parameters at a time, we have calculated the dependence of the breakthrough time as a function of these parameters. The result is summarized by the following expression:

$$T_B = (a_0)^{\frac{2n+1}{n-1}} \cdot \left(\frac{L^2\eta}{hc_{eq}}\right)^{\frac{n}{n-1}} \cdot k_n^{\frac{1}{n-1}} \cdot c(p,s) \qquad (26)$$

The constant $c(p,s)$ is dependent only on the properties of the initial fracture system. It depends on the occupation probability p and the geologic setting s. This equation resembles closely that of the one-dimensional case (eq. 20) provided the the length l of the conduit is replaced by the spatial dimension L of the fracture system.

Figure 10 represents a verification of eq. 26. Here we have plotted the breakthrough times calculated for various a_0, L^2/h, c_{eq} and k_4 in a double logarithmic plot as functions of the corresponding variables, whereby we have used results from the fracture system shown in Figure 8. The straight lines plotted through the calculated point shows the validity of the power law, and the exponent can be calculated from its slope. The exponents obtained are within ±10% those predicted from eq. 20. We have also calculated the breakthrough times in their dependence on the various parameters as defined above for a variety of different values of n between $n = 3$ up to $n = 11$ and have found eq. 20 to be valid in this range. We have also performed such calculations on a variety of different initial fracture systems with identical boundary conditions and different

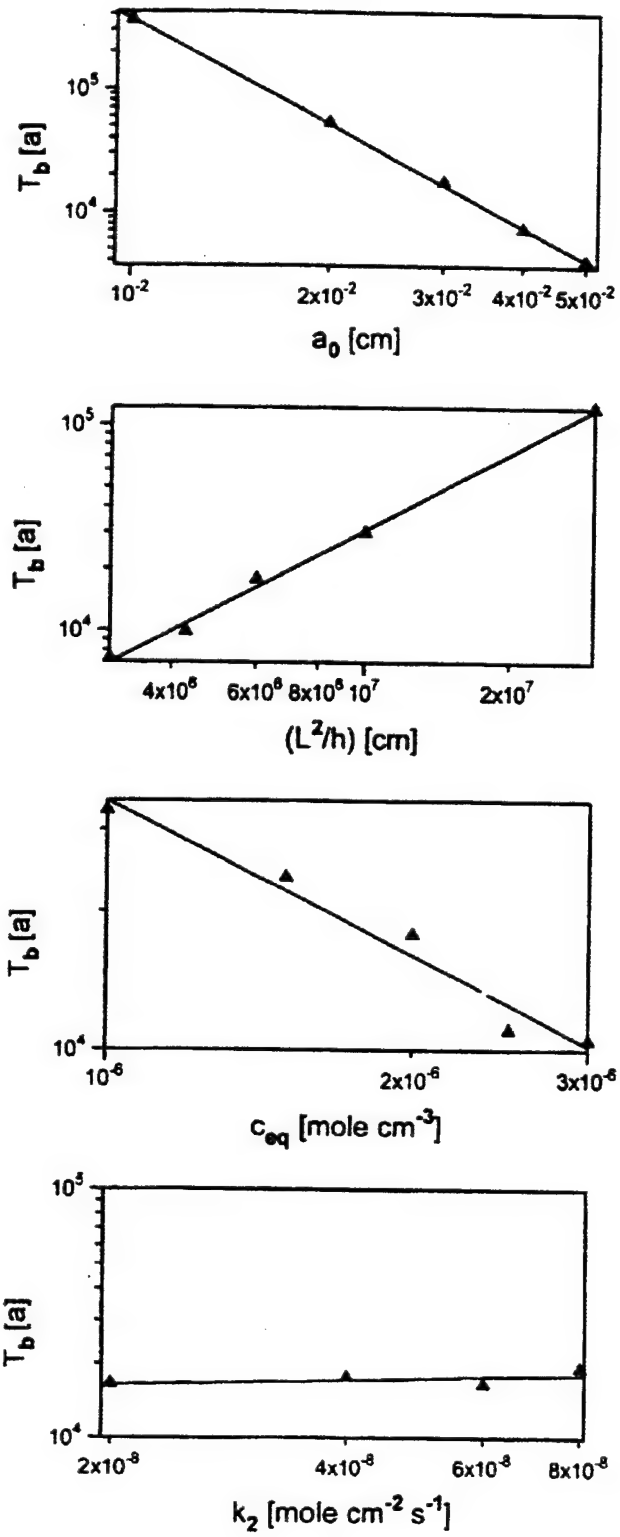

Figure 10: Double-logarithmic plot of breakthrough time as a function of a_0, (L^2/h), c_{eq}, and k_4 for $n = 4$ and p = 0.7, as obtained from comuter runs on the net of Figure 8.

occupation probabilities. These also have verified the predictions of eq. 20 (Siemers and Dreybrodt, 1998).

Discussion

One may consider the breakthrough time as a measure of the intensity of karstification in a limestone terrain. The shorter these times are, the higher is the degree of karstification. Thus, eq. 20 specifies the intensity of karstification in its dependence on the various specified parameters.

The hydrogeologic forces are reflected by the geometric parameters a_0, b_0, and l or L, but they are tied to the physical and chemical driving forces by the parameter group $[l^2\eta/(hc_{eq})]$ or $[L^2\eta/(hc_{eq})]$. In regions of low temperature, such as alpine or arctic karst, one expects low levels of CO_2 with P_{CO_2} from 0.1% up to 1% and consequently low equilibrium concentrations. In tropical karst P_{CO2} ranges from 0.2% up to 10% (Brook et al., 1983, Ford and Williams, 1989, White, 1988, Yuan Daoxian et al., 1991). Consequently calcite equilibrium concentrations are higher by at least a factor of two in tropical karst. Considering the temperature dependence of the viscosity, breakthrough times for otherwise identical settings are lower by about a factor of six in tropical karst compared to low-temperature karst.

One interesting feature is the fact that breakthrough times depend critically on n. For $n = 4$ an increase of l by a factor of only two extends the breakthrough time by a factor of six. Therefore, in areas of comparable hydraulic head h, one expects intensive karstification with many small caves, where geological setting allows comparatively short percolating pathways. In contrast, in regions of large l only few, but long, caves will be found.

Karstification times depend most sensitively on the initial fracture width. A variety of investigations using various methods report fracture widths between 5×10^{-3} and 10^{-1} cm with high probabilities in the region between 0.01 to 0.03 cm (Motyka and Wilk, 1984; Wilk et al., 1984; Böcker, 1969; Palliet et al, 1987; Palliet, 1988; Bandis et al, 1985; Johns et al, 1993). For wide fractures with $b_0 >> a_0$ and $a_0 = 2 \times 10^{-2}$ cm, breakthrough times are several tens of thousand of years for karst areas where i is high (0.1) and l is of the order of 100 m. Such times are realistic and have been reported by Ford (1988), Mylroie and Carew (1986), and Bakalowicz (1982) as minimum times required for the evolution of a karst aquifer to its maturity. For large systems with $l \approx 10$km and $i = 0.01$ correspondingly larger times in the order of ten million years are needed.

A further interesting point should be addressed. As we have shown, the breakthrough times are controlled by the dissolution rates at the exit of the fracture and therefore depend only k_n and n, but not on k_1. This leads to a most important conclusion. Since the kinetic length of the first-order kinetics at the entrance is extremely short, the concentration drops quickly to c_s, in most realistic cases after a distance of about $10^{-3} \cdot l$. From there on the higher-order kinetics takes over (cf. Figure 3c). Therefore higher-order kinetics practically acts along the entire tube, and consequently it does not matter whether the water entering the fracture has already dissolved limestone from the overlying soil. As long as the concentration c_0 remains below c_s, breakthrough times will not be influenced considerably. This is also the result of numerical calculations, which in comparison to $c_0 = 0$ show no more than an increase of about 10% for $c_0 = c_s$, provided c_{eq} is not altered. For these reasons, in contrast to current opinions, the initiation of karstification is not enhanced when allogenic water with low hardness enters a limestone terrain.

After breakthrough, however, turbulent flow sets in and the flow rates become restricted by the amount of water available at the surface. Due to the large flow velocities the concentration of Ca^{2+}, changes little along the entire flow path and stays close to its value at the input. Therefore dissolution rates are uniform throughout the conduit. These rates, however, depend on the concentration of the inflowing water and cave development in the mature state is enhanced when allogenic water of low calcium concentration enters the cave (Dreybrodt, 1996). Maximal rates are about 10^{-2} cm/year, but rates lower by one order of magnitude should be realistic (Dreybrodt and Buhmann, 1991; Liu and Dreybrodt,1997).

Conclusion

To conclude this work, Figure 11 illustrates the history of the formation of a mature conduit. It shows the conduit width at the exit as a function of time. Since during the initial phase it is of the order of 10^{-2} cm, its values are magnified by a factor of 5000 to become visible. During the gestation or initial phase the exit width varies extremely slowly until it has reached twice its initial width. Then shortly breakthrough sets in and turbulent flow is established. The concentration of Ca^{2+} drops to low values such that a uniform dissolution rate is active along the entire channel length. The initiation time depends critically on the length and the initial width of the fracture, and in realistic cases it covers the range from about ten thousand to ten million years.

After breakthrough, enlargement of the conduit proceeds under phreatic conditions at a rate of about 400 mm/ky with variations of about 200 mm/ky. In contrast to the initiation phase, the enlargement phase is similar for all phreatic conduits and independent of their former

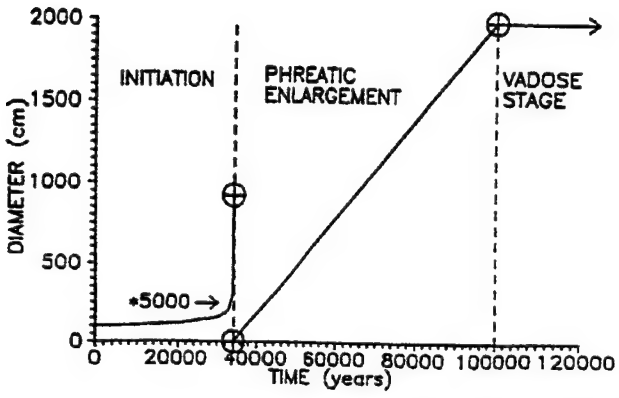

Figure 11: Schematic diagram of the evolution of a conduit from initiation to maturity. The encircled x symbols mark the transition from initiation to phreatic enlargement and from there to the vadose state.

development. Eventually the conduit will become vadose with a river flowing in it. Then entrenchment of canyons with similar rates will occur. Finally the passage becomes completely abandoned and growth stops until at a later time, because of varying external conditions, it may become active again and resume growth. The active phreatic phase is comparatively short, since it takes only about 100,000 years to create a passage about 30 m diameter, which is not often encountered in nature.

Finally, this work shows that to understand the evolution of cave systems one has to consider the dissolution kinetics of limestone. An understanding by only looking for the influence of calcite equilibrium in the system $H_20 - CO_2 - CaCO_3$ is not possible.

Acknowledgement

Franci Gabrovšek thanks the University of Bremen for financial support. This work was supported by the Deutsche Forschungsgemeinschaft.

References Cited

Bakalowicz, M., 1982, La genèse de l'aquifère karstique vue par un géochemiste: Reun. Monogr. Sobre Karst-Larra, v. 82, p. 159-174.

Balberg, I., 1986, Connectivity and conductivity in 2d and 3d fracture systems: Ann. of Israel Phys. Soc., v. 8, p. 89-101.

Bandis, S.C., A. Makurat, and G. Vik, 1985, Predicted and measured hydraulic conductivity of rock joints: Paper presented at the Int. Symp. on Fundamentals of Rock Joints, Int. Soc. of Rock Mechanics.

Beek, W.J. and K.M.K. Mutzall, 1975, Transport Phenomena: Wiley, New York.

Brook, G.A., M.E. Folkoff, and E.O. Box, 1983, A world model of soil carbon dioxide: Earth Surface proc. & Landforms *v.* 8, p. 79-88.

Böcker, T., 1969, Karstic water research in Hungary: Bull. Int. Assoc. Sci. Hydrol., v. 14, n. 4, p. 7-20.

Buhmann, D. and W. Dreybrodt, 1985, The kinetics of calcite dissolution and precipitation in geologically relevant situations of karst areas. 1. Closed system: Chem. Geol., v. 53, p. 109-124.

Dreybrodt W., 1988, Processes in karst systems - Physics, Chemistry and Geology, Springer Series in Physical Environments 5: Springer Berlin, New York.

Dreybrodt, W., 1990, The role of dissolution kinetics in the development of karstification in limestone: A model simulation of karst evolution: Journal of Geology, v. 98, p. 639-655.

Dreybrodt, W., 1992, Dynamics of karstification: A model applied to hydraulic structures in karst terranes: Applied Hydrogeol., v. 1, p. 20-32.

Dreybrodt, W., 1996 Principles of early development of karst conduits under natural and man-made conditions revealed by mathematical analysis of numerical models: Water Resources Research, v. 32, p. 2923-2935.

Dreybrodt, W. and D. Buhmann, 1991, A mass transfer model for dissolution and precipitation of calcite from solutions in turbulent motion: Chem. Geol., v. 90, p. 107-122.

Dreybrodt, W., J. Lauckner, L. Zaihua, U. Svensson, and D. Buhmann, 1996, The kinetics of the reaction $CO_2 + H_2O \Rightarrow H^+ + HCO_3^-$ as one of the rate limiting steps for the dissolution of calcite in the system $H_2O - CO_2 - CaCO_3$: Geochimica et Cosmochimica Acta, vol. 60, p. 3375-3381.

Eisenlohr, L., B. Madry, and W. Dreybrodt, W., 1997, Changes in the dissolution kinetics of limestone by intrinsic inhibitors adsorbing to the surface, *in* Proceedings of the 12th Int. Cong. of Speleology, La Chaux de Fonds, Switzerland, 6th Conference on limestone hydrology and fissured media v. 2, p. 81-84,

Ford D.C., 1988, Characteristics of dissolution cave system in carbonate rocks, *in* N.P. James and P.W. Choquette (eds.), Paleokarst: Springer Verlag.

Ford, D.C., and P.W. Williams, 1989, Karst geomorphology and hydrology: Unwin & Hyman, 601 p.

Groves, C.G., and A.D. Howard, 1994a, Minimum hydrochemical conditions allowing limestone cave development: Water Resources Research, v. 30, no. 3, p. 607-615.

Groves, C.G., and A.D. Howard, 1994b, Early development of karst systems. 1. Preferential flow path enlargement under laminar flow: Water Resources Research. v. 30, p. 2837-2846.

Jacobs, D., 1977, The State of the art in numerical analysis: Academic Press.

Johns, R.A., J.S. Steude, L.M. Castanier, and P.V. Robert, 1993, Nondestructive measurements of fracture aperture in crystalline rock cores, using X-ray computer tomography: Journal of Geophys. Res., v. 98, p. 1889 - 1900.

Liu, Z., and W. Dreybrodt, 1997, Dissolution kinetics of calcium carbonate minerals in H2O-CO2 solutions in turbulent flow: The role of the diffusion boundary layer and the slow reaction: Geochimica et cosmochimica acta, v. 61, p. 2879-2889.

Lowe, D.J., 1992, The origin of limestone caverns: in inception horizon hypothesis: PhD Thesis, Manchester Metropolitain University/Council for National Academic Rewards.

Motyka, I., and Z. Wilk, 1984, Hydraulic structure of karst-fissured Triassic rocks in the vicinity of Olkusz (Poland). Kras i speleologia: v. 14, n. 5, p. 11-24.

Mylroie, J.E., and J.L. Carew, 1986, Minimum duration of speleogenesis: Proc. 9th International Congress of Speleology, Barcelona v. 1, p. 249-251.

Paillet, F.L., A.E. Hess, C.H. Cheng, and E. Harding, 1987, Characterization of fracture permeability with high-resolution vertical flow measurements during borehole pumping: Ground Water, v. 25, p. 28-40.

Paillet, F.L., 1988, Fracture characterization and fracture-permeability estimation at the underground research laboratory in southeastern Manitoba, Canada: U. S. Geol. Survey, Water Resources Investigation, v. 88, p. 4009.

Palmer, A.N., 1984, Recent trends in karst geomorphology: Journal of Geological Education, v. 32, p. 247-253.

Palmer, A.N., 1991, The origin and morphology of limestone caves: Geol. Soc. of America Bull., v. 103, p. 1-21.

Sahimi, M., 1995, Flow and transport in porous media and fractured rock: Weinheim, VCH Verlag.

Siemers, J., and W. Dreybrodt, 1998, Early development of karst aquifers on percolation networks of fractures in limestone: Water Resources Research, in press.

Stauffer, D., 1985, Introduction to percolation theory: London and Philadelphia, Taylor & Francis Ltd.

Svensson, U., and W. Dreybrodt, 1992, Dissolution kinetics of natural calcite minerals in CO_2 -water systems approaching calcite equilibrium: Chem. Geol., v. 100, p. 129-145.

White, W.B., 1988, Geomorphology and hydrology of karst terrains: Oxford University Press, New York.

Wilk, Z., J. Motyka, and I. Józefko, 1984, Investigations of some hydraulic properties of karst solution openings and fractures: Annales Societatis Geologorum Poloniae Rocznik Polskiegotowarystwa Gelogicznego, v. 43, 1/2, p. 15-43.

Yuan D., 1991, Karst of China: Geological publishing house, Beijing.

POTENTIAL INFLUENCE OF APERTURE VARIABILITY ON THE DISSOLUTIONAL ENLARGEMENT OF FISSURES

Harihar Rajaram, Wendy Cheung, and Blair Hanna
Dept. of Civil Engineering, University of Colorado, Boulder, CO 80309

Introduction

Development of conduits and caverns in soluble rock occurs by sustained dissolution over large spatial scales. It is widely believed that the occurrence of extensive cave systems in carbonate rocks is largely due to the steep drop in the dissolution rate as the solubility limit is approached. White (1977) referred to the sudden rise in dissolution rate in a growing conduit as a "kinetic trigger" that leads to major cave development. In recent years, quantitative modeling of dissolutional growth of fractures in limestone (e.g. Dreybrodt, 1990, 1996; Palmer, 1991; Groves and Howard, 1994; Howard and Groves, 1995; Hanna and Rajaram, 1998) have contributed significantly to improved understanding of the morphology of cave systems and time-scales of evolution. Clemens et al. (1996) included natural boundary conditions such as springs and recharge into their model for a more complete understanding of karst development. Initiation of conduits during the early evolution of karst is of particular interest, because it is believed to be the slowest phase of cave development.

The dissolutional growth of a single one-dimensional fracture was modeled by Dreybrodt (1990, 1996), Palmer (1991), and Groves and Howard (1994). In all of these studies it was observed that once turbulent flow is initiated, further dissolutional growth occurs at a relatively rapid rate. In these works, the duration of the initial phase of karst evolution is quantified using the concept of "breakthrough time," which refers to the time at which turbulent flow is first encountered. As breakthrough is approached, the flow rate through the system increases rapidly, leading eventually to turbulent flow. After breakthrough occurs, conduits are expected to grow at a relatively rapid rate of a few millimeters a year (Dreybrodt, 1990, 1996; Groves and Howard, 1994). Thus the occurrence of breakthrough ensures further development of caverns. The time required for the onset of turbulent flow typically depends on the length of the fissure, the hydraulic gradient and the initial aperture. Typical breakthrough times estimated from one-dimensional studies by Dreybrodt (1990, 1996) and Groves and Howard (1994) range from 5×10^5 to 10^6 years (0.25 mm initial aperture, 1000 m long, hydraulic gradient of 4%). The mechanism by which conduits are initiated in one-dimensional systems is by progressive enlargement of the entrance and subsequent increase in flow rate (Dreybrodt, 1996).

Groves and Howard (1994) and Siemers and Dreybrodt (1998) simulated dissolutional growth of a network of fractures, illustrating the highly selective growth patterns that result during the initial phase (before breakthrough occurs). Hanna and Rajaram (1998) considered the dissolutional growth of a two-dimensional variable aperture fissure, motivated by the widespread recognition that natural fissures exhibit highly irregular geometries (e.g. Tsang and Witherspoon, 1981; Brown and Scholz, 1985; Power and Tullis, 1991; Zimmerman and Bodvarsson, 1994; Brown, 1995). Their computational experiments illustrated that highly selective channelized growth patterns occur in variable aperture fissures. Other important conclusions from their study are that (i) aperture variability leads to reduced breakthrough times and (ii) sustained dissolutional growth can occur even in the absence of a kinetic trigger. The fundamental mechanism leading to these features is the "reactive infiltration instability" identified by Ortoleva et al. (1987). The essence of the reactive infiltration instability is as follows: when a plane dissolution front is perturbed, dissolution fingers develop and advance ahead of the average dissolution front; since the permeability is larger within the fingers, more flow is focused into the fingers, leading to an increased rate of dissolutional enlargement within the fingers and slower enlargement outside the fingers. The irregular geometry of natural fissures will provide an inherent mechanism for initiating unstable growth and result in behavior significantly different from that of one-dimensional fissures.

In this paper we present some published results from Hanna and Rajaram (1998) and additional results related to the influence of the correlation scale of the aperture field. We also clarify some of the underlying features of dissolutional growth in variable-aperture fissures, such as progressive flow capture by the dominant dissolution channels. The influence of aperture variability on the breakthrough time is investigated based on simulations carried out in multiple realizations of the random-aperture field. For each set of statistical parameters, average breakthrough times are estimated based on multiple realizations and compared to the breakthrough time in a uniform-aperture fissure. Additional simulations are presented to illustrate that aperture variability can lead to sustained growth of conduits even in the absence of a kinetic trigger.

Stochastic model of a variable aperture fissure

To our knowledge, no field observations of aperture variability within a single fissure in a karst formation are reported in the literature. Dreybrodt (1990, 1996) cites field data obtained from a depth of about 150 m in a mine in Poland, wherein typical aperture values in networks of limestone fissures before karstification were found to be about 0.2 mm on the average, with extreme values larger than 0.5 mm. In the present study, we used hydraulic aperture values of about 0.25 mm, which is within the range suggested by Dreybrodt (1990). Different degrees of fissure variability were used to assess the sensitivity of the breakthrough time to the aperture variance. The logarithm of the initial aperture field within a single fissure is represented as an isotropic second-order stationary gaussian random field (i.e. the aperture values are log-normally distributed). These models have also been used in numerical studies of solute transport in rock fractures (e.g. Moreno et. al., 1988; Tsang and Tsang, 1989). Some other studies (e.g. Brown and Scholz, 1985; Power and Tullis, 1991; Brown, 1995) suggest that non-stationary models such as self-similar random fields are required for modeling the roughness of natural rock surfaces. However, even in these studies, the power-spectrum of the aperture field (modeled as the space between the two rough surfaces) takes on a constant value below a certain cutoff wavenumber. A finite value of the power-spectrum at zero wavenumber essentially implies stationarity. For this reason, we have chosen to employ a second-order stationary random field description of aperture variability. The influence of self-similar or multi-scale variability and anisotropy in the aperture field on dissolutional growth of fissures are topics which may be addressed separately at a future date. It should be noted further that a log-normal field cannot take on negative values. Therefore, contact areas are not represented if a lognormal distribution is used to describe the aperture field. Alternatively, we may view the hydraulic aperture at the scale of a grid block as log-normally distributed.

The natural logarithm of the aperture field, denoted as *lnb*, is represented as follows:

$$lnb(x,y) = \mu_l + f(x,y) \qquad (1)$$

In eq. 1, μ_l is the mean value of *lnb* and f(x,y) is a zero-mean, second-order stationary, isotropic random field with an exponential covariance function of the following form:

$$R(\xi_x,\xi_y) = E[f(x,y)f(x+\xi_x,y+\xi_y)] = \sigma_l^2 \exp\left(-\sqrt{\frac{\xi_x^2}{\lambda_x^2}+\frac{\xi_y^2}{\lambda_y^2}}\right) \qquad (2)$$

In eq. 2, $R(\xi_x, \xi_y)$ is the covariance function corresponding to separations ξ_x and ξ_y in the x and y directions respectively; σ_l^2 is the variance of *lnb*; E[ ] denotes the expectation operator; (x,y) refers to a spatial location; λ_x and λ_y are the correlation scales in the x and y directions respectively. When λ_x and λ_y are equal, an isotropic two-dimensional random field results. Random fields with the desired covariance function (eq. 1) are generated using a Fourier summation algorithm described by Shinozuka and Jan (1972). The mean (μ) and variance (σ) of the aperture field are related to those of the log-aperture field based on the familiar relationships between the moments of log-normal and normal distributions, i.e. $\mu = \exp(\mu_l + \sigma_l^2/2)$, $\sigma^2 = \exp(2\mu_l + \sigma_l^2)(\exp(\sigma_l^2 - 1))$. In this study, the coefficient of variation of the aperture field $\sigma/\mu = (\exp(\sigma_l^2 - 1))^{1/2}$ is used as a measure of the degree of heterogeneity.

Computational methods

A full description of the governing equations, computational methods, and validation exercises are presented in Hanna and Rajaram (1998). The computations involve solution of the two-dimensional flow (based on the cubic law) and reactive transport equations, invoking the low value of the ratio of solubility limit to the mineral density to simulate dissolutional growth via a sequence of quasi-steady states. This approximation was introduced previously by Ortoleva et al. (1987) and Lichtner (1988). The calcite dissolution kinetics was specified based on the empirical rate expressions presented by Palmer (1991).

The numerical solution of the quasi-steady equation to determine the head distribution is based on the conventional finite-difference approach (e.g. Bear, 1979, pp.450), which leads to a five-diagonal symmetric matrix system of equations. A pre-conditioned conjugate gradient algorithm was used to obtain the head solution. The preconditioning matrix was computed based on the modified implicit factorization (MIF) technique (Larabi and De Smedt, 1992). The flow solver requires that the mass-balance error (i.e. relative error between inflow and outflow rate) is less than 1%, and that the error norm is less than 10^{-16}. The quasi-steady state Ca^{2+} concentration field is computed using an upstream-weighted finite-difference approximation to the transport equation. Additional approximations used to speed up the transport solution and validation of the numerical solutions are described by Hanna and Rajaram (1998).

A grid size of 0.1 m in the x and y directions, used in the computations, adequately captures the sharp concentration front near the entrance to the fissure at early time, thus preventing numerical saturation and leading to reliable estimates of the breakthrough time. An alternative approach to grid design employed in reactive infiltration problems

involves adaptive gridding (e.g. Ortoleva, et al., 1987, Dreybrodt, 1996). Although it may be cumbersome to come up with an adaptive gridding scheme suitable for heterogeneous velocity fields, this is an important issue which merits further investigation. Experimentation with different values of Δt on fissures with σ/μ in the range of 0.0 to 2.0, for hydraulic gradients within the range considered in this study, revealed that the breakthrough time estimated using $\Delta t = 1.0$ year is not reduced by more than 6% as Δt is further refined. For this reason, a value of $\Delta t = 1.0$ year is used in all the simulations.

Computational results

In this section the influence of aperture variability on the breakthrough time is quantified based on detailed computations. The primary quantity of interest is the extent to which the breakthrough time is reduced, quantified by the ratio of time to breakthrough in a variable-aperture fissure to that in a uniform aperture fissure of the same length, and the same initial effective transmissivity. With the same initial effective transmissivity, the initial flow rate through the fissure is the same for a given hydraulic gradient. It is well established (see, e.g., Gelhar, 1987; Tsang and Witherspoon, 1981, Zimmerman and Bodvarsson, 1994) that the equivalent hydraulic aperture for a two-dimensional variable aperture-fissure with isotropic correlation structure and a log-normal aperture distribution, is the geometric average. For this reason, the geometric average of the initial aperture field was maintained the same in all cases compared against each other. The domain under consideration is a 15 m x 15 m fissure, with a hydraulic gradient of 20% imposed along two parallel boundaries, and no-flux boundary conditions on the other two parallel boundaries. Two sets of simulations were carried out to determine the influence of aperture variability. σ/μ values of 0.25, 0.5, 0.75, 1.0, 2.0 were considered, maintaining λ constant at 1.0. Values of λ used were 0.1, 0.5, 1.0, 2.0, and 5.0 with constant $\sigma/\mu = 0.5$. In the two sets of simulations that follow, 5 realizations of the random-aperture field were carried out for each σ/μ and λ.

In a fracture with uniform aperture, the dissolution pattern involves uniform enlargement of the whole width of the conduit near the entrance. In contrast, the dissolution is focused in a few high-permeability channels in variable-aperture fissures. For smaller values of σ/μ, the dissolution channels are wider and the dissolution is more diffuse; while for large values of σ/μ, the dissolution channels are narrow and more tortuous. The growth of the fissure occurs primarily along preferential flow paths, suggesting that the morphology of conduits is related to the structure (and number) of preferential flow paths (Figure 1). Figure 1 also suggest highly selective growth patterns -- only one dissolution channel eventually breaks through to the outflow end of the domain, and the growth of other dissolution channels is inhibited by the dominant channel. This feature is evident in the experimental studies of Ewers (cited by Ford and Williams, 1989) and Hoefner and Fogler (1988). A highly selective enlargement of fractures is also evident in numerical simulation studies of dissolutional growth in random networks (Groves and Howard, 1994) during the laminar flow regime and possibly explains the structure of caves in meteoric regimes. As noted by Meakin (1991), selective growth and dominance of a single channel is characteristic of a broad range of Laplacian growth models wherein fluid flow is described by a linear equation such as the Darcy equation.

The role of heterogeneity in fissures is critical to the early stages of karst growth and breakthrough time as shown in Figure 2. In comparison to $\sigma/\mu = 0.0$, or a uniform fissure, when σ/μ is increased to 2.0, the drop in breakthrough time is almost an order of magnitude. It is also observed that within each set of realizations, there is more variability with greater σ/μ. Figure 3 illustrates that with increasing σ/μ, less travel time through narrower channels results in smaller values of total mass removed at breakthrough. However, the rate of mass removed is apparently larger. The entrance flux for selected time periods (Figure 4) shows that for all σ/μ values, only one dominant flow channel exists. On the log-normal plot, while the dominant flow channel continues to increase with time, the flux drops in the surrounding region, a phenomenon which can be explained well by the mechanisms described by the reactive infiltration instability. The fluxes increase only in the dominant channels upward to 4 orders of magnitude. The development of dominant flow channels can only occur in 2-dimensional modeling, not 1-dimensional, as discussed later. This feature implies that a kinetic trigger is not really essential for breakthrough to occur. [Editor's note: "breakthrough" in the authors' context refers to the onset of turbulent flow. Most modelers use the change to low-order chemical kinetics, causing a sharp increase in reaction rate, as the criterion for breakthrough (e.g. Dreybrodt, this volume). In general, both changes take place at roughly the same time -- but not necessarily (as is demonstrated here).]

A second set of simulations was run while varying the correlation scale or λ to provide insight into the effect of spatial persistence on the development of flow channel. The size of the fracture modeled was 15 m x 15 m. With increasing correlation scale, the degree of connectivity of each grid block to its neighbor becomes greater. Figure 5 shows this results in wider channels and greater dominance of the leading dissolution channel. In Figure 6, the breakthrough time decreases as λ increases up to a value approximately that of domain length/6 before it begins to level off. There is only about a 30% reduction in

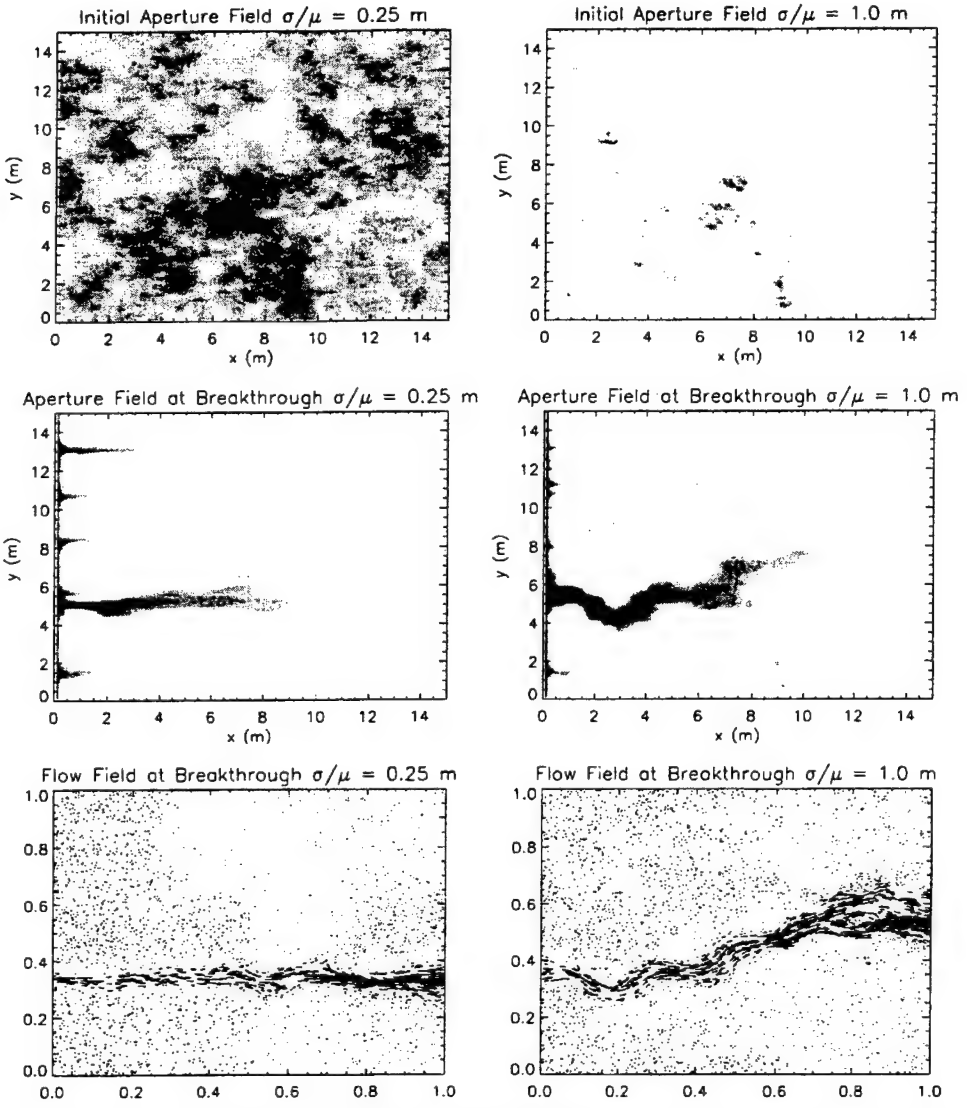

Figure 1: Comparison of aperture fields at t = 0 and breakthrough for $2\sigma/\mu$ cases. Darker shades correspond to larger aperture values. The flow field at breakthrough is also shown to illustrate focusing of flow into the dominant dissolution channel.

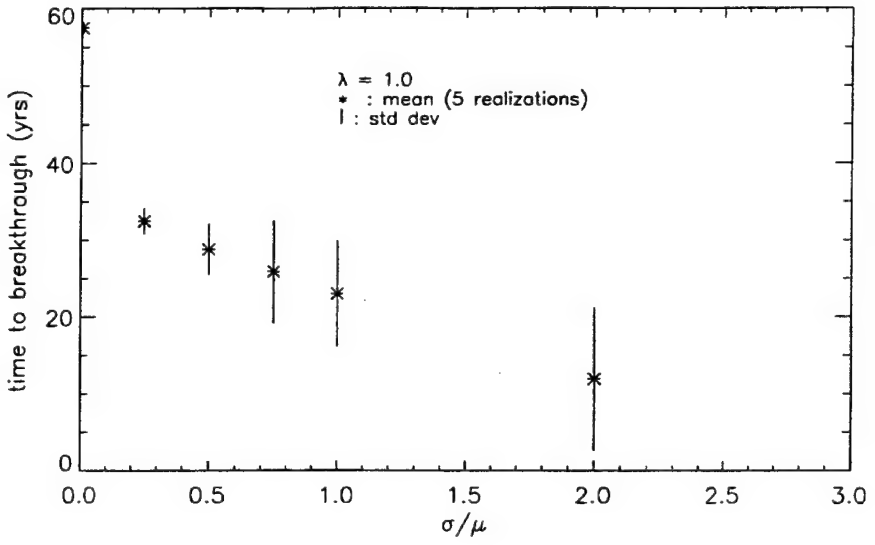

Figure 2: Average breakthrough time for varying $2\sigma/\mu$.

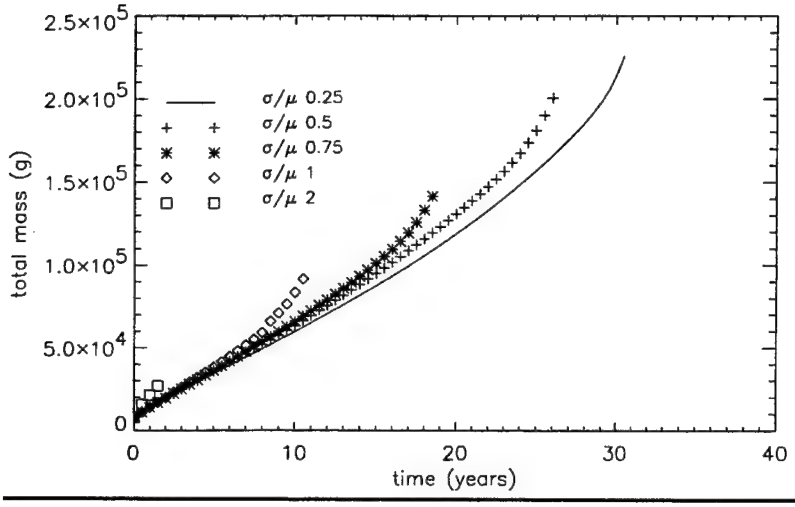

Figure 3: Average mass removed for varying $2\sigma/\mu$.

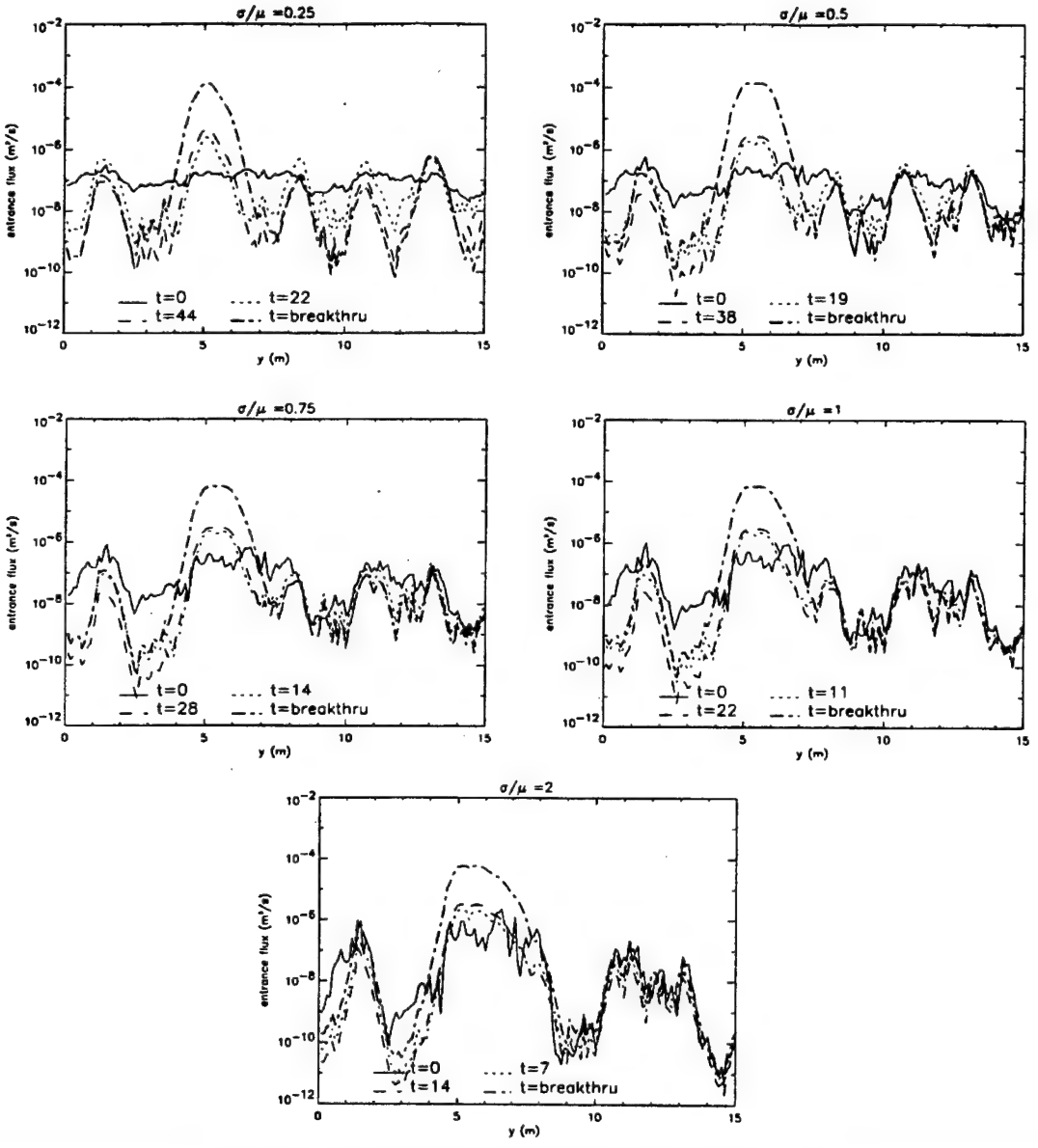

Figure 4: Entrance flux profiles for varying $2\sigma/\mu$ ($\lambda = 1$).

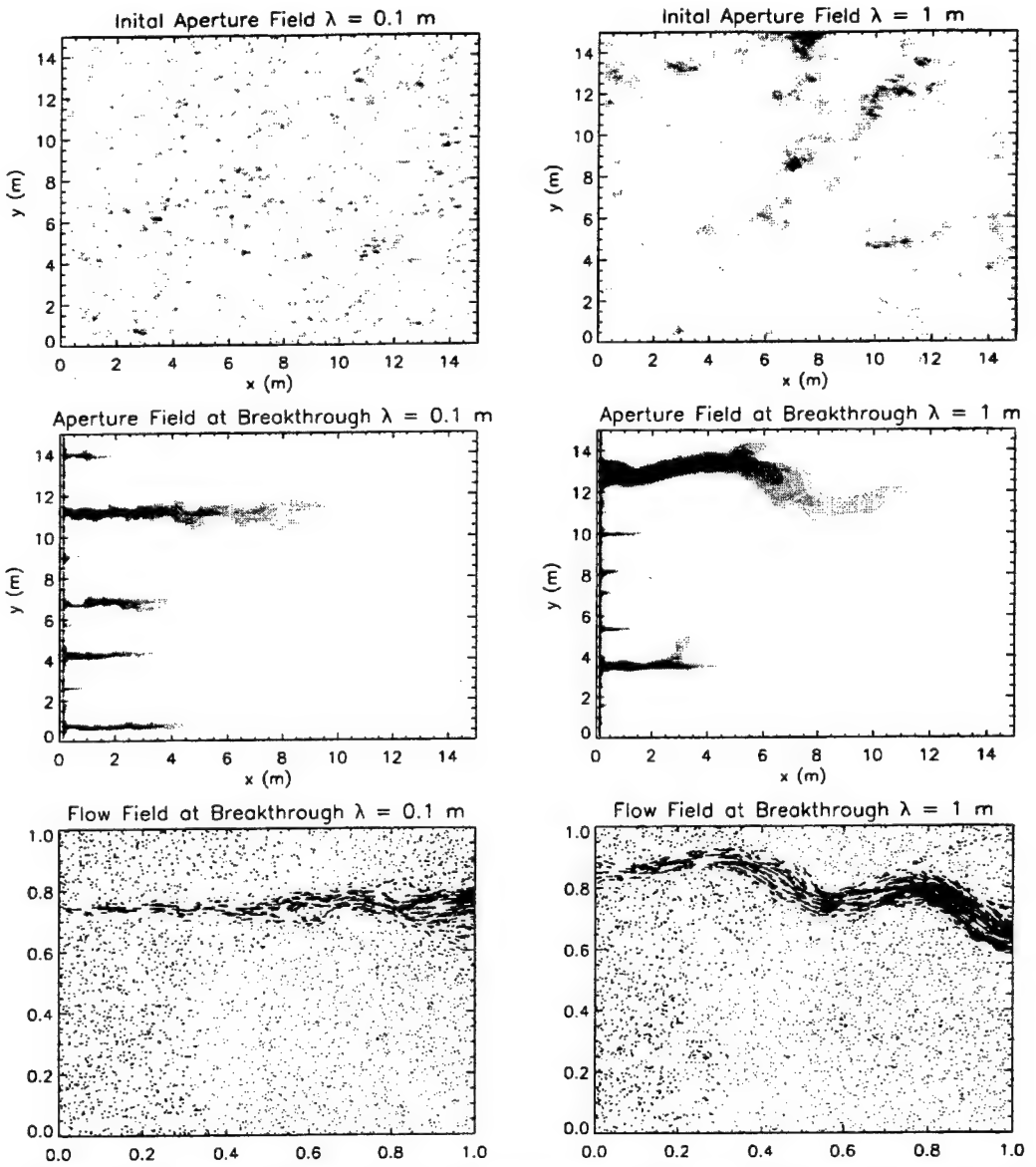

Figure 5: Comparison of aperture fields at t = 0 and breakthrough for 2λ cases. Darker shades correspond to larger aperture values. The flow field at breakthrough is also shown to illustrate focusing of flow into the dominant dissolution channel.

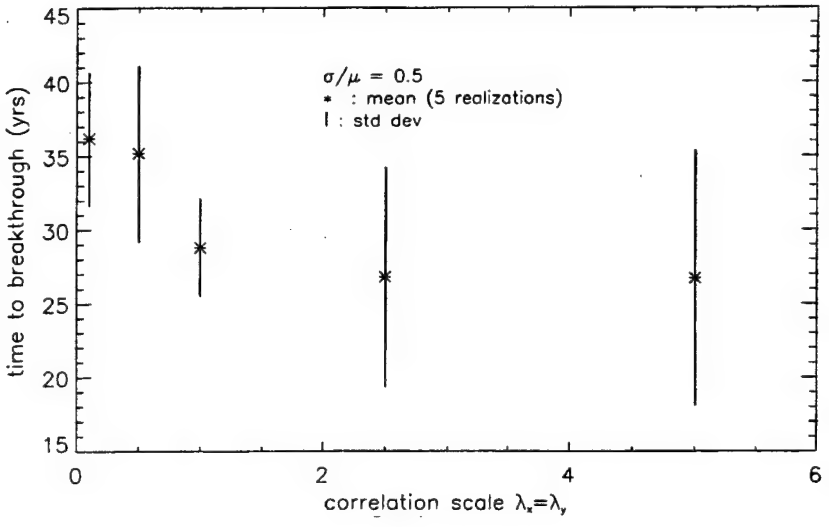

Figure 6: Average breakthrough time for varying λ.

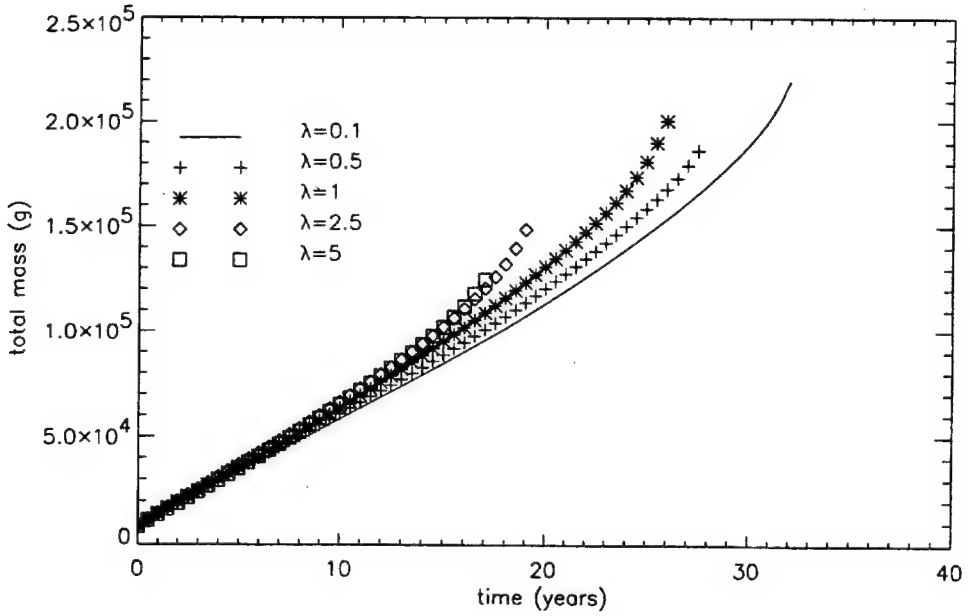

Figure 7: Average mass removed for varying λ.

breakthrough time from the smallest λ (0.1 m). Perhaps as λ increases even more and approaches the domain length, breakthrough time will increase since the fissure will be more uniform. The cumulative mass removal, shown in Figure 7, drops as λ increases. This effect is not as obvious as the simulations with varying σ/μ, whose breakthrough times were also more dramatic. There appears to be a widening of flow channels for increasing λ values up to those which correspond to the level-off of breakthrough times (Figure 8). Consistent with σ/μ results, for all λ values, a dominant flow channel does persist to breakthrough.

Dissolution rates and kinetics vary significantly between different minerals (Ford and Williams, 1989). For instance, gypsum is known to dissolve according to first-order kinetics over a large range of concentrations, at a relatively fast rate (James and Lupton, 1978). It is generally believed that waters which come in contact with a rapidly dissolving mineral will become saturated with respect to that mineral within a relatively short distance, inhibiting sustained conduit growth over large distances. As noted previously, the slower dissolution rate of calcite close to saturation, is widely believed to be the key to extensive karstification in limestone formations. Based on their one-dimensional experiments and computational studies, James and Lupton (1978) suggested that "runaway situations" (sustained dissolutional enlargement leading to breakthrough) are not expected to occur in gypsum, except at very high hydraulic gradients. In this section, we compare the breakthrough times obtained in uniform and variable aperture fissures over a wide range of first-order reaction. An aperture value of 0.25 mm was used for the uniform aperture fissure, and the variable aperture fissures had the same initial hydraulic aperture. A moderate value of 0.5 was used for the coefficient of variation of the aperture field (σ/μ). The same hydraulic gradient of about 19% was maintained across the fissure for both cases.

The influence of the reaction rate on the breakthrough time is shown in Figure 9 for both the uniform and variable-aperture fissures. The reaction rate is represented as K (mg/m^2/s) = 7.1 (mg/m^2) k (s^{-1}), and k is varied over a wide range. For small values of the reaction rate k, there is little difference between the breakthrough times in uniform and variable aperture fissures. When the reaction rates are slow, the fluid in contact with the rock is undersaturated within the entire fissure. As a result, dissolutional growth occurs throughout the fissure and flow is not focused by preferential growth into high flow channels. At large values of the reaction rate however, the behavior of a variable aperture fissure is dramatically different from that of a uniform aperture fissure. The time to breakthrough increases with reaction rate in a uniform fissure, whereas there is no change in breakthrough time in the case of a variable-aperture fissure.

In contrast to the uniform fissures, the growth of preferential flow channels within variable aperture fissures is sustained by their ability to progressively capture flow away from the surrounding regions. The difference between the behavior of uniform and variable-aperture fractures at high reaction rates is of practical significance. Dissolutional growth of conduits and caves in massive gypsum have been observed in the vicinity of dams such as the abandoned McMillan dam (James and Lupton, 1978). These cave systems were not detected before construction, and are therefore believed to have developed in a relatively short time. Whereas one-dimensional models of dissolutional

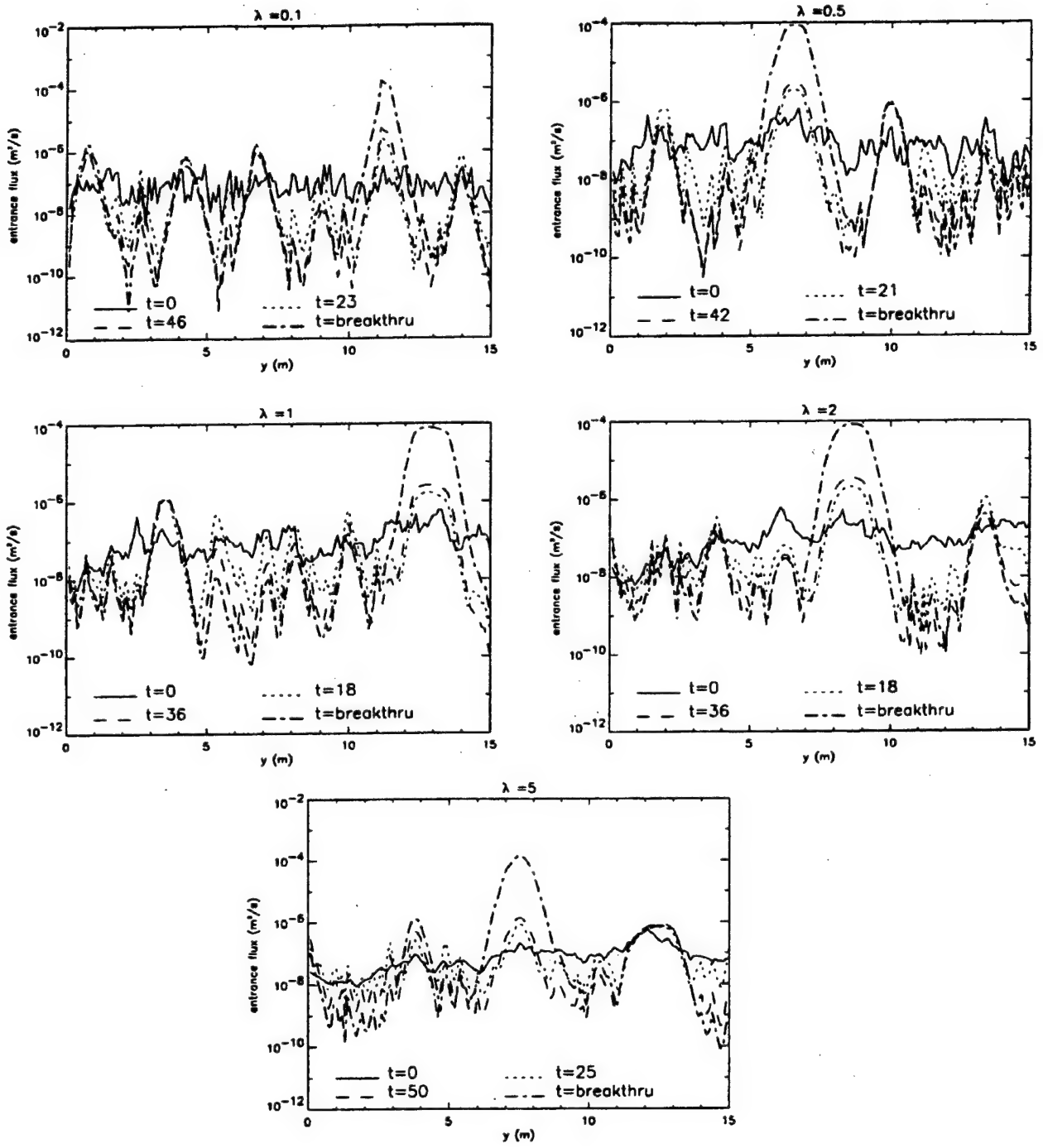

Figure 8: Entrance flux profiles for varying λ ($\sigma/\mu = 0.5$).

growth may predict that cave development will not occur within short time scales, cave development is almost sure to occur in reality, due to aperture variability within fissure systems. On a larger scale, variability between mean aperture values in networks of fissures can lead to a larger-scale preferential growth mechanism which leads to further acceleration in conduit development.

Summary and discussion

In this paper, we have illustrated the potential influence of aperture variability on the dissolutional enlargement of a fissure, based on numerical simulations. Our investigation focused on the initiation phase of conduit growth, wherein the flow is in a laminar regime. The duration of the initiation

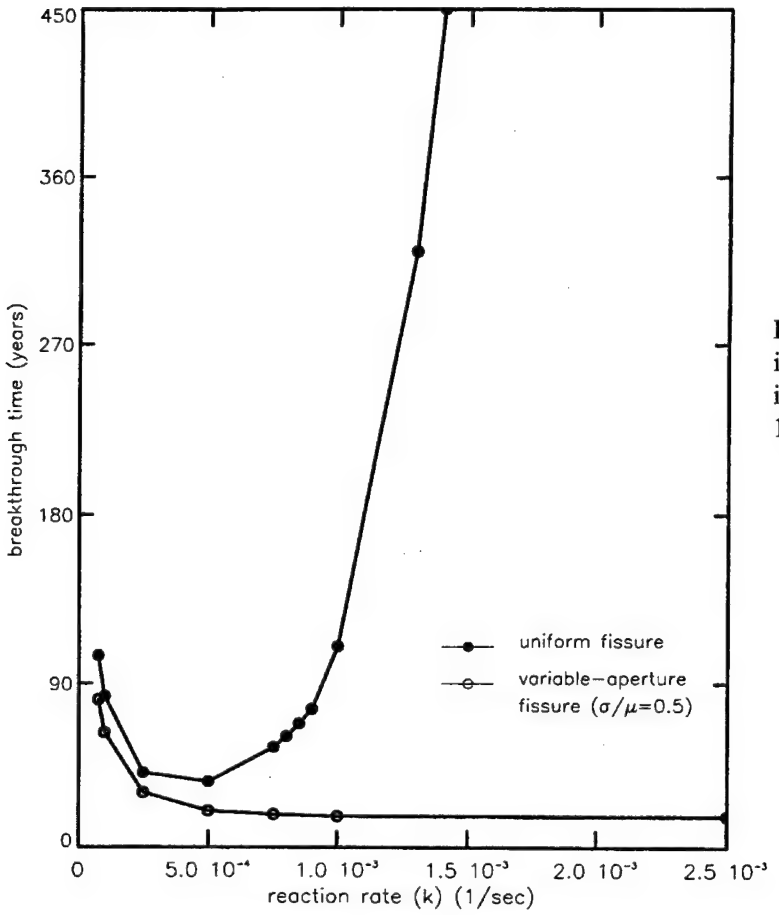

Figure 9: Comparison of breakthrough times in uniform and variable-aperture fields for varying linear reaction rates (Hanna and Rajaram, 1998).

phase is quantified using the concept of breakthrough time (time required for the first occurrence of turbulent flow within the fissure). The influence of aperture variability on the breakthrough time is examined based on numerical simulations in multiple realizations of random aperture fields. The logarithm of the aperture (ln b) is represented as an isotropic gaussian random field, with an exponential correlation structure. The size of the fracture modeled is 15 m x 15 m. The influence of the degree of aperture variability (quantified based on the coefficient variation (σ/μ) of the aperture field) and the correlation scale (λ) are examined. We also examined the dissolutional growth of a variable-aperture fissure in the absence of a kinetic trigger. The following points summarize our results:

(i) With correlation scales of 1 m ($\lambda_x = \lambda_y = 1$ m), aperture variability leads to a reduction in the time to breakthrough by a factor of two, even for very small degrees of heterogeneity ($\sigma/\mu = 0.1$) and by as much as an order of magnitude for large degrees of heterogeneity ($\sigma/\mu = 2.0$). At larger values of σ/μ, dissolution patterns suggest narrower and more tortuous conduits. As expected, the variability between breakthrough times in different realizations increases as σ/μ increases.

(ii) With a value of $\sigma/\mu = 0.5$, an increase in the correlation scale from 1 m to 2 m led to a reduction in breakthrough time by about 30%. Further increase in the correlation scale, up to 5 m, does not appear to reduce the breakthrough time further. As expected, the variability in breakthrough times between different realizations increases as the correlation scale increases. The dissolution channels are wider as the correlation scale increases.

(iii) The key mechanism contributing to accelerated conduit growth is the "reactive infiltration instability" identified by Ortoleva et al. (1987). In a variable aperture fissure, dissolution occurs at a faster rate in high-flow channels, leading to faster enlargement within these channels, and slower enlargement outside them. As a result, these high-flow channels progressively capture flow away from the surrounding regions and grow at a relatively fast rate.

(iv) As σ/μ or the correlation scale increases, less mass of calcite needs to be dissolved before the onset of turbulent flow. This results from a combination of a reduction in the breakthrough time and highly selective growth. However the overall rate of mass removal before the onset of turbulence is larger in both cases.

(v) With fast first-order dissolution reactions, rapid conduit growth can occur in a variable-aperture fissure, whereas in a uniform-aperture fissure the fluid becomes saturated with respect to the mineral very near the entrance and the breakthrough time becomes very large. It is widely believed that the change in reaction order leading to slower dissolution as saturation is approached is essential for sustained growth over large distances (Palmer, 1984). However, our results indicate that aperture variability can lead to sustained growth even with linear dissolution reactions. This is again due to the rapid growth along preferential flow paths, which leads to a progressive "capture" of flow away from the rest of the fracture and hence sustains growth. These results may partially explain why sustained conduit growth can occur in gypsum, whereas previous one-dimensional studies (e.g. James and Lupton, 1978) indicate otherwise.

A limited amount of data is available on the nature of aperture variability in fissures and faults (e.g. Brown and Scholz, 1985; Brown, 1995; Power and Tullis, 1991). However, the extent of heterogeneity that could occur in a karst formation before karstification is initiated is not adequately quantified. Based on the results presented in this study, we suggest that characterization of heterogeneity in soluble rock formations can be useful in refining estimates of breakthrough times and understanding the morphology of conduit systems. The study of dissolutional enlargement of fissures is also important in connection with the safety of nuclear waste repositories (e.g. Lichtner, 1996) and the impact of acid mine drainage or acid rain on carbonate terrains (Wicks and Groves, 1993). Variability in the hydraulic properties of rock fissures potentially impacts all of these phenomena. Additional field and computational studies will help to identify the influence of statistical parameters such as correlation scales relative to the domain length, anisotropy and self-similarity in aperture variations on the dynamics of dissolutional growth.

Acknowledgments

This research was supported partly by the National Science Foundation under grant number EAR 9734404 and the United States Department of Energy, Office of Basic Energy Sciences, through grant number DE-FG03-96ER14590.

References cited

Bear, J., 1979, Hydraulics of groundwater: McGraw Hill.

Brown, S. R., and C. H. Scholz, 1985, Broad Bandwidth Study of the Topography of Natural Rock Surfaces: Journal of Geophysical Research, v. 90, B14, p. 12575-12582.

Brown, S.R., 1995, Simple mathematical model of a rough fracture: Journal of Geophysical Research, v. 100, B4, p. 5941-5952.

Clemens, T., D. Hückinhaus, M. Sauter, R. Liedl, and G. Teutsch, 1996, A combined continuum and discrete network reactive transport model for the simulation of karst development, *in* Calibration and reliability in groundwater modeling, Proceedings of the ModelCARE 96 Conference held at Golden, Co., Sept. 1996: UAGS Publ. No. 237.

Dreybrodt, W., 1990, The role of dissolution kinetics in the development of karst aquifers in limestone: A Model Simulation of Karst Evolution: Journal of Geology, v.98, no. 5, p. 639-655.

Dreybrodt, W.,1996, Principles of early development of karst conduits under natural and man-made conditions revealed by mathematical analysis of numerical models: Water Resources Research, v. 32, no. 9, p. 2923-2935.

Ford, D. C., and P. Williams, 1989, Karst geomorphology and hydrology: Boston, Unwin Hyman Ltd.

Freeze, A.L., and J. Cherry, 1979, Groundwater: New York, Prentice-Hall.

Gelhar, L.W., 1987, Applications of stochastic models to solute transport in fractures rocks: Swedish Nuclear Fuel and Waste Management Company, SKB Tech. Rep. 87-05, Stockholm, Sweden.

Groves, C.G., and A.D. Howard, 1994a, Minimum hydrochemical conditions allowing limestone cave development: Water Resources Research, v. 30, no. 3, p. 607-616.

Groves, C.G, and A.D. Howard, 1994b, Early development of karst systems, 1. Preferential flow path enlargement under laminar flow: Water Resources Research, v. 30, no.10, p. 2837-2846.

Hanna, R.B., 1996, Genesis of hydraulic conduits in karst aquifers: a two-dimensional modeling approach: Masters Thesis, Department of Civil, Environmental, and Architectural Engineering, University of Colorado, Boulder, Colorado.

Hanna, R.B., and H. Rajaram, 1998, Influence of aperture variability on dissolutional growth of fissures in karst formations: Water Resources Research, v. 34, no. 11, p. 2843-2853.

Hoefner, M.L., and H.S. Fogler, 1988, Pore evolution and channel formation during flow and reaction in porous media: AIChE Journal, v. 34, no.1, p. 45-53.

Howard, A.D., and C.G. Groves, 1995, Early development of karst systems, 2. Turbulent flow: Water Resources Research, v. 31, no.1, p. 19-26.

James, A.N. and A.R.R. Lupton, 1978, Gypsum and anhydrite in the foundations of hydraulic structures: Geotechnique v. 28, no. 3, p. 249-272.

Larabi, A., and F. De Smedt, 1994, Solving three-dimensional hexahedral finite element groundwater models by preconditioned conjugate gradient methods: Water Resources Research vol. 30, no. 2, p. 509-521.

Lichtner, P.C.,1988, The quasi-stationary state approximation to coupled mass transport and fluid-rock interaction in a porous media: Geochimica et Cosmochimica Acta, vol. 52, p. 143-165.

Lichtner, P.C., 1996, Continuum formulation of multicomponent-multiphase reactive transport, *in* Reactive Transport in Porous Media: Reviews in Mineralogy vol. 34, Mineralogical Society of America.

Meakin, P., 1991, Fractal aggregates in geophysics: Reviews of Geophysics, vol. 29, no.3, p. 317-354.

Moreno, L., Y.W. Tsang, C.F. Tsang, F.V. Hale, and I. Neretnieks, 1988, Flow and tracer transport in a single fracture: A stochastic model and its relation to some field observations: Water Resources Research vol. 24, no. 12, p. 2033-2048.

Ortoleva, P., E. Merino, C. Moore, and J. Chadam, 1987, Geochemical Self-Organization I: Reaction-Transport Feedbacks and Modeling Approach, American Journal of Science, 287, 979-1007.

Palmer, A.N., 1984, Recent trends in karst geomorphology: Journal of Geological Education, v. 32, p. 247-253.

Palmer, A.N., 1991, Origin and morphology of limestone caves: Geological Society of America Bulletin, vol. 103, no. 1, p. 1-21.

Plummer, L.N., T.M.L. Wigley and D.L. Parkhurst, 1978, The kinetics of calcite dissolution in CO_2-water systems at 5-60° C and 0.0 to 1.0 atm CO_2: American Journal of Science, vol. 278, p. 179-216.

Power, W. L., and T. E. Tullis, 1991, Euclidean and fractal models for the description of rock surface roughness: Journal of Geophysical Research, vol. 96, B1, p. 415-424.

Shinozuka, M., and C.M. Jan, 1972, Digital simulation of random processes and its applications: Journal of Sound and Vibration Engineering, vol. 25, no. 1, p. 111-128.

Siemers, J., and W. Dreybrodt, 1998, Early development of karst aquifers on percolation networks of fractures in limestone: Water Resources Research, vol. 34, no.3, p. 409-419.

Tsang, Y.W., and C.F. Tsang, 1989, Flow channeling in a single fracture as a two-dimensional strongly heterogeneous permeable medium: Water Resources Research, vol. 25, no. 9, p. 2076-2080.

Tsang, Y.W., and P.A. Witherspoon, 1981, Hydromechanical behavior of a deformable fracture subject to normal stress: Journal of Geophysical Research, vol. 86, B10, p. 9287-9298.

Wicks, C.M., and C.G. Groves, 1993, Acidic mine drainage in carbonate terrains, geochemical processes and rates of calcite dissolution: Journal of Hydrology, vol. 146, no.13.

White, W. B., 1977, Role of solution kinetics in the development of karst aquifers: Memoirs of the International Association of Hydrogeology, vol. 12, p. 503-517.

Zimmerman, R.W., S. Kumar, and G.S. Bodvarsson, 1991, Lubrication theory analysis of the permeability of rough-walled fractures: International Journal of Rock Mechanics and Mining Engineering, vol. 28, p. 325-331.

Zimmerman, R.W., and G.S. Bodvarsson, 1996, Hydraulic conductivity of rock fractures: Transport in Porous Media, vol. 23, p. 1-30.

ENHANCEMENT OF EARLY KARSTIFICATION BY SUBTERRANEAN SOURCES OF CARBON DIOXIDE

Franci Gabrovšek and Wolfgang Dreybrodt
Institute of Experimental Physics, University of Bremen, 28334 Bremen, Germany

Abstract

When investigating early karstification by one-dimensional digital models, so far one has assumed that the CO_2 contents of the calcite-aggressive water stems entirely from the surface. Subterranean sources of CO_2, however, can rejuvenate the solutional power of the water already close to equilibrium with respect to calcite, and boost dissolution rates. In a first scenario we have investigated the influence of a point source of CO_2, for example release of volcanic CO_2, into a karstifiable region at some position kL from the entrance of the widening joint of length L (where $k<1$). The results show that only a small increase of the P_{CO2} in the solution to about 0.01 atm is sufficient to reduce the breakthrough times to about 0.3 with respect to the standard case, where no CO_2 is delivered. In a second scenario we assumed a constant rate of CO_2 input along parts of the fracture, as could be delivered by the activity of aerobic bacteria dwelling along its walls. In this case drastic reductions of the standard breakthrough time by about one order of magnitude are observed. These reductions are enhanced when the fracture width of the initial fracture decreases. The physico-chemical mechanisms of enhancement of karstification can be examined in detail by considering the evolution of the fracture width and of the dissolution rates in space and time. The results show that biological activity in primary fractures can exert a significant influence on the intensity of karstification.

THE INITIATION OF HYPOGENE CAVES IN FRACTURED LIMESTONE BY RISING THERMAL WATER: INVESTIGATION OF A PARALLEL SERIES OF COMPETING FRACTURES

Kevin A. Dumont, Hari Rajaram, and David A. Budd
Department of Geological Sciences, University of Colorado, Campus Box 399
Boulder, CO 80309

Abstract

Integrated cave systems can either form at or near the surface of the earth (epigenic) or at some depth below the earth's surface (hypogenic). For caves that form in fractured limestone, the two most common types of cave-system morphologies are branchwork and mazework. Branchwork caves are composed of tributaries that coalesce in the downstream direction, similar to surface streams.

Mazework caves exhibit two or more sets of parallel passages intersecting in a grid-like pattern. The majority of epigenic caves exhibit branchwork morphologies, which represent the dominance of individual flow paths. In contrast, mazework caves develop when dissolution occurs along numerous flow paths. Whereas most epigenic caves are related to surficial meteoric flow systems, some mazework caves are thought to have formed in hypogene environments where rising thermal water cools in response to the geothermal gradient.

Our objective is to examine the fundamental cause for the difference in morphology between epigenic and thermal hypogenic cave systems using numerical models. In particular, we are examining the competition between different flow paths in fractured limestone undergoing dissolutional enlargement. As noted in previous numerical studies, epigenic systems are characterized by the dominance of a single flow path, which is consistent with the structure of epigenic caves. So, in order to explain the structure of maze caves, one has to explain why no single flow path attains dominance. The retrograde solubility of calcite coupled with heat transfer from the fluid to the rock is hypothesized to provide the mechanism by which dissolutional power is distributed among all competing flow paths. Numerical models of fluid flow, heat transfer, and calcite dissolution chemistry are integrated to develop a model of hypogene cave initiation in fractured limestone. Flow is assumed to occur in the presence of a spatially variable rock temperature field that is constant through time. Preliminary numerical modeling results for a system of parallel fractures demonstrate the differences in the nature of competition between flow paths in epigenic (constant temperature) and hypogenic systems (flow in the presence of a negative thermal gradient).

Differences in results using various kinetic models for calcite dissolution are also presented. The role of aperture variation and distribution in a parallel set of fractures is also examined.

ON PREDICTING CONTAMINANT TRANSPORT IN CARBONATE TERRAINS: BEHAVIOR AND PREDICTION

W.K. Annable and E.A. Sudicky
Department of Earth Sciences, University of Waterloo
Waterloo, Ontario, Canada, N2L 3G1

Abstract

A three-dimensional numerical model was used to quantify the fate of conservative transport in carbonate terrains. Numerical flow and transport experiments were conducted in proto-conduit scale limestone terrains (conduits less than 10cm) which determined that *a priori* information on the 'spill' and/or 'tracer injection location' and discharge locations provided little insight in characterizing the complexity of the internal labyrinth of interconnected conduits. Scaling, aside from the characterization of the geologic media, was one of the most limiting factors in quantifying recharge tracers or contaminant distribution. However, if sufficient numbers of discharge locations (springs) are known, the extent of downstream contaminant migration can be characterized.

Introduction

Over the past several decades there has been significant advancement in the conceptual and theoretical understanding of karst land forms which include their surface topography, inter strata evolution, water resource capabilities and their susceptibility to contamination (see for example White, 1988; Ford and Williams, 1989). Correspondingly, advancements have also been made in the understanding of the physical and geochemical processes that have formed the primary and secondary porosity of many of the world's carbonate terrains (see for example Friedman and Sanders, 1978) whereby in this specific case secondary porosity represents the chemically altered state of the primary structure subsequent to deposition. Many other researchers have investigated the processes of geochemical dissolution which result in proto-conduit, conduit, and cave formation in carbonate terrains (Curl, 1965; Plummer et al., 1978; Dreybrodt, 1988, Arakaki and Mucci 1995, among others). Within the same time period, advancements in computing technology have made it possible to simulate many of the above principles in a rigorous numerical framework as an added tool in our evolving understanding of carbonate terrains. Defining the source and pathway of surface and/or groundwater inputs is a prerequisite to understanding the impact of contaminants originating at the surface or within carbonate terrains. Numerical models can provide a useful tool in evaluating possible flowpaths and the timing, duration, and magnitude of inputs to the system from various sources.

Much work has been done over the past thirty years in the development of numerical methods to evaluate carbonate terrains. However until recently, the body of this work as been limited to petroleum reservoir simulations and oil extraction techniques (see for example Fraser and Davis, 1998). Analogous to flow and transport in limestone conduits is the transport of water, contaminants and sediment in storm sewer drains which was born out of research which resulted in the development of the Darcy-Weisbach equation. Subsequent to this early research and more advanced methods, there has been a significant amount of research and application on storm sewer pipe network modeling in historical and modern day cities (see for example Daugherty and Franzini, 1965). Although the geochemical process of carbonate terrains cannot be quantified using such modeling approaches, routing and distributed runoff models can be generated which characterize areas of many square kilometers.

Kiraly and Morel (1976a, b) were likely among the first researchers to numerically simulate a geochemically evolving carbonate terrain. More recently in a series of papers by Groves (1993), Groves and Howard (1994) and Howard and Groves (1995) a two-dimensional model was introduced which integrated geochemical processes into a subterranean laminar and/or turbulent flow field. Flow and transport were simulated through a series of one-dimensional discrete pipes and coupled to a two-dimensional finite element mesh which accounted for diffusive geochemical matrix interaction. Modeling results showed significantly different conduit evolution over an approximate 1,000 year to a 100,000 year ranges in time spans under either laminar or turbulent flow conditions. The modeling domain used in all of the above simulations was set at 750m by 350m with a course level of discretization which lead to convergence thresholds of conduit sizes as outlined by Dreybrodt (1996).

Dreybrodt (1992, 1996, 1997, 1998) has conducted numerical experiments on the evolution of carbonate terrains using various 1-D and 2-D models. Dreybrodt (1992) illustrated the effects of enhanced geochemical dissolution at the faces of hydraulic structures constructed in carbonate terrains and showed that significant conduit evolution could occur under increased hydraulic heads from dam structures within approximately 100 years which can lead to the failure of such structures. The modeling

domain used in these experiments was set at 100 m. In further applications of a vast data base of investigated geochemical reaction rates of calcitic limestones , Dreybrodt (1996, 1997, 1998) demonstrated the geochemical evolution of conduits along well-defined 2-D conduit networks. In these cases modeling domains were less than 5 m.

In a separate series of numerical modeling experiments by Sauter (1992) and Clemens et al. (1996, 1997a, 1997b), another model was developed which incorporates discrete pipe networks into a 2-D dual-permeability porous matrix to describe flow and solute transport under laminar and turbulent flow conditions. Originally developed to quantify recharge distribution and tracer evolution along flow paths in a karstic aquifer in southern Germany (Sauter, 1992), the simulator has been further developed to account for geochemical interactions to study the formation of conduits in carbonate terrains. Dendritic conduit formations were investigated by Clemens et al. (1996, 1997b) and maze cave formations (Clemens et al., 1997a) as defined by Palmer (1991). Other than the regional-scale quasi-2D modeling by Sauter (1992), modeling domains were kept to approximately 1,350 m by 1,050 m.

In all of the above numerical experiments, modeling domains have been limited to approximately one kilometer or less in order to capture the important geochemical processes. However, it is well known that solutionally enhanced limestone terrains which occur along parting planes, sheeting structures, joints etc. can extend aerially for several kilometers. These units can also be connected vertically between many geochemically inactive units through vertical fractures or joints generating a complex three-dimensional network of possible flow routes. Adding further complexity to these systems is the addition of contaminants and / or tracers at particular locations. In a dissolutionally enhanced carbonate terrain, travel times over kilometer scales can occur within hours to a few days and the distribution of contaminant can be vast in aerial extent relative to what would be expected using an equivalent porous medium model. Moreover, most of the conduits have smaller secondary conduits as was described by Ford and Ewers (1978), which may, depending upon their orientation, result in 'dead-end conduits' similar to the dual permeability concept of dead end fractures as outlined by Smith and Schwartz (1993). Such conduits or 'immobile zones' can result in significant changes in the mass balance results in dye tracer experiments or can drastically hinder contaminant remediation. The presence of dead-end immobile zones was not accounted for in the above mentioned modeling techniques.

This study presents a modeling technique in three-dimensional space which can account for flow and transport in a network of interconnected conduits and dead end cavities. Diffusive exchange of solute mass between the conduits and immobile zones including diffusion in the rock matrix are also incorporated. Although not presented in this paper, decay chain transport of such species as tritium, deuterium, helium, chlorine etc. have also been integrated into the model. Numerical experiments presented herein investigate the effect of scale on mass recovery observations using a conservative tracer/contaminant.

Numerical model

The numerical model PipeMod (G.S.G., 1997) has been developed to simulate advective-dispersive transport through an arbitrarily structured network of interconnected one-dimensional pipes in three-dimensional space. In essence, PipeMod is based on a conceptualization that flow and transport in a three-dimensional rock mass containing a network of interconnected fracture planes can be reduced to that in a network of pipes, where the pipes represent the primary flow conduits through the fracture planes. Hanna and Rajaram (1998) recently demonstrated with a series of numerical experiments that flow along horizontal fracture planes is primarily channeled along conduits in a geochemically evolving matrix where natural variability exists in aperture size rather than parallel plates. Therefore, the pipe-flow hypothesis is considered valid in the present work. Furthermore, matrix interaction and more diffuse flow out of fractures can be accounted for using the immobile zone equations built into the existing simulator. The model also accommodates (1) diffusion from the pipes containing mobile groundwater into the surrounding rock matrix containing immobile groundwater, (2) diffusion into the immobile porewater within the fracture "plane" attached to a pipe containing the flowing groundwater, (3) diffusion from the mobile groundwater in a pipe to attached "dead-end" pipes that contain immobile groundwater, and (4) diffusion into fracture infilling or surface-coating material. Thus, in general, each pipe containing the flowing groundwater can be connected to multiple interacting immobile porosity zones. The model also allows for the sorption of the solutes onto the geologic materials within each immobile zone, including sorption onto the surfaces of the pipes in the network. Sorption is described by a linear Freundlich isotherm such that a retardation factor can be defined for each solute for each pipe and each immobile porewater zone.

The governing transport equation presented is based upon the pipe network conceptualization described above to describe solute migration through a fractured rock mass. Although the equations are solved using the Laplace Transform Galerkin (LTG) finite-element method (Sudicky, 1989; Sudicky, 1990; Sudicky and McLaren, 1992), the

equation presented is given in the real-time domain.

Assuming steady-state flow and a first-order approach to describe the diffusive mass transfer of a solute between the groundwater in a pipe and the multiple immobile porosity zones attached to it (see, e.g., Sudicky, 1990), the advective-dispersive transport of solute species k in a pipe network is given by:

$$A(\ell)\left[R_k(\ell)\frac{\partial C_k}{\partial t}+q(\ell)\frac{\partial C_k}{\partial \ell}-\frac{\partial}{\partial \ell}D_{\ell_k}(\ell)\frac{\partial C_k}{\partial \ell}+R_k(\ell)\lambda_k C_k-\sum_{j=1}^{m_k,\ k>1}\eta_{kj}\,R_j(\ell)\lambda_j C_j\right]$$

$$\pm\sum_{\ell'}\dot{M}\,\delta\,(\ell-\ell')+\sum_{\ell*}Q(C_k-C_k^*)\delta(\ell-\ell^*)$$

$$+\sum_{im=1}^{IM}P(im,\ \ell)\alpha_k(im,\ \ell)(C_k-C_k')\ =\ 0 \qquad (1)$$

where:

$A(\ell)$ = Pipe cross-sectional area [L^2]
$R_k(\ell)$ = Retardation factor [-]
$q(\ell)$ = Specific discharge (≡Pipe velocity v) [L/T]
$D\ell_k(\ell)$ = Dispersion coefficient = $\alpha v + D_k^\circ$ [L^2/T]
= Pipe longitudinal dispersivity [L]
D_k° = Free-solution diffusion coefficient [L^2/T]
λ_k = Decay constant [1/T]
m_k = Number of parents for species k (=1 for straight chain)
η_{kj} = Stoichiometric constant indicating fraction of parent species j that decays to daughter species *k*
= 1.0 for straight decay chain;
($0.0 < \eta_{kj} < 1.0$ for branching chain)
$\dot{M}(t)$ = Internal solute mass source/sink [M/T]
Q = External fluid source/sink [L^3/T]
$\delta(\ell - \ell')$, $\delta(\ell - \ell^*)$ = Dirac delta [1/L]
$P(im,\ell)$ = Immobile zone wetted perimeter for immobile zone "*im*" attached to pipe "ℓ" [L]
$\alpha_k(im,\ell)$ = Pipe/immobile zone transfer coefficient for immobile zone "*im*" attached to pipe "ℓ" [L/T]
C_k = Pipe concentration [M/L^3]
C_k' = Immobile zone concentration [M/L^3]
C_k^* = Concentration of injectate in external fluid source [M/L^3]
ℓ = Distance along interconnected pipe network [L]
ℓ' = Location of solute mass source/sink [L]
ℓ^* = Location of external fluid source/sink
im = Immobile zone class number (note: if desired *im* can equal 0) [-]
$IM(\ell)$ = Total number of immobile zones attached to pipe ℓ[-]
k = Species number [-],
m_k = Number of parent species decaying to species *k* [-],
t = time [T]

It should be further noted that if there is no flow along a particular conduit within the network (i.e. $q(\ell) = 0$), then the model allows for diffusive transport along the length of this conduit. It should also be pointed out that if fluid is withdrawn at a resident concentration $C_k^* = C_k$, then the term involving Q in (1) vanishes. If the injectate concentration is $C_k^* = 0.0$ then this term accounts for the dilution effect of the injection of solute-free water.

The initial concentrations of all species within the domain are assumed to be zero in the current version of PipeMod. For boundary conditions, they can be either of the Dirichlet-type where the input concentration history of each species is a specified function of time, or of the Cauchy-type where the advective input mass flux can be prescribed as a function of time.

In order to represent the diffusive exchange of solute mass between the pipes and within any of the *im* immobile zones attached to them, Pipemod uses a first-order approach was has been commonly used in the past (see, e.g., Sudicky, 1990, among others). Accordingly, the governing equation for the im^{th} immobile zone, allowing for chain decay and sorption according to a linear equilibrium Freundlich isotherm is described by:

$$\theta_{im}(im,\ \ell)V_{im}(im,\ \ell)\left[R_k'(im,\ \ell)\frac{\partial C_k'}{\partial t}+R_k'(im,\ \ell)\lambda_k C_k'-\sum_{j=1}^{m_k,\ k>1}\eta_{kj}\,\lambda_j\,R_j'(im,\ \ell)C_j'\right]$$

$$=\ P(im,\ \ell)\alpha_k(im,\ \ell)[C_k-C_k'] \qquad (2)$$

where:

$\theta_{im}(im,)$ = Immobile zone porosity for immobile zone "*im*" attached to pipe "ℓ" [-],
$V_{im}(im,\ell)$ = Immobile zone volume/unit pipe length for immobile zone "*im*" attached to pipe "ℓ" [L^2],
$R_k'(im,\ell)$= Immobile zone retardation factor for immobile zone "*im*" attached to pipe "ℓ" [-].

Note that PipeMod assumes the initial condition $C_k'(\ell,0) = 0$. With the formulation given by (1) and (2), the mass transfer coefficient α_k is interpreted to be:

$$\alpha_k = \frac{\theta_{im} D_k^o \tau}{d} \qquad (3)$$

where: τ = Tortuosity [-]
d = Diffusion distance [L]

If a particular immobile zone is fluid-filled, such as within an immobile water zone attached to a pipe within a fracture plane, then the immobile zone porosity, θ_{im}, would equal 1.0. Note that the definition of α_k given above differs from that used by Sudicky (1990) in that he uses d^2 in the denominator of (3).

The matrix equations arising from the Laplace transform solution algorithm when used in conjunction with the de Hoog et al. (1982) Laplace transform inversion scheme are complex-valued, and the coefficient matrix is sparsely populated for an arbitrary network of interconnected pipes. The WatSolv iterative sparse-matrix solver library (VanderKwaak et al., 1997) was employed and adapted to handle the complex system of matrix equations. The WatSolv library is based on an ILU factorization of the non-symmetric coefficient matrix with user-defined levels of infill and several alternative re-ordering methods, including Red/Black system reduction, and employs CGSTAB (van der Vorst, 1992) acceleration to solve the preconditioned system of matrix equations. It also uses a compact ia-ja data storage structure such that only the non-zero terms in the matrix equations are stored and operated on. Further details on the capabilities of WatSolv can be found in VanderKwaak et al. (1997).

Verification problems were conducted by GSG [1997] on single and double-porosity transport problems involving nonreactive and reactive solutes. Test cases were compared against results from Ogata-Banks analytic solution for the case of one-dimensional advective-dispersive transport on nonreactive solutes and matched with a high degree of accuracy. Additional verification problems were conducted for a non-sorbing (i.e. R=1) solute in a double-porosity system comprised of parallel fractures embedded in low-permeability, low-porosity rock matrix. Results were compared with the analytic solution of Sudicky and Frind (1982) at times equal to 1,000 and 10,000 days and at steady state. Comparison of results with a with a very coarse grid used in Pipemod yielded highly accurate results.

Flow and transport simulations

In this paper simulations were conducted on a 3-D network of interconnected conduits with immobile zones or 'dead end' conduits at varying scales as outlined in Table 1.

The computational domain was initially generated for each simulation using a dx = 20.0m by dy=5.0m spacing and the vertical layer boundaries as illustrated in Figure 1. The discretization was assumed to be analogous to an average fracture frequency occurrence of weathered limestone. The entire 3-D grid was initially filled with connecting elements on a regular lattice grid (i.e. conduits) and then elements were randomly removed based upon specified probabilities for both vertical and horizontal conduit occurrences. In the case of horizontal conduits, probabilities were specified for both longitudinal (x-direction) and transverse (y-direction) conduits recognizing that dissolutional enhancement would generally occur in the down gradient direction (x-direction) to a greater extent than across a given flow field. In all simulations, the probability of vertical and horizontal fractures were held constant.

Horizontal fractures were assumed to only occur along the contacts between the overlying dolomitic limestone and the vuggy limestone (z = 5.0m) and at the lower contact of the vuggy limestone and the underlying non-fractured dolomitic limestone (z = 5.5m). Solutional enhancement was assumed to be horizontally most dominant along the contacts of the different strata where pore water chemistry would maintain the highest chemical gradients. Cross-sectional areas of the remaining conduits, subsequent to elimination using a random probability grid field generator, were also specified. Mean conduit cross-sectional areas and variances were specified for both vertical and horizontal transverse conduits along the boundary of each stratigraphic unit. Based upon the mean conduit size specified and variance for each strata, random cross-

TABLE 1. Domain parameters for simulations

Simulation	X (m)	dX (m)	Y (m)	dY (m)	Z (m) at contact elevations **Bold values** represent contact elevations of solutionally enhanced zone	Final Nodes	Final Elements	CPU Solution Time (seconds)*
Small Scale	100	20	50	5	0.0 (Top) // **5.0** // **5.5** // 7.0 (Bottom)	27	25	0.031
Medium Scale	1000	20	500	5	0.0 (Top) // **5.0** // **5.5** // 7.0 (Bottom)	2758	2918	673
Large Scale	5000	20	1000	5	0.0 (Top) // **5.0** // **5.5** // 7.0 (Bottom)	66332	72029	1173

NOTE: CPU time referenced to a 400 Mhz Pentium II Dual processor (512Meg - RAM)

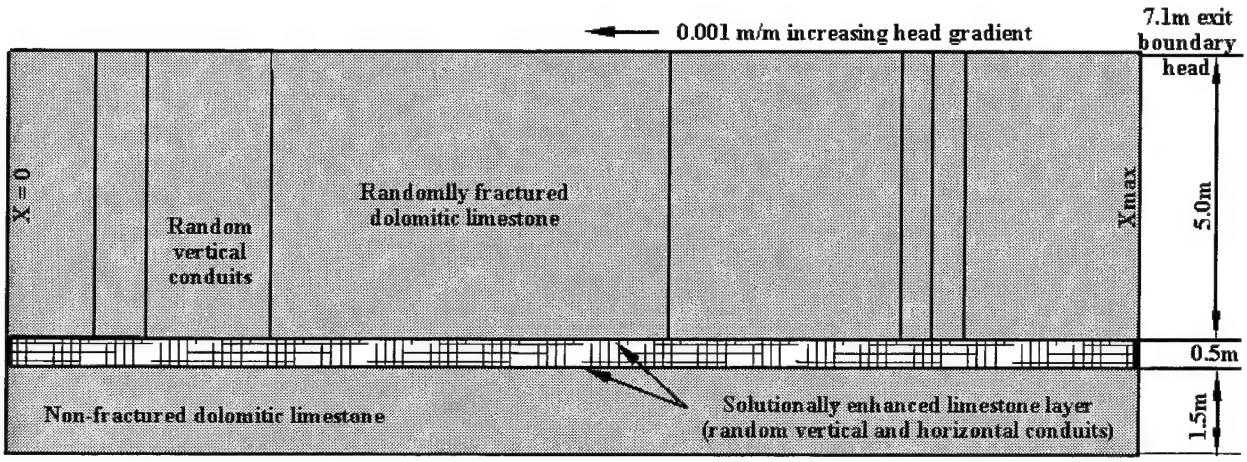

Figure 1: Modeling domain - vertical profile

sectional areas of each remaining conduit were calculated for input into Pipemod to calculate the flow velocity field. In the case of longitudinal horizontal conduits, a minimum conduit diameter, variance and maximum 'exit boundary' cross-sectional areas were specified. Studies by Curl (1965), Ford and Ewers (1978), and Palmer (1991), among others, have shown that geochemical dissolution along fracture planes has the greatest enlargement proximal to the locations where recharge to the confining layer occurs (i.e. conduits are largest close to the vertical fractures) and decrease in size downgradient from the vertical fractures as calcite solubility reaches saturation. In this paper, the geochemical enhancement of conduits at the intersection of vertical fractures is represented by an increase in cross-sectional area downgradient of each vertical fracture. The specific mean cross-sectional area at a given location along the flow field was scaled relative to the maximum flow field length and the largest conduit using the following equation:

$$A = \alpha + \beta(LOG(x_{max}) - LOG(x)) \qquad (4)$$

where A is the final mean cross-sectional area [L^2] for a given distance along x, α is the minimum cross-sectional diameter [L^2], x_{max} is the maximum domain length in the x-direction [L], x is the location of a discrete vertical fracture location occurring from z=0 and ≥ is a fitting parameter defined by:

$$\beta = \frac{A_{max} - \alpha}{LOG(x_{max})} \qquad (5)$$

where A_{max} is the maximum specified cross-sectional area [L^2] at the exit boundary of the domain.

The vertical domain is divided into three separate strata as illustrated in Figure 1. The top unit is considered to be a geochemically inactive dolomitic limestone 5.0m thick with random continuously penetrating conduits from the bedrock surface to the underling vuggy limestone. The location of the conduits are random in location and are originally based upon the 20m longitudinally (x-direction) and 5m transverse (y-direction) grid spacing as outlined in Table 1. Vertical fracture planes are considered to represent the discretization in the x and y directions. Within these planes it is assumed that the conduits represent joints at the intersection of two fracture planes with a mean conduit diameter of 0.02 m and a variance of 0.015 m. The probability of a vertical fracture occurring at any give node was set at 3% (i.e. 3% of all possible nodal connections may be vertically connected from the surface to the underling limestone layer). Bulk permeability of this layer was set at $1x10^{-7}$ m/s and it's porosity equals 5%.

Between depths 5.0 m and 5.5 m, a vuggy limestone exists as illustrated in Figure 1 with randomly occurring vertical and horizontal fractures throughout the unit. The probability of horizontal fractures occurring within this unit was set at 60% in the x-direction and 25% in the y-direction for each given node. The maximum conduit diameter was set at 0.10m and a mean diameter value of 0.03 m with a variance of 0.02 m. Vertical fracture probability within this unit was set at 20% with a mean aperture diameter of 0.02 m and a variance of 0.15 m. Bulk permeability of this layer was set at $1x10^{-6}$ m/s and its porosity is 10%. The unit below the vuggy layer is considered to be a non-fractured dolomitic limestone and treated as an impermeable boundary.

Three model scale domains were studied, as outlined in Table 2, and the random fracture generation field results for the x=100 m and x =1000 m simulations are illustrated in Figures 2a and 2b respectively.

The large simulation (x=5000 by y=1000 m) was visualized in 3-D in addition to figures 2a and 2b but not presented since the resulting network was too complex to be visually interpretable. It should further be mentioned that in Figures

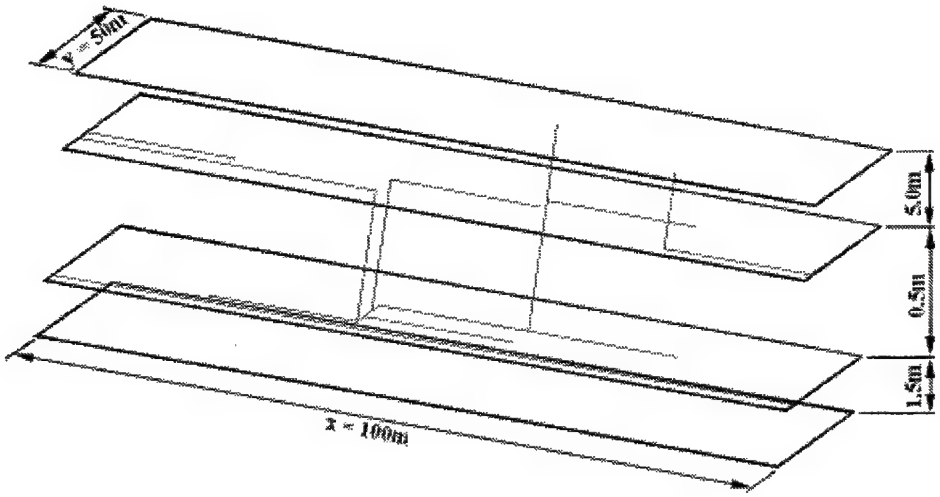

Figure 2a: Small scale grid (x = 100m, y = 50m, z = 7.5m)

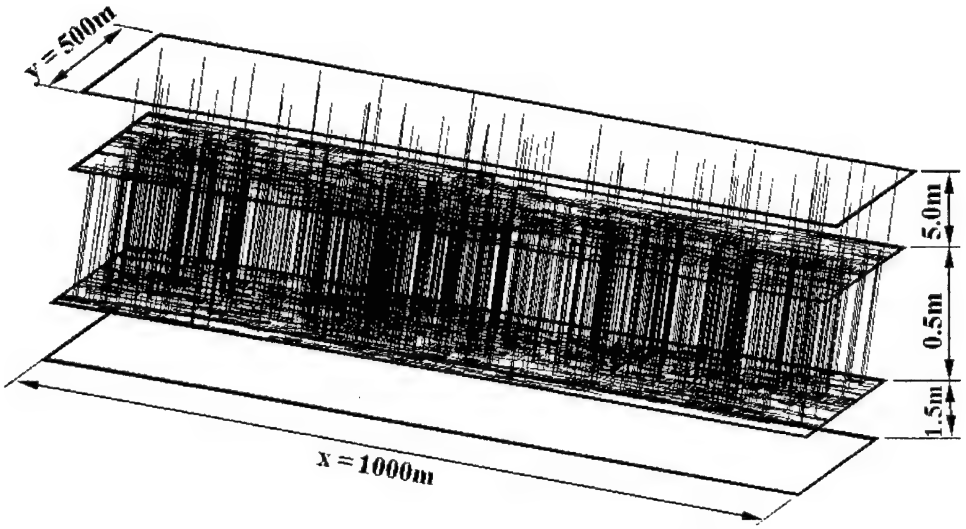

FIGURE 2b: Medium scale grid (x = 1,000m, y = 500m, z = 7.5m)

2a and 2b, the vuggy limestone layer between 5.0 m and 5.5 m was vertically exaggerated to view the connections between different contact layers, particularly in the case of Figure 2a. To provide further characterization of the three dimensional random network of conduits, particularly in the horizontal planes, Figures 3, 4 and 5 illustrate the resulting networks subsequent to random conduit generation in plan view. In Figures 3a, 4a and 5a, the bedrock surface at Z=0 illustrates the discrete locations where conduits from the bedrock surface penetrate to the 5.0 m elevation of the underlying vuggy limestone. The specific sizes of the conduits illustrated in these figures have been exaggerated to view the input locations to the underling unit. Variation in diameters of conduits, most visible in Figure 3a, provides further conceptual representation of the variability in diameters of the vertical conduits.

It should be further pointed out in Figures 3a, 4a, and 5a that a source-node location has been identified in each illustration. These are the specific locations where a conservative tracer or contaminant has been introduced into the network. To assure that an injection node would eventually exit the domain at any one of the observation nodes located on the x_{max} boundary (at either the z=5.0 or z=5.5m contacts), a form of particle tracking was used. Subsequent to the initial randomization of the computational domain, a discrete memory kernel was set at each of the three constant head boundaries (i.e. z_0, x_{max}, x_o). Any nodes (conduits) remaining along the constant head boundaries were assigned the respective kernels. An iterative procedure was then used to determine which nodes/ elements in the remaining domain, regardless of how complex the pathway or the number of 'dead-end conduits, were hydraulically connected to any of the three constant head boundaries. If hydraulically inactive nodes were

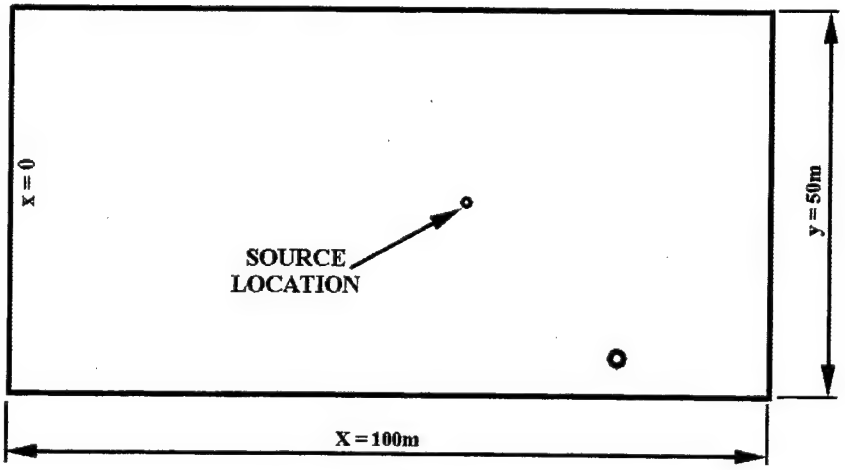

Figure 3a: Plan view of bedrock surface (z = 0) and vertical conduit locations of small scale grid (x = 1,000 m, y = 500 m, z = 7.5 m)

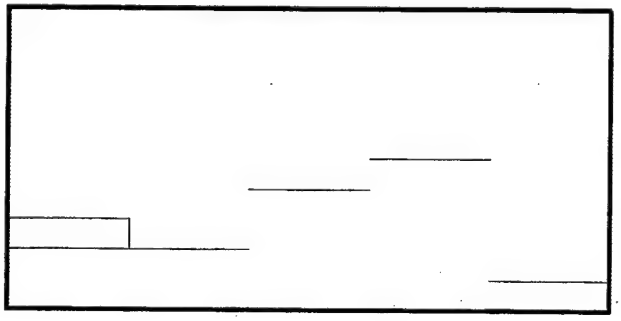

Figure 3b: Plan view of 5.0 m contact depth and horizontal conduit locations -Small scale grid (x = 1,000 m, y = 500 m, z = 7.5 m)

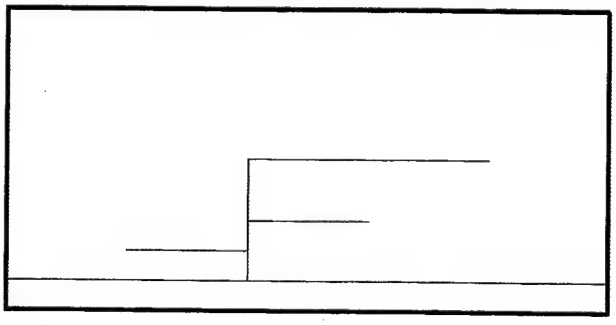

Figure 3c: Plan view of 5.5 m contact depth and horizontal conduit locations -Small scale grid (x = 1,000 m, y = 500 m, z = 7.5 m)

identified, they were eliminated from the domain for increased computational efficiency.

In all of the simulations, the hydraulic head was set at 7.1m on the exit boundary (x_{max}) and an average gradient of 0.001m/m (0.1%) was established across the domain in the x-direction. Therefore, for x domain lengths of 100m, 1000 m and 5000 m the (x=0) heads were set at 7.2 m, 8.1 m and 12.1 m respectively. Constant head nodes were assigned for the vertical conduits at the bedrock surface (z=0) based upon their longitudinal location (i.e. $Z_{head} = 7.1+0.001x$).

Observation nodes were set at each conduit that exited the domain at x_{max} on both the z=5.0 and z = 5.5 m horizontal contact planes. The observation nodes represent locations of springs or seepage faces along an exit boundary of the domain where sampling of groundwaters would typically occur.

Discussion of simulation results

The simulations investigated consist of the transport of a single nonreactive solute / tracer (retardation R=1.0, decay constant λ = 0.0) by advection and dispersion with the permeabilties and porosities for each unit identified above. The source of injectates as identified for each simulation in Figures 3a, 4a, and 5a were set as continuous sources which were initiated at t=0.

Figure 6 illustrates the results of the small-scale simulation. The modeling domain presented in Figure 6 illustrates the vertical projection of all horizontal fractures (i.e. Figures 3b and 3c combined), a similar representation if presented for the remaining illustrations. The random grid generation routine produced a single conduit that extended across the entire x domain with two vertical entry points from the bedrock surface. One hydraulically connected observation node at x_{max} was present at y = 5.0m and at the 5.5 m contact

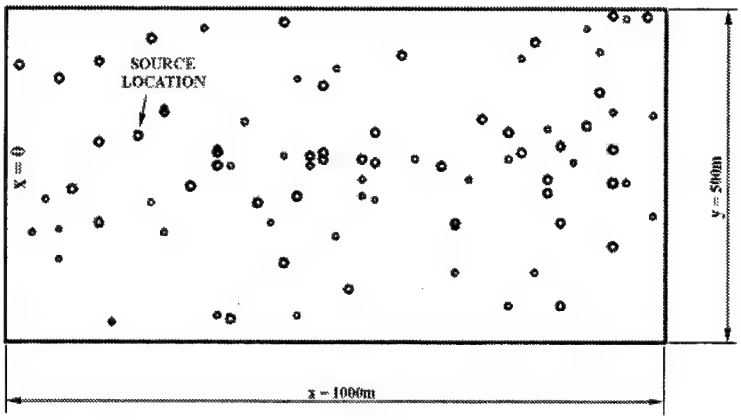

Figure 4a. Plan view of bedrock surface (z = 0) and vertical conduit locations of medium scale grid (x = 1,000 m, y = 500 m, z = 7.5 m

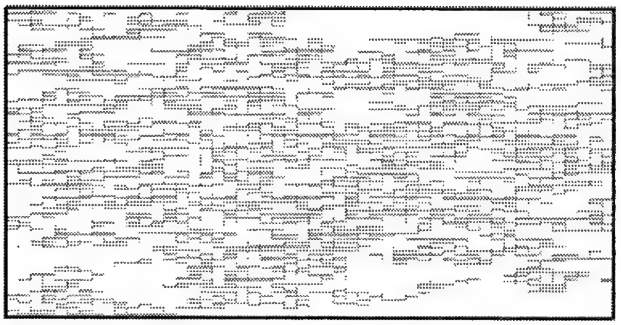

Figure 4b. Plan view of 5.0 m contact depth and horizontal conduit locations - Medium scale grid (x =1,000 m, y = 500 m, z = 7.5 m)

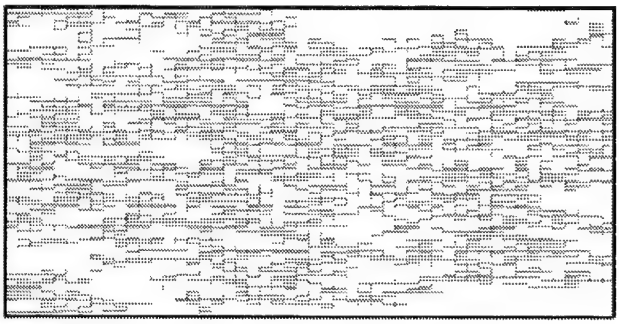

Figure 4c. Plan view of 5.5 m contact depth and horizontal conduit locations - Medium scale grid (x = 1,000m, y = 500m, z = 7.5m)

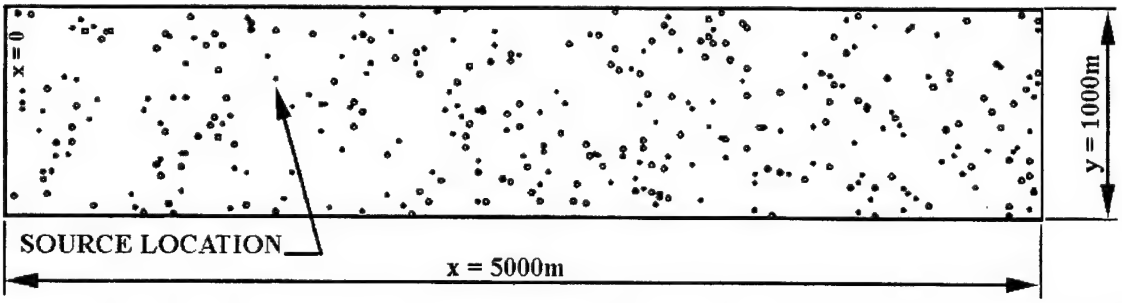

Figure 5a. Plan view of bedrock surface (z = 0) and vertical conduit locations of large scale grid (x = 10,000 m, y = 5,000 m, z = 7.5 m

Figure 5b. Plan view of 5.0 m contact depth and horizontal conduit locations - Large scale grid (x = 5,000 m, y = 1,000 m, z = 7.5 m)

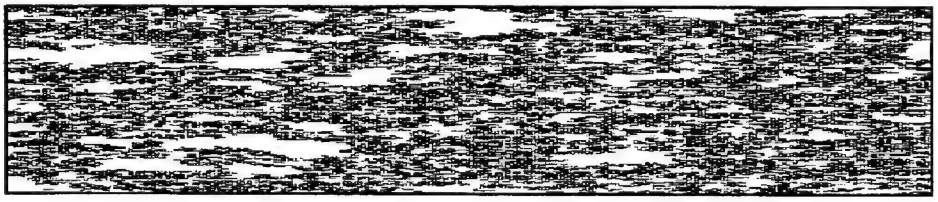

Figure 5c. Plan view of 5.5 m contact depth and horizontal conduit locations - Large scale grid (x = 5,000 m, y = 1,000 m, z = 7.5 m)

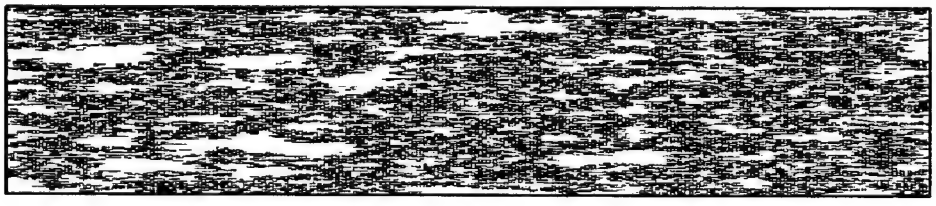

elevation. Although the source location is relatively close to the exit boundary, the arrival time is significantly longer than would be expected for such a short distance. One would typically expect first arrival of a tracer at an exit boundary for this distance within minutes to a few hours for a 2-cm diameter conduit. However, upon further inspection of Figure 2a, the particular flow path from the injection point must travel towards the left (x=0) boundary 20m before descending into a conduit along the lower 5.5 m contact where it then proceeds to exit the domain at the right boundary. The conduit from it's entry point to the upstream location of the vertical conduit which connects down to the 5.5 m elevation is hydraulically constrained as a dead-end conduit.

Therefore, the only process that controls the transport of solute in this instance to the lower vertical contact is diffusion. This is further characterized by the time of maximum concentration arrival at the observation node being greater than one month.

Figure 7 illustrates the results from the medium scale grid simulation. Randomization of the initial 20,604 node computational domain produced a final network which

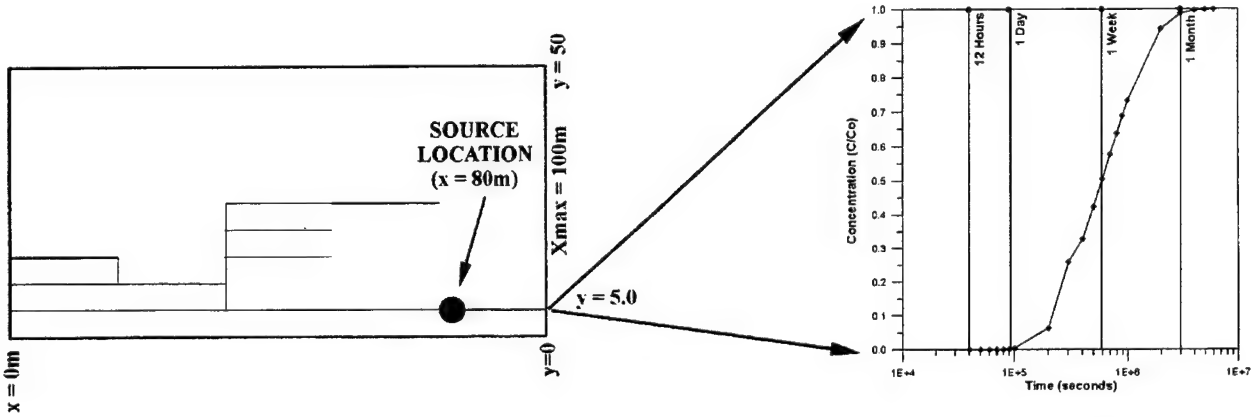

Figure 6. Simulation results - time of concentration to observation nodes - Small grid simulation (x = 100 m, y = 50 m, z = 7.5 m)

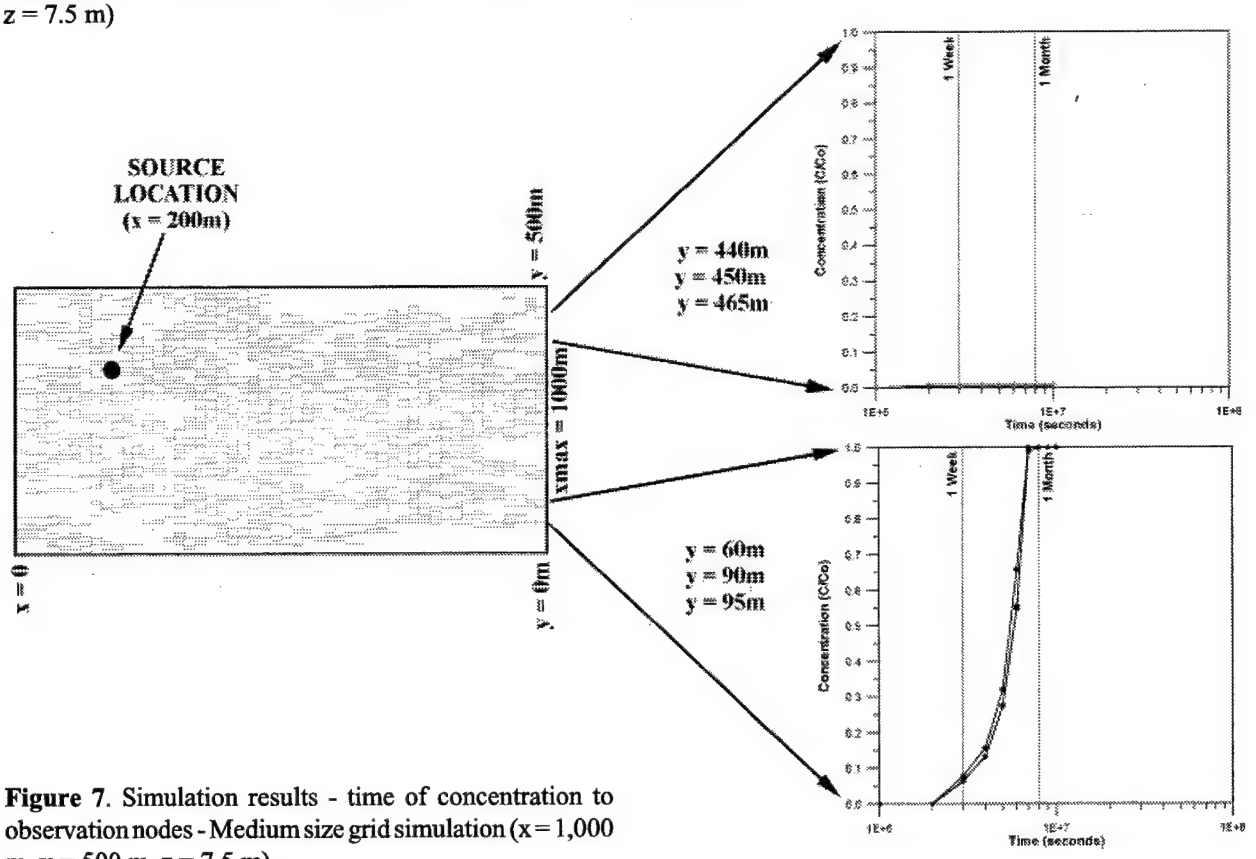

Figure 7. Simulation results - time of concentration to observation nodes - Medium size grid simulation (x = 1,000 m, y = 500 m, z = 7.5 m)

consisted of 84 bedrock surface entry points and 50 conduits that exited the boundary at x_{max}. The maximum simulation time was set to 30 years and at the end of that period, only six observation nodes showed a response to the contaminant injection. The most noteworthy observation with respect to this simulation is that, although the source injection point is located at x = 200 m and y = 310 m, breakthrough times and maximum concentration arrival were first observed at observation nodes between y = 60 m and y = 95 m at the exit boundary. Therefore, solute moved significantly transverse to the general flow direction to reach these locations. Initial arrival times for the three observation nodes between y = 60 m and y = 95 m were within two days following the injection, comparing relatively well with many dye tracer studies of similar distance. Maximum concentration arrival time for all three nodes was approximately one month. The time difference between the initial arrival time and the time of maximum concentration is affected by the number of immobile zones and dead-end conduits within the domain. If dead-end conduits and immobile zones did not exist, the concentration fronts would be relatively sharp. Since the concentration curves are almost identical for the observation nodes between y=60 m and y=95 m, it would seem likely that a single conduit pathway transported the injectate through much of the domain towards the x_{max} boundary. In nearing the x_{max} boundary, a branching of conduits was likely present close to the exit boundary which produced the three similar breakthrough curves at the distinct observation points on the exit boundary for transverse distances of y=60 m, 90 m, and 95 m. Although small quantities of tracer arrived at three other observation nodes on the exit boundary at y=440 m, 450 m , and 465 m, their relative concentrations were very low ($C/C_o = 0.006$). Although the duration of the simulation illustrated in Figure 7 is approximately three years, the time of arrival of the maximum concentration at the three nodes between 440m and 465 m occurred between 14 and 18 years.

Figure 8 illustrates the results from the large scale simulation. The computational domain, as outlined in Table 1, was originally set at 201,804 grid nodes and, after random conduit elimination, a computational domain of 66,332 nodes and 72,029 elements resulted. Three hundred and twenty four surface entry nodes remained out of a possible 50,451 nodes (3.4%) and 121 exit boundary nodes at x_{max} were present. The source node was located at x=800 m and y=725 m.

The simulation time was set to 100 years; however for presentation purposes, results for only the first three months ($1x10^7$ seconds) are presented. As illustrated in Figure 8, although the source node is located approximately 4km upstream of the exit boundary, tracer breakthrough was observed at three different observation nodes (y = 200 m, y = 900 m and y = 920 m) within one day of the injection. Moreover, the three observation nodes where breakthrough occurred at early times were not clustered in one location, but located across the entire Y domain. Two possible explanations exist which could have produced this early occurrence. Similar to the explanation used for the medium scale simulation, it is possible that a single conduit may be present along much of the domain (i.e. x-direction) in the direction of mean flow, but near the exit boundary a branching occurs which would lead to the tracer being observed in two very different y-locations at the exit boundary. However, considering that the domain is 1 km wide by 5 km long, this is an unlikely scenario because the conduit flow would have to bifurcate dramatically transverse to the general flow direction just prior to the exit boundary. If this were the case, breakthrough times should occur at other nodes between Y = 200 m and Y = 900 m in a similar time frame. As illustrated in the plot for y-distances between 701 m and 835 m, breakthrough times in this region lag by approximately one week, supporting the argument that this scenario did not occur. A more plausible explanation is that a single conduit carried the tracer for a relatively short distance away from the source node which then split into two distinct and different flow paths which were longitudinally continuous over most of the domain in the direction of bulk flow. This scenario is further supported when the response period between the first arrival time and maximum concentration arrival time at the three observation nodes (i.e. y = 200 m, 900 m, and 920 m) are considered. In the case of observation nodes located at y=920 and y=900, initial arrival times are virtually identical; however, there is a strong asymmetrical shape to the remainder of the curves leading up to time of maximum concentration. The y=920 m curve has a sharp front up to C/Co 0.3 whereas, in the case of the y=900 m curve, the response is very diffuse at first but then rises at late times. The y = 920 observation node discharges at the z = 5.0 m elevation whereas the y = 900 m node discharges at the 5.5 m elevation. The differences between the two curves can be explained by the additional flow paths taken by the lower conduit discharge point. There would likely be a greater number of secondary or dead-end conduits occurring along the primary flow path which would lead to a dispersed response. Until the tracer arrives in the conduits surrounding the primary flow tube, these secondary conduits would not have any affect on the concentration in the primary flow tube as illustrated for the breakthrough curve at y=900 m. In the case of the y=200 m, curve the discharge node is located at the z = 5.5 m elevation and the concentration increases most rapidly beyond C/Co 0.5. This would be typified by a smaller conduit with higher velocities and fewer secondary conduits along the flow path.

As further illustrated in Figure 8, other observation nodes

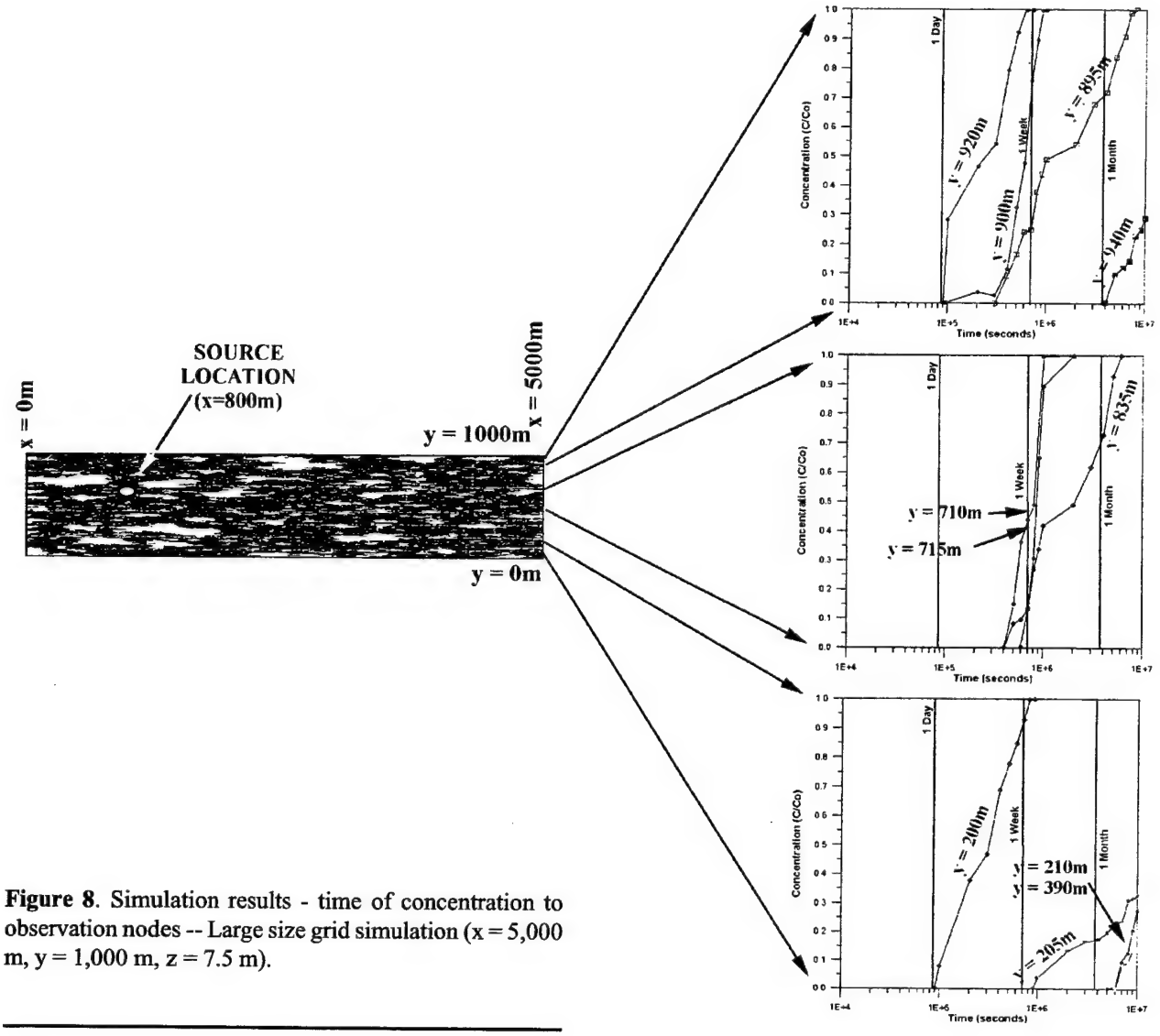

Figure 8. Simulation results - time of concentration to observation nodes -- Large size grid simulation (x = 5,000 m, y = 1,000 m, z = 7.5 m).

on the exit boundary experienced initial tracer arrival times between one week and one month (y= 205 m, 210 m, 390 m and 940 m). Through the course of the 100-year simulation, tracer concentrations at 17 other observation nodes reach the maximum value of $C/C_o = 1.0$ and were distributed across the entire exit boundary of the domain. These occurred mainly between y=400 and y=760 m. Furthermore, various lower levels of tracer concentrations were observed in 23 other exit conduits at the end of the simulation period, with peak values ranging from C/Co = 0.018 to 0.47. The gentle increase in tracer concentrations at these locations would be commensurate with the hypothesis of diffuse converging/diverging flow through the network.

Conclusions

A three-dimensional network model has been developed and presented which has been successfully applied to simulate flow and transport through a complex proto-conduit-scale carbonate terrain. As indicated by the results presented here, a conventional approach whereby equivalent porous medium concepts are used to interpret tracer migration in a complex network of solutionally enhanced carbonate terrains cannot capture the sporadic responses observed. Although at the small scale a carbonate system containing conduits may appear to be well behaved and predictable, the level of confidence for reliable prediction of tracer arrival times and concentration values decreases dramatically as the scale of the system, and hence the likelihood of conduit branching increases. Thus, the correlation between a specific contaminant injection point or spill location and the location of

discharge points decreases with an increase in scale. Furthermore, investigative procedures for characterizing the geologic system and the monitoring of the transport of contaminants may be severely compromised if conventional porous-medium approaches are exclusively employed. Depending on the interconnectivity of the conduits, the presence or absence of dominant "primary" channels and the scale of the system, tracer arrival times can range from hours to decades, and transverse spreading can be minimal to exceedingly large. Moreover, we would expect even less predictability in highly transient karstic systems exhibiting low storage capacity. If this is the case, then the system response with increasing temporal and spatial scales may be chaotic and therefore not amenable to conventional stochastic treatments.

Acknowledgments

The U.S. Environmental Protection Agency through its Office of Research and Development partially funded the research described herein under Cooperative Agreement CR-824654 with the University of Waterloo. It has not been subjected to Agency review and therefore does not necessarily reflect the views of the Agency, and no official endorsement should be inferred. Further funding was provided through an Ontario Graduate Scholarship.

References cited

Arakaki,. T., and A. Mucci, 1995, A continuous and mechanistic representation of calcite reaction-controlled kinetics in dilute solutions at 25°C and 1 Atm total pressure: Aquatic Geochemistry, vol. , no.1, p. 105-130.

Clemens, T., D. Hückinghaus, M. Sauter, and G. Teutsch, 1996, A combined continuum and discrete network reactive transport model for the simulation of karst development: Proceedings of the ModelCARE 96 Conference, Golden, Colorado, IAHS Publication No. 237, p. 309-318.

Clemens, T., D. Hückinghaus, M. Sauter, R. Liedl, and G. Teutsch, 1997a, Simulation of the evolution of maze caves:, 12th International Congress of Speleology and the 6th Conference on limestone hydrology and fissured aquifers, La Chaux-de-Fonds, Switzerland.

Clemens, T., D. Hückinghaus, M. Sauter, R. Liedl, and G. Teutsch, 1997b, Modeling the genesis of karst aquifer systems using a coupled reactive network model: Hard Rock Hydrosystems, Proceedings of Rabat Symposium S2, May, 1997, IAHS Publication No. 241, p. 3-10.

Curl, R.L., 1965, Solution kinetics of calcite: paper presented at the 4th International Congress of Speleology: Ljubljana, Slovenia.

Daugherty, R.L., and J.B. Franzini, 1965, Fluid mechanics with engineering applications: McGraw-Hill, New York, 564 p.

De Hoog, F.R., J.H. Knight, and A.N. Stokes, 1982, An improved method for numerical inversion of Laplace transforms: SIAM J. Sci. Stat. Comput. vol. 3, no. 3, p. 357-366.

Dreybrodt, W., 1981, Kinetics of the dissolution of calcite and its applications to karstification: Chemical Geology, vol. 31, p. 245 - 269.

Dreybrodt, W., 1988, Processes in karst systems: Springer-Verlag, New York, 288 p.

Dreybrodt,W., 1992, Dynamics of karstification: a model applied to hydraulic structures in karst terranes: Applied Hydrogeology, Vol. 3, p. 20-32.

Dreybrodt, W., 1996, Principles of early development of karst conduits under natural and man-made conditions revealed by mathematical analysis of numerical models: Water Resources Research, vol. 32, no. 9, p. 2923-2935.

Dreybrodt, W., 1997, Limestone dissolution rates in karst environments: 12th International Congress of Speleology and 6th Conference on limestone hydrology and fissured aquifers, La Chaux-de-Fonds, Switzerland.

Dreybrodt, W., 1998, Early development of karst aquifers on percolation networks of fractures in limestone: Water Resources Research, vol. 34, no. 3, p. 409-419.

Ford, D.C. and R.O. Ewers, 1978, The development of limestone cave systems in the dimensions of length and depth: Canadian Journal of Earth Science, vol. 15, p. 1783-1798.

Ford, D.C., and P.W. Williams, 1989, Karst geomorphology and hydrology: Chapman and Hall, Cambridge, Great Britain, 601 p.

Fraser, G.S., and J.M. Davis (eds.), 1998, Hydrogeologic models of sedimentary aquifers: Society for Sedimentary Geology, Tulsa, Oklahoma, 188 p.

Friedman, G.M. and J.E. Sanders, 1978, Principles of sedimentology: John Wiley & Sons, New York, 792 p.

Groundwater Simulations Group (GSG), 1997, A model for simulating advective-dispersive transport of a decay

chain through a network of interconnected pipes attached to multiple immobile porosity zones: Waterloo, Ontario, 13 p.

Groves, C.G., 1993, Early development of karst systems, Ph.D. thesis, University of Virginia, 253 p.

Groves, C.G., and A.D. Howard, 1994a, Minimum hydrochemical conditions allowing limestone cave development: Water Resources Research, vol. 30, no. 3, p. 607-615.

Groves, C.G., and A.D. Howard, 1994b, Early development of karst systems 1. Preferential flow path enlargement under laminar flow: Water Resources Research, vol. 30, no. 10, p. 2837-2846.

Hanna, R.B., and H. Rajaram, 1998, Influence of aperture variability on dissolutional growth on fissures in karst formations: Water Resources Research, vol. 35, no. 11, p. 2843-2853.

Howard, A.D., and C.G. Groves, 1995, Early development of karst systems 2. Turbulent flow: Water Resources Research, vol. 31, no. 1, p. 19 - 26.

Kiraly, L., and G. Morel, 1976a, Etude de régularisation de l'Areuse par modèle mathématique: Bulletin du Centre d'Hydrogéologie, vol. 1, p. 19-36.

Kiraly, L., and G. Morel, 1976b, Remarques sur l'hydrogramme des sources karstiques simulé par modèles mathématiques: Bulletin du Centre d'Hydrogéologie, vol. 1, p. 37-60.

Palmer, A.N., 1991, Origin and morphology of limestone caves: Geological Society of America Bulletin, vol. 103, p. 1-21.

Plummer, L.N., T.M.L. Wigley, and D.L. Parkhurst, 1978, The dissolution of calcite in CO_2 saturated solutions at 25°C and 1 atmosphere total pressure: Geochimica et Cosmochimica Acta, vol. 40, p. 191-202.

Sauter, M., 1992, Quantification and forecasting of regional groundwater flow and transport in a karst aquifer (Gallusquelle, Malm, SW Germany): Ph.D. thesis, University of Tübingen, Germany, 151 p.

Smith, L., and F.W. Schwartz, 1993, Solute transport through fracture networks, *in* J. Bear, C. Tsang, and G. De Marsily (eds.): Flow and contaminant transport in fractured rock: Academic Press, p. 129-164.

Sudicky, E.A., 1989, The Laplace transform Galerkin technique: A time-continuous finite element theory and application to mass transport in groundwater: Water Resources Research, vol. 25, no. 8, p. 1833-1846.

Sudicky, E.A., 1990, The Laplace transform Galerkin technique for efficient time-continuous solution of solute transport in double-porosity media: Geoderma, vol. 46, p. 209-232.

Sudicky, E.A., and E.O. Frind, 1982, Contaminant transport in fractured porous media: analytical solutions for a system of parallel fractures: Water Resources Research, vol. 18, no. 3, p. 1634-1642.

Sudicky, E.A., and R.G. McLaren, 1992, The Laplace transform Galerkin technique for large-scale simulation of mass transport in discretely fractured porous formations: Water Resources Research, vol. 28, no. 2, p. 499-514.

Van der Vorst, H., 1992. Bi-CGSTAB: A fast and smoothly converging variant of Bi-CG for the solution of nonsymmetric linear systems: SIAM, Jour. Sci. Stat. Comput., v. 13, p. 631-644.

Vanderkwaak, J.E., P. Forsyth, K. Macquarrie, and E.A. Sudicky, 1997, WatSolv:Sparse Matrix Iterative Solver, User's Guide for Version 2.16: Groundwater Simulations Group, Waterloo, Ontario, Canada.

White, W.B., 1988, Geomorphology and hydrology of karst terrains: Oxford University Press, New York, 464 p.

SUBSIDIARY CONDUIT SYSTEMS: A HIATUS IN AQUIFER MONITORING AND MODELING

Christopher C. Smart
Department of Geography, University of Western Ontario
London, Ontario N6A 5C2, Canada

Introduction

Karst aquifers are generally conceived and modeled as "diffuse" aquifers penetrated by trunk conduits. Head loss in conduits is much lower than in surrounding fractures or porous media (e.g. Jeannin and Maréschall, 1995). As a result, conduits control head distribution in the aquifer and permit exceptionally rapid transfer of water and contaminants. The diffuse aquifer is conceived of as a reservoir, slowly adjusting to autogenic (surface) recharge and backflooding from the primary conduits. Most karst hydrogeologists would recognize that this is an oversimplification; real karst aquifers constitute a network of fractures and ***subsidiary*** conduits.

The simplification arises because it permits aquifer modeling with reasonable demands for field parameterization. Cave mapping, groundwater tracing (e.g. Quinlan and Ray, 1981) and spring discharge monitoring (e.g. Smart, 1988) provide tools for diagnosis of the ***primary conduit*** structure of the aquifer, e.g. trunk conduits linking discrete stream sinks and springs. Conventional borehole water-level and testing techniques are available for porous and fractured media and can be used to characterize the diffuse aquifer.

Detailed characterizations of borehole hydrogeology reveal the presence of highly permeable horizons or points in karst aquifers. Presumably, these features correspond to small conduits and anastomosing horizons such as those observed in quarry faces and road cuts. While small in size, the hydraulics of these ***subsidiary conduits*** permit rapid transfer of water and contaminants, and distort the piezometry of the surrounding aquifer. Characterization of subsidiary conduits may permit development of more realistic aquifer models. Unfortunately, there seems to be little information on such features; they fall between testing wells and characterizing conduits. It therefore seems imperative to understand, identify, and characterize subsidiary conduits.

Exposures suggest that subsidiary conduits are focused on fractures and bedding planes and are therefore likely to have similar structure to primary conduits. They probably consist of dendritic or braided channels organized in vertical and size hierarchies. Unfortunately, exposures are not readily tested for their hydraulic function. Observation wells will permit some diagnosis of hydraulic function, but may not penetrate a subsidiary conduit. Data from observation wells must be regarded as a statistical sample, rather than characteristic of the aquifer.

As a first step in understanding the nature of subsidiary conduits, the relationship between a primary conduit, an observation well, and karst openings will be investigated using simple simulation models. The response of an observation well to hydraulic forcing of an adjacent conduit depends upon the link between the two. Differences in hydraulic head can be considered "errors" in representation of the conduit head, or can be regarded as diagnostic of the link between the well and conduit.

A subsidiary conduit model

The model is composed from two fundamental elements linked in a simple two-dimensional orthogonal array. Horizontal water-filled cylindrical pipes convey water between larger radius, variable volume, vertical pipes or reservoirs (Figure 1). Because head loss scales to radius to the fifth power, the latter large openings are considered frictionless. Each element is characterized by a length (l), radius (R) and vertical position. Rather than rendering each pipe in detail, an "equivalent pipe" is used.

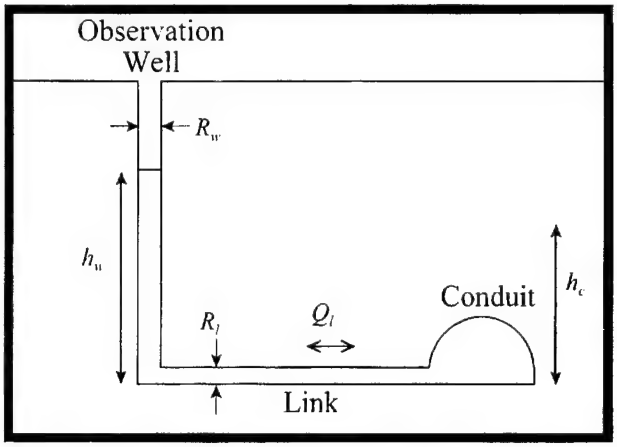

Figure 1: Definition diagram for the observation well connected to a conduit by a restrictive link.

A time-series approach is taken to investigate the response of karst systems to hydrological forcing. Recharge is modeled as an arbitrary characteristic hydrograph form, projected as an independent time sequence of hydraulic head in a major conduit.

Flow through each pipe segment is governed by the Darcy-Weisbach Equation:

$$Q = 2\ \pi g^{0.5} R^{2.5} ((h_2 - h_1)/f\ l)^{0.5} \qquad (1)$$

Where g is acceleration due to gravity, $h_2 - h_1$ is hydraulic head difference across the conduit element (treated as an absolute number), l is the length of the conduit element, and f is the Darcy-Weisbach friction factor. Model results are relatively insensitive to f and l, and they are held constant at 0.05 and 10 m, respectively.

The models operate by adopting a set of initial conditions of uniform steady head of two meters, and then gradually varying the head in the primary conduit. The head hydrograph adopted here is initialized with $h_c = 2$ m at 2 hours, peaking at $h_c = 10.4$ m at ~7.5 hours, and returning to 2 m around 30 hours. Flow is modeled as "gradually varying steady flow" in time steps of 1 second. Fluxes for each pipe element are computed from (1), based on difference in head across the connecting pipe. Pipe flow is initiated as the head at either end reaches the elevation of the pipe. When an active pipe emerges above current water level, the outlet head is taken as the elevation of the outlet. The volumetric water balance (ΔS) of free-surface storage elements (wells and reservoirs) is computed to provide change in head,

$$\Delta h = \Delta S/\pi R_r^2 = (\Sigma Q_{in} - \Sigma Q_{out})/\pi R_r^2 \qquad (2)$$

where ΔS is the volumetric change in storage, ΣQ_{in} and ΣQ_{out} are total inflow and outflow. Δh is applied to the current head to obtain the subsequent head at that point. Vertical storage elements are considered "hydrostatic." Results are expressed as five-minute time series of head on vertical elements, and of discharge through pipe elements.

The remainder of this paper describes the outcomes of various simple modeling experiments undertaken to learn something about subsidiary conduit systems.

Reservoir, observation well, and forcing conduit

A karst observation well is extremely unlikely to encounter a primary conduit. It follows that a distinctive *link* must exist between the well and the conduit. If the link is a subsidiary conduit, how will its form influence the representation of the conduit head in the observation well?

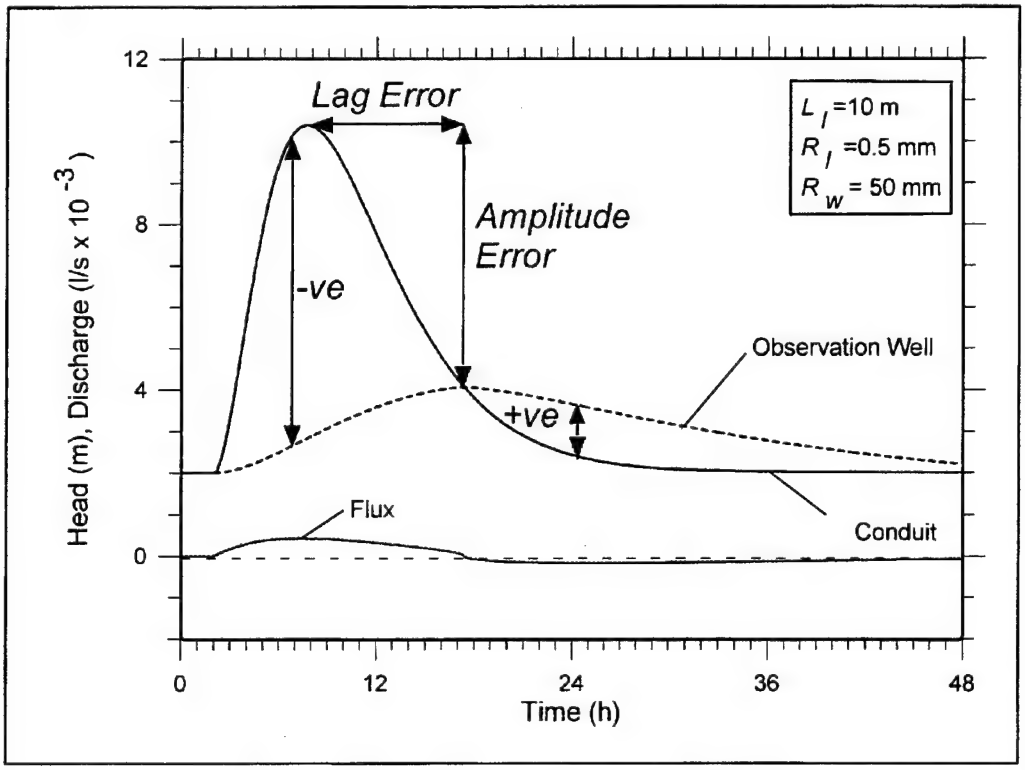

Figure 2: Head time series for a conduit and observation well with a 0.5 mm radius link and a 50 mm radius observation well. The conduit head series constitutes the "standard hydrograph" used in all subsequent simulations. Head differences between the conduit and well are considered to be "errors" of representation.

Figure 1 shows the model configuration adopted to tackle this question. It consists of a trunk conduit linked to a vertical observation well of radius R_w by a link of smaller radius, R_l. Head within the conduit (h_c in Figure1) is modulated to force the model with a simple hydrograph. Head in the observation well (h_w) adjusts by flux (Q_l) through the link, driven by the head difference between the conduit and the observation well.

Water flux through the link is limited, and therefore the head in the observation well lags behind and has a lower amplitude than that in the conduit (Figure 2). The departure of the observation-well signal from the conduit signal can be simply defined by differences in peak height and time lag, and by maximum absolute differences between the two (Figure 2). The influence of f and l on these errors is relatively minor; the link and well radii (R_l and R_w) are the dominant controls. Accordingly, the discrepancies, or "errors," have been determined for various values of R_l with all other factors held constant (Figure3). For example, the current conduit flood amplitude of ~8m translated through a 1 mm radius link has a phase error of ~4 hours, peak amplitude 2 m less than that on the conduit, and a maximum head difference of ~5m. Under current model conditions, large errors are seen at R_l of 1 mm, and "error" is negligible at R_l of 5 mm. These two values are taken in all following model scenarios as characterizing "poor" and "good" connections. A larger borehole radius increases the magnitude of the "errors."

A link between a primary conduit and an observation well will thus "translate" the conduit hydrograph, depending on the link radius. Such a well is likely to represent conditions in neither the conduit nor the diffuse aquifer. The water sampled at the entry point into an observation well during the rising stage of an event may be conduit water, albeit a little delayed in delivery. However, during falling stage, the well water is largely derived from the falling column of old conduit water in the well. This water is representative of neither conduit water nor diffuse aquifer water. Sampling and monitoring of karst observation wells are therefore fraught with uncertainty.

Observation well and vug

The necessity for a flux of water to represent hydraulic head changes is responsible for the observation-well problem. Accordingly, decreasing observation-well radius reduces the problem. Many wells installed in karst contain vugs and karst cavities. As water levels encounter such openings, more water is required to produce a given rise in head. If the flux through the link is restricted, then the rate of change in water level may drop. Is it possible to identify and characterize such features by analysis of the observation-well head time series?

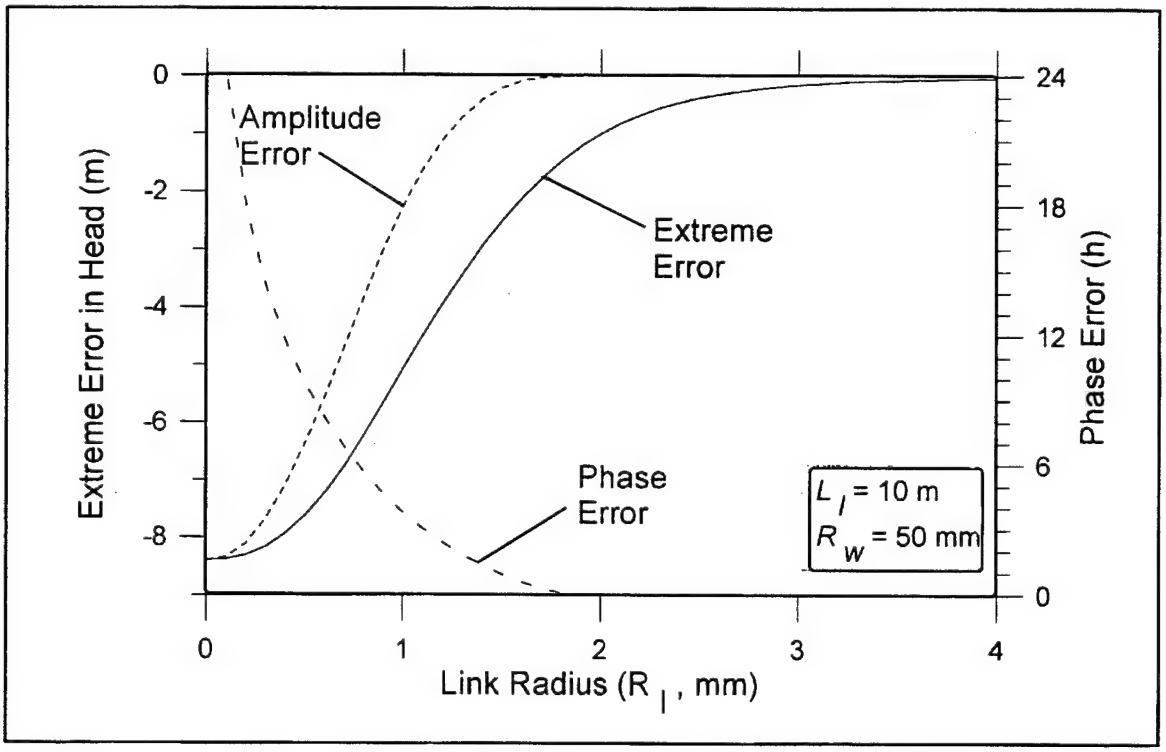

Figure 3: The phase, peak, and maximum absolute error between observation well and conduit plotted against link radius. See Figure 2 for definitions.

Figure 4 provides a simplified example where an observation well expands from R_w = 50 mm to R_{vug} = 100mm between 7 and 8 meters above datum. Figure 5 presents the results for R_l = 1, 2, 3, and 5 mm with the conduit forcing represented in Figure 2. When inflow is restricted by small R_l (Figure 5a), then a distinctive plateau appears in the time series of well water level (h_w), as the water level never passes above the top of the vug. At larger link radii (Figures 5b, c), the water level rises more slowly as it passes through the vug. At R_l = 5 mm, the well head follows the conduit head almost exactly, as the link is competent to deliver the additional water required to fill the vug.

Discharge through the link is governed by the head difference between the conduit and the well. As the link radius increases, subtle changes in this relationship result in a complex pattern of discharge through the link (Q_l, Figure 5). The spikes of discharge arise from the additional flux necessitated by the vug. At R_l = 5 mm, peak velocity is of the order of 0.22 m/sec during the rising stage, but less than half this on falling stage, a result of the asymmetry of the forcing hydrograph. Such velocity anisotropy will promote advection of clastic particles into the body of an aquifer rather than into a conduit. The sediment commonly occupying the floor of anastomoses and filling karst wells may thus have been derived from conduit floodwaters rather than internal residuum.

If the observation-well time series data are of sufficiently high frequency and resolution, the rates of change in water level across a transition can be used to obtain the effective radius of such a vug as follows:

$$R_2 = R_1 \sqrt{(\delta h/\delta t)_1/(\delta h/\delta t)_2} \qquad (3)$$

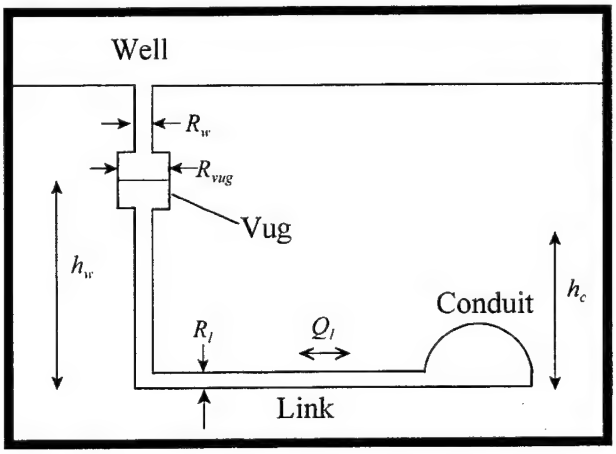

Figure 4: Vug definition diagram. The vug consists of a section of well R_{vug} = 0.10 m between 7 and 8 m elevation For all simulations, R_w = 0.05m, R_l = 5 mm, f = 0.05, L = 10 m. Standard hydrograph.

Where $\delta h/\delta t$ is the change of head with time, and subscripts 1 and 2 refer to known and unknown well radii, respectively.

It may be possible to determine if a conduit-well link is restricted and likely to cause errors. Absolute flux through the link is increased when the observation-well radius increases. A non-buoyant slug suspended in a well can be used to restrict the cross-sectional area. If during a flood event, the absolute rate of water-level change increases at the slug, then the link is implicitly restrictive and the well is under-representing the conduit hydraulics.

A poorly connected open observation well may generate misleading conduit stage data. A correctly installed pressure piezometer does not require a flux of water to generate a head signal. However, the signal will still be influenced by other karst elements attached to the connecting link, and only costly installations are able to withstand the extreme head changes.

Observation well and karst outlet

A cavity encountered in a well may be a karst *connection* (Figure 6), functioning as a simple overflow. How might this influence the observation-well head time series and resulting fluxes? Figure 7 presents the results of simulating this using a rather unrealistic constant head at the outlet of a 10 m long karst connection at 5 m above datum. This might arise if the overflow encountered a permanently air-filled shaft. Net flux out of the conduit through the observation well is the result. (The sign of discharge is positive into the well.) The overflow demonstrates how a karst reservoir with an independent, restricted link might be filled, only to drain very slowly

In general, overflows suppress h_w, head in the observation well, providing the overflow is of the same order as, or larger than, the link to the forcing conduit (Figure 7a, b, d). Where the overflow is large relative to the link, a characteristic overflow "plateau" (e.g. Figure 7b), or suppressed peak (e.g. Figure 7d) occurs in the well water-level series. The detachment points of the plateaus indicate the level of the overflow.

A large overflow suppresses head in the observation well, and large discharges can result (Figure 7d). Peak velocity is in excess of 1 m/sec, more than enough to initiate and sustain sediment transport. More subtle onset (Figure 7b) and steps (Figures 7c, d) in discharge also arise from the overflow. Head series are not sufficient to identify the overflow condition. However, the well mass-balance is distinctly different than with the vug model. Discharge data are also required to distinguish overflow from a vug.

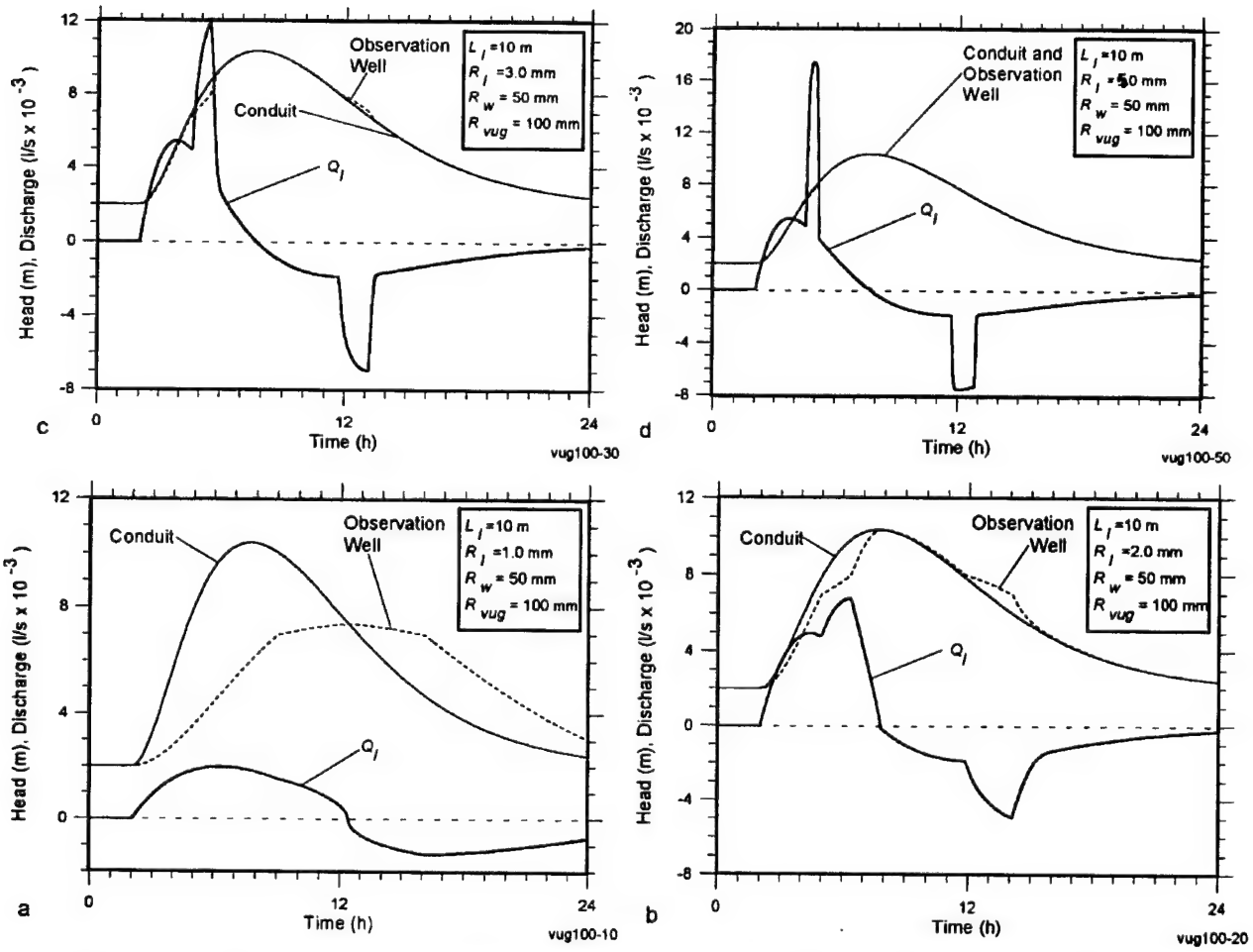

Figure 5: Vug-in-well results: **(a)** vug influence on response curve R_l = 1 mm; **(b)** vug influence on response curve R_l = 2 mm; **(c)** vug influence on response curve R_l = 3 mm; **(d)** vug influence on response curve R_l = 5 mm.

Overflow into a reservoir rather than a void

Overflow from a connection would more normally feed an adjoining karst system, and some back pressure would be developed. The simplest representation of this is to feed the outlet into the base of a reservoir of radius R_r which gradually fills and then drains back into the observation well during falling stage (Figure 8).

The models here adopt a large (R_l = 5 mm) link between the conduit and the well, so that exact matching of well and conduit heads would be expected (Figure 3). The overflow is positioned 5 m above base level. Under these circumstances, two primary variables control the response of the observation well to a reservoir: overflow radius and reservoir radius. The former determines the rate at which flux occurs in response to a developed hydraulic gradient. The latter governs the rate at which the reservoir head matches the well head.

Reservoirs have little impact on the well-head record unless they are large and well connected (e.g. Figure 9d). In contrast, the reservoir displays a wide variety of low-amplitude responses. Only in Figure 9c (small reservoir, large overflow) does the reservoir water level match that of the conduit. Surprisingly, Figures 9a and 9d give very similar reservoir water levels despite strong contrasts in overflow and reservoir form.

Small-scale reservoirs have relatively little effect on well water levels and discharges. The impact of intermediate-scale reservoirs (R_r = 0.10 m, Figures 9a and c) is highly dependent on the overflow radius. Larger overflow radius (Figure 9c) permits the reservoir head to match the well and conduit head. As the reservoir runs dry, discharge from the well back into the conduit (Q_l) is reduced dramatically, with no indication of this in the well head.

Large-radius reservoirs develop little back pressure, so they develop similar simulation histories to simple overflow (Compare Figures 7d and 9d, 7c and 9b.), except that there is a sustained reflux of the water stored in the reservoir.

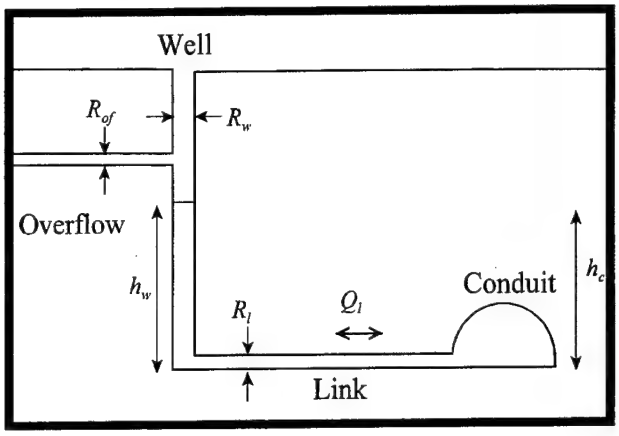

Figure 6: Overflow definition diagram. For all simulations, $R_w = 0.05$ m, $f = 0.05$, $l = 10$ m. Standard hydrograph.

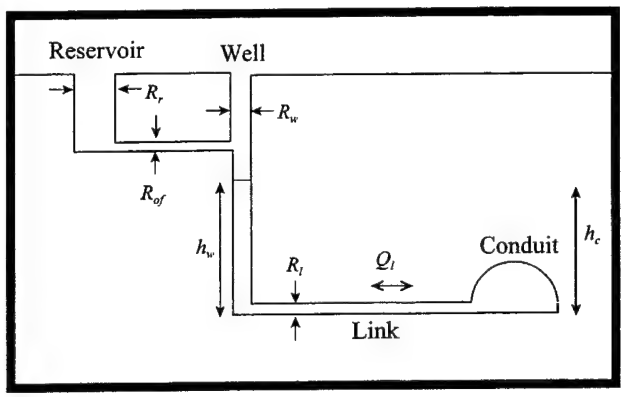

Figure 8: Definition diagram for overflow to adjacent reservoir. For all simulations, $R_w = 0.05$ m, R_l=5 mm, f = 0.05, $l = 10$ m. Standard hydrograph.

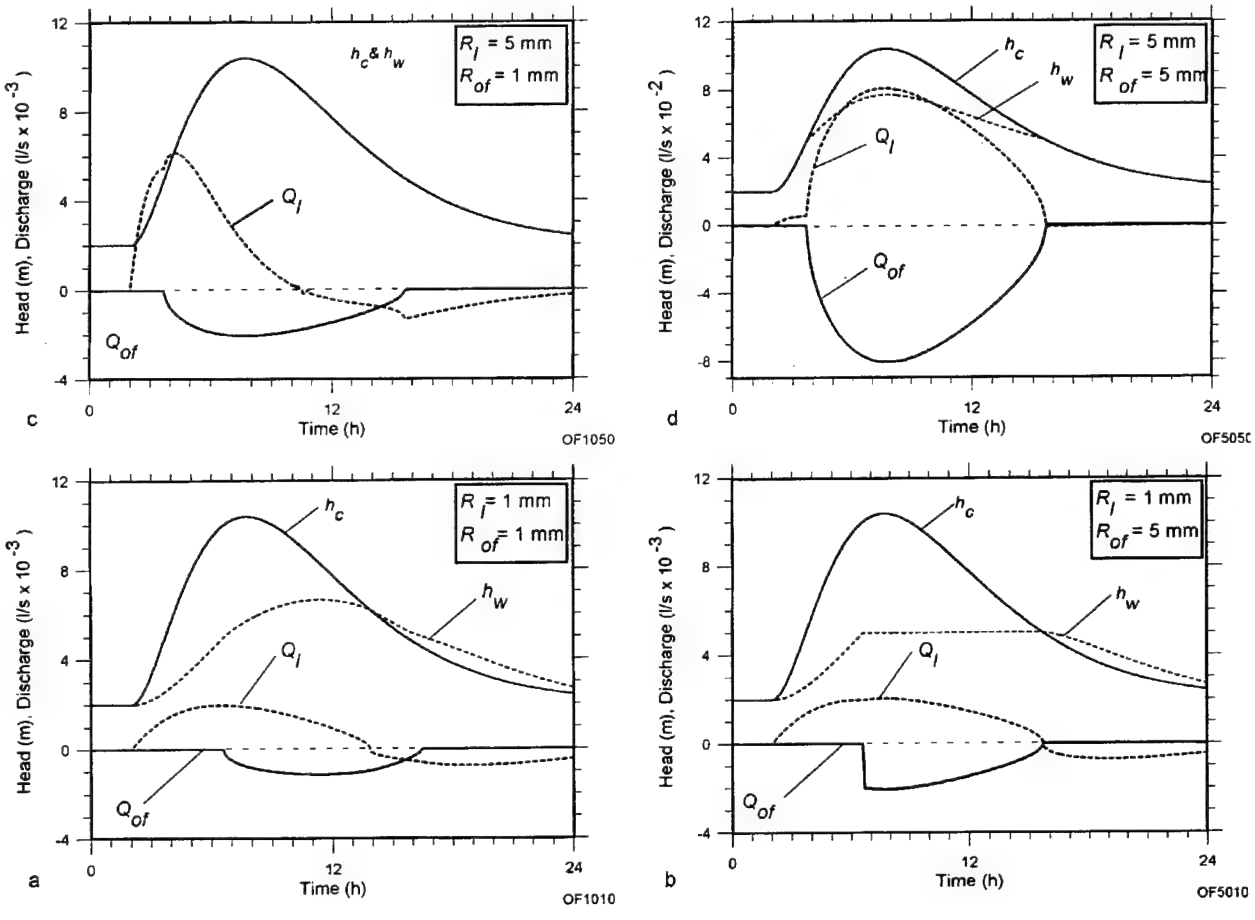

Figure 7: Overflow results: **(a)** Overflow results for link radius (R_l) = 1 mm, overflow radius (R_{of}) = 1 mm. **(b)** Overflow results for link radius (R_l) = 1 mm, overflow radius (R_{of}) = 5 mm. **(c)** Overflow results for link radius (R_l) = 5 mm, overflow radius (R_{of}) = 1 mm. **(d)** Overflow results for link radius (R_l) = 5 mm, overflow radius (R_{of}) = 5 mm. (Note discharge scale is an order of magnitude greater than in other graphs.)

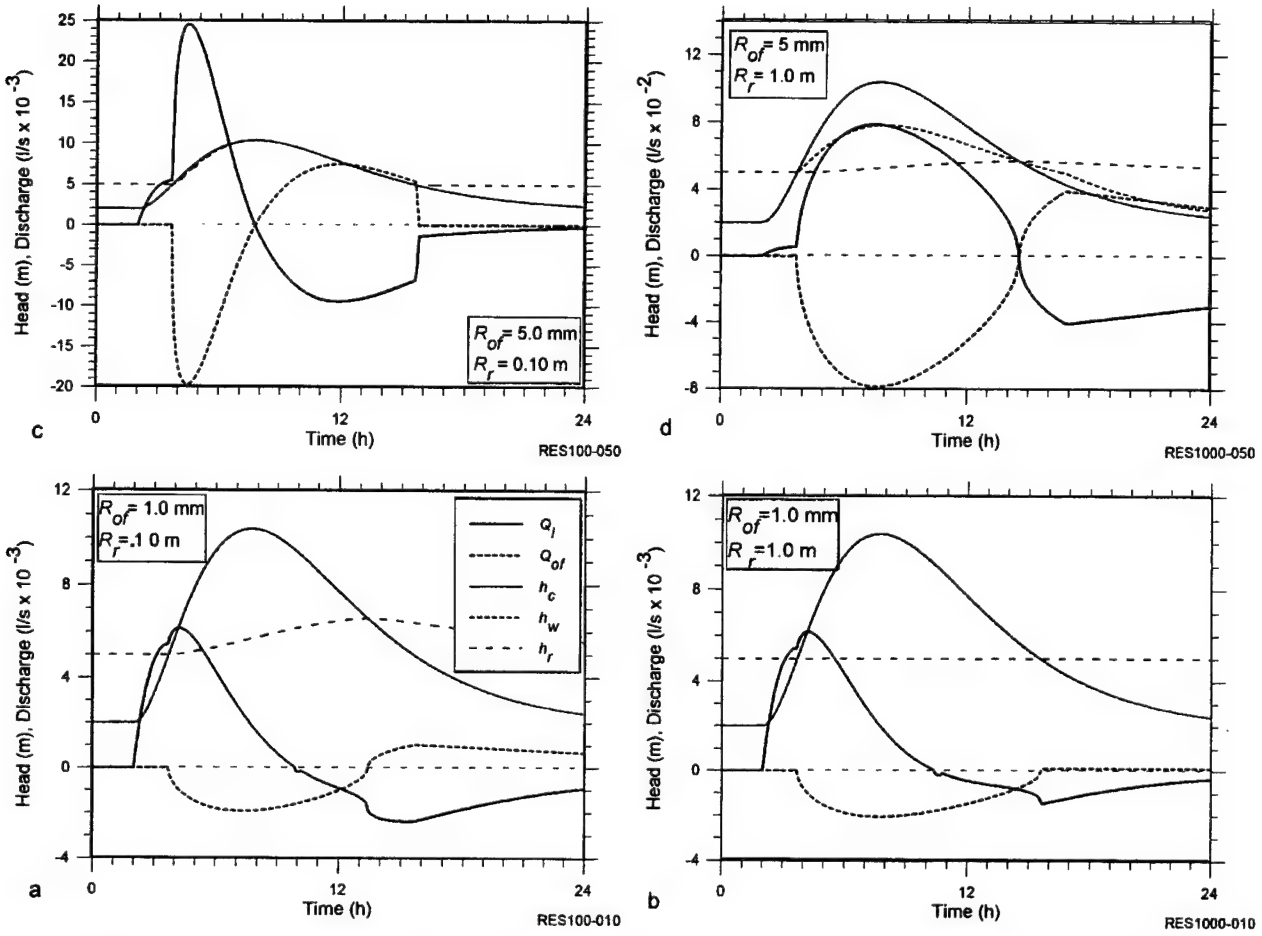

Figure 9: Results of overflow to adjacent reservoir: **(a)** Reservoir model results for overflow radius (R_{of}) = 1 mm, reservoir radius (R_r) = 100 mm. **(b)** Reservoir model results for overflow radius (R_{of}) = 1 mm, reservoir radius (R_r) = 1.0 m. **(c)** Reservoir model results for overflow radius (R_{of}) = 5 mm, reservoir radius (R_r) = 100 mm. **(d)** Reservoir model results for overflow radius (R_{of}) = 5 mm, reservoir radius (R_r) = 1.0 m. (Note discharge scale is an order of magnitude greater than in other graphs.)

Once more, well discharge patterns provide more useful diagnostic criteria than water levels. Significant breaks in discharge occur at overflow thresholds without any concomitant response in head. All larger reservoirs show distinctive steps in rising-stage discharge through the link, but only those with larger radii develop flows competent enough to transport sediment.

Multi-level links between conduit and well

Multiple linkages are likely to develop in well-bedded, low dip limestones. Returning to the simple original model, the impact of tandem links at different elevations can be investigated (Figure 10). When the lower link is large (R_1 = 5 mm, Figures 11c, d), the well water level follows the conduit water level. A small upper-level link has negligible effect on discharge (Figure 5c). When both links are small a subtle break in slope appears in the falling-stage well head (Figure 11 a) as the overflow ceases operation and the well suddenly is only draining through a single conduit. This feature is better developed in Figure 11b, where the rising stage analog is also present. It is suggested that multi-level conduits provide a physically rational explanation of multi-segment recession curves, in contrast to the conventional interpretation of progressive drainage of multi-permeability media (e.g. Shevenell, 1996; Smart, in prep.).

Where both conduits are pressurized and of identical size, their discharge is identical. Larger overflows result in a number of curious features (Figure 11b). When the well water level is below the outlet of the upper conduit, extreme discharges occur, albeit briefly (Figure 11b, maximum overflow discharge is 0.03 L/sec at 0.4 m/sec). Note that these are features "in principle;" the exact form of such "transients" is inadequately represented in the current model.

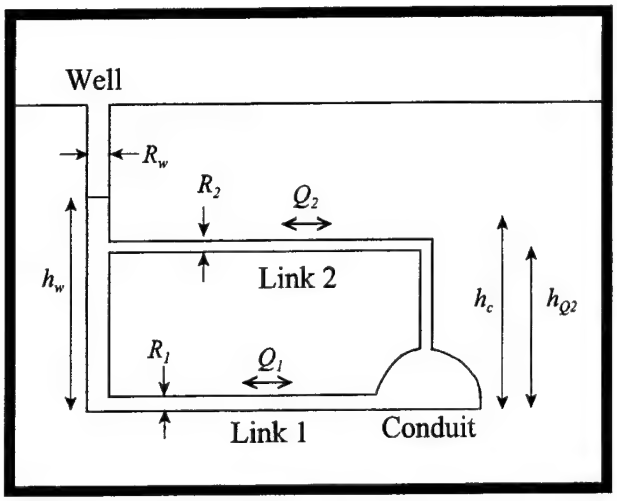

Figure 10: Tandem-link definition diagram. For all simulations, $R_w = 0.05$ m, $f = 0.05$, $l = 10$ m. Link 2 is 5m above link 1. Standard conduit hydrograph.

Tandem links between reservoir and well

The final logical step in this modeling progression is to consider the impact of tandem links between the well and reservoir (Figure 12). While the conduit-well link is maintained at $R_1 = 5$mm for all simulations, the remarkable sensitivities revealed have necessitated reporting separately for small and large reservoirs (Figures 13 and 14, respectively). The usual forcing hydrograph is applied, but sustained drainage of larger reservoirs requires extension of the time scale to 48 hours in Figures 14b and d.

With the smaller reservoir ($R_r = 0.1$ m, Figure 13), the only marked effect arises from a larger overflow (Figure 13c). Reservoir water level tends to match well water levels where any larger overflows are present. A larger reservoir (Figure 14) markedly depresses and modulates peak well water levels, if larger overflows are anywhere present. Larger reservoirs show very subdued water-level response.

Discharge patterns arising from tandem overflows are remarkable in terms of pattern and magnitude, but only a limited prospect is provided here. The complexity arises from the influence of multiple overflows on head matching between well and reservoir. In general, rising-stage fluxes are greater in absolute magnitude, sometimes remarkably so (e.g. Figures 13c and 14c). Velocities up to 1 m/sec occur (Figure 14b), and sometimes discharges change very suddenly (Figure 13c, d) and in very distinctive form (Figure 14d). An important feature identified here is the relative ease of recharging a reservoir by backflooding from a conduit, compared to its slow drainage.

Reliable sampling for tracers or water quality in tandem-linkage wells is very difficult. Variation in fluxes at different inlets in wells will alter the apparent hydrostratigraphy, confusing attempts to identify a coherent point of sampling. In addition, activation of a large overflow conduit may significantly reduce flow through a lower conduit, delaying tracer delivery (Smart, in preparation).

Surface recharge

Surface recharge into wells and reservoirs would contribute to the local water balance and enhance local head (Figure 15). There is precious little information on spatial patterns of recharge (e.g. Jeannin and Grasso, 1995; Smart and Friederich, 1986). It may be fair to assume that larger underground voids (reservoir cavities) will have correspondingly great surface catchments, and greater volumes of more rapid recharge. Such scaling will moderate the impact of surface recharge on local head. Nevertheless, in areas removed from primary pressure conduits, local recharge may be the primary source of head perturbation.

Attempting to model these effects significantly increases the proportion of *ad hoc* assignments in model design. This undermines both conviction and learning. As education and guidance were the objectives of this modeling campaign, these results will not be tackled here.

Conclusions

A forcing conduit and observation well have been used as an example of how information about the subsidiary conduit system might be obtained. It is difficult to generalize even from the limited results presented here. Overall, water levels have a complex relationship to water flux in subsidiary conduits. The main determinants of the pattern of response are the radii of conduits and reservoirs, and the elevation at which these are joined. Results are not so sensitive to distance and roughness, though the overall variability of these factors may be greater. Contrary to much opinion by karst hydrologists, flow regime and flow law are not of compelling significance.

The routing, storage and reflux of water through even simple subsidiary conduit systems suggests that water levels and water sampled from wells linked into the subsidiary conduit system is unlikely to characterize the aquifer. Similarly, a tracer cloud traveling through such a system may be fragmented, mixed, and delayed during unsteady conditions. Traces made away from primary conduits tend to show these features to the extent that breakthrough curves are often undefinable (e.g. Aley 1997). Flow velocities directed away from the primary conduit are generally greater than those returning. This

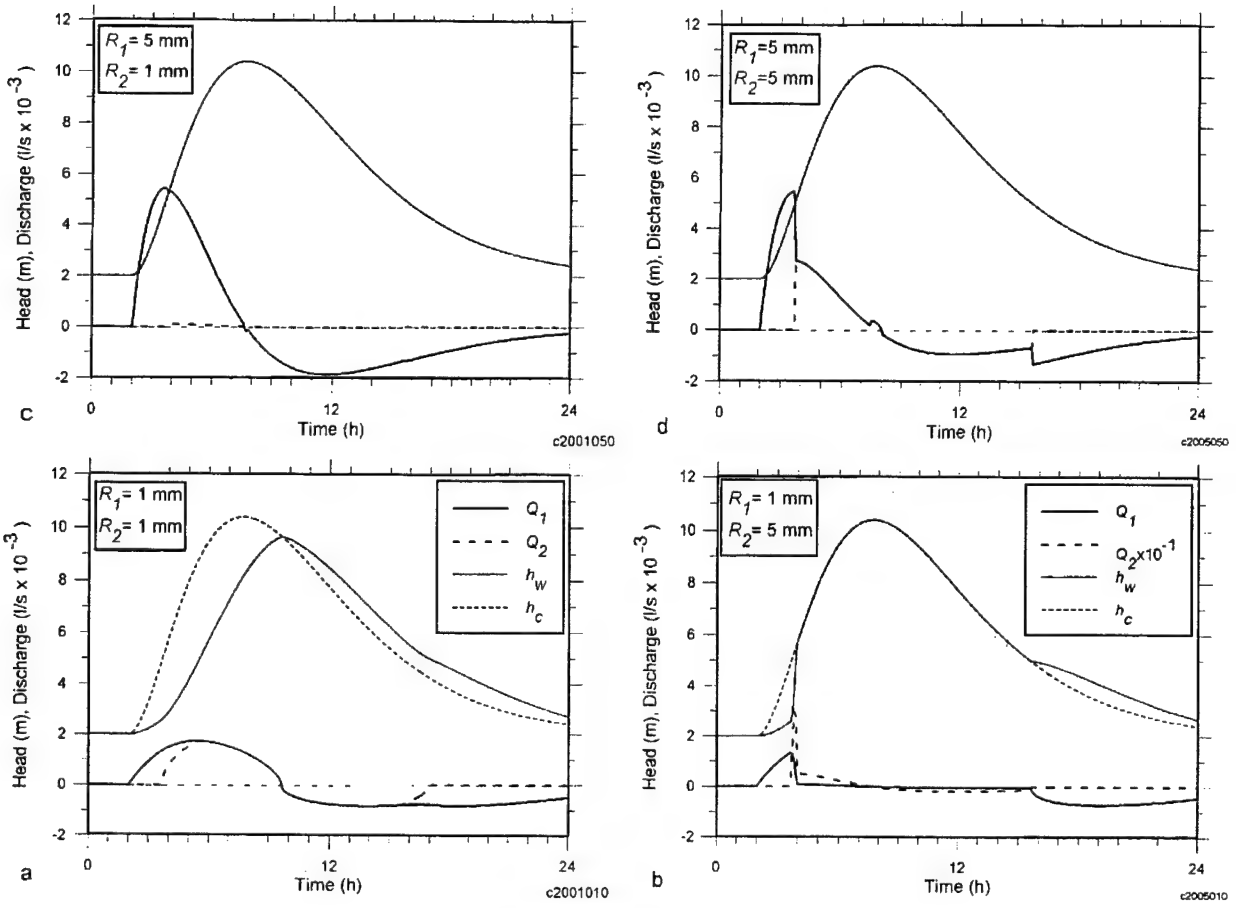

Figure 11: Tandem link results. **(a)** Tandem link results for R_1 = 1 mm, R_2 = 1 mm. **(b)** Tandem link results for R_1 = 1 mm, R_2 = 5 mm. Note: Q_2 is 10x axis scale. **(c)** Tandem link results for R_1 = 5 mm, R_2 = 1 mm. **(d)** Tandem link results for R_1 = 5 mm, R_2 = 5 mm.

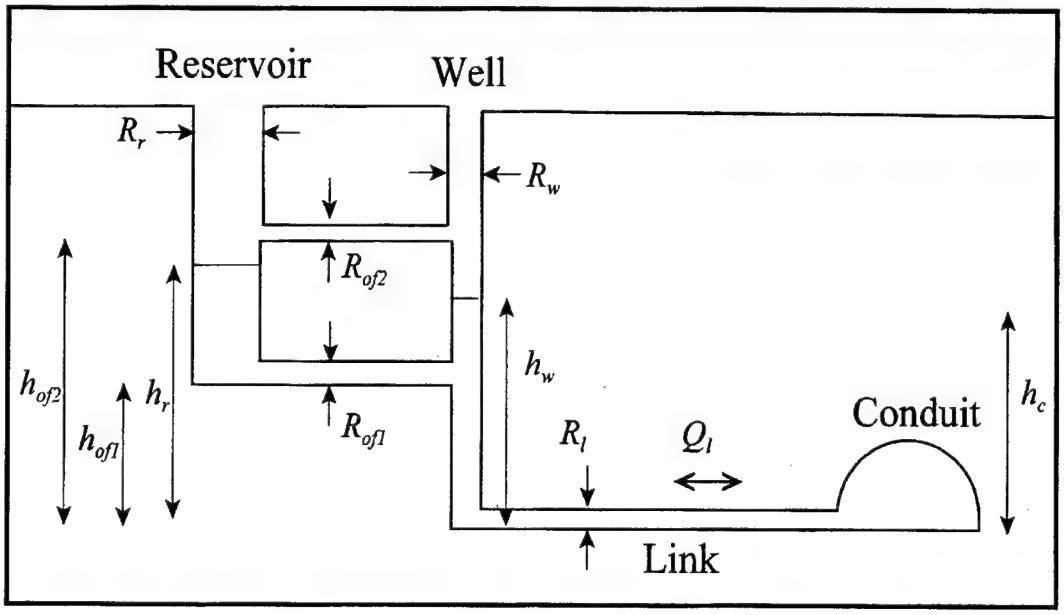

Figure 12: Tandem overflows between the reservoir and well. For all simulations, R_1 = 5 mm. R_w = 0.05m, f = 0.05, l = 10 m. Overflows lie 5 and 7 meters above link. Standard conduit hydrograph.

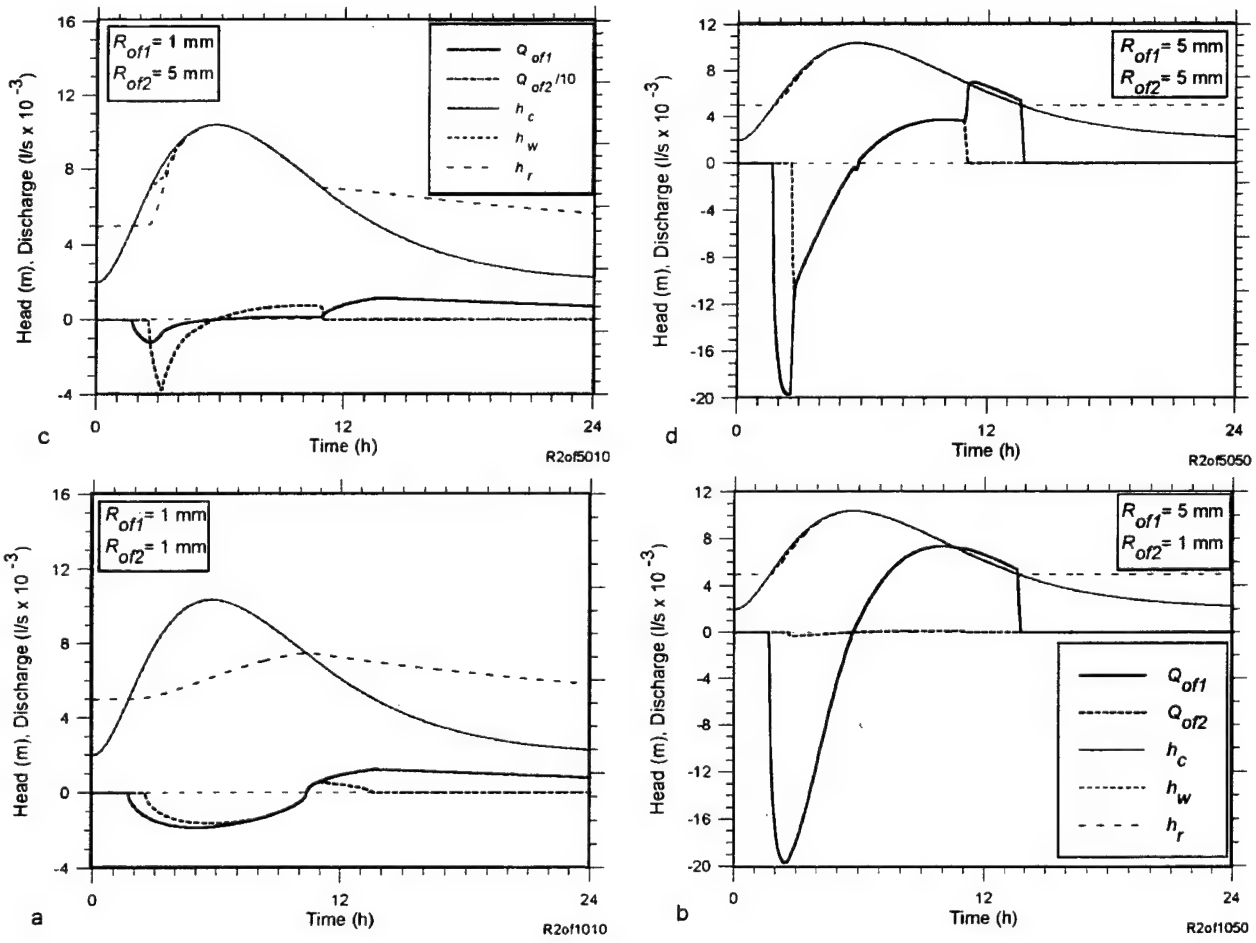

Figure 13: Results of tandem overflows between reservoir and well. For all simulations R_r = 0.1 m. **(a)** Lower overflow radius = 1 mm, upper overflow radius = 1 mm. **(b)** Lower overflow radius = 5 mm, upper overflow radius = 1 mm. **(c)** Lower overflow radius = 1 mm, upper overflow radius = 5 mm. **(d)** Lower overflow radius = 5 mm, upper overflow radius = 5 mm.

arises not only from the asymmetry of the forcing hydrograph, but is also a result of multiple conduits. Systemic anisotropy implies that clastic sediment will be transferred into the aquifer rather than out to the primary conduit.

From the monitoring perspective, it has long been known that low-frequency (e.g. bi-weekly) sampling of water levels will not identify event-driven variations in water level. Such data will not allow characterization of the subsidiary conduits and sustains the continued use of inappropriate groundwater models in karst. High-frequency, high-resolution monitoring of karst wells will increase costs -- so is it possible to derive useful parameters from high-resolution water level data? The present modeling indicates that observation-well data are likely to be highly ambiguous, representing neither the primary conduits nor the diffuse aquifer. Although water-level data from karst wells contain breaks and anomalies similar to those modeled here (e.g. Ray 1997), the modeling effort indicates that water-level effects are subtle and ambiguous in origin. In contrast, *discharge* patterns along the subsidiary conduits are remarkable in their variety and uniqueness. Adequate diagnosis of karst aquifers will require specialized methods, beyond conventional water-level observation, slug testing and packer testing. Discharge measurements seem to be the key.

Is there any prospect of incorporating subsidiary conduits into aquifer models? Probably not in the sense of physical realism. It is field information which is limiting, not computational power. Until we have effective underground remote sensing capability, observation wells provide our only window into the aquifer. Even if correctly interpreted, evidence from any well will be spatially idiosyncratic, a statistical sample rather than an absolute parameterization. However, it appears feasible to obtain information on the level and caliber of conduits, and the diameter and position

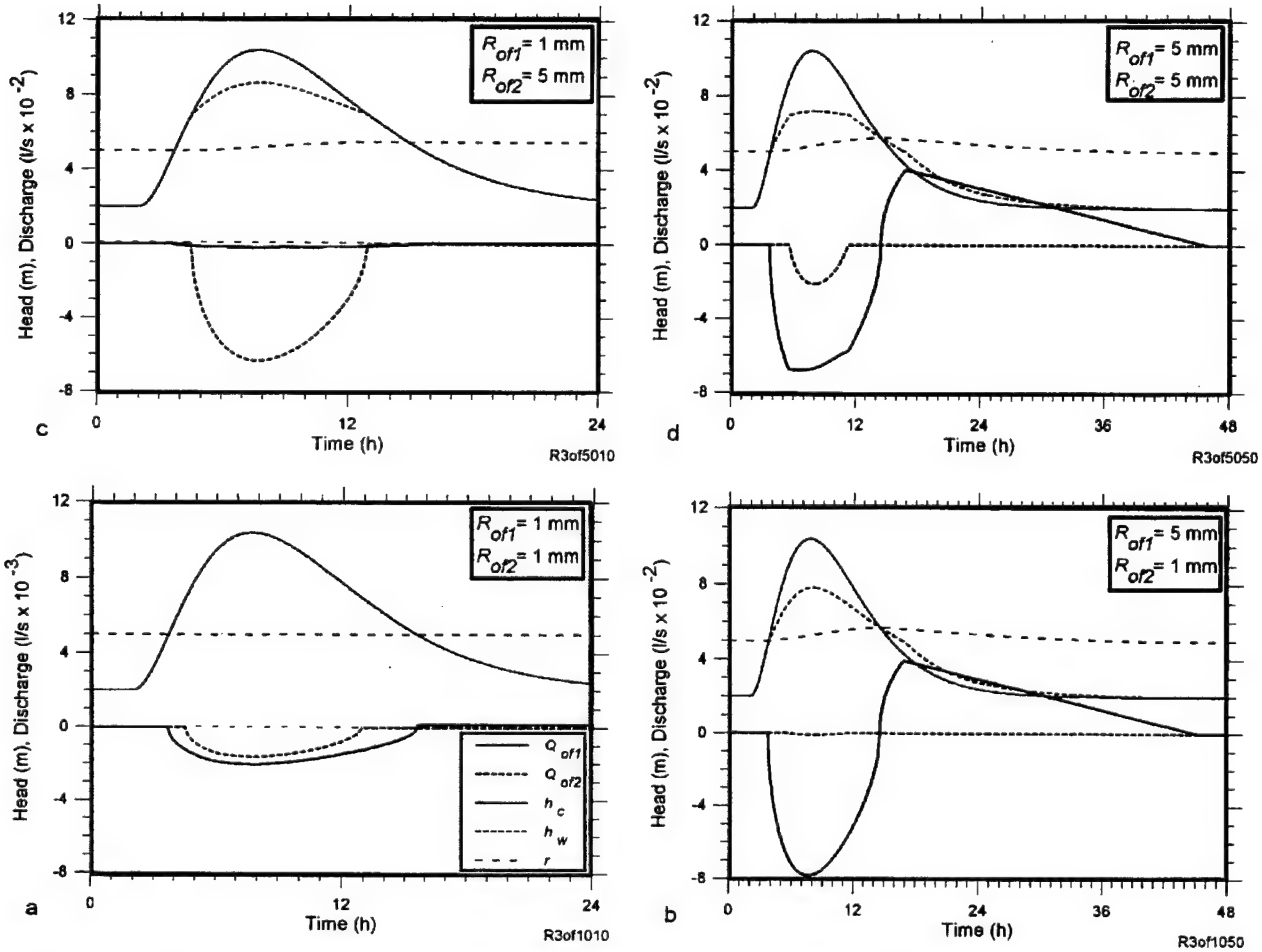

Figure 14: Tandem overflow results, with reservoir radius (R_r) of 1 m. **(a)** Lower overflow radius = 1 mm, upper overflow radius = 1 mm. **(b)** Lower overflow radius = 5 mm, upper overflow radius = 1 mm. **(c)** Lower overflow radius = 1 mm, upper overflow radius = 5 mm. **(d)** Lower overflow radius = 5 mm, upper overflow radius = 5 mm.

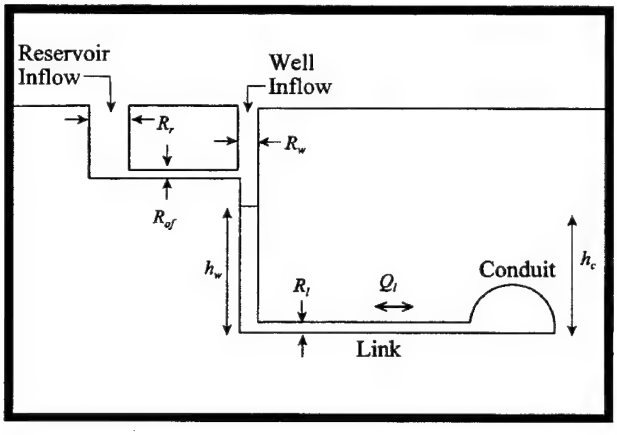

Figure 15: Definition diagram for surface recharge of the well and the reservoir. The recharge is likely to appear as a subsurface inflow.

of reservoirs, which may be key features in any successful karst aquifer model.

If subsidiary conduit systems are as sparse as those considered here, then few observation wells will be compatible with the model. If subsidiary conduit systems are of very high volumetric density, then near-continuum hydraulics will prevail and diagnostic testing may be impossible. Even if diagnostic testing is feasible, we may have to become reconciled to describing conduit form in "equivalent" terms, as absolute information on length, radius and roughness may never be resolvable.

References cited

Aley, T., 1997, Ground water tracing in the epikarst, *in* B.F. Beck and J.B. Stephenson (eds..), The Engineering geology and hydrogeology of karst terranes: New York, Balkema, p. 207-211.

Jeannin, P.-Y., and A.D. Grasso, 1995, Recharge respective des volumes de roche peu perméable et des conduits karstiques, rôle de l'épikarst: Bulletin d'Hydrogéologie, v. 14, p. 95-111.

Jeannin, P.-Y., and J.-C. Maréschall, 1995, Lois de pertes de charge dans les conduits karstiques: base théoretique et observations: Bulletin d'Hydrogéologie, v. 14, p. 149-176.

Quinlan, J.F., and J.A. Ray, 1981, Ground water basins of the Mammoth Cave Region, Kentucky: Friends of Karst Occasional Publication #1 (map).

Ray, J.A., 1997, Overflow conduit systems in Kentucky: a consequence of limited underflow capacity, *in* B.F. Beck and J.B. Stephenson (eds.), The Engineering geology and hydrogeology of karst terranes: New York, Balkema, p. 69-76.

Shevenell, L., 1996, Analysis of well hydrographs in a karst aquifer: estimates of safe yields and continuum transmissivities: Journal of Hydrology, v. 174, p. 331-355.

Smart, C.C., 1988, Artificial tracer techniques for the determination of the structure of conduit aquifers: Ground Water, v. 26, p. 445-453.

Smart, P.L., and H. Friederich, 1986, Water movement and storage in the unsaturated zone of a maturely karstified carbonate aquifer, Mendip Hills, England, *in* J.F. Quinlan (ed.), Proc. Conference on environmental problems of karst terranes and their solutions: National Water Well Association, Dublin, Ohio, p. 59-87.

SOLUTIONALLY ENHANCED LEAKAGE RATES OF DAMS IN KARST REGIONS

Sebastian Bauer, Steffen Birk, Rudolf Liedl, Martin Sauter
Applied Geology, University of Tuebingen, Sigwartstrasse 10
72076 Tuebingen, Germany

Abstract

This paper presents numerical model studies regarding the development of leakage rates of dams in karst regions due to solutional enlargement of conduits in the rock beneath the reservoir. A hybrid continuum-discrete flow model (CAVE) is used for the modeling. The fractured carbonate rock beneath the reservoir is represented by a network of initial conduits. The effects of a preferential flowpath and a grout curtain on leakage rates are studied in different scenarios. For the parameters considered in this paper, the simulation results suggest that dissolutional widening of the network leads in all scenarios to leakage rates endangering the reservoir within 100 years.

Introduction

In many regions of the world, recharge to groundwater is scarce or concentrated during just a few months of the year. Dams and reservoirs are means of ensuring the water supply of the population over an extended period of time. Some of these dams are located in karst areas, especially in the Mediterranean and the Middle East. The primary permeability of carbonate rocks consists of a network of fissures and cracks. If these are connected to form a flowpath, and if water enriched with CO_2 flows through the system, then solutional widening of the initial fissures leads to the development of secondary permeability, i.e. conduits, a process termed karstification. Under natural conditions, hydraulic gradients are low (<0.1), flowpaths are of the order of thousands of meters, and therefore karstification is generally a slow process. However, hydraulic structures in karst regions, such as dams and reservoirs, imply much higher gradients and shorter flowpaths, thus greatly enhancing dissolutional widening of conduits. These may lead to leakage shortening the lifetime of the dam considerably. This process has been analyzed by Palmer (1988) and Dreybrodt (1992) for individual fractures. They both arrived at comparable results, which demonstrated that hydraulic structures may seriously be affected by dissolution of the underlying carbonate rock within a time span of 100 years.

This paper studies the effect of dissolution of the underlying carbonate rock on the leakage rate of a dam. Compared to the work by Palmer (1988) or Dreybrodt (1992), dissolutional development of a conduit network and water exchange between the conduits and the surrounding fissured rock are considered. This type of interaction has been shown to be characteristic of the flow in karst systems and essential if realistic karst modeling is to be attempted. The employment of various strategies to prolong the lifetime of a dam or a reservoir, e.g. a grout curtain, is considered.

Modeling approach

In order to model the characteristic flow patterns of karst aquifers, the dualistic structure of the flow system has to be considered. Conceptually, the flow system of a karst aquifer consists of a conduit system, which is characterized by low storage and high hydraulic conductivity, and a fissured system with high storage and a much lower conductivity. Karst genesis models also have to consider ionic transport in the conduits, dissolution from the conduit walls, and thus enlargement of the conduits. These processes have been implemented in the model CAVE by coupling the discrete continuum flow calculation to a carbonate dissolution model. Groundwater flow in the fissured system is modeled by a continuum approach using Boussinesq's equation. Flow in the conduit system, represented by cylindrical tubes intersecting at nodes, is governed by Kirchhoff's rule, stating that total inflow and total outflow balance at each node. The relationship between hydraulic head difference and discharge is adapted to the flow conditions, i.e. the model distinguishes between laminar and turbulent flow. Exchange of groundwater between the fissured and the conduit system is modeled by a linear steady-state exchange term (Barenblatt et al., 1960), i.e. the water flux is assumed to be proportional to the head difference between the flow systems. The corresponding proportionality factor is termed the exchange coefficient.

Transport of calcium in the conduit system is described by the 1D advection equation, with an additional source term accounting for the increase in concentration due to calcite dissolution at the conduit walls. At the nodes of the conduit system, additional inflow of dissolved calcium from the fissured system is considered, and instantaneous and complete mixing of all inflow concentrations is assumed. Modeling of carbonate dissolution is based on experimental findings by Buhmann and Dreybrodt (1985), which show that dissolution kinetics is fast if the dissolved

calcium concentration is far from saturation with respect to calcite, and slow if it is close to saturation. The amount of carbonate mass dissolved from the conduit walls is used to determine the increase of conduit diameter with time. Flow in the fissured system is simulated by central finite differences using MODFLOW (McDonald and Harbaugh, 1988). Flow in the conduit system is solved utilizing the iterative Newton-Raphson method in order to deal with the nonlinearities occurring in turbulent flow conditions. Transport of calcium is modeled by employing an upwind-finite-difference scheme with integrated reaction kinetics. The model supports a wide variety of boundary conditions, thus enabling a good approximation of natural situations. For more details and model verification see Clemens et al. (1996).

Model area and scenarios

A model dam was designed to examine the enhanced dissolutional widening of conduits under high gradients. The model consists of a 2-D cross section of the carbonate aquifer below the dam, i.e. dissolution in the carbonate rock underlying the dam and the reservoir is considered. The cross section is a slice of 10 m thickness and contains one plane of solutionally enlargable conduits. The conduit system thus represents a region of fractures every 10 meters. The bottom boundary represents a different lithological layer, which is assumed to be much less permeable and not soluble, e.g. a clay layer. Different hydraulic scenarios are studied to investigate the effects of a grout curtain and a preferential flowpath, and the model was designed accordingly.

Model dimensions, boundary conditions and geometry of the conduit network are shown in Figure 1. The model area is 500 m long, 10 m wide and 55 m deep. The reservoir is modeled by fixed-head cells with a potential head of 40 m, and downstream of the dam the potential is fixed at 0 m. The left, right, and bottom sides of the model domain are considered no-flow boundaries. The hydraulic conductivity of the fissured system is set to 10^{-6} m/s, and the aquifer is considered to be confined. The exchange coefficient is set to 10^{-6} m/s. The dam base is 90 m long with a hydraulic conductivity of 10^{-8} m²/s. The conduit system has equal spacings of 10 m between the nodes and initial diameters of 0.4 mm. The grout curtain is located in the middle under the dam and has the same conductivity as the dam. It reaches to 30 m depth below the dam and is 10 m thick. A preferential flow path right under the dam is included and has a larger initial diameter of 1 mm. This preferential flowpath is intercepted by the grout curtain in Scenario 4 (Figure 1b).

Calcium equilibrium concentration is 1 mmol/L, the fast first-order kinetic rate constants for laminar flow and turbulent flow are 2.5 x 10^{-5} cm/s and 5 x 10^{-5} cm/s, respectively. If the calcium concentration is near saturation (>90%) with respect to calcite, a slow fourth-order kinetic is applied with only one constant for laminar and turbulent

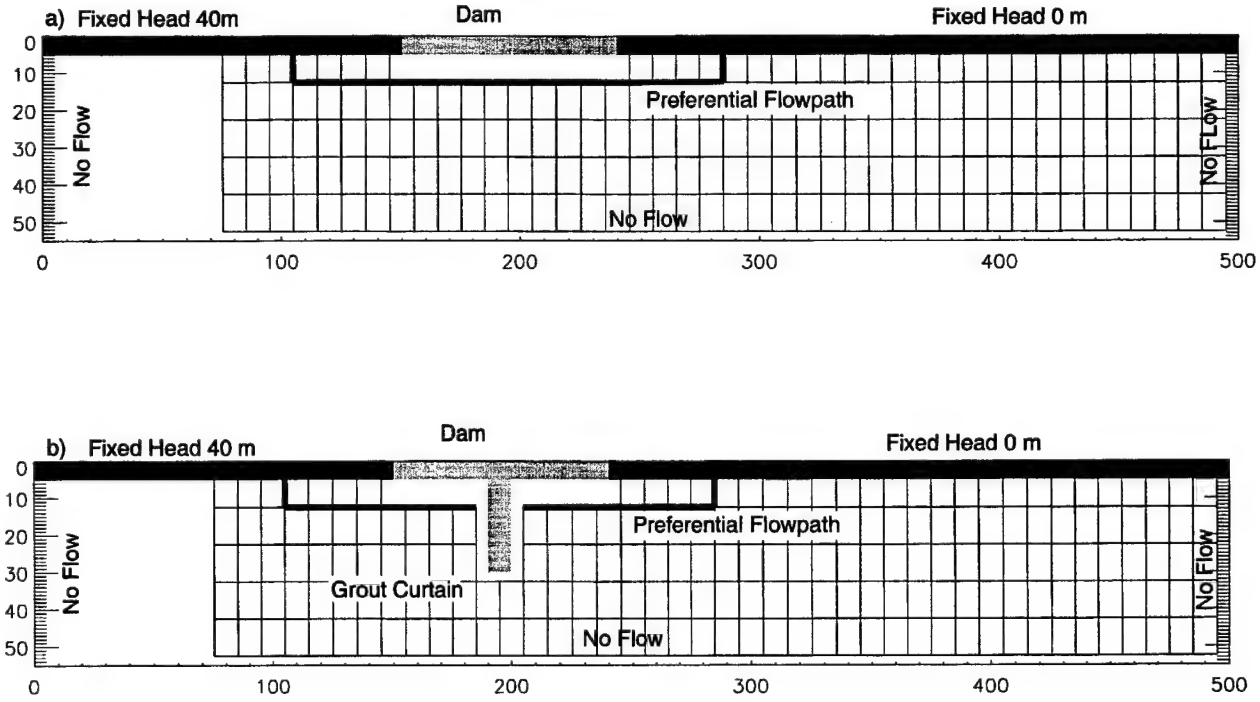

Figure 1: Model domain with geometry of the conduit network for **(a)** Scenarios 1 and 2, **(b)** Scenarios 3 and 4. The preferential flowpaths in Scenarios 2 and 4 are depicted by fat lines.

flow of 1.3 x 10^{13} $cm^{10}/(mol^3 \cdot sec)$. The calcium concentration of water entering the conduit system from the reservoir is zero, and the water entering the conduit system from the fissured system has equilibrium concentration.

The influence of a grout curtain and a preferential flow path on leakage flow from the reservoir is studied in four different scenarios: Scenario 1 with neither preferential flowpath nor grout curtain; Scenario 2 with preferential flowpath but no grout curtain; Scenario 3 with no preferential flowpath but a grout curtain; and Scenario 4 with both preferential flow path and grout curtain.

The preferential flowpath and the grout curtain are shown in Figures 1a and b. As a design criterion a critical leakage rate under the dam was calculated, above which the dam would lose more water than is supplied by recharge to its catchment area. A catchment area of 10 km^2 and a groundwater recharge rate of 0.2 m/a are assumed for the calculation of a critical leakage rate of 0.06 m^3/s (230 m^3/h). The critical leakage rate is thus scaled to a catchment area of 10 km^2 and a dam width of 10 m, which enables comparison to dams with other dimensions. If the dam is 100 m wide with a catchment area of 50 km^2, the critical leakage rate would be 0.03 m^3/s (115 m^3/h).

Simulation Results

Figure 2 shows the development of the conduit system with time for Scenario 1 of 15, 30, and 50 years. Widening of the conduit system begins at the reservoir, from which aggressive water is entering the system. Conduits under high hydraulic gradients are enlarged first, because they display highest flow rates and thus the most aggressive water. Conduit diameters decrease with increasing flow length, as calcium concentrations increase due to dissolution, and slower kinetics becomes active. The flowpath closest to the dam, which is most rapidly widened by dissolution, changes from a laminar to turbulent flow regime after 15 years. After 30 years the conduit system is widened more or less uniformly under the dam, even down to the impermeable base at 55 m depth. Most of the tubes are now turbulent and fast first-order kinetics is active in most of the widened conduits. After 50 years the conduit system shows further enlargement and slowly extends further downgradient. Most of the tubes now have

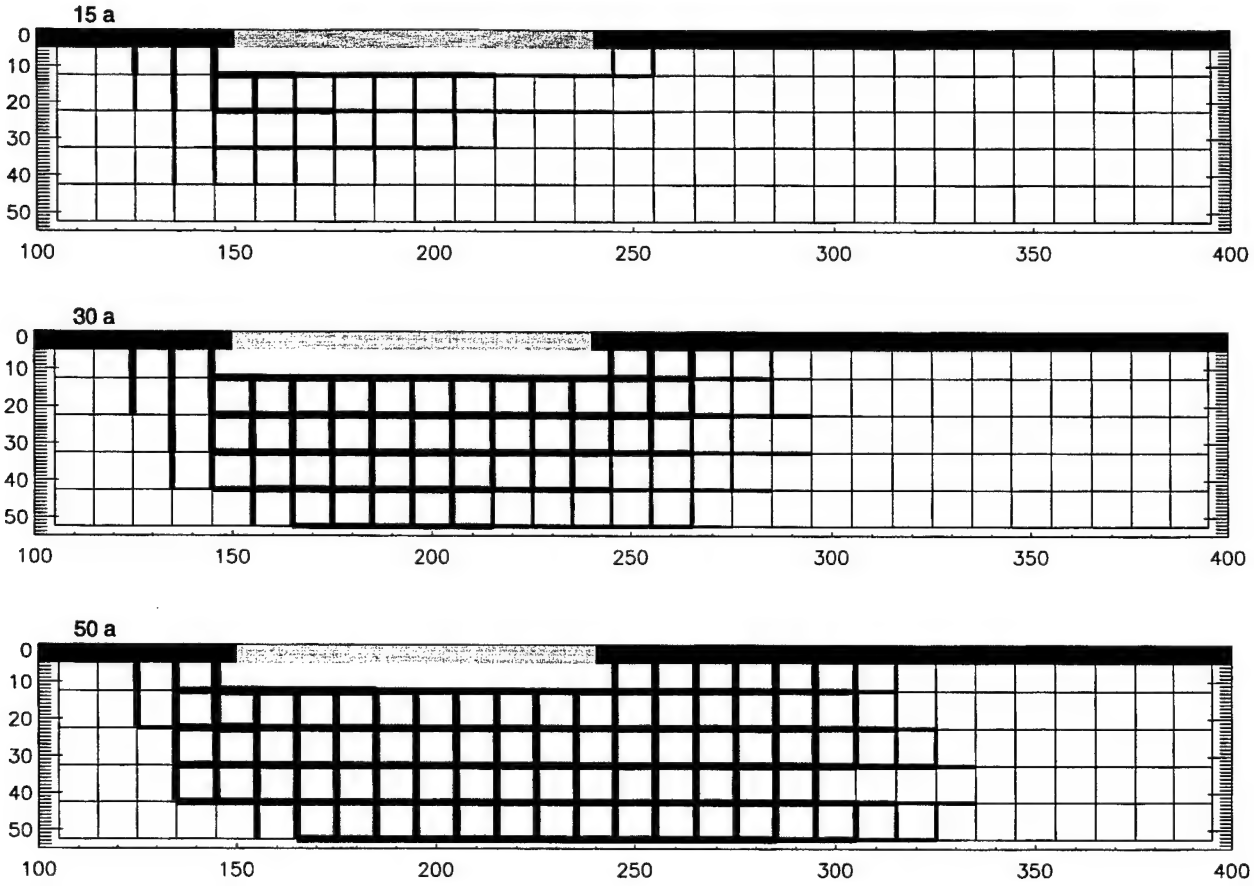

Figure 2: Model results for Scenario 1, depicting the conduit network after 15, 30, and 50 years. The line thicknesses represent conduit diameters of >0.4 mm, >1 mm, >5 mm, >1 cm and >5 cm respectively.

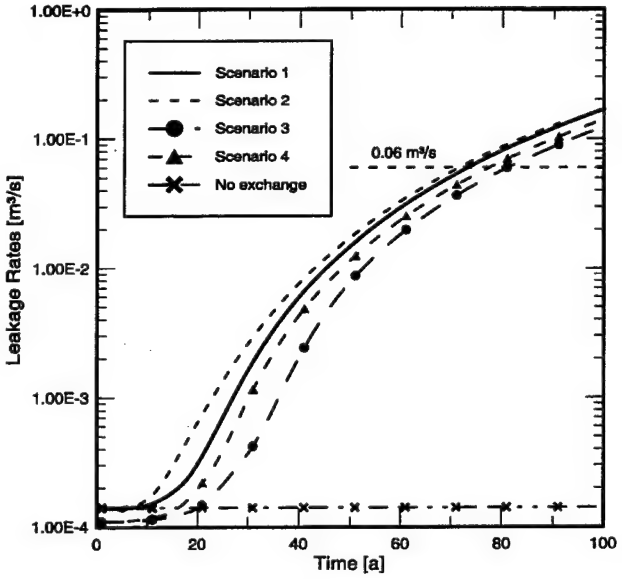

Figure 3: Development of leakage rates with time for the different scenarios. Also included is the leakage rate for a model with boundary conditions of Scenario 1, but no exchange between the fissured and conduit system.

diameters between 1 and 5 cm, and the conduits upgradient from the dam have grown to just above 5 cm diameter. After 73 years the leakage rate has risen to the critical rate of 0.06 m^3/s, i.e. the catchment cannot supply enough recharge water to refill the reservoir. Similar patterns of dissolutional widening arise from the other scenarios.

Figure 3 shows leakage rates over time for the different scenarios. At the beginning of the simulation all leakage rates are approximately 10^{-4} m^3/s. Leakage rates for Scenarios 3 and 4 are a little lower, due to the presence of the grout curtain. In the early stages, flow occurs mainly in the fissured system and flow through the conduit system is lower by approximately 4 orders of magnitude. Flow through the fissured system remains nearly constant throughout the simulation for all scenarios, since the hydraulic conductivity of the fissured system does not change. Leakage rates for Scenario 1 start to rise after 15 years. Breakthrough time to first-order kinetics, defined as the time when the first tube at the outlet at the lower head boundary shows a calcium concentration lower than 90% of the equilibrium concentration, is 11 years. The first turbulent flowpath from the reservoir to the outlet is established after 15 years. From then on the flow rate through the conduit system is comparable to that in the fissured system. It rapidly grows with increasing dissolutional widening of the conduits and eventually dominates the leakage rate. Due to the presence of an initial preferential flow-path leakage rates rise first for Scenario 2 (Figure 3). Breakthrough time is 2 years, the first turbulent flow path is established after 9 years and the critical leakage rate is reached after 72 years. Leakage rates in Scenario 3 are lowest compared to the other scenarios, due to the grout curtain. Breakthrough is achieved after 23 years, the first turbulent flow path after 28 years, and the critical leakage rate after 82 years. For Scenario 4, which includes both grout curtain and a preferential flowpath, the corresponding times are 14, 21, and 78 years, respectively. Conduit diameters at the critical leakage rate vary between 6 and 9 cm for all scenarios.

Discussion and conclusions

A close analysis of Figure 2 shows that nearly all conduits under the dam are enlarged simultaneously. Solution first enlarges tubes near the reservoir, from which water with a calcium concentration of zero enters the conduit system and follows the path of highest hydraulic gradient in the conduit network. Thus dissolution spreads to depth as well as downgradient and quickly reaches the impervious bottom boundary. The turbulent flow conditions combined with a fixed-head potential in the reservoir lead to a uniform enlargement of the conduit system, because even conduits with a longer flowpath still receive a constant supply of water. There is no selective mechanism developing, which, in the case of limited water supply, leads to evolution of the fastest evolving conduit only (e.g. Clemens et al., 1996; Groves and Howard, 1994). All tubes that are turbulent at the time of the critical leakage have diameters varying only between 6 and 9 cm. This type of uniform enlargement is also reported by Howard and Groves (1995) for turbulent-flow conditions with fixed heads. The reason is that under fixed-head boundary conditions all conduits are solutionally enlarged. After turbulent flow is established, the calcium mass dissolved from the conduit walls per unit time remains nearly constant. Therefore, as the conduit surface area grows with time, the increase in conduit diameter is gradually slowing down.

In the scenarios considered here, both grout curtain and initial preferential flowpath have no significant effect on the development of the leakage rate with time (Figure 3). All scenarios reach the critical leakage rate within a time span of 10 years from 72 years onward. As can be expected from the boundary conditions, Scenario 2 with no grout curtain and an initial preferential flow path has highest leakage rates, while Scenario 3 without an initial flowpath but with a grout curtain shows the lowest leakage rates. The uniform widening of the conduit system eventually overrides differences that arise in the early stages of the conduit development. Although breakthrough time for Scenario 2 is only 2 years, compared to 14 years of Scenario 4, this initial difference in conduit conditions does not result in corresponding differences between leakage rates.

Figure 3 also shows the leakage rate for a model run with the boundary conditions of Scenario 1 but no exchange between fissured and conduit system. Almost no dissolutional widening is taking place, only the first few conduits directly beneath the reservoir are enlarged, and there is no breakthrough or turbulent flow. The reason is that the special boundary conditions arising when modeling a dam lead to highly enhanced dissolution, if exchange between fissured and conduit system is accounted for: from the beginning of the simulation, the hydraulic conductivity of the conduit network is higher than that of the fissured system. Therefore, downgradient of the reservoir the hydraulic heads in the conduit system are higher than in the fissured system and exchange flow is directed into the fissured system. As a result, the conduit system loses water with high calcium concentration to the fissured system at each node below the reservoir. This amount of water flowing into the fissured system is resupplied to the conduit system from the fixed-head reservoir with a calcium concentration of zero, i.e. by highly aggressive water. Therefore this exchange provides a sink for water high in calcium and acts as an additional source for aggressive water. This effect strongly enhances the development of the conduit system.

The model results presented here show that dissolution of small conduits under man-made structures like a dam can have serious effects on the performance of the reservoir. The depth of 30 m for the grout curtain used in the simulations seems too small to effectively prohibit the strong increase of the leakage rate. The model results also suggest that small conduits with initial diameters of 0.4 mm can be solutionally enlarged within tens of years and may cause serious water losses, if the effect of the fissured system is accounted for.

References cited

Barenblatt, G.E., I.P. Zheltov, and I.N. Kochina, 1969, Basic concepts in the theory of seepage of homogeneous liquids in fissured rocks: Journal of Applied Mathematics and Mechanics, v. 24, p. 1286-1303.

Buhmann, D., and W. Dreybrodt, 1985, The kinetics of calcite dissolution and precipitation in geologically relevant situations of karst areas. 1. Open systems: Chemical Geology, v. 48, p. 189-211.

Clemens, T., D. Hückinghaus, M. Sauter, R. Liedl, 1996, A combined continuum and discrete network reactive transport model for the simulation of karst development: Calibration and Reliability in groundwater modeling, IAHS Publ. 237, p. 309-318.

Dreybrodt, W., 1992, Dynamics of karstification: A model applied to hydraulic structures in karst terranes: Applied Hydrogeology, v. 3, p. 20-32.

Groves, C.G., and A.D. Howard, 1994, Early development of karst systems 1. Preferential flow path enlargement under laminar flow: Water Resources Research, v. 30, p. 2837-2846.

Howard, A.D., and C.G. Groves, 1995, Early development of karst systems 2. Turbulent flow: Water Resources Research, v. 31, p. 19-26.

McDonald, M.G., and A.W. Harbaugh, 1988, A modular three-dimensional finite difference groundwater flow model: Techniques of Water-Resources Investigation 06-A1, USGS.

Palmer, A., 1988, Solutional enlargement of openings in the vicinity of hydraulic structures in karst regions: Association of Ground Water Scientists and Engineers, 2nd Conference on Environmental Problems in Karst Terranes and their Solutions, Proceedings, p. 3-15.

QUANTITATIVE ANALYSIS OF TRACER BREAKTHROUGH CURVES FROM TRACING TESTS IN KARST AQUIFERS

Malcolm S. Field
National Center for Environmental Assessment
U.S. Environmental Protection Agency
Washington, D.C. 20460

Abstract

Numerical analysis of tracer-breakthrough curves allow quick reliable estimates for many of the basic hydraulic and geometric parameters. Tracer-breakthrough curve analysis relies on the application of a continuous mass balance model for transport parameter estimation. Readily obtained hydraulic parameters required for modeling include peak arrival time and peak velocity, longitudinal dispersion, and Péclet number. Geometric parameters include volume, cross-sectional area, and diameter. Some boundary-layer effects can also be roughly estimated.

Introduction

Groundwater flow and contaminant transport in fractured-rock aquifers are very complex, and considerably more complex in karst aquifers. This is because flow and transport in karst aquifers are often rapid, may be nearly parallel to regional equipotential lines, or even appear to be traveling against the regional hydraulic gradient. Darcy's law is not readily applicable because flow tends to occur in discrete channels, and apparent hydraulic conductivities can approach infinity if evaluated for laminar flow conditions (*e.g.* similar to the hydraulic conductivity of a lake), or are nonlinear for turbulent-flow conditions (*e.g.* hydraulic conductivity of a fast flowing river). These problems can only be addressed by conducting quantitative groundwater tracing studies and applying mathematical models to analyze the results (Field and Nash, 1997; Field, 1997), but there is considerable need to ensure that the initial parameter estimates obtained from the tracer tests are reliable.

This paper illustrates how reliable parameter estimates may be obtained from tracer-breakthrough curves. Tracer-breakthrough curve analyses provide a basis for estimating total tracer recovery and such hydraulic parameters as residence times, flow velocities, longitudinal dispersion, Reynolds number, and Froude number. Karst-conduit geometric parameters that may be estimated include conduit volume, cross-sectional area, diameter, and sinuous length. Boundary-layer effects can also be estimated.

Tracer-breakthrough-curve parameters

Tracer analyses plotted, preferably in conjunction with discharge measurements, constitute a "true" breakthrough curve. Typically, tracer-breakthrough curves appear as a positively-skewed histogram. The positive skewness is often considered to be a result of longitudinal dispersion effects, but has been shown to be more realistically a result of immobile-flow regions (Field et al., 1998).

Tracer residence times from tracer-breakthrough curve inspection

Tracer-breakthrough curves can be inspected visually for some important parameters. Such inspection can be very useful in developing an initial assessment of solute behavior in the aquifer system. Some parameter estimates from inspection of the tracer-breakthrough curve can be highly reliable while others may be highly unreliable.

Initial tracer arrival (first arrival) is a highly unreliable parameter that is often used by water managers to estimate how quickly a pollutant may reach a community water supply. It is based on the first appearance of tracer in water samples. First arrival is based greatly on the sensitivity of analytical instruments used to analyze for the tracer, and the prevailing hydrology at the time of the tracing test. It is also strongly affected by interpolation algorithms.

Peak tracer arrival is a more reliable parameter that best represents the residence time of the tracer during a tracer test. It is also dependent on the prevailing hydrology and mass injected, but not on the sensitivity of the analytical instruments, provided adequate tracer masses are used. Comparison with theoretical models typically shows the peak arrival to be very representative of subsurface conditions affecting solute transport.

Elapsed residence time is also an unreliable parameter that relates the length of time that the tracer could be observed in the system. Water managers use this parameter to estimate the length of time that a community water supply will be affected by a pollutant. This parameter is greatly affected by the sensitivity of the analytical instruments,

prevailing hydrology, and mass of tracer injected. It is also strongly affected by extrapolation algorithms.

Analysis of tracer-breakthrough curves

Numerical analysis of tracer-breakthrough curves relies primarily on the method of moments. Integrating tracer-breakthrough curves provides reasonable estimates for mass recovery, mean residence time, and mean flow velocity. However, the method of moments will tend to seriously overestimate longitudinal dispersion.

Tracer mass recovery

Assuming complete mixing within the karst conduit, estimation of tracer recovery for individual sampling stations is obtained by

$$M_O = \int_0^\infty C(t)Q(t)dt \tag{1}$$

and total tracer recovery from all downgradient sampling stations may be estimated by

$$M_T = \sum_{i=1}^{n} M_{O_i} \tag{2}$$

Tracer recovery is essential for evaluating groundwater monitoring systems and contaminant-transport processes. Tracer recovery must be quantified to ensure that all relevant discharge locations have been monitored for the discharge of contaminants. A low-percent recovery of tracer mass may occur as a result of inadequate sampling of downgradient tracer discharge locations. A high-percent recovery suggests that most downgradient discharge locations were adequately monitored for the tracer.

Quality of tracer mass recovery

The quality of the tracer experiment may be quantified in terms of mass recovered. Usually, the quality of the trace experiment is given as percent of mass recovered, but this affords little insight. An accuracy index given by (Sukhodolov et al., 1997)

$$A_I = \frac{M_{in} - M_T}{M_{in}} \tag{3}$$

provides more insight into the quality of the tracing experiment. An $A_I = 0$ indicates a perfect tracing experiment. A positive A_I indicates more mass injected than was recovered, while a negative A_I suggests more mass apparently recovered than was injected. As A_I moves further away from zero, the quality of the tracing experiment gets poorer.

Mean tracer residence time

Mean tracer residence time is the length of time required for the centroid of the tracer mass to traverse the entire length of the karst conduit. The centroid generally lags behind the peak concentration of the tracer mass of the tracer-breakthrough curve, but the more the groundwater flow is constrained to discrete conduits the less obvious the difference between the centroid and the peak concentration.

Mean tracer residence time may be estimated by

$$\bar{t} = \frac{\int_0^\infty tC(t)Q(t)dt}{\int_0^\infty C(t)Q(t)dt} \tag{4}$$

with a standard deviation

$$\sigma_t = \left[\frac{\int_0^\infty (t-\bar{t})^2 C(t)Q(t)dt}{\int_0^\infty C(t)Q(t)dt} \right]^{1/2} \tag{5}$$

Equations (4) and (5) assume that tracer residence time will vary from nearly zero for instantaneous exit of tracer mass from the karst conduit upon injection to apparent infinity for tracer mass that is stored in micropores within the aquifer system. Equation (4) contributes relevant information on the time required for the centroid of a nonreactive pollutant mass spilled in the vicinity of the injected tracer to be discharged. Equation (5) is a measure of the possible range of travel times weighted for tracer concentration, sampling-time interval, and discharge.

Time to peak concentration t_p and peak tracer concentration C_p may generally be considered more reliable parameters for describing transport processes and are easily read directly from the tracer-breakthrough curve. However, no level of uncertainty may be established for these two parameters except by conducting multiple tracer tests in the same system.

Mean tracer velocity

Mean tracer velocity is a measure of the velocity of the tracer centroid estimated by

$$\bar{v} = \frac{\int_0^\infty \frac{x_s}{t} C(t)Q(t)dt}{\int_0^\infty C(t)Q(t)dt} \quad (6)$$

with a standard deviation

$$\sigma_v = \left[\frac{\int_0^\infty x_s \left(\frac{1}{t} - \frac{1}{\bar{t}}\right)^2 C(t)Q(t)dt}{\int_0^\infty C(t)Q(t)dt} \right]^{1/2} \quad (7)$$

Investigations of numerous caves throughout the world have shown that most cave passages average about 1.5x their straight-line distance. This average sinuosity estimate is also considered to be representative of most karst conduits even though they may be much smaller in terms of length and breadth than mapped cave passages.

Equation (6) assumes that tracer residence time varies from nearly zero for instantaneous exit of tracer mass from the karst conduit upon injection to virtually infinity for tracer mass that is stored in micropores within the aquifer system. Mean tracer velocity is more useful for defining the hydraulic geometry of the karst conduit than is maximum velocity and is necessary for conducting acute and chronic toxicity risk assessments.

Longitudinal dispersion

Flow in karst conduits may occur as open-channel or closed-conduit flow and exhibit longitudinal effects typical of surface-water streams or storm sewers. Estimation of longitudinal dispersion is best accomplished using open-channel or closed-conduit flow models. Studies of longitudinal dispersion, mostly with respect to open-channel flow, have led to the development of various models that generally ignore non-Fickian effects. A method for determining longitudinal dispersion that applies to both open-channel and closed-conduit flow and affords a visual assessment of non-Fickian effects can be obtained from (Chatwin, 1971)

$$\left[t \ln \left(\frac{A_p}{C t^{1/2}} \right) \right]^{1/2} = \left[\frac{x_s}{2D_{x_s}^{1/2}} - \frac{\bar{v}t}{2D_{x_s}^{1/2}} \right] \quad (8)$$

where the constant of proportionality A_p is estimated from peak tracer concentration C_p and the peak time of arrival t_p (Day, 1975):

$$A_p = C_p \sqrt{t_p} \quad (9)$$

The first term on the right-hand side of Equation (8) is the y intercept and the second term on the right-hand side of Equation (8) is the gradient. Either term on the right-hand side allows solution for the longitudinal dispersion coefficient, D_{x_s}, provided that a plot of the left-hand side of Equation (8) against early-time data reasonably falls on a straight line (Day, 1975).

The late-time data will depart from the straight line due to non-Fickian dispersion characteristics that result from immobile-flow regions. Typically, longitudinal dispersion is estimated using the method-of-moments, which tends to greatly overestimate longitudinal dispersion because the method-of-moments does not allow for exclusion of immobile-flow regions.

Karst conduit volume

Tracer mass recovery at a spring where discharge has been measured during a tracer study allows a rough estimate of the maximum volume of the karst conduit traversed by the tracer cloud. This is achieved by

$$V = \int_0^{\bar{t}} Q dt \quad (10)$$

If a single discharge value is used as a mean spring discharge, then the karst-conduit volume may be estimated by

$$V = \overline{Q}t \quad (11)$$

A maximum volume estimate based on the sum of each individual conduit traversed by the tracer cloud may be determined from

$$V_T = \sum_{i=1}^{n} V_i \quad (12)$$

Equation (10) is a more realistic estimation method for the conduit volume than is (11). Both (10) and (11) are more reliable methods for estimating karst-conduit volume than the conventional method of taking the product of the mean spring discharge, $\overline{Q}$, and the time to peak concentration, t_p. By far the majority of volume space will be occupied by micropores, but these contribute little to groundwater flow and solute transport in conduit-dominated karst aquifers.

Aquifer volume estimation using (12) will be a coarse approximation at best. Summing the volumes of individual karst conduits to achieve an estimate of total volume space occupied by karst conduits should not be expected to produce very accurate estimates because it represents an

oversimplification of the aquifer system. For example, (12) may be used to sum the volumes of several karst conduits that are presumed to be distinct but in reality may actually be connected along significant segments of their total lengths. However, the sum of the individual karst conduits does provide some indication of the aquifer volume occupied by conduits.

Empirical fluid dynamics models

Experiments with fluid dynamics have led to the development of many models of flow for specific geometries. These geometries will not necessarily reproduce those of the actual karst conduits or fracture systems, which cannot be reliably approximated whether or not physical measurements can be made. However, by making some simple assumptions, reasonable parameter estimates may be obtained. For karst conduits, it may be assumed that the phreatic conduit will best be approximated by assuming a cylindrical geometry. Such an assumption is reasonable for phreatic conduits developed in flat-lying sedimentary rocks and may not be unreasonable for other structural and stratigraphic conditions.

Karst conduit geometries

The easiest and probably most reliable geometric parameter that can be estimated is cross-sectional area. Because the karst conduit volume V could be estimated from (10) or (11), the cross-sectional area may be estimated from

$$A = \frac{V}{x_s} \tag{13}$$

which is based on a sinuous distance and hence less than the straight-line distance would suggest.

By assuming a cylindrical karst conduit it is possible to estimate a karst conduit diameter from a tracer-breakthrough curve. Because the system volume has been estimated the karst conduit diameter may be obtained by

$$D_c = 2\sqrt{\frac{A}{\pi}} \tag{14}$$

where V/x_s has been used to reliably estimate cross-sectional area. Obviously (14) can be used to estimate the karst conduit radius, which is typically used in many modeling endeavors.

If open-channel flow is assumed to occur in the karst conduit, then a hydraulic depth may be estimated by

$$D_H = \frac{A}{D_C} \tag{15}$$

which is a reasonable approximation.

Péclet Number

The Péclet number is a measure of the relative contribution of mechanical dispersion and diffusion to solute transport. It relates the effectiveness of mass transport by advection $\left(-\frac{\bar{v}x_s}{D_{x_s}}\frac{\partial C}{\partial x_s} = -Pe\frac{\partial C}{\partial x_s}\right)$ to the effectiveness of mass transport by either dispersion or diffusion $\left(\frac{\partial^2 C}{\partial x_s^2}\right)$ (Schiesser and Silebi, 1997, p. 372). Péclet numbers below 0.4 indicate diffusion/dispersion control; 0.4 – 6.0 suggest that diffusion/dispersion and advection are in transition and thus approximately equal to each other; and >6.0 indicate advection control. Large Péclet numbers indicate strongly advective systems.

Estimation of a Péclet number may be obtained from the estimated longitudinal dispersion and mean tracer velocity by

$$Pe = \frac{\bar{v}x_s}{D_{x_s}} \tag{16}$$

Dynamic flow equations

Open-channel and closed-conduit flow phenomena are usually described by dimensionless equations for flow behavior. The Reynolds number furnishes a means for determining if flow is laminar or turbulent. The Froude number is used to determine if the flow is subcritical or supercritical.

Reynolds Number

The resistance of flow depends upon the conduit geometry and magnitude of the Reynolds Number. The smaller the Reynolds number, the more resistance there is to flow. Assuming a cylindrical conduit, a rough approximation of the Reynolds number for each individual sampling station may be obtained from

$$N_R = \frac{\rho\bar{v}D_C}{\mu} \tag{17}$$

where ρ represents fluid density, D_c the conduit diameter, and μ the dynamic viscosity.

Froude Number

The ratio of the mean flow velocity to the linear dimension of flow (hydraulic mean depth, D_H) is useful for determining if flow is in the subcritical or supercritical range. The parameter describing the effect is the Froude number, given by

$$N_F = \frac{\bar{v}}{\sqrt{gD_H}} \quad (18)$$

Estimation of the Froude number by (18) will be a rough approximation mainly for the same reasons that apply to the Reynolds number estimation. The Froude number is used to explain flow behavior for streams with a free surface, which may increase uncertainty because karst conduits may exhibit either open-channel flow, closed-conduit flow, or both flow types depending on stage. An estimated Froude number for karst conduits exhibiting closed-conduit flow is not appropriate. Also, as presented, the calculation for the Froude number assumes that the cross-sectional area of the karst conduit divided by the diameter of the conduit is equal to the mean hydraulic depth, which may not always be true.

Boundary-layer effects

While not generally considered in tracing studies, boundary-layer effects can substantially impact the study results. Karst conduit walls are often assumed to be smooth, which is unreasonable. Cave exploration has revealed that conduit walls are often covered with scallops, making them very rough. Additionally, sediment coating on cave walls and layers on cave floors greatly add to roughness and surface area. Cave breakdown is an extreme case, which causes significant roughness.

Friction-factor estimation

When flow is believed to be laminar, a friction factor may be estimated by (White, 1988, p. 163)

$$f_f = \frac{64}{N_R} \quad (19)$$

and for when flow is turbulent, a friction factor may be estimated by (White, 1988, p. 163)

$$\frac{1}{\sqrt{f_f}} = 2\log\frac{D_C}{\epsilon} + 1.14 \quad (20)$$

where the relief of surface irregularities ϵ is a controlling factor and depends on the nature of the conduit through which the flow is occurring.

Laminar-flow sublayer

It is well documented by empirical studies that turbulent flow occurs as a core that is surrounded by a laminar flow sublayer. The thickness of the laminar flow sublayer is dependent on the degree of conduit wall roughness. If a typically very rough karst conduit is assumed, then the laminar flow sublayer may be estimated by (White, 1988, p. 163)

$$\frac{\delta}{D_C} = \frac{32.8}{N_R\sqrt{f_f}} \quad (21)$$

which is an important parameter for assessing the extent of solute sorption to conduit walls and the possibility of matrix-diffusion effects. Matrix diffusion can only occur from the laminar-flow sublayer.

Hydraulic head loss

When flow is laminar, the hydraulic head loss along the conduit can be estimated by (modified from White, 1988, p. 162)

$$h_L = \frac{8.04\mu\bar{v}x_s}{\rho g r^2} \quad (22)$$

and for when flow is turbulent, the hydraulic head loss along the conduit may be estimated by (White, 1988, p. 163)

$$h_L = \frac{f_f x_s \bar{v}^2}{4gr} \quad (23)$$

which emphasizes the influence of friction on head loss.

Quantitative example

Figure 1 shows a typical original version and modification of a tracer-breakthrough curve for Quarry Spring in Tennessee. Quarry Spring was the recovery site for a Rhodamine WT tracer test initiated at a monitoring well drilled at a nearby Superfund site. The spring is located in an unused formerly flooded quarry and discharges approximately 0.02 m^3/sec. The site is underlain by Cambrian limestones and dolostones of the Conasauga Group. A natural-potential survey was used to site the monitoring well in or near a flooded karst conduit. Monitoring-well depth was 18 m below land surface. During drilling, circulation was lost, and Quarry Spring (300 m distant along the strike) was observed to discharge turbid water, representing substantial sediment transport, whereas all previous discharges had been relatively clear. Dye slugs were injected as rapidly as possible into the monitoring well with approximately 1500 L of potable

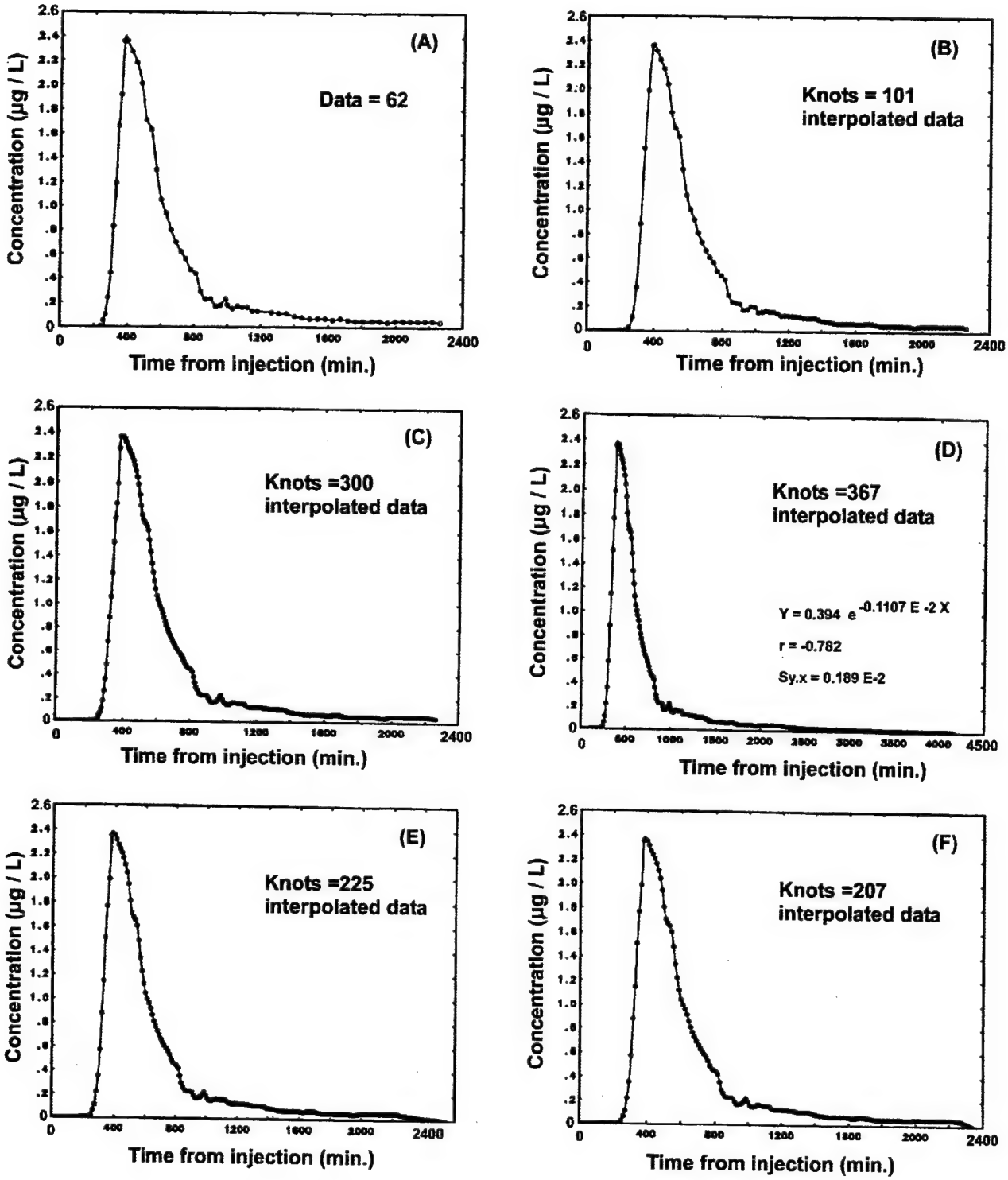

Figure 1: Tracer-breakthrough curve for Quarry Spring, Tennessee. **A** represents the original data; **B** and **C** represent interpolated data using ≥100 and ≥300 knots, respetively; and **D**, **E**, and **F** represent interpolated/extrapolated data using ≥200 knots applied to an exponential decay function, cubic Hermite function, and a statistical determination method, respectively. The cubic Hermite function is a piecewise interpolation procedure with a continuous derivative. Knots are the abscissa values of the interpolated points.

water to flush the dye out of the well for each trace. Initial dye recoveries occurred within 3 hours of the injections at Quarry Spring. The two tracing events were initiated approximately 48 hours apart and were separated by a storm event.

Tracer mass recovery

Results of numerical integration of the tracer-breakthrough curves, shown in Figure 1, are listed in Table 1. Mass recovery was excellent and only slightly affected by interpolation/extrapolation of the data. Data extrapolation using an exponential decay function had the most effect because it resulted in the greatest extension of the time data.

Hydraulic parameters

The basic hydraulic parameters estimated from the tracer-breakthrough curves shown in Figure 1 are listed in Tables 2 and 3. Results were not greatly different even when interpolation/extrapolation methods were applied. The greatest change again occurred when an exponential decay function was applied.

Geometric and flow dynamics

Table 4 depicts the geometric parameter estimates and fluid-dynamics estimates. Relatively small volume, area, and diameter estimates were obtained. Turbulent flow conditions were also estimated. The greatest effect was caused by the exponential decay function.

Estimates of boundary-layer effects

Table 5 lists the estimates for the basic boundary-layer effects. Small values for the laminar flow sublayer and hydraulic head loss were obtained, as expected. A very large surface area and insignificant sorption coefficient were also obtained. The greatest effect was caused by the exponential decay function.

Table 1. Estimated tracer mass recovery and related parameters.

Method of Analysis	Maximum Integration (h)	Tracer Mass Recovered (g)	Accuracy Index (dimen.)	Percent Recovered
Straight Data (no interp.)	37.75	6.77×10^3	3.29×10^{-2}	96.7
Interpolated Data ($\geq$ 100 knots)	37.75	6.76×10^3	3.42×10^{-2}	96.6
Interpolated Data ($\geq$ 300 knots)	37.75	6.77×10^3	3.30×10^{-2}	96.7
Extrapolated Data (exponential decay)	69.25	6.86×10^3	1.97×10^{-2}	98.0
Extrapolated Data (cubic Hermite)	42.28	6.79×10^3	2.99×10^{-2}	97.0
Extrapolated Data (statistical)	38.96	6.78×10^3	3.17×10^{-2}	96.8

All extrapolated data $\geq$ 200 knots.

Table 2. Estimated tracer-transport times and peak concentration.

Method of Analysis	Initial Tracer Breakthrough (h)	Time to Peak Concentration (h)	Peak Arrival Concentration ($\mu g\ L^{-1}$)	Mean Tracer Residence Time (h)
Straight Data (no interp.)	4.27	6.25	2.35	10.41±5.79
Interpolated Data ($\geq$ 100 knots)	4.15	6.42	2.35	10.41±5.80
Interpolated Data ($\geq$ 300 knots)	4.15	6.29	2.35	10.41±5.79
Extrapolated Data (exponential decay)	4.12	6.52	2.35	10.81±6.79
Extrapolated Data (cubic Hermite)	4.15	6.42	2.35	10.50±6.00
Extrapolated Data (statistical)	4.15	6.42	2.35	10.44±5.87

All extrapolated data $\geq$ 200 knots.

Table 3. Estimated tracer-flow velocities and dispersion effects.

Method of Analysis	Peak Tracer Flow Velocity ($m\ h^{-1}$)	Mean Tracer Flow Velocity ($m\ h^{-1}$)	Shear Velocity ($m\ h^{-1}$)	Logitudinal Dispersivity (m)	Peclet Number (dimen.)
Straight Data (no interp.)	72.00	43.24±2.04	20.66	17.40	25.86
Interpolated Data ($\geq$ 100 knots)	70.12	43.21±2.04	20.64	17.10	26.13
Interpolated Data ($\geq$ 300 knots)	71.52	43.22±2.04	20.65	18.41	24.45
Extrapolated Data (exponential decay)	69.01	41.63±1.96	19.65	18.26	24.65
Extrapolated Data (cubic Hermite)	70.12	42.86±2.02	20.42	18.24	24.67
Extrapolated Data (statistical)	70.12	43.09±2.03	20.57	18.14	24.80

All extrapolated data $\geq$ 200 knots.

Table 4. Estimated karst-conduit geometries and flow dynamics.

Method of Analysis	Conduit Volume (m^3)	Conduit Area (m^2)	Conduit Diameter (m)	Hydraulic Depth (m)	Reynolds Number (dimen.)	Froude Number (dimen.)
Straight Data (no interp.)	524.52	1.17	1.22	9.57×10^{-1}	1.28×10^{4}	3.92×10^{-3}
Interpolated Data ($\geq$ 100 knots)	524.89	1.17	1.22	9.57×10^{-1}	1.28×10^{4}	3.92×10^{-3}
Interpolated Data ($\geq$ 300 knots)	524.68	1.17	1.22	9.57×10^{-1}	1.28×10^{4}	3.92×10^{-3}
Extrapolated Data (exponential decay)	544.79	1.21	1.24	9.75×10^{-1}	1.26×10^{4}	3.74×10^{-3}
Extrapolated Data (cubic Hermite)	529.14	1.18	1.22	9.61×10^{-1}	1.28×10^{4}	3.88×10^{-3}
Extrapolated Data (statistical)	526.35	1.17	1.22	9.59×10^{-1}	1.28×10^{4}	3.91×10^{-3}

All extrapolated data $\geq$ 200 knots.

Table 5. Estimated karst-conduit boundary-layer effects parameters.

Method of Analysis	Friction Factor (dimen.)	Laminar Flow Sublayer (m)	Hydraulic Head Loss (m)	Surface Area (m^2)	Sorption Coeficient (m)
Straight Data (no interp.)	5.81×10^{-1}	4.08×10^{-3}	1.58×10^{-3}	4.22×10^{5}	4.23×10^{-5}
Interpolated Data ($\geq$ 100 knots)	5.81×10^{-1}	4.09×10^{-3}	1.58×10^{-3}	4.22×10^{5}	4.41×10^{-5}
Interpolated Data ($\geq$ 300 knots)	5.81×10^{-1}	4.09×10^{-3}	1.58×10^{-3}	4.22×10^{5}	4.24×10^{-5}
Extrapolated Data (exponential decay)	5.67×10^{-1}	4.29×10^{-3}	1.40×10^{-3}	4.09×10^{5}	2.68×10^{-5}
Extrapolated Data (cubic Hermite)	5.78×10^{-1}	4.13×10^{-3}	1.54×10^{-3}	4.19×10^{5}	3.89×10^{-5}
Extrapolated Data (statistical)	5.80×10^{-1}	4.10×10^{-3}	1.56×10^{-3}	4.21×10^{5}	4.10×10^{-5}

All extrapolated data $\geq$ 200 knots.

Notation

A	karst conduit cross-sectional area (L^2)
A_I	accuracy index (dimensionless)
A_p	constant of proportionality for amount of diffusing material ($M T^{1/2} L^{-3}$)
C	tracer concentration ($M L^{-3}$)
C_p	peak tracer concentration ($M L^{-3}$)
D_C	karst conduit diameter (L)
D_H	karst conduit hydraulic depth (L)
Dx_s	longitudinal dispersion coefficient ($L^2 T^{-1}$)
f_f	friction factor (dimensionless)
g	gravitational acceleration ($L T^{-2}$)
h_L	hydraulic head loss (L)
M_{in}	mass of tracer injected (M)
M_O	mass of tracer recovered (M)
M_T	total tracer mass recovered from all sampling stations (M)
N_F	Froude number (dimensionless)
N_R	Reynolds number (dimensionless)
Pe	Péclet number (dimensionless)
Q	groundwater discharge ($L^3 T^{-1}$)
$\bar{Q}$	mean groundwater discharge ($L^3 T^{-1}$)
t	time of sample collection (T)
t_p	time to peak concentration (T)
$\bar{t}$	mean tracer residence time (T)
v	mean tracer velocity ($L T^{-1}$)
$\bar{x_s}$	radial distance to sampling station (L)
V	volume of individual karst conduits (L^3)
V_T	total volume space occupied by karst conduits in karst aquifer (L^3)
$\bar{x}$	straight-line tracer migration distance (L)
x_s	sinuous tracer migration distance = 1.5∞ (L)
δ	laminar flow sublayer (L)
ϵ	relief of karst conduit wall surface irregularities (L)
μ	dynamic viscosity ($M L^{-1} T^{-1}$)
ρ	fluid density ($M L^{-3}$)
σ_t	standard deviation for mean residence time (T)
σ_v	standard deviation for mean flow velocity ($L T^{-1}$)

References cited

Chatwin, P. C., 1971, On the interpretation of some longitudinal dispersion experiments: Jour. of Fluid Mech. v. 48, p. 689–702.

Day, T. J., 1975, Longitudinal dispersion in natural channels: Water Resources Res., v. 11, p. 909–918.

Field, M. S., 1997, Risk assessment methodology for karst aquifers: (2) Solute-transport modeling: Environmental Monitoring and Assessment, v. 47, p. 23–37.

Field, M. S. and S. G. Nash, 1997, Risk assessment methodology for karst aquifers: (1) Estimating karst conduit-flow parameters: Environmental Monitoring and Assessment, v. 47, p. 1–21.

Field, M. S., P. F. Pinsky, and G. J. Davies, 1998, Solute-transport parameter estimation for karst conduits using a two-region nonequilibrium model [in press]

Schiesser, W. E., and C. A. Silebi, 1997, Computation Transport Phenomena: Cambridge University Press, 457 p.

Sukhodolov, A. N., V. I. Nikora, P. M. Rowiski, and W. Czernuszenko, 1997, A case study of longitudinal dispersion in small lowland rivers: Water Envir. Res., v. 97, p. 1246–1253.

White, W. B., 1988, Geomorphology and Hydrology of Karst Terrains: Oxford University Press, 464 p.

Disclaimer: The views expressed in this paper are solely those of the authors and do not necessarily reflect the views or policies of the U.S. Environmental Protection Agency.

NONEQUILIBRIUM SOLUTE-TRANSPORT MODELING IN KARST AQUIFERS

Malcolm S. Field
National Center for Environmental Assessment
U.S. Environmental Protection Agency, Washington, D.C. 20460

Solute-transport modeling in karst aquifers using a two-region nonequilibrium model that accounts for partitioning of solute into mobile- and immobile-fluid regions in karst conduits may be used to refine initial parameter estimates more accurately than traditional equilibrium modeling (Figure 1). Solute partitioning into mobile- and immobile-fluid regions causes an increase in average real velocity and a decrease in longitudinal dispersion estimates. Assumptions include flow through a Type I karst network (single flow channel), 100% volumetric water content for flooded karst conduits, and no sorption sites available to the mobile fluid.

Improved estimates for average real velocity and longitudinal dispersion over initial estimates and advection-dispersion model estimates can be obtained. In addition, ranges for the solute partitioning parameters that describe the degree of nonequilibrium and mass transfer can be obtained to a reasonable degree. While improvements in velocity estimates may be small, dispersion estimates will exhibit significant improvements because the adverse influence imparted by immobile-fluid regions on dispersion will be negated. Unfortunately, parameter estimates that describe the immobile-fluid region are identifiable only in terms of ratios describing solute partitioning. However, knowledge of the physical properties of the model provide constraints on allowable ranges for the nonidentifiable parameters. As a result, these ranges will be sufficiently narrow that the nonidentification problem becomes trivial.

Disclaimer: The views expressed in this paper are solely those of the author and do not necessarily reflect the views or policies of the U.S. Environmental Protection Agency.

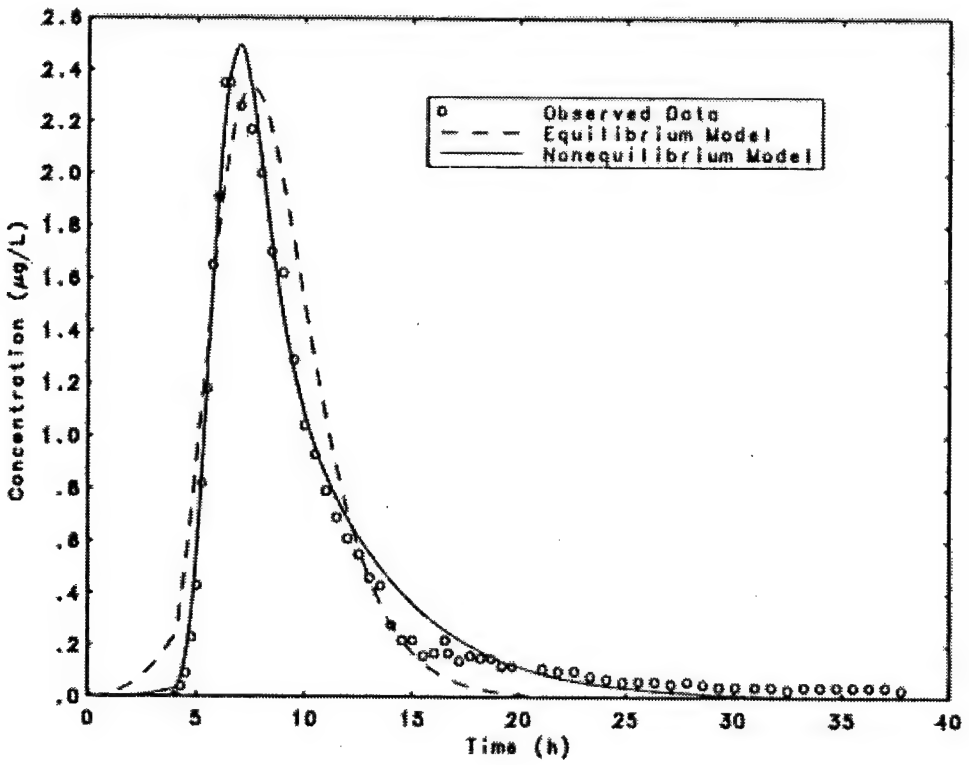

Figure 1: Comparison of equilibrium and nonequilibrium model fits to tracer-breakthrough curve data for Quarry Spring, Tennessee.

MODELING BREAKTHROUGH CURVES OF TRACING EXPERIMENTS IN A KARST ENVIRONMENT

Pierre-Yves Jeannin, Michael Hauns, and Olivier Atteia
Center of Hydrogeology, University of Neuchâtel, Rue Emile-Argand 11, CH-2007 Neuchâtel, Switzerland

During the past ten or fifteen years the development of sampling and analysis techniques has considerably improved the possibility of quantitatively measuring breakthrough curves during tracing experiments. In Europe it is now common to record fluorescence more or less continuously at springs or wells using field fluorometers and data loggers.

Analysis and interpretation methods of these curves are still under development. Many codes have been developed, but almost all of them for modeling tracing experiments in porous media (1, 2, or 3D analytical or numerical solutions of solute transport equations). If these codes are applied to karst or fissured aquifers, then a retardation of the observed data with respect to the model is often present along the falling limb of the breakthrough curve. Some of the codes have been improved in order to be able to fit real data. For this purpose, processes like adsorption/desorption, or diffusion of the tracer into the rock matrix have been introduced. Although such codes can fit observed data very well, it can hardly be believed that these processes are of great significance in karst systems where flow can be very fast and surface contact area between conduits and surrounding clays (for adsorbtion) or matrix rock (for diffusion) is pretty low.

Furthermore, none of these models reproduce the "scale effect" on apparent dispersivity that has been observed by many authors in heterogeneous aquifers, karst included. This scale effect is characterized by an increase of the apparent dispersivity when observation scale increases.

We have developed a new approach. We assumed that retardation and scale effects could result from the special features present in karst conduits, like cascades, pools (enlargement of a conduit's cross section), solution pockets, rapids, etc. For testing this hypothesis, we used a computational fluid dynamic (CFD) model, a laboratory model, and we made several tracing experiments in a cave. This approach made it possible to demonstrate that a significant retardation can result from any of these features, especially from pools, because of the presence of recirculation zones (eddies) which keep part of the tracer trapped for a certain time (Figure 1).

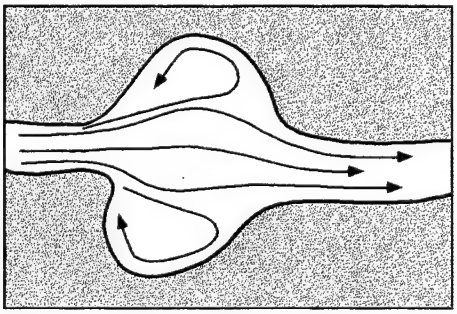

Figure 1: Flow routes in a pool.

On the basis of CFD models and convolution techniques, we were able to look at the effect of several of these features (like pools) repeated along the course of an underground flow path. The aim here was to investigate the scale effect on apparent dispersivity. The convolution models reproduced the scale affect with a good approximation.

It can be concluded that one pool induces retardation (or "tailing") due to recirculation in eddies. When several pools separated by channels with turbulent flow conditions are traversed by a tracer, there is a statistical compensation of the retardations in each pool, leading to a general increase of the dispersivity when the number of pools (e.g. the investigation length) increases. This adequately reproduces the "scale effect on dispersivity" generally observed in karst systems (Figure 2).

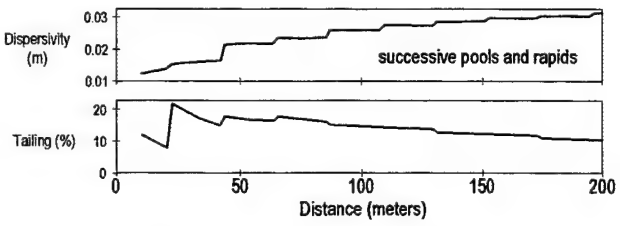

Figure 2: Scale effect on dispersivity and compensation of the tailing along the course of successive pools and rapids (results from the convolution approach based on CFD models).

HYDROLOGIC INSIGHTS FROM A FINITE-ELEMENT MODEL OF THE YIGO-TUMON SUB-BASIN, NORTHERN GUAM LENS AQUIFER

J. M. U. Jocson and J. W. Jenson
Water & Environmental Research Institute of the Western Pacific
University of Guam, Mangilao, Guam 96923

D. N. Contractor
Dept. of Civil Engineering & Engineering Mechanics
University of Arizona, Tucson, AZ 85721

Abstract

The Northern Guam Lens Aquifer (NGLA) is a Pleistocene karst aquifer in an uplifted Cenozoic limestone sequence forming a plateau about 60 to 180 meters high. Climate is tropical wet-dry, with average rainfall about 2.5 m/a (100 in/a), 80% of which falls between July and January. Monthly recharge estimates for 1982 through 1995, based on positive-definite daily differences of rainfall minus pan evaporation, suggest a relationship between monthly precipitation and recharge of N = max(0, -1.7+0.87P), where N and P are estimated minimum monthly recharge and precipitation, respectively, in inches. We used a two-phase fresh-water/saltwater flow model to simulate transient regional-scale responses of the fresh-water lens to monthly variations in natural recharge in the Yigo-Tumon sub-basin of the NGLA. Boundary conditions included monthly-averaged mean sea-level changes. Recharge rates were based on the assumption that 100% of monthly recharge infiltrated to the fresh-water lens within each one-month time step. Comparison of observed well-water elevations with elevations simulated for various values of hydraulic conductivity, K, suggest a regional K of about 6100 m/day (20,000 ft/day), consistent with previous studies. Variations of +/-20% around this value produced calculated water levels consistent with observed water levels. The most significant result from the modeling study, however, is that even for best-fit simulations, simulated water levels are consistently higher than observed levels for wet-season months and lower than observed levels during the dry-season months. The simplest explanation is that vadose storage is sufficient to dampen monthly-scale variations in recharge.

Karst Modeling
Karst Waters Institute Special Publication 5

SIMULATED EFFECT OF A KARSTIC VADOSE ZONE ABOVE THE NORTHERN GUAM LENS ON WELL-WATER LEVELS

Dinshaw N. Contractor
CEEM Dept.,University of Arizona,Tucson, AZ 85721

John W. Jenson
WERI, University of Guam, Mangilao, Guam 96923

Abstract

Saltwater intrusion in the Northern Guam lens has been simulated in the past using a finite-element, sharp-interface computer model, SWIG2D. Comparison of measured and computed water levels in several wells indicated systematic differences between the two. The computed peaks were higher and the computed lows were lower than the measured levels. This suggested that there was some storage in the vadose zone during peak inflows, with a subsequent higher release into the lens during low inflows. Hence, it was decided that the vadose zone should be modeled so as to reduce the error between the measured and computed water levels. The vadose zone was simulated using a one-dimensional, finite-element, unsaturated-flow program, UNSAT1D, in the vertical direction above each finite element in the SWIG2D network. The van Genuchten model was chosen to characterize the unsaturated properties of the karstic vadose zone. The parameters of this model were not known *a priori* and hence were obtained by calibration.

The two programs, UNSAT1D and SWIG2D, were combined into one large program, VADOSWIG. The input to VADOSWIG was the rainfall excess at the ground level and the output was the computed water levels in the observation wells. Calibration of the unknown parameters of the vadose zone was performed using a global optimization technique called the Shuffled Complex Evolution (SCE-UA) Method. Hydrologic data from 1982 through 1995 were used in the calibration. Water levels in four observation wells were used to calculate the errors in the calculated response. The sum-of-the-squared-errors between computed and measured water levels in the four wells was reduced by 35% when the vadose zone was modeled.

The conclusions reached in this study are that the vadose zone is capable of storing a considerable amount of rainfall excess. The vadose zone recharges the aquifer at a rate significantly different from the rainfall input. The storage and recharge rates are functions of the moisture content of the vadose zone. When the vadose zone is 500 feet thick and relatively dry, the peak recharge rate is shown to occur five months after the rainfall, and the recharge will be completed about a year later. When the vadose zone is relatively wet, the peak recharge is shown to occur two months after the rainfall, and the recharge is completed in five months. Understanding this phenomenon is necessary in predicting the response of the water levels in the wells to rainfall inputs. It is also important when analyzing the travel times of pollutants through the vadose zone.

SCALE MODELS

Most researchers have been tempted at one time or another to build scale models (i.e., hardware models) to evaluate physical processes that have too large a spatial or temporal scale, or are too difficult of access, to study conveniently in the field. Few succeed, because there is more involved than simply reducing the scale: the ratio of forces must also be kept similar to those in the field.

For example, in closed-conduit flow, the ratio of inertial to viscous forces, expressed by the Reynolds Number ($\rho vL/\mu$ -- units defined below), must be about the same in the model as it is in the field. Since the size of the model is much smaller than the field scale, other factors such as fluid velocity, density, or viscosity must be adjusted to make the Reynolds Numbers equivalent. In open-channel flow the Froude Number (v^2/gL) must be similar to that in the field. If surface tension is a dominant factor, the Weber Numbers ($\rho v^2 L/\sigma$) must be similar. Furthermore, in scale models the hydraulic gradients must be the same as in the field, unless special compensation is made.

Example: A model boat 0.5 m long is built to determine the stability and efficiency of the real thing, which will be 8 m long. The real boat will travel up to 10 m/sec. At what velocity should the model be towed across a water surface to simulate the dynamics of the real boat? Towing the model at 10 m/sec would produce very exciting results! The problem involves a water surface, so the Froude No. in the real boat = $(10^2/(8g) = 1.27$. To achieve this same Froude No. in the model its velocity must be about 2.5 m/sec.

Ignoring the issue of dynamic similarity has led to blunders such as attempting to simulate river meanders with trickles of water running down glass plates (disparity in Weber Number), or by using small sand models for erosional studies. In sand models the ratio of erosive force (a function of v^2) to resistive force (a function of the weight of the sand grains) falls far below that in the field, because the erosive force is greatly reduced but the resistive force remains the same. Tilting the model to increase erosive force violates the need for similar gradients, and linear trenches appear instead of meanders.

In laminar-flow models the exact Reynolds Number is unimportant, as long as it falls within the fully laminar range. Most scale models of early karst evolution are valid for this reason, and even where turbulent flow develops in the models their Reynolds and Froude Numbers may not deviate greatly from those in the field, except where large conduits are involved.

The best-known karst models are those of Ewers (1982), who simulated the development of karst aquifers by forcing water through artificial partings made by the contact of transparent media pressed against blocks of gypsum and salt. One can argue that the chemical dynamics differed from those of carbonate rocks, and that the hydraulic gradients were more akin to floodwater conditions than normal groundwater flow; but the growth, competition, and linkage of conduits that Ewers observed in the models led to a conceptual view that has been verified many times over in the field (see examples illustrated in the paper by Ford in the section on Conceptual Models). These experiments have been given wide exposure in the landmark paper on cave origin by Ford and Ewers (1978).

The paper that begins on the next page, our single brave excursion into the field of scale modeling, describes a recent approach to modeling the flow of water through conduits surrounded by a porous matrix.

Units

L = representative dimension (e.g. length, width, etc.) and the model and of the real object
v = fluid velocity (or velocity relative to object)
g = gravitational field strength (9.81 m/sec^2)
ρ, μ = density and dynamic viscosity of fluid
σ = surface tension of fluid

References cited

Ewers, R.O., 1982, Cavern development in the dimensions of length and breadth: Ph.D. thesis, McMaster University.

Ford, D.C., and R.O. Ewers, 1978, The development of limestone cave systems in the dimensions of length and breadth: Canadian Jour. of Earth Sci., v. 15, p. 1783-98.

BENCH-SCALE KARST MODELS

Lee J. Florea and Carol M. Wicks
Department of Geological Sciences, University of Missouri
Columbia, MO 65201

Approaches to mathematical modeling in karst aquifers

Modeling the transport of solutes through karst aquifers is difficult due to their complex nature. Traditional groundwater modeling in porous media uses a Darcian approach to describe flow though porous media. Flow though karst aquifers does not display Darcian behavior, as a large portion of the flow is through conduits and not the matrix. Use of a Darcian approach may be not appropriate.

Another approach to karst aquifer modeling is by the application of a pipe-network model. This approach requires knowledge of the internal geometry and flow conditions at all locations in the aquifer. The internal geometry is determined through cave mapping. It is not possible to use cave mapping in many karst aquifers for several reasons. Curl (1966) states that the statistical probability that a cave is enterable is low. Therefore, many karst aquifers exist for which there is no human-size entrance. Even with an entrance, the aquifer may not be enterable because many of the largest karst aquifers are perennially under phreatic flow conditions. Even if the aquifer is enterable, the resolution of the mapping is limited by the size of the surveyor. This biases the perception of the conduit geometry. A pipe-network model is useful if details can be obtained, but impossible to use if that information is lacking or unobtainable.

The linear systems approach is a "black box" model that relates a known input function to a known output function through a kernel function (Dreiss, 1982). The values of the solute-transport kernel function, y_m, can be calculated according to:

$$y_m = \frac{q_m C_m \Delta t}{\sum_{m=0}^{N} q_m C_m \Delta t} \qquad m = 1,2,...,N \tag{1}$$

where q_m are the values for the discharge from the spring, C_m are the concentrations of the solutes corrected for background, and Δt is the incremental time (Dreiss, 1989). The shape of the kernel function might correlate with the physical processes and properties within the aquifer and might provide an understanding of the internal workings of the aquifer.

Cave systems tend to follow one of four conduit morphology patterns (Palmer, 1991). Branchwork morphologies compose about 55-60% of the total observed in nature, and network morphologies represent about 15-20% of the total observed in nature (Palmer, 1991). It is reasonable to assume that karst aquifers also follow the four morphologic patterns described by Palmer (1991). Therefore, the internal geometries of karst aquifers that cannot be entered and mapped can be assumed to be branchwork or network systems. Branchwork and network morphologies are emphasized because of their statistical predominance and hydrogeologic importance.

The question to be answered in this study is: Do the kernel functions change as a function of conduit morphology, or as a function of the distance from the injection location to the spring?

Approach and methods

While field studies are very useful, their use in investigating the relation between conduit morphology and kernel function would be cumbersome and very time-consuming. The approach used in this study was to perform a laboratory study using scale models of karst aquifers. This decision led to two other questions: Is it possible to design and construct a bench-scale karst model including typical karst characteristics (e.g. sinkholes and conduits)? Are the results from the scale models consistent with results derived from field studies?

The models constructed for the study measure 16 cm by 16 cm by 3.8 cm. Two models were built: one representing branchwork morphology and the other representing network morphology. Both models were created using the same construction methods and materials.

Materials

The first aspect of the karst models investigated was the choice of modeling material. The material must be easily molded yet have hydraulic characteristics of karstic aquifers. Ceramic clays were selected. Three types of ceramic clays were available: 35-mesh Hawthorn, 20-mesh fireclay, and red earthenware clay. Nine cylinders were made of each type of clay (27 total). Of each set made of

ceramic clay, three were fired at each of the following temperatures: 970° C, 1100° C, and 1300° C. After firing, the porosity and permeability were determined and compared to values typical of karstic aquifers. From these test results, the 20-mesh fireclay fired at a temperature of 970° C was shown to provide the best choice of porosity (12 %) and permeability (0.00015 darcys).

Sinkholes, conduits, path length, and efficiency

Karst aquifers receive recharge via diffuse flow in the bedrock and rapid recharge through sinkholes and swallets. The locations of sinkholes on the models were determined by creating a Cartesian grid of 1-cm spacing on the surface of the model with the grid intersections representing possible sinkhole locations. The distribution for the diameters of sinkholes was calculated by using the depth-distribution function with the coefficient for Missouri karst (White, 1988). Results for the distribution were grouped into six classes of sinkholes such that the largest diameter class had the lowest frequency of occurrence. The locations of each sinkhole of each class were determined by drawing random numbers representing grid locations on the surface of the model (Figure 1). The spatial distribution of sinkholes and the diameters of the sinkholes were the same on both of the models.

The number of segments of conduits within a given cross-sectional area was calculated using fractal statistics and a fractal dimension of 2.5 (Curl, 1986). A conduit segment connected two adjacent grid locations on the model. The results were grouped into five segment orders, each containing a range of percentages of the cross-sectional areas. The locations of segments of a given order were determined by the distribution of sinkholes (as larger conduits are needed to carry the extra recharge provided by larger sinkholes) and by a hierarchization of flow (many small conduits joining and increasing in size in the direction of groundwater flow) (Padilla and Pulido-Bosch, 1995). Both models were created with the same numbers of conduit segments of a given order.

For each model and for each path, the number and order of the conduit segments along each path were known, and therefore the path length and the theoretical pore volume could be calculated. The combination of path pore volume and path length provided information about the openness of each path and was defined as the path efficiency (PE):

$$PE = \frac{path\ pore\ volume}{path\ length} \qquad (2)$$

A higher value for path efficiency results from solute paths containing greater numbers of higher-order segments. Higher-efficiency paths are less constricted.

Experimental setup, experiments, and data analyses

A recharge delivery system designed for the solute-injection experiments provided recharge evenly distributed across the top of the model. The system consisted of 256 pipette tips that were fed from a bifurcating system of tubes leading from a peristaltic pump. The rate of recharge was controlled with the pump. Distilled water was used to decrease the background concentration.

A syringe pump was used to inject the solute onto the top of the model at ten discrete locations. The injection locations were located along five rays that originated at the outlet of the model. The angles between adjacent rays were equal. Along each ray there were two injection locations: one proximal and the other distal relative to the location of the outlet (Figure 1). Path efficiencies were calculated for the only path leading from any injection location to the

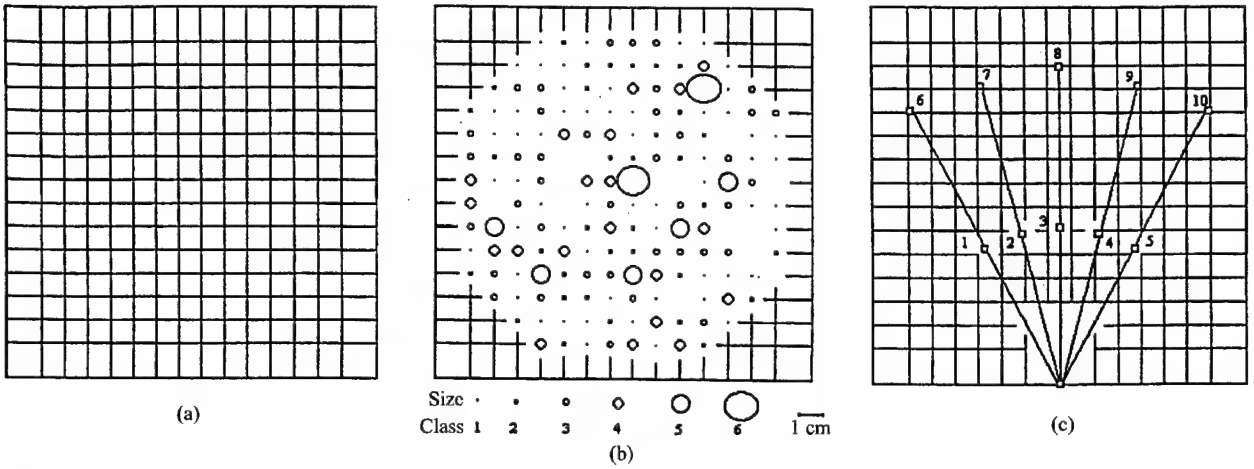

Figure 1: Schematic diagrams **(a)** of the grid pattern, **(b)** of the location and size of sinkholes, and **(c)** of the injection locations,

spring for the branchwork model and for the three shortest paths from each injection location to the spring for the network model.

A one-molar NaCl solution was used as the solute solution. The solution that discharged from the outlet of the model (the spring) flowed through a voltage probe. The voltage was recorded on a strip chart and the data were digitized. The voltage was converted to concentration through the use of a calibration curve that was developed for each probe. Probes were calibrated before and after each set of experiments. The experiments were conducted under steady-state conditions.

For both models, triplicate experiments were performed for each of the ten injection locations using a short-duration input function. The changes in concentration of the solution that discharge from the spring were used to derive kernel functions (eq. 1). For each of the derived kernels, the following statistical parameters were calculated: the time lag between the start of an injection and the breakthrough of solute at the spring, the time lag between the start of an injection and the time at which the maximum value of kernel occurred, the mean residence time (first moment about the mean), and the variance (second moment about the mean). The resultant kernel functions were grouped according to path length and averaged. Statistical differences between the two models (conduit morphologies) were tested by performing two-sided t-tests at the 95% confidence interval.

Results

The path lengths in the branchwork model are similar to the shortest paths in the network model (Table 1). Branchwork proximal and network proximal paths have the highest PE (0.16). Branchwork distal sites have an intermediate PE (0.14). Network distal sites have the lowest PE (0.12). The standard deviation of the PE is 0.01.

The results of the solute-transport experiments show a distinct difference due to path length (Table 1). Injections at distal locations tend to have higher lag times, times to maximum value of kernel, mean residence times, and variances than do injections made at proximal locations. There is a linear relation between path efficiency and lag times, time to maximum value of kernel, mean residence time, and variance (Figure 2). For paths that are less efficient, these measures are shown to be greater.

Discussion

The results from the solute-transport experiments show that there are differences in the parameters of the kernel

Table 1: Results for the branchwork and network models.

	Path Length (cm)	Path Efficiency	Lag Time (seconds)	Time to Maximum (seconds)	Residence Time (seconds)	Variance (seconds)
Branchwork Model						
Location						
B1	10	0.14	4.7	14.0	23.2	19.1
B2	8	0.15	4.3	11.0	13.2	8.8
B3	7	0.17	3.3	11.0	24.2	24.6
B4	7	0.17	3.7	10.3	22.5	20.1
B5	8	0.15	3.3	11.7	13.0	8.6
B6	18	0.12	7.7	15.3	38.4	29.9
B7	16	0.14	9.0	16.0	39.0	29.3
B8	19	0.14	7.7	17.3	38.7	29.5
B9	17	0.15	7.7	16.7	26.3	15.9
B10	21	0.13	7.3	15.0	49.1	37.4
Network Model[1]						
Location						
N1	8	0.15	5.7	11.8	33.7	31.1
N2	8	0.15	5.6	11.3	28.5	26.7
N3	7	0.17	4.7	11.9	29.4	26.5
N4	9	0.15	5.0	11.1	27.8	27.1
N5	8	0.16	5.3	11.2	25.8	23.9
N6	19	0.12	12.3	24.3	53.5	34.1
N7	16	0.11	10.8	25.8	55.9	33.6
N8	20	0.12	7.7	22.8	52.1	38.2
N9	17	0.12	8.3	27.8	60.9	40.5
N10	21	0.11	6.3	15.3	38.0	31.7

[1]Path lengths and efficiencies shown for most efficient network path.

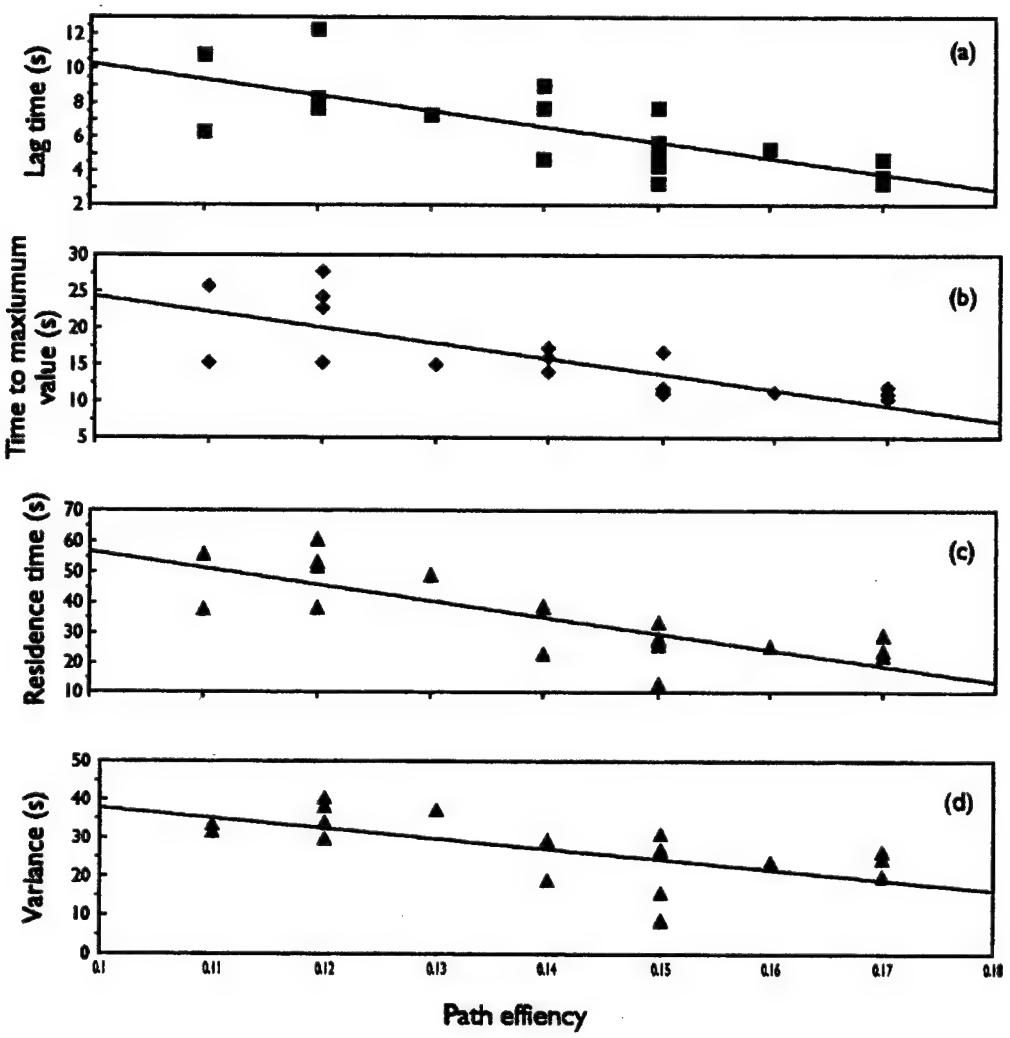

Figure 2: Correlations between model properties and path efficiency.

functions that can be attributed to conduit morphology. The variance of the kernel and the time to the maximum value of the kernel function for the network morphology tends to be higher than for the branchwork morphology (Table 1). Though differences between morphologies were detected, it may not be possible to determine the morphology of an aquifer based only on its output response. But when compared to the path efficiency, the kernel functions can provide us with information about the openness of the aquifer (Figure 2).

The experimental kernel functions were compared to kernel functions derived from three field sites. The first kernel was derived from concentration and discharge data that were gathered during a fertilizer pipeline break (Hoke, 1998). The other two kernels were derived from two dye traces: one at Dyer Spring and the other at City Spring, both in Elizabethtown, Kentucky (Mull and others, 1988). The field sites were more complex than a simple branchwork model (Figure 3). The peaks of the kernel functions from field locations were not damped like the distal kernel functions from the model, indicating a proximal-like response.

Conclusions

The bench- scale karst models created in this study provide a means to test solute transport in a laboratory setting. The kernel functions have different values of statistical properties due to the length of transport path. By correlating the statistical properties of the kernel functions to path efficiency, the model was described in terms of openness of conduits. Conduit morphology did have some effect on the kernel functions attained in this study. The derived kernel functions have similar statistical properties to those derived from field sites. Therefore, these bench-scale karst models lend insight to how real karst aquifers behave and provide a basis for continued physical karst aquifer modeling.

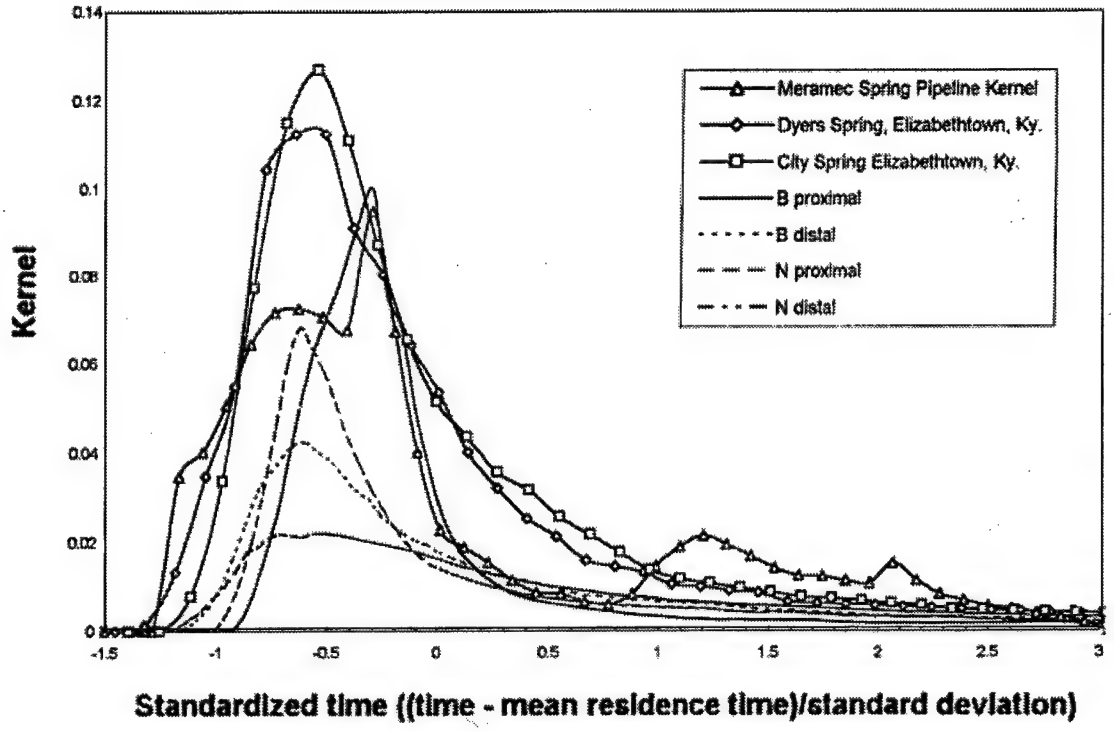

Figure 3: Graph showing match among kernels derived from bench-scale models (lines with no symbols) and from three field sites (lines with symbols),

Acknowledgments by the first author

As with any academic pursuit, several people have influenced the direction and form of this study. The following is a list of those who had a significant effect upon the completion of this study. Many thanks to Dr. Bede Clark in the Department of Fine Arts at the University of Missouri-Columbia for allowing the use of his facilities and aiding in the creation of clay samples and the models used in this study; the University of Missouri Research Board and Department of Geological Sciences, University of Missouri-Columbia for financial assistance; Dr. Joseph Engeln and Dr. Lee Peyton for serving on this thesis committee; and Dr. Carol Wicks for serving as thesis supervisor and for her support and guidance.

References cited

Curl, R. L., 1966, Caves as a measure of karst: Journal of Geology, v. 74, p. 798-830.

Curl, R. L., 1986, Fractal dimensions and geometries of caves: Mathematical Geology, v. 18, p. 765-783.

Dreiss, S.J., 1982, Linear Kernels for Karst Aquifers: Water Resources Research, v. 18, p. 865-876.

Dreiss, S.J., 1989, Regional scale transport in a karst aquifer, 2. Linear systems and time moment analysis: Water Resources Research, v. 25, p. 126-134.

Hoke, J. A., 1998, Modeling groundwater flow and solute transport, Maramec spring basin, Missouri: unpublished M.S. Thesis, University of Missouri-Columbia, 68 p.

Mull, D. S., J.L. Smoot, and T.D. Liebermann, 1988, Dye tracing techniques used to determine ground-water flow in a carbonate aquifer system near Elizabethtown, Kentucky: USGS Water-Resources Investigations Report 87-4174, 95 p.

Padilla A., and A. Pulido-Bosch, 1995, Study of hydrographs of karstic aquifers by means of correlation and cross-spectral analysis: Journal of Hydrology, v. 168, p. 73-89.

Palmer, A. N., 1991, The origin and morphology of limestone caves: Geological Society of America Bulletin, v. 103, p. 1-21.

White, W. B., 1988, Geomorphology and Hydrology of Karst Terrains: Oxford University Press, New York, 464 p.

STATISTICAL MODELS

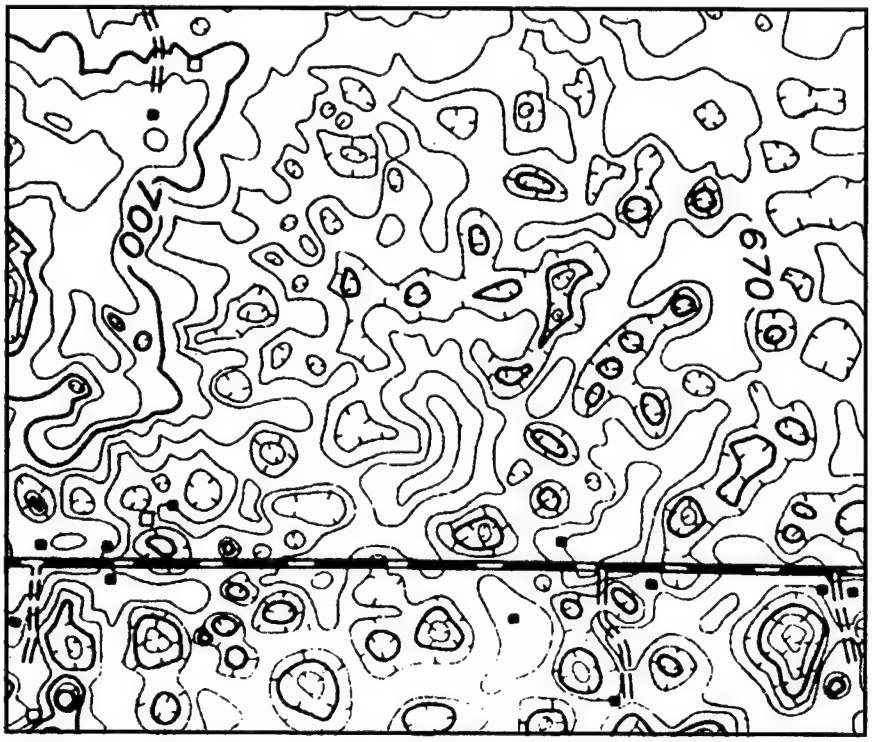

Statistical karst models are designed to fit measured field data to ideal distributions. If successful, such a model allows the distribution of karst features to be predicted or extrapolated with a degree of confidence that depends on how well the data fit the ideal.

The most common statistical ideal is the normal distribution, the well-known bell-shaped curve, which plots as a straight line on probability paper. Some data, such as fracture widths, have a discrete lower limit close to the mean value (for example, fractures cannot have widths less than zero). These data usually fit a log-normal distribution, in which the logs of the data values fit the normal curve. Karst porosity gives the impression of fractal distribution, and a a few researchers have pursued the goal of characterizing caves and lesser pores in this manner.

As shown by the following papers, field data often fail to fit the mathematical ideals. In some cases the data are so far from ideal that they can be interpreted only in terms of cumulative frequency, a method that does not allow confident extrapolation. Yet the very deviations from the ideal curves by themselves are of interest, because they lead to genetic questions about what accounts for the discrepancies.

Most statistical work in karst has taken the form of morphometric analysis of features such as sinkhole dimensions and interrelationships (e.g. Williams, 1972). Less has been done on hydrological aspects. This is a promising field that in the future may allow environmental scientists to answer site-specific questions in terms of probability and confidence intervals, rather than in qualitative terms.

Reference cited

Williams, P.W., 1972, The analysis of spatial characteristics of karst terrains, *in* R.J. Chorley (ed.), Spatial analysis in geomorphology: London, Methuen, p. 136-163.

ENTRANCELESS AND FRACTAL CAVES REVISITED

Rane L. Curl
Department of Chemical Engineering, University of Michigan,
Ann Arbor, MI 48109-2136

Abstract

Cave geometric properties have been studied between 1958 and today as statistical or fractal objects. These studies have divulged some degree of order in such properties as the distribution of cave lengths in a region and the distribution of cave passage sizes, and exhibiting some degree of self-similarity, suggesting a fractal nature, or moderate departures from self-similarity, suggesting geological mechanisms that introduce particular scales. The studies have also produced methods for estimating roughly the number of entranceless caves and the length distribution of all caves in regions, and the volume of caves as a function of the size of cave passages, first steps in a more complete description of karst aquifers.

A cave is a hole in the ground. That caves generate so much popular and scientific interest is not surprising, considering that the earth is, in most places, solid. It is not just relative rarity but also their present environment and contents, and questions about the origins of caves and their contents, which lead people to visit, study and write about them. This is my own story of the exploration of a group of facets of the cave puzzle (in what follows, my publications will be cited just by date).

The first issue is, how does one describe caves, measure them, and generalize about their shapes and sizes? My interest in these questions arose soon after I started exploring caves and was triggered by a nearly facetious observation: there are lots of caves with one entrance, some with two, fewer with three, and four-entrance caves are very rare. Could counts of caves with n entrances be plotted and extrapolated back to $n = 0$? An explorer's dream! It wasn't hard to plot and extrapolate, but it appeared to have little basis in geological processes. A model was needed.

A few years later I attended an extension course in statistics and learned of the Erlang stochastic process that describes telephone trunking -- in particular, the probability that an exchange will have n trunks occupied if subscribers call and hang up at random. The concept and the model transferred directly to the number of entrances to caves in the following manner: entrances form and are lost randomly over time by geological processes. If one postulates that the rate at which caves gain entrances is proportional to their length and that the rate at which they lose entrances is proportional to the number of entrances they have, caves will, after the process reaches equilibrium, be distributed over n by a Poisson distribution conditional on length. The model has only one parameter (λ), the ratio of the rate constants for caves gaining an entrance (per unit length of cave) to the rate constant for caves losing an entrance (per entrance). All that was necessary was to measure the lengths and numbers of entrances of caves in some region, estimate λ by fitting the mathematical model to the data, and extrapolate to $n = 0$. This was done for two sets of cave data, from West Virginia and Pennsylvania (1958), which fitted very closely by the model. A result for West Virginia (data from Davies, 1949, *Caverns of West Virginia*) was that for caves longer than 100 feet, 257 with one or more natural entrances were described, while the model predicted 2,405 with no entrances. In addition, the model also took the measured length distributions of surveyed caves and predicted the length distribution of entranceless caves. In more thorough studies conducted some years later (1966, 1987), the caves in eleven regions were analyzed, including with alternative models, and the caves of all regions were fitted best by the simple conditional Poisson model. It has been shown than the number and lengths of entranceless caves in many regions can be predicted.

There is no question that there are many naturally entranceless caves. A recent dramatic documentation of this was by Wilson (1994), who studied wells that penetrated caves in the Orange County (FL) aquifer, and concluded that there are at least 7,600 miles of (entranceless) cave per cubic mile of limestone. However, the existence of entranceless caves is not the essential problem. It is, what is meant by cave and cave entrance in a context in which the only available data (apart from well data) come from caves that are explorable and entrances that are negotiable, by people. Does this relate to karst hydrological systems, which don't care about people?

In a pair of studies following the 1958 work, I explored the questions of why the predicted distribution of the lengths of all caves (including those without entrances) appeared to fit a hyperbolic distribution (1960 - inversely proportional to some power of length) and afterward, how to de-

fine a cave (1966). The most significant conclusion of the latter was that it is not meaningful to limit what one considers a cave to spaces necessarily large enough for people. Cave spaces exist at all scales, from microns to hundreds of meters. The term *proper* was introduced to denote caves large enough for people (because most with *proper entrances* have proper names), and the term *cave modulus* was introduced for the size of an explorer that defines the cave space it can explore. It has been observed (in these terms) that *non-proper* cave space, with scales smaller than the *proper modulus*, (i.e. *subproper*) is the vast majority of the habitat for cave organisms.

As an amusing footnote, prior to 1997 the *Glossary of Speleology* defined a cave as "A natural cavity, recess, chamber, or series of chambers and galleries beneath the surface of the earth, *large enough for a person to enter*" (emphasis added). This must have been one of the few geological definitions to be essentially political in nature. The current definition in the Glossary (Jackson, 1997) is merely schizophrenic: "(a) natural underground open space, large enough for a person to enter; spaces large enough to enter are *proper caves*, entrances large enough to transit are *proper entrances*."

Time passed. Although it was recognized that non-proper cave was probably the majority of cave volume, it could not be studied except by the very unsatisfactory method of drilling. Then, between 1977 and 1983, Mandelbrot published versions of his book , *The Fractal Geometry of Nature*, and another block fell into place. Fractals are geometric objects irregular at all scales, often showing self-similarity and distributions of sizes (scales) that are hyperbolic. Proper cave lengths are approximately hyperbolically distributed (1966), and caves are certainly irregular at all scales. Caves are fractal objects! The problems were to invent a description and method of measurement that would reveal, if possible, whatever self-similarity is expressed by caves and to determine their fractal dimension for comparison with natural (and mathematical) phenomena. A model for doing this was reported in 1986.

The technique that was developed was to "fill" a cave with (spherical) *linked modular elements* (LME), touching each other and the nearest walls of the cave. This could be implemented on a computer by placing a LME at each survey station that was the size of the distance to the nearest wall (lesser of the survey left-right and up-down distances), and then interpolating more LME between stations. The sum of the sizes of all the LME is the "length" of the cave. The statistical distribution of the sizes of the LME could be determined. The first cave studied, Little Brush Creek Cave in Utah, exhibited self-similarity (the distribution of the sizes of the LME was hyperbolic), and a *fractal dimension* of 2.8 (which means, physically, that the cave is more than plane filling -- it has an area approaching infinity due to the many irregularities -- but is not space filling). The data truncated at a lower LME size of about 0.6 meters -- the *proper modulus*. The cave volume in chosen modulus ranges was estimated by assuming that the self-similarity extended to zero size, and with information from the known distribution of proper cave lengths in various regions. For example, it was estimated that, in limestone regions of Pennsylvania, there is a total of 2.1×10^7 cubic meters of cave space, 37% of which has a modulus below 1.0 meter, and 14% of which has a modulus below 1.0 centimeter.

The model and method involve several important questions, indeed limitations, which have not been resolved:

1. The LME do not fill the entire cave volume. The LME are fitted along a "string survey" of the cave, so they represent the survey data, but not the full three-dimensional structure of the cave volume. If one filled the total volume with LME and added up their sizes to determine the "length" of the cave, an enormous number would be created in caves with high and narrow (or low and wide) passages -- the same passage "length" would be counted many times. However one might well ask exactly what one means by the "length" of a cave? The concept applies only anthropometrically to complex three-dimensional (spatial) objects like caves. Putting aside the subjective use of the concept of "length," what is a better fractal measure of the structure of a cave? To be determined....

2. The LME method was subsequently applied to Stagebarn Crystal Cave in South Dakota, again with apparent self-similarity and a fractal dimension of 2.5 (1991). A more recent application by William Howcroft (personal communication), to be presented at this symposium, exhibits an apparent departure from self-similarity. This raises some interesting new questions. If the departures from self-similarity are real, what do they mean geologically? One must accept that observing self-similarity is the *unexpected* result, as there are many ways in which scale dependencies can enter into geological phenomena, but departures from self-similarity can also arise from measurement biases and data truncation. If the departures are real, mathematics have been developed to describe what is called multi-fractal behavior (e.g. Belfield, 1994), but a greater challenge is to identify the responsible geological process.

3. Neither descriptions of the distribution of cave lengths or of LME sizes contribute anything to describing the three-dimensionality and connectivity of a cave. They are rather like trying to describe a forest by only marginal statistical description of trunk and branch sizes. Something is learned about the forest, but not enough to reveal its vastly greater complexity than revealed by such a measure. There is still required a technique to put true spatial three-dimensional-

ity and connectivity into these statistical models. A lot of similar considerations are involved in trying to describe the hydrology of karst aquifers. Attempts related to that are numerous and include many topics such measurement techniques and the application of percolation theory (e.g. Benson, et al., 1993; Berkowitz, 1995). It is not known which, if any, of these techniques now under development will be fruitful in adding three-dimensionality to the current fractal description of karst aquifers.

References cited

Belfield, W. C., 1994, Multifractal characteristics of natural fracture apertures: Geophysical Research Letters, vol. 21, no. 24, p. 2641-2644.

Benson, R.C., and L. Yuhr, 1993, Spatial sampling considerations and their applications to characterizing fractured rock and karst systems: Environmental Geology, vol. 22, p. 296-307.

Berkowitz, B., 1995, Analysis of fracture network connectivity using percolation theory: Mathematical Geology, vol. 27, no. 4, p. 467-483.

Curl, R.L., 1958, A statistical theory of cave entrance evolution: National Speleological Society Bulletin, vol. 20, p. 9-21.

Curl, R.L., 1960, Stochastic models of cavern development: National Speleological Society Bulletin, vol. 22, p. 66-76.

Curl, R.L., 1964, On the definition of a cave: National Speleological Society Bulletin, vol. 26, p. 1-6.

Curl, R.L., 1966, Caves as a measure of karst: Journal of Geology, vol. 74, no. 5, part 2, p. 798-830

Curl, R.L., 1986, Fractal dimensions and geometries of caves: Mathematical Geology, vol. 18, no. 2, p. 765-783.

Curl, R.L., 1987, Entranceless caves of the Fiborn Karst Preserve, Michigan (abstract): Proceedings of 1987 annual meeting, National Speleological Society, *in* NSS Bulletin, vol. 50, no. 1, p. 31.

Curl, R.L., and J.A. Nepstad, 1991, Fractal analysis of Stagebarn Crystal Cave, South Dakota (abstract): Proceedings of 1991 annual meeting, National Speleological Society, *in* NSS Bulletin, vol. 53, no. 1, p. 44.

Jackson, J.A. (ed.,), 1997, Glossary of Geology, 4th ed.: Annapolis Junction, Md., American Geological Institute.

Mandelbrot, B. B., 1983, The Fractal Geometry of Nature: New York, W.H. Freeman.

Wilson, W. L., 1994, The extent of unexplored caves in the Floridian aquifer; Notes and Figures: presented at 26th Annual Cave Diving Seminar: North Florida Junior College, 19 November 1994.

FRACTAL CHARACTERISTICS OF CONDUIT SYSTEMS

William D. Howcroft and John W. Hess
Water Resources Center, Desert Research Institute, 7010 Dandini Boulevard, Reno, Nevada 89512,
and Graduate Program of Hydrologic Sciences
University of Nevada, Reno, Nevada 89512

Abstract

Cave survey data from California, New Mexico, South Dakota, and Tennessee are being examined to determine the fractal characteristics of conduit systems within karst aquifers. Linked Modular Element (LME), box counting, and Richardson's Law type fractal analyses are being applied to elucidate self similarities in conduit length, size distribution, and pattern in 3-D space. Different types of conduit systems, including branchwork caves, anastomotic mazes, network mazes, and ramiform/spongework caves, are being analyzed to deduce similarities between one conduit type and another. In addition, data from individual caves within the same aquifer are being examined to ascertain whether data from an individual cave may be representative of the entire flow system. Contrary to work performed by other researchers, results thus far obtained in this study indicate that not all cave systems exhibit fractal size characteristics.

VOLUMETRIC FRACTAL DIMENSION AS A QUANTITATIVE DESCRIPTOR FOR SATURATED CAVE MORPHOLOGY

Todd R. Kincaid
Department of Geology and Geophysics, University of Wyoming
Laramie, WY 82071

Abstract

A method is presented for calculating a volumetric fractal dimension from three-dimensional cave survey data that describes a particular cave's volume-filling capacity or "bulkiness." A modified box-counting technique is utilized to sample cave volume at varying scales of investigation. Using this technique results in $3 <= D <= 4$ because D describes the clustering of the cave volume, where a perfect cube yields $D = 3$. The lower limit of the scaling range is dependent on the resolution of the cave survey. The upper limit is dependent on the conduit dimensions of the cave system being sampled.

The method has been tested on five saturated cave systems. Three-dimensional models were constructed from detailed survey data consisting of azimuth, depth, width, and height measurements collected at closely spaced survey stations along linear paths through the conduits. Cartesian coordinates were determined for points along the cross-sectional perimeter of the cave at each survey station. Additional cross sections were generated between survey stations by linear interpolation. The Cartesian coordinates were then gridded in three dimensions with a 1 x 1 x 1 m spacing and exported as regularly spaced coordinate data files from which a box-counting method could be used to determine the volumetric fractal dimension. The caves include Wakulla Spring in the Floridan aquifer of north Florida, Duden Spring in the Antalya Travertine aquifer of southern Turkey, and Kirkgoz-1 Spring, Finike-Suluin, and Kirkgoz-Suluin in the Taurus Mountain aquifer of southern Turkey. The spring caves display dendritic morphologies while the other two caves display spongework morphologies.

For these five caves, D ranges between 3.16 and 3.92 with an approximate error of 0.05. The dendritic caves displayed D values of 3.48 and up, while the spongework caves were characterized by lower values of 3.16 and 3.23. These results indicate that the volumetric fractal dimension provides a quantitative descriptor for saturated cave morphology. Further work is being conducted to determine how these results relate to surface and boundary fractal dimensions calculated for the same cave systems.

A STATISTICAL EVALUATION OF THE STRUCTURAL INFLUENCE ON SOLUTION-CONDUIT PATTERNS

Arthur N. Palmer
Department of Earth Sciences, State University of New York
Oneonta, NY 13820-4015

Abstract

Geologic mapping of accessible vadose and phreatic cave passages in a variety of carbonate aquifer types has quantified the relation between conduit trends and the local stratal dip. Gravitational flow in the vadose zone tends to follow the dip of the strata, with varied degrees of downward discordance across the strata according to the distribution of cross-cutting fractures. This trend is strongest in prominently bedded strata of low dip. Likewise there is a distinct tendency for phreatic flow to follow paths nearly parallel to the local strike. This pattern is most favored in bedded rocks of all types, especially those of high dip. However, in prominently fractured strata the dip orien-tation of vadose channels is faint, and there is no significant preference for strike orientation of phreatic conduits. The data and interpretive methods described in this report pertain only to unconfined karst aquifers, and only to major flow paths that are capable of forming discrete solution conduits.

Introduction

A glance at a typical cave map is enough to demonstrate that geologic structure plays an important role in the patterns of solution conduits in karst aquifers. Other papers in this volume, including those by Sasowsky, Jancin, Ford, and Kastning, emphasize this relationship. The most obvious manifestation is the guidance of solvent groundwater by fractures.

The effects of stratal dip and strike are more subtle. Although they are widely recognized, little has been done to quantify their effect in a systematic manner. In many caves the relationship is conspicuous, especially where the dip is steep, but in massive rocks it is far less clear. In gently dipping strata, where the true dip directions and angles cannot be discerned by eye, the relationship must be measured by precise geologic mapping.

Toward the goal of quantifying the geological influences on patterns of solution conduits, approximately 100 km of cave passages have been mapped in a variety of settings by the author and M. V. Palmer with an automatic surveyor's level, hand level, or tripod-mounted Brunton compass, the choice depending on the nature of the cave. The data presented in this report are derived from that study.

A practical goal of quantifying groundwater flow directions is to enable one to evaluate paths of potential contaminant movement. Tracer tests can show quite clearly the paths between selected inputs and their spring outlets. However, they do not show the exact paths between these points, which may be equally important in some studies. Occasionally it is not possible to conduct tracer tests at all.

The method presented here is a complementary approach that can be used in conjunction with tracing, by which it is possible to predict flow patterns in both the downstream and upstream directions. It also demonstrates a promising tool in geologic and hydrologic studies -- the use of statistics to provide an approximate probability of hydrogeologic conditions, so that predictions or explanations of field conditions can be made in the same manner as a weather report, in terms of probability.

This is an update of an earlier report (Palmer, 1986). It applies only to epigenic caves -- the "common" caves formed by meteoric ground-water flowing between upland karst areas and springs at lower elevations.

The ideal unconfined groundwater flow pattern

As an ideal, consider a prominently bedded limestone aquifer with a moderate dip (Figure 1). Vadose solution channels are formed by gravitational flow that follows the steepest available openings. In the absence of prominent fractures, virtually all of these openings consist of dipping bedding-plane partings. Vadose passages should therefore have a strong down-dip orientation that underscores their gravitational origin. In real aquifers, however, even in the most prominently bedded strata, the flow tends to cut across the bedding in places, usually along scattered fractures. In vadose channels this discordance is almost invariably downward across the strata, producing gradients that are steeper than the dip. The typical result is a stair-step pattern in which dip-oriented canyons or perched tubes alternate with shafts discordant to the strata. Floor entrenchment by free-surface streams can cause secondary

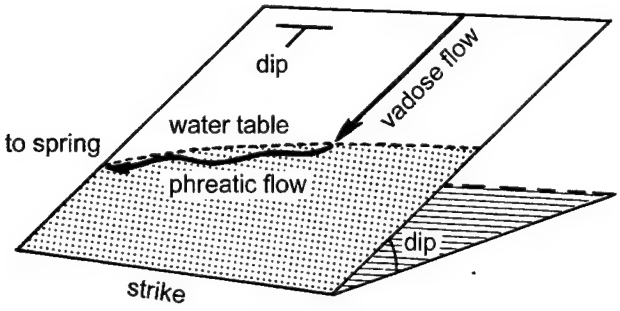

Figure 1: Ideal pattern of vadose and phreatic flow in a prominently bedded unconfined aquifer. Actual flow patterns deviate from this ideal in different amounts according to the structural setting.

discordance to the strata, but only the primary flow paths, prior to entrenchment, are included in the data for this paper.

Once the water reaches the potentiometric surface (water table, in this case), the incoming vadose flow loses its gravitational tendency, because gravity is offset to varying degrees by the downward increase in hydrostatic pressure. So the orientations of phreatic flow paths are generally independent of the stratal dip, and this is true also for the resulting conduits. Phreatic flow is concentrated along the most efficient paths -- those that offer the least resistance to a given discharge. In the ideally bedded example of Figure 1, these paths are unlikely to cut across the strata, and since the incoming vadose water already occupies favorable partings, there is a very strong tendency for the water to remain within them. Penetration beneath the water table is an option, but only if it affords an efficient path to the surface at a lower elevation. This likelihood is greatly suppressed by the decrease in width and spatial frequency of openings with depth as a result of lithostatic pressure. This decrease can be disrupted by structural deformation, for example in tectonic belts, but even in those areas the tendency persists for the majority of efficient flow paths to be shallow. As a result, in the well-bedded case shown in Figure 1, the major phreatic flow paths are nearly parallel to the local strike of the strata. This outcome is dictated by the combination of stratal concordance and shallow flow. The direction along the strike (left or right with reference to the incoming vadose flow) is that which affords the most efficient outlet (usually, but not always, the one with the steepest gradient).

In the well-bedded example, the distinction between initial vadose and phreatic conditions is clear, even in abandoned conduits. Vadose channels are relatively steep with down-dip trends having no rises in the downstream direction. Passages consist mainly of canyons and perched tubes, perhaps interrupted by discordant shafts. At the present (or former) water table, most passages change to tube-shaped conduits with a strong tendency for strike orientation. Undulatory profiles are common in tubes, as are overall low gradients and certain segments that rise in the downstream direction.

The reader's reaction at this point is probably one or more of the following: (1) Isn't this obvious? (2) This is no 'rule' -- it's an exception; or (3) Cave origin is too complex to allow such simple relationships. One serious objection to this scheme might be that the earliest phase of cave origin is thought to be deep beneath the surface along favorable *inception horizons* (Lowe, 1992). The importance of initial deep flow as a factor in conduit development is revealed by the many large regional karst flow systems that discharge sulfate-rich water from depth (Worthington, 1991). The impact of deep artesian flow on emerging carbonate aquifers, even those that are now fed by shallow meteoric water, has been emphasized by Klimchouk (in press). Therefore analysis of the field data is necessary to assess the validity of the idealized flow paths of Figure 1, as well as the objections to it.

Field data

To assess these relationships, the local stratal dip within each conduit must be precisely surveyed, especially in low-dip settings, because geologic maps based on surface exposures rarely provide sufficient detail. Small structural irregularities (tectonic or sedimentary in origin) superimposed on the regional structure can produce local dip directions that differ greatly from regional patterns. Dips can vary from bed to bed in response to irregular stratal thickness, so the exact bedding-plane parting(s) that originally controlled the passages must be mapped. In vadose canyons these are usually interpreted to be the uppermost partings at or near ceiling level. In phreatic tubes they are considered to be the partings exposed in the walls at the widest parts of the passage cross section. Determining the vadose or phreatic nature of each passage is not as subjective as it sounds, thanks to the genetic clues described earlier. The few passages of ambiguous origin are not included in the statistical summary.

The geologic structure in representative caves has been mapped in a variety of unconfined karst aquifers throughout much of North America, Europe, and a few other locations. A list of aquifers from which the earliest data were acquired is given in Palmer (1986). A disproportionate amount of field effort has been expended in low-dip settings, because the relationships are most subtle there and require more careful mapping to reveal the structures. However, equally as many caves have been examined in deformed strata, e.g. in the Rockies and Appalachians.

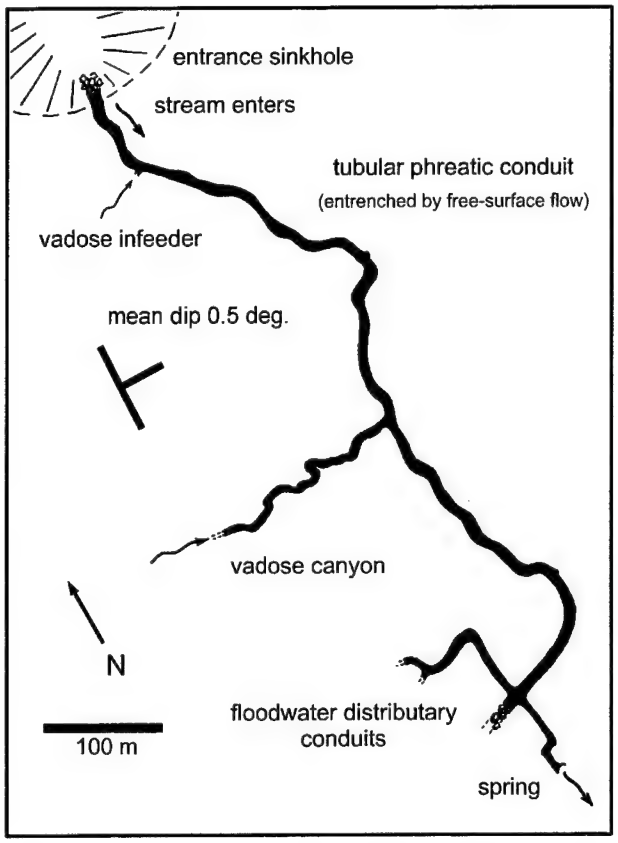

Figure 2: Pattern of vadose and phreatic conduits in a typical epigenic cave formed by unconfined meteoric water (Shiloh Cave, Indiana). Although the regional dip is to the southwest, a local dip reversal is responsible for the eastward trend of vadose infeeders. Distributary routes at the downstream end are independent of the dip, having formed under floodwater conditions in response to collapse of the spring outlet. Map courtesy of Central Indiana Grotto, National Speleological Society.

A typical example is shown in Figure 2, a cave located in the prominently bedded upper Salem Limestone of Indiana. The vadose infeeders enter from the west, which is contrary to the WSW regional dip shown on geologic maps. Field measurements show that the mean dip within the cave is actually to the east at about half a degree. The main passage, of phreatic origin (although modified by vadose water) is nearly parallel to the local strike. Another example is shown in Figure 3 of Kastning in the section on Conceptual Models. However, the clarity of these examples should not be taken to mean that this pattern is inevitable.

Statistical summaries of field data

Preliminary investigations (Palmer, 1986) show that the data fall into three major groups according to the structural setting: **(1)** prominently bedded strata of low dip, such as the Ste. Genevieve, St. Louis, and Monteagle Limestones of the east-central U.S.; **(2)** prominently bedded but tectonically disturbed strata (folded and faulted), such as the Jefferson Limestone of the Rockies and Onondaga Limestone along the Hudson Valley, New York; and **(3)** prominently fractured strata, generally massive, in which more than 50% of cave passages are fracture-guided, linear fissures, e.g. the main strata of the Salem Limestone in Indiana, epigenic karst zones in the Madison Limestone in the Rockies, and the Hauptdolomit of the Alps. The low dip of group 1 is considered to be less than 5 degrees. The prominently fractured strata of group 3 generally have an average bed thickness greater than 2 m. Aside from this general grouping, the exact magnitude of the dip angle appears to have little effect on cave trends. The structural character of an aquifer can vary geographically, or from one stratigraphic interval to another.

The surveyed sample was divided into vadose and phreatic passages. The mean trend of each passage was determined by the overall direction from its most upstream accessible point to its farthest downstream accessible point, or where it merged with another passage. Where appropriate, the upstream or downstream end was instead considered to be the point where the passage changed character from vadose to phreatic.

Several relationships were derived from the geologic data:

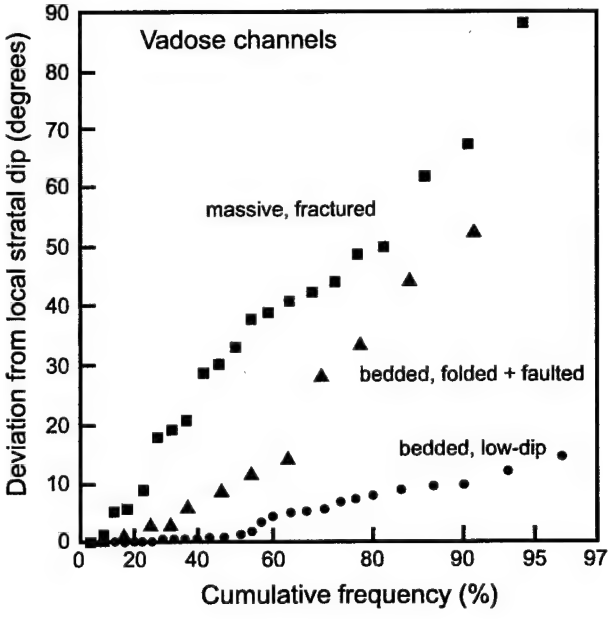

Figure 3: Cumulative frequency plot of vadose passage trends, with respect to deviation from the local dip direction.

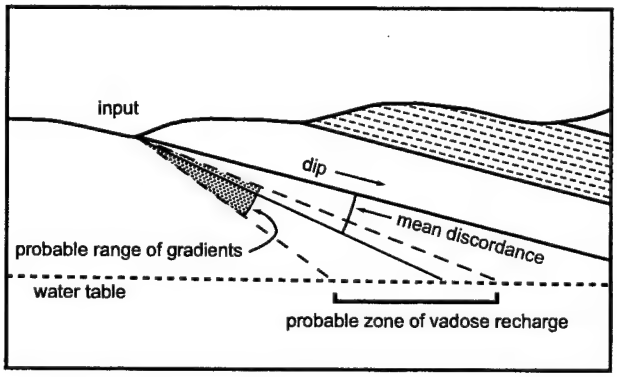

Figure 4: Discordance of vadose flow to dipping strata. In the measured sample the discordance is almost invariably downward (gradient of flow > dip), except in a few places in prominently fractured aquifers. For each structural type, the scatter around the mean discordance has an approximately log-normal distribution (see Figure 5).

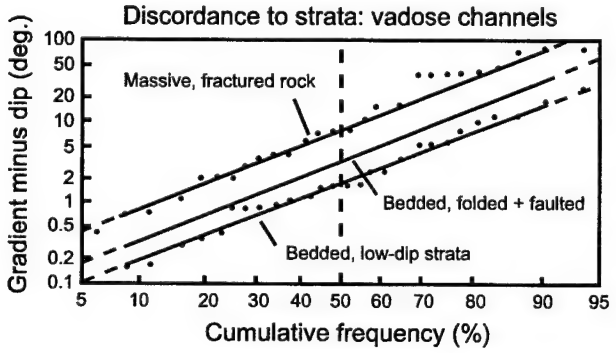

Figure 5: Discordance of vadose cave passages to stratal dip (gradient minus dip), plotted on a log-normal scale.

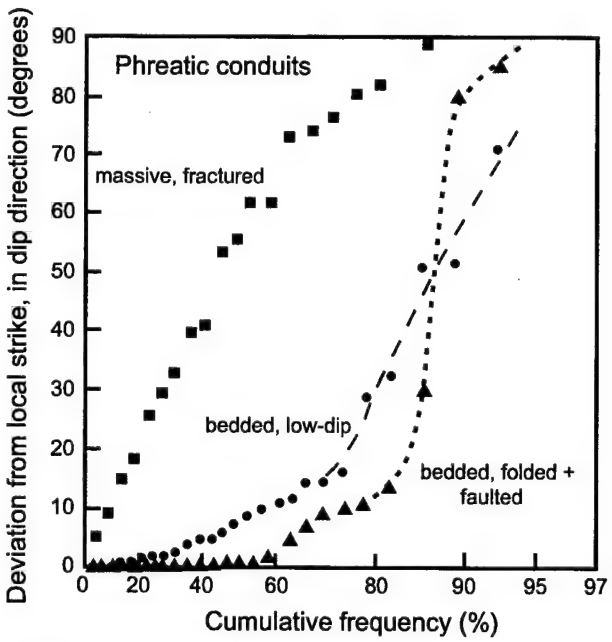

Figure 6: Cumulative frequencly plot of deviation of phreatic conduits from the local strike of the strata.

1. Direction of vadose conduits relative to the local dip direction. The direction of each conduit was compared to that of the measured local dip, and the deviation of the passage from the true dip direction was measured in degrees. The data are compiled in a cumulative frequency plot (Figure 3). The vertical scale shows deviation from the mean dip direction in a one-tailed normal (Gaussian) distribution, although the data deviate somewhat from the normal, as shown by their non-linearity in Figure 3. A few vadose trends in massive and steeply dipping strata are against the dip, and although they were included in the statistics, they plot outside the graph.

2. Discordance of the gradients of vadose conduits to the local dip angle (Figure 4). The gradient of the initial flow path of each conduit was compared to the measured local dip angle, and the deviation from the dip angle was recorded in degrees (+ = dip steeper than gradient; - = gradient steeper than dip). These measurements give the overall trends for paths that in detail usually consist of irregular stair-step patterns. The data fall rather well on a log-normal probability plot (Figure 5). This is the only data set to show clearly either a normal or log-normal distribution. To avoid congestion, individual data points for the middle line (bedded, deformed strata) are not plotted. A few vadose passages cut across the strata in the up-dip direction, so their discordance is greater than 90°, and therefore they plot off the graph. They represent less than 2% of the data. More data points plot beyond the limits of Figure 3 than they do in Figure 5, causing a slight disparity in the number of points on the two graphs.

3. Direction of phreatic conduits relative to the local strike. The difference in direction between each phreatic conduit and the local strike was measured and found to be almost invariably in the direction of the dip. Left and right orientation relative to the incoming vadose flow path was not included, as this is determined more by geomorphic and hydrologic factors than by structure. The results are compiled on a cumulative frequency plot in Figure 6. The data have a maximum in the strike orientation, with diminishing frequencies toward the dip direction, and hardly any data opposite the dip direction. Some conduits that clearly follow irregularities in local strike, but whose mapped trends happen to fall slightly updip of the mean strike direction, were assigned values of zero. The few samples that clearly deviate in the updip direction are included in the statistics, in the same manner as Figure 3, but fall outside the limits of the graph.

Evaluation of data

Figures 3, 5, and 6, in combination with the original geologic data, show that the ideal model of down-dip vadose flow and strike-oriented phreatic flow is most applicable in prominently bedded low-dip strata. Bedded but steeply dipping strata showed greater deviation from the ideal model, but not as much as one might expect. Conduits in massive, prominently fractured strata were least likely to follow the dip-strike pattern. In these aquifers the dip tendency of vadose flow is still present though subdued, but there is a poor correlation between phreatic passages and the strike. Details are summarized below.

Prominently bedded, low-dip strata

In well-bedded rocks lacking many prominent discordant fractures, most conduit-forming flow follows bedding-plane partings, or, in some cases, a myriad of small fractures within favorable beds. Concordance of flow routes to the strata is greater than in any other structural setting. Vadose water easily perches on insoluble beds, even rather thin ones. Phreatic water also tends to follow paths that are strongly concordant with the bedding. There are many similarities to the ideal model in Figure 1. In low-dip settings, at least within the field sample, 90% of the vadose passages fall within 10° of the local dip direction; and 82% have a discordance to the strata of less than 10°. Phreatic passages deviate from the strike by only 10° at the 50th percentile but as much as 60° at the 90th percentile.

Prominently bedded, deformed strata

In bedded, deformed strata, vadose passages are less apt to follow the dip than they are in low-dip rocks. Although at the 50th percentile the deviation from the dip is only 10°, it is 60° at the 90th percentile. Vadose discordance to the strata is about 35-40° at the 90th percentile. Phreatic passages show the greatest tendency toward strike orientation of any data set, even more than in low-dip strata. This is due to the fact that to follow any other direction, water would have to follow paths with considerable discordance to the strata. At the 90th percentile the deviation of phreatic passages from the strike is about the same as in low-dip bedded strata, but at the 50th percentile the deviation is a mere 2 degrees.

Prominently fractured strata

Prominently fractured strata, regardless of dip angle, show the greatest disparity to the ideal flow pattern of Figure 1. At the 50th percentile, vadose channels deviate from the dip as much as 30°, which shows only a faint influence of dip on vadose flow direction. The deviation is more than 60° at the 90th percentile. Discordance of vadose flow to the strata is also greater than in any other structural setting. At the 50th percentile the discordance is less than 10°, but at the 90th percentile it is about 90°. Phreatic conduits show great deviation from the strike direction. At the 50th percentile the deviation is nearly 60°, indicating no significant relationship to the strike direction.

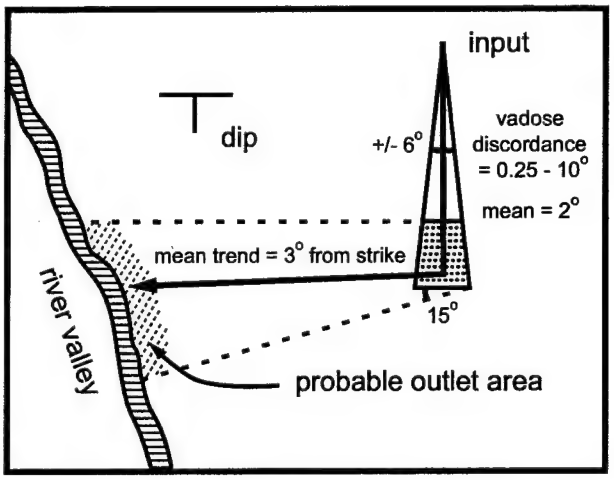

Figure 7: Composite predicted zone of conduit flow in a prominently bedded, low-dip aquifer, with a 70% probability, on the basis of field data shown in Figures 3, 5, and 6. The prediction is less precise in prominently fractured aquifers.

Although there are some large deviations from the exact dip and strike direction, particularly in fractured aquifers, only about 5% of the passages in the total sample follow a direction opposite to that of the dip. This shows an overwhelming structural influence on major flow paths. Deflection from the exact dip or strike direction is caused mainly by discordant fractures. The geologic mapping shows that passage sinuosity, such as that shown in Figure 2, can not only be caused by intersecting fractures but also by local irregularities in dip or strike orientation (Palmer, 1976, 1989).

A composite view of conduit patterns

The results of this study can be applied to several common field problems. (1) A contaminant spill occurs at a known point. What path is it likely to follow, and where is its most likely point of emergence at the surface? (2) Contaminants are detected in a well or spring. What is the most likely source? (3) Well-head protection areas are being mapped. What areas are most and least likely to supply the wells?

To guide such field investigations, a probability plot can be devised that shows the most likely paths of flow, at least on the basis of this data sample. Figure 7 shows the result of combining the data from Figures 3, 5, and 6 in a well-

bedded aquifer of gently dipping strata, with a probability of 70% (a bit more than +/- one standard deviation from the mean). Zonations showing greater and lesser probabilities can also be shown if desired.

In Figure 3, at 70% cumulative frequency, the data fall within a 6-degree deviation in both directions from the dip. This is shown by the angle expanding outward from the input point on Figure 7. In Figure 5 the mean discordance of vadose flow to the bedding is about 2 degrees (at cumulative frequency = 50%), and 70% of the data fall approximately between 0.25 and 10 degrees (cumulative frequency = 15-85%). This range, in combination with the range of probable deviation from the dip direction, produces a trapezoidal zone at the water table where the incoming vadose water is likely to arrive. Its exact position is determined by projecting the probability zone downward to the water table at the appropriate angle, which depends on the dip angle and thickness of the vadose zone. Figure 4 shows an idealized profile through this zone.

Finally, the probable paths of phreatic outflow to the outlet river valley are determined from Figure 6. A cumulative frequency of 70% spans the range 0-15 degrees deviation from the strike, in the direction of the dip. The mean value, at a cumulative frequency of 35%, is about 3 degrees. This range is shown by the diverging lines emanating from the shaded trapezoidal zone. The probable zone of emergence of the water is shown with a cross-hatched pattern along the valley wall. The ideal path, with no deviation from the mean, is shown as the bold arrow-headed line.

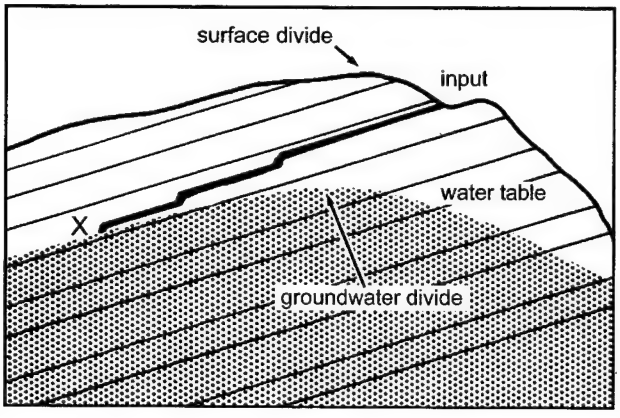

Figure 8: Perching of vadose flow can cause substantial down-dip deflection from the commonly assumed vertical paths. Potentiometric data from wells can detect the groundwater divide, but dye tracing is the only reliable method for detecting the deflection of flow across the groundwater divide. In water-budget studies, delineation of well-head protection zones, or predicting contaminant transport, this tendency should be anticipated, especially in prominently bedded strata.

The method can be applied to prominently fractured strata, but although the mean conduit trends are similar to those of Figure 7, the range of uncertainty is far greater. There is some chance (about 5%) that the vadose flow will not even be in the dip direction, and an even greater probability that the phreatic flow will deviate from the strike in the direction opposite to the dip.

It is also possible to trace flow paths upstream to potential source areas, although with less precision. For example, if contaminants are detected in a well or spring, the most likely source areas can be determined, potentially reducing the amount of required field work needed to identify the exact source.

Ironically, the lower the dip, the greater its importance in controlling conduit patterns, because discordance to the strata is small, allowing vadose perching to extend for great distances (kilometers in some cases). Vadose flow can easily cross groundwater divides, as shown in Figure 8.

Interpretive problems

Many examples of these conduit trends can be cited on the basis of geologic mapping (e.g. Palmer, 1972, 1976, 1989). However, many other studies appear to contradict these findings. In particular, Ford (1965, 1971, and in this volume) gives examples of dip-oriented flow that continues discordantly in the down-dip direction through the phreatic zone. His type example is that of the Mendip Hills, England, which contain steeply dipping, prominently fractured limestones, with favorable outlets only in the dip direction. However, he cites many other examples of both dip and strike orientation as well (e.g. Ford and Ewers, 1978). In general, these seemingly contrary observations do not conflict with the results presented here. They differ mainly in emphasis.

Many researchers favor the view that the initial water table in a carbonate aquifer is at or near the surface, so that the vadose zone is virtually absent (see Ford in this volume). This may be a valid assumption in certain aquifers, especially in areas of rapid tectonic uplift or where a thick insoluble caprock is being breached. However, in terms of cave development, the sample for this paper shows that even the earliest vadose passages have a prevailing down-dip trend in nearly all cases, with evidence for a rather deep water table.

The geomorphic setting has a strong influence on the structural attributes of an aquifer. For example, Sasowsky and White (1994) give examples from the deeply entrenched Obey River Gorge, Tennessee, where openings are favored by stress release caused by local erosion. Dip and strike relationships are greatly subdued in such areas,

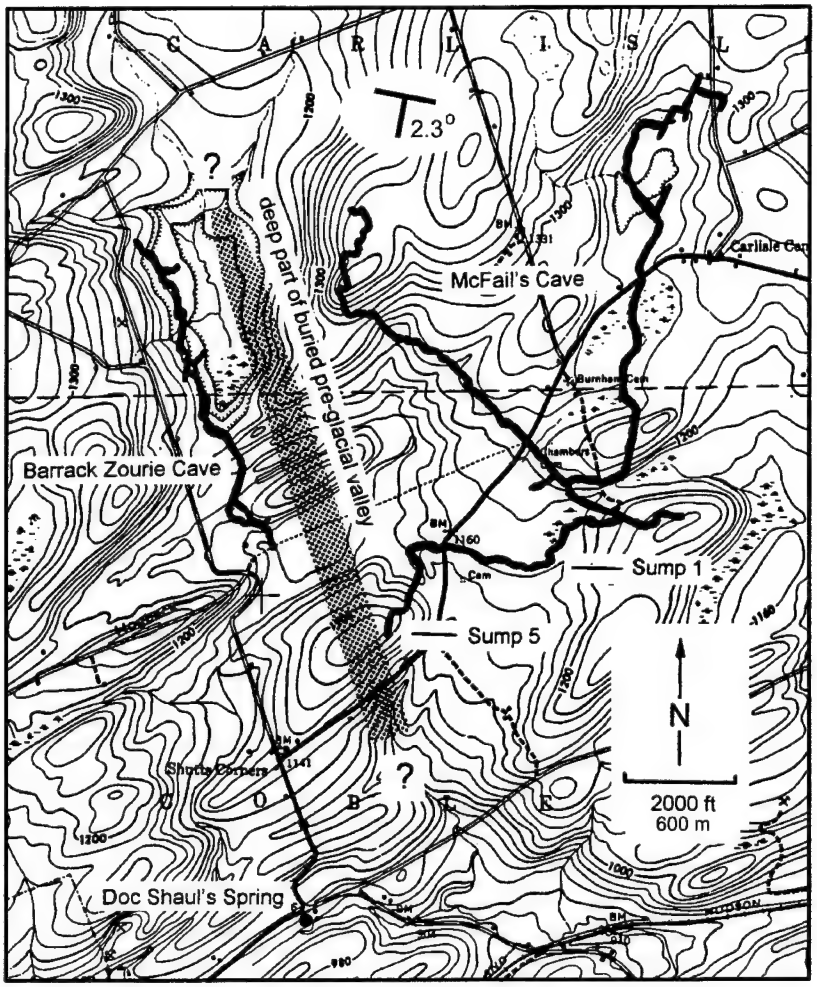

Figure 9: Plan view of two New York caves in prominently fractured Silurian-Devonian strata that dip 2.3 degrees to the south-southwest. McFail's Cave, to the east, consists of a down-dip canyon that merges with a nearly strike-oriented tube. Despite conspicuous jointing, much of the cave is guided by a few major bedding-plane partings and low-angle thrust faults. The southern extension is a relatively recent diversion passage. Barrack Zourie Cave, to the west, follows the contours of a buried pre-glacial valley (shaded) and has more prominent fracture control. If its vadose passages had followed the dip direction, it would have extended beneath an undissected plateau capped by less soluble strata. Stress release along the walls of the valley has provided a more favorable route. In such highly fractured strata this deviation of vadose passages away from the dip is more probable than in prominently bedded rocks. Some of the strata here are thin bedded, but discordant fractures cut across entire rock formations and transmissive bedding-plane partings are sparse. Linear cave trends along fractures are masked on these small-scale, generalized maps.

even in well-bedded strata. The influence of floodwaters on cave origin in these settings also helps to obscure the relationships to dip and strike. Another example is shown in Figure 9, where stress release along the steep walls of a pre-glacial valley has favored cave development along the valley margin, independent of the dip, despite the fact that other caves in the area show prominent dip and strike relationships.

One should anticipate that the dip configuration may have changed since the origin of the solution conduits. There are many examples in the Madison Limestone of the Rockies, where late Cretaceous or Tertiary tectonism has disrupted the original structure in which many now-relict caves were formed during the Paleozoic. The problem is more subtle in caves that were formed in the present geomorphic setting, but where tectonics, isostatic movements, or erosional unloading have disrupted the original structure. This problem is likely only in low-dip settings, where tiny changes in bedding attitude can have a large effect on local dip directions. This possibility should be investigated wherever measurements show a poor correlation between what otherwise should be clear dip-oriented vadose trends.

It is common for field researchers to attribute cave trends simply to the prevailing hydraulic gradient, without reference to stratal dip effects. Many of these statements are backed by specific examples. However, these examples are rarely based on actual structural mapping within the caves. The cave in Figure 2 is a good example that seems to defy the influence of dip on vadose passages. However, leveling surveys show that the dip is reversed in this area. The seemingly erratic conduit patterns in low-dip strata are largely the result of variations in local dip, which are rarely discernible on surface geologic maps. Many examples have been demonstrated in the Mammoth Cave region (Palmer, 1989). As a further complication, dip-influenced vadose development in many caves has superseded phreatic development as the result of a drop in base level. It must not be assumed that the lowest passages in a cave are invariably phreatic.

Some caves show no relation to the ideal pattern of Figure 1. In general they formed under hypogenic or confined con-

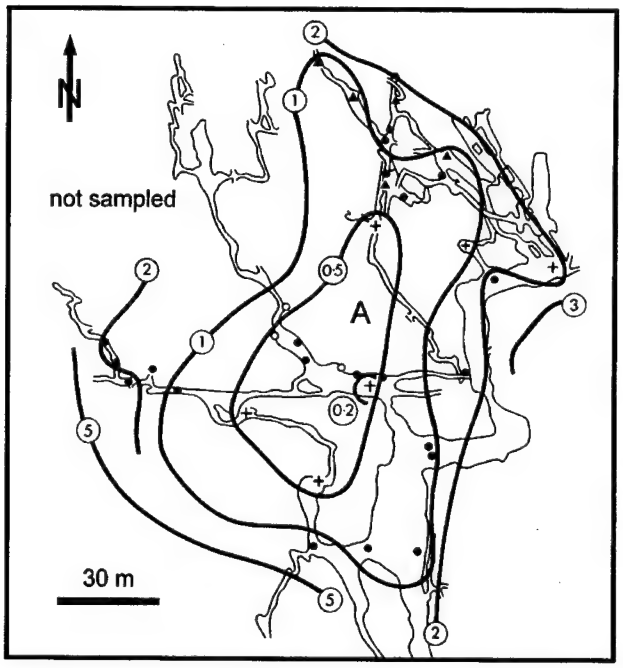

Figure 10: Distribution and first-arrival time (days) or vadose seepage into underlying cave passages in GB Cave, Mendip Hills, U.K., as determined from dye injection at point A (from Smart and Friederich, 1986). The carbonate units are prominently fractured and dip steeply southward. Vadose seepage tends to be highly dispersed, in contrast to the flows that are capable of forming conduits.

ditions and lie outside the scope of this paper. They reveal very little about the patterns of meteoric groundwater flow.

The observations in this paper apply only to major flow paths that have the potential of forming solution conduits. Small amounts of vadose seepage are capable of dispersing among many different flow routes as the result of overflow into, or leakage through, neighboring fissures. Tracer studies often show great dispersion of flow through karst aquifers, especially in the vadose zone (Figure 9). Thrailkill and Robl (1981) distinguished between vadose seepage and vadose flows, where only the latter are able to form cave passages. They suggested a minimum discharge of about 1 cm^3/sec for flows. Phreatic seepage, in contrast, tends to be tributary to the major conduits, at least during low flow. It consists of laminar flow through fissures with little or no solutional enlargement. A knowledge of conduit trends is thus vital to the interpretation of the surrounding laminar flow.

What of the deep-basinal flow described earlier as the precursor to epigenic cave development? Evidence for its influence on accessible caves is scant, even in aquifers in which deep flow has been presently documented. For example, the Illinois Basin contains deep flow paths along sulfate zones within the St. Louis Limestone (Krothe and Libra, 1983). Around the perimeter of the Illinois Basin, the St. Louis also contains some of the longest caves in the U.S. (e.g. Hidden River Cave, Kentucky). Presumably, if deep flow once occurred in the same strata, it must have created preferential paths for cave development. Careful mapping has been aimed specifically toward identifying passages out of adjustment with the present shallow groundwater pattern, but there is very little evidence of early, deep flow paths. Why not? There are several possible reasons: (1) The deep flow paths may be very sparse. (2) Deep sulfate-hosted openings may collapse and thus be represented only by intrastratal breccias. (3) The early flow paths may be so out of adjustment with shallow meteoric flow that they tend to be bypassed by meteoric groundwater flow and eventually become filled with sediment. (4) The sulfate-rich beds that favor deep flow may not have extended into the marginal parts of the basin where the presently accessible caves are. Local zones of former sulfate nodules produce minor pockets in cave walls in certain stratigraphic horizons, which have no significant influence on the cave origin or pattern. Thus it appears that this fourth hypothesis is at least partially valid. (5) Or perhaps they *are* utilized and are simply modified to look as though they were formed by shallow flow. But if so, they should not possess the strong relation to the local dip and strike that has been demonstrated here. Deep-seated dissolution must have some effect in guiding the paths of presently accessible caves formed by unconfined meteoric water, but in most karst areas its influence is limited and subtle.

Many caves show clear evidence of having concentrated along relatively few bedding-plane partings. Much of McFail's Cave (Figure 8) follows a few major partings near the contact between the Manlius Limestone and the overlying Coeymans Limestone. Do these represent inception horizons that have been prepared by deep flow for preferential cave development by shallow water? This is unlikely because of the strong relationship of the passages to the dip and strike. These zones are favored by cave development because thin shaly beds have allowed prominent partings to appear along certain bedding planes in an otherwise highly fractured unit.

Conclusions

This paper gives a simple but effective first approximation of vadose and phreatic conduit trends in unconfined karst aquifers fed by meteoric groundwater. It probably also represents the major pre-conduit flow patterns. Exact numerical values should not be taken literally, because a larger data base and more detailed analysis is warranted. However, in the absence of any other data, there is no harm in using this as a rough guide to the major flow patterns in

karst. It is not likely that further sampling will greatly change the results shown here.

An interesting aspect of the control of stratal attitude on passage orientation is the enormous range of scales that it spans. At the largest scale, for example that of entire carbonate massifs, much groundwater flow is oriented down the dip slopes of tectonic uplifts (Maire, 1990). Many of the world's deepest caves are vadose systems perched within steeply dipping beds and concentrated along synclinal axes. At the smallest scale, structural mapping shows that the individual bends within many sinuous passages are simply following the contours of minor depositional irregularities (Palmer, 1989; see also Figure 2).

Some puzzles remain, such as the relation between deep early flow and shallow cave development, which invite further field investigation. For this study to be considered statistically valid, despite its large sample size, the question must be addressed as to whether it is representative of the entire population of caves in each category (a very slippery concept, since the total population will never be known), and whether the members of each sampling group are sufficiently homogeneous and random.

References cited

Ford, D.C., 1965, The origin of limestone caverns: a model from the central Mendip Hills, England: National Speleological Society Bulletin, v. 22, no. 1, p. 109-132.

Ford, D.C., 1971, Geologic structure and a new explanation of limestone cavern genesis: Transactions of the Cave Research Group of Great Britain, v. 13, no. 2, p. 81-94.

Ford, D.C., and R.O. Ewers, 1978, The development of limestone cave systems in the dimensions of length and depth: Canadian Journal of Earth Sciences, v. 15, p. 1783-1798.

Klimchouk, A., in press, Spelogenesis under deep-seated and confined settings, *in* A. Klimchouk, D.C. Ford, A.N. Palmer, and W. Dreybrodt (eds.), Speleogenesis: evolution of karst aquifers: Huntsville, Ala., National Speleological Society.

Krothe, N.C., and R.D. Libra, 1983, Sulfur isotopes and hydrochemical variations in spring waters of southern Indiana, U.S.A.: Journal of Hydrology, vol. 61, p. 267-283.

Lowe, D.J., 1992, The origin of limestone caverns: an inception horizon hypothesis: Ph.D. thesis, Manchester Metropolitan University, U.K.

Maire, R., 1990, La haute montagne calcaire: Karstologia-Mémoires no. 3, La Ravoire, France, Editions Gap, 731 p.

Palmer, A.N., 1972, Dynamics of a sinking stream system, Onesquethaw Cave, New York: National Speleological Society Bulletin, v. 34, no 3., p. 89-110.

Palmer, A.N., 1976, Geologic influence on passage orientation in Ludington Cave, Greenbrier County, West Virginia: Proceedings of Fourth Conference on Karst Geology and Hydrology, West Virginia Geological and Economic Survey, p. 33-40.

Palmer, A.N., 1986, Prediction of contaminant paths in karst aquifers: Proceedings of First Conference on Environmental Problems in Karst Terranes and Their Solutions, Dublin, Ohio, National Water Well Association, p. 32-53.

Palmer, A.N., 1989, Stratigraphic and structural control of cave development and groundwater flow in the Mammoth Cave region, *in* W.B. White and E.L. White (eds.), Karst Hydrology: concepts from the Mammoth Cave area: New York, Van Nostrand Reinhold, p. 293-316.

Sasowsky, I.D., and W.B. White, 1994, The role of stress release fracturing in the development of cavernous porosity in carbonate aquifers: Water Resources Research, v. 30, no. 12, p. 3523-3530.

Smart, P.L., and H. Friederich, 1986, Water movement and storage in the unsaturated zone of a maturely karstified carbonate aquifer, Mendip Hills, England: Proceedings of First Conference on Environmental Problems in Karst Terranes and Their Solutions, Dublin, Ohio, National Water Well Association, p. 59-87.

Thrailkill, J., and T.L. Robl, 1981, Carbonate geochemistry of vadose water recharging limestone aquifers: Journal of Hydrology, vol. 54, p. 195-208.

Worthington, S.R.H., 1991, Karst hydrogeology of the Canadian Rocky Mountains: Ph.D. dissertation, McMaster University, Hamilton, Ont., 227 p.

ACQUISITION AND APPLICATION OF FIELD DATA

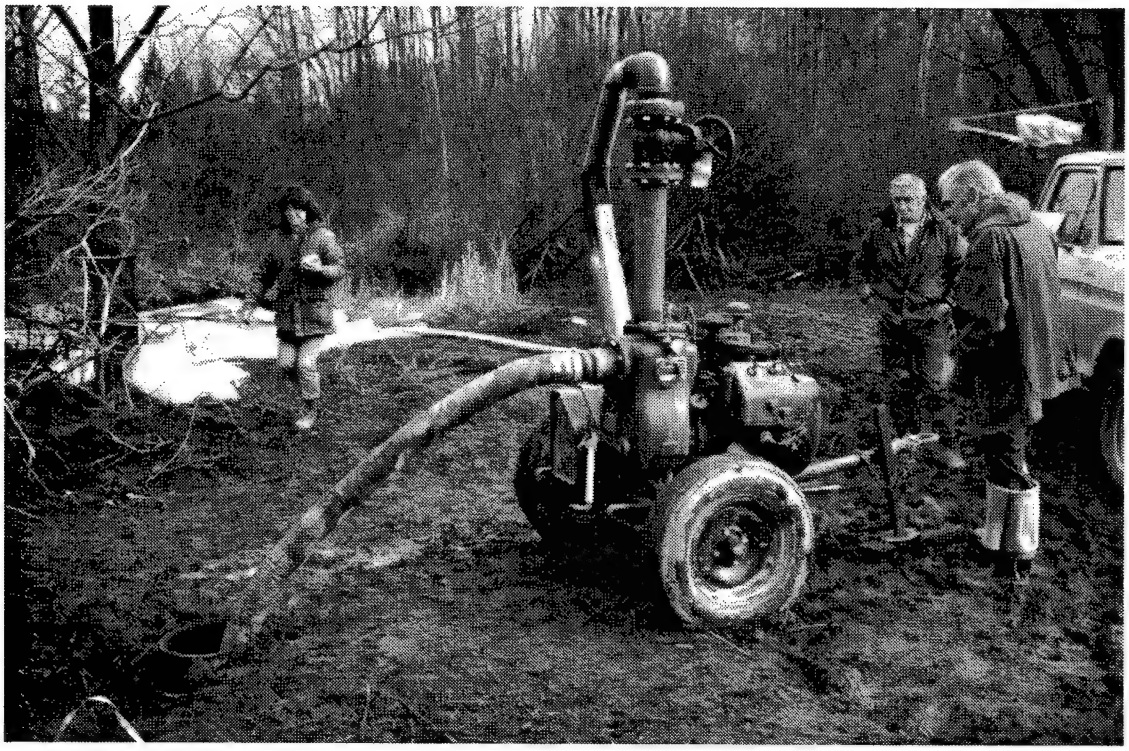

It is essential that models be based on solid field evidence, and that any conclusions from the model be validated in the field. The acquisition of appropriate field data should be not only the first step in modeling, but a continuing process throughout the project. That is the explicit message of several of the papers in this concluding section.

There are many different kinds of karst, as the papers in this volume show. When beginning a field project, the most fundamental piece of information to ascertain is the geomorphic province in which the karst area lies. Within each province the nature of karst tends to be similar. At a smaller scale, the specific stratigraphic units that host the karst determine the nature of the pre-solutional porosity. The geomorphic layout of the aquifer determines the pattern of groundwater recharge and discharge.

Although the nature of the karst hydrology tends to be rather uniform within the same formation and physiographic setting, it can differ a great deal from that in other provinces and strata. Simple as this observation may seem, it is surprising how many field studies focus on local details without much thought as to the overall picture.

At this broad scale, most of the appropriate information is available from state geological surveys and from published reports and maps. Specific details about local carbonate aquifers must be obtained from a combination of well tests, tracer tests, cave information, spring hydrographs, thermographs, and chemographs, and similar quantitative methods. Examples are described in the papers that follow. Additional guidelines can be found in the references at the end of the Introduction.

Throughout any field investigation, especially in karst, it is wise to avoid too narrow an approach. Any study that is based solely on one or two of the above approaches is certain to overlook critical information at other scales within the aquifer.

BRIDGING THE GAP BETWEEN REAL AND MATHEMATICALLY SIMULATED KARST AQUIFERS

Chris Groves[1], Joe Meiman[2], and Alan D. Howard[3]

[1]Center for Cave and Karst Studies, Department of Geography and Geology
Western Kentucky University, Bowling Green, KY 42101
[2]Division of Science and Resource Management, Mammoth Cave National Park,
Mammoth Cave, KY 42259
[3]Department of Environmental Sciences, University of Virginia, Charlottesville, VA 22903

Abstract

Although several numerical codes have been developed to study the patterns of karst aquifer evolution and behavior, in the current generation of models simplifying assumptions must be made because of incomplete quantitative understanding of key processes. A one-year, high-temporal-resolution study of carbonate chemistry with Mammoth Cave's Logsdon River, designed to investigate details of these processes, reveals that limestone dissolution rates vary appreciably over storm and seasonal time scales due to variations in the flux of CO_2-rich waters that wash through, and flood, conduits during storm events. This undersaturated storm water dissolves rock within a flood zone 25-30 m thick. Through the year, waters were undersaturated only 31% of the time. Time scales of actual karst development may thus be impacted by time-varying processes different from the constant-input chemistry assumed in current published numerical codes.

A dual approach, coupling quantitative modeling and refinement of the models by careful measurement of processes within real karst aquifers, provides a framework for developing a comprehensive understanding of karst system behavior.

Introduction

Significant progress has been made in the development of mathematical models of karst aquifers, particularly for those that study long-term evolution of flow patterns and conduit sizes. These models use coupled expressions describing fluid flow and limestone dissolution kinetics to shed light on details and time scales of the karst development process, and have included, for example, models of single conduits (Dreybrodt, 1988, 1990; Palmer, 1991; Groves and Howard, 1994a); and network development (Figure 1; Kraemer, 1990; Groves and Howard, 1994b; Howard and Groves, 1995; Clemens et al., 1996; Annable and Sudicky, 1997; Siemers and Dreybrodt, 1998). Although this work is theoretical and abstract, it represents a critical step in the ultimate development of models aimed at solving applied karst environmental problems because it *helps us understand how karst systems work.* Without this understanding, we are just fumbling in the dark when we attempt either environmentally related planning or remedial actions. Not only do the histories of water resource development and engineering in karst landscapes bear this out, but in some cases legal regulations are still based on an inadequate understanding of karst groundwater flow.

What are the limitations of the modeling approach? Because they start from first principles, models of this type are necessarily idealized constructs that attempt to capture flow-system behavior in a way that is realistic enough to provide meaningful inferences about long-term processes and patterns of dissolution. However, numerous simplifying assumptions must be made. The first is to simplify the physics and chemistry in the interest of mathematical tractability and computational efficiency. The "numerical fluids" within the conduit systems of Howard and Groves (1995), for example, are subject to a variety of assumptions concerning incompressibility, constant properties, certain negligible gradients, and fully developed, steady-state flow. Input chemical conditions,

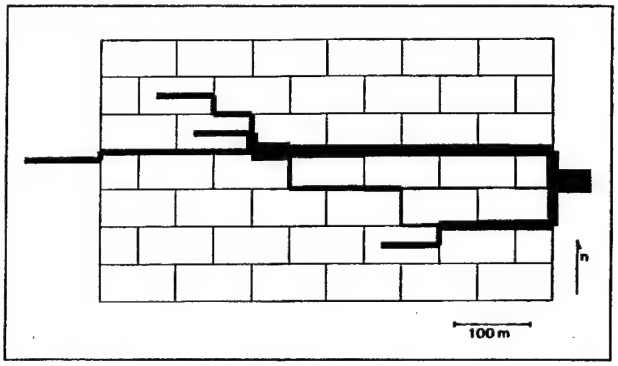

Figure 1: Mathematically simulated karst flow system designed with coupled expressions describing fluid flow and limestone dissolution kinetics to study factors that determine conduit selectivity (Groves and Howard, 1994b).

specified by CO_2 pressure and temperature, are constant, and the conduits are kept fully saturated. In the continuing evolution of this work, limitations due to these types of assumptions are a temporary problem only, with the rapidly evolving memory capacities of personal computers, and as future investigators develop new generations of codes evolving from the earlier efforts.

Another, more difficult problem is that we still have incomplete understanding and quantitative descriptions of many of the important processes that in real aquifers may significantly impact carbonate chemistry, conduit growth rates, and transport of dissolved species, contaminants, and sediment. To better understand these we have to go into the caves themselves. A dual approach, which couples quantitative modeling and refinement of the models by careful measurement of processes within real karst aquifers, provides a framework within which we can ultimately develop a comprehensive understanding of karst system behavior.

Motivated by this need, an ongoing hydrologic research program is currently underway at Mammoth Cave National Park by a consortium of scientists and students from the National Park Service, the Center for Cave and Karst Studies at Western Kentucky University, and the Cave Research Foundation. This work is taking place in various parts of the Mammoth Cave System, primarily in Losgdon River, especially near its confluence with Hawkins River in the Proctor Cave section of the system, and the Echo River/ River Styx Complex within Mammoth Cave Ridge.

The assumption of a system of continually phreatic conduits with constant input conditions may be a reasonable approximation of the earliest stages of evolution of a karst flow system, but as the aquifer evolves, changes inevitably occur that compromise the relatively restrictive assumptions of the current generation of published numerical models. As conduits enlarge and overall flow resistance decreases, flow and chemical conditions can fluctuate rapidly in response to storm recharge. Dissolution and the associated evolution of the aquifer framework increasingly takes place within a floodwater zone, where water levels can fluctuate rapidly over as much as tens of meters, and at any moment individual fractures and conduits can be saturated, partly filled, or dry. Analysis of the locations and elevations of 47 km of surveyed cave passages within Kentucky's Martin Ridge Cave System (Glennon, 1998), for example, reveal that about 30% of the conduits contain perennial, free-surface streams that only partially fill the conduits during low-flow conditions, 10% vary from dry to saturated (and thus potentially dissolving) throughout a 25 m thick floodwater zone, and the remainder are permanently abandoned.

A key goal of our field program is to understand the distribution of water/rock interactions, and thus aquifer development, within the floodwater zone of the Mammoth Cave karst aquifer. This paper reports on the results of a one-year sampling program (May 5, 1995 to May 4, 1996) designed to evaluate the spatial and temporal distribution of the flow and carbonate chemistry of aquifer fluids in the vicinity of the confluence of the Logsdon and Hawkins River. These are two of the major underground rivers of the humid-temperate south-central Kentucky karst aquifer.

Field site

The south-central Kentucky karst is located within the broad karst region that extends through the Interior Low Plateaus of the southeastern United States, and is among the most extensively developed, well explored, and intensively studied of the world's karst landscapes (White *et al.*, 1970; Hess, 1974; White and White, 1989). Within one part of this region, beneath an area of about 100 km^2 between the Green and Barren Rivers of south-central Kentucky, over 800 km of cave passages have been explored and surveyed. This includes 560+ continuous km in the Mammoth Cave System, the world's longest known cave. The aquifer is developed within a 160 m thick section of nearly horizontal, Upper Mississippian limestones of the St. Louis, Ste. Genevieve, and Girkin Formations (Pohl, 1970; White *et al.*, 1970; Palmer, 1981). The limestones are intermixed with minor chert and dolomite layers, and in the northern part of the study area, are covered by flat-lying clastic caprocks (primarily the Big Clifty Sandstone) that form the dissected Mammoth Cave Plateau.

Logsdon River is one of the major underground streams of the south-central Kentucky karst. Within the Proctor Cave section of the system, near the southwestern currently explored edge of Mammoth Cave, Logsdon River converges with Hawkins River, which drains about 75 km^2 near Park City, Kentucky. About 100 m upstream from the confluence of the two rivers are two sets of 15 cm diameter, 145 m deep observation wells, with two wells intersecting each river. At each location, one well is equipped with a compressor-driven pump for collecting water samples from the surface, and through the other electronic probes deliver high-resolution (two-minute) data on stage, velocity, temperature, and specific conductance. The bottoms of the wells can be reached underground (for pump and probe installation and maintenance) through the Doyel Valley Entrance to Mammoth Cave, requiring a 3 km round-trip through the cave.

The conduit at the Logsdon River well site is about 3 m tall and 7 m wide (Figure 2), and lies near the downstream end of one of the world's longest known sections of accessible underground river passage, continuously traversable for

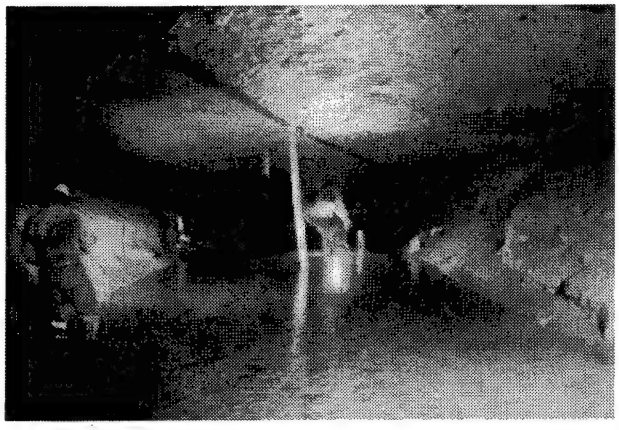

Figure 2: Losgdon River, Mammoth Cave Kentucky, showing the bottom three meters of a 145 m deep well through which water samples are collected under varying conditions. Another well, just out of the picture in the sediment alcove along the left side of the passage, delivers probes that measure temperature, stage, specific conductance, and velocity with two-minute resolution. Photo by Chris Groves.

over 8 km. At the Logsdon wells the river drains an area of about 25 km^2. Waters at the Logsdon River site reflect the recharge characteristics of this dissected plateau region, with 38% of the flow draining the clastic rocks, and 62% reaching the aquifer as direct recharge onto the karst surface, primarily through sinkholes.

Methods

The primary objective of the research has been to collect sufficient high-resolution data on both flow and chemical characteristics of the river to quantitatively evaluate the magnitudes and rates of change of carbonate chemistry and water/rock interactions at a variety of time scales. Four probes were installed into the river through one of the 145 m deep wells that intersect Logsdon River, including temperature, specific conductance, stage, and velocity. A Campbell 21X multichannel data logger queries the probes every thirty seconds and averages these readings every two minutes. The logger is programmed to record data at varying intervals, from every two minutes during rapidly changing flow or chemical conditions in the rivers to hourly during static conditions.

Hourly water-chemistry measurements have also been made during storms of various magnitudes by sampling from the surface through the second well using a compressor-driven Bennett pump (Hall, 1997; Meiman and Groves, 1997; Anthony, 1998). With this information we have used regression analysis to relate high-resolution specific conductivity data from within the river to calcium, magnesium, and bicarbonate concentrations, as well as hydrogen-ion activities. These derived parameters, along with direct temperature measurement, then allow calculation of several important components of carbonate system behavior with high temporal resolution, including the saturation state of the groundwater with respect to the calcite making up the limestone bedrock, carbon dioxide pressure, and calcite dissolution rates.

We have also studied sediment samples collected in late summer from the bed of Logsdon River and examined individual grains using scanning electron microscopy.

Analyses

Values describing the carbonate system used in our calculations were obtained by regression between specific conductance (spC), measured in Logsdon River with two-minute resolution, and direct measurements of Ca, Mg, HCO_3, and pH under a wide range of conditions. Significant linear relations were found for bicarbonate and the cations, and a third-order expression was fit to hydrogen activities. Water samples used in the regressions have been collected during storms at various seasons, and there does not appear to be a seasonal dependence on any of the relationships. Continuing study of the seasonal changes in carbon flux and impacts on carbonate water chemistry at the site is underway (Anthony, 1998).

Because of the relationships between carbonate mineral dissolution rates and the relatively short residence times for waters within many karst flow systems, these waters are often out of thermodynamic equilibrium with respect to the limestone aquifer framework. Both equilibrium chemistry and kinetics of the dissolution reactions must thus be considered in order to understand the evolution of the systems, as well as the waters that flow through them. An instantaneous measure of the state of the fluid/rock interaction with respect to this equilibrium condition is provided by the calcite saturation index (SI_{cal}):

$$SI_{cal} = \log_{10}\left(\frac{[Ca^{2+}][CO_3^{2-}]}{K_{cal}}\right) \qquad (1)$$

where activities are designated by square brackets, and K_{cal} is the equilibrium constant for calcite dissolution. Carbonate activities are generally very low at the pH ranges of karst groundwaters, and were calculated from HCO_3^-, pH, and temperature, using appropriate equilibria. Negative and positive S.I. values predict undersaturated and oversaturated conditions, respectively, while a value of zero predicts thermodynamic equilibrium. Expressions for the temperature dependence of calcite and carbonate system equilibria developed by Plummer et al. (1976) and Plummer and Busenberg (1982), were used in our cal-

culations. Activity corrections used the extended Debye-Hückel limiting law (Stumm and Morgan, 1981), and our aqueous model assumes that the impact of ion pairing and complexation on calculated results is negligible.

Carbon dioxide pressure (PCO_2[atm]), was also calculated for each observation

$$PCO_2 = \frac{[H_2CO_3^*]}{K_H} \quad (2)$$

where K_H is the Henry's Law constant for dissolution of CO_2 gas in water (Plummer et al., 1976; Plummer and Busenberg, 1982), and H_2CO_3* is the sum of H_2CO_3 and aqueous CO_2 (Stumm and Morgan, 1981).

Calculation of limestone dissolution rates assumed reaction-limited kinetics, and used the expression of Plummer et al. (1978):

$$RATE = k_1[H^+] + k_2[H_2CO_3^*] + k_3[H_2O] - k_4[Ca^{2+}][HCO_3^-] \quad (3)$$

where the k values are temperature-dependent rate constants (Plummer et al., 1978), and rates are given in mass per surface area of mineral/fluid contact per time. Assuming a limestone density of 2.7 g/cm^3, we report dissolution rates in mm/yr of wall retreat. With data resolution varying from two minutes during storms to hourly during static conditions, these values were calculated for 21,473 observations between May 5, 1995 to May 4, 1996. Equipment problems led to a loss of 19.9 days (5.4% of the period) of conductance data during the year. With the large number of conductance chemographs during storms over the rest of our study period, however, we were able to closely estimate these missing periods using a procedure analogous to unit-hydrograph analysis (Chow, 1964). In addition, electrical problems created offsets of the data (29.2 days, or 8.0%) that were corrected by calibration and translation.

Results and discussion

Fifty-six storm events caused measurable changes in the flow or chemistry within Logsdon River during the study (Figure 3), with thirteen of the storms flooding the conduit to the ceiling. The lower, horizontal line across Figure 3, at

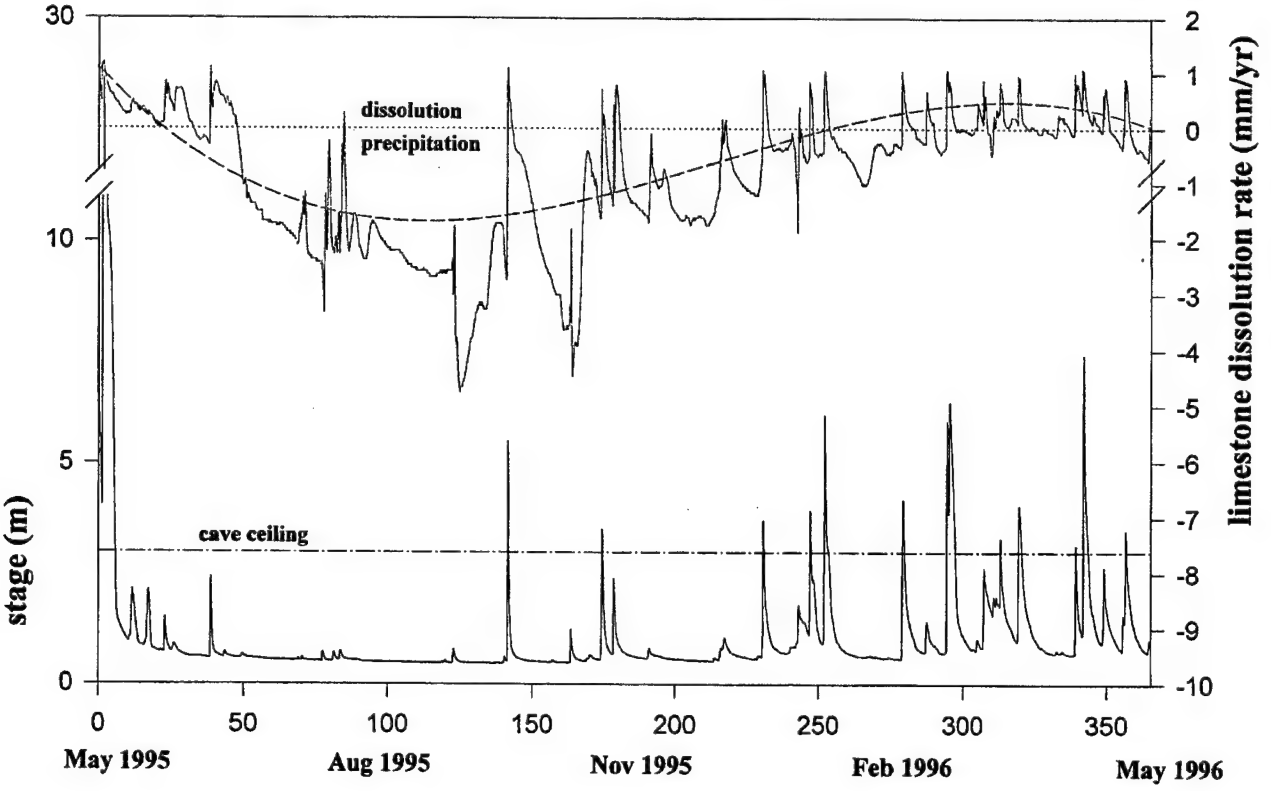

Figure 3: Stage and calculated limestone dissolution rates for 21,473 observations between May 5, 1995 to May 4, 1996 in Logsdon River. Measurements were made with two minute resolution, recorded hourly during static conditions. Rate calculations used the expressions of Plummer et al. (1978). The horizontal line in the bottom figure shows the level of the cave ceiling at the study site, and that in the upper figure indicates calculated equilibrium with respect to calcite dissolution. Negative dissolution rates predict calcite precipitation.

3 m stage, corresponds to the cave ceiling. During the largest storm, on May 8, 1995, the water level reached a maximum height of 28.2 m, with a maximum rate of rise of 6.03 m/hr. The ceiling of the conduit under these conditions is about 25 m below the water table, and the conduit remained totally flooded for 114 hours.

Calculated calcite saturation indices for the year show that at various times the water at this point in the river may be either undersaturated or oversaturated, thus conduit enlargement is episodic, and closely associated with storms, as passages are washed with relatively undersaturated, high-PCO_2 waters. The waters were undersaturated, and thus capable of enlarging the conduit, only for 113.6 days, or 31.6%, of the year, with saturation indices ranging from -1.11 to a maximum of +0.67. These showed both storm- and seasonal-scale patterns and are closely related to the distribution of CO_2 pressures. The fractures and conduits throughout the floodwater zone above local base level experience flow only periodically, with a decreasing probability higher above base level, but when fluids do reach these areas, they are relatively high in CO_2 and undersaturated with respect to calcite.

Calcite dissolution rates also have a flashy, storm-scale pattern (Figure 3), with instantaneous calculated rates during the year ranging from around one mm/year to predicted precipitation of up to four mm/yr. Negative dissolution rates on the upper part of Figure 3 predict precipitation. The mean condition is 0.13 mm/year of precipitation, which would suggest an overall net deposition over the year. Several observations, however, suggest that precipitation is limited. It has been reported in other settings that SI_{cal} values on the order of about +1 are required to exceed kinetic thresholds required for the initiation of calcite precipitation (e.g., Herman and Lorah, 1988), and the maximum calculated SI values during the study period were less than 0.7. No macroscopic physical evidence of travertine depostion, such as rimstone dams, is present at the site. We have examined bed-sediment grains collected at the end of the fall dry period (October, 1996) under a scanning electron microscope, and washed sediment in acid to identify increased calcium concentrations, and have found evidence for calcite coatings. It is not clear, however, whether this precipitation occurred at the site, or when the grains were further upstream, where rimstone is common in some areas. Making the assumption that solutions do not become sufficiently oversaturated during the year to initiate calcite precipitation at the site, by setting all negative rates to zero, the mean calculated rate becomes 0.36 mm/year of dissolution.

Dissolution rates (Figure 3), saturation indices, and CO_2 pressures each show a sinusoidal seasonal pattern with a minimum dissolution rate in the dry months of late summer and early fall, and a peak in the early spring. Our data suggest that CO_2 pressures at this point in the river system, in the lower end of the basin, are influenced primarily by the relative contributions of high-PCO_2 recharge from discrete inputs and during storms, and lower-PCO_2 diffuse flow inputs. The latter have been in close, prolonged contact with limestone, and much of the gas has been consumed by the resulting carbonate mineral dissolution. This seasonality in CO_2 pressures, and thus dissolution rates, is more closely in phase with seasonal hydrologic changes (including the influence of both precipitation and evapotranspiration rates) than changes in seasonal soil CO_2 levels, which are in general highest in the warm seasons.

With regard to the development of quantitative models of karst aquifer behavior and development, we conclude that fluctuations in both flow and chemical conditions at a variety of time scales may significantly influence aquifer behavior. As these models (and the questions we are able to investigate with them) evolve, they should be calibrated with the results from studies of the dynamics of real karst systems. It is only through these types of quantitative observations that we can ultimately determine which processes are important, and how they might impact the success with which quantitative models (and what they teach us) reflect the real systems that we set out to study in the first place.

Acknowledgments

The authors would like to express their appreciation to Darlene Anthony, Phil Bodanza, Rachel Bosch, Deven Carigan, John Fry, Alan Glennon, Deana Groves, Cliff Hall, Marlowe Howard, Beth Miracle Meiman, Ryan Smith, Kevin Vaughan, and the Division of Science and Resource Management at Mammoth Cave National Park for assistance with this research. Financial support of this work has been provided by Western Kentucky University and the National Park Service.

References cited

Annable, W., and E. Sudicky, 1997, Simulation of karst genesis: hydrodynamic and geochemical rock-water interactions in partially-filled conduits: 6th Conference of Limestone Hydrology and Fissured Aquifers: Modeling in Karst Systems, p. 1-7.

Anthony, D.M., 1998, Seasonal effects on the geochemical evolution of the Logsdon River, Mammoth Cave, Kentucky: M.S. thesis, Center for Cave and Karst Studies, Department of Geography and Geology, Western Kentucky University, 140 p.

Chow, V.T., 1964, Runoff, *in* V.T. Chow (ed.), Handbook of applied hydrology: New York, McGraw-Hill, p. 14.1-14.54.

Clemens, T., D. Hückinghaus, M. Sauter, R. Liedl, and G. Teutsch, 1996, A combined continuum and discrete network reactive transport model for the simulation of karst development, *in* Calibration and Reliability in Groundwater Modeling. Proceedings of the ModelCARE 96 Conference: Colorado, I.A.H.S. publication 237, p. 309-318.

Dreybrodt, W., 1988, Processes in karst systems: New York, Springer-Verlag, 288 p.

Dreybrodt, W., 1990, The role of dissolution kinetics in the development of karst aquifers in limestone: a model simulation of karst evolution: Journal of Geology, vol. 98, p. 639-655.

Glennon, J.A., 1998, Hydrogeology and morphometric analysis of the Martin Ridge Cave System, Edmonson County, Kentucky: M.S. thesis, Center for Cave and Karst Studies, Department of Geography and Geology, Western Kentucky University.

Groves, C.G., and A. D. Howard, 1994a, Minimum hydrochemical conditions allowing limestone cave development: Water Resources Research, vol. 30, p. 607-615.

Groves, C., and A.D. Howard, 1994b, Early development of karst systems: 1. Preferential flowpath development under laminar flow: Water Resources Research, vol. 30, p. 2837-2846.

Hall, C., 1996, Assessment of karst groundwater quality relative to contaminant transport within the Turnhole Spring Groundwater Basin, Mammoth Cave National Park, Kentucky: M.S. thesis, Department of Geology, Eastern Kentucky University.

Herman, J., and M. Lorah, 1988, Calcite precipitation rates in the field: measurement and prediction for a travertine-depositing stream: Geochimica et Cosmochimica Acta, vol. 52, p. 2347-2355.

Hess, J., 1974, Hydrochemical Investigations of the Central Kentucky Karst Aquifer System: Ph.D. thesis, Department of Geosciences, The Pennsylvania State University.

Howard, A.D., and C.G. Groves, 1995, Early development of karst systems: 2. Turbulent flow: Water Resources Research, vol. 31, p. 19-26.

Kraemer, S., 1990, Modeling of regional groundwater flow in fractured rock aquifers: Ph.D. dissertation, School of Public and Environmental Affairs, Indiana University, Bloomington.

Meiman, J. and C.G. Groves, 1997, Frequency/magnitude study of cave passage development in the Central Kentucky Karst: Proceedings of the Sixth Mammoth Cave Science Conference, Mammoth Cave, KY

Palmer, A., 1981, A geological guide to Mammoth Cave National Park: Teaneck, NJ: Zephyrus Press, 196 p.

Palmer, A., 1991, The origin and morphology of limestone caves: Geological Society America Bulletin, vol. 103, p. 1-21.

Plummer, L.N., and E. Busenberg, 1982, The solubilities of calcite, aragonite, and vaterite in CO_2-H_2O solutions between 0 and 90°C , and an evaluation of the aqueous model for the system $CaCO_3$-CO_2-H_2O: Geochimica et Cosmochimica Acta, vol. 46, p. 1011-1040.

Plummer, L.N., T.M.L. Wigley, and D.L. Parkhurst, 1978, The kinetics of calcite dissolution in CO_2-water systems at 5 to 60°C and 0.0 to 1.0 atm CO_2: American Journal of Science, vol. 278, p. 179-216.

Pohl, E.R., 1970, Upper Mississippian deposits of south-central Kentucky: Kentucky Academy of Science Transactions, vol. 31, p. 1-15.

Quinlan, J.F., and R.O. Ewers, 1981, Hydrogeology of the Mammoth Cave region, Kentucky, *in* T.G. Roberts (ed.), GSA Cincinnati '81 Field Trip Guidebook 3, Falls Church: American Geological Institute, p. 457-506.

Siemers, J., and W. Dreybrodt, 1998, Early development of karst aquifers on percolation networks of fractures in limestone: Water Resources Research, vol. 34, p. 409-419.

Stumm, W., and J. Morgan, 1981, Aquatic chemistry, an introduction emphasizing chemical equilibria in natural waters: New York, John Wiley and Sons, 780 p.

White, W.B., and E. White, 1989, Karst hydrology: concepts from the Mammoth Cave area: New York, Van Nostrand Reinhold, 364 p.

White, W.B., R.A. Watson, E.R. Pohl, and R. Brucker, 1970, The central Kentucky karst: Geographical Review, vol. 60, p. 88-115.

THE DEVELOPMENT OF BASIN-SCALE CONCEPTUAL MODELS OF THE ACTIVE-FLOW CONDUIT SYSTEM

Joe Meiman
Office of Science and Resource Management, Mammoth Cave National Park, KY 42259

Martin T. Ryan
ERM Southeast, Brentwood TN 37027

Abstract

In the development of a conceptual model for conduit flow, the most fundamental aquifer unit, the groundwater basin, defines the spatial boundary of the model while storm-scale responses provide temporal limits. Within the basin, the framework of the model develops as the relationships between recharge (sinking streams and sinkholes), transfer mechanisms (conduits), and discharge points (springs) are revealed. Several investigative methods are used, including rigorous qualitative dye tracing, and intensive monitoring of physical and chemical properties of the groundwater during storm-pulse activity. The combination of these techniques may reveal details that could be missed if only one method were used. Three basin-scale conceptual models were developed at Mammoth Cave National Park. Methods used were largely dictated by access points to the active conduits within aquifer.

Introduction

At the core of modeling is the ability to predict or interpolate, with a relatively high degree of certainty, the outcome of an unknown based upon a set of known variables and assumptions. The best models are derived from large and accurate data bases and mathematical expressions that give a detailed description of the known conditions and variables. In the best-understood karst setting, the most detailed and accurate information on the flow conduits is described by a cave survey. A survey team, with compass, tape, and book, creates a descriptive graphic and spatial narrative of the traversable cave. Passage dimensions and orientations are measured, physical appearance described, tributaries plotted, and other attributes located. Such a detailed inventory yields a realistic picture of the cave but a limited representation of the karst aquifer, as one can only map caves that are large enough to permit passage of human-sized particles — which are considerably larger than cave fish, sediment, chlorinated hydrocarbons, and water molecules. For every kilometer of accessible, "meter-scale" active conduit, there may exist tens of kilometers of active flow conduits that are is simply inaccessible due to sumps and collapses, and hundreds or thousands of kilometers of conduits on the scale of centimeters and millimeters. The question becomes: How can we predict (model) the hydrogeology of inaccessible conduit portions of the karst system?

Although there have been steady advances in the development of mathematical models to predict karst flow, they are still somewhat limited in applicability in a real-word setting, especially if the investigator is interested in flow properties of a specific karst groundwater basin. Data generated by using a variety of techniques can greatly increase our understanding of the inaccessible portions of the karst aquifer as a conceptual model of the aquifer takes shape. A conceptual model of the karst flow network, based primarily on the collection and interpretation of detailed hydrogeologic data, can be thought of as a schematic representation of the aquifer. In the construction of any model, we must start with the simplest predictable entity, usually the one with the most descriptive data. This paper deals with conceptual modeling of the basin-scale active conduit system alone. Although absolutely essential to understanding and predicting the overall behavior of a karst aquifer, diffuse recharge/storage mechanisms are not within the scope of this paper.

Three case studies

Each of the following case studies is located within Mammoth Cave National Park, Kentucky, north of the Green River (Figure 1). In this part of the Park, caves are numerous but generally short. Sinkholes and karst valleys are present but not with great ubiquity or size. The regional dip is generally away from the Green River, which hindered the development of extensive karsted recharge areas. Only the uppermost portion of the thick Mississippian carbonate sequence (which contains the Mammoth Cave System south of the Green River) is exposed, and only along the deepest valley bottoms. The valley walls and ridges are composed of an alternating sequence of perched karst aquifers and siliciclastic strata. Water generally flows overland across the siliciclastics and through the limestones, ultimately sinking into the upper Girkin Formation, which is the top of the basal karst aquifer (Figure 2).

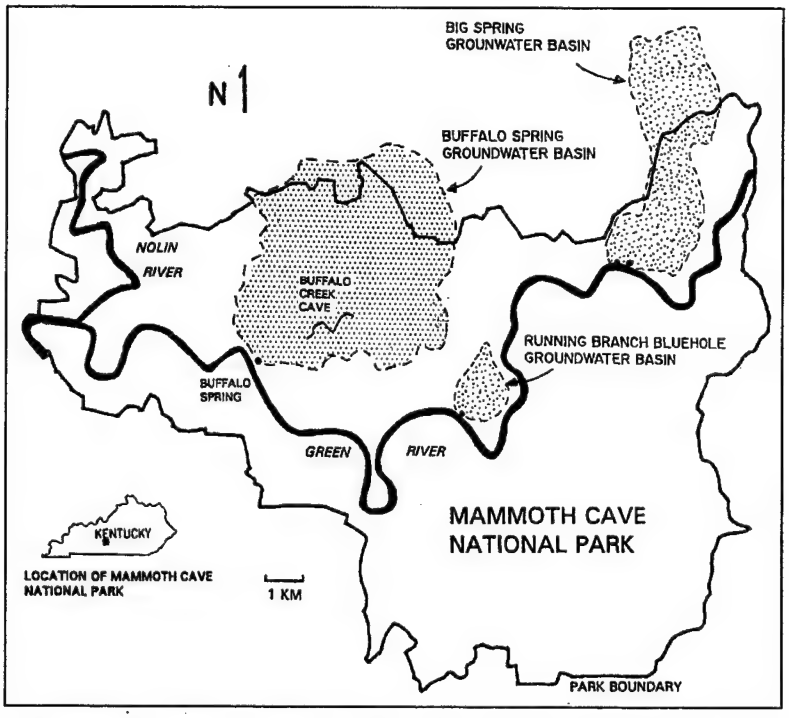

Figure 1: Location of Buffalo Spring, Running Branch Bluehole, and Big Spring groundwater basins, Mammoth Cave National Park, Kentucky.

The boundaries of each basin were defined by qualitative dye traces — the fundamental step to understanding, and thus producing any conceptual model (Kentucky Karst Atlas, 1998). Several different methods of developing a conceptual model of the active conduit networks of these basins were used: quantitative dye tracing with flow-through fluorometers; high-resolution monitoring of aquifer conditions; and circum-storm monitoring with storm-pulse tracing. Fluorometers for these studies were developed and built in-house (Ryan, 1992). Linked to a digital datalogger, these battery-powered filter units, when submersed in a spring or cave spring, recorded the concentrations of dyes at 15-minute intervals. Stage pressure transducers (Druck PDCR 80) and a variety of other probes were also coupled to the datalogger (Campbell 21X). A program that automatically senses changing conditions was written to record stage conditions as frequently as every two minutes, and as seldom as once per hour. Circum-storm monitoring combines the high-resolution electronic monitoring of physical and chemical properties of the groundwater with water-quality parameters. Storm-pulse tracing involves the injection of dye into a sinkpoint immediately prior to or during a runoff event, and the recovery of dye, as well as water quality samples, at a spring or cave stream. This method required the use of discrete automatic water samplers.

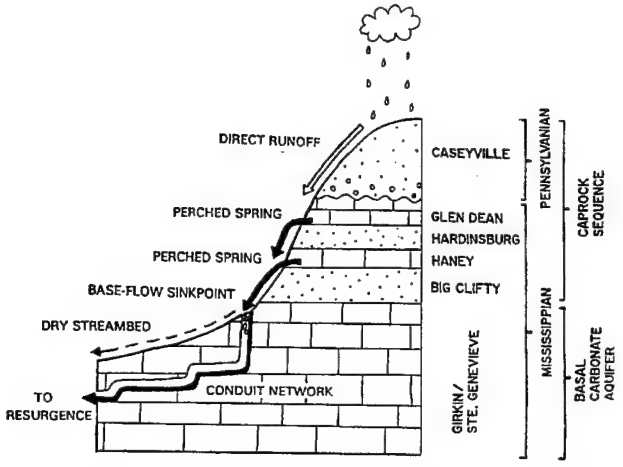

Figure 2: Typical hydrostratigraphy of the karst groundwater basins north of the Green River within Mammoth Cave National Park.

The Buffalo Spring Basin (Ryan and Meiman, 1992) — *multiple aquifer access points; multiple quantitative dye traces; pipe-diagram model*

Buffalo Spring, a rise-pit with an average discharge of about 500 L/s, is located at the mouth of Buffalo Creek at the Green River (Figure 3). The spring is stratigraphically situated in the middle of the Girkin Formation. The primary tributaries to Buffalo Creek, the Wet Prong and the Dry Prong, are oriented roughly northeast-southwest, along the regional strike. Surface flow in the tributaries typically sinks into the Girkin Formation just downstream from the contact of the overlying Big Clifty Sandstone. The recharge area for Buffalo Spring (25 km^2) is nearly identical to the Buffalo Creek surface catchment. During the Buffalo Spring study, nine quantitative traces were completed and up to three fluorometers were deployed at a given time, taking advantage of multiple conduit-access points.

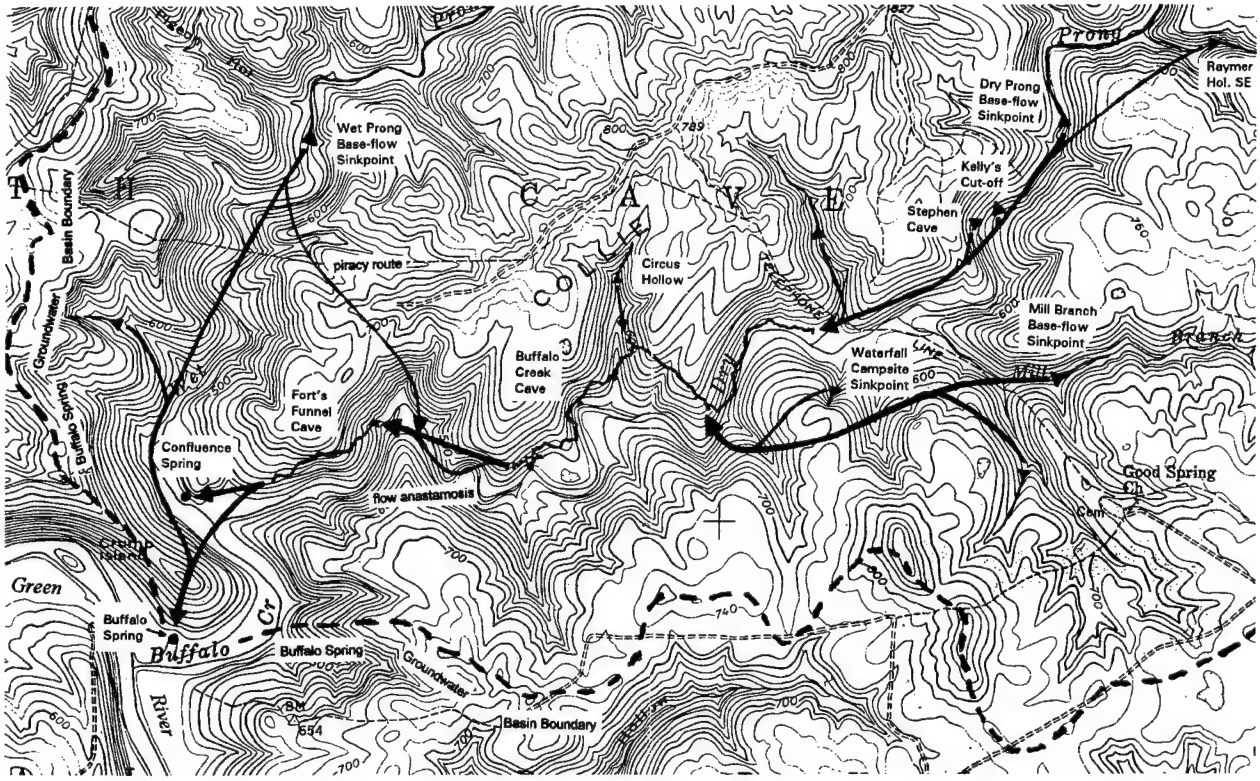

Figure 3: Map of the lower portions of the Buffalo Spring groundwater basin, showing key surface and subsurface features. Solid lines represent hypothesized groundwater flow routes. (1" = 2700'.)

Rhodamine WT was injected at the Wet Prong terminal sinkpoint at exactly the same time fluorescein was injected into the cave stream of Fort's Funnel (Figure 3). The dye cloud from the Wet Prong arrived at the sampling site at Buffalo Spring ahead of the dye from the much closer Fort's Funnel. These results seemed to conflict with qualitative tracer tests, which had shown that water sinking in the Wet Prong passes through Fort's Funnel on its way to Buffalo Spring. From quantitative traces it became apparent that the Buffalo Spring basin includes two major trunk conduits — the Wet Prong and the Dry Prong trunk (the latter accessible through Fort's Funnel and Buffalo Creek Cave). Furthermore, the two trunks join somewhere between Fort's Funnel and Buffalo Spring. A minor conduit must pirate a small portion of flow from the Wet Prong trunk into the Dry Prong trunk upstream from Fort's Funnel. Since the distance between the Wet Prong sinkpoint and Buffalo Spring is greater, and the travel times less, than between Fort's Funnel and Buffalo Spring, the Wet Prong trunk gradient must be steeper. It is apparently this head difference between the two trunks upstream from Fort's Funnel that is responsible for the piracy upstream from Fort's Funnel. These relationships are schematically displayed in the pipe-diagram (following the example of Smart, 1988) of Figure 4.

Double-peaked recovery curves were recorded at Fort's Funnel and Buffalo Spring during several traces from both Mill Branch and the Dry Prong sinkpoint (Figure 5). There were no double-peaks recorded in Buffalo Creek Cave. The double-peaked curves suggest the presence of a bifurcated flow path — an anastomose. The absence of a double-peaked curve at Buffalo Creek Cave implies that the anastomose must be located between Buffalo Creek Cave and Fort's Funnel. This section of trunk is inaccessible in these caves due to terminal sumps.

It is possible to further infer the nature of the anastomose through the interpretation of mapped passages of Buffalo Creek Cave. Mapping of the stream passage of Buffalo Creek Cave revealed an abundance of similar flood cut-arounds ranging between 50 to 300 meters in length. During moderate to high flow they serve as auxiliary flow paths. The anastomose responsible for the double dye peaks at Fort's Funnel is a similar flood cut-around. This interpretation is supported by a series of repeated traces during falling discharge. The dual peaks eventually disappear and only one peak remains under lower flow conditions; one of the routes is apparently abandoned at some point during receding flow.

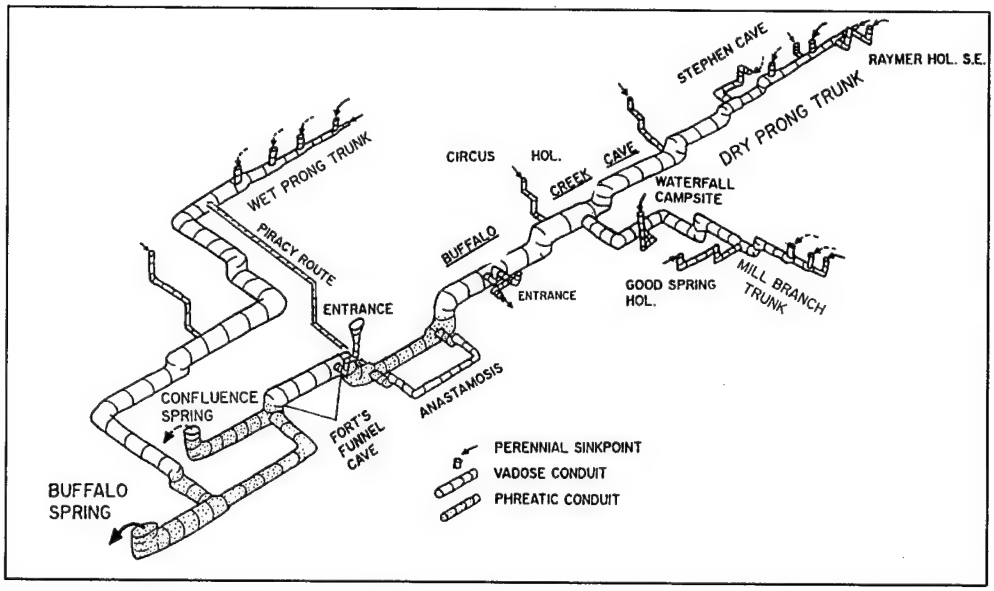

Figure 4: Pipe diagram of the Buffalo Spring groundwater basin active conduit flow system.

Running Branch Bluehole Basin (Ryan and Meiman, 1997) — *single aquifer access point; instrumentation, multiple quantitative dye traces; schematic cross-section model*

The Running Branch basin (2.5 km²) features its namesake cave (with a perennial stream in its lowest level) at the basin's midpoint and an intermittent bluehole spring about 60 m from the Green River (Figure 6). The channel connecting the spring to the Green River is completely floored with alluvium with limestone exposed only in the side wall.

A series of four quantitative dye traces was performed with flow-through fluorometers deployed in Running Branch Cave and Running Branch Bluehole. Both sites, as well as the Green River, were equipped with pressure transducers to measure stage. The dye-recovery curves shown in Figure 7 are typical of all four traces. The leading edge of the dye slug arrived at the cave stream (670 m straight-line distance) in only 4.5 hours, while it then took an additional 38 hours to traverse the remaining 610 m to the bluehole. An additional trace was initiated after the fluorometer was removed from the cave, and as the dye traveled toward the river, the spring's discharge dropped to zero — the level of the bluehole surface was lower than the spring run. The fluorometer remained in the spring and, surprisingly, recorded the passage of the dye cloud even though there was no flow issuing from the bluehole (Figure 8).

Simultaneous stage data for the cave stream, the bluehole and the Green River are shown in Figure 9. The hydrographs were nearly identical in response to the day-14 storm pulse until the river stage began falling at a faster rate on day 21. The elevation at which the inflection occurs is of particular importance here because it also corresponds to the level of the bluehole spill-over point along the spring run. Note that the river peak of the day-25 event caused a subtle increase in bluehole stage some 4 hours later.

During times of low flow, up to 100% of the basin's groundwater was discharged to the Green River through floodplain alluvium. That is, although there was measurable flow in the basin (evident by flow in the cave stream), the bluehole was not flowing -- at least on the

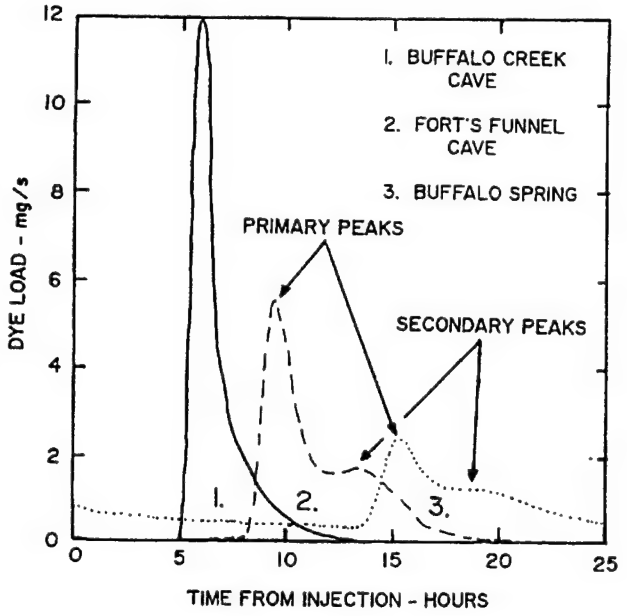

Figure 5: Double-peaked recovery curves along a common conduit. This signature was only present during moderate to high flow conditions as a high-level flow anastomose becomes active between Buffalo Creek Cave and Fort's Funnel Cave.

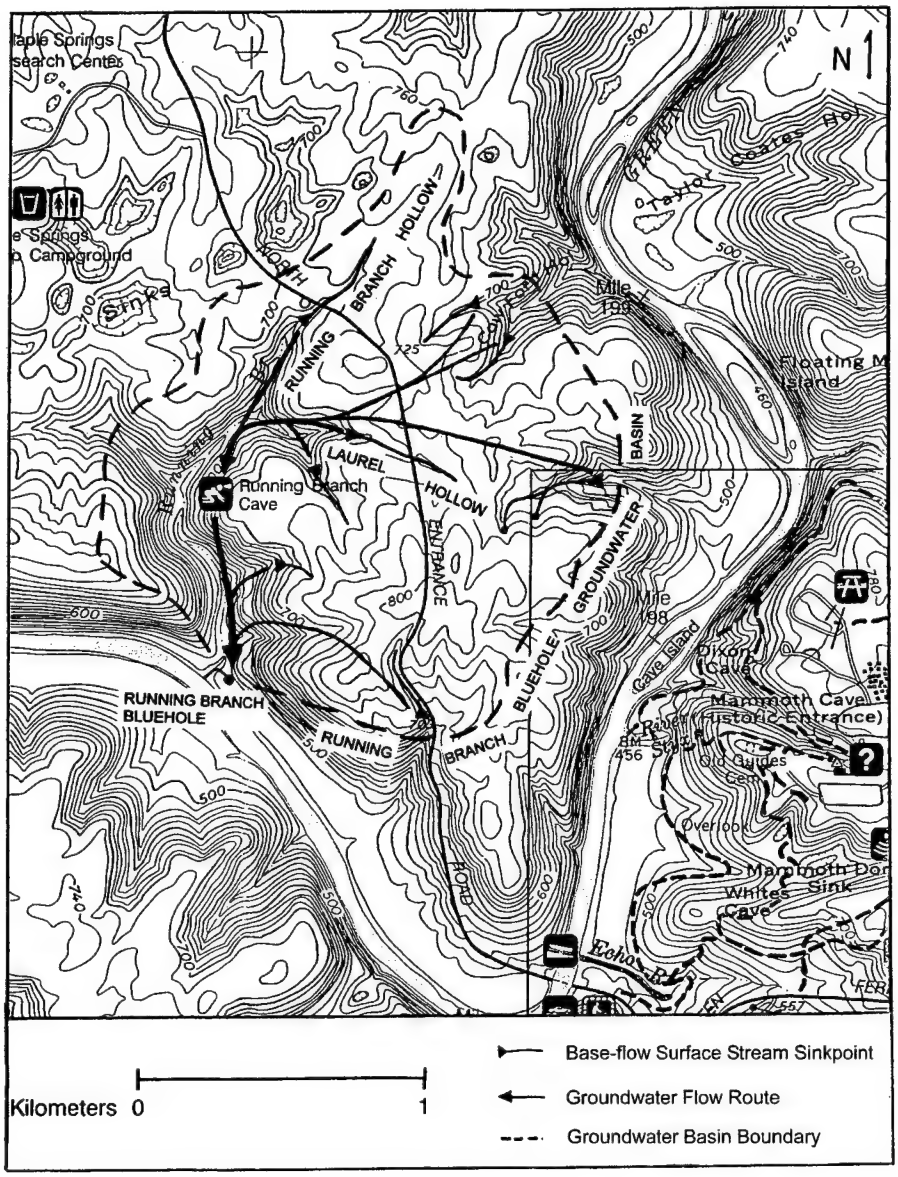

Figure 6: Map of Running Branch Bluehole groundwater basin, showing key surface and subsurface hydrologic features.

surface. Initially it was believed that a submerged distributary spring might be pirating flow from the bluehole. Upon further review, the alluvial flow model stands to reason: (1) the slight increase in river stage on day 25 was recorded in the bluehole four hours delayed; there would have been an instantaneous response through an open conduit; (2) a difference in head of 24 cm was measured between the bluehole and the river during baseflow conditions; such a steep gradient would be difficult to maintain through a significant open conduit; and, perhaps conclusively, (3) although a filled conduit might produce a similar response, the nearest limestone is approximately 12 meters beneath the aggraded river channel.

Discharge from the bluehole occurs in three ways, depending on flow conditions: (1) pooled overflow, (2) riffled overflow plus alluvial underflow, and (3) alluvial underflow only. Pooled overflow occurs when the river stage is higher than the spring spill-over point, causing pooled flow along the spring channel (Figure 10a). Under this flow condition the gradient through the alluvium is essentially zero, so there is no underflow component. Also, any stage increase in the river is immediately recorded in the bluehole and the cave stream, as it is linked to the spring through a phreatic conduit. Riffled overflow occurs when the river stage drops below the spring spill-over point elevation (Figure 10b). The inflection point seen on the day 14-21 hydrographs mark the beginning of riffled overflow as the river stage drops rapidly (Figure 9). Under these flow conditions a gradient begins forming through the alluvium and underflow commences. At some point, as the river continues to drop (increasing the gradient through the alluvium) and as the discharge of the basin decreases,

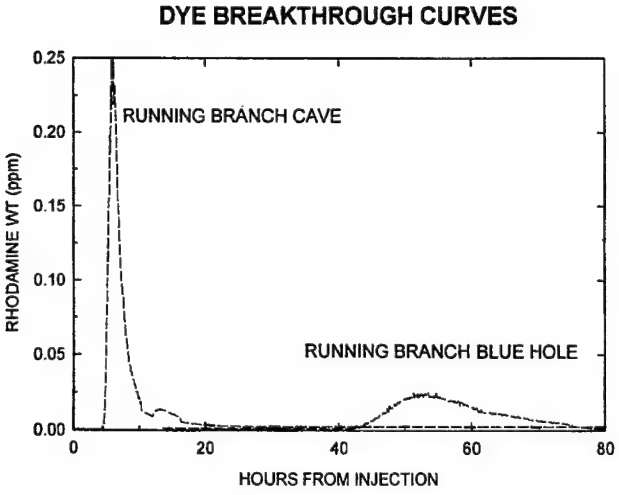

Figure 7: Results from a single quantitative dye trace through the Running Branch Bluehole groundwater basin initiated from the baseflow terminal sinkpoint in Running Branch Hollow (see Figure 6) and monitored at two locations along a common conduit.

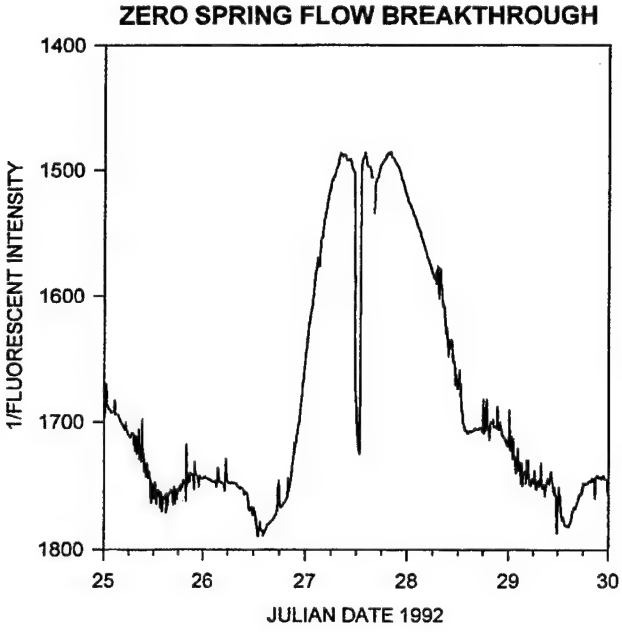

Figure 8: Dye-recovery curve recorded at Running Branch Bluehole initiated at Laurel Hollow (see Figure 6). There was no flow along the spring run during the passage of this cloud. The negative inflections near the peak are the result of the fluorometer being temporarily out of the water.

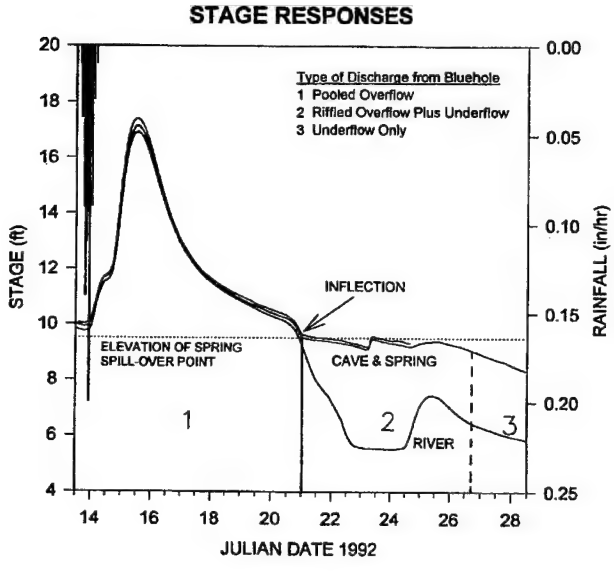

Figure 9: Stage responses simultaneously recorded at Running Branch Cave, Running Branch Bluehole, and Green River following a storm event. Note bluehole flow conditions labeled within graph (see Figure 10).

spring overflow ceases and all discharge is through the alluvium (Figure 10c). The "zero-flow" recovery curve shown on Figure 8 was recorded at the bluehole under this flow condition.

Quantitative tracer test data show that the main conduit segment upstream from Running Branch Cave is very different from the downstream portion (Figure 11). Upstream the conduits are composed of a number of convergent tributaries, one for each sinking stream. These segments are free-flowing, high-gradient cave streams, which rarely, if ever, fill with water as they are high within the vadose zone. The conduit segment downstream is largely phreatic, and where it is not phreatic, in the lowest part of Running Branch Cave, it is pooled. Stage-response hydrographs from the pooled water in the cave were identical in timing, shape, and magnitude to hydrographs at the bluehole. Although groundwater travel through this segment is rather slow due to the low gradient, flood waves are propagated virtually instantaneously through the filled conduit.

It is important to note that if a fluorometer had not been placed in the cave stream, and only the bluehole monitored, the true character of the conduits in most of the basin would be unknown. The much-longer dye travel times of the

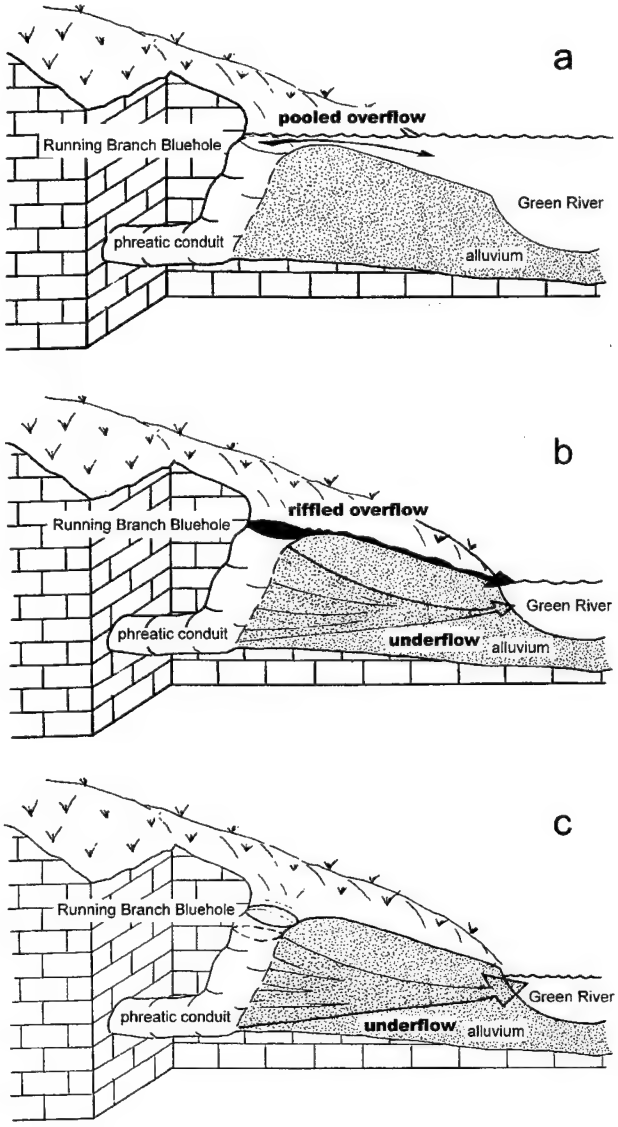

Figure 10: (a) At high stages, there may be little gradient between the bluehole and the river. During these times, deep, pooled overflow results (Zone 1, Figure 9). **(b)** As stage drops in the Green River, riffled overflow occurs as the pool elevation of the bluehole is higher that the spring run, which is in turn higher than the river. Alluvial underflow begins as well (Zone 2, Figure 9). **(c)** As stage continues to drop, all groundwater flow is through the alluvium (Zone 3, Figure 9).

---

downstream end of the basin would have masked the rapid travel times through the upstream portion. One should be careful, when interpreting quantitative trace data from only one monitoring point, not to make unwarranted inferences about the entire conduit network.

Big Spring Basin (Ryan and Meiman, 1996) — *no aquifer access points; circum-storm monitoring, storm-pulse tracing; schematic cross-section model*

When there is no access to the conduit system of the karst aquifer, the investigator must rely on observations made at the spring to predict the hydrogeology upstream. As demonstrated in the Running Branch study, interpreting dye travel times from a single recovery point may yield an erroneous model of the conduit system. We have found that rigorous circum-storm sampling and storm-pulse quantitative dye tracing can disclose important clues concerning the plumbing of the inaccessible conduit system.

The Big Spring groundwater basin (14 km^2) is roughly bisected by the northeast boundary of Mammoth Cave National Park (Figure 12). The basin discharges into the Green River primarily through Big Spring and, to a lesser degree, through its distributary Mile Five Spring.

Data were recorded during two separate storm events, one each in September and March, representative of summer and winter antecedent flow conditions. This paper will discuss the aquifer response of the March event (for details of the September event and the water quality responses, see Ryan and Meiman, 1996). An automatic water sampler was positioned on the floodplain above Big Spring and programmed to collect 24 samples at two-hour intervals (although samples were retrieved every 24 hours). Sampling commenced eight hours before the onset of precipitation. Samples were collected and analyzed for fecal coliform bacteria, turbidity, dye concentration, and specific conductivity. The stage height at Big Spring was measured using a pressure transducer and datalogger (as used at Running Branch) which recorded as often as every two minutes. A discharge rating curve was made which allowed the conversion of stage data into continuous discharge data. Hourly rainfall was recorded at a weather station one kilometer south of Big Spring.

Shortly before the March runoff event, rhodamine WT was injected into the stream of Logsdon Cave and fluorescein into a sinking stream in the Big Woods (both situated at the top of the Girkin Formation) (Figures 2 and 12). Four hours later the rain gauge noted the arrival of the storm event as 0.65 cm of precipitation were recorded in the first hour (Figure 13). Because of the nearly saturated soil conditions, most of the precipitation resulted in runoff that promptly increased the volume of recharge entering the aquifer through stream swallets. The discharge of Big Spring increased almost immediately in response to the storm-induced recharge. Even though discharge rose rapidly from its antecedent level of 200 L/s, specific conductance, turbidity and fecal coliform remained at their

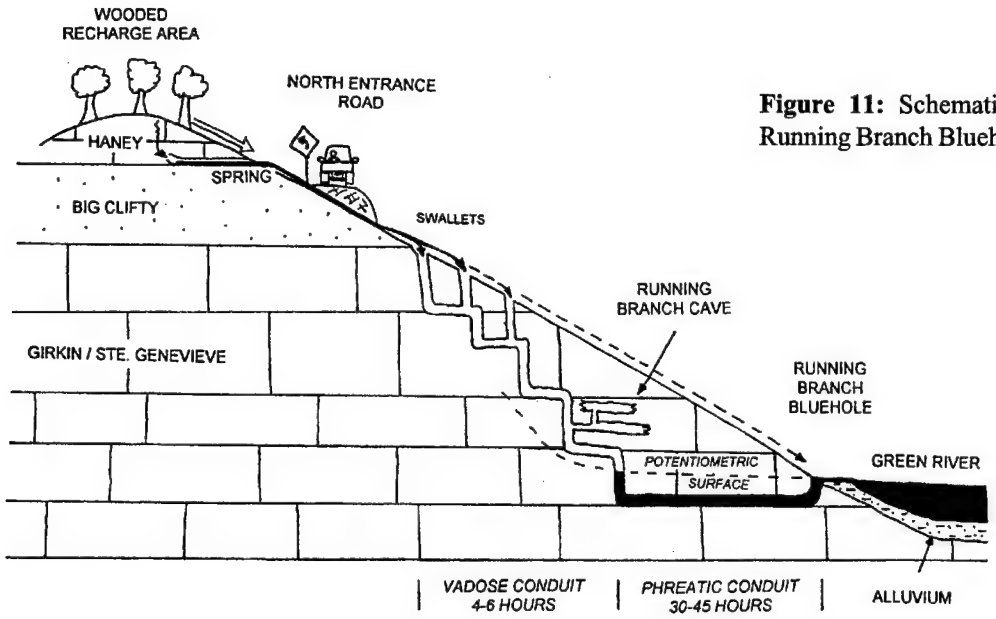

Figure 11: Schematic cross section of the Running Branch Bluehole groundwater basin.

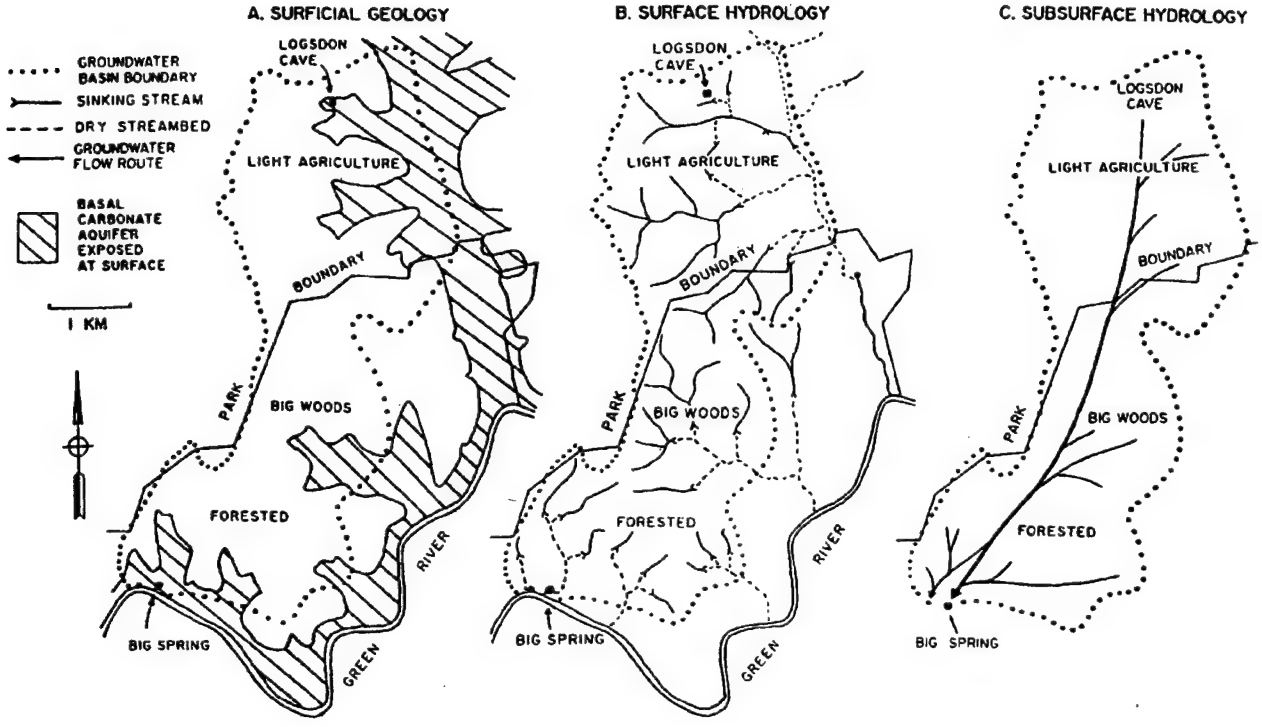

Figure 12: Comparisons of the (A) surface geology, (B) surface hydrology, and (C) subsurface hydrology of the Big Spring groundwater basin.

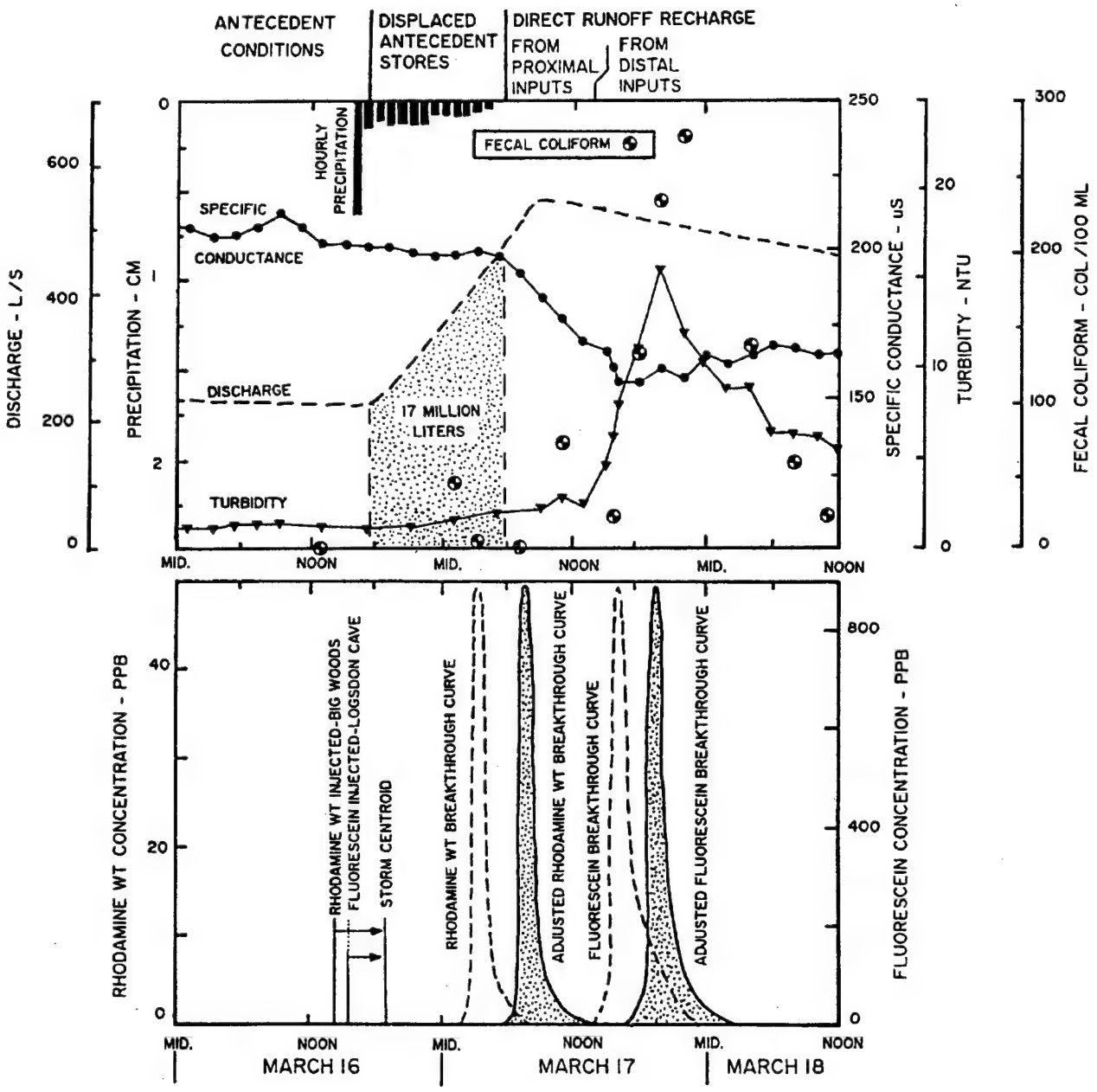

Figure 13: March runoff-event sampling, including storm-pulse tracing results.

pre-storm levels of 205 µS, 2 ntu, and 5 col/100ml respectively.

Not until 14 hours after the initiation of the runoff event did specific conductance begin decreasing from its antecedent level. The drop in specific conductance denoted the arrival of the relatively low-ionic-strength stormwater runoff at Big Spring. Driess (1989), Hess and White (1988), and Meiman (1989) also observed similar delays between the initial discharge response and the arrival of storm-derived waters. They suggest that this delay was the time required for the displacement of antecedent (pre-storm) water in the conduit system between the inputs and the spring.

The discharge hydrograph and the timing of water-quality variations revealed the presence of a significant phreatic conduit immediately upstream from Big Spring. The discharge response to the storm runoff was nearly immediate at Big Spring, even though there was no immediate corresponding change in water quality. This was caused by direct runoff arriving, shortly after the onset of precipitation, at the upstream end of a major phreatic conduit, and the hydrostatic head of the flood wave was instantaneously propagated through the phreatic conduit to Big Spring (similar to Running Branch). There was no significant change in water quality at the spring until a volume of 17 million liters had been displaced from the

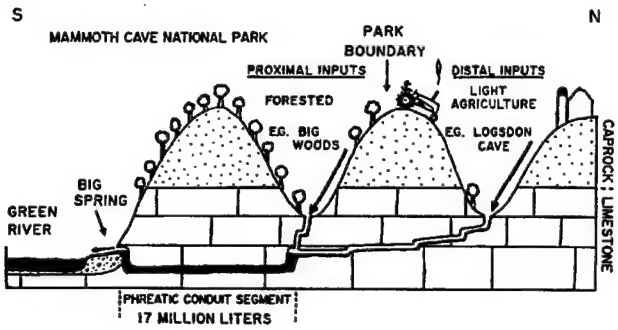

Figure 14: Schematic cross section of the Big Spring groundwater basin, showing land-cover distribution and subsurface conditions, including the long phreatic segment.

conduit through Big Spring. This volume was determined by integrating the storm-response discharge curve between the time of the first increase in discharge and the first drop in specific conductance (Figure 13), a technique used also by Ashton (1966) and Atkinson (1977). It represents the volume of antecedent phreatic water in transitory storage in the trunk conduit between Big Spring and the nearest major input(s) (Figure 14). This technique was repeated over several storm events, and the volume of this phreatic conduit was repeatedly calculated to be 17 million liters.

Note that although the specific conductance dropped as the storm runoff arrived at Big Spring, there was no significant increase in turbidity or bacteria (Figure 13). Sources of this water are likely to be relatively close to the phreatic section of conduit (and thus be in the first large dose of storm waters to arrive), and derived from land uses low in these contaminants. This rationale was supported by the coincidental arrival of the fluorescein trace from the Big Woods.* Likewise, the rhodamine WT from Logsdon Cave arrived coincidentally with the pulse of high turbidity and fecal coliform, reflective of the agricultural land uses around this distal input. The arrival of physically and chemically very distinct waters, supported by storm-pulse tracing, allowed the construction of a conceptual model of the basin (Figures 13 and 14).

*Since the runoff centroid could not be predicted ahead of time, the dye-recovery curve was time-adjusted to the centroid in order to mimic, as closely as possible, a dye injection at peak runoff. The adjustment translated the recovery curves, as well as the elapsed time between the dye injection and the runoff centroid. The time adjustment did not take into account the probable effects that changing flow velocities, caused by the flood wave, have on travel times. This same technique was used with success in a number of additional traces.

References Cited

Ashton, K., 1966, The analysis of flow data from karst drainage systems: Trans. Cave Res. Group of Great Britain, v. 7, p. 161-203.

Atkinson, T.C., 1977, Diffuse flow and conduit flow in limestone terrain in the Mendip Hills, Somerset (Great Britain): Journal of Hydrology, v. 35, p. 93-110.

Driess, S.J., 1989, Regional scale transport in a karst aquifer, 1. Component separation of spring flow hydrographs: Water Resources Research, v. 25, no. 1, p, 117-125.

Hess, J.W., and W.B. White, 1988, Storm response of the karstic aquifer on south-central Kentucky: Journal of Hydrology, v. 99, p. 235-252.

Kentucky Karst Atlas, 1998, Mapped karst groundwater basins in the Beaverdam 30 X 60 minute quadrangle: Kentucky Geologic Survey map.

Meiman, J., 1989, Investigation of flood-pulse movement through a maturely karstified aquifer at Mammoth Cave, Kentucky: M.S. thesis, Eastern Kentucky Univ., 343 p.

Ryan, M.T., 1992, Using newly-developed dye tracing techniques to determine the karst hydrology of the Buffalo Creek Groundwater Basin of Mammoth Cave National Park, Kentucky: M.S. thesis, Eastern Kentucky University, 123 p.

Ryan, M.T., and J. Meiman, 1992, Hydrogeology of Buffalo Creek, Mammoth Cave National Park: Cave Research Foundation Newsletter, v. 20, no. 3, p. 1, 12-13.

Ryan, M.T., and J. Meiman, 1996, An examination of short-term variations in water quality at a karst spring in Kentucky: Ground Water, v. 34, no. 1, p. 23-30.

Ryan, M.T., and J. Meiman, 1997, Notes on the hydrology of the Running Branch Bluehole Groundwater Basin: Proceedings of the Sixth Annual Mammoth Cave National Park Science Conference, p. 153-166.

Smart, C. C., 1988, Artificial tracer techniques for the determination of the structure of a conduit aquifers: Ground Water, v. 26, no. 4, p. 445-453.

ROLE OF CAVE INFORMATION IN ENVIRONMENTAL SITE CHARACTERIZATION

Mark Jancin
USFilter, 120 Radnor Rd., State College, PA 16801

Abstract

For consultants concerned with developing site-specific conceptual models for flow and transport in karst, cave information can be worth accessing. At the scale of the basin, caves often display patterns that correlate with both the flow and recharge characteristics of their aquifers. Characterization of overall basin hydrology bolsters predictions and monitoring recommendations which address the site. Although the presence of caves beneath or near sites is rare, site-based information such as water-table maps (under both natural and pumping conditions), well water-level fluctuations, well turbidity observations, borehole-void yields during drilling, and dye-trace results, are potentially useful in defining conduit-flow boundaries to diffuse-flow blocks. The appropriate choice of dye-tracer methods should acknowledge whether most site conduits (or borehole voids, or even caves) are within the epikarst, the vadose zone, the phreatic zone, or the oscillation zone. For inferences on site flow directions, it is useful to compare the directional frequencies of cave passages and joints, faults, and photolinears in the area. There is evidence that where caves are well developed, there tends to be a low correlation between photolinear locations and relatively high well yields. LNAPL migration will be retarded where main conduits are well beneath the water table, but an extensive overlying system of saturated epikarstic pores serve as traps. Karst with high seasonal or storm variations in water level will tend to repeatedly remobilize LNAPLs. Given sufficient volume, DNAPLs can penetrate vertically integrated networks of pores, fractures, or solution conduits to great depth. However, where such pathway networks are lie above relatively tight lithologies at shallow depth, and are not sediment filled, lateral movement can greatly exceed vertical movement. Characterization of the 3-D nature of pores and pathways is an important element in understanding the migration of free product, and therefore in understanding the evolution of associated aqueous plumes.

Introduction

This paper is written from the perspective of a hydrogeological consultant concerned with site-specific environmental characterization in karst terranes. Emphasis is on using cave information in developing conceptual site models (CSMs) for groundwater flow and contaminant transport and fate. If cave information is available and geographically relevant, it is almost always useful in developing a fuller context for CSMs and for characterization of the drainage basin or sub-basin. Good hydrogeological context-development promotes good, and relatively comprehensive, CSMs, which in turn promote testable predictions and defensible monitoring recommendations.

Issues touched on include: potential sources of cave information; cave types associated with various carbonate aquifer systems; interpreting the hydrologic significance of cave locations on the scale of the basin; complementary information from inventories of sinkholes, sinking streams, and springs; implications of nearby caves for distinguishing diffuse versus conduit flow at the scale of the site; dye-tracer methods for vadose versus phreatic conduits; inferring flow directions from trends of cave passages, joints, faults, and photolinears; conduits and NAPL migration; and how the acquisition of cave information can foster more thorough and defensible CSMs.

Key definitions and distinctions

Cave: natural subsurface void in rock that is large enough for human access. Filled by air or water; often partially occupied by sediment.

Borehole void: subsurface void located along a borehole, with a presence either inferred (e.g. rod drops during drilling) or observed (e.g. downhole camera). Human entry is not possible, regardless of void size. Filled with air, water, or sediment.

Conduit: either (1) elongate subsurface void of any size (may be synonymous with cave); or (2) elongate void of cross-sectional size too small to permit human entry, but arbitrarily more than ~1 cm wide or tall; or (3) inferred, hidden parts of underground drainage networks.

Cavity: inferred subsurface void of any size >1 cm (arbitrarily) with either (1) indeterminate three-dimensional form, or (2) roughly equant three-dimensional form. Filled with air, water, or sediment.

Candidate geophysical signatures: possible (but unproved) cavities or conduits inferred from various types

of surface geophysical surveys, including natural potential, microgravity, ground temperature, shallow seismic reflection, ground-penetrating radar, and resistivity surveys.

Potential sources of cave information

Desirable information includes cave entrance locations, cave maps, stratigraphic locations, and structural features observed in caves. Such information may be available from printed sources retrievable at a good geology library. General sources include regional cave surveys and cave catalogs, topographic and geologic maps, and field searches.

Regional surveys generally are systematic inventories of all known caves in a specific geographic area. Such areas may be at the scale of the state, county, or a geographic district of particular interest to the compilers. Some surveys are conducted by formal groups that publish their results in journals or monographs. Other surveys work with formal state geological groups which publish the results. Some surveys are very informal (and sometimes small) groups that may either never publish their results, or only publish limited information within, for example, guidebooks for conventions of cavers. White (1988, his table 3.2) has summarized recent, major regional and state cave surveys in the United States.

Informal survey groups, or groups that otherwise do not publish their information comprehensively, generally must be sought out by the consultant desiring cave information. In such situations, it may be difficult to access their (private) information, unless the consultant is a member of a recognized caver group, such as the National Speleological Society. It is important not to divulge cave locations or maps without specific permission from the survey. If cave information is accessed but locations are not provided on a map from the survey, the consultant will need to use any available location control (e.g. latitude and longitude) to plot the cave entrances on topographic and geologic maps.

Topographic maps often contain useful information on the locations of sinkholes, sinking streams, springs, underdrained areas, karst windows, and so forth. However, such maps virtually never show all such features -- in many karst investigations it is vital to do field reconnaissance for such landforms. Many topographic maps have proven unreliable in distinguishing perennial versus intermittent streams, but this distinction is often essential for understanding the groundwater hydrology of the drainage basin.

Geologic maps are useful because they show the locations of the soluble rocks. Stratigraphy and structure often guide the locations and types of caves in an area. Groundwater flow regimes will reflect these factors in proportion to the degree of local or regional karstification of the aquifers.

Topographic maps are used to delineate the boundaries of the catchment basin surrounding the site. Then one can use geologic maps to see the basin layout of soluble versus nonsoluble rocks. Of course, in fairly mature karst basins the actual groundwater divides may not coincide with the surface divides, and the groundwater divides may shift location due to variations in recharge. Still, it is important to have at least a first-order depiction of the catchment-basin boundaries in order to place the site into a meaningful context for hydrogeological characterization.

Rarely, one can locate caves in an area of interest by talking to local residents and doing field searches. Even in an area with a fairly large number of caves, it is very unlikely the consultant will locate more than a few in this way. Topographic maps, geologic maps, and aerial photos can help limit the areas targeted for investigation. Most industrial sites are small enough that it is exceedingly unlikely an accessible cave will be on the property, even in rather mature karst.

Cave types in various carbonate aquifer systems

White (1969) outlined a classification of diverse types of groundwater behavior in carbonates by relating the flow type to particular hydrogeologic environments, each (ideally) having characteristic cave morphology. White's scheme is shown in Table 1, as applied to regions of low to moderate topographic relief.

White referred to three main classes of carbonate aquifers: diffuse flow, free flow, and confined flow (Table 1). Diffuse-flow aquifers are those in which the rocks have undergone little dissolution. To varying degrees, flow approximates Darcian conditions (ideally meaning that flow rates are proportional to hydraulic gradients). Solution cavities are limited and fairly randomly located, while caves are rare and generally small and poorly integrated. Where the carbonate rock reaches the surface, there is little geomorphic expression of karst landforms. The lithologic associations are with solution-retarding carbonates, such as shaly limestones and dolomites.

Where maturely karsted, free-flow aquifers have been dissolved to form well-integrated conduit systems, White subdivided this aquifer class into perched and deep flow systems (Table 1). Flow is non-Darcian and often turbulent. The conduit systems (sometimes caves) tend to be of branchwork form and often serve as subsurface continuations of surface streams. In the absence of

TABLE 1
Hydrologic Classification of Carbonate Aquifers (after White, 1969)

Flow Type	Hydrological Control	Associated Cave Type
I. DIFFUSE FLOW	GROSS LITHOLOGY Shaley limestones; crystalline dolomites; high primary porosity.	Caves rare, small, have irregular patterns.
II. FREE FLOW	THICK, MASSIVE SOLUBLE ROCKS	Integrated conduit cave systems.
A. PERCHED	Karst system underlain by impervious rocks near or above base level.	Cave streams perched--often have free air surface.
1. Open	Soluble rocks extend upward to level surface.	Sinkhole inputs; heavy sediment load; short channel morphology caves.
2. Capped	Aquifer overlain by impervious rock.	Vertical shaft inputs; lateral flow under capping beds; long integrated caves.
B. DEEP	Karst system extends to considerable depth below base level.	Flow is through submerged conduits.
1. Open	Soluble rocks extend to land surface.	Short tubular abandoned caves likely to be sediment-choked.
2. Capped	Aquifer overlain by impervious rocks.	Long, integrated conduits under caprock. Active level of system inundated.
III. CONFINED FLOW	STRUCTURAL AND STRATIGRAPHIC CONTROLS	
A. Artesian	Impervious beds which force flow below regional base level.	Inclined 3-D network caves.
B. Sandwich	Thin beds of soluble rock between impervious beds.	Horizontal 2-D network caves.

impervious capping beds, karst landforms tend to be well developed. The lithologic association is with thick, massive, fairly pure limestones.

Confined-flow aquifers are associated with stratigraphic and structural controls dominating the hydraulics. In the artesian subclass (Table 1), tilted impervious confining layers force flow below the regional baselevel -- associated caves are usually inclined, three-dimensional network mazes with joint control. In White's sandwich subclass, thin horizontal beds of soluble rock (often <12 m thick) occur between impervious confining layers -- associated caves are typically horizontal, two-dimensional network mazes with joint control. White noted that caves with this pattern often are located near major streams, where backflooding may contribute to their development. White (1988) later referred to sandwiched, 2-D network caves as a type of interstratal karst. Jancin and Ewart (1995) proposed such 2-D conduit networks can form within steeply inclined, thin-bedded sequences of soluble and nonsoluble layers, under the action of diffusely recharging waters. Confined-flow aquifers tend to have little geomorphic expression, since the soluble layers intersect the surface over very limited areas, or not at all.

White (1977) later expanded his 1969 classification scheme to include factors of relief, structure, and aquifer size. Palmer (1991) presented an interesting classification of cave patterns related to three main types of groundwater recharge: focused (point), diffuse, and hypogenic. Palmer also emphasized that artesian aquifers have no inherent tendency for the development of maze caves.

Cave locations on the scale of the basin

It is important to locate all known caves on maps of the drainage basin encompassing the site -- it is preferable to do the same with surrounding basins or sub-basins. This exercise allows one to address a key first-order question: are the caves overall acting as approximately dendritic feeders to the main baselevel streams? If the apparent answer is "yes," then there is a follow-up question: is the site close enough to the main streams to have a significant chance of pronounced subjacent or nearby conduit

influence, or is the site far enough from these streams that such is less likely (or even demonstrably not the case)? From this basin-wide perspective, the goal is to evaluate the evidence for a fluviokarst setting and cave distribution.

Within autogenic systems, caves acting as dendritic feeders to surface streams tend to grow headward, and become increasingly well integrated, over geologic time. One manifestation of this progression is the rather common observation that groundwater in the headwater portions of a predominantly autogenic basin often behaves in a slow-flow, diffuse manner, while groundwater in the lower reaches of the same basin can show fast flow reflecting the presence of large, hydraulically efficient caves or conduits (e.g., Currens, 1995). Where the main base-level streams are incised into carbonate rock, there may be a tendency for the development of meander-cutoff caves (e.g., Mylroie and Mylroie, 1990).

Along steep topographic faces, especially plateau rims, there sometimes can be a tendency for cave development subparallel to, and within, the faces (Sasowsky and White, 1994). This configuration probably represents the predominance of solution along stress-release joints, which form from expansion of the rock mass during erosion. These so-called Cumberland-style caves are associated with the margins of the Cumberland/Allegheny Plateau, where they are usually developed on the downdip valley walls but not elsewhere (Sasowsky and White, 1994). It is likely that stress-release fracturing has controlled cave development in other fluviokarst settings, and one should check for possible concordance in orientations of valley walls and underlying caves.

Where cave and stream locations show little correlation, cave genesis is probably unrelated to more-or-less modern groundwater circulation in an epigenic, fluviokarst setting. This negative correlation makes it harder to infer the likely presence or absence of sizable conduits beneath or nearby a site. For example, caves deriving from a paleokarstic origin may be exhumed by eventual erosion -- their locations need not bear a clear spatial association with modern basin boundaries, baselevel streams, or major springs. Another example comprises hypogenic caves in the Guadalupe Mountains of New Mexico-Texas -- these relict caves have little or no genetic relation to the present landscape and surface recharge (e.g. Ford and Williams, 1989).

Inventories of sinkholes, sinking streams, and springs

Although the frequency of natural ground-subsidence events is low compared to those induced by human activities, the possible presence of surface depressions within the site's drainage basin is worth investigating. Sinkhole occurrence implies either that there is sufficient underlying void space to accept the displaced debris, or that conduits are well enough developed to permit groundwater flow sufficient for lateral transport of the debris sediments (under either natural or induced hydraulic gradients). Sinkhole spacing also is an indication of whether recharge over a given area tends to be distributed (diffuse) or concentrated (focused). As well, evaluating area and regional sinkhole occurrences allows one to develop a sense of whether sinkhole development might be a hazard on site property (for example, via pumping-induced drawdown).

Where surface streams lose much or all of their flow to the subsurface along discrete points, the karst is moderately to very mature. Sinkholes, integrated conduits, and springs are likely to occur in parts of the drainage basin. Plotting the locations of such features on a map of the site's basin permits one to see whether the site falls within an area that is likely to have conduit-influenced drainage and flow. This information forms an important qualitative part of the eventual CSM, and it should be integrated with site-specific information such as the degree of definition of the water table, storm and seasonal well water-level fluctuations, well-water turbidity responses to storms, and the locations, yields, and frequency of borehole voids.

It is important to gather the fullest possible information regarding the basin spring locations and discharge characteristics. These characteristics include flashiness, turbidity, variation in water conductivity, peak-to-base-flow ratios, and so forth (e.g. Quinlan et al., 1991; Rovey, 1994). For basin hydrologic characterization, and therefore site context, karst springs are the most revealing features regarding integrated characteristics of aquifer recharge, storage, flow, and discharge. Unfortunately, most regions will not have this sort of spring information compiled in a single source, if at all. The researcher or consultant generally has to ascertain much of this information by direct observation and measurement within limits dictated by time, cost, and the degree of concern regarding potential groundwater impacts to people and the environment.

Inventories of the above sorts of information are complementary to cave information. On the one hand, if known caves act as significant groundwater flow channels, most or all of the above karst features should be expected within the relatively mature basin -- their absence should be looked upon as a curiosity requiring further investigation. Conversely, the presence of most or all of the above karst features indicates a relatively mature basin, and the absence of known caves should not be taken as a hard indication that hydrologically significant conduits are not, in fact, present. This sort of investigative approach amounts to marshalling the key evidence, reviewing it for consistency,

and then targeting any unexpected feature correlations or gaps for further consideration. In some cases, reevaluation of previously drawn groundwater-basin boundaries may be in order (though definitive boundary delineation requires dye tracing).

Diffuse versus conduit flow at the scale of the site

The presence of conduits (including caves) beneath or near a site should not be taken as a basis to dismiss the role of diffuse flow in the site groundwater system. Conduit flow is always localized, in that the conduits are embedded within more diffuse-flow parts of the rock mass and aquifer. This has important implications for development of defensible CSMs and groundwater monitoring programs. The concepts of diffuse versus conduit flow (e.g. White, 1969, 1988) must always be scale-qualified, and the same is true for gathering and interpreting the evidence upon which aquifer flow regimes may be labeled as diffuse or mixed or conduit.

Even in rather mature karst aquifers, caves (and, by extension, conduits and proto-conduits) comprise a rather small part of the total storage -- such conduit storage might be roughly 1/30th of the total storage (Atkinson, 1977; Ford and Williams, 1989). Though many groundwater flow lines in contiguous diffuse-flow volumes will tend to converge on transmissive, integrated conduits, other flow lines will not, and flow can reverse direction during high recharge events. If recharge over an area or site tends to be distributed (diffuse), significant aquifer volumes with diffuse or mixed-flow behavior may never drain into nearby conduits, but instead will flow toward diffuse discharge (seeps) along base-level streams or shorelines, or perhaps along tight rock perched above baselevel. However, point discharge tends to dominate in most carbonate terranes.

With sufficient well coverage at a particular site, one can try to get a handle on the locations and sizes of approximately diffuse-flow blocks (separated by conduit-flow zones) from the following information: (1) steep, local potentiometric gradients may indicate conduit influence; (2) local potentiometric troughs may align along conduits; (3) fluctuations in well water levels of more than ~10 m may indicate conduit influence; (4) borehole-void intervals with sustainable yields greater than (arbitrarily) 100 gpm indicate conduit flow (though no trend direction can usually be determined); (5) well water turbidity during recharge events generally shows conduit flow to the wellbore; (6) blowouts at a separate location during the drilling or development of a well imply conduit connection; and (7) dye-trace travel times and reception locations can prove conduit flow between points (although the actual flow routes must be inferred).

Dye-tracer methods for vadose versus phreatic conduits

Any water-bearing caves beneath or nearby a site potentially make excellent locations for either injecting tracer dye or monitoring for dye that has been injected elsewhere. Of course, they also are useful monitoring points for constituents of site-related interest. Introduction of dye into sinking surface streams or cave streams generally provides a direct input to part of the conduit-flow system in the vadose zone, with potential for throughput into the phreatic zone. Point-to-point connections and travel rates determined from dye traces in karst have mostly focused on such dye-introduction locations, with such results skewed toward the fast-flow components of the aquifer located relatively near springs.

Less commonly, entirely phreatic caves have been dye traced (e.g. the Leon Sinks Cave System in the Woodville Karst Plain of Florida). Such tracing generally involves penetration by divers to an interior point of strong flow, where the dye is released.

Recently, attention has turned to dye injection at locations lacking focused recharge or cave streams and which may be located relatively far from springs. Aley (1997) has defined and used Epikarstic Dye Introduction Points (EDIPs) for dye injection. He has used either selected monitoring wells or specially constructed wells as the EDIPs, in both cases targeting borehole voids. He has referred (p. 207) to the epikarstic zone as, "...the dissolutionally weathered upper portion of the bedrock in carbonate landscapes; it has sometimes been called the subcutaneous layer." In this sense, the term epikarst refers to the top-of-bedrock and the uppermost part (typically ~10 m) of the underlying bedrock. Aley (1997) defined three hydrologic classes of epikarst, based on whether such zones are mostly dry through time, seasonally saturated, or perennially saturated.

It is worth noting that this idea of "perennially saturated epikarst" seems to represent a recent expansion of the original meaning of the term epikarst (and its synonym, the subcutaneous zone). For example, Williams (1983) stated, "The subcutaneous zone is the upper weathered layer of rock beneath the soil, but above the permanently saturated (phreatic) zone." Such earlier usage of the term epikarst (subcutaneous zone) referred to a relatively high permeability zone, generally with temporary storage, having a base above the phreatic zone.

Aley (1997) has emphasized that most water tracing reported in the literature has used dye introduction points that poorly characterize the functioning of the seasonally or perennially saturated epikarstic zones. He argued that

many karst industrial sites are associated with release of contaminants into such epikarst, where dye-recovery rates are lower, and groundwater-travel rates are slower, by one or two orders of magnitude (or more) than those generally reported in the literature.

Inferring flow directions from caves and structural elements

For many CSMs, an essential component is inference of the direction(s) of flow. Groundwater flow is biased in directions of decreasing head but controlled by available pathways. Even at sites where the water table is quite well defined, solution and fracture conduits can promote local flow oblique to, or even almost parallel to, potentiometric contours. In forming a CSM while reasoning from evidence that will never be complete, it is useful to compare known cave-passage trends with the strike orientations of joints, faults, and photolinears. Where one or more of these classes of features are available for measurement on the site, the inferred flow direction may be compelling. Where most of these measured features are offsite, the inferred flow direction is quite circumstantial and can only become compelling by the acquisition of other information (e.g. dye- trace results, or detection of constituents of interest at monitoring points).

Cave maps are needed for evaluation of the frequency distribution of the passage trends. One procedure is to plot cumulative passage length versus azimuth as a rose diagram (e.g. Deike, 1969). More qualitatively, one can generalize the overall trend frequencies, by rank, as orientation sets with reference to general compass directions.

This same sort of orientation analysis and summary is done for any available data regarding joint and fault populations. Unlike cave passages, joints and faults are planar features. Where most of these planes are subvertical, rose diagrams are suitable for depicting the orientations. Where many of these planes are off the vertical, their orientations are best analyzed using stereographic projections (such as an equal-area net diagram). It is useful to supplement these orientation data with any available information (e.g. from published reports or quarry observations) regarding preferred directions of solutioning along certain joint sets, and any suggestions that larger faults in the region have tended to act as groundwater conduits, or barriers, or both, or neither.

Maps of natural photolinears in an area will allow orientation analysis and depiction in rose diagrams. It seems that some photolinears trace deep, steeply inclined zones of enhanced solution or fracture permeability. Others are likely to trace elevated-permeability zones that are bed-delimited (not penetrating to great depth); others are likely to trace faults (possibly unrecognized in surface mapping); and some are likely to be artifacts of perception. Without ground-truthing or investigative follow-up, no hydrologic significance should be attached to most photolinears. Among others, Zewe and Rauch (1991) have reported interesting results from correlations of photolinear locations, the degree of cave development, and well yields. Generally, they found that where caves were well developed, there was little correlation between photolinear locations and relatively high well yields. Conversely, where known caves were poorly developed or absent, photolinear locations correlated with relatively high well yields. They proposed that poorly cavernous carbonate rocks are productive diffuse-flow aquifers with networks of fractures and small solution conduits that are well integrated along photolinear zones. This jibes with the idea that the best development of karst features, including caves, tends to occur where joints are spaced relatively widely.

With the above orientational information compiled, one evaluates the degree of correlation between the different features. For example, if the direction of greatest cave-passage frequency correlates with the direction of greatest joint-strike frequency, and independent information suggests this same joint set tends to be preferentially solutioned in the area or region, it is reasonable to view this direction as a candidate for preferred flow pathways beneath the site. Next, consider any other available site-specific information which may correlate; for example: do any potentiometric contours form a zig-zag pattern along one or more correlative directions? Do any surface geophysical anomalies (e.g. natural potential) correlate in direction? Do inferred (straight-line) dye-travel paths correlate in direction? Do any pumping tests show drawdown contours elongate in this same direction?

Such correlations build a circumstantial case for preferred directions of groundwater flow. As with other aspects of CSMs, it is best to view such ideas as hypotheses which may eventually be supported or refuted by the acquisition of new site information.

Conduits and NAPL migration

The presence or absence of conduits has implications for the migration of nonaqueous phase liquids (NAPLs). According to Ewers et al. (1991), the following conditions decrease the likelihood of light NAPL (LNAPL) movement in conduit-bearing karst aquifers: (1) the limestone is thick and conduits are well beneath the water table; (2) the limestone is covered by a thick soil mantle fostering slow, non-turbulent recharge; (3) the aquifer is not recharged by sinking streams so that conduit-flow

turbulence is minimized; and (4) an extensive system of epikarstic pores, overlying the main conduits, provides cavities for LNAPL trapping. Mobilization of LNAPLs trapped within the epikarst could be fostered by intense rainfall, sinkhole development, excavations through the soil mantle, and sufficiently deep pumping-induced drawdown. Free-product migration within the phreatic conduits is fostered by any conditions which promote turbulent flow, or any water-level declines that could allow free-surface stream flow. Karst with high seasonal or storm variations in water level (approximately 10-30 m or more) will tend to repeatedly remobilize LNAPLs.

Not all LNAPLs move as floating product or entrained globules. Where fractures or solution conduits are integrated vertically, it is possible for LNAPLs with sufficient volume and head to migrate well beneath the water table, especially along narrow pathways (Cooley, 1991). Evaluation of the potential for LNAPL movement is also important for understanding the distribution of the associated aqueous plume.

Dense NAPL (DNAPL) migration is driven mostly by gravity (density contrasts leading to negative buoyancy). Capillary forces also play a strong role in migration; hydrodynamic forces generally play a very restricted role. Given sufficient volume, DNAPLs can penetrate vertically integrated networks of pores, fractures, or solution conduits to great depth. Of course, where conduits are sediment filled they do not serve as migration pathways. Sediment-filled conduits located in the uppermost phreatic zone may eventually be flushed open by artificially induced or natural causes. Filled conduits deep in the phreatic zone are likely to remain nontransmissive.

Beneath many sites with DNAPL surface sources one must infer the presence of subsurface DNAPLs from chemical concentrations in groundwater samples. DNAPLs often move along such narrow, filamentous bedrock pathways that they are not directly intercepted by site monitoring wells. If background information allows key surface source areas to be located, and a relatively dense network of monitoring wells exists, one can constrain the three-dimensional DNAPL distribution at depth. If such information suggests limited lateral components of DNAPL movement relative to surface source areas, it is fair to suspect that no laterally persistent, transmissive conduits have been utilized during migration.

Gravitative DNAPL migration can occur along very gently inclined pathway networks. Where such networks are on top of relatively tight lithologies at shallow depth, and the DNAPL volume is sufficient, lateral movement can greatly exceed vertical movement. Lateral movement along horizontal pathways can be driven by DNAPL thickness variation (pressure-induced spreading).

Along wide bedrock pathways, DNAPLs tend to migrate as drops or in a steady stream to points of entrapment where the pathways pinch out. Along narrow fissure and joint pathways, considerable residue often remains from globule entrapment by snap-off or bypassing mechanisms, or by catchment in offshoots from the main migration routes. Residual DNAPL saturation values in the phreatic zone generally exceed those in the vadose zone. Such residues tend to persist indefinitely, acting as secondary product sources for vapor or aqueous phases. These residues are immobile and tend to defy remediation where located deep within the saturated zone. Shallower DNAPL residues can be amenable to volatilization by sparging or if pumping drawdown allows air to infiltrate the pores.

There often is a variation between the predominant horizontal direction of groundwater flow and any lateral-migration direction(s) of DNAPL. This should foster aqueous-phase plumes that tend to evolve via advance in both the direction of groundwater flow and the direction of DNAPL migration.

Conclusions

Caves are conspicuous and interesting features of relatively mature karst terranes, but it is challenging to incorporate cave information into site-specific environmental characterizations. This is not surprising, given the very small areas of most sites and the heterogeneity inherent in the development of conduit porosity. Even in mature karst, it is very uncommon to have accessible caves located beneath or nearby sites.

Cave information generally is most useful in furthering the conceptual characterization of the hydrogeology of the site's drainage basin. This is valuable, since the basin constitutes the physical context within which the smaller site exists. For the consultant concerned with developing conceptual site models (CSMs) for flow and transport, it is vital to flesh out the hydrology of the basin as much as possible in order to make, and defend, predictions and monitoring recommendations which address the site. As well, the consultant who proposes CSMs while ignorant of the existence of any noteworthy caves in the vicinity of the site can, during eventual regulatory review, be viewed as having "left a major stone unturned" during his karst investigation.

Given the spectrum of recharge, storage, flow, and discharge characteristics demonstrated by carbonate aquifers, it is difficult to systematize how one can productively incorporate cave and conduit information into CSMs. Nonetheless, this paper provides some key topical

and analytical associations between cave information and CSM development. There are associations between particular cave patterns and both the flow and recharge characteristics of their aquifers. In autogenic karst basins there is a tendency for diffuse, slow flow in the headwater areas and conduit, and fast flow in the discharge (spring) areas. It can be useful to place some sites into such a basin-wide context in order to infer the likely nature of flow near the site. Site-based information such as water table maps, well water-level fluctuations, well turbidity observations, borehole-void yields during drilling, and dye-trace results, are potentially useful in delineating conduit-flow boundaries to relatively diffuse-flow blocks. If significant conduit flow beneath the site is demonstrated by such information, one should suspect there are caves in the vicinity -- if no caves are known, one should try and explain why. Conversely, if caves are known near the site, but considerable evidence indicates no conduit flow beneath the site, one should try and explain why. The appropriate choice of dye-tracer methodology should include considerations of whether most site caves (or conduits or borehole voids) are within the epikarst, the vadose zone, the phreatic zone, or within the oscillation zone. In inferring flow directions for CSMs, it can be useful to compare the directional frequencies of cave passages with those of nearby joints, faults, and photolinears. At NAPL contamination sites, evaluation of the three-dimensional role played by fracture and solution conduits in free-product migration will greatly aid understanding the evolution of the associated aqueous plume.

Acknowledgment

Walter F. Ebaugh made helpful comments on this manuscript.

References cited

Aley, T., 1997, Groundwater tracing in the epikarst, *in* Beck, B.F. and J.B. Stephenson (eds.), The Engineering geology and hydrogeology of karst terranes: A.A. Balkema, Rotterdam, p. 207-211.

Atkinson, T.C., 1977, Diffuse flow and conduit flow in limestone terrain in the Mendip Hills, Somerset (Great Britain): Journal of Hydrology, vol. 35, p. 93-110.

Cooley, T.C., 1991, Approaches to hydrogeologic assessment and remediation of hydrocarbon contamination in clay-covered karsts with shallow water tables: Proceedings of the Third Conference on Hydrogeology, Ecology, Monitoring, and Management of Ground Water in Karst Terranes, National Ground Water Association, Dublin, Ohio, p. 95-111.

Currens, J.C., 1995, Mass flux of agricultural nonpoint-source pollutants in a conduit-flow-dominated karst aquifer, Logan County, Kentucky, *in* B.F. Beck (ed.), Karst geohazards: engineering and environmental problems in karst terrane: A.A. Balkema, Rotterdam, p. 179-187.

Deike, R.G., 1969, Relations of jointing to orientation of solution cavities in limestones of central Pennsylvania: American Journal of Science, vol. 267, p. 1230-1248.

Ewers, R.O., A.J. Duda, E.K. Estes, P.J. Idstein, and K.M. Johnson, 1991, The transmission of light hydrocarbon contaminants in limestone (karst) aquifers: Proceedings of the Third Conference on Hydrogeology, Ecology, Monitoring, and Management of Ground Water in Karst Terranes, National Ground Water Association, Dublin, Ohio, p. 287-306.

Ford, D., and P. Williams, 1989, Karst Geomorphology and Hydrology: Chapman and Hall, London, 601 p.

Jancin, M., and J. Ewart, 1995, Prediction and testing of hydraulic parameters in interstratal karst of the Valley and Ridge Province, Pennsylvania, *in* Beck, B.F. (ed.), Karst Geohazards: Engineering and Environmental Problems in Karst Terrane: A.A. Balkema, Rotterdam, p. 125-130.

Mylroie, J.E., and J.R. Mylroie, 1990, Meander cutoff caves and self piracy: the consequences of meander incision into soluble rocks: National Speleological Society Bulletin, June 1990, v. 52, p. 33-44.

Palmer, A.N., 1991, Origin and morphology of limestone caves: Geological Society of America Bulletin, vol. 103, p. 1-21.

Quinlan, J.F., P.L. Smart, G.M. Schindel, E.C. Alexander, A.J. Edwards, and A.R. Smith, 1991, Recommended administrative/regulatory definition of karst aquifer, principles for classification of carbonate aquifers, practical evaluation of vulnerability of karst aquifers, and determination of optimum sampling frequency at springs: Proceedings of the Third Conference on Hydrogeology, Ecology, Monitoring, and Management of Ground Water in Karst Terranes, National Ground Water Association, Dublin, Ohio, p. 573-635.

Rovey, C.W., 1994, Assessing flow systems in carbonate aquifers using scale effects in hydraulic conductivity: Environmental Geology, v. 24, p. 244-253.

Sasowsky, I.D., and W.B. White, 1994, The role of stress release fracturing in the development of cavernous

porosity in carbonate aquifers: Water Resources Research, vol. 30, p. 3523-3530.

White, W.B., 1969, Conceptual models for carbonate aquifers: Ground Water, vol. 7, p. 15-21.

White, W.B., 1977, Conceptual models for carbonate aquifers: revisited, *in* S.C. Csallany and R.R. Dilamarter (eds.), Hydrologic Problems in Karst Regions: Western Kentucky University, Bowling Green, p. 176-187.

White, W.B., 1988, Geomorphology and Hydrology of Karst Terrains: Oxford University Press, 464 p.

Williams, P.W., 1983, The role of the subcutaneous zone in karst hydrology: Journal of Hydrology, vol. 62 , p. 45-67.

Zewe, B.T., and H.W. Rauch, 1991, Influence of hydrogeologic setting and lineaments on water-well yield in the Great Valley karst terrain of eastern West Virginia, *in* E.H. Kastning and K.M. Kastning (eds.), Appalachian Karst: National Speleological Society, Huntsville, Alabama, p. 223-230.

VARIATION OF KARSTIC PERMEABILITY BETWEEN UNCONFINED AND CONFINED AQUIFERS, GRAND CANYON REGION, ARIZONA

Peter W. Huntoon
Department of Environmental Studies, University of Nevada at Las Vegas
Las Vegas, NV 89154-4030

Abstract

Most of the ground water in the Grand Canyon region circulates to springs in the canyon through the thick, deeply buried, karstified Cambrian through Mississippian carbonate section. These rocks are collectively called the lower Paleozoic carbonates and comprise the Redwall-Muav aquifer where saturated.

The morphologies of the caves are primarily a function of whether the carbonates are unconfined or confined, a distinction that has broad significance for groundwater exploration and which appears to be generally transferable to other carbonate regions. Caves in unconfined high-gradient environments tend to be highly localized, partially saturated, simple tubes, whereas those in confined low-gradient settings are saturated 2- or even 3-dimensional mazes. The highly heterogeneous distribution of the unconfined conduits makes for difficult drilling targets, whereas the more ubiquitously distributed confined mazes are far easier to target.

The distinctions between the storage characteristics within the two classes is probably even more important. There is minimal groundwater storage in the unconfined systems because they are well drained. In contrast, the saturated mazes exhibit maximal storage. Consequently, system responses to major storm recharge events in the unconfined systems is often dominated by flow-through rather than the pulse-through hydraulics as found in the confined systems. Spring discharges from the unconfined systems tends to be both flashy and highly variable from season to season, but total dissolved solids are small. In contrast, the pulse-through hydraulics in the artesian systems causes spring discharge responses to be highly moderated and, in the larger basins, remarkably steady. Both total dissolved solids and temperatures in the waters from the confined aquifers tend to be elevated because most of the water is derived from storage.

Karst permeability is created by the flow system, consequently predicting where the permeability is best developed in a carbonate section involves determining how circulation should be ideally organized through an examination of the geometry of the flow system. The areas where flow concentrates are the areas where karstification will maximize, provided enough time has elapsed to allow dissolution to adjust to the imposed boundary conditions. The rate of adjustment in the Grand Canyon region appears to be related to the degree of saturation. The artesian systems are far better adjusted to hydraulic gradients than the unconfined systems, a finding that probably implies that there is greater contact between the solvent and rock in the saturated confined systems.

ANISOTROPY IN CARBONATE AQUIFERS

Arthur N. Palmer
Department of Earth Sciences, State University of New York
Oneonta, NY 13820-4015

Introduction

Anisotropy, or directional permeability, is characteristic of most bedrock aquifers and can have considerable effect on patterns and rates of contaminant transport. Horizontal anisotropy is especially common in strongly fractured rocks, owing to variations in relative abundance and prominence of different fracture sets. This is less likely in thin-bedded strata in which bedding-plane partings are dominant, but in these rocks the contrast between vertical and horizontal permeability is greater.

At any given point in an aquifer, ***anisotropy*** represents the variation of hydraulic conductivity with direction, which differs from ***heterogeneity***, which is the variation from place to place. Most bedrock aquifers are both anisotropic and heterogeneous, and without a great deal of well-test information it can be difficult to distinguish between them. The two are combined in such a chaotic way in some karst aquifers that no meaningful distinction can be made at all.

The main concern in this brief summary is the recognition and evaluation of horizontal anisotropy -- how to detect variations in hydraulic conductivity and their effect on piezometric data. The concepts are derived from basic groundwater flow equations and well-test data and are easily verified with digital models, but detailed information on the subject is rarely encountered in textbooks.

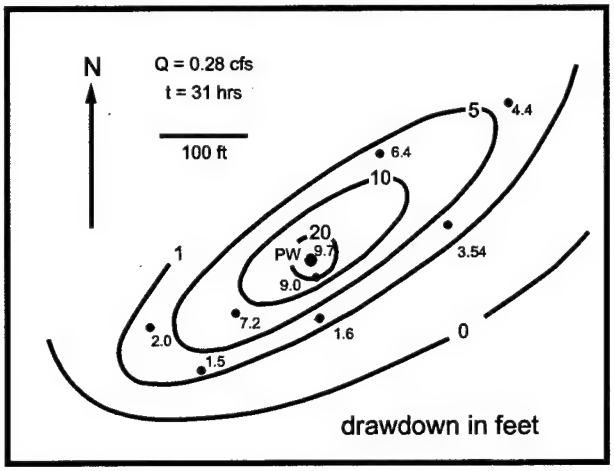

Figure 1: Elongate cone of depression in an anisotropic carbonate aquifer (Beekmantown Fm., Pennsylvania). PW = pumping well.

Recognition of anisotropy

Horizontal anisotropy can be recognized most easily by cones of depression that are elongate in the direction of maximum hydraulic conductivity (K_{max}). However, few pump tests are accompanied by enough observation wells to delineate the theoretically ideal elliptical cone. Usually the anisotropy is manifest simply as erratic distance-drawdown relationships (see the well data of Jones later in this section). A common puzzler for newcomers to the field is to find that the drawdown in a remote observation well is greater than that in a nearby one.

If sufficient data are available, the cone of depression can simply be contoured. Figure 1 shows the combined results of two pump tests in the steeply dipping, highly fractured Beekmantown Formation (mainly limestone), in a location that must remain anonymous. The plot was generated by the kriging routine of SURFER (Golden Software Corp., Golden, Colo.) without manipulation. Figure 2 is an idealized view that identifies the appropriate parameters. The following procedure can be used to determine the mean, maximum, and minimum K values:

1. Determine the ratio between the maximum and minimum cone diameters (d_{max}/d_{min}), taking an average if the data are not consistent. In Figure 1, the diameter ratios for the two widest closed contours are 2.7 for the 10-foot and 3.5 for the five-foot contour.

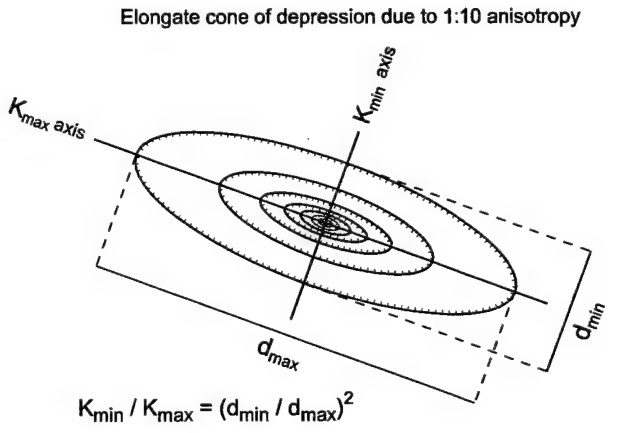

Figure 2: Elongation of cone of depression vs. axes of hydraulic conductivity in an anisotropic aquifer.

2. Calculate the anisotropy ratio $(K_{max}/K_{min}) = (d_{max}/d_{min})^2$. In Figure 1 the conductivity ratio in the vicinity of the well is between 7.5 and 12 (i.e. the square of the diameter ratios), with K_{max} aligned with the local strike of the beds.

3. Use the Theis or Jacob method to evaluate the effective transmissivity (T_{calc}). In the example shown in Figure 1, the mean of several calculations gave T = 0.46 cm²/sec with the Jacob and Theis methods (with misgivings, since the formation contains numerous solutional voids). These methods are designed for confined aquifers but can also be applied to unconfined aquifers if the drawdown is only a small proportion of the saturated thickness (b), where $K_{calc} = T_{calc}/b$. The aquifer in Figure 1 is unconfined, and although the bottom was not reached by the wells, their depth of penetration below the water table averaged about 40 m, which, if used for b, gives a lower limit of 1.2×10^{-4} cm/sec for K_{calc}. It is best to determine T_{calc} or K_{calc} from drawdown in a well that is aligned in the K_{max} direction, because its response to pumping will be more rapid and there is less chance that boundaries will have interfered with the drawdown. It is surprising how many well tests in karst give nearly ideal drawdown curves that can be evaluated by these methods, which are valid only for Darcian flow. Occasionally the results are difficult to interpret, as one might expect in a karst aquifer (see, for example, the Jones data).

4. In an anisotropic aquifer, K_{calc} is the geometric mean of the maximum and minimum K: that is, $(K_{calc})^2 = (K_{max}K_{min})$. Since $K_{min} = K_{max}(d_{min}/d_{max})^2$, therefore $K_{calc} = K_{max}(d_{min}/d_{max})$. The same is true for T values. The actual K_{max} and K_{min} (or T_{max} and T_{min}) can be found in the following way: $K_{max} = (K_{calc})(d_{max}/d_{min})$, and $K_{min} = (K_{calc})(d_{min}/d_{max})$. In Figure 1, if the mean $d_{max}/d_{min} = 3.1$, then $K_{max} = (1.2 \times 10^{-4})(3.1) = 3.7 \times 10^{-4}$ cm/sec, and Kmin = 3.9×10^{-5} cm/sec.

Papadopulos (1965) presents a method for determining anisotropy from the drawdown in 3 or more observation wells (see condensed review in Dawson and Istok, 1991) without the need to define the sometimes-uncertain elongation of the cone of depression. K or T values intermediate between the maximum and minimum can be calculated from the conductivity ellipsoid (e.g. Freeze and Cherry, 1979, p. 174), but in bedrock aquifers the results are suspect.

Oddly enough, the calculated T or K in an anisotropic aquifer is independent of the direction of the observation well with respect to the pumping well. One might expect them to be greater in the K_{max} direction. Yet in a homogeneous anisotropic aquifer the slopes of log time vs drawdown are identical, regardless of direction. At any given distance from the pumping well, the drawdown in the K_{min} direction will simply be delayed. In the example given by Jones, the vast differences in T_{calc} represent heterogeneity, and although anisotropy is also present, it is not the reason for the discrepancies in calculated T.

Anisotropy can also be recognized, although not necessarily quantified, by anomalous piezometric data under natural (non-pumping) conditions, since the groundwater drainage will be more efficient in the K_{max} direction. Maps of static water levels in carbonate aquifers typically show isolated points of unusually low head. These may be associated with anisotropy but are more commonly the result of encountering solution conduits. An actual field example from the anonymous Beekmantown aquifer is shown in Figure 3. The well at **A** shows an extraordinarily low head, even though it was not being pumped at the time of measurement. SURFER produced a plot that makes the well look like the vortex of a tornado. Such data are often omitted from final potentiometric maps in the assumption that they are blunders or meaningless outliers. In this example there was heavy pumping west of the field site, and this single point appears to represent a communicating conduit or fracture zone. The conduit is not aligned with the axes of anisotropy. Although the conduit itself is certainly anisotropic, from the standpoint of the surrounding aquifer it serves more as a potentiometric boundary rather than an expression of either anisotropy or heterogeneity.

Interpretation of anisotropy from geologic data and cave maps

Anisotropy can be anticipated, even before well data are available, from local joint patterns. Rose diagrams of joints give a clear idea of the directions of maximum and mini-

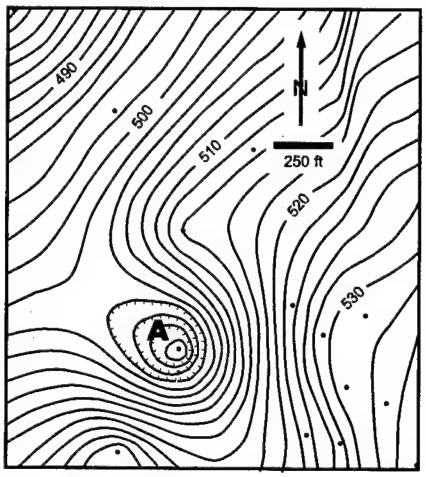

Figure 3: Anomalous point (A) in static potentiometric data in the Beekmantown Fm., Pennsylvania, interpreted as a conduit or fissure zone connecting with area of pumping to the west. This has no direct bearing on anisotropy. Contour interval = 2 feet. Data points shown as dots.

mum K, and to some extent the degree of anisotropy. Measurement of joints in quarries, outcrops, and roadcuts is encouraged (see papers by Sasowsky and Jancin in this volume). Lineaments on aerial photos are also feasible sources of information, although the results can be ambiguous, subjective, and difficult to quantify.

Cave maps provide a ready source of information on anisotropy. Nearly every known cave of substantial size has been mapped, and their patterns alone can provide a clear indication of anisotropy and preferred groundwater flow directions. A rose diagram of the passage segments from survey shots can quantify the anisotropy to some extent. Some examples are given below:

Beekmantown caves, Pennsylvania

The asymmetrical drawdown from the pump test in Figure 1 shows that the local Beekmantown Formation has a prominent K_{max} trend along joints parallel to the strike of the steeply dipping beds. Caves in the region are small, complex, and fragmentary, with highly varied patterns. They nevertheless show the dominant fracture trends and suggest the direction and amount of anisotropy.

No local caves are known, but there are two caves in nearby counties in the same formation where it has similar amounts of deformation. They also show a distinctly dominant strike-oriented alignment (Figure 4). Along with their rose diagrams, simplified outlines of the two caves are shown, reduced from maps by Bernard Smeltzer (Stone, 1953; Reich, 1974). Caves witha clear rectilinear joint pattern are best for this purpose. Those with only a few passage segments are not appropriate candidates.

The cumulative lengths of passage segments for each cave were plotted on rose diagrams (Figure 4), and the cumulative length of the longest trend was divided by that of the longest trend normal to it. In Goods Cave, the major trends occur within individual 10-degree sectors, but in Emigs Cave the major trends span 20 degrees each, and so the values of the two adjacent sectors were summed for the following calculations. The length ratios (major vs. minor axes) were 2.7 for Emigs and 4.6 for Goods. If these ratios are treated in the same manner as the d_{max}/d_{min} of a cone of depression in an anisotropic aquifer, squaring them gives values of 7.3 and 21, which can, with only a few reservations, be considered indicators of local anisotropy. The results are compatible with the well data in Figure 1, in which the anisotropy is between 7.5 and 12. Goods Cave lies along the crest of an anticline, where stresses are highly directional, and its high ratio is atypical (compare with Figure 5a).

Blue Spring Cave, Indiana

Most of Blue Spring Cave, Indiana, is located in massive, prominently jointed Salem Limestone of Mississippian age. The dominant regional joint patterns are very clear in the rose diagram of the trends of passage segments (Figure 5a). The pattern of the rose diagram is virtually identical to that of joints measured in surface exposures. High-yield wells in the area show an alignment along the direction of the largest peak in the rose diagram (Palmer, 1969). The probability of drilling a new high-yield well in proximity to a known high-yield well is increased about 3-4 times if the new well is situated in the direction of the dominant joint direction shown on the rose diagram. Well yields in this formation cluster at either high or low values, with few at intermediate values. This clustering has no direct bearing on whether the aquifer is anisotropic, but it is a characteristic that usually accompanies that condition in

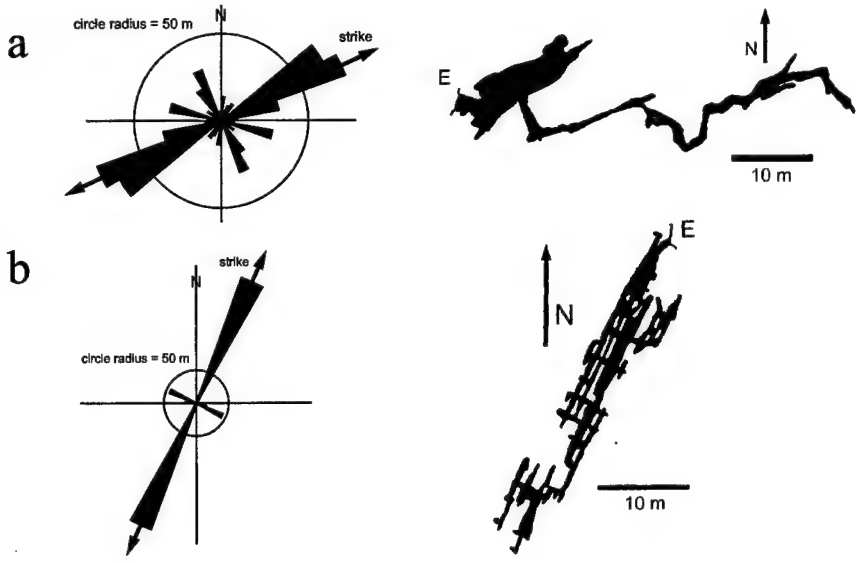

Figure 4: Rose diagrams of passage trends in caves in the Beekmantown Formation, Pennsylvania: **(a)** Emigs Cave, **(b)** Goods Cave (both from survey data by B. Smeltzer). The dominant strike-oriented joint patterns are clearly portrayed and provide a rough indicator of anisotropy ratios (see text for details). The outlines of the caves alone are sufficent to portray the preferred directions of groundwater movement.

bedrock aquifers.

Where two major joint sets intersect, as indicated by the conduit trends in Figures 4 and 5a, the dominant peak is the K_{max} direction and the secondary peak is considered the K_{min} direction. Flow in other directions is thus considered to encounter intermediate K values that are a composite of the K_{max} and K_{min}, because the water is expected to follow irregular paths that zig-zag between the two major joint sets.

Blue Spring Cave, Tennessee

Where bedding-plane partings dominate, well tests show little if any anisotropy. Blue Spring Cave, Tennessee, is located in prominently bedded Monteagle Limestone of Mississippian age. The lack of prominent jointing is shown by the scatter in the rose diagram of passage segments (Figure 5b). Passages are sinuous and have generally been guided by bedding-plane partings. The broad, low peak in the NE-SW direction is caused by alignment of many passages sub-parallel to the strike. The cave patterns suggest no anisotropy, nor do the pump tests elsewhere in this formation.

Effects of anisotropy on laminar flow patterns

Groundwater flow lines are traditionally drawn normal to equipotential lines, i.e. in the direction of steepest hydraulic gradient. If the anisotropy axes are not orthogonal to the equipotentials, the flow is deflected away from the paths of steepest gradient in the direction of K_{max}. If anisotropy is ignored, estimated routes of contaminant movement can be highly inaccurate, even within the laminar-flow parts of bedrock aquifers.

The traditional method for adjusting flow directions to account for anisotropy is to reduce the scale of the equipotential map in the K_{max} direction by the square root of the K_{max}/K_{min} ratio, then draw the flow lines perpendicular to the equipotential lines and finally stretch the map back out to its original scale. This method, though long known, had not been embraced with enthusiasm because of the labor involved. But computer-aided design software turns the exercise into a game. Some digital groundwater models are able to produce similar results, but without the personal insight that free-hand drawing gives.

For example, Figure 6a shows an equipotential diagram for an aquifer in which K_{max}/K_{min} =10. Shrinking the K_{max} dimension by a factor of 3.16 (square root of 10) gives the strangely attenuated version of Figure 6b. Flow lines are drawn orthogonal to the equipotential lines at this distorted aspect ratio, and then the map is expanded back to its original scale, giving the flow pattern shown in Figure 4c.

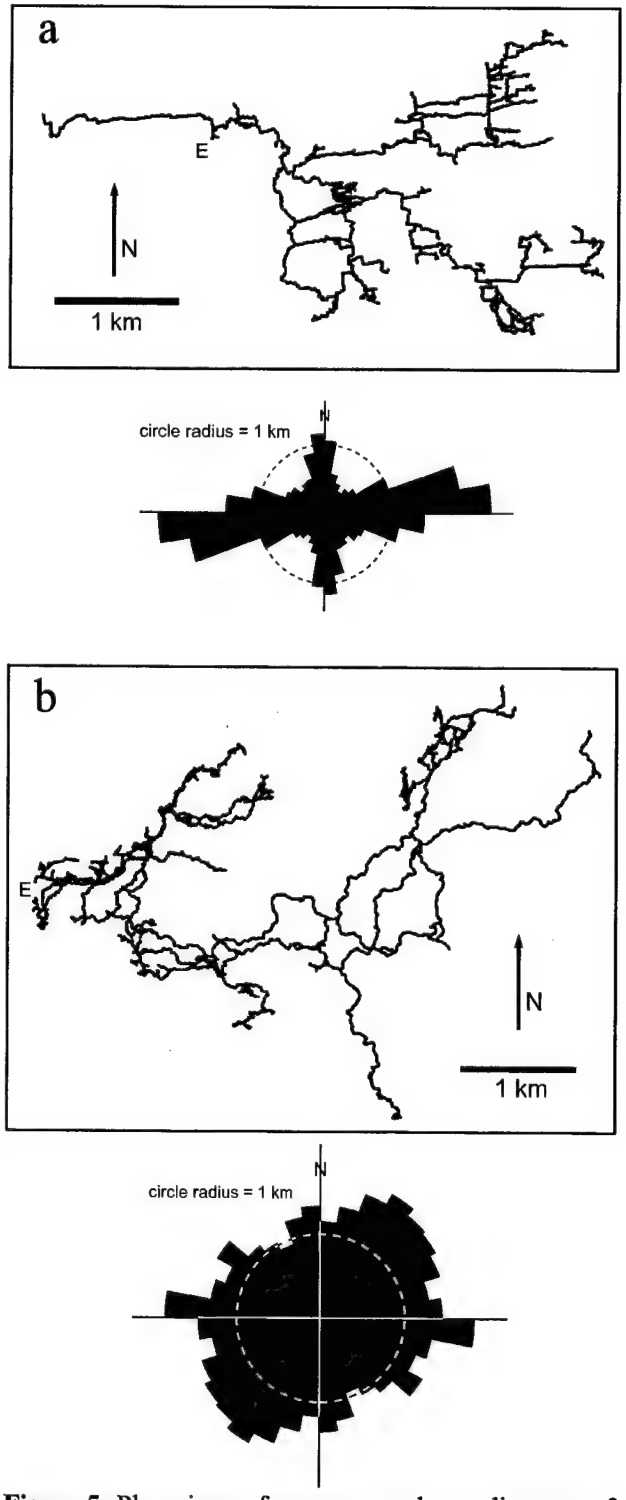

Figure 5: Plan views of passages, and rose diagrams of cave-passage survey shots, in the two longest caves in Indiana and Tennessee, which happen to share the same name: **(a)** Blue Spring Cave, Indiana, located mainly in prominently fractured Salem Limestone; total surveyed length 33 km. (from Palmer, 1969); **(b)** Blue Spring Cave, Tennessee, in prominently bedded Monteagle and upper St. Louis Limestones; total surveyed length 52 km. (from survey data supplied by W. Walter and M. Yocum).

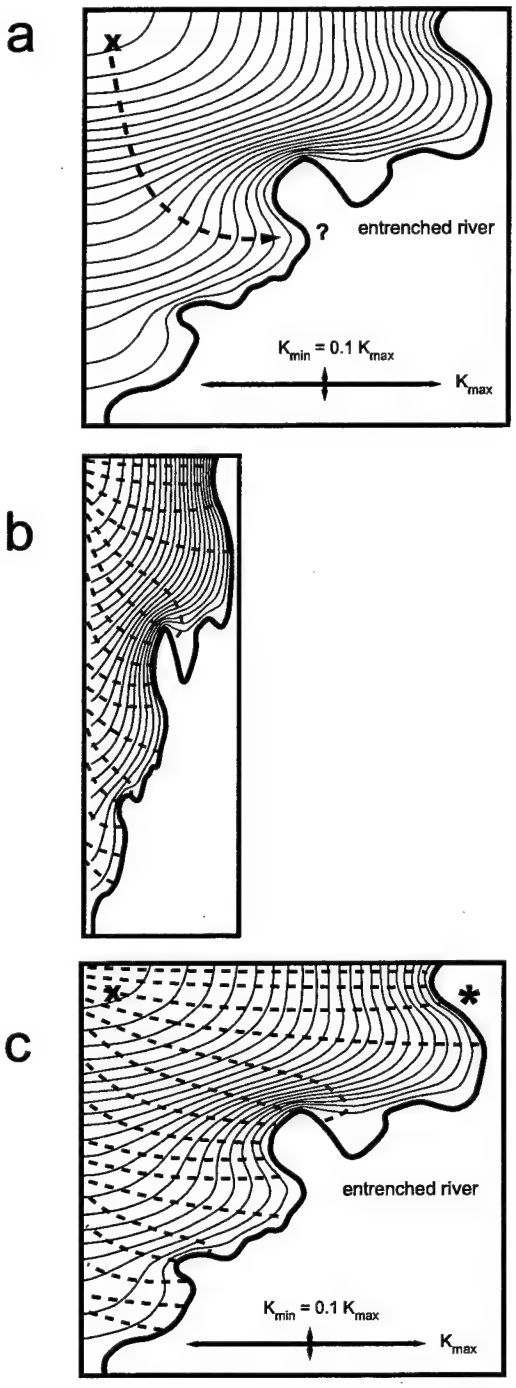

Figure 6: Influence of anisotropy on groundwater flow paths: **(a)** Equipotential diagram based on static water levels in wells. If the aquifer is anisotropic, drawing the flow lines perpendicular to the equipotental lines would be inaccurate. Contaminants at **X** might be expected to arrive at the point marked "**?**". **(b)** Instead, the scale is reduced in the K_{max} direction by the square root of K_{max}/K_{min} and orthogonal flow lines are drawn. **(c)** The map is stretched back to its original shape to show the corrected flow pattern. Flow from point **X** is now predicted to arrive in the vicinity of the asterisk.

The result can help to clarify flow patterns and contaminant movement within the laminar-flow parts of bedrock aquifers. Although it has no direct bearing on flow in existing conduits, this flow-path adjustment may relate to certain aspects of conduit origin.

Significance of recognizing anisotropy

Knowledge of anisotropic conditions is most significant to estimations of contaminant paths and well-head protection areas. Refer to the paper by Spangler (later in this section) for examples of the difficulty of estimating time-of-travel zones in carbonate aquifers. Transmissivity or conductivity data from pump tests are generally limited to the simple T_{calc} or K_{calc} values described earlier, which, in anisotropic aquifers, have been shown to represent only the geometric means of T_{max} or K_{max}. Although the maximum and minimum values are rarely determined from pump tests, they can easily be at least an order of magnitude greater or less than the calculated values. Since estimates of groundwater velocity depend linearly on the K values in the direction of flow, this oversight can cause large errors in estimating travel times and contaminant transport.

As shown in Figure 6, failing to recognize anisotropy can cause substantial errors in prediction of contaminant paths, even in the laminar-flow portions of karst aquifers. Often there is insufficient pump-test information to reveal anisotropy, let alone quantify it. Thus it must be anticipated, and one of the most direct ways of doing so is to make use of structural field data and cave maps.

References cited

Dawson, K.J., and J.D. Istok, 1991, Aquifer testing: Chelsea, Mich., Lewis Publishers, 344 p.

Freeze, R.A., and J.A. Cherry, 1979, Groundwater: Englewood Cliffs, N.J., Prentice-Hall, 604 p.

Palmer, A.N., 1969, A hydrologic study of the Indiana Karst: unpublished Ph.D. thesis, Indiana University, 181 p.

Papadopulos, I.S., 1965, Nonsteady flow to a well in an infinite anisotropic aquifer: International Association of Scientific Hydrology Symposium, Dubrovnik, vol. 1, no. 73, p. 21-31.

Reich, J.R., 1974, Caves of southeastern Pennsylvania: Pa. Dept. of Environmental Resources, General Geology Report 65, 120 p. + map folder.

Stone, R.W., 1953, Caves of Pennsylvania: National Speleological Society Bulletin, vol. 15, 143 p.

MODERN DYE-TRACING DATA AS FUNDAMENTAL INPUT FOR KARST MODELING

Thomas Aley
Ozark Underground Laboratory, 1572 Aley Lane
Protem, MO 65733

Abstract

Modern dye-tracing approaches provide fundamental data for karst modeling. Groundwater tracing studies which yield such data typically have the following characteristics:

1) There are numerous sampling stations which often include both natural groundwater discharge points (such as springs) and monitoring and/or pumping wells. Dyes are recovered from multiple sampling stations.

2) Dye sampling occurs at regular intervals for periods of up to several months, and sampling stations are not dropped after one or two positive dye recoveries.

3) Sampling uses both activated carbon samplers and water samples. Some of the water samples may be collected with programmable automatic samplers.

4) Dye analysis is quantitative and utilizes instruments such as spectrofluorophotometers operated under synchronous scan protocols. With careful study designs, with the aid of such instruments, multiple dyes can be used concurrently and their concentrations credibly calculated.

5) Dye introduction points are chosen to characterize the aquifer and its interactions with the epikarstic zone.

ON THE IMPORTANCE OF STOCK DYE CONCENTRATIONS FOR ACCURATE PREPARATION OF CALIBRATION STANDARDS

Malcolm S. Field
National Center for Environmental Assessment
U.S. Environmental Protection Agency, Washington, D.C. 20460

Fluorescent dyes are commonly used in tracing surface- and groundwater flow, especially in karstic terranes. However, no effort has been made in the past to ascertain the actual pure dye content of the stock solution. In general, stock dye solutions are incorrectly assumed to be 20% or 100% strength, depending on dye type. As a result, fluorometric instrument calibration is incorrect. In particular, calibration standards are prepared that have been excessively diluted beyond that which is noted and recorded (Figure 1). The high dilutions used as standards cause fluorometric instruments to be incorrectly calibrated with a bias towards weaker concentrations.

By calibrating with standards that are more diluted than intended, all subsequent water samples tend to be measured at inferred concentrations that are weaker than the actual concentration. Fluorometric water-sample analyses based upon a calibration curve that is weaker than recorded concentrations translates into a reduced tracer-breakthrough curve and serious-mass balance errors.

In addition, incorrect specific-gravity estimates applied to liquid dyes can further exacerbate incorrect fluorometric instrument calibration. Incorrectly high specific gravities raise stock concentration estimates, while incorrectly low specific gravities lower stock concentration estimates.

Reliable fluorometric instrument calibration can be achieved by preparing dye standards using dry powders that account for the manufacturer's standards and individual batch percentages. Preparation of dye standards using liquid dyes can be reliably achieved by noting the percent pure dye content, batch percent, and specific gravity of the dye. For example, the actual stock concentration of a dry powder sample of Acid Yellow 73 with an 82% manufacturer's standard and a batch percent equal to 99.5% can be reasonably estimated by

$$C_s = 82.0 \times 0.995 = 81.6\% \quad (1)$$

and the actual stock concentration of a liquid sample of Acid Yellow 73 with a 30.0% pure dye content, a batch percent of 98.7%, and a specific gravity of 1.19 g/cm^3 can be reliably estimated by

$$C_s = 30.0 \times 0.987 \times 1.19 = 35.2\% \quad (2)$$

where the units for specific gravity are accounted for elsewhere in the dilution process.

When obtaining fluorescent dyes for tracing studies, a certificate of analysis should be obtained that details the manufacturer's standard for dry powders, or percent pure dye content for liquid dyes, and the batch percent. This information is not always readily available, but can and should be demanded prior to purchase.

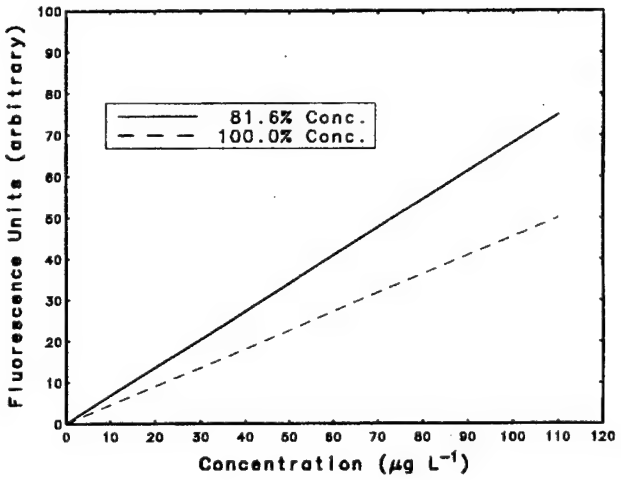

Figure 1: Simulated calibration curves for a dry powder sample of Acid Yellow 73.

Disclaimer: The views expressed in this paper are solely those of the author and do not necessarily reflect the views or policies of the U.S. Environmental Protection Agency.

DELINEATION OF SOURCE-PROTECTION ZONES FOR CARBONATE SPRINGS IN THE BEAR RIVER RANGE, NORTHEASTERN UTAH

Lawrence E. Spangler
U. S. Geological Survey, Salt Lake City, UT 84104

Dye tracing to determine recharge areas and residence times for water from carbonate springs in the Bear River Range in northeastern Utah indicates that pathways of increased groundwater velocity need to be considered when source-protection zones (zones of contribution) are delineated. Drinking-water source-protection zones for springs in fractured-rock terrains are commonly delineated using hydrogeologic mapping and time of travel (TOT) based on Darcy flow equations. Aquifers in these terrains, however, are often assumed to behave as uniform, porous media at the scale of the study area.

Dewitt spring, near Logan, Utah, discharges from Paleozoic carbonate rocks into the Logan River, which is the base level for groundwater that discharges from this alpine region (Figure 1). Discharge from the spring ranges from a low flow of about 10 cubic feet per second (cfs) during the winter to a peak flow of as much as 35 cfs in late spring during snowmelt. The aquifer supplying water to this spring can be characterized as a mixed diffuse-conduit flow system.

On the basis of other studies, 250-day, 3-year, and 15-year TOT zones for Dewitt Spring were delineated using an average linear velocity of 9.3 feet per day (ft/day). these travel times correspond to distances of about 2300, 10,200, and 51,000 feet from the spring, respectively. Dye tracing within these zones of contribution indicates considerably faster travel times than those that were calculated. Maximum ground-water travel times of less than 31 days were determined for reaches of losing stream 4.3, 5.6, and 7.2 miles upgradient from Dewitt spring, within the 15-year TOT zone, and indicate that average groundwater velocities exceed 1000 ft/day (Table 1). These results show that TOT may be substantially overestimated when delineations in these hydrogeologic settings are based on porous-media assumptions.

Dye tracing also can be used to help determine recharge areas and residence times of groundwater in carbonate terranes that behave primarily as porous-media aquifers. Maple spring supplies water for fishery and irrigation purposes and generally discharges between 5 and 10 cfs from Paleozoic carbonate rocks. The flow system supplying water to this spring is predominantly diffuse (Figure 2). On the basis of tritium age dating, the mean residence time of ground water discharging from Maple Spring was determined to be between 4 and 12 years. Dye tracing to the spring from point sources 2.65 miles upgradient and outside of the delineated recharge area, however, indicates a flow path with a travel time of about 5 days, or an average gound-water velocity of about 2700 ft/day. These results indicate that in part of the groundwater basin a high-velocity component of flow is superimposed upon the base flow of the spring during snowmelt.

These two examples illustrate the use of dye tracing as an effective method of determining zones of contribution and, most importantly, that pathways of increased ground-

SUMMARY OF DYE TRACES

Dye-Input Site	Elevation (feet)	Date-Time of Dye Injection		Type of Dye	Quantity	Dye-Recovery Sites	Elevation (feet)	Date-Time of Dye Recovery		Detector	Maximum Travel Time (days)	Linear Distance (feet)	Average Velocity (feet/day)	Average Spring Discharge (cubic feet/sec)
Maple Spring														
Devils Gate Valley	6,400	6/28/91	1430	Fluorescein	2.2 lbs (1.0 kg)	Maple Spring upper and lower (pond)	5,210	7/4/91	1530	Activated charcoal	6.04	14,050	2,325	7.0
Devils Gate Valley	6,400	7/10/93	1530	Rhodamine WT	0.26 gal (1 liter)	Maple Spring upper and lower (pond)	5,210	7/15/93	1930	Automatic sampler	5.17	14,100	2,725	7.0
Devils Gate Valley	6,400	5/7/94	1200	Fluorescein	3.2 lbs (1.4 kg)	Maple Spring upper and lower (pond)	5,210	5/21/94	0945	Activated charcoal	13.91	14,150	1,015	8.8
Dewitt Spring														
South Fork of Cottonwood Canyon	7,160	9/15/95	1700	Fluorescein	2.4 lbs (1.1 kg)	Dewitt Spring channel	5,040	10/9/95	1745	Activated charcoal	24.03	29,550	1,230	25
Upper Wood Camp Hollow	7,120	9/13/96	1800	Fluorescein	2.0 lbs (0.91 kg)	Dewitt Spring channel	5,040	10/14/96	1415	Activated charcoal	30.84	22,700	735	23
Upper Cottonwood Canyon	7,920	7/5/98	1800	Fluorescein	4.4 lbs (2.0 kg)	Dewitt Spring overflow	5,040	7/27/98	1740	Activated charcoal	21.99	38,200	1,735	28

Table 1: Summary of dye-tracing results to Maple Spring and Dewitt Spring, Bear River Range, Utah.

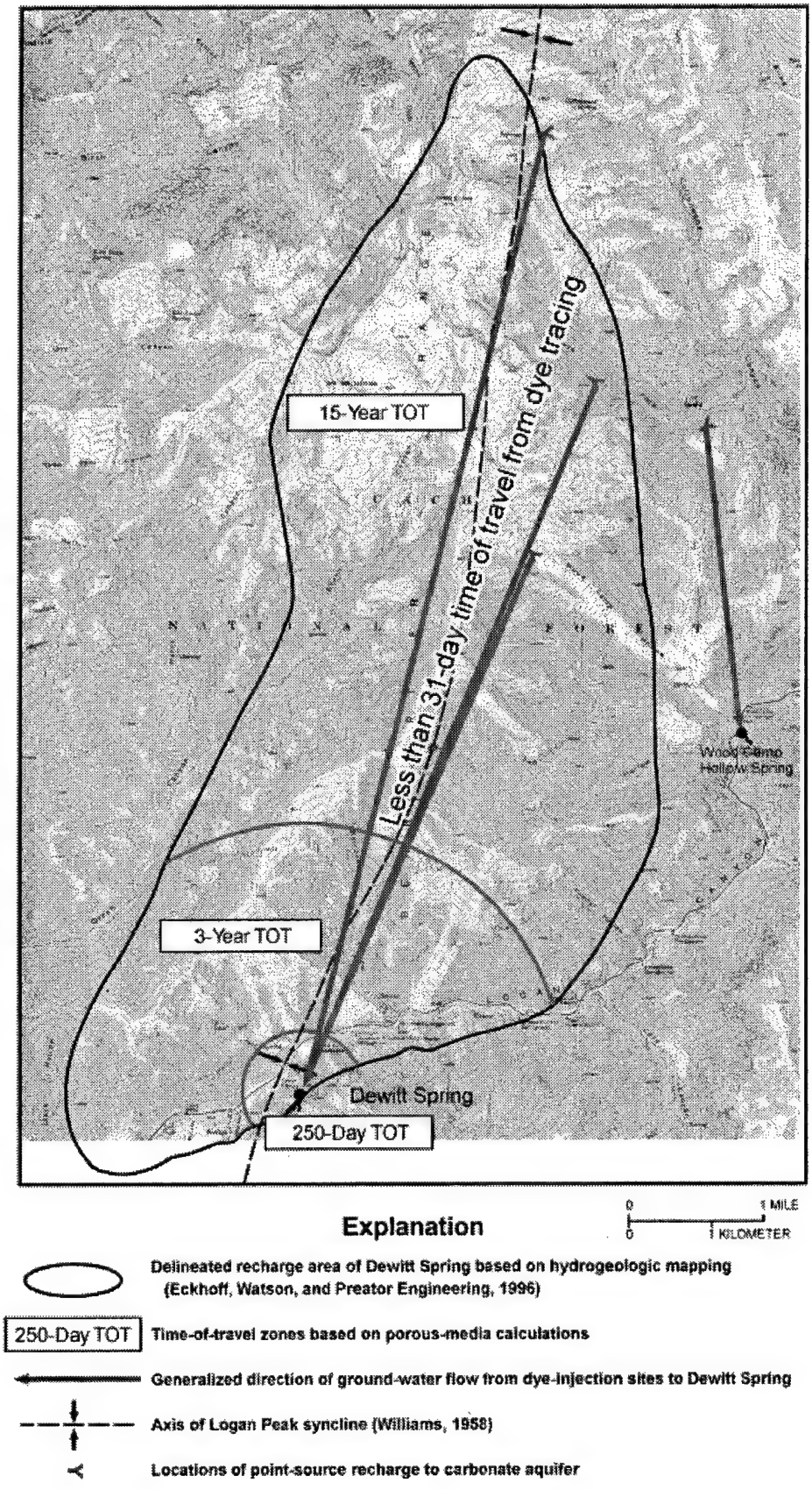

Figure 1: Time-of-travel estimates to Dewitt Spring, assuming porous-media flow, compared to dye-tracing results.

water velocity to springs in fractured-rock terrains that do not behave as porous-media aquifers. Because dissolution along fractures in carbonate terrains results in increased ground-water velocity, conceptual models of ground-water movement based on porous-media flow may not be applicable when source-protection zones are delineated. Recognition of these pathways also is crucial to predicting the transport and fate of contaminants to public-water supplies developed in these settings.

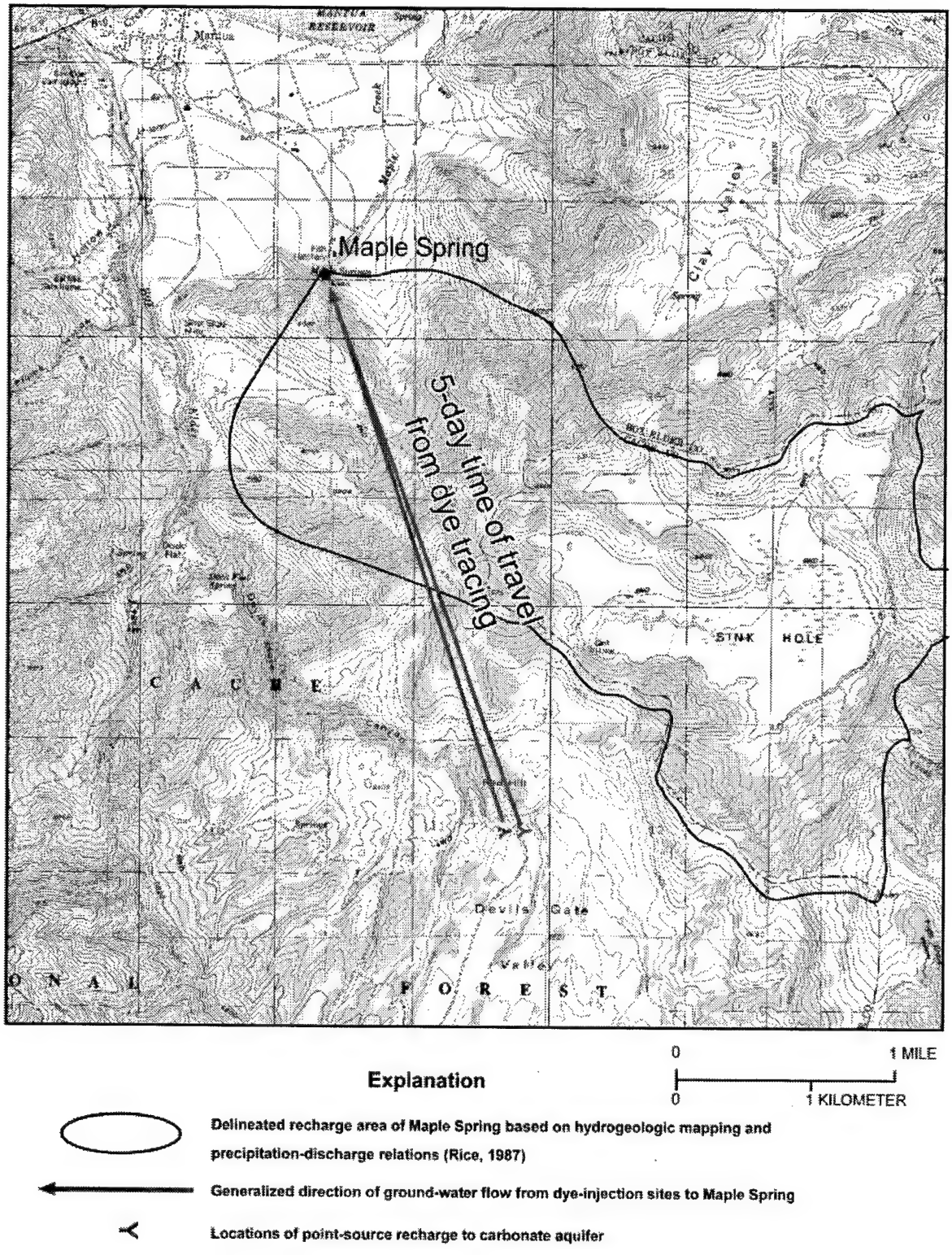

Figure 2: Time-of-travel estimates to Maple Spring, assuming porous-media flow, compared to dye-tracing results.

GEOCHEMICAL AND ISOTOPIC EVIDENCE FOR MULTIPLE RESIDENCE TIMES IN THE SAME AQUIFER

E. Calvin Alexander, Jr., Scott C. Alexander, Sheila R. Grow[1], Betty J. Wheeler[1], Roy A. Jameson, Lifeng Guo[2], and Daniel H. Doctor
Department of Geology and Geophysics, University of Minnesota, Minneapolis, MN, 55455.

[1] Minnesota Department of Health, 121 E. 7th Place, P.O. Box 64975, St. Paul, MN 55164.
[2] Minnesota Pollution Control Agency, 520 Lafayette Rd. St. Paul, MN 55155

Abstract

Modern agriculture significantly changes the bulk ionic chemistry of waters recharging through cultivated areas. In southeastern Minnesota's shallow carbonate aquifers current recharge waters contain up to 6 meq/kg of a Ca+ Mg/Cl+NO_3 component in addition to the natural background of 4 to 6 meq/kg of Ca+Mg/HCO3. This anthropogenic component results from application of nutrients to the fields. The nutrients are modified by complex bio-mediated reactions, primarily in the root zone, to produce the observed recharge compositions. In domestic and municipal water wells the absence of detectable tritium correlates remarkably well with the absence of any anthropogenic components. The atmospheric testing of thermonuclear weapons in the 1950s and 1960s, which produced the tritium signal, coincidentally occurred at the same time that modern intensive agriculture was developed. The anthropogenic component, therefore, can be a chronological marker of groundwater residence times. This component can be detected with conductivity probes and characterized with cation/anion analyses -- both of which are much more economical than traditional isotopic residence-time chronological measures; and conductivity measurements are readily adapted to continuous monitoring with data loggers.

Numerous workers all over the world have documented the large and complex chemical changes displayed by many springs that drain carbonate aquifers -- and the absence of such changes in other such springs. The presence or absence of such changes in individual springs forms the basis of Shuster and White's (1971) classic classification of carbonate aquifers. Shuster and White (1971) emphasized annual cycles of seasonal changes as revealed by biweekly sampling. They and many other workers have documented the complex chemical hydrographs produced by recharge events in many carbonate springs at the time scale of minutes to days. Several workers have used tracing techniques to document that the flow paths feeding adjacent ceiling drips in caves can have radically different residence times.

At the karst basin scale, a three-year study of the water quality in two karst springs in Fillmore County, Minnesota, documented both minutes-to-days scale, recharge-event-driven changes, and longer time-scale changes in the nitrate and atrazine levels in these springs. The longer time-scale changes occur on the months-to-years scale but are not seasonal. The longer-term changes correlate with periods of above- and below-average precipitation. The nitrate and atrazine levels in the springs decrease during dry periods (nitrate by factors of two or more and atrazine by much larger factors) and rebound during wet periods. Although several hydrogeochemical models might explain these data, the simplest explanation postulates variable-residence-time reservoirs in the same aquifer. The spring flows during wet periods are dominated by short-residence-time discharge, but the lower levels of anthropogenic components in the spring water during dry periods indicates that the residence times of the dry-period flows predate the rise of modern high-input agriculture. The time response of these carbonate aquifers is highly non-linear. A few months into a dry period the base flow in the springs contains major flow components that are several decades old.

In a local-scale study, two speleothem drips in Mystery Cave, Fillmore Co., Minnesota, have been monitored for several years. Continuous records of the drip rates, conductivity and temperature are complemented by periodic chemical and isotopic analyses of the drip waters. The two drips are about 50 m apart and about 20 m below the surface. While the flow in both drips responds rapidly to surface recharge events, the chemistries of those responses are different. Both drips display very little temperature variation. The more rapid drip's chemical hydrograph resembles that of a mixed surface spring. The slower drip's chemical hydrograph is marked by conductivity peaks associated with recharge events followed by conductivity decreases as the drip rate returns to base flow on the weeks-to-months time scale. The conductivity peaks are due to the addition of an anthropogenic Ca+Mg/Cl component to the base flow's

Ca+Mg/HCO3 composition. The challenge at this drip is not to explain the high-flow component because the cave is under and adjacent to agricultural fields. The challenge is to understand the composition of the base-flow component. A key question is: where and when did the water infiltrate that is in the drips during base flow? Again, the simplest among several possible models postulates that the base flow is older than modern high-intensity agriculture. This model has the advantage of being testable with tritium analyses of selected samples. Such measurements are in progress but results are not available at this time.

This research has been supported by a series of grants from the Legislative Commission on Minnesota Resources. Minnesota Department of Natural Resources staff have supported this research in many ways. We are especially grateful to Forestville State Park Manager Mark White and Mystery Cave Specialist Warren Netherton.

MASS BALANCE AS A TOOL FOR THE MODELING OF MIXING ZONES AT KARST SPRINGS, USING MANITOU SPRINGS AND CAVE OF THE WINDS, COLORADO, AS AN EXAMPLE

Fred Luiszer
Department of Geological Sciences, University of Colorado
Boulder. CO 80309-0399

Abstract

In this day and age of the super-computers and complex 3D modeling software, we sometimes forget about simple mathematical models that can be used to solve complex problems. The deciphering of the mixing zone at Manitou Springs is a good example. A mass-balance equation was constructed with the cation and anion input and output of the springs. All of the outputs and one of the inputs of the spring system were well constrained. The underground inputs, however, were not well known. Setting up mass-balance equations on a computer spreadsheet facilitated the modeling of the composition of the underground inputs. By trail and error it was quickly determined that there were three underground sources and that these sources probably had compositions similar to three known springs. The variable anion and cation ratios of the springs enabled the construction of three unique equations with three variables. A computer spreadsheet was used to solve for the flow rates of the three underground sources. When these figures were put into the original mass-balance equation it indicated that mixing corrosion in the mixing zone below Manitou Springs has the ability to dissolve ~70 tons of limestone every year. The mass balance also indicated that dissolved manganese and iron are lost in the mixing zone. The nearby Cave of the Winds, with its manganese and iron oxide deposits, is strong evidence that this mixing-zone model is robust.

GEOCHEMISTRY OF THE SPRINGS OF MISSOURI

Carol M. Wicks
Department of Geological Sciences, University of Missouri
Columbia, MO 65211

Abstract

The big springs of Missouri drain the Salem Plateau. The groundwater basins range from several hundreds to a thousand square miles. The discharge from the springs can be up to several hundred cfs. Whereas a good understanding of the areal extent of the basins is available, an understanding of the depth to which groundwater flows is not. The Salem Plateau is a thick sequence of Cambrian and Ordovician carbonates (Roubidoux, Gasconade, Eminence, and Potosi Formations). These units are underlain by the Davis-Derby-Doerun Formation, a regional confining unit, and the Lamotte Sandstone. The entire sedimentary package is up to 2000 feet thick.

The purpose of this study was to use the molar ratio of SO_4 /Cl and saturation indices (SI) to elucidate the depth to which groundwater circulates through the Salem Plateau. The molar ratio of well water collected from known stratigraphic horizons was calculated and showed that the molar ratio in water from the one stratigraphic horizon was distinct from that from other. The molar ratio of spring water was determined and compared to that of the fingerprinted horizons. The saturation indices of the water with respect to the carbonate and sulfate minerals was used because the Potosi Formation hosts a barite deposit through a portion of the area. Groundwater that flows through the Potosi Formation might be equilibrated with respect to barite.

In addition, well yields for the stratigraphic horizons were compiled from a variety of sources. The well yield of the Potosi Formation is at least an order of magnitude greater than that of other formations in the sequence. It is believed that the groundwater that discharges at the karst springs in the Salem Plateau has flowed through the Potosi Formation.

TEMPERATURE AS A NATURAL TRACER OF SHORT RESIDENCE TIMES FOR GROUNDWATER IN KARST AQUIFERS

Jonathan B. Martin and Randolph W. Dean
Department of Geology, University of Florida, P.O. Box 112120
Gainesville, FL 32611-2120

Abstract

Chemistry of karst waters is controlled by reactions with aquifer rocks, the extent of mixing between water sources, and variations in the composition of recharged water. The extent of reactions and mixing may be determined uniquely if compositions of both recharged and discharged water are known, such as where sinking streams are linked to resurgent springs, and if residence time in the subsurface can be measured. Such a linked system occurs along the Santa Fe River in north-central Florida, where the river flows underground for approximately 5.2 km as it crosses from confined to unconfined portions of the Floridan Aquifer. Temporal variations in temperature can be correlated between the river sink, the river rise, and Sweetwater Lake, a karst window approximately midway between the sink and rise. Delays in the arrival time of temperature maxima and minima from the sink to Sweetwater Lake and from Sweetwater Lake to the Rise reflect the residence time of the river water in the subsurface. Residence time correlates with the river stage and ranges from approximately 12 hours to more than four days at high and low stage, respectively between the river sink and Sweetwater Lake, and from about six hours to nearly two days at high and low stage, respectively, between Sweetwater Lake and the river rise. These short residence times reflect minimum flow rates of between 1.3 and 9 km/day, indicating conduit flow. Knowing the residence time at any stage allows sampling of water as it enters the aquifer, and then again as it discharges. Changes in the chemistry of water as it passes through the subsurface should reflect chemical reactions, mixing, or both.

Introduction

Karst covers a substantial portion of the earth's continental surface and provides an important source of potable water. Regions with karst typically are characterized by direct links between groundwater and surface water through sinkholes, swallets, and highly permeable rocks. These links make karst groundwater particularly vulnerable to contamination (Field, 1988; White et al., 1995), and in some karst regions, complex and extensive mixing between groundwater and surface water blurs the distinction between the two (e.g. Kincaid, 1997). Thus contaminants such as pesticides (Pasquarell and Boyer, 1997), and nitrate from animal waste and fertilizer (Andrews, 1994; Iqbal and Krothe, 1995; Boyer and Pasquarell, 1996; Katz et al., 1997) are carried rapidly into the groundwater. Karst aquifers are characterized by pore sizes that range from cavernous to small fractures to micropores, and permeability of the aquifers can be equally heterogeneous. Consequently, flow in karst aquifers is unpredictable and difficult to model with standard numerical flow models, making it difficult to trace sources of pollutants. Furthermore, groundwater divides may not coincide with surface-water divides, and thus surface hydrology does not provide constraints on the subsurface hydrogeology (Bonacci and Zivaljevic, 1993; Greene, 1997; Katz et al., 1997).

One common technique to characterize subsurface flow is through observations of water discharging from springs. Observations include variations in the volume of spring discharge and the chemical and isotopic composition of the discharged water. Physically, variations in discharge have been used to identify sources of water within the aquifer, e.g. from conduits, micropores, fractures, or the epikarst layer (Felton and Curry, 1994; Padilla et al., 1994). Chemically, the saturation of carbonate minerals has long been used to estimate the residence time of water in the subsurface and whether flow is predominately diffuse or through conduits (Pitty, 1968; Ternan, 1972; Shuster and White, 1971, 1972; Hess and White, 1988). More recently, temporal variations in the chemical composition of spring discharge, along with its quantity, has been shown to reflect the origin of discharge water, particularly whether water is stored in the saturated or unsaturated zones, and how much is mixed with recently recharged water following storms (Dreiss, 1989; Lakey and Krothe, 1996).

Most observational studies of spring discharge rely on temporal deviations from baseline values of either the volume of water being discharged from springs or its chemical composition. Such deviations are used, rather than comparing values for recharged and discharged water, because the volume and composition commonly are unknown for the water entering the aquifer. Where perennial sinking streams are linked to resurgent springs, however, variations in the natural chemical composition of both the recharge and discharge water can be measured. Comparison of these values could provide information on the extent and type of chemical reactions in the subsurface,

as well as the amount of mixing of surface and groundwater if the composition of groundwater is known. A few studies have previously attempted this technique. For example, Thrailkill et al. (1991) injected dyes into several swallets and determined that a significant amount of flow bypasses the spring on the basis of the dye returns and discharge measurements at springs. Greene (1997) linked several sinking streams to discharge points at springs using stable-isotopic composition of the water. Vervier (1990) showed that for all measured components except silica, the composition of water of the La Planche Creek in southern France matches that of discharge of a nearby spring, indicating little mixing or reactions in the subsurface. Composition was measured approximately every two weeks, however, which is significantly longer than the time for water to flow the 3300 m from the sink to the spring. In addition, samples were collected simultaneously from the sink and the spring, and thus any differences in chemistry between the two sampling sites could reflect a temporal variation in the composition of water in La Planche Creek.

In order to identify variations in chemical composition caused by mixing or reaction in the subsurface, samples must be collected as the water in a stream sinks, and then again when the same batch of water returns to the surface. If no mixing or reactions occur in the subsurface, these linked samples should have identical compositions. The ability to collect such linked samples, however, requires detailed information on the residence time of water in the subsurface (i.e., the time it takes for water to flow from it entry point into the aquifer to its discharge point). As demonstrated in this paper, the residence time between a river sink, river rise and intermediate karst windows can be measured by correlation of variations of the water temperature at each sampling location. Temperature provides a good tracer because it can be measured automatically and continuously (e.g. Shuster and White, 1971, 1972), providing detailed and frequent information about the residence time of water in the subsurface. We use this information to address additional questions of how residence time varies with river stage, and to speculate on the relationship between residence time, stage, and the nature of the subsurface conduits.

Regional geology and hydrology

The geology of north-central Florida can broadly be divided into the pre-Miocene carbonate rocks that comprise the Floridan aquifer, and Miocene and younger mixed siliciclastic and carbonate rocks that act as the confining unit for the Floridan aquifer (Scott, 1988, 1992; Groszos et al., 1992). Miocene and younger rocks (primarily of the Hawthorn Group) have been removed by erosion from the western portion of northern peninsular Florida. The erosional edge of the Miocene rocks is the boundary between the confined and unconfined Floridan aquifer, which extends through the study area (Figure 1). The boundary is referred to as the Cody Scarp and

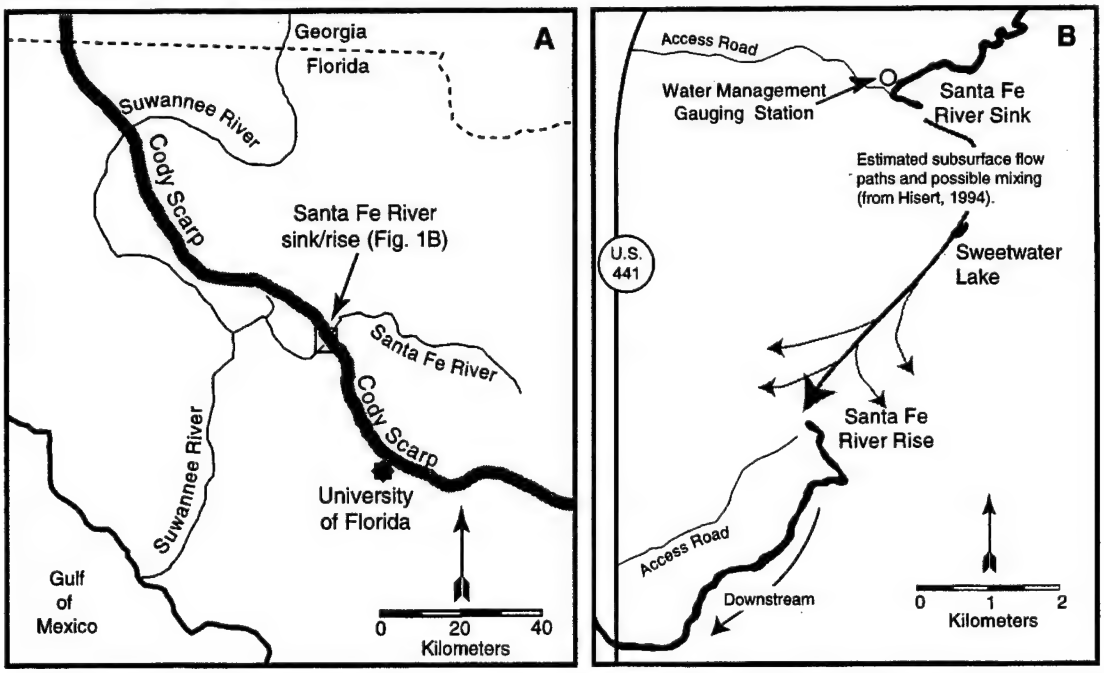

Figure 1: (A) Regional location map showing the location of the Cody Scarp, the Santa Fe sink and rise, and the major streams in the region. The Cody Scarp represents the western limit of the Hawthorn Group and the boundary between the confined and unconfined Floridan Aquifer. **(B)** Details of the Santa Fe sink/rise area showing locations of the river sink, Sweetwater Lake, and river rise. The gauging station upstream from the river sink is where the stage data presented in Figure 3 is collected.

represents one of the steepest land surface slopes in Florida, approximately 25 m vertical relief over approximately 10 km lateral distance (Puri and Vernon, 1964). In the confined area to the northeast of the scarp, surface water is common, but it is mostly missing in the unconfined area to the southwest. Most streams that cross the Cody Scarp either become losing streams, sink underground and then re-emerge, or completely sink underground with no clear point of emergence (Hunn and Slack, 1983).

Groundwater in Florida resides in three separate aquifers: The Surficial, Intermediate, and Floridan aquifers (Scott, 1992). The Surficial aquifer is a water-table aquifer comprised of Pleistocene and Holocene unconsolidated sands. The Intermediate aquifer consists of disconnected carbonate units within the Hawthorn Group. The Floridan aquifer is composed of Oligocene and Eocene carbonate rocks and extends from South Carolina across the entire Florida Platform (Ryder, 1985; Tibbals, 1990). The Floridan aquifer is the primary water supply for northern Florida, and thus mixing between groundwater and surface water along the Cody Scarp is critical to the quality and quantity of the regional water supply. In addition, surface water is undersaturated with respect to carbonate minerals and drives extensive dissolution when it sinks along the Cody Scarp (Upchurch and Lawrence, 1984).

One of the major streams in the region is the Santa Fe River, which discharges an average of 10.3 m^3/sec as it flows across the Cody Scarp. Along this stretch the river flows into a sinkhole at the sink and temporarily re-emerges at the rise approximately 5.2 km from the sink (Figure 1B). Although tracer studies have been conducted, no direct link between the sink and rise has been made; instead the Sink was linked to the rise in two steps, first between the sink and Sweetwater Lake, an intermediate karst window, and then subsequently between the Sweet-water Lake and the rise (Hisert, 1994). Nonetheless, Hisert (1994) showed rapid flow on the order of 1-3 km/day, indicating that subsurface flow is through conduits. Hisert (1994) also concluded that the river rise is the primary resurgence of the underground flow of the Santa Fe River.

Temperature as a tracer

Dye tracing is a useful tool for linking sources of water with their discharge points (e.g. Hisert, 1994; Thrailkill et al., 1991), but the complex logistics involved with these types of studies limits the frequency with which they can be conducted. In karst regions, the elevation of the free water surface in conduits can change rapidly following storms because of rapid influx of recharge water. As elevations of the water surfaces change, water may use different conduits as flow paths, or conduits may become completely filled. Consequently, dye trace studies would have to be conducted frequently and at various stages of water level in order to accurately determine the residence time of water in the subsurface, as well as the relationship of residence time to river stage or water-table elevation. Therefore it is critical to find a technique that measures the residence time of water in the subsurface at high frequency.

The approach we take here is to measure residence time by correlating variations in the water temperature at the river sink, Sweetwater Lake, and the river rise. Temperature is measured automatically using waterproof commercial temperature loggers manufactured by Onset Computer Corporation. The loggers have temperature and time accuracies of 0.1° C and 0.01% respectively. The temperature loggers are encased in 3-inch-diameter PVC pipe, open at both ends. The loggers and PVC pipe are attached to floats and anchored to the bottom of the river in such a way that the loggers float approximately 1.5 m off the bottom. Between January and July 1998, the temperature loggers measured temperature every 90 seconds, and we downloaded the data every two weeks. Between July and November 1998, the loggers measured the temperature every 3 minutes, and we downloaded the data once a month. The resulting temperature records from January 13, 1998, through November 2, 1998, are shown in Figure 2. River stage is measured daily at a gauging station located approximately 1 km upstream from the river sink by personnel at O'Leno State Park (Figure 1B).

An abnormal amount of rain fell in the region during the winter months of 1998, and as a result the Santa Fe River experienced a 100-year flood during February (Figure 3). When river stage reaches >14.3 m above mean sea level, such as during the February flood, a portion of the river flows overland as well as enters the sink. Below this stage, all water in the river enters the sink. Regardless of stage, the temperature records at the sink, Sweetwater Lake and the rise show numerous distinct maxima and minima of several days' duration that occur most commonly when the river stage is high. As the air temperature warmed and the river stage dropped in late spring and early summer, the longer-periodicity variations in temperature were replaced with a gradual warming trend overprinted by diurnal fluctuations in temperature at the river sink (Figure 2). These diurnal fluctuations are less pronounced, but are still present at Sweetwater Lake, and are reduced further, but occasionally recognizable, at the river rise. Most of the longer maxima and minima can be correlated between the three sampling locations. The diurnal fluctuations can also be correlated in certain portions of the records, particularly where there are longer variations such as at the end of July and beginning of August, and in the middle of October. The systematic lack of diurnal temperature fluctuations during high river stage suggests that the river water equilibrates with air temperature only during slow flow.

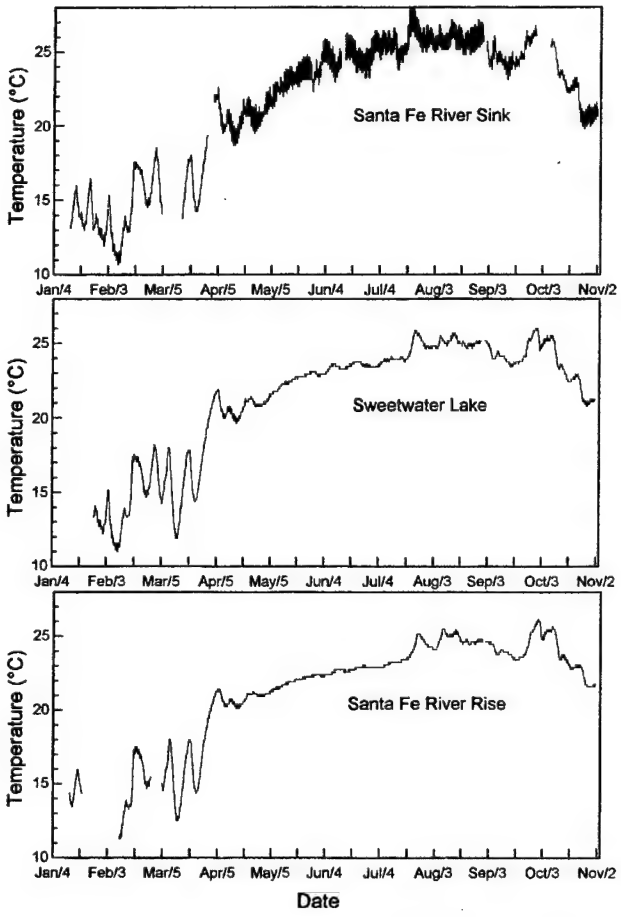

Figure 2: Records showing the temperature of water at the Santa Fe River sink, Sweetwater Lake, and river rise between January 13, 1998 and November 2, 1998. Gaps in the data are when temperature loggers failed or were lost. Correlations between the records were made from significantly larger-scale figures, which are not shown here in order to save space.

Correlations of maxima and minima in temperature shown on Figure 2 reflect a systematic time lag in maxima and minima of temperature measured at the river sink and Sweetwater Lake and at Sweetwater Lake and the river rise. These time lags may reflect the residence time of the water in the subsurface. Several processes may change the temperature of the water during passage through the subsurface, however, such as heat exchange with the aquifer rocks, diffusion of heat into or out of the groundwater, heating and cooling as the water passes through the karst windows in its passage from the sink to the rise, and physical mixing of water in the pore spaces with river water as it flows through the subsurface conduits (Figure 1B). Mixing is likely to control the temperature during low-flow conditions in the summer. As shown in Figure 2, the temperature maxima that occur in July through August decrease in value from the sink to Sweetwater to the rise, where the temperature approaches the average value of approximately 22° C for groundwater in the region. These decreases in temperature imply that there has been some mixing, but the temperature does not change between the sampling locations during flooding in February or October, which suggests that there is less mixing during floods. There is also little observable change in the temperature between the sink, Sweetwater Lake, and the rise during low-flow conditions at the end of the record in October, because the surface and groundwater temperatures are nearly identical.

There is a good correlation between the stage of the river and the residence time in the subsurface, with significantly faster flow occurring during higher river stage, but the change in residence time with stage does not vary smoothly (Figure 4). At river stage <11, residence time decreases rapidly as stage increases from >4 days to approximately 1.5 days between the sink and Sweetwater Lake, and from nearly two days to approximately 12 hours between Sweetwater Lake and the rise. At river stages between 11 and 12.5 m, residence time decreases more slowly with increasing stage than at river stages <11 m. At these intermediate stages, residence times decrease from approximately 1.5 days to approximately 12 hours between the sink and Sweetwater Lake and from 12 to 6 hours between Sweetwater Lake and rise. At stages >12.5, residence time changes little, even when the river begins to flow overland at a stage of 14.3 m. The straight-line distances between the river sink and Sweetwater Lake, and between Sweetwater Lake and the river rise are 3 and 2.2 km, respectively. These distances indicate that minimum flow velocities in the subsurface range between approximately 1 and 9 km/day, depending on the river stage. The slowest flow rates match those found by Hisert (1994) and must reflect conduit flow.

The dependence of residence time on stage may reflect variations in the flow character of the subsurface conduits. At low stage, the large variation in residence time with small increases in stage may indicate that portions of the conduits are not completely filled with water or that there may be additional conduits that the river spills into as stage increases. At stages above 11 m, the less-rapid increase in residence time with increasing river stage may reflect conduits that are completely filled with water. The slight decrease in residence time as stage increases may reflect the increased hydrologic gradient between the sink and rise.

By knowing the relationship between residence time and stage (e.g. Figure 4), it is possible to sample water when it enters the sink, re-emerges at karst windows such as Sweetwater Lake, and when it permanently re-emerges at

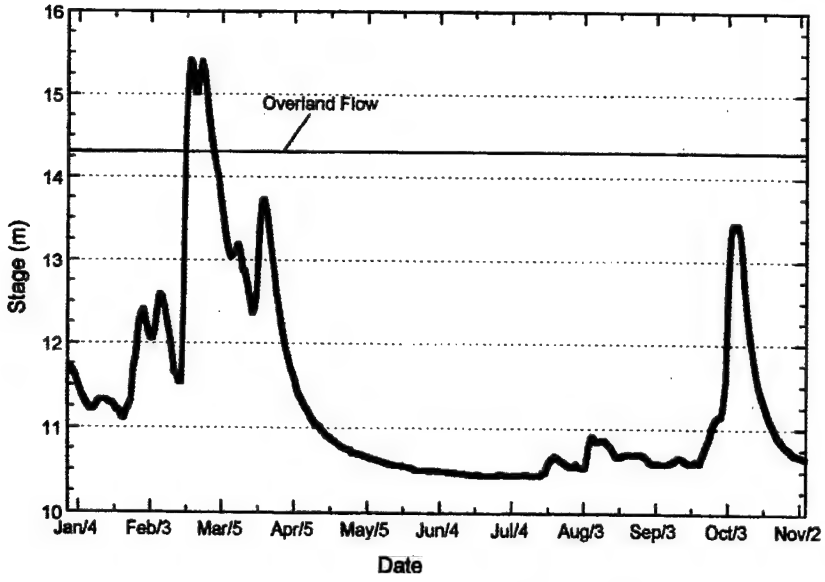

Figure 3: Stage of the Santa Fe River between January 1, 1998, and November 5, 1998. The flood during February and March, the normal dry season, was a result of that winter's El Niño weather patterns, and the flood in October resulted from Hurricane Georges.

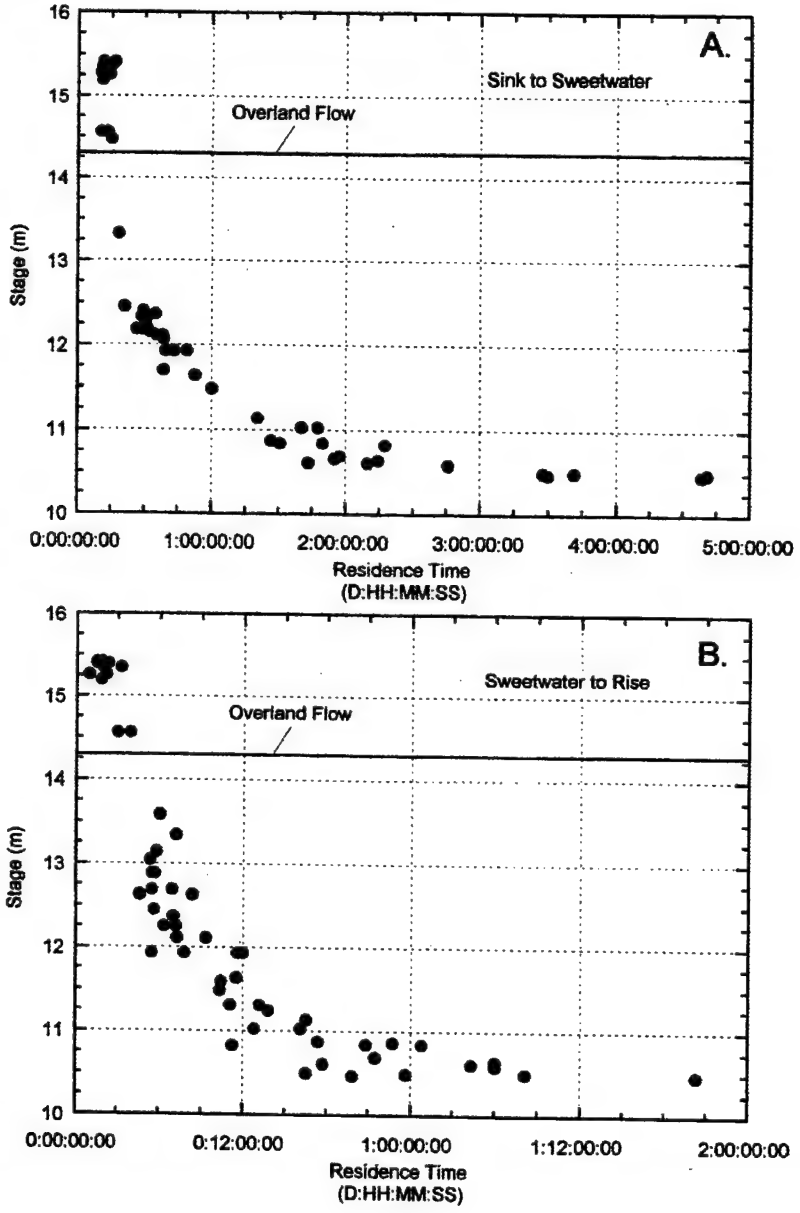

Figure 4: The relationship between residence time and river stage for **(A)** flow between the river sink and Sweetwater Lake, and **(B)** flow between Sweetwater Lake and the river rise. There is a good correlation between stage and residence time, but the slope of the correlation changes at stages of ~11 m, possibly reflecting changes in the flow paths, or that the conduits become completely filled with water.

the rise. The chemical composition of water sampled in this manner will only vary because of mixing with groundwater and through reactions in the subsurface. Mixing proportions can be calculated by comparing values of conservative tracers such as Cl concentrations and ^{18}O and D values of water at the sink, Sweetwater Lake, and the rise with groundwater obtained from water-supply wells in the region. Thus by measuring changes in the chemistry at the river sink, Sweetwater Lake, and the rise, it will be possible to calculate the relative proportions of water discharging at the rise that represents groundwater and water that flows from the sink. It should also be possible to determine how the extent of mixing varies with stage. Changes in the chemistry that are not caused by mixing must result from reactions in the subsurface and may be a useful way to measure rates of karstification in the region.

Conclusions

Temperature appears to be a useful natural tracer in areas characterized by rapid flow through karst aquifers. This tracer is useful because it can be accurately measured at high resolution, which allows frequent determination of residence time. Consequently, this information allows observations of the changes in residence time relative to river stage, which may be related to the nature of the conduits. In addition, by knowing the relationship between residence time and stage, it is possible to sample water as it enters the aquifer and again as it discharges to the surface. Chemical changes in the water as it passes through the subsurface should provide information on mixing between the surface and groundwater, as well as chemical reactions in the subsurface.

Similar to temperature, the chemical composition, including conductivity of the water, is likely to provide useful natural tracers for residence time in the subsurface. Using these tracers will require development of techniques either to automatically measure the tracer or automatically collect water samples at high resolution. Nonetheless, it will be particularly useful to use two or more distinctly different natural tracers simultaneously. Different tracers are likely to be controlled by different environmental variables, and this could provide complementary information about the system. For example, conductivity should change after storms and flood events through dilution by lower-conductivity rainwater, although temperature may remain fairly constant. In contrast, temperature will mimic seasonal air-temperature patterns, but the temperature will not alter the conductivity of the water. High-resolution measurements of conservative chemical and isotopic components in the water, such as Cl or stable isotopes of water, may also be useful for determining the residence time. Changes in the composition of the reactive components may reflect small spatial and temporal heterogeneity of the mixing of various water sources and possibly reactions in the subsurface. Combining two or more tracers should thus precisely constrain the residence time of water in the subsurface.

Acknowledgments

We thank the staff at O'Leno State Park, in particular Mr. Dale Kendrick, for allowing us to sample frequently and at times when the park is normally closed to the public. By granting us frequent access to the park, Mr. Kendrick has made this work possible. We also thank Liz Screaton for reviewing an early version of the manuscript. The work was supported by NSF grant EAR-9725295 to Martin.

References cited

Andrews, W.J., 1994, Nitrate in ground water and spring water near four dairy farms in North Florida, 1990-1993: U.S. Geological Survey, Water Resources Investigation 94-4162, 63 p.

Bonacci, O., and R. Zivaljevic, 1993, Hydrological explanation of the flow in karst: example of the Crnojevica spring: Journal of Hydrology, v. 146, p. 405-419.

Boyer, D.G., and G.C. Pasquarell, 1996, Agricultural land use effect on nitrate concentrations in a mature karst aquifer: Water Research Bulletin, v. 32, p. 565-573.

Dreiss, S.J., 1989, Regional scale transport in a karst aquifer 1. Component separation of spring flow hydrographs: Water Resources Research, v. 25, p. 117-125.

Felton, G.K., and J.C. Currens, 1994, Peak flow rate and recession-curve characteristics of a karst spring in the Inner Bluegrass, central Kentucky: Journal of Hydrology, v. 162, p. 99-118.

Field, M.S., 1988, The vulnerability of karst aquifers to chemical contamination: Environmental Protection Agency, 600/D-89/008, 13 p.

Greene, E.A., 1997, Tracing recharge from sinking streams over spatial dimensions of kilometers in a karst aquifer: Ground Water, v. 35, p. 898-904.

Groszos, M.R. C., D. Allison, R. Cooper, M. Weinberg, M. Macesich, M.M. Enright, and F. Rupert, 1992, Carbonate units of the intermediate aquifer system in the Suwannee River Water Management District, Florida: Florida Geological Survey, Open File Report no. 54, 22 p.

Hess, J.W., and W.B. White, 1988, Storm response of the karstic carbonate aquifer of south-central Kentucky: Journal of Hydrology, v. 99, p. 235-252.

Hisert, R.A., 1994, A multiple tracer approach to determine the ground and surface water relationships in the western Santa Fe River, Columbia County, Florida: unpub. Ph.D. dissertation, University of Florida, 212 p.

Hunn, J.D., and L.J. Slack, 1983, Water resources of the Santa Fe River Basin, Florida: U.S. Geological Survey, Water Resources Investigation 83-4075, 111 p.

Iqbal, M.Z., and N.C. Krothe, 1995, Infiltration mechanisms related to agricultural waste transport through the soil mantle to karst aquifers of southern Indiana, U.S.A.: Journal of Hydrology, v. 164, p. 171-192.

Katz, B.G., and T.D. Bullen, 1997, The combined use of $^{87}Sr/^{86}Sr$ and carbon and water isotopes to study the hydrochemical interaction between groundwater and lake water in mantled karst: Geochimica et Cosmochimica Acta, v. 60, p. 5075-5087.

Kincaid, T.R., 1997, Ground water - surface water exchange in the unconfined karstified Floridan aquifer, *in* G.G. Johnson (ed.), Karst Waters and Environmental Impacts: Rotterdam, A.A. Balkema, p. 405-412.

Lakey, B., and N.C. Krothe, 1996, Stable isotopic variation of storm discharge from a perennial karst spring, Indiana: Water Resources Research, v. 32, p. 721-731.

Padilla, A., A. Pulido-Bosch, and A. Mangin, 1994, Relative importance of baseflow and quickflow from hydrographs of karst spring: Ground Water, v. 32, p. 267-277.

Pitty, A.F. , 1968, Calcium carbonate content of water in relation to flow-through time: Nature, v. 217, p. 939-940.

Puri, H.S., and R.O. Vernon, 1964, Summary of the geology of Florida and a guidebook to the classic exposures: Florida Geological Survey Special Publication 5, 312 p.

Ryder, P.D., 1985, Hydrology of the Floridan aquifer system in west-central Florida: U.S. Geological Survey Professional Paper 1403-F, 98 p.

Scott, T.M., 1988, The lithostratigraphy of the Hawthorn Group (Miocene) of Florida: Florida Geological Survey Bulletin 59, 147 p.

Scott, T.M., 1992, A geologic overview of Florida: Florida Geological Survey, Open File Report, no. 50, 78 p.

Shuster, E.T., and W.B. White, 1971, Seasonal fluctuations in the chemistry of limestone springs: A possible means for characterizing carbonate aquifers: Journal of Hydrology, v. 14, p. 93-128.

Shuster, E.T., and W.B. White, 1972, Source areas and climatic effects in carbonate groundwaters determined by saturation indices and carbon dioxide pressures: Water Resources Research, v. 8, p. 1067-1073.

Ternan, J.L., 1972, Comments on the use of a calcium hardness variability index in the study of carbonate aquifers, with reference to the central Pennines, England: Journal of Hydrology, v. 16, p. 317-321.

Thrailkill, J.S., B. Sullivan, and D.R. Gouzie, 1991, Flow parameters in a shallow conduit-flow carbonate aquifer, Inner Bluegrass karst region, Kentucky, USA: Journal of Hydrology, v. 129, p. 87-108.

Tibbals, C.H., 1990, Hydrology of the Floridan aquifer system in east-central Florida: U.S. Geological Survey, Professional Paper 1403-E, 98 p.

Upchurch, S.B., and R.W. Lawrence, 1984, Impact of ground-water chemistry on sinkhole development along a retreating scarp, *in* B.F. Beck (ed.), Sinkholes: their geology, engineering and environmental impact: Rotterdam, B.A., Balkema, p. 189-195.

Vervier, P., 1990, Hydrochemical characterization of the water dynamics of a karstic system: Journal of Hydrology, v. 121, p. 103-117.

White, W.B., D.C. Culver, J.S. Herman, T.C. Kane, and J.E. Mylroie, 1995, Karst lands: American Scientist, v. 83, p. 450-459.

USING TEMPERATURE VARIATION AT SPRINGS TO CHARACTERIZE FLOW IN CARBONATE AQUIFERS

Gareth J. Davies
Cambria Ground Water Inc., 109 Dixie Lane, Oak Ridge, TN 37830

Sidney W. Jones
Tennessee Department of Environment and Conservation, 761 Emory Valley Road
Oak Ridge, TN 37830

Abstract

Daily temperature measurements were taken for more than a year at several springs discharging from the Knox aquifer into Scarboro Creek in Oak Ridge, Tennessee. The data exhibit a delayed response to the annual harmonic temperature variation, but no apparent correlation between amplitude of the signal and the lag time (with respect to the daily air temperature for the year). The lag times appear to be almost identical, while the amplitudes vary significantly. The springs have variable discharges and some are known to involve deep flow paths.

A hypothetical model of heat conduction through aquifer materials having similar thermal properties predicts both lower amplitude and significantly larger lag time for deeper flow paths than for shallower flow paths. An analytical model which included both conduction and an advective heat flux based upon typical average aquifer recharge rates was used to show that uniform heat advection due to aquifer recharge was not sufficient to change the inverse correlation between the predicted amplitude and lag time.

Interpretation of the temperature data using these single-continuum heat-transfer models would require significant variations in thermal properties between adjacent portions of the Knox aquifer. Given that the thermal diffusivity of similar geological materials does not vary greatly, such a hypothesis would not seem tenable. Alternatively, apparent variations in the bulk average thermal properties of the aquifer may be hypothesized as being primarily due to thermal disequilibrium between rapid-flow and slow-flow portions of the aquifers discharging at the springs. If the advective heat flux into the aquifer is modeled using concentrated rapid recharge and groundwater flow through fissures, the lag time would not necessarily correlate inversely with amplitude. An analytical model of a thermal signal carried into the aquifer via advection through a fracture with conduction into the adjacent rock matrix can demonstrate that heat carried by rapid flow through dissolutionally enlarged fractures can penetrate the aquifer much more rapidly than the thermal signal transferred by conduction. This effectively lowers the bulk aquifer heat capacity, since the thermal signal can be carried relatively large distances along the major flow paths while penetrating only short distances into the matrix.

During the period of maximum evapotranspiration the advective component of the heat flux into the aquifer would be diminished relative to the conductive flux, and would be negligible except perhaps after a few major storms. The conductive heat flux is thus thought to dominate throughout the growing season. The downturn of the spring temperatures appears to correspond roughly to the initiation of significant recharge of cooler water and hence indicates a more important role for the advective flux in the cold season. Springs with larger base flows show less seasonal temperature change during the growing season. The Oak Ridge data support a hypothesis that springs with larger recharge areas have deep average flow paths and are less influenced by the conductive heat flux.

DELINEATION AND CHARACTERIZATION OF THE GROUNDWATER BASINS OF FOUR CAVE SYSTEMS OF SOUTHWESTERN ILLINOIS' SINKHOLE PLAIN

S. V. Panno and C. P. Weibel
Illinois State Geological Survey, 615 E. Peabody Drive
Champaign, IL 61820

Abstract

An approximation of the boundaries of the groundwater basins associated with four of the largest cave systems in Illinois was initiated in 1996 using limited data on tracer experiments and existing cave maps, and by characterizing the size, morphology and distribution of sinkholes in the vicinity of the caves.

Clusters of relatively large sinkholes were found overlying and near the state's largest known cave systems. Sinkholes can approach one-half kilometer in areal extent in the vicinity of large caves. The size and morphology of these sinkholes are different from that in the vicinity of smaller cave systems. That is, sinkholes associated with large cave systems are larger and more complex than those associated with smaller conduit systems. We suggest that, at least in Illinois, the size of a sinkhole is an indicator of conduit-system size.

The mechanism for this relationship is erosion of relatively thick loess deposits that mantle the karst areas. The higher the energy of runoff flowing through the sinkholes, the more erosion that occurs. Erosive growth of a sinkhole is limited by the rate at which the underlying conduit system can discharge incoming water. Too small a conduit system, and its storage capacity will be exceeded, causing sinkhole flooding. The flooding, in turn, creates a low-energy environment that is more depositional that erosive, and growth of the sinkhole is inhibited. Conversely, if the inflow of water through a sinkhole is uninhibited, the energy of inflowing water can remain high and continue to erode the sinkhole margins via gullying.

KARST INVENTORY OF THE NORTHERN GUAM LENS AQUIFER

Danko S. Taborosi
Water & Environmental Research Institute of the Western Pacific University of Guam
Mangilao, Guam 96923

Abstract

Guam is a rapidly developing island with over 70% of its water supply drawn from the carbonate Northern Guam Lens Aquifer. This project is the first attempt to comprehensively inventory, map, and interpret the aquifer's karst features. Guam exhibits characteristic island karst features, but karst evolution and hydrologic behavior have been influenced in important ways by rapid uplift (up to 180 m in Pleistocene time). Moreover, in spite of the aquifer's relatively small size and young age, it also exhibits, on some terrain, some well-developed classic karst features more typical of continental settings (e.g., blind valleys and disappearing streams). Features on which this investigation is focused include epikarst, closed depressions, caves, and coastal springs. Epikarst on Guam appears to be identical to that of other carbonate islands. Dissolutional closed depressions include large sinkholes mimicking cockpit karst, small collapsed sinkholes, and blind valleys. The largest closed depressions are probably constructional. Exposed caves on Guam include pit caves, stream caves and flank margin caves. Numerous pit caves vary widely in size and reach depths up to 50 meters. Stream caves are associated with allogenic rainwater catchment by volcanic rocks. Flank margin caves are exposed on the cliffs in Northern Guam and indicate previous sea-level still stands. Additional types of caves include voids created on the top, bottom and within the freshwater lens. These voids, not exposed at the surface, are often intercepted during well drilling. Coastal springs include discharging caves, fractures, and underwater vents along cliff lines, and springs and seep fields along beaches.

THE KENTUCKY KARST ATLAS: A COOPERATIVE PROJECT BY KENTUCKY DIVISION OF WATER AND KENTUCKY GEOLOGICAL SURVEY

Joseph A. Ray
Kentucky Division of Water
Frankfort, KY 40601

Abstract

More than half of Kentucky is underlain by soluble rocks such as limestone and dolomite, which produce karst groundwater drainage. Karst terrane may include features such as sinkholes, caves, underground streams, karst windows, and large springs. Also, a general absence of perennial surface drainage in karst terrane can cause public water-supply sources to be localized, poorly understood, and difficult to protect.

The Kentucky Karst Atlas consists of maps compiled from groundwater tracer studies over the last 60 years. They provide much-needed information about the occurrence of karst groundwater basins and their hidden underground streams. The maps are vital to the Division of Water's emergency response to spills of hazardous materials, and the protection of karst water supplies. The volume of a spring and the location of its recharge area can be inferred from the mapped groundwater basin.

These atlas sheets are a result of one of the most comprehensive statewide karst-basin compilation projects in the nation. This atlas series features on-demand digital maps that will be periodically revised and updated as new data become available. The mapping style is based on the map: *Groundwater Basins in the Mammoth Cave Region, Kentucky,* by Quinlan and Ray (1981). Innovations include the delineation of karst and non-karst areas; the use of Division of Water *AKGWA* numbers to identify spring basins; the identification of surface overflow routes and known intermittent lakes; and the illustration of overflow springs with open circles.

HOW DID THE FIBORN KARST FORM IN ONLY 5000 YEARS?

Rane L. Curl
Department of Chemical Engineering, University of Michigan
Ann Arbor, MI 48109-2136

The Fiborn Karst in Michigan is an integrated system of caves, some extending over 2 km, with at least five active stream inputs, on a portion of the Niagaran Escarpment with a total hydrologic relief of 10 meters. There is no other area known like it in Michigan. The Wisconsinan glaciation uncovered the area barely 11,000 ybp, and then the high stand of Lake Algonquin deposited more than a meter of glacial sand and cobbles across the area. The water inputs are all from an extensive peat bog, but the runoff now never gets more acidic than pH = 6.5 and the flow is negligible for over half the year. It is possible that karst initiation did not even begin until 5000 ybp, when the climate turned cooler and wetter and many depressions developed bogs. Unanswered questions are how and when did the initial porosity develop, and how were cave conduits excavated to depths of up to five meters in 5,000 years, if the water was not more acidic than now.

THE HYDROGEOLOGY CONSORTIUM

David Loper
Geophysical Fluid Dynamics Institute, Florida State University
Tallahassee FL 33431

Groundwater is the source of over 90% of drinking water in Florida and of most of the water used by industry and agriculture. However, it also serves as the repository for many waste products, particularly storm-water runoff. There is a strong need for better scientific knowledge of groundwater behavior in Floridan-type karstic aquifers and for better mechanisms to transfer such knowledge into practice. To facilitate this transfer, a new scientific organization called the Hydrogeology Consortium has recently been established. Its mission is to cooperatively provide scientific knowledge applicable to groundwater resource management and protection.

The Hydrogeology Consortium was established in May 1998 in response to two needs related to groundwater issues in general, and to those of Florida and its karstic aquifers in particular. The general need is for better coordination of activities and better transfer of knowledge among the diverse groups and agencies dealing with our water resources. The more specific need is for better scientific understanding of flow and transport in aquifers having multi-scale porosity, as exemplified by Floridan-type karst.

The Consortium is a semi-autonomous component of the Florida Center for Environmental Studies based at Florida Atlantic University, but it functions independently, having its own set of Bylaws and Statement of Purpose. It has more than 100 scientific members affiliated with all major universities and water-management districts within Florida, the Florida Department of Environmental Protection, the USGS, NWS, USAF, several municipalities, and many private companies.

To quote from its Statement of Purpose, "The vision of the *Hydrogeology Consortium* is to have an abundant supply of clean water for human use while maintaining a healthy natural environment. To help achieve that vision, the Consortium has chosen as its mission *to cooperatively provide scientific knowledge applicable to ground water resource management and protection*. The primary goal is improved effectiveness and efficiency of management and protection of water resources, particularly ground water, through better understanding and application of scientific knowledge. The activities of the Consortium will include, but not be limited to:

- "endeavoring to develop the necessary scientific knowledge and collect field data, when and where they are found to be lacking, in order to continuously improve our conceptual understanding of hydrogeological environments and associated models.

- "fostering the cooperative development of valid scientifically based models of ground water: including its flow and the behavior of waterborne contaminants, as critical factors in determining the health of complex three-dimensional ecosystems.

- "coordinating the development and implementation of specific pilot studies and laboratory simulations designed to calibrate and test these models."

General membership in the Consortium is open to any individual, group, association, or business that is interested in providing or promoting scientific knowledge applicable to water-resource management and protection. For further information, contact the Consortium's communications officer, Dr. Steve Bortone at sbortone@ces.fau.edu or sbortone@uwf.edu.

THE SAVOY EXPERIMENTAL WATERSHED -- EARLY LESSONS FOR HYDROGEOLOGIC MODELING FROM A WELL-CHARACTERIZED KARST RESEARCH SITE

J.V. Brahana[1], P.D. Hays[2], T.M. Kresse[3], T.J. Sauer[4], and G.P. Stanton[2]

[1]U.S. Geological Survey and University of Arkansas, Fayetteville, Arkansas
[2]U.S. Geological Survey, Little Rock, Arkansas
[3]Arkansas Department of Pollution Control and Ecology, Little Rock, Arkansas
[4]U.S. Department of Agriculture, Agricultural Research Service, Fayetteville, Arkansas

Abstract

Karst hydrogeology does not lend itself to easy interpretation, and many well-respected researchers consider it unlikely that numerical tools and models will be developed that will accurately predict groundwater flow and transport in karst aquifers at less than regional scales (from kilometers to tens of kilometers). Unfortunately, most of the groundwater problems faced today are at these much smaller, site-specific scales—typically on the order of meters to tens of meters -- are relevant for most of the groundwater problems faced today, thus expending considerable effort toward developing numerical tools for use at smaller scales is circumspect and prudent. This paper describes the results of a multidisciplinary, long-term effort to fully characterize a typical mid-continent shallow karst basin, which was initiated in 1996 at the Savoy Experimental Watershed, a 1250-hectare University of Arkansas research property typical of shallow karst basins in the southern Ozarks of Arkansas. The Savoy Experimental Watershed is an integrated research effort between the University of Arkansas, Arkansas Department of Pollution Control and Ecology, Agricultural Research Service and the Natural Resources and Conservation Service of the U.S. Department of Agriculture, and the U.S. Geological Survey. Important objectives of the preliminary collaboration the first two years were to establish baseline water quality, to fully characterize the hydrogeologic framework and to identify and quantify important components of the hydrologic budget at field scale. Data collected thus far have reinforced our initial concept that an integrated well-characterized study site is the optimum approach to studying karst hydrogeology and is the keystone to developing meaningful models that can be used to test hypotheses of karst flow and transport in other, less well-characterized settings. The emphasis at Savoy is on process assessment and hypothesis testing models. Models of this sort can be valuable tools in extending our understanding of observed hydrologic behavior elsewhere. Predictive models are still viewed with caution because most flow boundaries and flow paths in karst aquifers are not accessible, and one single undefined boundary or flow path can render model calculations meaningless at site-specific scales. Examples of interbasin diversion of groundwater only under high-flow conditions, long-term (about 6 months) storage and remobilization of dye along flow paths, and continuous water-quality monitoring at springs from the Savoy Experimental Watershed provide specific lessons on the strengths and weaknesses of different kinds of modeling

Introduction

Karst aquifers, by their very method of formation, are highly nonhomogeneous and anisotropic. Groundwater flow is concentrated along unpredictable, preferred flowpaths that are typically open and much more permeable than the surrounding rock matrix. Hydrologic studies in areas underlain by limestone and other easily dissolvable karst rocks generally take a more regional approach (Imes and Emmett, 1994), because at a larger scale, (1) unknown and unpredictable flowpaths become more integrated, (2) discrete conduits become less influential for specific hydrologic-budget components, (3) flow more closely obeys Darcy's Law, and 4) prediction thus becomes more tractable from an empirical and theoretical point of view. Environmental questions in karst, on the other hand, typically require site-specific, watershed-scale answers that are commonly 3 to 5 orders of magnitude more refined than the 10 kilometer (km) scale typical of regional studies (Quinlan et al., 1995). The following research effort is the first step in bridging the gap between regional reality and site-specific need, in tipping the scale in karst research toward watershed-scale problem solving, and in assessing the suitability of using models to study karst systems.

The Savoy Experimental Watershed (SEW) is a University of Arkansas (UofA) property occurring on the mantled karst of the Springfield Plateau (Figure 1). The SEW is approximately 1250 hectares (ha), and lies approximately 24 km west of the UofA campus at Fayetteville. The site is bound on the north and west by the Ozark National Forest,

and on the south and east by small private cattle and poultry farms. The SEW encompasses parts of 6 watersheds (Figure 2) and is contiguous to and discharges directly into the Illinois River. These basins cover a range of settings including riparian, pasture, forest, and dissected upland. Only one of the watersheds within the SEW (watershed 6, in the northeast corner) has been exposed to extensive human activities or development, and at this point in time, watersheds 1-5 represent relatively unstressed hydrologic environments.

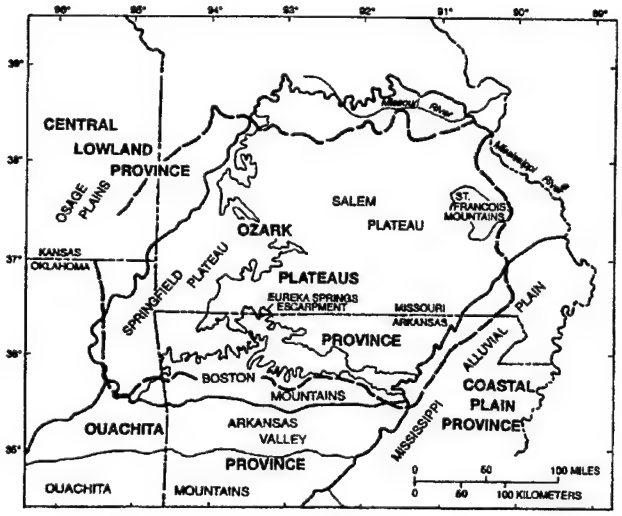

Figure 1: Location of the Springfield Plateau and other major geomorphic features of the southern Ozarks.

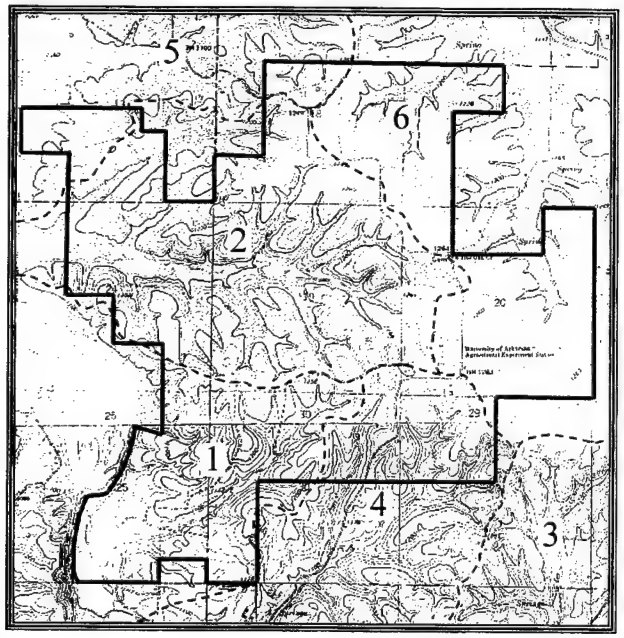

Figure 2: Boundary and general topographic setting of the Savoy Experimental Watershed (SEW), with numbers and dashed lines showing location of 6 watersheds that lie within or nearby. This paper describes results from basin 1, which lies in the southwest corner of SEW.

The SEW is the site of an integrated research effort at watershed scales between the Animal Science Department, the Agronomy Department, the Geology Department, and the Geography Department of the UofA, the Arkansas Department of Pollution Control and Ecology (ADPCE), the Agricultural Research Service (ARS) of the U.S. Department of Agriculture (USDA), and the U.S. Geological Survey (USGS) to develop a long-term, interdisciplinary field laboratory to evaluate processes, controls, and hydrologic and nutrient-flux budgets in surface-water, soil, and shallow groundwater environments. The importance, need, and practical application of studies of this nature are well-documented in the literature (Steele, 1995; Davis et al., 1996; Sauer et al., 1997).

The vision for the SEW is to develop a long-term, interdisciplinary field laboratory similar to Hubbard Brook Experimental Forest (HBEF) in New Hampshire—for the main purpose of evaluating processes, controls, budgets, modeling, and management practices related to animal production in a mantled karst setting. Such studies advance our knowledge by providing a more accurate and reliable conceptualization from which numerical simulations, risk-based management strategies and other assessment and predictive tools can be implemented. More accurate representation of flow and contaminant movement will provide information necessary to make informed risk-based decisions related to human health and ecosystems in karst terrain used for human activities. This study site offers extraordinary promise to address meaningful, relevant questions of land use and agricultural practices on water quality, including such diverse topics as nutrient cycling (nitrogen compounds, phosphorus compounds), pathogen transport, testing of management practices, tracer development and applicability, karst hydrogeology, transport modeling, trace constituent transport associated with sediments and colloids, and pharmaceutical compound transport in karst flow systems.

Site characterization of SEW was initiated in the spring of 1997 to define baseline water quality for discrete hydrologic-budget components, to describe controlling influences affecting nutrient and pathogen transport at the site, and to develop a preliminary conceptual model of hydrologic flow and transport at a site-specific scale of the watershed. The current data-collection infrastructure includes:

- 2 continuous spring sampling stations (Langle Spring and Copperhead Spring), with 20-minute monitoring for stage, water temperature, specific conductivity, and pH;
- 1 surface runoff sampling station in a (normally) dry drainage basin;
- incorporation of an existing USGS stream gaging station on the Illinois River at Highway 16,

approximately 400 meters upstream from the southwest corner of SEW, and upstream with the confluence with Clear Creek

- 33 augered boreholes, with observation-well completion within regolith at or above the epikarst;
- 7 rotary-drilled wells, with observation-well completion within the indurated, shallow carbonate aquifer;
- karst inventory, including field location and hydrogeologic characterization of sinkholes, sinking streams, caves, and springs;
- 7 fluorescent field dye-tracing experiments, to determine recharge areas of specific springs and time of travel from input to resurgence points;
- well inventory of SEW and contiguous areas to a distance of 5 kilometers, including compilation of geologic logs from existing wells, existing records of water quality, and geophysical logging of 7 rotary-drilled wells, and 2 additional wells contiguous to the SEW property;
- complete weather station, including continuous precipitation record, utilizing a tipping-bucket rain gages within SEW;
- verification of previous field mapping of soils and geology within SEW;
- determination of infiltration using double-ring infiltrometers on selected soil types and geomorphic settings within SEW; and
- determination of selected water-quality parameters sampled from 52 different surface and subsurface locations.

This data network has been initially directed at site characterization—subsequent studies will add to that original ongoing data base, but more importantly, will address very specific environmental problems dealing with animal production in karst terrrane. As additional data are accrued, accurate water and element balances will be constructed, providing (1) insight into ecosystem function, (2) empirical data for testing models and generating hypotheses, (3) a record of extreme or unusual events and karst hydrologic system response, and (4) process identification. Any activity related to water or animal production can be a potential research topic. Data from each study conducted at the SEW will be synthesized and incorporated into a GIS data base (Center for Advanced Spatial Technologies—UofA).

Selected field results

The following paragraphs briefly highlight field results that show the complexity of the karst hydrogeologic systems at SEW, and point to benefits using models for hypothesis testing, and illustrate drawbacks using models for predictive flow and transport conditions. Data and interpretations presented herein are based on: unpublished UofA Master of Science theses by Al-Rashidy (1999) and Shirley (1999); unpublished data from continuous water-quality monitors (T.J. Sauer, USDA-ARS, written commun., 1999); unpublished data from UofA Field Hydrogeology courses (J.V. Brahana, USGS/UofA, written commun., 1999); and published reports (Brahana, 1997; Sauer et al., 1997; Brahana et al., 1998; Marshall et al., 1998)

The boundaries of the surface drainage in watershed 1 (Figure 2) do not coincide with the boundaries of groundwater drainage. Langle Spring and Copperhead Spring occupy contiguous basins in watershed 1, and share a common boundary that is nearly linear; during periods of high precipitation, the valley may carry surface runoff (fewer than 12 hours total in 1998). For most of the year no surface flow occurs in this valley, except for a segment of about 100 meters, where flow occurs at all times (Figure 3). The flowing segment occurs at a major permeability contrast in the bedrock where a thick chert layer perches shallow groundwater flow. Continuously flowing seeps emerge from the regolith near the top of this contact, flow along the surface for about 100 meters, and disappear into gravel below the chert layer. Based on fluorescent dye-tracing studies at conditions of low flow, Langle Spring receives all of the water flowing at the surface in this part of the valley. This flow is pirated from the surface into the gravel, and then into the St. Joe Limestone, where it moves beneath the topographic divide to Langle Spring. Based on tracing at low flow, none of the surface flow emerges at Copperhead Spring—all flows to Langle Spring.

Copperhead Spring drains a smaller area than Langle Spring, based on low-flow discharge and the method of normalized base flow (Brahana, 1997). At high flow conditions, however, Copperhead displays a more rapid and larger flow than Langle, suggesting that (1) Copperhead captures a larger percentage of surface water than Langle, or (2) the Copperhead conduit system is more open and permeable than that of Langle, and thereby able to pass a larger quantity of water more rapidly. Low flow conditions show no interbasin transfer of groundwater, but dye tracing under high-flow conditions indicates that groundwater moves across the groundwater basin divide in either direction; the mechanism of interbasin diversion is thought to be overflow across a groundwater dam along the linear valley.

Computations by Al-Rashidy (written commun., 1999) and Shirley (written commun., 1999) provide further documentation on interbasin transfer. Although Langle has about 4 times larger baseflow discharge than Copperhead, Copperhead shows increasingly larger flows than Langle during high-flow conditions. Computations of basin size for Copperhead yield 0.114 mi^2, and for Langle, 0.537 mi^2,

based on low flow. Discharges

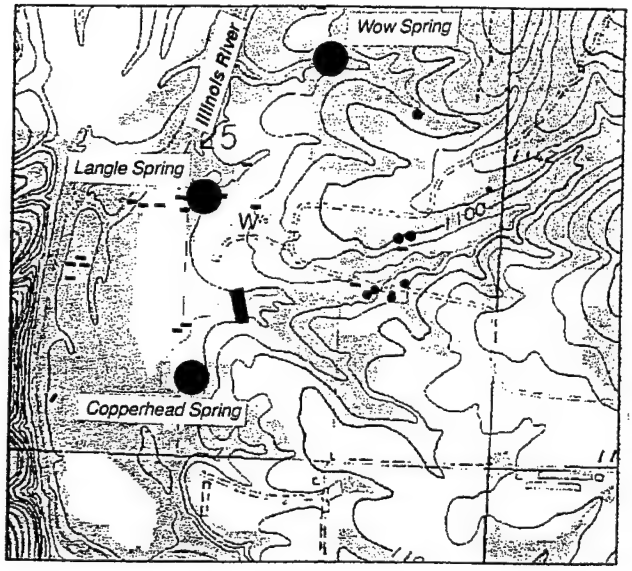

Figure 3: Location of Langle and Copperhead Springs in basin 1 of the Savoy Experimental Watershed, including topography of the area. The northeast trending linear valley is monitored by a weir (rectangular bar), and the springs are monitored by transducers and floats (stage), and water-quality (pH, specific conductance, and temperature). A precipitation and weather station is represented by the letter W.

for both springs for the January 4-5, 1998 storms were 26.4 ft^3/s for Copperhead, and 8.3 ft^3/s for Langle. If storm volume is distributed over computed basin size for this or any other storm, and the total outflow from the storm is integrated from the hydrograph, it becomes obvious that Langle Spring basin is becoming smaller -- not considered a realistic possibility -- or that subsurface flow from Langle Spring basin is being captured by Copperhead Spring -- considered as the best explanation. Modeling of these variations is valuable, and aids understanding of the flow system based on site-specific scale measurements.

Dye tracing has proven to be a valuable tool to empirically define point-to-point flow paths in karst, and to provide time-of-travel through otherwise unobservable settings (Figure 5). Background sampling in seeps emerging from the Copperhead Spring basin gave an unexpected positive response in a location heretofore not connected (more accurately, not anticipated) with any dye injection at SEW. Careful scrutiny of dye-trace work in the previous five years indicated that the only viable source was dye injection into a dug well upgradient from the seeps almost 6 months prior to detecting dye at the seeps. The injection site was on the opposite side of the valley as the background seeps, although it was at a higher elevation than the seeps. Scrutiny of precipitation data indicates that a storm occurring about a week prior to the dye detection at the seeps was the first major storm event since the preceding spring (about 6 months). Dye tracing from a year earlier had established a direct connection down the valley. Water levels from some wells in the carbonate aquifer have been documented to show no response to more minor storms during the growing season, due primarily to large losses of shallow groundwater to evapotranspiration. Although not proved at this point, it is suspected that the dye was stored within the aquifer during this period, and not remobilized until a storm of sufficient recharge was able to thoroughly flush the aquifer.

Although Langle and Copperhead Springs lie next to one another and appear to be similar in many respects, continuous monitoring of chemical quality of the water indicates that the springs also have distinctly different flow characteristics, different basin size, different geometry of input points and flow-path character, and a different ratio of components that make up their hydrologic budgets. To illustrate (and for the purpose of brevity, only temperature data from the two springs will be discussed here) temperature is compared with rainfall for December 1997 (Figure 4). On cloudless days with intense solar radiation, Copperhead Spring shows a noticeable diurnal variation , whereas Langle Spring does not. We hypothesize that point input from pirated surface water that lying near the mouth of Copperhead Spring represents a larger component of the spring-flow budget at Copperhead than this type of source does at Langle. Moreover, during the storms of December 8 and December 24, temperature at Langle decreased about 0.6° C and 0.2° C, whereas temperature at Copperhead increased 1.5° C and 0.5° C. Actual water temperatures for water from the two springs for these storms was about 14.0° C. The interpretation is that stormwater on the surface, which was about 14.0° C, was captured at point input sources along surface-drainage channels fairly near the resurgence of both springs. The relative amount of captured surface flow from Copperhead is significantly more of the total budget of the spring when compared to Langle. The warmer water temperature in Langle represents predominance of slightly older groundwater that has equilibrated with the subsurface environment and is therefore warmer in comparison to Copperhead, which shows cooler water with larger diurnal temperature variations from the recent storms. The continuous sampling data contains a huge amount of information useful for unraveling the complex controls on the flow of these springs (Figure 4).

Discussion and summary

Karst hydrogeology does not lend itself to easy interpretation, and many well-respected researchers consider it unlikely that numerical tools and models will be developed that will accurately predict groundwater flow

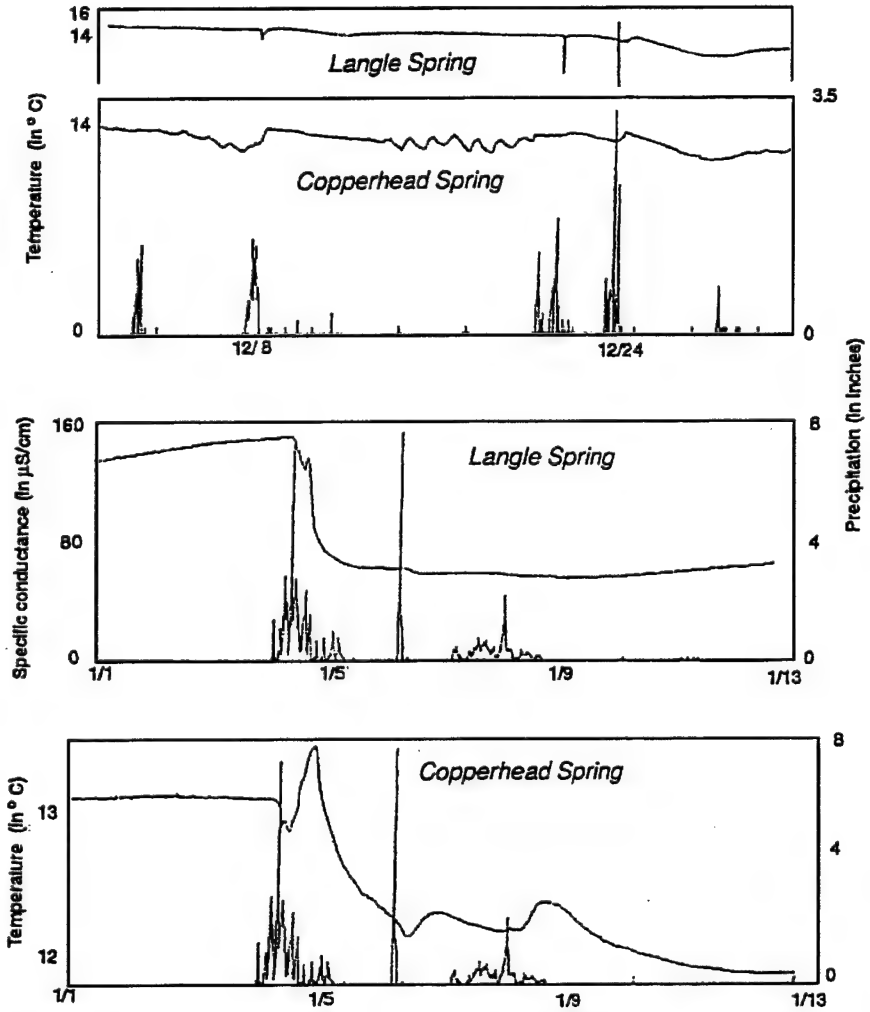

Figure 4: Responses of water-quality parameters in response to precipitation at Copperhead and Langle Springs.

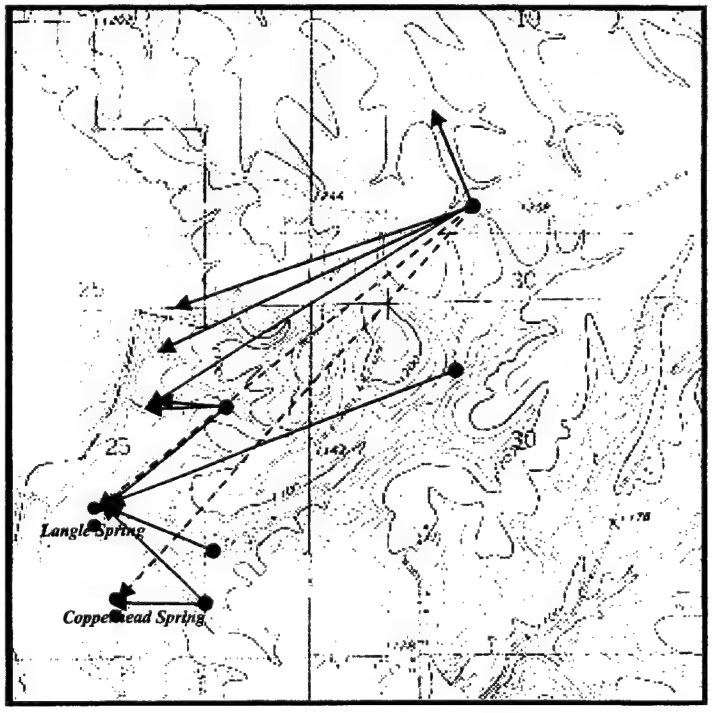

Figure 5: Dye-tracing results showing results at both high-flow and low-flow conditions.

and transport in karst aquifers at less than regional scales. Unfortunately, smaller, site-specific scales—typically on the order of meters to tens of meters -- are relevant for most of the groundwater problems faced today, thus expending considerable effort toward developing numerical tools for use at smaller scales should be productive. Data collected at the Savoy Experimental Watershed have reinforced our initial concept that an integrated, well-characterized study site is the optimum approach to studying karst hydrogeology and is the keystone to developing meaningful models that can be used to test hypotheses of karst flow and transport in other less well-characterized settings. The emphasis at Savoy is on process assessment, conceptual models, and hypothesis-testing models. Models of this sort can be valuable tools in extending our understanding of observed hydrologic behavior elsewhere. Predictive models, on the other hand, are still viewed with utmost caution, however, because most flow boundaries and flow paths in karst aquifers are not accessible, and one single undefined boundary or flow path can render model calculations meaningless at site-specific scales. Examples of interbasin diversion of groundwater only under high-flow conditions, long-term (about 6 months) storage and remobilization of dye along flow paths, and continuous water-quality monitoring at springs from the Savoy Experimental Watershed provide specific lessons about unexpected results that can come from a fairly well-characterized research site.

Modeling to test alternate hypotheses likewise gives quantitative testing of empirical data—and is a valuable tool. It is our opinion that predictive modeling may or may not be meaningful, depending on how much is known about the system at the time of the simulation. Under most conditions, we feel predictive modeling should be viewed with extreme skepticism.

References cited

Adamski, J.C., 1987, The effect of agriculture on the quality of ground water in a karstified carbonate terrain, Northwest Arkansas: unpublished M.S. thesis, University of Arkansas, Fayetteville, 124 p.

Adamski, J.C., 1997, Geochemistry of the Ozark aquifer in Arkansas, Kansas, Missouri, and Oklahoma: Geological Society of America, Abstracts with Programs, v. 29, no. 6, p. 326.

Al-Rashidy, S.M., 1999, Hydrogeologic controls of the shallow mantled karst aquifer, Copperhead Spring, Savoy Experimental Watershed, Northwest Arkansas: unpublished M.S. thesis, University of Arkansas, Fayetteville, 69 p.

Bartholmey, E.C., and J.V. Brahana, 1995, Influence of fractures and faults on the hydrogeology of springs of the Springfield Plateau in northwestern Arkansas: Geological Society of America Abstracts with Programs, v. 27, no. 7.

Bartholmey, E.C., J.W. Martin, T.M. Kresse, and J.V. Brahana, 1995, Influence of fractures and faults on the hydrogeology of springs in the Springfield Plateau of northwestern Arkansas: Geological Society of America, Abstracts with Programs, v. 27, no. 6, p. A-100.

Bostian, Rick, and J.V. Brahana, 1996, Regional tectonic and structural control on the hydrogeology of the Boone-St. Joe aquifer, Northwest Arkansas: Geological Society of America Abstracts with Programs, v. 28, no. 1, p. 5-6.

Brahana, J.V., 1993b, Dominant factors affecting groundwater flow and transport in the carbonate-rock aquifers of northwestern Arkansas, in Proceedings of Abstracts, December 9, 1993, Sixth Annual AWRA/AGWA Symposium, Ground Water Issues of the 90's—Quantity and Quality, p. 5-6.

Brahana, J.V., 1995a, Field Hydrogeology—Theory, techniques, and applications or How we spent our summer vacation: University of Arkansas Teaching Academy, 3rd Annual Teaching and Research Ideas Exchange Workshop, Abstracts, p. 50.

Brahana, J.V., 1995b, Controlling influences on groundwater flow and transport in the shallow karst aquifer of northeastern Oklahoma and northwestern Arkansas: Proceedings Volume, Hydrologic Problems Along the Arkansas-Oklahoma Border, Arkansas Water Resources Center Publication No. MSC-168, p. 25-30.

Brahana, J.V., 1995c, Hydrogeological delineation and continuous monitoring of the shallow karst aquifers of northern Arkansas—Practical implications for land-use planning: Proceedings of the 6th Biennial State Water Conference and 8th Annual American Water Resources Association and Arkansas Ground-Water Association Joint Symposium, p. 21-22.

Brahana, J.V., 1996, The role of fractures as tectonically-controlled ground-water flow boundaries in deep aquifers of the northern Mississippi embayment: Geological Society of America Abstracts with Programs, v. 28, no. 1, p. 6.

Brahana, J.V., 1997, Rationale and methodology for approximating spring-basin boundaries in the mantled karst terrane of the Springfield Plateau, northwestern Arkansas: in Beck, B.F., and B.J. Stephenson, (eds.), The Engineering Geology and Hydrogeology of Karst Terranes—Proceedings of the Sixth Multidisciplinary Conference on Sinkholes and the Engineering and Environmental Impacts

of Karst, Springfield, Missouri: Balkema, Rotterdam, p. 77-82,

Brahana, J.V., G.J. Gonthier, and L.M. Remsing, 1991, Hydrogeologic data for Boone County, Arkansas: U.S. Geological Survey Open-File Report 91-518, 36 p.

Brahana, J.V., and E.F. Hollyday, 1988, Dry stream reaches in carbonate terranes: Surface indicators of ground-water reservoirs: Water Resources Bulletin, v. 24, no. 3, p. 577-580.

Brahana, J.V., E.F. Hollyday, M.W. Bradley, and G.E. Hileman, 1991, Lithologic controls on the evolution of permeability in chert-bearing carbonate rocks of Mississippian Age from the southern United States: Geological Society of America Abstracts with Programs, v. 23, p. A266.

Brahana, J.V., V.A. Leidy, J. Lindt, and S.A. Hodge, 1993, Hydrogeologic data for Carroll County, Arkansas: U.S. Geological Survey Open-File Report 93-150, 32 p.

Brahana, J.V., and J.W. Martin, 1994, Temporal variability in discharge and water quality from large springs in northwestern Arkansas—Implications for data collection: Geological Society of America Abstracts with Programs, v. 26, p. A-286.

Brahana, J.V., G.P. Stanton, P.D. Hays, and R.H. Davis, 1996, Field Hydrogeology—Theory, Techniques, and Applications: Workbook: University of Arkansas Geology Department, Fayetteville, 56 p.

Brahana, J.V., and D. Walters, 1994, Methodology development and preliminary field assessment of host-specific viruses as tracers in shallow karst aquifers: Conference Proceedings of Breakthroughs in Karst Geomicrobiology and Redox Geochemistry, Colorado Springs, Colorado, p. 2-3.

Brahana, J.V., T.J. Sauer, T. Kresse, S. Al-Rashidy, T. Shirley, and P. McKee, 1998, Tipping the scale in long-term karst research—Hydrogeologic characterization of the Savoy Experimental Watershed: Proceedings Volume, Water Quality of Surface and Ground Water and Best Management Practice, Arkansas Water Resources Center, p. 9-17.

Davis, R.K., N.J. Sinor, and T.G. Monk, 1996, Impacts to ground-water quality of selected springs in Northwest Arkansas: in Steele, Kenneth F., ed., Diversity of Arkansas Water Resources Research: Arkansas Water Resources Center Publication No. MSC-195, p. 7-14.

Doherty, E., and J.V. Brahana, 1996, Use of remote-sensing data and GIS models for mapping hydrogeology and structure in the karst terrain of northwestern Arkansas: Geological Society of America Abstracts with Programs, v. 28, no. 1, p. 11.

Fanning, B. J., 1995, Geospeleologic analysis of cave and karst development within the Boone and St. Joe Formations of Benton and Madison Counties, Northwest Arkansas: unpublished M.S. thesis, University of Arkansas, Fayetteville, 144 p.

Fanning, B. J., and J.V. Brahana, 1993, Hydrogeologic factors affecting cavern morphology within rocks of Mississippian Age in Northwestern Arkansas: Geological Society of America Abstracts with Programs, v. 25, p. 13.

Freiwald, D.A., 1985, Average annual precipitation and runoff for Arkansas, 1951-80: U.S. Geological Survey Water-Resources Investigations Report 84-4363, 1 sheet.

Freiwald, D.A., 1987, Streamflow gain and loss of selected streams in northern Arkansas: U.S. Geological Survey Water-Resources Investigations Report 86-4185, 4 sheets.

Imes, J.L., and L.F. Emmett, 1994, Geohydrology of the Ozark Plateaus aquifer system in parts of Missouri, Arkansas, Oklahoma, and Kansas: U.S. Geological Survey Professional Paper 1414-D, 127 p.

Marshak, S. and T. Paulsen, 1996, Midcontinent U.S. fault and fold zones: A legacy of Proterozoic intracratonic extensional tectonism?: Geology, v. 24, no.. 2, p. 151-154.

Marshall, D., J.V. Brahana, and R.K. Davis, 1998, Resuspension of viable sediment-bound enteric pathogens in shallow karst aquifers, *in* Brahana, J.V., Y. Eckstein, L.K. Ongley, R. Schneider, and J.E. Moore (eds.), Gambling with groundwater—Physical, chemical, and biological aspects of aquifer-stream relations: Proceedings Volume of the International Association of Hydrogeologists Congress XXVIII and the Annual Meeting of the American Institute of Hydrology, Las Vegas, p. 179-186.

Martin, J. W., 1999, Controls on ground-water flow and quality in the Boone-St. Joe aquifer in north-central Benton County, Arkansas: : unpublished M.S. thesis, University of Arkansas, Fayetteville, 110 p.

Martin, J. W., and J.V. Brahana, 1995, Comparative hydrogeology of large springs of the Springfield Plateau in northwestern Arkansas: Geological Society of America, Abstracts with Programs, v. 27, no. 6, p. A-181.

Monk, R.G., R.K. Davis, and J.V. Brahana, 1996, Fault

control of ground-water flow to Decatur Spring, Northwest Arkansas: Geological Society of America Abstracts with Programs, v. 28, no. 1, p. 54.

Orndorff, H.A., R.K. Davis, and J.V. Brahana, 1997, Comparison of shallow aquifer flow systems in Northwest Arkansas: Geological Society of America Abstracts with Programs, v. 29, no. 6, p. 328.

Peterson, E.W., R.K. Davis, and J.V. Brahana, 1997, The use of regression analysis in predicting nitrate-nitrogen concentrations in springs of Northwest Arkansas: Geological Society of America Abstracts with Programs, v. 29, no. 6, p. 182.

Quinlan, J.F. and J.A. Ray, 1995, Normalized base-flow discharge of groundwater basins: A useful parameter for estimating recharge area of springs and for recognizing drainage anomalies in karst terranes, *in* Beck, B.F., (ed.), Karst geohazards: A.A. Balkema, Rotterdam, p. 149-164.

Quinlan, J.F., J.A. Ray, and G.M. Schindel, 1995, Intrinsic limitations of standard criteria and methods for delineation of groundwater-source protection areas (springhead and wellhead protection areas) in carbonate terranes: Critical review, technically-sound resolution of limitations, and case study in a Kentucky karst, *in* Beck, B.F. (ed.), Karst geohazards: A.A. Balkema, Rotterdam, p. 525-537.

Ray, J. A., 1997, Overflow conduit systems in Kentucky: A consequence of limited underflow capacity: in B.F. Beck, and J.B. Stephenson, (eds.), The Engineering Geology and Hydrogeology of Karst Terranes—Proceedings of the Sixth Multidisciplinary Conference on Sinkholes and the Engineering and Environmental Impacts of Karst, Springfield, Missouri: A. A. Balkema, Rotterdam, p. 69-76.

Roggio, R. G., G.L. Ford, and J.V. Brahana, 1996, Hydrogeologic controls of the springs in northern Arkansas: Geological Society of America Abstracts with Programs, v. 28, no. 1, p. 61.

Sauer, T.J., J.V. Brahana, T.M. Kresse, P.A. Moore, Jr., S.D. Logsdon, K.P. Coffey, T.C. Daniel, C.V. Maxwell, C.P. West, and S.M. Braum, 1997, Using landscape position and soil information to optimize manure application: Soil and Water Conservation Society Proceedings, Managing Manure in Harmony with the Environment and Society, Ames, IA, p. 9-18.

Schindel, G. M, J.A. Ray, and J.F. Quinlan, 1995, Delineation of the recharge area for Rio Springs, Kentucky: An EPA Demonstration Project in Wellhead (Springhead) protection for karst terranes, *in* Beck, B.F., (ed.), Karst geohazards: A.A. Balkema, Rotterdam, p. 165-176

Shirley, Tracy, 1999, Basin-scale hydrogeologic characterization of Langle Spring, Savoy Experimental Watershed, Northwest Arkansas: unpublished M.S. thesis, University of Arkansas, Fayetteville, 88 p.

Sinor, N., R. Davis, and K. Steele, 1995, Spring monitoring to assess the impacts from land application of animal wastes to groundwater quality in Northwest Arkansas: Geological Society of America, Abstracts with Programs, v. 27, no. 6, p. A-42.

Sinor, N., R. Davis, C. King, and K. Steele, 1995, Monitoring springs in Northwest Arkansas to determine the impact of land application of animal wastes to groundwater quality: Proceedings of the 6th Biennial State Water Conference and 8th Annual American Water Resources Association and Arkansas Ground-Water Association Joint Symposium, p. 21-22

Stanton, G.P., 1993, Processes and controls affecting anisotropic flow in the Boone-St. Joe aquifer in northwestern Arkansas: unpublished M.S. Thesis, University of Arkansas, Fayetteville, 212 p.

Stanton, G.P. and J.V. Brahana, 1996, Structural control on hydrogeology of a mantled karst aquifer in northwestern Arkansas: Geological Society of America, Abstracts with Programs, v. 28, no. 6.

METHODOLOGY TO STUDY THE EFFECTS OF ANIMAL PRODUCTION IN MANTLED KARST AQUIFERS OF THE SOUTHERN OZARKS

Jaysson Funkhouser[1,2], Paul Little[2], Van Brahana[1,2], Tim Kresse[3], McCree Anderson[4], Sandi Formica[3] and Tom Huetter[4]

[1]U.S. Geological Survey
[2]University of Arkansas, Fayetteville, Arkansas
[3]Arkansas Department of Pollution Control and Ecology, Little Rock, Arkansas
[4]Arkansas Department of Pollution Control and Ecology, Jasper, Arkansas

Abstract

Concentration of animal wastes in aquifers is one of the major ongoing hydrogeologic problems in karst areas. Typically the poor soils and dissected land surface are conducive to few other land-uses than animal production. Coupled with the relatively rapid flow systems of karst aquifers, and the general overall lack of attenuation of contaminants, wastes from poultry, cattle, swine, and humans become a complex problem of: animal density, economic sustainability of specific animal-production practices that likely will impact water quality, environmental sustainability of animal-production practices that likely will impact water quality, and the ultimate ability of the environment to assimilate the wastes. The main point of this recently-initiated project is not to describe a site study, but to characterize a methodology that incorporates intensive field study coupled with numerical modeling of alternative hypotheses. The methodology is not novel, but in many karst studies it becomes overlooked for any number of reasons. All available data that can be reasonably collected in the field should be—these are the basis of ground truth, and although expensive, provide the constraints by which real understanding is gained. The modeling may be simple, no more than analytical computation of end-member mixing or storm-discharge computations, or it may be sophisticated and involve flow-path evolution of chemical constituents, and three-dimensional flow in highly anisotropic and heterogeneous aquifers. Accurate definition of flow paths, recharge areas, ground-water solute budgets, and conceptual models are essential. Integrated study of each system requires an interdisciplinary, intensive field reconnaissance at a scale appropriate to allow quantitative testing (modeling) of all known attributes of the system. Such modeling efforts, combined with a hybrid data-collection program, provide the key hypothesis testing that leads to understanding the system.

Introduction

The karst area of the Springfield Plateau in northwestern and north-central Arkansas is subject to numerous and varied land-use practices that impact water quality. (For location map, see Figure 1 in the preceding paper by Brahana et al.) In this region of the U.S., animal production (poultry, swine, and cattle) and human activities concentrate wastes within an environmentally-sensitive karst hydrogeologic setting. Karst hydrogeology in this area includes limestone and dolomite aquifers covered by a thin, rocky soil, and a variable thickness of regolith (residuum). The karst ground-water system is underdrained by carbonate-rock aquifers that have been dissolved to form an open network of caves, enlarged fractures, bedding planes, conduits, sinkholes, swallets, sinking streams, and springs. Flow in these aquifers is typically rapid, flow directions are difficult to predict, interaction between surface and groundwater is typically extensive, and processes of contaminant attenuation that characterize many other ground-water settings are typically absent (White, 1988; Ford and Williams, 1989). Some of the most environmentally-sensitive water-quality issues in the Springfield Plateau deal with nutrients and microbes, most notably, with elevated amounts of phosphate, nitrate, bacteria and other microorganisms that are transported into shallow ground-water aquifers and bodies of water in contact with the aquifers (Peterson and others, 1998).

The production of dairy cattle and swine concentrates manure and other solid and liquid waste on the land surface, and rainfall mobilizes the waste and transports it into both surface-water and groundwater supplies. When rainfall occurs, the waste transported into the groundwater may be in either dissolved or suspended phases, moving along discrete but not always obvious pathways from input points (fields and sinking streams) to points of discharge (springs and drains) within the local hydrologic system. Many cases of high nutrient and microbial levels in ground-water have been reported at wells and springs downgradient from intense animal-production activity in the region, but unequivocal contaminant-source identification and cause-effect documentation of specific cattle-raising activities on

water quality have not been well established.

In an effort to define effects of various animal-producing activities on water-quality in the region, the Arkansas Department of Pollution Control and Ecology (ADPCE) has undertaken a series of long-term projects to assess current water-quality conditions near large animal-production operations, and to evaluate, assess, and demonstrate water-quality changes resulting from the implementation of best-management practices [BMPs] (Sandi Formica, ADPCE, Little Rock, written commun., 1998; Tim Kresse, ADPCE, Little Rock, written commun., 1998). One such project deals specifically with dairy-cattle operations in the Springfield Plateau southeast of Harrison, Arkansas, in Boone and Searcy Counties, and this paper is a preliminary description of the early phase of that larger project.

Purpose and scope

The overall purpose of this study is to demonstrate the effectiveness of BMPs on ground-water quality at three dairy-cattle operations in the karst Springfield Plateau of Newton and Searcy Counties, Arkansas. Specific objectives include:

8delineation of ground-water basin boundaries within and contiguous to three site-specific study areas (dairy-cattle farms);
8determination of ground-water flow paths and approximate times of travel for variable hydrologic conditions at the three site-specific study areas;
8characterization of pre-BMP ground-water quality within and contiguous to each of the three site-specific study areas, for base flow and storm flow conditions;
8characterization of post-BMP ground-water quality within and contiguous to each of the three site-specific study areas, for base flow and storm flow conditions.

The scope of this study includes ground-water-discharge determination and ground-water-quality assessment of the nutrients phosphorus and nitrogen, and the microbial components fecal coliform, fecal streptococcus, and *e. coli*, and the physical properties temperature, specific conductance, and pH at each of the three site-specific study areas.

Methodology

1. Ground-water basin boundaries will be delineated using the following methodologies:
a. in-depth, site-specific study-area reconnaissance, karst inventory, spring inventory, seepage investigations, and hydrologic boundary delineation (Quinlan, 1989);
b. application of standard ground-water fluorescent dye-tracing techniques applicable to karst terrane (Aley, 1997; Quinlan, 1989; Davis and others, 1998);
c. determination of overall size of the basin contributing recharge will be approximated using normalized base flow techniques in which low flow of springs is proportional to basin size, given specific hydrogeologic and climatic variables (Quinlan and Ray, 1995; Brahana, 1997);
d. compilation of driller's logs, geophysical wireline logs, soils maps, geologic maps, topographic maps, relevant published reports, and aerial photography (Brahana, 1997);
e. development of an integrated conceptual model of ground-water flow and transport for each of the three sites (Brahana, 1995)

2. Determination of ground-water flow paths and approximate times of travel will be accomplished using the following methodologies:
a. ground-water fluorescent dye-tracing applicable to karst terrane techniques (Aley and Fletcher, 1977; Quinlan, 1989; Aley, 1997; Davis and others, 1998);
b. ground-water basin boundary delineation for springs in karst terrane (Brahana, 1997; Davis and others, 1998);

3. Characterization of pre-BMP water quality (selected parameters—nutrients, microbes emphasized, as well as any identified anomalies) base- and high-flow conditions will be accomplished using the following methodologies:
a. construction and installation of automated data-collection samplers for storm sampling, including weirs on dominant springs, and 4-parameter continuous monitoring (Davis and others, 1998; Al-Rashidy, 1999; Shirley, 1999; Brahana and others, 1998);
b. collection of grab samples under base flow conditions—[selected emphasized parameters, as well as majors, minors, trace constituents, others as appropriate] (Brahana and others, 1998);
c. utilization of existing wells, springs, seeps, and streams as appropriate (Brahana and others, 1998);
d. installation of tipping bucket rain gage for precise definition of input stresses (Davis and others, 1998; Brahana and others, 1998;
e. construction of epikarst wells as appropriate, with attention to QW evolution along flow lines (Aley, 1997; Brahana and others, 1998).

4. Characterization of post-BMP water quality (selected parameters—nutrients, microbes emphasized, as well as any identified anomalies) base- and high-flow conditions will be accomplished using the following methodologies:

a. Operation of automated data-collection samplers for storm sampling, including weirs on dominant springs, and 4-parameter continuous monitoring (Davis and others, 1998; Al-Rashidy, 1999; Brahana and others, 1998);
b. collection of grab samples under base flow conditions—

[selected emphasized parameters, as well as majors, minors, trace constituents, others as appropriate] (Brahana and others, 1998);
c. utilization of existing wells, springs, seeps, and streams as appropriate (Brahana and others, 1998);
d. operation of tipping bucket rain gage for precise definition of input stresses (Davis and others, 1998; Brahana and others, 1998);
e. utilization of epikarst wells as appropriate, with attention to QW evolution along flow lines (Aley, 1997; Brahana and others, 1998).

5. Integration of all relevant data into a conceptual model that facilitates quantitative testing of all alternative hypotheses (Brahana, 1995; Taylor, 1997).

6. Numerical simulation of flow and transport scenarios, based on an intensive, real-world constraints imposed by high-quality field data (Franke and others, 1998; Greene, 1997; Knochenmus and Robinson, 1996; and Davis, 1996).

Discussion and summary

The main point of this recently-initiated project is not to describe a site study, but to characterize a methodology that incorporates intensive field study coupled with numerical modeling of alternative hypotheses. The methodology is not novel, but in many karst studies it becomes overlooked for any number of reasons. All available data that can be reasonably collected in the field should be—these are the basis of ground truth, and although expensive, provide the constraints by which real understanding is gained. The modeling may be simple, no more than analytical computation of end-member mixing or storm-discharge computations, or it may be sophisticated and involve flow-path evolution of chemical constituents, and three-dimensional flow in highly anisotropic and heterogeneous aquifers. Later emphasis of the project will be on assessing the impact of practices that are cost effective and that optimize natural breakdown of the most troublesome contaminants, especially nutrients such as nitrates and phosphates. Accurate definition of flow paths, recharge areas, ground-water solute budgets, and conceptual models are essential. Integrated study of each system requires an interdisciplinary, intensive field reconnaissance at a scale appropriate to allow quantitative testing (modeling) of all known attributes of the system. Such modeling efforts, combined with a hybrid data-collection program, provide the key hypothesis testing that leads to understanding the system.

References cited

Aley, Thomas, and M.W. Fletcher, 1976, The water tracer's cookbook: Missouri Speleology, v. 16, p. 1-32.

Aley, T., 1997, Groundwater tracing in the epikarst, *in* B.F. Beck and J.B. Stephenson (eds.), 1997, The engineering geology and hydrogeology of karst terranes: A. A. Balkema, Rotterdam, p.207-211.

Al-Rashidy, S. M., 1999, Hydrogeologic controls of the shallow mantled karst aquifer, Copperhead Spring, Savoy Experimental Watershed, Northwest Arkansas: unpublished M.S. thesis, University of Arkansas, Fayetteville, 69 p.

Brahana, J.V., 1997 Rationale and methodology for approximating spring-basin boundaries in the mantled karst terrane of the Springfield Plateau, northwestern Arkansas. *in* B.F. Beck and J.B. Stephenson (eds.), 1997, The engineering geology and hydrogeology of karst terranes: A.A. Balkema, Rotterdam, p. 77-82.

Brahana, J.V., T.J. Sauer, T. Kresse, S. Al-Rashidy, T. Shirley, and P. McKee, 1998, Tipping the scale in long-term karst research—Hydrogeologic characterization of the Savoy Experimental Watershed: Proceedings Volume, Water Quality of Surface and Ground Water and Best Management Practice, Arkansas Water Resources Center, p. 9-17.

Davis, H., 1996, Hydrogeologic investigation and simulation of ground-water flow in the Upper Floridan aquifer of north-central Florida and southwestern Georgia and delineation of contributing areas for select city of Tallahassee, Florida, water-supply wells: U.S. Geological Survey Water-Resources Investigations Report 95-4296. 56 p.

Davis, R.K., J.V. Brahana, and J.S. Johnston., 1998, Ground water in northwest Arkansas: Minimizing nutrient contamination from non-point sources in karst terrane: Final Report for Tasks 94-300 and 95-300 to Arkansas Soil and Water Conservation Commission for U.S. Environmental Protection Agency Projects numbers C9996103-02 and C9996102-03, 56 p.

Ford, D.C. and P.W. Williams, 1989, Karst geomorphology and hydrology: Unwin Hyman, London, 601 p.

Franke, O.L., T.E. Reilly, D.W. Pollock, and J.W. LaBaugh, 1998, Estimating areas contributing recharge to wells—Lessons from previous studies: U.S. Geological Survey Circular 1174, 14 p.

Greene, E.A., 1997, Tracing recharge from sinking streams over spatial dimensions of kilometers in a karst aquifer: Ground Water, v. 35, no. 5, p. 898-904.

Imes, J.L. and L.F. Emmett, 1994, Geohydrology of the Ozark Plateaus aquifer system in parts of Missouri, Arkan-

sas, Oklahoma, and Kansas: U.S. geological Survey Professional Paper 1414-D, 127 p.

Knochenmus, L.A., and J.L. Robinson, 1996, Descriptions of anisotropy and heterogeniety and their effect on groundwater flow and areas of contribution to public supply wells in a karst carbonate aquifer system: U.S. Geological Survey Water-Supply Paper 2475, 47 p.

Petersen, J.C., J.C. Adamski, R.W. Bell, J.V. Davis, S.R. Femmer, D.A. Freiwald, and R.L. Joseph, 1998, Water quality in the Ozark Plateaus, Arkansas, Kansas, Missouri, and Oklahoma, 1992-95: U.S. Geological Survey Circular 1158, 33 p.

Quinlan, J.F., 1989, Ground-water monitoring in karst terranes: Recommended protocol and implicit assumptions U.S. Environmental Protection Agency, Environmental Monitoring Systems Laboratory, Las Vegas, Nevada, EPA/600/X-89/050, 88 p.

Quinlan, J.F., and J.A. Ray, 1995, Normalized base-flow discharge of groundwater basins: A useful parameter for estimating recharge area of springs and for recognizing drainage anomalies in karst terranes, *in* B.F. Beck (ed.), 1995, Karst geohazards—engineering and environmental problems in karst terrane: A. A. Balkema, Rotterdam, p. 149-164.

Shirley, T., 1999, Basin-scale hydrogeologic characterization of Langle Spring, Savoy Experimental Watershed, Northwest Arkansas: unpublished M.S. thesis, University of Arkansas, Fayetteville, 88 p.

Taylor, C.J., 1997, Delineation of ground-water basins and recharge areas for municipal water-supply springs in a karst aquifer system in the Elizabethtown area, northern Kentucky: U.S. Geological Survey Water-Resources Investigations Report 96-4254, 22 p.

White, W.B., 1988, Geomorphology and hydrology of karst terrains: Oxford University Press, New York, 464 p.

PUMP TESTS OF WELLS AT THE NATIONAL TRAINING CENTER NEAR SHEPHERDSTOWN, WEST VIRGINIA

William K. Jones
Environmental Data, P. O. Box 490
Charles Town, WV 25414

Abstract

Five-hour pumping tests were conducted on a water-supply well (well 4a, Figure 1) situated about 1000 ft (300 m) south of the Potomac River in Jefferson County, West Virginia. The well is 760 ft (230 m) deep and develops a steady-state drawdown of about 500 ft (152 m) within 30 minutes of pumping at 100 gpm (6.3 L/sec). The drawdown effects extend north to the Potomac River and the cone of depression is highly anisotropic in the direction of the stratigraphic strike. The results show some of the complexities of pump-test analysis in carbonate rocks.

Discussion

Wells developed for the water supply at the National Training Center (U. S. Fish and Wildlife Service) near Shepherdstown, West Virginia, were tested by the U. S. Army Corps of Engineers and Dames and Moore, Inc., during late December 1997 - early January 1998. The NTC is situated south of the Potomac River and west of Terrapin Neck in northern Jefferson County, on about 540 acres (approx. 2 km^3) entirely underlain by Cambrian carbonates of the Conococheague Formation. The rocks are folded almost vertically and strike about N20°E near the southern edge of the property, shifting to due north near the river. These carbonate rocks have little primary porosity, so almost all of the groundwater flow is through secondary fractures. The most important fractures are along vertically inclined bedding planes, so the hydraulic conductivity is strongly directional in the NNE strike direction. This paper presents a brief description of the wells, test results, and a preliminary analysis of aquifer characteristics.

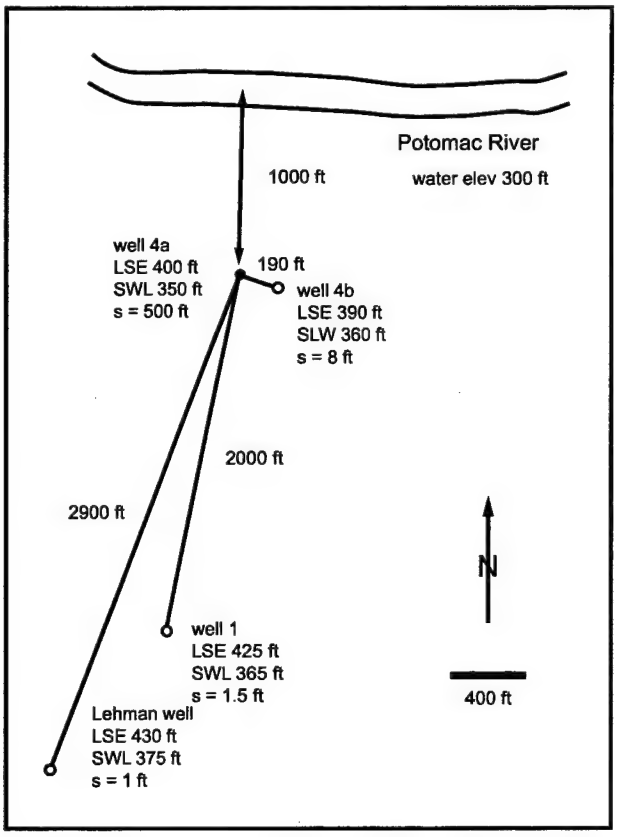

Figure 1. Location sketch for wells used in the multiwell pump-test analysis.

The static water level (SWL) in the wells at the site averages about 50 ft (15 m) below land surface (BLS). Wells 1 and 4a are the primary supply wells for the Center with a daily pumpage of 30,000-60,000 gallons (1.14 - 2.28 x 10^5 L). The wells are not normally pumped simultaneously. Pumping rates average 100 gallons per minute (6.3 L/sec) at each well . The working drawdown during pump tests in June, 1997, was about 390 ft (120 m) at well 1 and about 500 ft (152 m) at well 4a. These are unusually deep drawdowns for wells in this area, partly because the wells are drawing water mainly from deep fractures. Well 1 appears to receive water from fractures at elevations of 60 to -75 ft (18 to -23 m) relative to sea level, which indicates weathering far deeper than the regional base level of 300 feet would suggest. Due to the unknown factor of "well loss," the exact drawdown in the aquifer at the pumping wells is unknown, but it is below the level of the Potomac River, which represents regional base level.

A series of 5-hour pump tests was conducted on well 4a to simulate the expected production pumping schedule of this well. These were the only tests conducted using monitoring wells, but five hours did not allow sufficient development of drawdown curves at the observation wells for a good mathematical analysis. The hydrogeologic setting is so complex that the best of aquifer tests will present data that are very difficult to model or analyze. Figure 1 is a sketch map showing the location of wells studied in this report, and Table 1 gives details on the wells.

Table 1: Well descriptions.

Well	Depth (FT)	Yield (GPM)	SWL (FT)
1	529	100	59
2	400	500	??
4a	760	100	50
4b	645	38	30
3a	305	60	??
Lehman	120	??	55

Table 2, Figure 2, and Figures 3 - 6 present the analyses of the results of several of the pump tests. The single-well calculation uses the Jacob time-drawdown analysis and is based on the early part of the curve before the effects from the recharge boundary fully develop. The physical limits of the fractures are probably felt instantaneously as impermeable boundaries. The single-well tests were analyzed using the recovery part of the curve to minimize the effects of variable discharge during the early parts of the tests. Jacob time-drawdown and distance-drawdown techniques were used to calculate transmissivities (T) and storage coefficients (S) from the observation-well data for the five-hour pump test on well 4a on January 1, 1998. Steady-state conditions had not begun to develop in the observation wells after five hours of pumping, so these are very rough estimates at best. Note that the transmissivity calculated for well 4b, at right angles to the stratigraphic strike from the pumped well, was 230 ft^2/day (2.5 cm^2/sec) compared with about 2300 ft^2/day (25 cm^2/sec) for well 1 and the Lehman well situated parallel to the strike from the pumped well.

Calculated tranmissivities are at the low end of the range reported in the county by Kozar and others (1991) and Trainer and Watkins (1975). The storage coefficients presented are two to three orders of magnitude lower than generally reported for this area. These small values are representative of a confined aquifer, but for this site they appear to represent deep fracture zones that are closed on the top and bottom but which may have considerable horizontal reach. The storativity values are probably even less reliable than the transmissivity values.

Table 2: Summary of aquifer parameters.

Well	Drawdown/Time	T (ft^2/day)	Storativity
Single well tests			
1 125 gpm	388 ft/48 hrs	150	
4a 128 gpm	566 ft/72 hrs	80	
3a 50 gpm	237 ft/72 hrs	300	
5-hr test on 4a			
4b	8 ft/5 hrs	230	0.001
1 and Lehman		2300	0.00003

References cited

Hobba, W. A., Jr., 1981, Ground-water hydrology of Jefferson County, West Virginia: WV Geol. and Econ. Surv., EGB 16, 21p.

Jones, W. K., 1997, Karst hydrology atlas of West Virginia: Karst Waters Institute, 111p.

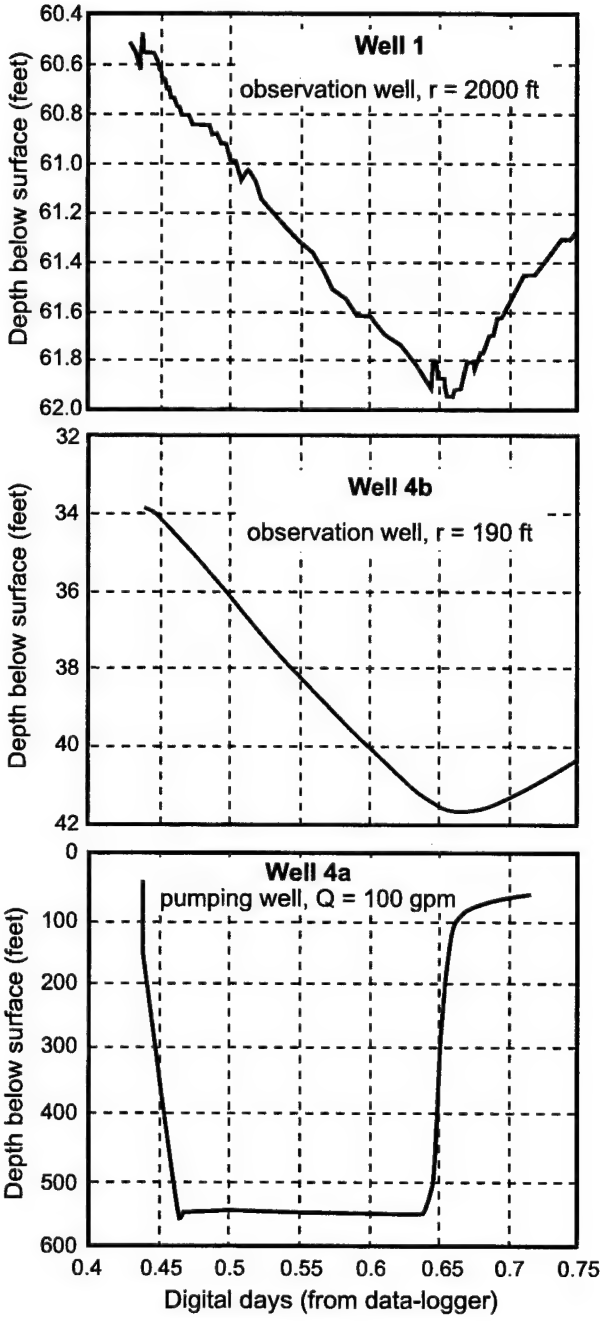

Figure 2. Drawdown and recovery in pumping well 4a and observation wells 4b and 1. Duration of pumping = 5 hours.

Kozar, M. D., W. A. Hobba Jr., and J.A. Macy, 1991, Geohydrology, water availability, and water quality of Jefferson County, West Virginia: USGS WRIR 90-4118, 93p.

Trainer, F. W., and F.A.Watkins, Jr., 1975, Geohydologic reconnaissance of the upper Potomac River Basin: USGS WSP 2035, 68p.

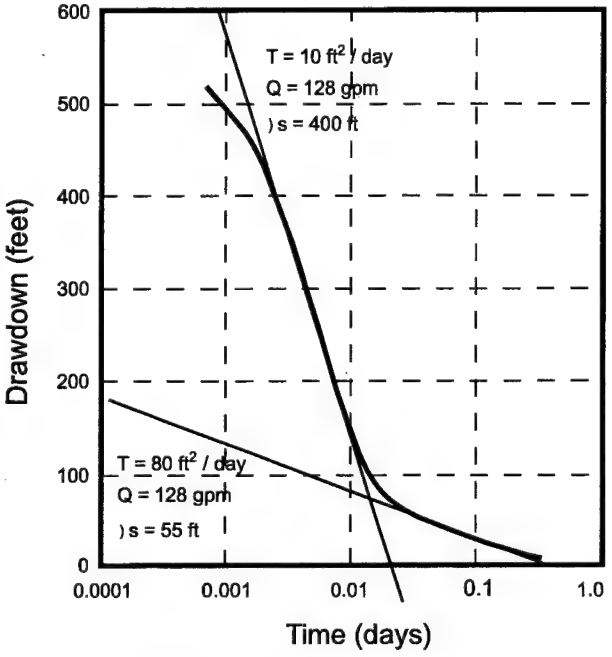

Figure 3: Analysis of recovery data from 72-hour test in well 4a (pumping well), 9-19-97.

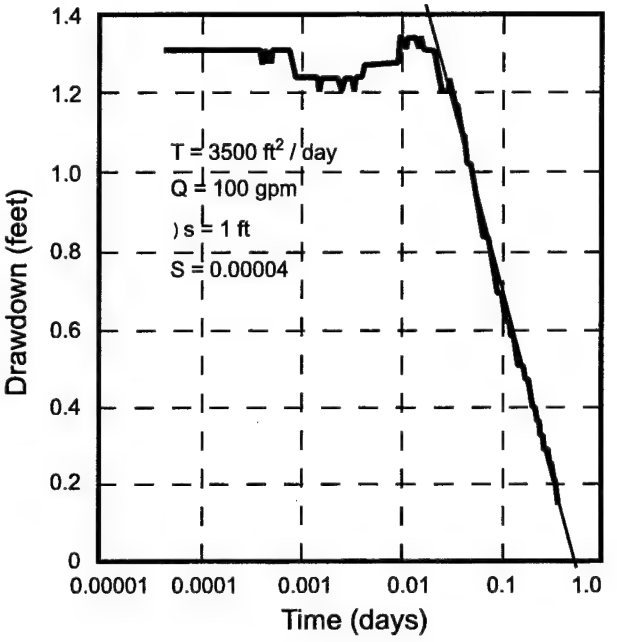

Figure 5: Analysis of recovery in well 1, from 5-hour test on well 4a, 1-1-98.

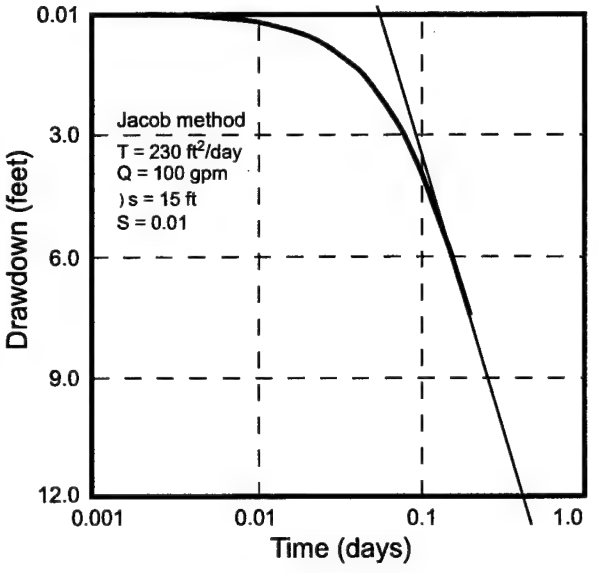

Figure 4: Analysis of drawdown in well 4b, from 5-hour pump test in well 4a, 1-1-98.

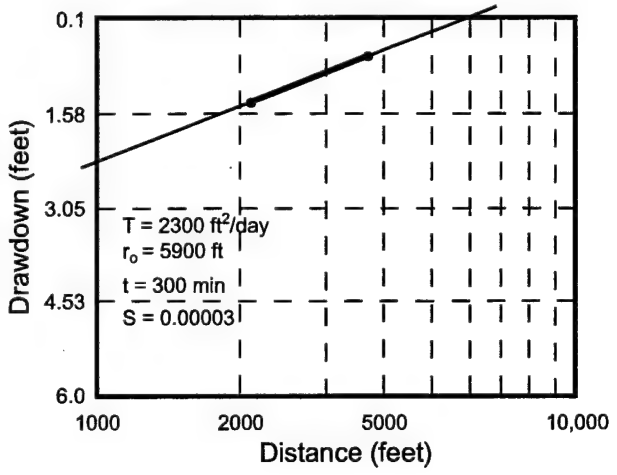

Figure 6: Distance-drawdown graph. well 1 and Lehman well, during 5-hour pump test on well 4a, 1-1-98.

FIELD TRIP TO ENDLESS CAVERNS, NEW MARKET, VIRGINIA

William K. Jones
P.O. Box 490, Charles Town, WV 25414-0490

The following field trip, held during the Karst Modeling Symposium, illustrates many of the characteristics of subsurface dissolution features in carbonate rocks.

Tour Route: The tour follows I-64 west from Charlottesville, Virginia, to Staunton and then proceeds north on I-81 to New Market. Charlottesville is situated in the Piedmont physiographic province on Precambrian metamorphics (Lynchburg gneiss). About 10 miles (16 km) west of Charlottesville, I-64 climbs over the Blue Ridge at Rockfish Gap. The Catoctin greenstones (Eocambrian metabasalts) are exposed in several roadcuts on the north side of I-64 on the east flank of the Blue Ridge. The west flank of the Blue Ridge is underlain by lower Cambrian clastics (Chilhowee group) and the Cambro-Ordovician carbonates are exposed throughout most of the Valley of Virginia. The course of I-81 between Staunton and New Market is on carbonates with Massanutten Mountain (Devonian clastics) rising to the east and North Mountain (Devonian and Silurian clastics) to the west. The Shenandoah Valley (Valley and Ridge physiographic province) lies within the Massanutten synclinorium, where the rocks are generally steeply dipping to overturned. The field-trip route is sketched on the accompanying map (Figure 1) from Gathright (1976). A more detailed description of the karst features of the Shenandoah Valley is presented on a 1:250,000 scale map by Hubbard (1983).

Endless Caverns: Endless Caverns is in Rockingham County, Virginia, a few miles south of New Market. The cave was discovered in 1879 and was first opened as a commercial venture in 1920. Several studies of the cave were conducted by the Explorers Club and the American Museum of Natural History in 1925 and 1940 (Hubbard, 1995). More than 8000 meters of passage have been surveyed and exploration continues. The commercial tour covers about 1200 meters (Figure 2). Endless Caverns is developed primarily in middle Ordovician New Market and Linclonshire Limestones exposed along the base of the western flank of Massanutten Mountain. The cave is developed along several levels in an anticlinal fold trending NNW with most passage development along the strike on the eastern flank of the anticline. The rocks commonly dip about 20 to 30 degrees to the east. A small stream flows north and west through the lower level and resurges in a spring below the gift shop. One measurement of a magnetic reversal in the sediment record reported by G. S. Springer (Hubbard, 1995) suggests that the cave is at least 788,000 years old.

Endless Caverns contains numerous secondary deposits of calcium carbonate, including shields and rimstone dams. Geologically, the main interest of the cave is in its variety of solution features, which appear to have formed under different hydraulic conditions. Much of the upper level part of the cave appears to have formed under phreatic (closed-conduit) flow conditions with latter imprinting of vadose stream activity. Vadose features include canyon passages and deposits of stream gravels. Ceiling domes, pendants (between anastomosing ceiling channels) and half-tubes (individual ceiling channels) formed under closed-conduit flow conditions. Several classic papers on speleogenesis refer to solution features in Endless Caverns to support various hypotheses (Davis, 1930, p. 607-610; Bretz, 1942, p. 740-742; Bögli, 1980, p. 159). Hydologically, the cave offers a well-preserved record of dissolution activity and a chance to enter a small part of a complex limestone aquifer.

New Market Well Field: The town of New Market has developed a well field along the North Fork of the Shenandoah River in the lower Ordovician carbonates (Beekmantown Group and Chepultepec Formation). Several wells were determined to be "surface-water influenced" by the Virginia Department of Health and were thus not acceptable as water sources for the town. Well 6 was sited at the intersection of two fracture traces oriented N15°W and N30°E. Well 6 was drilled to a depth of 309 feet and cased to 249 feet. The 15-inch-diameter well (cased to 10 inches) showed a yield in excess of 1500 gpm (5,700 L/min). Pumping the well for five days at 900 gpm (3,400 L/min) resulted in the sudden appearance of several cover-collapse sinkholes in the field adjacent to the well (Brown, 1996). These sinkholes have been covered and the well is currently online.

References cited

Bögli, Alfred, 1980, Karst hydrology and physical speleology: Spring-Verlag, New York, 284p.

Bretz, J H., 1942, Vadose and phreatic features of limestone caverns: Journal of Geology, v. 50, p. 675-811.

Brown, Terri, 1996, Cover-collapse sinkhole development, Shenandoah County: Memorandum to Town of New Market, Aug. 16, 1996.

Davis, W. M., 1930, Origin of limestone caverns: Geol. Soc. of America. Bull., v. 41, p. 475-628.

Gathright, T. M., II, 1976, Geology of the Shenandoah National Park, Virginia, VA Div Mineral Resources, Bull 86, 93p.

Holsinger, J. R., 1975, Descriptions of Virginia caves: VA Div. of Mineral Resources, Bull. 85, 450p.

Hubbard, D. A., Jr., 1983, Selected karst features of the northern Valley and Ridge province, Virginia: VA Div. of Mineral Resources, Pub. n. 44, one sheet.

Hubbard, D. A., Jr., 1995, Endless Caverns, *in* Kastning, Kass, D.A.Hubbard, Jr., E.H.Kastning, and K.M. Kastning (eds.), Origin of caves and karst in the Shenandoah Valley, Rockingham and Agusta Counties, Virginia: 1995 NSS Field Trip Guidebook, 50p.

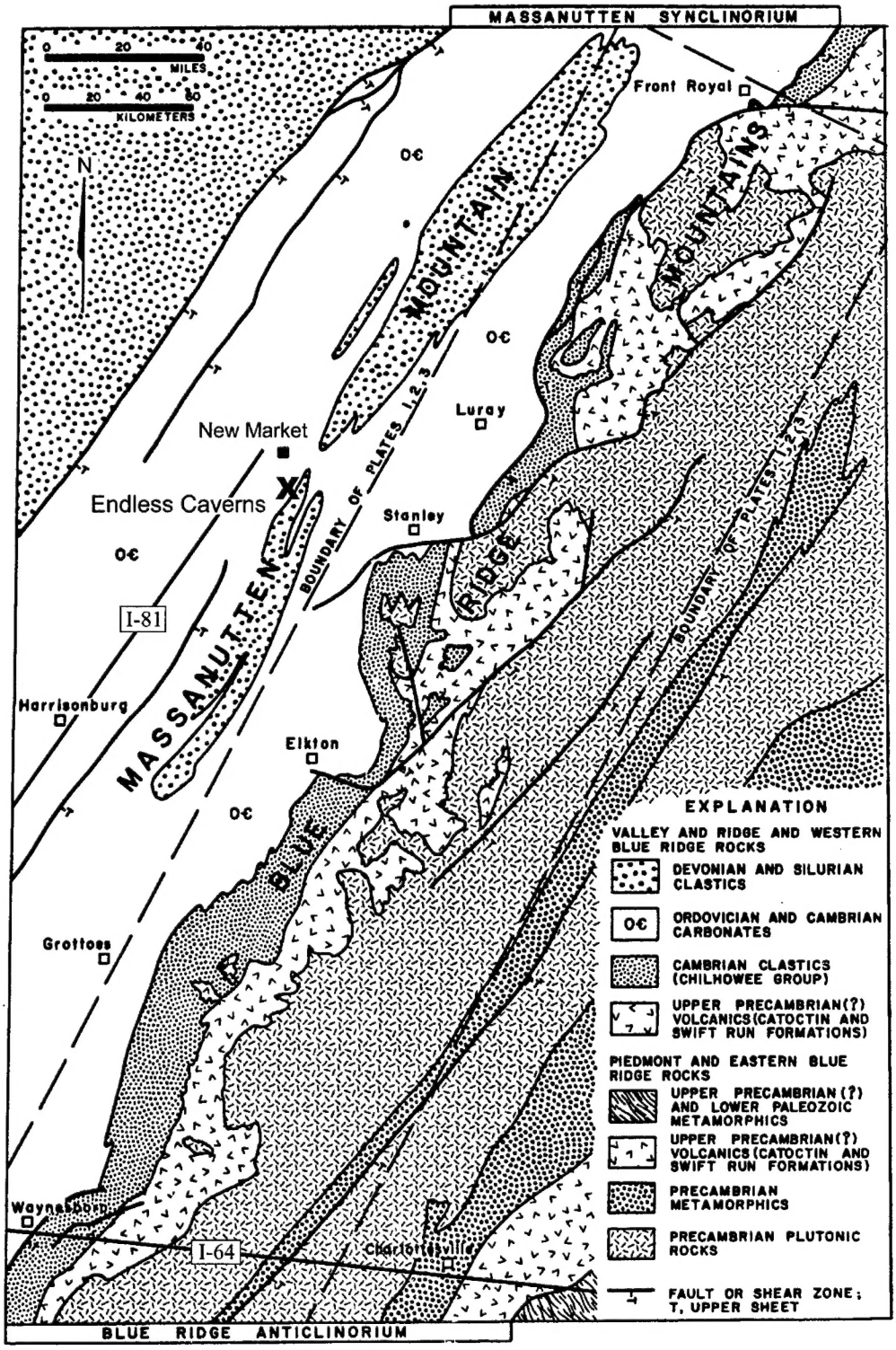

Figure 1: Generalized geologic map of field-trip area, from Gathright (1976).

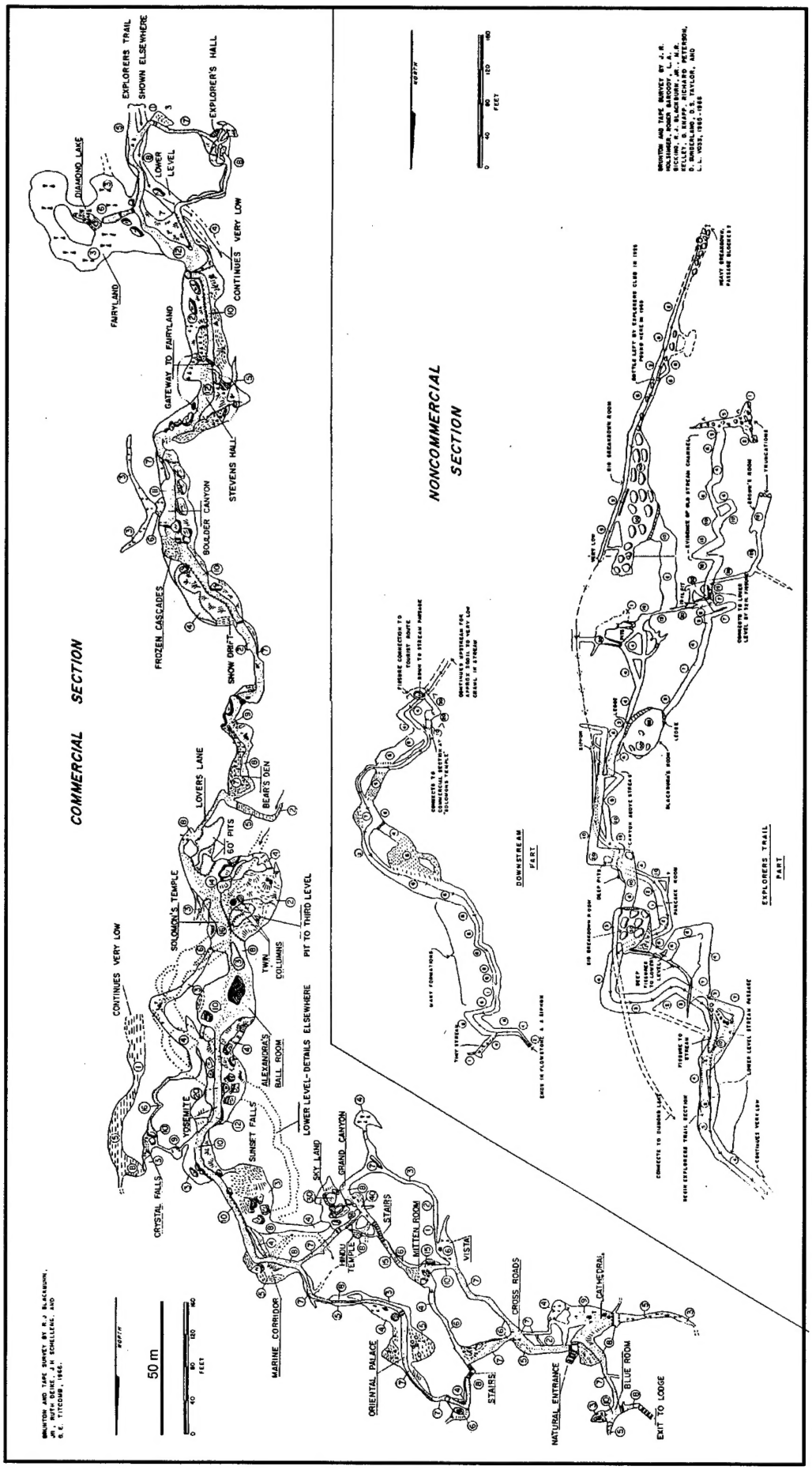

Figure 2: Map of Endless Caverns (1966) from Holsinger (1975).

Author Index